Covalently Bound Fluorine-Containing Monolayers on Silicon and Oxides

Formation, Stability and Tribology

Sidharam Pundlik Pujari

Thesis committee

Promotors

Prof. Dr H. Zuilhof
Professor of Organic Chemistry
Wageningen University

Prof. Dr C.J.M. van Rijn
Professor of Microsystem and NanoTechnology for Agrofood and Health
Wageningen University

Other members

Prof. Dr F.A.M. Leermakers, Wageningen University
Prof. Dr E. Sudhölter, Delft University of Technology
Prof. Dr W. Browne, University of Groningen
Dr E. Gelinck, TNO Science and Industry, Eindhoven

This research was conducted under the auspices of the Graduate School VLAG (Advanced studies in Food Technology, Agrobiotechnology, Nutrition and Health Sciences).

Covalently Bound Fluorine-Containing Monolayers on Silicon and Oxides

Formation, Stability and Tribology

Sidharam Pundlik Pujari

Thesis

submitted in fulfillment of the requirements for the degree of doctor
at Wageningen University
by the authority of the Rector Magnificus
Prof. Dr M.J. Kropff,
in the presence of the
Thesis Committee appointed by the Academic Board
to be defended in public
on Friday 6 September 2013
at 4 p.m. in the Aula.

Sidharam Pundlik Pujari
Covalently Bound Fluorine-Containing Monolayers on Silicon and Oxides: Formation, Stability and Tribology.
304 pages.

PhD thesis, Wageningen University, Wageningen, NL (2013)
With references, with summaries in English and Dutch.

ISBN: 978-94-6173-651-2

Table of Contents

Chapter 1	General Introduction	1
Chapter 2	Hexadecadienyl Monolayers on Hydrogen-terminated Si(111): Faster Monolayer Formation and Improved Surface Coverage Using the Enyne Moiety	25
Chapter 3	Mono-Fluorinated Alkyne-Derived SAMs on Oxide-Free Si(111) Surfaces: Preparation, Characterization and Tuning of the Si Workfunction	55
Chapter 4	Ultra-Low Adhesion and Friction of Fluoro-Hydro Alkyne-Derived Self-Assembled Monolayers on H-terminated Si(111)	93
Chapter 5	Highly Wear-Resistant Ultra-Thin Per-fluorinated Organic Monolayers on Silicon (111) Surfaces	135
Chapter 6	Covalently Attached Organic Monolayers onto Silicon Carbide from 1-Alkynes: Molecular Structure and Tribological Properties	149
Chapter 7	Organic Monolayers from 1-Alkynes Covalently Attached to Chromium Nitride: Alkyl and Fluoroalkyl Termination	185
Chapter 8	Tribology and Stability of Organic Monolayers on CrN: A Comparison among Silane, Phosphonate, Alkene, and Alkyne Chemistries	213
Chapter 9	Superoleophobic and Highly Stable Perfluorinated Monolayers on Polymer Surfaces	241
Chapter 10	General Discussion	275
Summary		287
Samenvatting		291
Overview of completed training activities		295
Acknowledgments		297
List of publications		300
About the author		303

CHAPTER 1

General Introduction

The formation of fluorinated monolayers with a minimized surface energy and an improved chemical stability on specific substrates will enable outstanding tribological properties and is the main goal of the research described in this thesis. Inorganic substrates, such as Si(111), silicon carbide (SiC), chromium nitride (CrN), and organic nano-micro-textured substrates such as PMMA, PDMS, PS and PEEK have been studied. Both fluorinated and non-fluorinated monolayers with a high packing density were obtained using functionally different surface attaching groups like alkenes, alkynes, enynes, silanes, and phosphonates. Most of these attaching moieties have been used before, but the deepening understanding of the factors that determine monolayer qualities allowed the development of even better attaching groups, like the ynenes.

Newly synthesized fluorinated alkyne-derived monolayers will be described exhibiting a minimized surface energy and an exceptionally low critical surface tension. The chemical stability in various aqueous media at different temperatures was also studied. Nano-tribology measurements were performed using atomic force microscopy (AFM) to verify a minimum in adhesion, friction and wear. The organic monolayers obtained on various surfaces in this study will be useful in MEMS/NEMS high performance industrial applications.

Table of Contents

1 General Introduction 1
1.1 Introduction 3
1.2 Organic Monolayers on Silicon-Rich Surfaces 4
1.2.1 Silicon Surfaces 4
1.2.2 Silicon nitride (SiN) surfaces 5
1.2.3 Silicon carbide (SiC) surfaces 7
1.3 Organic Monolayers on Oxide Surfaces 8
1.4 Superoleophobic Surface Modification 9
1.5 Tribology 12
1.5.1 Surface roughness, hydrophobicity and tribological properties 14
1.5.2 Tribological properties of self-assembled monolayers 15
1.6 Aim of this Research 17
1.7 Outline of this Thesis 17
1.8 References 20

1.1 Introduction

Micro/Nano Electro Mechanical Systems (MEMS/NEMS) are becoming increasingly important for a wide range of products, including airbag sensors, digital light projector chips (beamers), microfluidic devices, car tire pressure monitoring systems, etc. Given their potential, several industrial and governmental roadmaps[1] are forecasting the "imminent broad-based impact of MEMS/NEMS technology in modern society" or "the world we are living is fashioned by interfaces, surfaces and ultra-thin films"[2] suggesting that MEMS/NEMS devices should by now be as common as the personal computer. Tremendous progress has been made in micro-fabrication techniques using monocrystalline silicon both as an electronic and a mechanical bulk material. Miniaturization of mechanical/electronic devices is a lot more than just scaling down the device components. The design engineer needs to weigh for instance the magnitudes of the possible consequences from the reduction on both the volume and surface of the particular device. An increase of the friction force with respect to the inertial force is inherent to an increase in the ratio between surface and bulk material. Also wear imposes severe constraints on how much material may erode before miniaturized hightech devices stop working. The development of highly robust surfaces with a reduced adhesion, friction, and resistance against wear is therefore important for many of these MEMS/NEMS devices. However, large-scale implementation of MEMS and NEMS is still highly challenging, and significantly limited by incomplete control over the relevant surface parameters.

Since the invention of the transistor in 1947, there has been a widespread and continuing interest in understanding the physical and chemical properties of monocrystalline silicon semiconductor surfaces.[3, 4] Also outside the field of microelectronics, such as genomic, proteomic,[5] lab-on-chip,[6] microfluidic[7] and other BioMEMS applications require adequate control of surface characteristics by applying suitable monolayers. The enormous resources of (bio-)organic surface chemistry can be used to permit access to a broad range of surface functionalities.[8-10]

Surface modification by organic monolayers was pioneered in 1946 by Zisman et al.,[11] who used long-chain hydrocarbons with polar end groups to form monolayer films on several polar surfaces. After that Sagiv[12] introduced the concept of Self-Assembled Monolayers (SAMs) in 1980. These monolayers have thicknesses in the range of a few nanometers, but they are able to significantly transform the physical properties (electrical and mechanical) of the substrates. Some unique properties of SAMs are due to their highly ordered and oriented structure, and the flexibility to incorporate almost any groups

in the chain (or at the terminal position of the anchoring molecules). This makes them a highly versatile tool in making a variety of surfaces with tuned chemical and physical properties. SAMs have thus found application in areas such as protective layers, analytical sensor layers, and catalytic structures.[13] Many types of SAMs have been studied over the last three decades, with thiolates on gold as likely the most studied ones due to their high order and ease of formation.[14]

The most important criteria in the formation of SAMs are the choice of the surface and a chemically compatible grafting molecule to control various monolayer parameters such as density, orientation, stability, etc. There are three main structural features of SAM-forming monomers. a) Terminal functional group, which dictates the new surface properties, b) hydrocarbon linker chain (typically polyethylene), which assists in the packing and organization of the monolayer, and c) an anchoring group, linking this 'linker-functionality' system to the substrate by specific interactions. A wide variety of anchoring groups have been studies over the years, such as thiols, alcohols, alkynes, alkenes, siloxanes and phosphonates. They are known to self-assemble on a wide variety of active surfaces by forming covalent linkages on the surface having hydrogen, metal, hydroxyl and/or oxide termination.

1.2 Organic Monolayers on Silicon-Rich Surfaces

1.2.1 Silicon Surfaces

A variety of surface passivation methods has been investigated to preserve the nearly ideal electrical properties of oxide-free Si(111) surfaces in ambient conditions.[8] The formation of in particular Si-C bonds has attracted considerable interest due to the kinetic inertness of these bonds as compared to Si-O or Si-H bonds. The almost non-polar Si-C bond is chemically more stable than Si-O bonds on oxidized Si surfaces, and less susceptible to hydrolysis and other nucleophilic substitution reactions.[15] Hydrogen-terminated Si(111) surfaces have been functionalized by a variety of methods using alkenes, alkynes, –OH,[16] –C(O)H, $–NH_2$, –Br, –C(O)Cl, and –SH reactive groups.[17] For the formation of Si-C bonds various methods are used, like radical initiator, thermal, photochemical UV and white light-initiated reactions, catalytic coupling using Grignard chemistry on halide-terminated surfaces to obtain novel mechano-chemical and electrochemical surface modification routes as shown in **Figure 1**.[8]

For molecules with just one binding site the resultant layer will typically be a monolayer. Furthermore, as the underlying silicon surface can be tuned both electronically and topographically this system has a huge versatility. Si(111) faces can be prepared to be

atomically flat with a combination of mechanical and chemical polishing, and Si(111) and Si(100) faces can also be provided with a micro and nanoscale roughness using a range of isotropic and anisotropic wet and dry etching techniques.[18]

The challenge with this covalently coated Si is to achieve high-quality layers without the formation of silicon oxide. As (partly) oxidized surfaces will be detrimental for electronic properties of electronic devices, applications in aqueous media thus require to prepare oxide-free modified substrates of substantial stability. Amongst other conditions this requires that the surface modification is performed in an inert atmosphere with degassed chemicals of high purity (typically in GC/MS >99.99%). The difficulty of this challenge is demonstrated by many examples in the literature where visible SiO_x peaks are observed in X-ray photoelectron spectroscopy (XPS) scans of the Si 2p region of the spectrum binding energy at 102 - 103 eV.

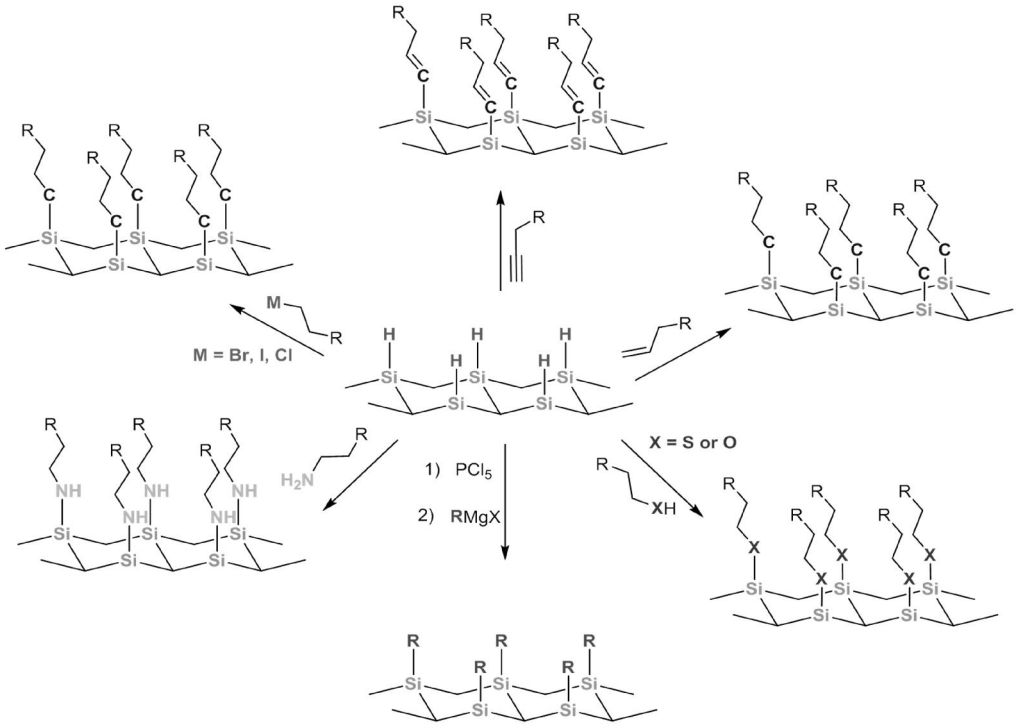

Figure 1. Several modification routes for hydrogen-terminated Si(111) surfaces.[10, 19, 20]

1.2.2 Silicon nitride (SiN) surfaces

Silicon nitride surfaces have been extensively studied due to their remarkable dielectric properties and resistance to chemical and mechanical attack (wear resistance) enabling good tribological performance under a wide range of conditions.[21] During the last 20 years

the surface chemistry of SiN and also SiC has been greatly developed (**Figure 2**), particularly because of its increasing application in the semiconductor industry.

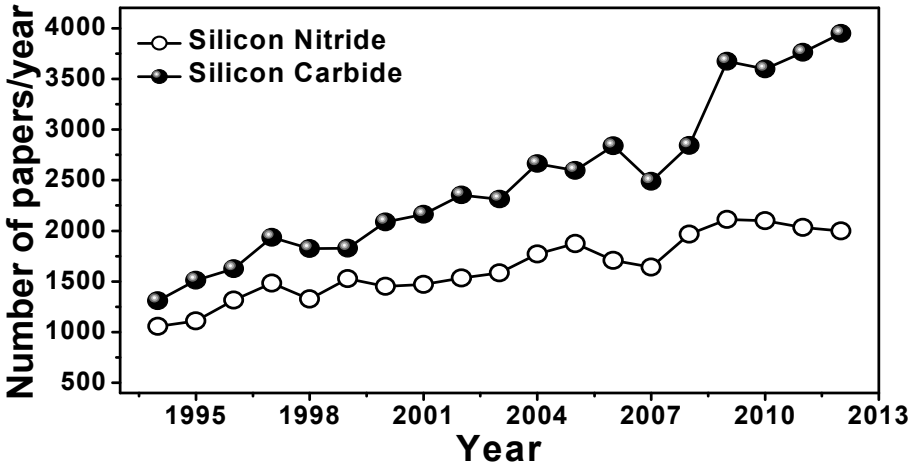

Figure 2. Annual trends in the number of publications for silicon carbide (SiC) and nitride (SiN). (from: www.scopus.com, with the terms "Silicon Nitride" and "Silicon Carbide")

Well-controlled and stable modification of un-oxidized SiN has been made possible with the covalent attachment of organic monolayers.[22, 23] This has opened up many new opportunities for optoelectronic applications, including optoelectronics, biosensors, and waveguide material with a refractometric or fluorescence detection technique. In addition, the mechanical robustness and electrical resistance of SiN allow for the development of micro- and nano-electromechanical systems (MEMS and NEMS) and for use as coating material in sensors based on electrical impedance or vibrating micro-cantilevers.[24] Examples of silicon nitride as modified with different organic monolayers are shown in **Figure 3**.

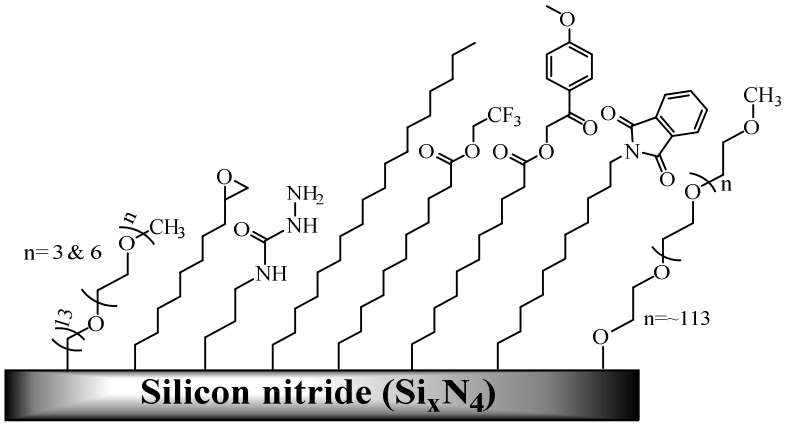

Figure 3. Examples of silicon nitride surface modified with different organic monolayers.[22, 25-27]

1.2.3 Silicon carbide (SiC) surfaces

Silicon carbide is being increasingly studied, due to its outstanding mechanical hardness (Mohr's Index = 9) and excellent chemical stability. As a result, it is also heavily investigated for use in high-temperature tribological systems.[28, 29] To this aim, more detailed information on its tribological behavior is required, in particular, information on friction coefficients and wear rates under different conditions to ensure efficient and reliable performance. Furthermore, a deeper understanding of the wear mechanisms and of the relationship between these mechanisms and the nanostructure of the material is needed to develop improved materials with an enhanced performance.[30]

SiC with a chemically modified surface layer is also used in, for example, refractometers and biosensors.[31] Some theoretical studies have been reported on the chemisorption of organic molecules onto clean or SiC surfaces, which show the potential of this material to form hybrid structures for bio(techno)logical applications. This is of interest, since the high biocompatibility of SiC itself allows its use in medical applications, for instance as a supporting material of bioactive layers for sensing or as a passivation coating for prostheses or microelectrodes. Both such sensing and biomedical applications would benefit from specific surface modification.[32]

With an eye to such chemistry, our group reported recently on the thermal and UV light-induced modification of poly-SiC hydroxyl-terminated surfaces as shown in **Figure 4**. In this manner Markovnikov addition was obtained, yielding highly stable and good-quality monolayers from several simple alkenes (e.g., contact angles up to 107° for octadecene-derived monolayers on SiC).[31] This reaction also works well on the probably the best studied silicon-rich material, namely glass,[33] which leads us to the topic of the next paragraph.

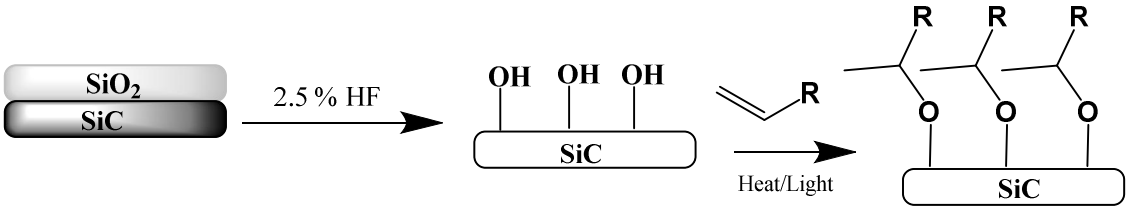

Figure 4. Attachment of alkyl monolayers on hydroxyl-terminated SiC surfaces.[31]

1.3 Organic Monolayers on Oxide Surfaces

Hydroxyl-terminated oxidic substrates provide a highly interesting class of materials, which have been used for a plethora of fundamental studies and applications. Surface modification thereof by organic monolayers can be aimed for in various different manners, several of which have become rather routine practices. **Figure 5** shows different anchoring groups provided on a hydroxyl-terminated inorganic substrate.

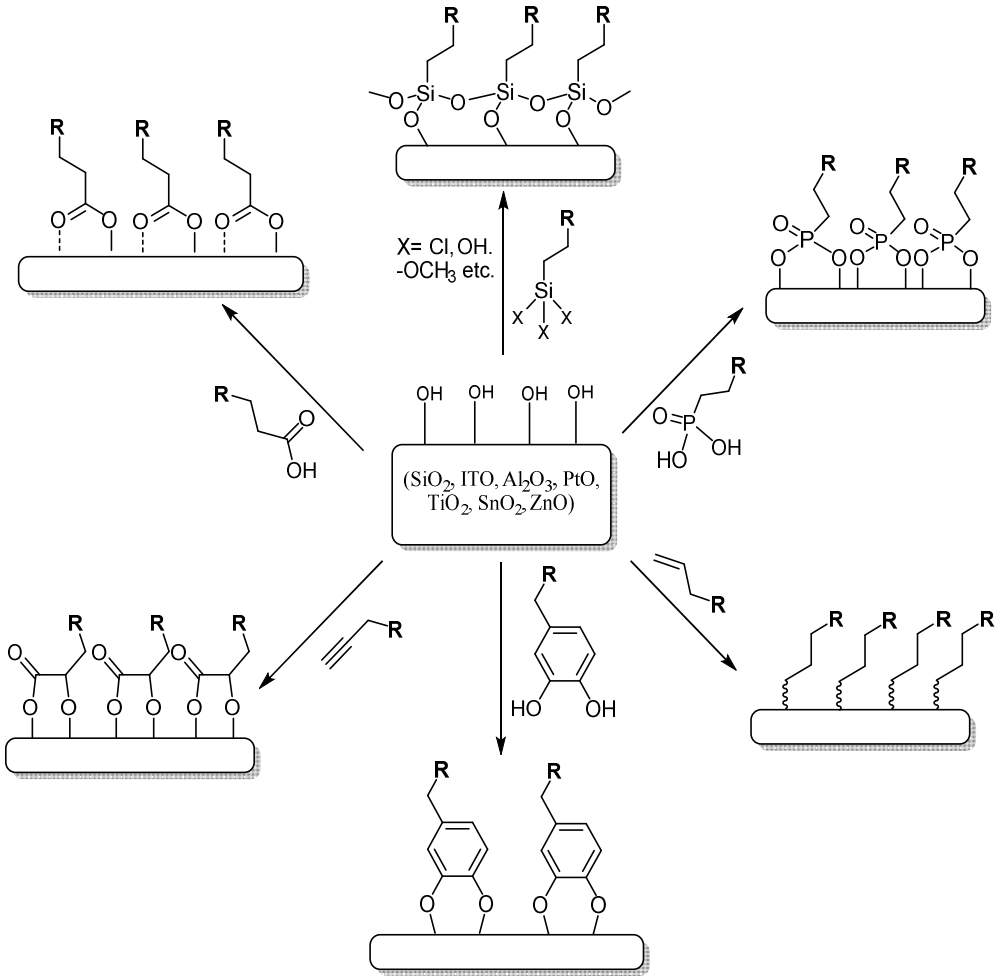

Figure 5. Alkyl monolayers using different anchoring groups for the modification of metal oxide surfaces.[34-36]

Over the years several researchers have worked on tailoring the anchoring molecules to tune their properties in order to understand and further improve the formation of SAMs. Knowledge is thus obtained in the underlying mechanism of competing reactions such as intermolecular, molecular-substrate and molecular-solvent interactions. Selection of the right surface and anchoring molecules provides a flexible tool to develop materials with

desired properties at both the molecular and material level. As far as surface modification of oxidic materials is concerned, topics of interest require the possibility to use easy-to-synthesize, apolar molecules to provide high chemical stability to the modified surface, by using mild, non-corrosive reaction conditions, possibly combined with light-induced reactivity to allow non-contact patterning. Such chemistry using terminal alkenes has initially been developed by our group and that of Hamers[34,35] on glass, hydroxyl-terminated SiC and TiO_2. More recently, this has been extended to surfaces like aluminum oxide, ITO and ZnO, and of course the question arose whether it can be extended even further, so as to provide other materials with fundamentally new surface properties. In fact, the chemistry outlined in this thesis on the modification of chromium nitride is an example of precisely this. A review of this topic is forthcoming.[37]

1.4 Superoleophobic Surface Modification

Surfaces and materials that are to a very high degree repellent to fluids are of great interest for numerous commercial and specialty applications, including non-fouling,[38] self-cleaning,[39] and stain-resistant clothing.[40] The primary measure of wetting of a liquid on a non-textured (or smooth) surface is the static or equilibrium contact angle θ. It is given by Young's relation as follows:

$$\cos\theta = \frac{\gamma_{SV} - \gamma_{SL}}{\gamma_{LV}}$$

Here, γ refers to the interfacial tension and S, L and V refer to the solid, liquid and vapor phases, respectively. The solid–vapor interfacial tension (γ_{SV}) and the liquid–vapor interfacial tension (γ_{LV}) are also commonly referred to as the solid surface energy and the liquid surface tension, respectively. Surfaces that display contact angles $\theta > 90°$ with water are considered hydrophobic, while surfaces that display contact angles $\theta < 90°$ with water are considered hydrophilic.

Relatively recently, a new classification, known as superhydrophobic surfaces, has emerged. Superhydrophobic surfaces display water contact angles greater than 150° along with low contact angle hysteresis.[41] Here, contact angle hysteresis refers to the difference between the advancing and the receding contact angles. Water droplets can easily roll-off and/or bounce on such surfaces. Note that all superhydrophobic surfaces are nano or micro textured (or rough), as the maximum water contact angle measured thus far on a textured surface is ~160°.[42] The Cassie-Baxter model or Wenzel model are needed to describe the corresponding contact angles depending on the wetting state (see **Figure 6**):

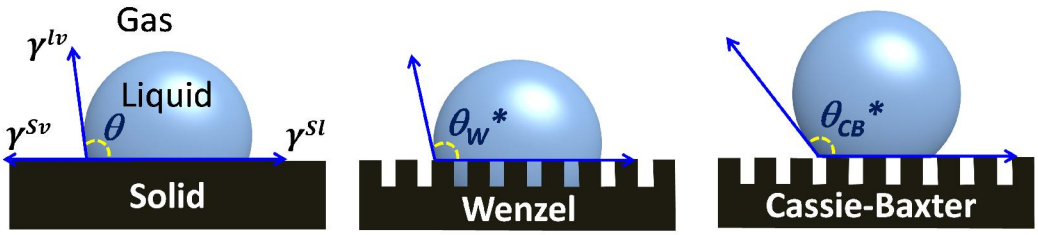

Figure 6. The micro/nano texture of the substrate will co-determine the corresponding contact angle. Wenzel model (middle) whereby the water droplet penetrates the protuberances down to the surface, and Cassie-Baxter model (right side) which assumes the water droplet retains its shape whilst perched on top of the structures.

Superhydrophobic surfaces are pervasive in nature with various plant leaves, gecko's feet, water strider, troughs on the elytra of desert beetles and insect wings, displaying extreme water repellency. Inspired by natural superhydrophobic surfaces, several researchers have also engineered artificial (or synthetic) superhydrophobic surfaces, as displayed in **Figure 7**.[43, 44]

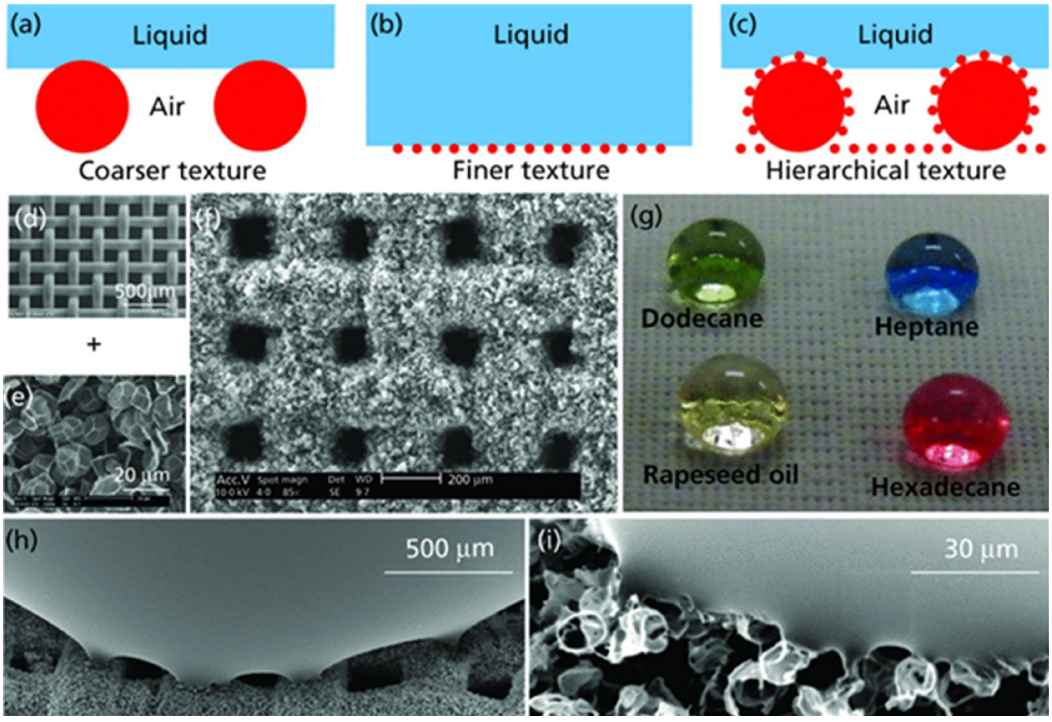

Figure 7. (a–c) Schematic of a liquid droplet in the Cassie-Baxter state on a coarser textured surface, a finer textured surface and a hierarchically textured surface, respectively. (d–f) SEM images of the coarser texture, finer texture and the hierarchically textured surface fabricated by overlaying the finer texture on the coarser texture. (g) Droplets of various low surface tension liquids displaying very high contact angles on the hierarchically textured surface. (h and i) SEM images showing the vicinity of the

contact line along the coarser length scale texture and the finer length scale texture, respectively, on top of the hierarchically structured surface. The distortions in the contact line are evidence of air trapped at both the length scales.[44] The vicinity of the contact line was imaged using a PDMS droplet that was cross-linked on top of the hierarchically textured superoleophobic surface. [44]

In a similar manner, based on their respective contact angles with oils, it is possible to classify surfaces as oleophilic ($\theta < 90°$), oleophobic ($\theta > 90°$) or superoleophobic ($\theta^* > 150°$ and low contact angle hysteresis). Here, θ^* refers to the apparent contact angle, that is the contact angle on a textured surface. In contrast with the numerous naturally occurring superhydrophobic surfaces (see e.g. Figure 8), there are not known natural superoleophobic surfaces. This is because oils possess significantly lower surface tension values than water and consequently spread on most natural and synthetic surfaces. Previous work[42] has explained how re-entrant surface textures, in conjunction with surface chemistry and roughness, can be used to engineer superoleophobic surfaces, even with extremely low surface tensions liquids such as oils and alcohols.

As an example of a low surface energy material octameric fluorinated polyhedral oligomeric silsesquioxane (Fluoro-POSS) nano-composite can be mentioned. Fluoro-POSS constitutes a new class of materials, in which the silsesquioxane cage is surrounded by fluorinated alkyl groups. A number of different molecules with various fluoroalkyl groups have been developed, as shown in Figure 8C. Fluoro-POSS have been studied on various textured and non-textured materials. The high concentration of perfluorinated carbons in the alkyl chains leads to extremely low surface energies for surfaces decorated with these molecules.[45] Additionally covalently bound monolayers are more stable as compared to non-covalently bonded films.[46]

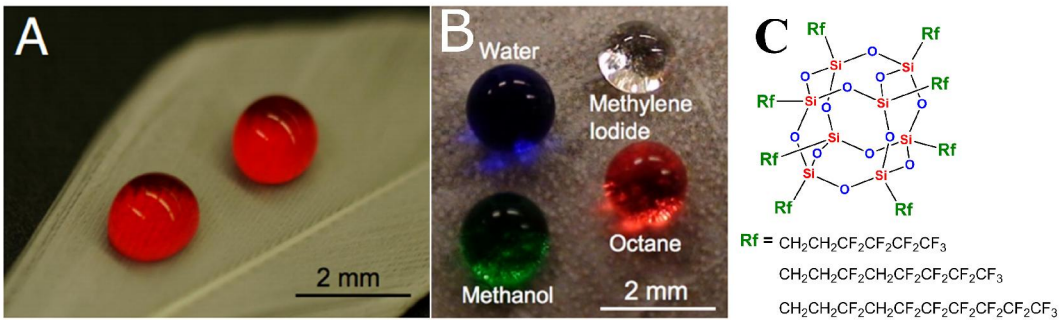

Figure. 8. Imbuing oleophobicity to natural surfaces. (A) Droplets of rapeseed oil (γ/v = 35.7 mN/m), colored with oil red O, on a duck feather dip-coated in a solution of fluorodecyl POSS. (B) Droplets of water (γ/v = 72.1 mN/m), methylene iodide (γ/v = 50.1 mN/m),methanol (γ/v = 22.7 mN/m), and octane (γ/v = 21.7 mN/m) on a lotus leaf surface covered with electrospun fibers (beads-on-strings morphology) of PMMA + 44 wt% fluorodecyl POSS. A reflective surface is visible underneath all droplets, indicating the presence of microscopic pockets of air and the formation of a composite interface.[47] (C) Extremely low surface energy POSS compounds.[45]

1.5 Tribology

The word 'tribology' is derived from the ancient Greek word *tribos, which means rubbing*, and the suffix *-logy* from –logia, *study of*. Tribology is the science of interacting surfaces in relative motion and of related subjects and practices. Wear resistance is an important subject in tribology. Tribological knowledge helps to improve lifetime, safety and reliability of interacting machine components, and yields substantial economic benefits as well as long-term reliability.[48]

Two recent developments have allowed tremendous progress in the systematic study of interfacial effects with high resolution. First of all, the development of proximal probes, in particular tip-based scanning probe microscopies (such as scanning tunneling microscopy (STM), atomic force microscopy (AFM)), and surface force apparatus (SFA)), has allowed the study of surface forces, typically down to the range of picoNewtons. This has stimulated the development of various methods and means for modifying and manipulating micro-nanostructures. Secondly a range of computational methods for simulating the interactions between tips and substrates have been developed, which have allowed detailed interpretation and suggestions for further experiments.[2]

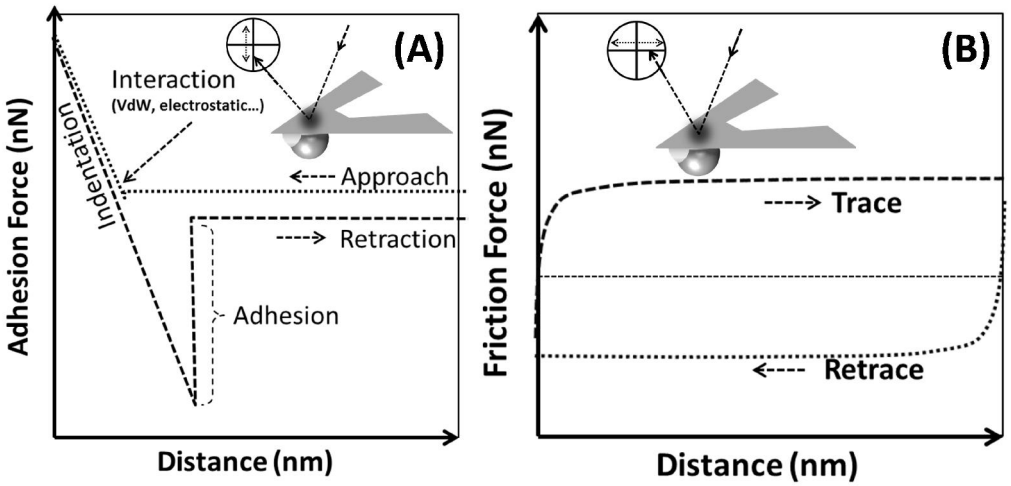

Figure 9. (A) A typical force-distance curve describing a single approach-retraction cycle of the AFM tip, (B) Representative AFM lateral friction force depicting trace and retrace curves of a laterally 90º (laterally is along the surface) moving AFM cantilever.

There are many innovative applications that involve detailed understanding of the tribological basics and related industrial processes on macro- to nano-scales. For the first time in 1984 the tribology of the magnetic storage device has become an important keystone in the field of tribology. Thereafter tribological studies were fully explored on

Micro/nano-ElectroMechanical Systems (MEMS/NEMS), Micro/Nano-Opto ElectroMechanical Systems (MOEMS/NOEMS), bio-MEMS/NEMS and radio-frequency (RF-MEMS/RF-NEMS), which brought many challenges in the field of tribology.

The adhesion forces between two solid surfaces approaching and separating each other has been studied experimentally with the help of AFM (See figure 9A). This has brought much understanding of interactions between surfaces, and the way in which these forces are modified by the presence of a monolayer, a polymer film, or a thin liquid. The friction properties in these systems have been studied by moving an AFM tip with a colloidal probe laterally with respect to the substrate, and these experiments provide fundamental insights into operation of lubricants at the molecular-scale (See figure 9B). The experiments show the relationship between friction, surface roughness, velocity and/or surface condition (dry and wet) and it is not always simple or obvious to measure them with any other method. The AFM studies have also revealed much about the nano-scale nature of wear and indentation of the material interacting with the hard probe.

For experiments on wear resistance related to organic monolayers on different surfaces at the micro or nano levels various modern surface-sensitive techniques will be employed. We will emphasize on hard solid surfaces ranging from diamond-like carbon surfaces to transition metal carbide and nitride surfaces. Many of these solid surfaces are grown by both chemical and physical thin film vapor deposition methods.

For application in high performance technological devices studies on no-wear and low friction surfaces are important. In particular, the nano-tribological behavior of fluorocarbon-hydrocarbon based organic monolayers has been widely studied in order to produce durable low-friction lubricants.[49] These monolayers on Si surfaces improved their tribological properties including wear.[50] Silicon is the primary substrate material for many MEMS/NEMS micro-components whose dimensions are typically between 1 and 100 microns as shown in **Figure 10**.

In MEMS and NEMS devices the numerous relevant forces related to their application are dependent on the size of device. E.g. when the length of the device decreases from 1 mm to 1 μm, the surfaces area will decrease by a factor of million while the volume decrease by factor of a billion. As a result surface forces such as adhesion, friction, capillary forces, viscous drag and surface tension, that are linearly dependent to area, become a thousand times bigger than the forces proportional to the volume such as the inertial and gravitational forces. At these small scales surface properties, such as van der Waals forces, thus greatly influence the performance. Several types of organic monolayers

have been proposed, which have considerably enhanced the tribological properties of silicon at the micro/nano scale.[51]

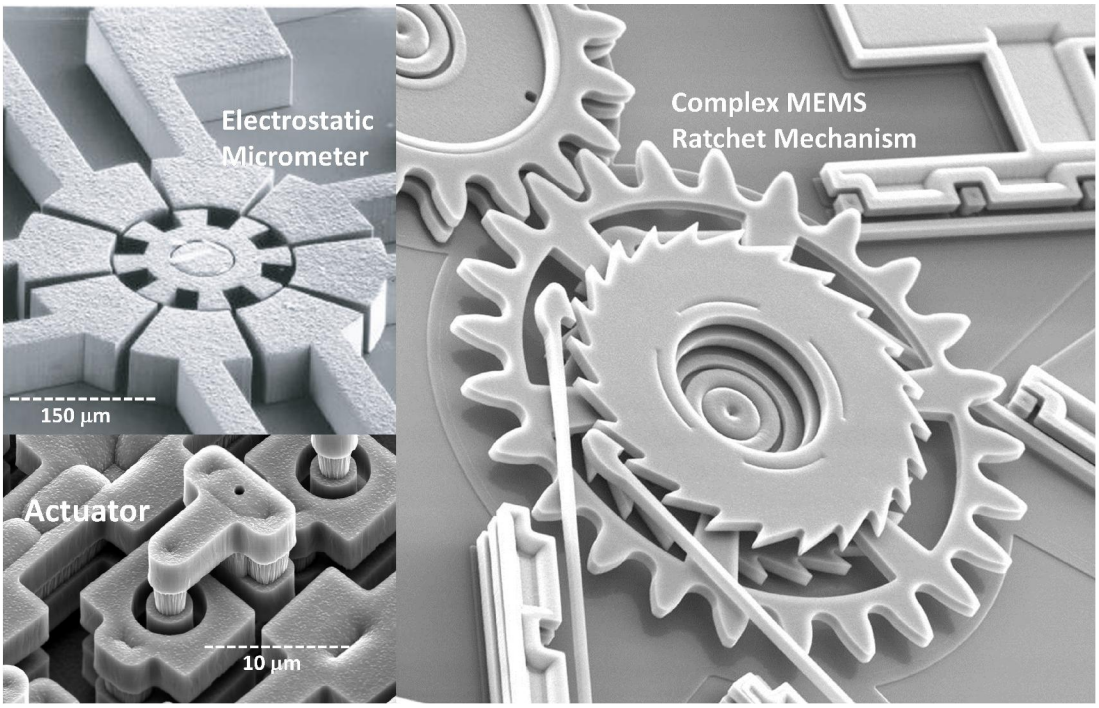

Figure 10. Applications of nanotechnology that operate at high sliding velocities and ditto wear: top left electrostatic micromotor; left bottom actuator (http://www.memx.com/); and right side Complex MEMS ratchet mechanism (http://www.sandia.gov/).

1.5.1 Surface roughness, hydrophobicity and tribological properties

Many tribological studies are carried out on smooth surfaces, using highly polished surfaces with mean roughness well below 10 nm, sometimes even below 1 nm, approaching the typical surface roughness of a polished atomically flat silicon surface. This provides detailed information on the tribological effects of these coatings, as flat surfaces are typically the most easily to study and to understand in detail. Subsequently structuring the surface is an effective way on further lowering the frictional force or changing the contact angle to either more hydrophobic or more hydrophilic.[2, 52-54] It has been useful to classify rough surfaces into three types: irregular rough surfaces,[55] designed rough surfaces,[56] and hierarchical multi-level surfaces.[57]

Structuring the surface can yield tribological benefits. It has, for example, been shown that micro-structuring of read/write heads in magnetic disks results in lower friction.[57] Another biological example is the very low sliding friction at natural synovial joints,

which have friction coefficients of < 0.002 at pressures up to 5 megaPascals or more, a value that has not been attained in human-made joints or in model surfaces in aqueous environments.[58]

The effect of roughness in the macro to nano scale has also been theoretically examined by various groups.[59, 60] The effects were not always easy to understand when varying surface roughness, humidity, etc. A recent study on graphite, MoS_2, and NaCl in ambient conditions using an AFM and a tribometer in combination with a scanning electronic microscope showed that roughness can surprisingly lead to a higher friction due to a change of slope[61, 62] (**Figure 11**). In **Figure 11(a)** a color-coded image of the topography is shown on top; in the middle a double, a fivefold, and a single step; and at the bottom a higher frictional increase for upward scans is shown clearly. **Figure 11(b):** plots of frictional increase, as observed at three different step edges, as a function of the load in upward panel; the frictional increase grows linearly with load, while it is constant for downward scans, as shown in bottom panel.[62]

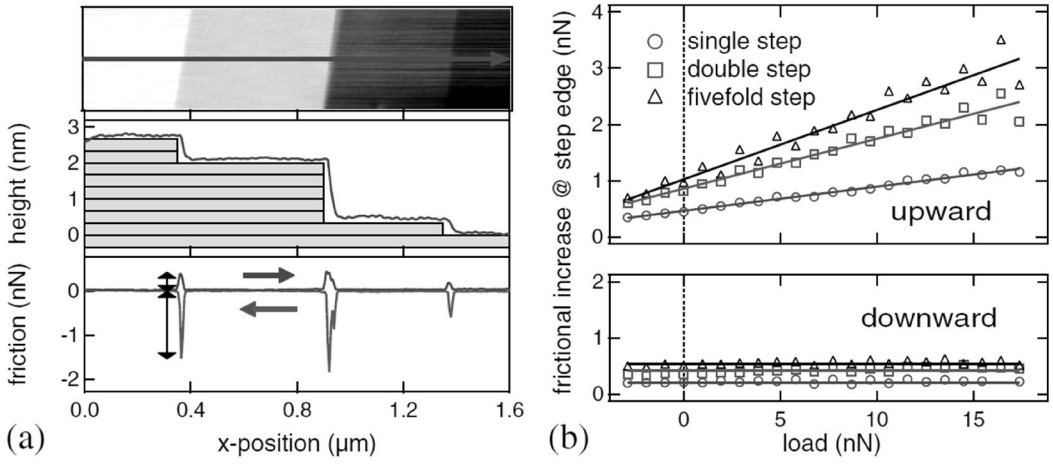

Figure 11. The frictional behavior of graphite at atomic scale surface steps.[62]

1.5.2 Tribological properties of self-assembled monolayers

For molecular force measurements on a laterally small scale, atomic force micro/nano-scopic (AFM) methods have been used. To obtain a well-defined probe geometry, spherical probes have been attached to AFM cantilevers. **Figure 12** depicts both AFM adhesion force-distance curves and a typical lateral friction force trace and retrace curve. Monolayer films offer distinct advantages over many standard strategies for lubrication of MEMS devices, because the molecular components can assemble onto the targeted the

surface, even in the presence of nano scale gaps between moving components.[48, 63] Specific surfaces can be addressed by matching the adsorbate head group with the surface.

Fluorocarbon-based films are generally preferred in low-friction tribological applications.[64, 65] In addition, most MEMS devices are fabricated from silicon,[66] and therefore, there is a growing interest in fluorocarbon-based, wear-resistant surfaces. This has led to several studies on the tribological properties of fluorine-coated silicon surfaces.[54, 67-69] Tribological properties of monolayer films are also dependent on their internal stabilities, which are influenced by interchain interactions (Van der Waals) and the adsorbate-substrate bond.

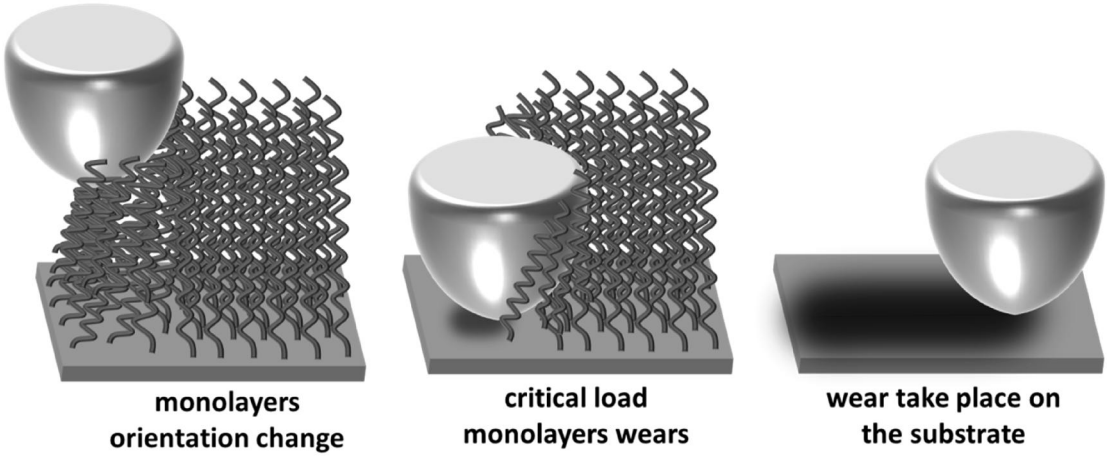

Figure 12. Schematic representations of the wear mechanisms in monolayers with an increasing normal load.[49]

By scanning the sample in two dimensions with the AFM, wear scars are generated on the surface. High-quality monolayers with long carbon chains exhibit excellent tribological properties especially characterized by improved wear properties.[70] Most of the monolayers only change orientation when normal loads are exerted below a critical value. However, at a certain critical load the monolayer may show wear or abrasion, due to severe changes in the interfacial intermolecular bond strengths as shown in Figure **12**.[49] Bhushan et al.[71] reported that longer chain methyl-terminated alkylsilane or phosphate organic monolayers exhibit a significant decrease in friction and a reduced tendency to wear compared to shorter chain monolayers. They have shown that alkylsilane monolayers having a chain length of at least more than 12 carbon atoms, and preferably rather 18 or more, are recommended for tribological applications. The disorder of the alkyl chains in short chain hydrocarbon disulfide SAMs was found to result in a noteworthy increase in friction, due to a less crystalline structure and an enhanced lateral cohesion. However, they were found less compliant in shearing .[72]

1.6 Aim of this Research

Despite the fundamental scientific importance of organic monolayers, many questions about their formation, structure and behavior remain unanswered. Answering these questions is therefore highly relevant, also in view of the ever growing industrial interests: How will a change of anchoring moieties alter the binding mode of a monolayer? How do the polar moieties in a monolayer affect the overall surface dipole forces, and thereby electrical properties like the work function? Which reaction mechanisms occur during formation of monolayers? How stable are these monolayer under different chemical and mechanical (tribological) conditions? How do chemical and physical properties change if hydrogen is substituted to fluorine or vice versa? While several of these questions have been answered for a selected series of monolayers, systematic studies are still rare. The aim of the research described in this thesis is to partly fill this gap, largely by focusing on three aspects: to examine monolayer formation for different flat and nanostructured surfaces, to determine the structure and stability of these monolayers in relation to the terminal functional groups, and finally, to evaluate and optimize the tribological properties of both fluorinated and non-fluorinated monolayers, with the aim to make truly low-friction surfaces. Fortunately, these goals have come within reach.

1.7 Outline of this Thesis

In this thesis the surface modification, stability and tribology properties will be studied of several inorganic substrates: Si(111), silicon carbide (SiC), and chromium nitride (CrN), as well as of various organic substrates: PMMA, PDMS, and PEEK. We will focus on the formation of dense monolayers, investigate their structure in great detail, and determine changes in surface energy, tribological properties and chemical stability.

In Chapter 2 to 3 the formation of dense monolayers on Si(111) are described, whereas chapter 4, 5, 6, 7, and 8 deal with the relation between the obtained monolayers and its tribological properties. Chapter 9 deals with superoleophobic nanotextured organic substrates (PMMA, PDMS, PS, and PEEK).

In Chapter 2 we investigated the use of a novel functional group, ynenes, for monolayer formation on silicon. This nucleophile reacts faster with H-Si(111) than alkynes and is shown to be a better reagent for dense monolayer formation. The kinetics of the surface attachment reactions were followed by studying partially complete monolayers obtained after fixed times. Next, in order to reveal the influence of the structurally different linkages (Si-C=C-C=C versus Si-C=C) to the H-Si(111) substrate the

quality, structure and surface coverage of the resultant monolayers have been studied both experimentally and theoretically.

In Chapter 3 we describe the formation of self-assembled monolayers with five different ω-fluorinated 1-alkynes of different lengths (F-$(CH_2)_{8-16}$-C≡CH), onto an oxide-free, H-Si(111) surface. Characterization was based on XPS, IRRAS, ellipsometry, NEXAFS and water contact angle measurements. The thickness, tilt angle and surface coverage was determined, and compared with the result of molecular modeling. Finally charge transport was measured across a metal/monolayer-semiconductor junction, and it is concluded that via fluorination the charge transport can be fine-tuned through modulation of the surface potential (work function).

In Chapter 4 we investigated the tribological properties of a number of newly synthesized fluorine-containing fixed chain length terminal alkynes, which were attached onto H-Si(111) substrates. We showed by a series of experimental measurements and theoretical calculations that an increasing number of fluorine atoms in the main chain decreases the surface tension, the work of adhesion and also the friction coefficient. We had set ourselves the goal to get something significantly better than Teflon coated unmodified substrates, and we really achieved this (we got the lowest friction and adhesion currently reported for *any* flat surface!)

In **Chapter 5** we focused on the surface chemistry and wear resistance of perfluorinated monolayers coated on Si(111) by using AFM and SEM measurements. Such wear resistance of modified Si is of increasing importance, as outlined in section 1.2.1 above. A comparison is made of the wear properties on a varying number of fluorine atoms (#F atoms = 0 - 17) at a constant chain length (C_{16}).

In **Chapter 6** we describe newly discovered insights in the structural and tribological properties of fluorinated and non-fluorinated monolayers bound to SiC surfaces. The mode of attachment for 1-alkynes onto SiC was studied using various physical characterization techniques in detail. It is also demonstrated using extensive AFM experiments that the fluorinated monolayers show excellent tribological properties compared with non-fluorinated surfaces, which render them particularly interesting for the development of new coating materials in high-performance microelectromechanical devices.

Chapter 7 outlines for the first time, the formation of stable fluorinated-non-fluorinated alkyne derived organic monolayers on plasma-activated, hydroxyl-terminated CrN surfaces through covalent bond formation with anchoring alkyne molecules. Subsequently, the kinetics of alkyne- and alkene-derived monolayers was discussed. We describe the use of various fluorinated and non-fluorinated 1-alkynes to form monolayers

onto hydroxyl-terminated CrN surfaces via Cr-O-C linkages under thermal conditions. Various chain lengths and degrees of fluorination were used, to study the influence on the packing density of the monolayer, and the resulting hydrophobic properties. To probe the binding to the surface more deeply, monolayers derived from 1-hexadecene and 2-hydroxyhexadecanoic acid (2HHDA) were also studied. The resulting modified surfaces were characterized in detail to elucidate their binding mode and various physical properties using static water contact angle measurements, infrared spectroscopy, and X-ray photoelectron spectroscopy (XPS) have been obtained.

In Chapter 8 we investigated the chemical stability and tribological performance of a variety of organic monolayers on chromium nitride, as derived from different anchoring groups and with varying chain length. To study the chemical stability, we used three different media such as strong acid (pH = 3), strong base (pH = 11) and in water at 65 °C. The replacement of the methyl group by the fluorinated terminal groups to enhance the performance in tribology was also studied. In addition, wear resistance on fluorinated surfaces was studied using DLC (diamond like carbon) coated probes, and they show low wear resistance. The obtained results provide a valuable reference for the development of high-performance devices.

In Chapter 9 we combine the plasma-induced nanotexturing of polymeric surfaces of polymethyl methacrylate (PMMA), polyether ether ketone (PEEK), and polydimethyl siloxane (PDMS) with a covalently attached perfluorinated monolayer. The resulting hierarchically ordered surfaces were characterized in detail by SEM, IR and XPS analyses. Static contact angles and concomitant hysteresis are measured with a variety of liquids, ranging from water to hexadecane and soya oil, on freshly prepared samples, but also after prolonged (> 1 month) exposure to aqueous media. The resulting data show for the first time that non-degrading (surfaces are stable for > 40 days in water!) superoleophobicity can be produced on polymeric surfaces using a simple and generic technology suitable for most polymers.

Chapter 10 summarizes the most important achievements and places them in a wider context. Furthermore, we will comment on currently on-going and likely or desired future research, and address the potential of MEMS/NEMS applications of surface-modified hard and soft materials.

1.8 References

1. Pelesko, J. A.; Bernstein, D. H., *Modeling MEMS and NEMS*. CRC Press: 2002.
2. Bhushan, B., *Handbook of Nanotechnology*. 2 ed.; Springer-Verlag New York, LLC: 2007; p 1222.
3. Waltenburg, H. N.; Yates, J. T., Surface-chemistry of silicon. *Chem. Rev.* **1995,** 95, (5), 1589-1673.
4. Casady, J. B.; Johnson, R. W., Status of silicon carbide (SiC) as a wide-bandgap semiconductor for high-temperature applications: A review. *Solid-State Electronics* **1996,** 39, (10), 1409-1422.
5. Hirschman, K. D.; Tsybeskov, L.; Duttagupta, S. P.; Fauchet, P. M., Silicon-based visible light-emitting devices integrated into microelectronic circuits. *Nature* **1996,** 384, (6607), 338-341.
6. Pallandre, A.; de Lambert, B.; Attia, R.; Jonas, A. M.; Viovy, J. L., Surface treatment and characterization: Perspectives to electrophoresis and lab-on-chips. *Electrophoresis* **2006,** 27, (3), 584-610.
7. Dittrich, P. S.; Schwille, P., An integrated microfluidic system for reaction, high-sensitivity detection, and sorting of fluorescent cells and particles. *Anal. Chem.* **2003,** 75, (21), 5767-5774.
8. Buriak, J. M., Organometallic chemistry on silicon and germanium surfaces. *Chem. Rev.* **2002,** 102, (5), 1271-1308.
9. Scheres, L.; Giesbers, M.; Zuilhof, H., Organic Monolayers onto Oxide-Free Silicon with Improved Surface Coverage: Alkynes versus Alkenes. *Langmuir* **2010,** 26, (7), 4790-4795.
10. Li, Y.; Calder, S.; Yaffe, O.; Cahen, D.; Haick, H.; Kronik, L.; Zuilhof, H., Hybrids of Organic Molecules and Flat, Oxide-Free Silicon: High-Density Monolayers, Electronic Properties, and Functionalization. *Langmuir* **2012,** 28, (26), 9920-9929.
11. Bigelow, W. C.; Pickett, D. L.; Zisman, W. A., Oleophobic monolayers. I. Films adsorbed from solution in non-polar liquids. *Journal of Colloid Science* **1946,** 1, (6), 513-538.
12. Sagiv, J., Organized monolayers by adsorption. 1. Formation and structure of oleophobic mixed monolayers on solid surfaces. *J. Am. Chem. Soc.* **1980,** 102, (1), 92-98.
13. Onclin, S.; Ravoo, B. J.; Reinhoudt, D. N., Engineering silicon oxide surfaces using self-assembled monolayers. *Angewandte Chemie - International Edition* **2005,** 44, (39), 6282-6304.
14. Ulman, A., Formation and structure of self-assembled monolayers. *Chem. Rev.* **1996,** 96, (4), 1533-1554.
15. Reddy, S.; Assad, P. O.; Haick, H., Highly stable organic modification of Si(111) surfaces: Towards reacting Si with further functionalities while preserving the desirable chemical properties of full Si-C atop site terminations. *J. Am. Chem. Soc.* **2008,** 130, (29), 9184-+.
16. Harada, Y.; Koitaya, T.; Mukai, K.; Yoshimoto, S.; Yoshinobu, J., Spectroscopic Characterization and Transport Properties of Aromatic Monolayers Covalently Attached to Si(111) Surfaces. *The Journal of Physical Chemistry C* **2013,** 117, (15), 7497-7505.
17. Wayner, D. D. M.; Wolkow, R. A., Organic modification of hydrogen terminated silicon surfaces1. *Journal of the Chemical Society, Perkin Transactions 2* **2002,** 0, (1), 23-34.

18. Huang, Z.; Geyer, N.; Werner, P.; de Boor, J.; Gösele, U., Metal-Assisted Chemical Etching of Silicon: A Review. *Adv. Mater.* **2011,** 23, (2), 285-308.
19. Tian, F.; Teplyakov, A. V., Silicon Surface Functionalization Targeting Si–N Linkages. *Langmuir* **2012,** 29, (1), 13-28.
20. Jin, H.; Kinser, C. R.; Bertin, P. A.; Kramer, D. E.; Libera, J. A.; Hersam, M. C.; Nguyen, S. T.; Bedzyk, M. J., X-ray Studies of Self-Assembled Organic Monolayers Grown on Hydrogen-Terminated Si(111). *Langmuir* **2004,** 20, (15), 6252-6258.
21. Fischer, T. E.; Mullins, W. M., Chemical aspects of ceramic tribology. *J. Phys. Chem.* **1992,** 96, (14), 5690-5701.
22. Arafat, A.; Giesbers, M.; Rosso, M.; Sudholter, E. J. R.; Schroen, K.; White, R. G.; Yang, L.; Linford, M. R.; Zuilhof, H., Covalent biofunctionalization of silicon nitride surfaces. *Langmuir* **2007,** 23, (11), 6233-6244.
23. Rosso, M. Modification of silicon nitride and silicon carbide surfaces for food and biosensor application. PhD Wageningn University, Wageningen, 2009.
24. Shekhawat, G.; Tark, S. H.; Dravid, V. P., MOSFET-embedded microcantilevers for measuring deflection in biomolecular sensors. *Science* **2006,** 311, (5767), 1592-1595.
25. Coffinier, Y.; Boukherroub, R.; Wallart, X.; Nys, J. P.; Durand, J. O.; Stievenard, D.; Grandidier, B., Covalent functionalization of silicon nitride surfaces by semicarbazide group. *Surf. Sci.* **2007,** 601, (23), 5492-5498.
26. Manova, R. K.; Pujari, S. P.; Weijers, C. A. G. M.; Zuilhof, H.; van Beek, T. A., Copper-Free Click Biofunctionalization of Silicon Nitride Surfaces via Strain-Promoted Alkyne–Azide Cycloaddition Reactions. *Langmuir* **2012,** 28, (23), 8651-8663.
27. Suo, Z. Y.; Arce, F. T.; Avci, R.; Thieltges, K.; Spangler, B., Dendritic structures of poly(ethylene glycol) on silicon nitride and gold surfaces. *Langmuir* **2006,** 22, (8), 3844-3850.
28. Peter Friedrichs; Tsunenobu Kimoto; Lothar Ley; Pensl, G., *Silicon Carbide*. WILEY-VCH: Weinheim, 2010; Vol. 1.
29. Gao, D.; Carraro, C.; Howe, R. T.; Maboudian, R., Polycrystalline silicon carbide as a substrate material for reducing adhesion in MEMS. *Tribology Letters* **2006,** 21, (3), 226-232.
30. Sasaki, S., The effects of the surrounding atmosphere on the friction and wear of alumina, zirconia, silicon-carbide and silicon-nitride. *Wear* **1989,** 134, (1), 185-200.
31. Rosso, M.; Giesbers, M.; Arafat, A.; Schroen, K.; Zuilhof, H., Covalently Attached Organic Monolayers on SiC and SixN4 Surfaces: Formation Using UV Light at Room Temperature. *Langmuir* **2009,** 25, (4), 2172-2180.
32. Gonzalez, P.; Serra, J.; Liste, S.; Chiussi, S.; Leon, B.; Perez-Amor, M.; Martinez-Fernandez, J.; de Arellano-Lopez, A. R.; Varela-Feria, F. M., New biomorphic SiC ceramics coated with bioactive glass for biomedical applications. *Biomaterials* **2003,** 24, (26), 4827-4832.
33. ter Maat, J.; Regeling, R.; Yang, M.; Mullings, M. N.; Bent, S. F.; Zuilhof, H., Photochemical Covalent Attachment of Alkene-Derived Monolayers onto Hydroxyl-Terminated Silica. *Langmuir* **2009,** 25, (19), 11592-11597.
34. Shah, S.; Benson, M. C.; Bishop, L. M.; Huhn, A. M.; Ruther, R. E.; Yeager, J. C.; Tan, Y.; Louis, K. M.; Hamers, R. J., Chemically assembled heterojunctions of SnO2 nanorods with TiO2 nanoparticles via "click" chemistry. *J. Mater. Chem.* **2012,** 22, (23), 11561-11567.

35. Franking, R.; Kim, H.; Chambers, S. A.; Mangham, A. N.; Hamers, R. J., Photochemical Grafting of Organic Alkenes to Single-Crystal TiO2 Surfaces: A Mechanistic Study. *Langmuir* **2012,** 28, (33), 12085-12093.
36. Rodenstein, M.; Zürcher, S.; Tosatti, S. G. P.; Spencer, N. D., Fabricating Chemical Gradients on Oxide Surfaces by Means of Fluorinated, Catechol-Based, Self-Assembled Monolayers†. *Langmuir* **2010,** 26, (21), 16211-16220.
37. Pujari, S. P.; Wadwha, K.; Scheres, L.; Zuilhof, H., Covalently bound organic Monolayers on Metal Oxide Surfaces. *Angew. Chem. Int. Ed.* **2013**, In Preparations (Invited Review).
38. Cheng, G.; Xue, H.; Zhang, Z.; Chen, S.; Jiang, S., A Switchable Biocompatible Polymer Surface with Self-Sterilizing and Nonfouling Capabilities. *Angew. Chem.* **2008,** 120, (46), 8963-8966.
39. Blossey, R., Self-cleaning surfaces [mdash] virtual realities. *Nat Mater* **2003,** 2, (5), 301-306.
40. Leng, B.; Shao, Z.; de With, G.; Ming, W., Superoleophobic Cotton Textiles. *Langmuir* **2009,** 25, (4), 2456-2460.
41. Pan, S.; Kota, A. K.; Mabry, J. M.; Tuteja, A., Superomniphobic Surfaces for Effective Chemical Shielding. *J. Am. Chem. Soc.* **2012,** 135, (2), 578-581.
42. Tuteja, A.; Choi, W.; Ma, M.; Mabry, J. M.; Mazzella, S. A.; Rutledge, G. C.; McKinley, G. H.; Cohen, R. E., Designing Superoleophobic Surfaces. *Science* **2007,** 318, (5856), 1618-1622.
43. Sun, T.; Feng, L.; Gao, X.; Jiang, L., Bioinspired Surfaces with Special Wettability. *Acc. Chem. Res.* **2005,** 38, (8), 644-652.
44. Kwon, G.; Kota, A. K.; Li, Y.; Sohani, A.; Mabry, J. M.; Tuteja, A., On-Demand Separation of Oil-Water Mixtures. *Adv. Mater.* **2012,** 24, (27), 3666-3671.
45. Mabry, J. M.; Vij, A.; Iacono, S. T.; Viers, B. D., Fluorinated Polyhedral Oligomeric Silsesquioxanes (F-POSS). *Angew. Chem. Int. Ed.* **2008,** 47, (22), 4137-4140.
46. Zhou, H.; Wang, H.; Niu, H.; Gestos, A.; Wang, X.; Lin, T., Fluoroalkyl Silane Modified Silicone Rubber/Nanoparticle Composite: A Super Durable, Robust Superhydrophobic Fabric Coating. *Adv. Mater.* **2012,** 24, (18), 2409-2412.
47. Tuteja, A.; Choi, W.; Mabry, J. M.; McKinley, G. H.; Cohen, R. E., Robust omniphobic surfaces. *Proceedings of the National Academy of Sciences* **2008**.
48. Bhushan, B.; Israelachvili, J. N.; Landman, U., Nanotribology: friction, wear and lubrication at the atomic scale. *Nature* **1995,** 374, (6523), 607-616.
49. Liu, H. W.; Bhushan, B., Nanotribological characterization of molecularly thick lubricant films for applications to MEMS/NEMS by AFM. *ULTRAMICROSCOPY* **2003,** 97, (1-4), 321-340.
50. Singh, R. A.; Pham, D. C.; Kim, J.; Yang, S.; Yoon, E. S., Bio-inspired dual surface modification to improve tribological properties at small-scale. *Appl. Surf. Sci.* **2009,** 255, (9), 4821-4828.
51. Tsukruk, V. V., Molecular lubricants and glues for micro- and nanodevices. *Adv. Mater.* **2001,** 13, (2), 95-108.
52. Hans-Jürgen Butt, M. K., *Surface and Interfacial Forces*. Wiley-VCH: 2010; p 436.
53. Lyklema, J., *Fundamentals of Interface and Colloid Science: Fundamentals*. Academic Press Ltd, London. : 1991; Vol. 1.

54. Liu, Y. H.; Wang, X. K.; Luo, J. B.; Lu, X. C., Fabrication and tribological properties of super-hydrophobic surfaces based on porous silicon. *Appl. Surf. Sci.* **2009,** 255, (23), 9430-9438.
55. Lua, Y. Y.; Niederhauser, T. L.; Wacaser, B. A.; Mowat, I. A.; Woolley, A. T.; Davis, R. C.; Fishman, H. A.; Linford, M. R., Chemomechanical production of submicron edge width, functionalized, similar to 20 mu m features on silicon. *Langmuir* **2003,** 19, (4), 985-988.
56. Shastry, A.; Case, M. J.; Bohringer, K. F., Directing droplets using microstructured surfaces. *Langmuir* **2006,** 22, (14), 6161-6167.
57. Bhushan, B.; Gupta, B. K.; Azarian, M. H., Nanoindentation, microscratch, friction and wear studies of coatings for contact recording applications. *Wear* **1995,** 181, 743-758.
58. Chen, M.; Briscoe, W. H.; Armes, S. P.; Klein, J., Lubrication at Physiological Pressures by Polyzwitterionic Brushes. *Science* **2009,** 323, (5922), 1698-1701.
59. Meine, K.; Schneider, T.; Spaltmann, D.; Santner, E., The influence of roughness on friction Part I: The influence of a single step. *Wear* **2002,** 253, (7-8), 725-732.
60. Meine, K.; Schneider, T.; Spaltmann, D.; Santner, E., The influence of roughness on friction Part II. The influence of multiple steps. *Wear* **2002,** 253, (7-8), 733-738.
61. Singh, R. A.; Yoon, E. S., Friction of chemically and topographically modified Si (100) surfaces. *Wear* **2007,** 263, 912-919.
62. Holscher, H.; Ebeling, D.; Schwarz, U. D., Friction at Atomic-Scale Surface Steps: Experiment and Theory. *Phys. Rev. Lett.* **2008,** 101, (24).
63. Carpick, R. W.; Salmeron, M., Scratching the surface: Fundamental investigations of tribology with atomic force microscopy. *Chem. Rev.* **1997,** 97, (4), 1163-1194.
64. Bhushan, B.; Cichomski, M.; Hoque, E.; DeRose, J. A.; Hoffmann, P.; Mathieu, H. J., Nanotribological characterization of perfluoroalkylphosphonate self-assembled monolayers deposited on aluminum-coated silicon substrates. *Microsystem Technologies-Micro-and Nanosystems-Information Storage and Processing Systems* **2006,** 12, (6), 588-596.
65. Sung, J. C.; Kan, M. C.; Sung, M., Fluorinated DLC for tribological applications. *International Journal of Refractory Metals & Hard Materials* **2009,** 27, (2), 421-426.
66. Maboudian, R.; Ashurst, W. R.; Carraro, C., Tribological challenges in micromechanical systems. *Tribology Letters* **2002,** 12, (2), 95-100.
67. Lorenz, C. D.; Webb, E. B.; Stevens, M. J.; Chandross, M.; Grest, G. S., Frictional dynamics of perfluorinated self-assembled monolayers on amorphous SiO2. *Tribology Letters* **2005,** 19, (2), 93-99.
68. Kim, H. I.; Graupe, M.; Oloba, O.; Koini, T.; Imaduddin, S.; Lee, T. R.; Perry, S. S., Molecularly specific studies of the frictional properties of monolayer films: A systematic comparison of CF3-, (CH3)(2)CH-, and CH3-terminated films. *Langmuir* **1999,** 15, (9), 3179-3185.
69. Kim, H. I.; Koini, T.; Lee, T. R.; Perry, S. S., Systematic studies of the frictional properties of fluorinated monolayers with atomic force microscopy: Comparison of CF3- and CH3-terminated films. *Langmuir* **1997,** 13, (26), 7192-7196.
70. Lee, D. H.; Oh, T.; Cho, K., Combined Effect of Chain Length and Phase State on Adhesion/Friction Behavior of Self-Assembled Monolayers. *The Journal of Physical Chemistry B* **2005,** 109, (22), 11301-11306.
71. Bhushan, B., Nano- to microscale wear and mechanical characterization using scanning probe microscopy. *Wear* **2001,** 250-251, (PART 2), 1105-1123.

72. Schonherr, H.; Vancso, G. J., Tribological properties of self-assembled monolayers of fluorocarbon and hydrocarbon thiols and disulfides on Au(111) studied by scanning force microscopy. *Materials Science & Engineering C-Biomimetic and Supramolecular Systems* **1999,** 8-9, 243-249.

CHAPTER 2

Hexadecadienyl Monolayers on Hydrogen-terminated Si(111): Faster Monolayer Formation and Improved Surface Coverage Using the Enyne Moiety

To further improve the coverage of organic monolayers on hydrogen-terminated silicon (H-Si) surfaces with respect to the hitherto best agents (1-alkynes), it was hypothesized that enynes (H-C≡C-HC=CH-R) would be even better reagents for dense monolayer formation. To investigate whether the increased delocalization of β-carbon radicals by the enyne functionality indeed lowers the activation barrier, the kinetics of monolayer formation by hexadec-3-en-1-yne and 1-hexadecyne on H-Si(111) were followed by studying partially incomplete monolayers. Ellipsometry and static contact angle measurements indeed showed a faster increase of layer thickness and hydrophobicity for the hexadec-3-en-1-yne-derived monolayers. This more rapid monolayer formation was supported by IRRAS and XPS measurements that for the enyne show a faster increase of the CH_2 stretching bands and the amount of carbon at the surface (C/Si ratio), respectively. Monolayer formation at room temperature yielded plateau values for hexadec-3-en-1-yne and 1-hexadecyne after 8 and 16 h, respectively.

Additional experiments were performed for 16 h at 80° to ensure full completion of the layers, which allows comparison of the quality of both layers. Ellipsometry thicknesses (2.0 nm) and contact angles (111 - 112°) indicated a high quality of both layers. XPS, in combination with DFT calculations, revealed terminal attachment of hexadec-3-en-1-yne to the H-Si surface, leading to dienyl monolayers. Moreover, analysis of the Si_{2p} region showed no surface oxidation. Quantitative XPS measurements - obtained via rotating Si samples - showed a higher surface coverage for C_{16} dienyl layers than C_{16} alkenyl layers (63% vs. 59%). The dense packing of the layers was confirmed by IRRAS and NEXAFS results. Molecular mechanics simulations were undertaken to understand the differences in reactivity and surface coverage. Alkenyl layers show more favorable packing energies for surface coverages up to 50 - 55%. At higher coverages this packing energy rises quickly, and there the dienyl packing becomes more favorable. When the binding energies are included the difference becomes more pronounced, and dense packing of dienyl layers

becomes more favorable by 2-3 kcal/mol. These combined data show that enynes provide the highest-quality organic monolayers reported on H-Si onto now.

This Chapter has been published as:

"*Hexadecadienyl Monolayers on Hydrogen-Terminated Si(111): Faster Monolayer Formation and Improved Surface Coverage Using the Enyne Moiety*" Bart Rijksen*, /Sidharam P. Pujari*, Luc Scheres, Cees J. M. van Rijn, J. E. Baio, Tobias Weidner, and Han Zuilhof. *Langmuir* **2012** 28 (16), 6577-6588 (*contributed equally)

Table of Contents

2 Hexadecadienyl Monolayers on Hydrogen-terminated Si(111): Faster Monolayer Formation and Improved Surface Coverage Using the Enyne Moiety 25
2.1 INTRODUCTION 27
2.2 MATERIALS AND METHODS 30
2.2.1 Materials 30
2.2.2 Equipment 30
2.2.3 Synthesis of hexadeca-3-ene-1-yne 30
2.2.4 Hydrogen-terminated Si(111) surfaces 30
2.2.5 Preparation of 3-en-1-ynes and 1-alkynes Derived Monolayers on H-Si(111) 31
2.2.5.1 Kinetic studies 31
2.2.5.2 Quality studies 31
2.3 MONOLAYER CHARACTERIZATION 31
2.3.1 Contact Angle Measurements 31
2.3.2 Ellipsometry 32
2.3.3 X-ray Photoelectron Spectroscopy (XPS) 32
2.3.4 Near Edge X-ray Absorption Fine Structure (NEXAFS) 33
2.3.5 Infrared Reflection Absorption Spectroscopy (IRRAS) 33
2.3.5 Infrared Attenuated Total Reflectance (IRATR) 33
2.3.6 Computational Procedures 34
2.3.6.1 XPS binding energies 34
2.3.6.2 Monolayer simulations 34

2.4 RESULTS AND DISCUSSION 34
2.4.1 Reactivity difference of 3-en-1-ynes and 1-alkynes onto H-Si(111) 34
2.4.2 High-quality 3-en-1-yne and 1-yne monolayers on H-Si(111) 38
2.4.3 Molecular modeling 43
2.5 CONCLUSIONS 47
2.6 REFERENCES 47

2.1 INTRODUCTION

Long-term passivation of oxide-free silicon surfaces can be achieved by the covalent attachment of self-assembled monolayers onto hydrogen-terminated silicon surfaces (H-Si). Not only can these thin organic layers protect the surface from oxidation, they also form a versatile scaffold for (bio)functionalization.[1-6] Many methods and procedures to produce these layers have been described in literature, including thermal[7, 8] and UV[9-12] methods, electrochemistry,[13, 14] and chemomechanical scribing.[15, 16] However, under those reaction conditions side reactions might occur, thereby reducing the quality of the produced layers.[17, 18] Milder methods, which invoke a substantially lower energy input, have been shown to overcome these issues, though at cost of longer reaction times.[19, 20] Hence, a reduction of the reaction time under these mild reaction conditions, while maintaining the oxide-free nature of the organic monolayer-silicon interface, might bring application of these layers in (bio)electronic devices within reach.[21-25]

For these potential applications the stability of the oxide-free monolayer-silicon interface is one of the most important properties, for which oxidation is a hampering factor both during and after the modification process.[26, 27] During the formation of the – not yet complete – monolayer, oxidation by traces of oxygen present in the precursor or reaction flask might be relatively fast, and competes with the precursors for reactive surface sites. After completion of the monolayer the oxidation rate is relatively slow due to the limited diffusion of oxygen through the monolayer[28] but even there, only a small fraction of defects in the monolayer is already sufficient to cause detectable amounts of oxide after prolonged storage in ambient conditions.[29] In order to further improve the stability of the oxide-free monolayer-silicon interfaces, both oxidation routes need to be suppressed via a combination of faster attachment and a higher packing density.

One of the current theories that explain mild attachment involves initiation by nucleophilic attack of the precursors to delocalized silyl radical cations at the H-Si surface (see Scheme 1).[5, 6, 30] Hence, better nucleophiles will improve the initial attack on the

delocalized radical cations and therefore facilitate C-Si bond formation. In addition, recent studies have shown that stabilizing the β-carbon radical intermediate by a neighboring π-system speeds up the propagation of the radical chain mechanism and thereby monolayer formation.[31-33] In accordance with the above, a significant higher reactivity of ω-alkynes compared to ω-alkenes has been demonstrated on H-Si(100) and H-Si(111) surfaces.[34, 35]

Besides the reactivity, also the shape and footprint of the precursor are important parameters, as both can have a tremendous influence on the packing, and thus on the stability of the layer.[36] Limited by steric constraints and unfavorable conformations of the carbon chains near the surface, numerous studies have reported a maximum surface coverage of 50-55% for alkyl monolayers on Si(111).[7, 9, 35, 37-42] However, by introducing moieties with a smaller Van der Waals radius than a regular CH_2-group, i.e., a smaller footprint, packing densities as high as ~67% have been obtained for long alkoxyl (Si-O-C) monolayers[40, 43, 44] and for C_{18} alkenyl (Si-C=C) monolayers on H-Si(111).[19, 35, 36] Obviously, this is a clear indication that even minor structural differences in the linkage can have a major effect on the overall monolayer structure. In addition, regarding the long term stability of the oxide-free interface, we note that a higher surface coverage will not only slow down diffusion of water and oxygen through the monolayer, but will also result in slightly reduced numbers of unreacted H-Si sites at the interface.

All these findings encouraged us to design two new precursors with a further increased reactivity and the proper geometrical requirements. As can been seen in Scheme 1, both candidate structures (hexadec-3-en-1-yne and 1,3-hexadecadiyne) possess a conjugated reactive terminal functionality, which is expected to enhance the nucleophilic attack at the silicon surface and might improve subsequent stabilization of the β-carbon radical intermediate by the neighboring π-system. Furthermore, since CH=CH moieties have a significantly smaller footprint than CH_2-CH_2 moieties, the smaller Van der Waals radius of both linkages to the silicon surface (Si-HC=CH-HC=CH- and Si-HC=CH-C≡C-, respectively) meet the requirements to obtain high surface coverage organic monolayers.

In a recent photospectroscopic study the reactivity of these two candidate structures towards silyl radicals has been investigated.[31] It was shown that hexadec-3-en-1-yne and 1,3-hexadecadiyne are both at least 30 times more reactive than 1-alkynes. However, preliminary results of monolayer-forming experiments showed that diynes polymerize under monolayer-forming conditions, which precludes their use in this.

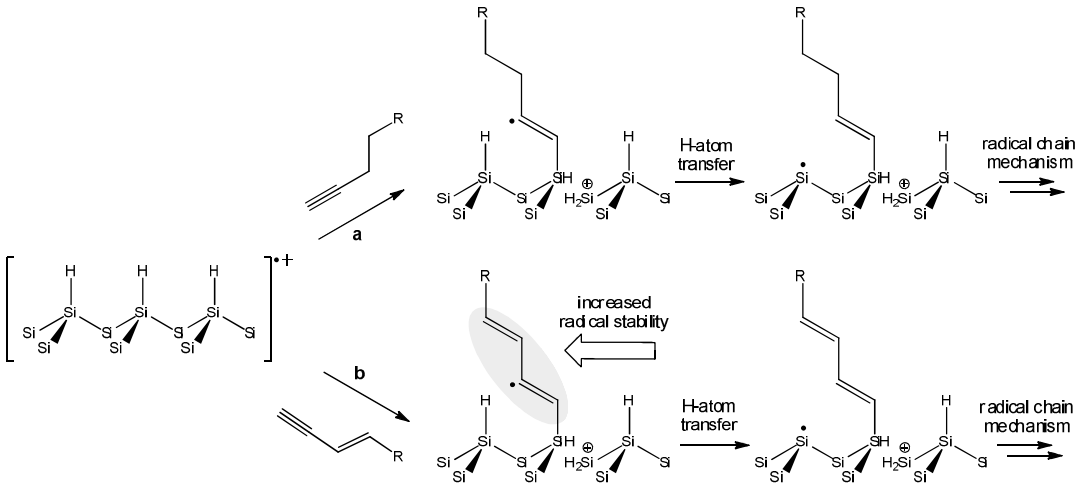

Scheme 1. Mechanistic hypothesis that initiated study of enynes for monolayers on H-Si(111): Nucleophilic attack of (a) 1-alkynes and (b) 3-en-1-ynes to delocalized radical cations at the silicon surface result in the formation of β-carbon radicals. Subsequent transfer of a hydrogen atom from a neighboring Si-H site then results in the formation of a surface-centered radical.

The above ideas and results stimulated us to investigate the kinetics of monolayer formation with hexadec-3-ene-1-yne on hydrogen-terminated Si(111) in detail. To visualize a possible enhanced reactivity of the 3-ene-1-yne functionality compared to 1-alkynes, 1-hexadecyne-derived monolayers were used as a reference. The kinetics of the surface attachment reactions were followed by studying partially complete monolayers obtained after fixed times by static contact angle measurements, ellipsometry, infrared reflective absorption spectroscopy (IRRAS), and x-ray photoelectron spectroscopy (XPS). Next, in order to reveal the influence of the structurally different linkage to the H-Si(111) substrate (Si-C=C-C=C versus Si-C=C) on the quality and structure of the final monolayers, fully completed hexadecadienyl and hexadecenyl monolayers were thoroughly studied by additional quantitative XPS measurements involving rotating Si samples to exclude crystal reflection effects,[35,39] DFT calculations and near-edge x-ray absorption fine structure (NEXAFS) measurements. Finally, a combined *ab initio* and molecular mechanics molecular modeling study was undertaken to provide insight into the subtle chemical and structural differences responsible for the observed reactivity and quality difference between alk-3-ene-1-yne and in 1-alkyne-derived monolayers. The resulting picture clarifies the potential of novel, high-reactivity moieties for the attachment of organic monolayers onto H-Si surfaces.

2.2 MATERIALS AND METHODS

2.2.1 Materials

Bis(trimethylsilyl)-1,3-butadiyne (96%), 1-bromododecane (99%), potassium fluoride dihydrate, dimethylformamide (DMF), hexamethylphosphoramide (HMPA), methyllithium/LiBr in diethylether (1.6 M), di-isobutylaluminumhydride in pentane (1.6 M), dimethoxyethane (DME) (anhydrous), and n-butyllithium in pentane (1.6 M), acetone (semiconductor grade VLSI PURANAL Honeywell 17617) and sulfuric acid (95-97%) were obtained from Sigma-Aldrich. From other sources we purchased hydrogen peroxide (Acros Organics, 35%) ammonium fluoride (Riedel-de Haën, 40%, semiconductor grade VLSI PURANAL Honeywell 17600), deionized water (resistivity 18.3 MΩ cm), pentane (VWR, 95%). 1-Hexadecyne (90%, ABCR, Germany) was purified by column chromatography (hexane) to remove trace amounts of 1-bromoalkane, and subsequently distilled twice under reduced pressure before use. Silicon wafers were (111)-oriented, single-side or doubly polished (500-550 μm thick, n-type doping by phosphorus), and have a resistivity of 2.0 - 8.0 Ω cm (Siltronix, France).

2.2.2 Equipment

NMR spectra were recorded on a Bruker Avance III with an inverse broadband probe running at 400 MHz, with C_6D_6 as solvent. Hexadeca-3-ene-1-yne was purified by HPLC (Shimadzu, ALLTIMA C18 5U column, MeOH, 15 mL/min, UV detection at 215 nm).

2.2.3 Synthesis of hexadeca-3-ene-1-yne

This compound was synthesized according to a literature procedure,[45] using 1-tris(trimethyl)silyl-1,3-hexadeca-di-yne[46, 47] as precursor, and purified by prep-HPLC (C_{18} reversed phase/MeOH) to achieve 99.9% purity as determined with GC-MS. Yield: 90%. ^{1}H-NMR (400 MHz, C_6D_6) δ 0.91 (t, J = 6.8 Hz, 3H), 1.13-1.29 (m, 20H), 1.82 (m, 2H), 3.01 (s, 1H), 5.52 (d, J = 15.6 Hz, 1H), 6.18 (m, 1H). ^{13}C-NMR (100 MHz, C_6D_6) δ 14.39 (CH_3), 23.15, 29.00, 29.14, 29.42, 29.59, 29.85, 30.01, 30.13, 30.16, 30.74, 33.31, 92.79 (HC≡C-), 105.08 (HC≡C-), 110.58 (≡C-CH=), 146.12 (C=CH-CH_2). MS (EI) m/z(%) 220 (1) [M^+], 135 (23), 121 (37), 107 (38), 93 (74), 79 (100), 67 (54), 55 (54).

2.2.4 Hydrogen-terminated Si(111) surfaces

H-Si(111) was prepared by chemical etching as previously reported.[48, 49] All liquid reagents were continuously purged with an argon flow. An n-type Si (111) wafer with a 0.2° miscut angle along <112>, was first cut (10 × 10 mm^2) and subsequently cleaned in a

sonication bath with acetone and then with Milli-Q water (resistivity >18 MΩ cm). The Si wafer was oxidized in freshly prepared piranha solution (H_2SO_4/H_2O_2 3:1) for at least 20 min. After piranha treatment, the substrates were immersed immediately in water and rinsed thoroughly, followed by drying with a stream of argon. Subsequently, the substrates were etched in an argon-saturated 40% aqueous NH_4F solution for 15 min, rinsed by Milli-Q water, and finally dried with a stream of argon. The H-Si surfaces were studied by X-ray photoelectron spectroscopy (XPS) and atomic force microscopy.

2.2.5 Preparation of 3-en-1-ynes and 1-alkynes derived monolayers on H-Si(111)

2.2.5.1 Kinetic studies

After being etched, the samples were rinsed with argon-saturated water, and finally blown dry with a stream of argon. These samples were then immediately transferred to the inert atmosphere glove box. Next, the surface was covered with a few drops of neat 1-hexadecyne or hexadeca-3-ene-1-yne. The reactions were performed at room temperature under ambient light (i.e., standard fluorescent lamps in the fume hood were on). To stop the reaction, the sample was removed from the glovebox and immediately extensively rinsed with pentane and CH_2Cl_2. The sample was then sonicated for 5 min in CH_2Cl_2 to remove physisorbed molecules, after which the samples were blown dry with a stream of dry argon.

2.2.5.2 Quality studies

High-quality monolayers were produced in a fume hood setup described in literature.[35, 48] A three-necked flask was charged with 2 mL of 1-hexadecyne or hexadeca-3-ene-1-yne, and was purged with argon under reduced pressure for 30 min, while being heated up to 80 °C. The freshly etched and dried surface was then quickly transferred into the flask, which was immediately depressurized again. The reaction mixture was kept at 80 °C overnight. The sample was then removed from the flask and immediately extensively rinsed with pentane and CH_2Cl_2, sonicated for 5 min in CH_2Cl_2 to remove physisorbed molecules, and blown dry with a stream of dry argon.

2.3 MONOLAYER CHARACTERIZATION

2.3.1 Contact Angle Measurements

Contact angle measurements were performed on a Krüss DSA 100 contact angle goniometer with an automated drop dispenser and image video capture system. The static

contact angles of six small droplets, (3.0 μL volume of deionized water) dispensed on modified silicon surfaces, were determined using the implemented Tangent 2 fitting model. The digital drop images were processed by the image analysis system, which calculated both the left and right contact angles from the drop shape with an accuracy of ±1.0°.

2.3.2 Ellipsometry

The thickness of the modified silicon surfaces (in the dry state) was measured using a rotating analyzer ellipsometer of Sentech Instruments (Type SE-400), operating at 632.8 nm (He–Ne laser), and an angle of incidence of 70°. The optical constants of the substrate were determined with a piece of freshly etched H-Si(111) (n = 3.819 and k = 0.057). The thicknesses of the monolayers were determined with a planar three-layer (ambient, monolayer, substrate) isotropic model with a refractive index for the organic monolayers of 1.46. The reported values for the layer thickness are the average of eight measurements taken at different locations on the substrate with an error < 1 Å.

2.3.3 X-ray Photoelectron Spectroscopy (XPS)

XPS measurements were performed using a JPS-9200 photoelectron spectrometer (JEOL, Japan). A monochromatic Al Kα X-ray source (h_v = 1486.7 eV) 12 kV and 20 mA using an analyzer pass energy of 10 eV was used. The base pressure in the chamber during measurements was 3×10^{-7} Torr, and spectra were collected at room temperature. The intensity of XPS core level electron was measured as the peak area after standard background subtraction according to the linear procedure. The takeoff angle φ (angle between sample and detector) of 80° is defined with a precision 1°. The typical sample size was 1 × 1 cm^2. For a precise determination of the atomic C/Si ratio of organic monolayers on Si(111), the influence of X-ray photo diffraction (XPD) on the XPS signal had to be accounted for.[35, 39] Therefore, the samples were rotated 360° around the surface normal, yielding rotationally averaged C_{1s} and Si_{2p} emissions to obtain a truly quantitative C/Si ratio which is now independent of the orientation of the sample. As our sample holder only allows rotation of the samples at a takeoff angle of 90°, we used non-monochromatic Al-Kα ray radiation (twin source) at 10 kV and 15 mA with analyzer pass energy of 50 eV and a takeoff angle of 90° for these measurements. All spectra were corrected with a slight linear background before fitting. All XPS spectra were evaluated using the Casa XPS software (version 2.3.15). All binding energies are referenced relative to the main hydrocarbon (CH_2) peak with a binding energy of 285.0 eV.

2.3.4 Near Edge X-ray Absorption Fine Structure (NEXAFS)

NEXAFS spectra were collected at the National Synchrotron Light Source (NSLS) U7A beamline at Brookhaven National Laboratory, using an elliptically polarized beam with ~85% p-polarization. This beam line utilizes a monochromator and 600 l/mm grating providing a full-width at half-maximum (FWHM) resolution of ~0.15 eV at the carbon *K*-edge. The monochromator energy scale was calibrated using the intense C 1s - π^* transition at 285.35 eV of a graphite transmission grid placed in the path of the X-rays. Partial electron yield was monitored by a detector with the bias voltage maintained at -150 V. Samples were mounted to allow rotation and allow changing the angle between the sample surface and the synchrotron X-rays. The NEXAFS angle is defined as the angle between the incident light and the sample surface. The spectra were brought to the standard form by linear pre-edge background subtraction and normalizing to the unity edge jump defined by a horizontal plateau 40–50 eV above the absorption edge.

2.3.5 Infrared Reflection Absorption Spectroscopy (IRRAS)

IRRAS spectra were recorded on a Bruker Tensor 27 FT-IR spectrometer using a variable angle reflection unit (Auto Seagull, Harrick Scientific). A Harrick grid polarizer was installed in front of the detector and was used to record spectra with p-polarized (parallel) radiation with respect to the plane of incidence at the sample surface. All spectra were obtained at an incident angle of 68° (2048 scans). The resolution was set at 1 cm^{-1} per modulation center. The final spectra were obtained using a piranha-oxidized reference surface as background. Data were collected as differential reflectance versus wavenumber. All spectra were recorded at room temperature in dry atmosphere. A linear baseline correction was applied.

2.3.5 Infrared Attenuated Total Reflectance (IRATR)

Infrared spectra were acquired using a Bruker spectrometer (model Tensor 27) equipped with a Harrick ATR accessory (Harrick Scientific Co.) and an FTIR spectrometer equipped with liquid nitrogen cooled mercury cadmium telluride (MCT) detectors. A wire-grid Harrick polariser was placed in front of the sample to measure p- (parallel) or s-(perpendicular) polarization with respect to the light incidence plane. The spectrometer was purged with dry nitrogen to minimize the contribution of moisture and CO_2 to the recorded spectra. Double side polished single crystal n-Si(111) wafers were cut into pieces of 5 × 1 cm^2 and polished to obtain ATR crystals with 45° angles with respect to the large parallel bevel faces, producing approximately 100 internal optical reflections of the incident beam. The reflection spectra of the samples were in the wavenumber range

4000 to 560 cm^{-1} and resolution of 1 cm^{-1} spectra where the average of 10000 scans. The unit of absorbance intensity was defined as −log(R/Ro), where R and Ro are the reflectivity of the substrate with and without the monolayer, respectively.

2.3.6 Computational Procedures

2.3.6.1 XPS binding energies

XPS binding energies were estimated by calculating the orbital energies of molecular analogues of C_{16} chains attached to a silicon surface. A $Si(SiH_3)_3$ group was attached to specifically mimic the Si-C bond.[50] The geometries were optimized with B3LYP/6-311G(d, p), using the Gaussian 09 package.[34] The carbon binding energies were then estimated by calculating the 1s core energy versus the average of the 2p valence orbital energies (mimicking the Fermi level).

2.3.6.2 Monolayer simulations

Unit cells were constructed, and expanded to supercells of 12 × 12 units (33, 50, 67 and 75% surface coverage) and 10 × 15 units (60% surface coverage), following literature procedures.[35] The geometries were optimized using the polymer consistent force field (PCFF) (bottom two rows of Si atoms were constrained) as implemented in the Discover package in Materials Studio, using the ultrafine settings of the smart minimizer routine (line width 0.01 and convergence 10^{-5}, VdW and coulomb, atom centered and long-range correction switched off).[35] All G3 calculations of the binding energies of the chains to the surface were performed using the Gaussian 09 package.

2.4 RESULTS AND DISCUSSION

2.4.1 Reactivity difference of 3-en-1-ynes and 1-alkynes onto H-Si(111)

To study the reactivity difference of alkynes and alk-3-en-1-ynes towards oxide-free hydrogen-terminated Si(111) (H-Si(111)) surfaces, the kinetics of monolayer formation under ambient conditions were explored by analyzing the resulting (partial) monolayers after different reaction times. To minimize the effect of competing oxidation reactions induced by water and oxygen, the experiments were performed in a glovebox under argon atmosphere. Precursors and freshly etched H-Si(111) were deoxygenized by three or more freeze-pump-thaw cycles before transferring them into the glovebox. The reaction was started by covering the freshly etched surfaces with 1 or 2 drops of precursor. The surfaces were then allowed to react for the appropriate time at a constant temperature of

20 °C. Subsequently, the resulting (partial) monolayers were analyzed by water contact angle measurements (static, advancing and receding angles), ellipsometry and x-ray photoelectron spectroscopy (XPS) and infrared reflection-absorption spectroscopy (IRRAS). As shown in Figure 1A, for both precursors, the static contact angles gradually increase in time, while monolayer formation proceeds faster with hexadec-3-en-1-yne than with 1-hexadecyne. With hexadec-3-en-1-yne, the plateau value of 111 - 112°, indicative of hydrophobic and densely packed organic monolayers,[7, 19, 35, 48, 51] was already reached after 8 h, while for 1-hexadecyne these values were only obtained after increasing the reaction time to 16 h. This demonstrates a considerable reactivity difference between both precursors. As expected, this difference in reactivity was also displayed by the ellipsometry measurements (See Figure 1B), which show significant differences in the growth of the layer thickness over time. The hexadecadienyl monolayers reached a thickness of 1.9 nm after 2 h,, while hexadecenyl monolayers were then only 1.5 nm thick. The plateau value 2.1 (± 0.1 nm) nm for hexadec-3-en-1-yne was reached after 8 h, whereas it took the 1-hexadecyne at least 16 h.

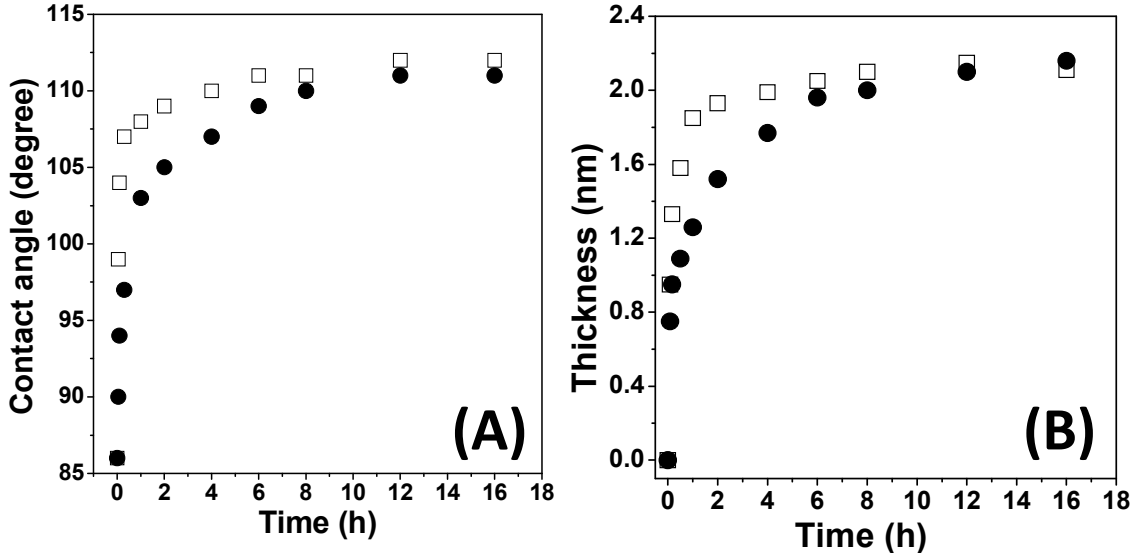

Figure 1. (A) Static water contact angles (± 1°), and (B) layer ellipsometric thicknesses (± 0.1 nm) of hexadec-3-en-1-yne (□) and 1-hexadecyne (●) layers versus the reaction times at room temperature. Each data point represents the average value of two separately prepared monolayers.

In order to monitor the actual formation of the organic monolayer, the contributions of the Si_{2p} and C_{1s} core levels were studied in time by XPS narrow scans. For both precursors, the Si_{2p} signal rapidly decreases in time, which coincides with an increase of the carbon signal at 285 eV (Figure 2A and B). This is a clear indication of the formation of an organic monolayer. Furthermore, the Si_{2p} narrow scans of both partial and complete

organic monolayers, show no visible traces of oxygen at the silicon surface, demonstrating the success of the stringent oxygen-excluding conditions required to study the kinetics of monolayer formation in detail, and to obtain high-quality organic monolayers on oxide-free H-Si (see Figure 2C and D).[20, 35] Finally, from Figure 2E (which shows the C1s/Si2p ratios in time) it becomes clear that the carbon build-up of the 3-en-1-yne layers is faster than of the 1-yne counterpart. In fact the amount of carbon after 16 hours of reaction of 1-yne, is in the case of the 3-en-1-yne already achieved after 6-8 hours of reaction. This indicates a speed-up of a factor ~2, which is in agreement with the contact angles and the ellipsometric thicknesses discussed earlier.

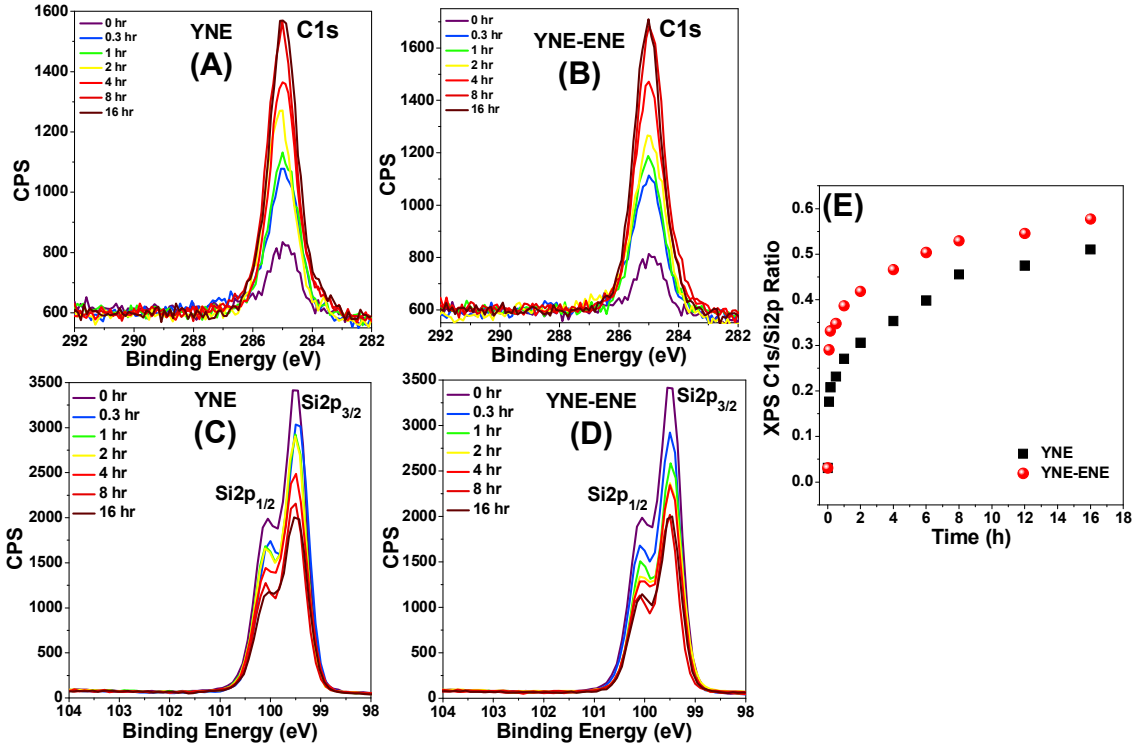

Figure 2. XPS spectra of the C1s (A and B) and Si2p region (C and D) of monolayers on H-Si(111) derived from 1-hexadecyne and hexadec-3-en-1-yne, respectively; and C1s/Si2p ratios in time (E).

To obtain detailed information about the molecular order of the (partial) monolayers in time, IRRAS measurements were carried out. As can be seen in Figures 3A and 3B, the intensities of the antisymmetric (ν_a) and symmetric (ν_s) methylene stretching vibrations grow gradually in time for both precursors, clearly displaying the increasing amount of carbon chains at the surface. Furthermore, upon completion of the monolayers, for both types of monolayer the antisymmetric and symmetric CH_2 stretching frequencies shift

from 2923 to 2918 cm^{-1} and from 2853 to 2848 cm^{-1}, respectivelyThese optimal frequencies were obtained after 4 h for the hexadec-3-en-1-yne and after 8 h for the 1-hexadecyne. This difference of speed (~factor 2) is in line with the contact angle an ellipsometry data in Figure 1. We note that these frequencies correspond to highly ordered organic monolayers and are for 1-hexadecyne in good agreement with literature.[51-53] Moreover, the gradual disappearance of a detectable Si-H stretching vibration at 2083 cm^{-1} (Fig. 3C and D) confirms the formation of a monolayer by adsorption of the precursors onto H-Si(111).[19, 35] The initial rate difference is in line with the speed-up demonstrated earlier. However, loss of a detectable Si-H stretching vibration prevents accurate comparison of the speeds at longer reaction times.

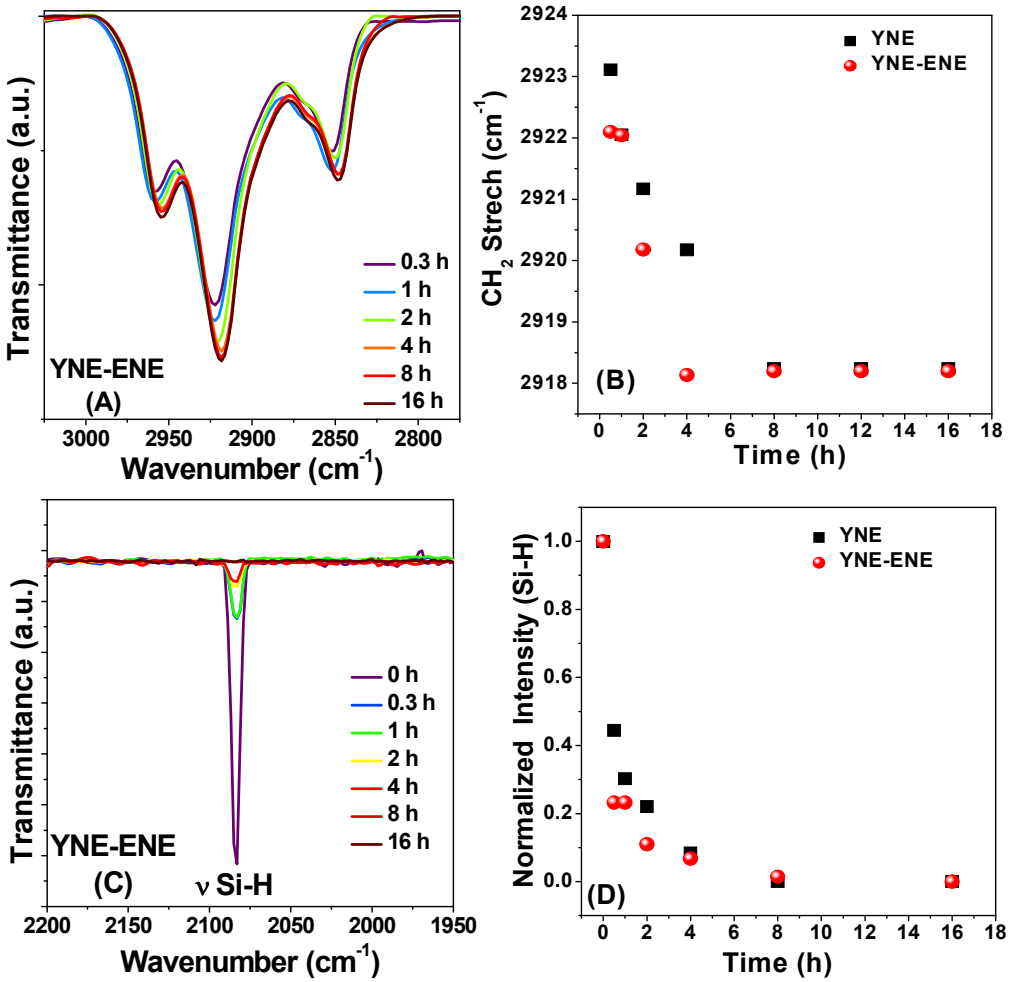

Figure 3. IRRAS data of 1-alkyne-derived and 3-en-1-yne-derived monolayers on H−Si(111) at ambient condition as a function of reaction time: (A) CH_2 stretch region of 3-en-1-yne in time, (B) CH_2 stretch frequencies of 3-en-1-yne and 1-yne monolayers in time, (C) Si-H stretch region of 3-en-1-yne in time, and (D) Si-H stretch normalized peak areas in time.

2.4.2 High-quality 3-en-1-yne and 1-yne monolayers on H-Si(111)

After confirming the considerably higher reactivity of the 3-en-1-yne moiety towards H-Si(111) compared to the 1-yne moiety, the quality of the both final monolayers was studied in more detail. To ensure completion of the monolayer formation, i.e., to minimize the number of defects, more stringent reaction conditions (16 h at 80 °C) were chosen. Static water contact angles of 111 - 112°, advancing contact angles of 116 - 117°, receding contact angles of 109 - 110°, and ellipsometric thicknesses of 2.1 ± 0.1 and 2.2 ± 0.1 nm for monolayers derived from hexadec-3-en-1-yne and 1-hexadecyne, respectively, compare well with literature values (111° and 2.1 nm for 1-hexadecyne) and confirm the high quality of both organic monolayers.[35] The theoretical layer thickness can be determined via equation 1, and 2. By inserting a tilt angle (θ) of 30°, which is the experimentally determined tilt angle of high-quality organic monolayers on gold,[54] a theoretical thickness of 1.90 nm for hexadecenyl and 1.89 nm for hexadecadienyl monolayers was calculated. This is somewhat lower than the ellipsometric values, which is likely caused by the assumed tilt angle of 30°. A smaller tilt angle, indicating more upright positioned chains, will result in thicker layers.

1-hexadecyne (nm):

$$d_{Th} = 0.188 + 1.772\cos\theta + 0.156\sin(35.5 + \theta) \qquad (1)$$

hexadeca-3-en-1-yne (nm):

$$d_{Th} = 0.188 + 1.765\cos\theta + 0.156\sin(35.5 + \theta) \qquad (2)$$

ATR measurements show the anti-symmetric and symmetric CH_2 stretching vibrations at 2918.8 cm^{-1} and 2849.4 cm^{-1} (hexadecenyl), and 2917.6 cm^{-1} and 2847.5 cm^{-1} (hexadecadienyl), respectively for both monolayers (see Figure 4). The value for hexadecenyl monolayers is in line with literature values,[35] and indicative of a highly ordered monolayer. In this regard it should be noted that that these hexadecadienyl monolayers have two methylene groups less for favorable interchain Van der Waals interactions compared to hexadecenyl monolayers and even four methylene groups less compared to hexadecyl monolayers. Therefore it is remarkable that such a highly ordered organic monolayer can be obtained with only 12 CH_2 groups (cf. dodecyl termination),

especially when comparing these low wavenumbers with those of a dodecyl monolayer on H-Si(111) (2922 cm^{-1}).[35]

In addition ATR measurements proved sensitive enough to capture the C=C stretch vibrations around 1600 cm^{-1}. A clear single peak is visible in the hexadecenyl spectrum, whereas hexadecadienyl gives two peaks. Simulations (vibrations obtained from G3 calculations) show that the denyl moiety gives rise to two peaks, and that one is indeed shifted to higher wavenumbers, which is in good agreement with the ATR results (see Figure 4b). This result indicates terminal attachment of the 2-en-1-yne with retention of the double bonds upon monolayer formation. The C-H stretch vibration, however, is only visible in the hexadecadienyl layer (3016 cm^{-1}), which may be explained by the higher concentration (2 double bonds instead of 1).

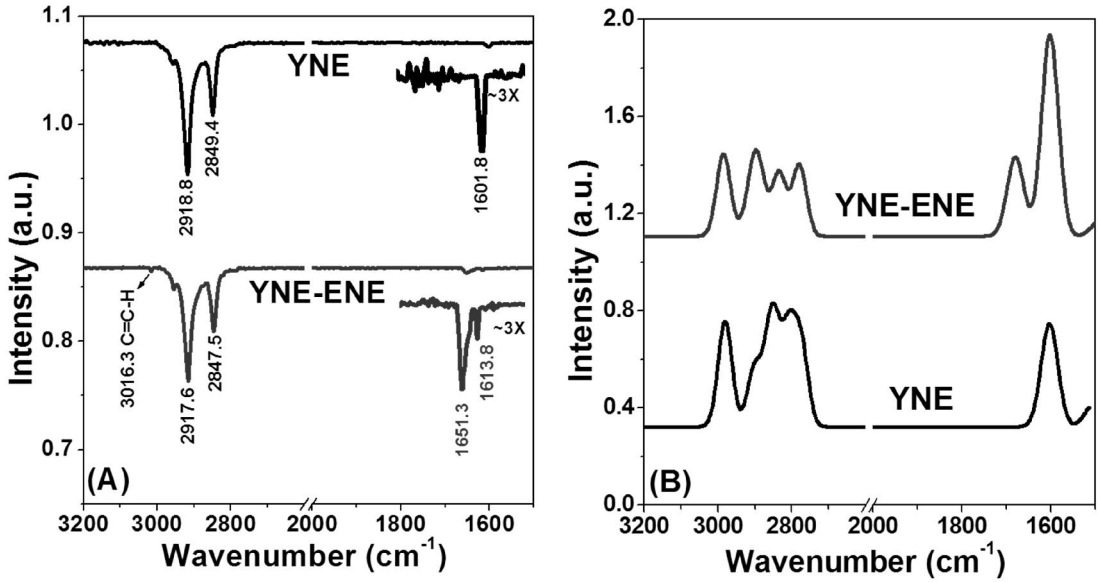

Figure 4. (A) ATR of hexadec-3-en-1-yne (black) and 1-hexadecyne (red) derived monolayers on H-Si(111) at 80 °C; and (B) frequencies from G3 calculations of carbon chains attached to silicon clusters.

To study the linkage to the Si(111) substrate in more detail, XPS C_{1s} narrow scans were recorded. In addition, density functional theory (DFT) calculations were used to calculate the binding energies of the distinct carbon atoms in the linkage. As shown in Figure 5A and B, both C_{1s} spectra are deconvoluted into three contributions. The components at 283.8, 285.0 and 285.7 eV have been assigned to the carbons directly attached to the relatively electropositive silicon (C-Si, E_{calc} = 283.9 eV), the aliphatic carbons (C-C, E_{calc}

= 285.0 eV), and the more electronegative sp^2 hybridized carbons (C=C, E_{calc} = 285.6 and 285.8 eV), respectively. In combination with DFT calculations on other possible binding conformations (see *Supporting Information S.2.2*), the relative intensities of these distinct carbons disclose the linkage of both monolayer types to the H-Si(111) surface, i.e., 1 : 12 : 3 for hexadec-1-en-3-yne-derived monolayers with a Si-C=C-C=C linkage and 1 : 14 : 1 for 1-hexadecyne-derived monolayers with a Si-C=C linkage. In addition, in the Si $_{2p}$ narrow scans obtained for the dienyl and alkenyl layers (see Figure 5C and D), no silicon oxide was identified in the 101 - 103.5 eV region. This again confirms the monolayer quality and its ability to prevent appreciable oxidation of the underlying Si substrate.[36]

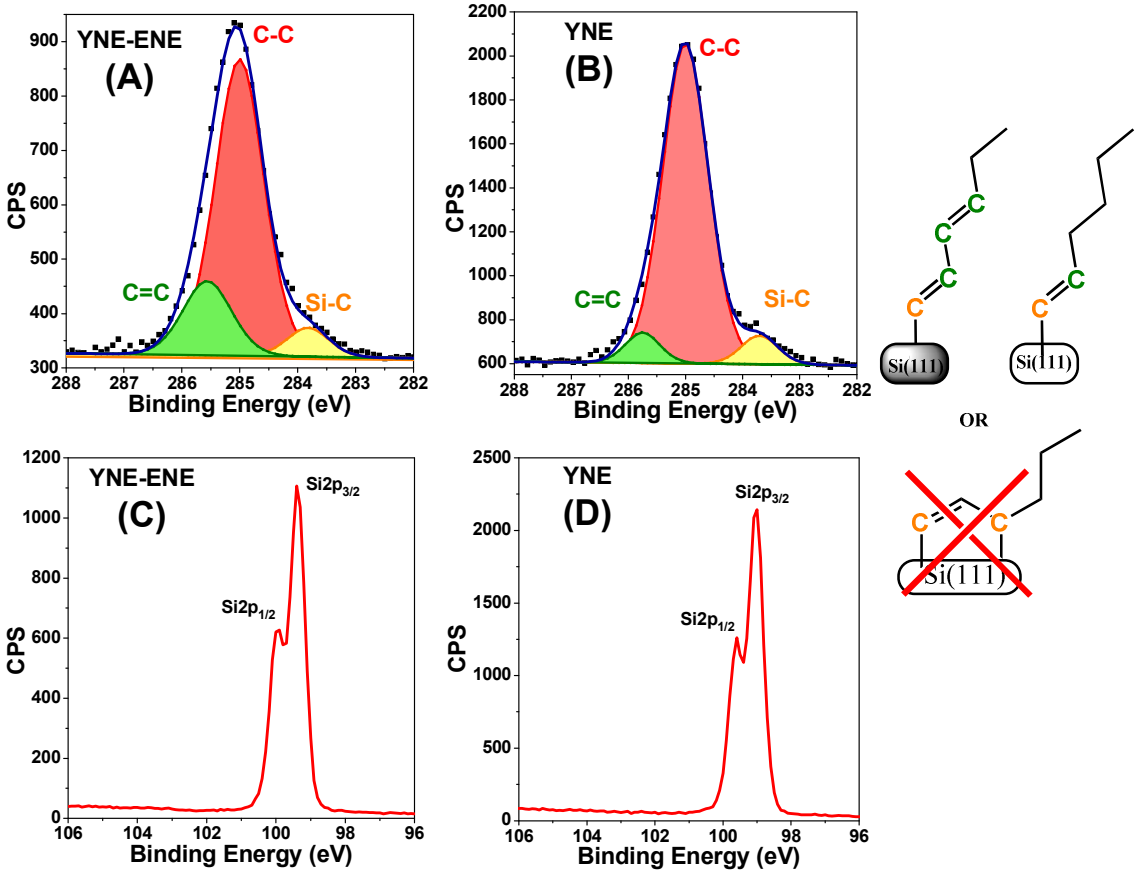

Figure 5. C_{1s} (A,B) and Si_{2p} (C,D) XPS narrow scan spectra of the H-Si(111) surface after modification (80 °C, 16 h) with hexadec-3-en-1-yne and 1-hexadecyne, respectively.

Moreover, in order to extract the packing densities, also the exact composition of monolayers was determined by quantitative XPS measurements. To overcome the signal dependency on the orientation of the crystal, i.e., to remove any influence of X-ray

diffraction, the XPS samples were rotated 360° around the surface normal, in steps of 10°.[35, 39] The obtained C/Si ratios display the expected periodicity of 120°, and reveal an increased amount of carbon for the hexadecadienyl monolayers as compared to the hexadecenyl monolayers (Table 1). The surface coverage and monolayer thickness were calculated from these C/Si ratios using the following equations:[27,56]

Thickness: $$d_{ML}\,(\text{Å}) = \lambda_{ML}^{Si}\,\sin(\varphi)\,\ln(1 + {}^{C}/_{Si}) \quad (3),$$

Surface coverage: $$\theta_{ML} = \frac{d_{ML}\,x\,D_{Au}}{d_{TH(30)}\,x\,D_{Si}} \quad (4),$$

In which λ_{ML}^{Si} is the attenuation length of Si_{2p} photoelectron in the organic monolayer (39.5 Å), and φ is the angle between the surface plane and the detector (90°). The surface coverage is estimated by comparison to the literature value of a fully characterized alkanethiol monolayer on gold, where d_{TH} is the theoretical thickness of an organic monolayer on H-Si(111) with a tilt angle of 30° (1.90 and 1.89 nm for alkenyl and dienyl layers, respectively), and D_{Si} and D_{Au} are the number of sites per cm (7.8×10^{14} cm^{-2} and 4.65×10^{14} cm^{-2}, respectively).[35, 39] From the results in Table 1, it shows that the dienyl layers, with a surface coverage of 63% (± 1%), are significantly more densely packed than the hexadecenyl monolayers, while the XPS-derived thickness of both layers is the same within the experimental error (1.9 ± 0.1 and 2.0 ± 0.1 nm, for enyne-derived and alkyne-derived C_{16} monolayers, respectively). The thickness and surface coverage of 59% for the hexadecenyl monolayers are in excellent agreement with previous findings.[35] These results clearly show that, besides an increased reactivity, the 3-en-1-yne moiety also leads to a significant higher surface coverage, fulfilling both prerequisites for improvement of quality in monolayers.

Table 1. Quantitative XPS Data; Atomic C/Si ratios, resulting monolayer thickness and surface coverage of hexadecadienyl and hexadecenyl monolayers on H-Si(111).

Reactant	XPS C_{1s}/Si_{2p} ratios	Surface coverage %
C_{16} Enyne	40.2/59.8	63%
C_{16} Alkyne	37.7/62.3	59%

Finally, to investigate the ordering of the monolayer in more detail, high-quality Near Edge X-Ray Absorption Fine Structure (NEXAFS) measurements were performed. NEXAFS spectra provide information about the electronic structure of the surface species

by measuring characteristic absorption resonances corresponding to electronic transitions from atomic core levels to unoccupied molecular orbitals.[55] Carbon *K*-edge spectra for the hexadecadienyl and hexadecenyl layers on silicon, acquired at 70°, 55° and 20°, are presented in Figure 6 along with the difference between the 70° and 20° spectra. Since radiation damage from the X-ray would also be visible in this spectral range,[56] a careful beam damage study was performed to rule out this possibility.[57] The adsorption near 285.0 eV, π^*(C=C) clearly indicates resonance of the aromatic alkene moieties, whereas the strong Rydberg/C-H (*R**) resonance near 287.9 eV and the broad σ^* resonances are related to the alkyl chains and the C-C bonds at higher photon energies, respectively. The spectra show neither signs of chemical impurities such as C=O, nor any traces of unreacted C≡C moieties (expected near 285.9 eV) for any of the monolayers.[55, 58-61] The pronounced linear dichroism for the C=C, C-C and C-H related resonances (highlighted by the 70° – 20° difference spectra) indicates significant order and molecular alignment in both monolayers. The positive polarity of the observed difference peaks for the π^* resonance implies a strongly tilted orientation of the π^*(C=C) orbitals, which is expected for an upright chain orientation, since the π^*(C=C) orbitals are perpendicular to the C=C-C plane. The R* features also show an appreciable positive linear dichroism while the C-C difference peaks are negative, which is again a clear indication of an upright orientation of the alkyl chain.

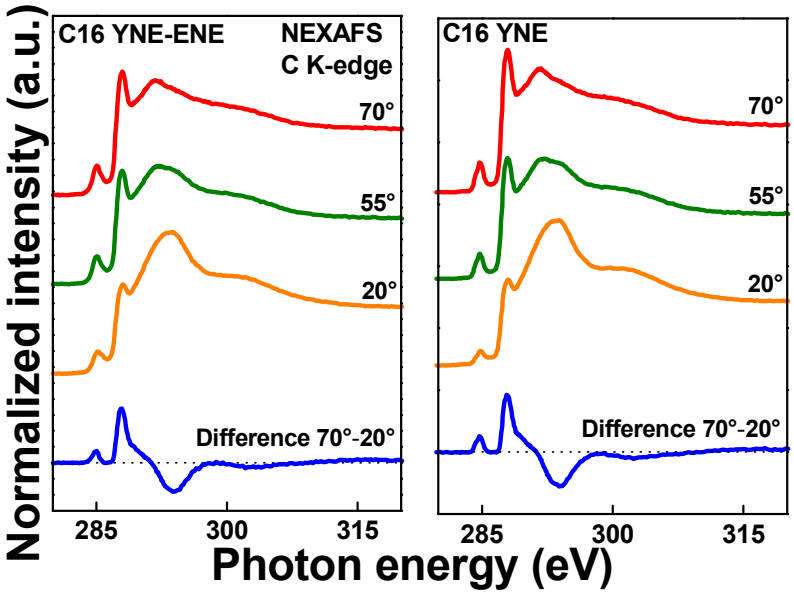

Figure 6. NEXAFS carbon K-edge spectra for hexadecadienyl and hexadecenyl monolayers on Si(111), acquired at 70°, 55° and 20°. The difference spectra between the 70° and the 20° data are shown in blue.

A quantitative analysis of the C *K*-edge NEXAFS spectra was performed to determine the average molecular tilt and twist angles. The orientation of the carbon chains with respect to the surface normal were determined using the *R** transitions. The intensities of these resonances as a function of the X-ray incidence angle Θ were evaluated using literature procedures for a planar orbital.[55] This analysis yields average tilt angles versus the surface normal of 28° ± 5° and 25° ± 5° for dienyl and alkenyl layers, respectively. These values are slightly similar to those observed for alkane thiols on gold (28°).[62] In addition, these NEXAFS data can be used (via Eq. 2) to derive monolayer thicknesses, and these agree within experimental error with the XPS thicknesses.

The tilt angle of the alkene π^*(C=C) orbitals was determined using the π^* resonance intensity variations and a standard methods for vector orbitals.[55] The orientations of the orbitals (ρ) were found to be 66° ± 5° and 76° ± 5° for dienyl and alkenyl chains, respectively. These values can be used, together with equation 5, to determine the twist angle of the chains.[63] The twist angle ψ can be described as the rotation over the long molecular axis of the chains.

$$\rho = \arccos(\sin\phi\cos\psi) \qquad (5)$$

This evaluation yields twist angles of ψ = 60° and ψ = 45° for dienyl and alkene chains, respectively. These values are in line with geometries observed for related alkanethiols on gold (53°) and other metal surfaces.[54] Overall, the NEXAFS data indicate that the structure of the hexadecadienyl and hexadecenyl layers is very similar. Both are densely packed, highly ordered and contamination free. The structure and orientation of the monolayers are also very similar to the binding geometry observed for alkanethiols on gold.

2.4.3 Molecular modeling

The obtained difference in surface coverage stimulated us to perform a comparative molecular modeling study of monolayers derived from 1-hexadecyne and hexadec-3-en-1-yne. Unit cells containing hexadecadienyl and hexadecenyl (both C_{16}) chains were constructed, and used to create large simulation cells with various substitution percentages and substitution patterns analogous to those described in literature.[38, 40, 41, 64-66] Energy minimizations were performed using a polymer consistent force field (PCFF) with high-convergence criteria and periodic boundaries conditions to eliminate the edge effects and to mimic an infinitely large monolayer.

The structure of the resulting optimized monolayers was compared in detail with the available experimental data. Reported data are the average observed for the chains (48 at 33% coverage to 108 at 75% coverage) in the periodically repeating unit cells at a specific substitution pattern. As shown in Table 2 for one of the substitution patterns (arbitrarily labeled A; see for other patterns and corresponding data the *Supporting Information S.2.1*), at a coverage of approximately 60 – 67%, the alkenyl and dienyl layers display a calculated thickness of 1.9 and 2.0 nm, respectively. These values agree with the thicknesses derived from the XPS and NEXAFS measurements discussed above (1.9 ± 0.1 nm for both layers). The differences between both types of layers become clear after comparison of the tilt and the layer thicknesses at the various surface coverages. At low coverage (33-50%), the dienyl chains are more upright oriented than the alkenyl chains, resulting in a higher layer thickness. However, the tilt angles for alkenyl layers decrease rapidly when going to a higher surface coverage, while the dienyl layers show a more gradual decrease. This behavior can be explained by the rigidity of the dienyl moiety, which is caused by the two double C=C bonds and their overlapping p-orbitals, which keep the four carbons in an almost planar conformation (typical dihedral C=C-C=C ~ 170° for 33 - 60% coverage). At low coverage, the dienyl will thus keep its upright orientation, whereas the alkenyl moiety has more rotational freedom, resulting in a more flat orientation of alkyne-derived monolayers. Both layers show a slight increase of the Si-C=C bond angles with increasing coverage, likely caused by the optimization of the interchain Van der Waals interactions between CH_2 moieties at the expense of such minor distortions at the surface.

Table 2. Calculated characteristics of hexadecenyl and hexadecadienyl monolayers on H-Si(111).

Unit Cell	Hexadecenyl			Hexadecadienyl		
	Thickness (nm)	Tilt angle chain	∠Si-C=C (in °)	Thickness (nm)	Tilt angle chain	∠ Si-C=C (in °)
33A	1.2	61 ± 2	123 ± 1	1.3	56 ± 2	121 ± 1
50A	1.7	48 ± 2	123 ± 2	1.8	26 ± 4	124 ± 2
60A	2.0	19 ± 6	125 ±3	1.8	27 ± 3	124 ± 4
67A	2.0	17 ± 2	124± 3	2.0	11 ± 4	126 ± 3
75A	2.1	8 ± 3	124 ± 3	2.0	5 ± 3	127 ± 2

Next to the structural parameters of the monolayers, also the packing energies were determined. After optimization of the layer, the chains were cut loose from the surface.

The carbon atoms that were attached to silicon were left uncapped since capping with hydrogen led to distortion of the geometry. The resulting dangling carbon bonds were subsequently neglected by the used PCFF forcefield. The average packing energy per chain was then calculated according to:

$$E_{packing} = \frac{E_{chains}}{n} - E_{single} \qquad (5),$$

in which E_{chains} is the total packing energy of the layer, n is the number of chains in the layer, and E_{single} is the energy of a separately optimized chain.[64] The resulting average packing energies per chain are shown in Figure 7 (dotted lines). At low surface coverage, hexadecenyl layers are energetically more favorable than dienyl layers. This difference can be explained by the upright position of the rigid dienyl moiety that pushes the CH_2 chain up, to an orientation in which the π-π overlap of the resulting diene moiety competes with the interchain Van der Waals interactions between CH_2 moieties. For the alkyne-derived monolayer, such competition is absent, yielding a more flat orientation of the CH_2 chains with concomitantly increased attractive Van der Waals interactions.

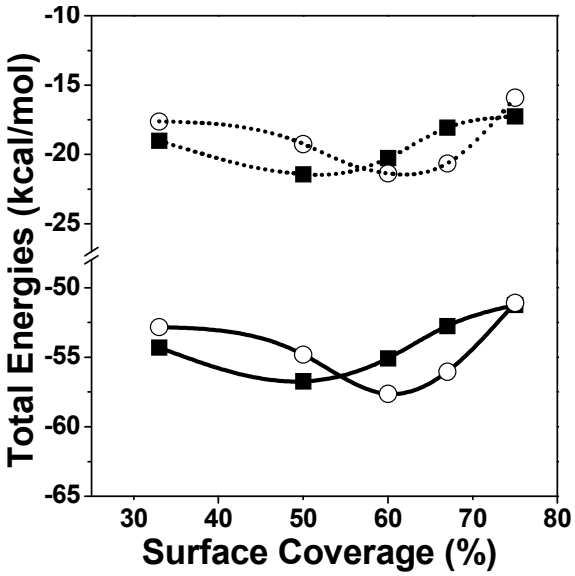

Figure 7. Packing energy (dotted lines) and total energy (solid lines) per chain for hexadecenyl (■) and hexadecadienyl (○) monolayers, as a function of surface coverage.

The optimum for the C_{16} alkenyl layers is found around 50% coverage, while for the C_{16} dienyl monolayer this is close to 60%. This difference corresponds to the experimental

finding that hexadecadienyl layers can achieve a higher surface coverage (63%) than hexadecenyl layers (59%). This can largely be attributed to the volumes of the atoms close to the silicon surface (-CH=CH-CH=CH- versus -CH=CH-CH_2-CH_2-), which for the -CH=CH-CH=CH- moiety is ~5% smaller, with concomitant reduction of steric repulsions as increased surface coverages.

The optimum packing, however, is still lower than the experimentally observed packing of both the alkenyl and dienyl layers. The likely dominant part of the explanation for this phenomenon lies in the fact that the binding of the chains to the surface is energetically highly favorable and irreversible, yielding an experimental density that is higher than the optimum for the non-covalent interchain interactions.

The second aspect controlling the experimentally observed packing density relates to the Si-C binding energy. For the monolayers under study this was calculated via high-quality G3 *ab initio* calculations of the reaction of 1-pentyne and pent-3-en-1-yne with a small hydrogen-terminated silicon cluster ($HSi(SiH_3)_3$), analogous to literature procedures.[64, 65] For fully relaxed structures this would favor the reaction of the enyne by 2.6 kcal.mol^{-1}. However, the situation is slightly more complicated, as for varying coverages the precise structures near the surface vary slightly. To take this into account properly, the product geometries for the G3 calculations were isolated from the PCFF-optimized monolayer structures discussed earlier. Isolated Si_4 clusters were cut out of the surface slabs, and the chains were truncated to five carbon atoms, in order to lower the computational cost. The atoms were then constrained, in order to perform single-point G3 energy calculations. The binding energy was then calculated as the difference of the energy of the chain attached to the surface and the fully relaxed reactant complexes, and corrected for the energy contribution of the deformation of the C_5 chain, according to literature procedures.[64] Figure 7 (continuous lines) then shows the sum of packing and binding energies at the various degrees of surface coverage for enyne-derived and alkyne-derived C_{16} monolayers. This profile of the total energy resembles the profile of the packing energy, but show a more distinct preference for the reactivity of the C_{16} enyne. For the calculated total energies of 60% and 67%, i.e., close to what is experimentally observed, the energy gap between the alkenyl and the dienyl layers increases to 2.5 and 3.2 kcal mol^{-1}. This overall higher reaction exothermicity and higher optimum packing density for enyne-derived monolayers fits very well with the experimental observation of the faster reaction of the C_{16} enyne than of hexadecyne (Figure 1), and the observed higher denser packing of the dienyl layers (Figure 4).

2.5 CONCLUSIONS

In summary, we successfully developed a novel precursor, hexadeca-3-en-1-yne ($HC{\equiv}C\text{-}HC{=}CH\text{-}C_{12}H_{25}$), for the formation of high-quality monolayers on H-terminated silicon surfaces. Detailed kinetics studies show that this enyne reacts faster than the corresponding C_{16} alkyne, while quantitative XPS studies show that the resulting dienyl monolayers also display a higher packing density than had been reported up to now on H-Si(111). Infrared and NEXAFS measurements confirm the formation of highly ordered, densely packed enyne-derived monolayers. Finally, a molecular modeling study (combination of molecular mechanics calculations on complete monolayers and G3 *ab initio* calculations on well-defied model systems) shows that for C_{16} monolayers an enyne-derived monolayer is both more stable and more densely packed than the monolayer derived from the corresponding C_{16} alkyne (hexadecyne).

This enhanced monolayer quality and rate of formation of enyne-derived monolayers, compared with the best performing reagent up to now (1-alkynes), makes enynes $HC{\equiv}C\text{-}HC{=}CH\text{-}R$ the agent of choice if a supreme monolayer quality is desired, which also enhances the stability of the oxide-free silicon interface. This development further increases the chance of a successful application of organic monolayers on silicon in electronic and biosensor devices.

2.6 REFERENCES

1. Gooding, J. J.; Ciampi, S.; Harper, J. B., Wet chemical routes to the assembly of organic monolayers on silicon surfaces via the formation of Si-C bonds: surface preparation, passivation and functionalization. *Chem. Soc. Rev.* **2010,** 39, (6), 2158-2183.
2. Buriak, J. M., Organometallic chemistry on silicon and germanium surfaces. *Chem. Rev.* **2002,** 102, (5), 1271-1308.
3. Yonezawa, T.; Shirahata, N.; Hozumi, A., Monolayer-derivative functionalization of non-oxidized silicon surfaces. *Chem. Rec.* **2005,** 5, (3), 145-159.
4. Gooding, J. J.; Ciampi, S., The molecular level modification of surfaces: from self-assembled monolayers to complex molecular assemblies. *Chem. Soc. Rev.* **2011,** 40, (5), 2704-2718.
5. Rijksen, B.; Caipa Campos, M. A.; Paulusse, J. M. J.; Zuilhof, H., In *Encyclopedia of Radicals in Chemistry, Biology and Materials*, Chatgilialoglu, C.; Struder, A., Eds. Wiley: Chichester, 2012.
6. Scheres, L.; ter Maat, J.; Giesbers, M.; Zuilhof, H., Microcontact Printing onto Oxide-Free Silicon via Highly Reactive Acid Fluoride-Functionalized Monolayers. *Small* **2010,** 6, (5), 642-650.
7. Linford, M. R.; Fenter, P.; Eisenberger, P. M.; Chidsey, C. E. D., Alkyl Monolayers on Silicon Prepared from 1-Alkenes and Hydrogen-Terminated Silicon. *J. Am. Chem. Soc.* **1995,** 117, (11), 3145-55.

8. Sieval, A. B.; Huisman, C. L.; Schoenecker, A.; Schuurmans, F. M.; Van der Heide, A. S. H.; Goossens, A.; Sinke, W. C.; Zuilhof, H.; Sudhölter, E. J. R., Silicon surface passivation by organic monolayers: minority charge carrier lifetime measurements and Kelvin probe investigations. *J. Phys. Chem. B* **2003,** 107, (28), 6846-6852.
9. Cicero, R. L.; Linford, M. R.; Chidsey, C. E. D., Photoreactivity of Unsaturated Compounds with Hydrogen-Terminated Silicon(111). *Langmuir* **2000,** 16, (13), 5688-5695.
10. Shestopalov, A. A.; Clark, R. L.; Toone, E. J., Catalytic Microcontact Printing on Chemically Functionalized H-Terminated Silicon. *Langmuir* **2010,** 26, (3), 1449-1451.
11. Terry, J.; Mo, R.; Wigren, C.; Cao, R. Y.; Mount, G.; Pianetta, P.; Linford, M. R.; Chidsey, C. E. D., Reactivity of the H-Si (111) surface. *Nucl. Instrum. Meth. B.* **1997,** 133, (1-4), 94-101.
12. Wang, X. Y.; Ruther, R. E.; Streifer, J. A.; Hamers, R. J., UV-Induced Grafting of Alkenes to Silicon Surfaces: Photoemission versus Excitons. *J. Am. Chem. Soc.* **2010,** 132, (12), 4048-4049.
13. G. Robins, E.; P. Stewart, M.; M. Buriak, J., Anodic and cathodic electrografting of alkynes on porous silicon[dagger]. *Chem. Commun.* **1999**, (24), 2479-2480.
14. Belanger, D.; Pinson, J., Electrografting: a powerful method for surface modification. *Chem. Soc. Rev.* **2011,** 40, (7), 3995-4048.
15. Niederhauser, T. L.; Jiang, G. L.; Lua, Y. Y.; Dorff, M. J.; Woolley, A. T.; Asplund, M. C.; Berges, D. A.; Linford, M. R., A new method of preparing monolayers on silicon and patterning silicon surfaces by scribing in the presence of reactive species. *Langmuir* **2001,** 17, (19), 5889-5900.
16. Yang, L.; Lua, Y.-Y.; Tan, M.; Scherman, O. A.; Grubbs, R. H.; Harb, J. N.; Davis, R. C.; Linford, M. R., Chemistry of olefin-terminated homogeneous and mixed monolayers on scribed silicon. *Chem. Mater.* **2007,** 19, (7), 1671-1678.
17. Buriak, J. M.; Stewart, M. P.; Geders, T. W.; Allen, M. J.; Choi, H. C.; Smith, J.; Raftery, D.; Canham, L. T., Lewis Acid Mediated Hydrosilylation on Porous Silicon Surfaces. *J. Am. Chem. Soc.* **1999,** 121, (49), 11491-11502.
18. Jin, H.; Kinser, C. R.; Bertin, P. A.; Kramer, D. E.; Libera, J. A.; Hersam, M. C.; Nguyen, S. T.; Bedzyk, M. J., X-ray Studies of Self-Assembled Organic Monolayers Grown on Hydrogen-Terminated Si(111). *Langmuir* **2004,** 20, (15), 6252-6258.
19. Scheres, L.; Arafat, A.; Zuilhof, H., Self-assembly of high-quality covalently bound organic monolayers onto silicon. *Langmuir* **2007,** 23, (16), 8343-8346.
20. Caipa Campos, M. A.; Paulusse, J. M. J.; Zuilhof, H., Functional monolayers on oxide-free silicon surfaces via thiol-ene click chemistry. *Chem. Commun.* **2010,** 46, (30), 5512-5514.
21. Popoff, R. T. W.; Asanuma, H.; Yu, H. Z., Long-Term Stability and Electrical Performance of Organic Mono layers on Hydrogen-Terminated Silicon. *J. Phys. Chem. C* **2010,** 114, (24), 10866-10872.
22. Seitz, O.; Bocking, T.; Salomon, A.; Gooding, J. J.; Cahen, D., Importance of monolayer quality for interpreting current transport through organic molecules: Alkyls on oxide-free Si. *Langmuir* **2006,** 22, (16), 6915-6922.
23. Seitz, O.; Vilan, A.; Cohen, H.; Hwang, J.; Haeming, M.; Schoell, A.; Umbach, E.; Kahn, A.; Cahen, D., Doping molecular monolayers: Effects on electrical transport through alkyl chains on silicon. *Adv. Func. Mat.* **2008,** 18, (14), 2102-2113.
24. Yaffe, O.; Scheres, L.; Puniredd, S. R.; Stein, N.; Biller, A.; Lavan, R. H.; Shpaisman, H.; Zuilhof, H.; Haick, H.; Cahen, D.; Vilan, A., Molecular Electronics at

Metal/Semiconductor Junctions. Si Inversion by Sub-Nanometer Molecular Films. *Nano Lett.* **2009,** 9, (6), 2390-2394.
25. Zigah, D.; Herrier, C.; Scheres, L.; Giesbers, M.; Fabre, B.; Hapiot, P.; Zuilhof, H., Tuning the Electronic Communication between Redox Centers Bound to Insulating Surfaces. *Angew. Chem. Int. Ed.* **2010,** 49, (18), 3157-3160.
26. Chatgilialoglu, C., *Organosilanes in Radical Chemistry* **2004**.
27. Chatgilialoglu, C.; Guarini, A.; Guerrini, A.; Seconi, G., Autoxidation of tris(trimethylsilyl)silane. *J. Org. Chem.* **1992,** 57, (8), 2207-2208.
28. Wayner, D. D. M.; Wolkow, R. A., Organic modification of hydrogen terminated silicon surfaces1. *J. Chem. Soc., Perkin Trans. 2* **2002**, (1), 23-34.
29. Lehner, A.; Steinhoff, G.; Brandt, M. S.; Eickhoff, M.; Stutzmann, M., Hydrosilylation of crystalline silicon (111) and hydrogenated amorphous silicon surfaces: A comparative x-ray photoelectron spectroscopy study. *J. Appl. Phys.* **2003,** 94, (4), 2289-2294.
30. Sun, Q.-Y.; de Smet, L. C. P. M.; van Lagen, B.; Wright, A.; Zuilhof, H.; Sudhölter, E. J. R., Covalently Attached Monolayers on Hydrogen-Terminated Si(100): Extremely Mild Attachment by Visible Light. *Angew. Chem. Int. Ed.* **2004,** 43, (11), 1352-1355.
31. Rijksen, B.; Zuilhof, H., *Submitted*.
32. Takeuchi, N.; Kanai, Y.; Selloni, A., Surface reaction of alkynes and alkenes with H-Si(111): A density functional theory study. *J. Am. Chem. Soc.* **2004,** 126, (48), 15890-15896.
33. Lalevée, J.; Blanchard, N.; Graff, B.; Allonas, X.; Fouassier, J. P., Tris(trimethylsilyl)silyl versus tris(trimethylsilyl)germyl: Radical reactivity and oxidation ability. *J. Organomet. Chem.* **2008,** 693, (24), 3643-3649.
34. Frisch, M. J. T., G. W.; Schlegel, H. B.; et al, *Gaussian 09, Revision A.1*, Gaussian, Inc., Wallingford CT.: 2009.
35. Scheres, L.; Giesbers, M.; Zuilhof, H., Organic Monolayers onto Oxide-Free Silicon with Improved Surface Coverage: Alkynes versus Alkenes. *Langmuir* **2010,** 26, (7), 4790-4795.
36. Puniredd, S. R.; Assad, O.; Haick, H., Highly stable organic modification of Si(111) surfaces: Towards reacting Si with further functionalities while preserving the desirable chemical properties of full Si-C atop site terminations. *J. Am. Chem. Soc.* **2008,** 130, (29), 9184-9185.
37. Nemanick, E. J.; Solares, S. D.; Goddard, W. A.; Lewis, N. S., Quantum Mechanics Calculations of the Thermodynamically Controlled Coverage and Structure of Alkyl Monolayers on Si(111) Surfaces. *J. Phys. Chem. B* **2006,** 110, (30), 14842-14848.
38. Sieval, A. B.; van den Hout, B.; Zuilhof, H.; Sudhölter, E. J. R., Molecular Modeling of Covalently Attached Alkyl Monolayers on the Hydrogen-Terminated Si(111) Surface. *Langmuir* **2001,** 17, (7), 2172-2181.
39. Wallart, X.; De Villeneuve, C. H.; Allongue, P., Truly quantitative XPS characterization of organic monolayers on silicon: Study of alkyl and alkoxy monolayers on H-Si(111). *J. Am. Chem. Soc.* **2005,** 127, (21), 7871-7878.
40. Pei, Y.; Ma, J.; Jiang, Y., Formation Mechanisms and Packing Structures of Alkoxyl and Alkyl Monolayers on Si(111): Theoretical Studies with Quantum Chemistry and Molecular Simulation Models. *Langmuir* **2003,** 19, (18), 7652-7661.
41. Zhang, L.; Wesley, K.; Jiang, S., Molecular Simulation Study of Alkyl Monolayers on Si(111). *Langmuir* **2001,** 17, (20), 6275-6281.

42. Barone, V.; Cacelli, I.; Ferretti, A.; Monti, S.; Prampolini, G., Organic Functionalization and Optimal Coverage of a Silicon(111) Surface in Solvent: A Computational Study. *J. Phys. Chem. C* **2011,** 115, (10), 4145-4154.
43. Sano, H.; Maeda, H.; Ichii, T.; Murase, K.; Noda, K.; Matsushige, K.; Sugimura, H., Alkyl and Alkoxyl Monolayers Directly Attached to Silicon: Chemical Durability in Aqueous Solutions. *Langmuir* **2009,** 25, (10), 5516-5525.
44. Hacker, C. A.; Anderson, K. A.; Richter, L. J.; Richter, C. A., Comparison of Si−O−C Interfacial Bonding of Alcohols and Aldehydes on Si(111) Formed from Dilute Solution with Ultraviolet Irradiation. *Langmuir* **2004,** 21, (3), 882-889.
45. Miller, J. A.; Zweifel, G., Hydroalumination of 1-(trimethylsilyl)-1,3-diynes. Syntheses of stereodefined enynes and dienes. *J. Am. Chem. Soc.* **1983,** 105, (5), 1383-1384.
46. Kim, T.; Crooks, R. M., Polymeric self-assembling monolayers. 1. Synthesis and characterization of υ-functionalized n-alkanethiols containing a conjugated diacetylene group. *Tetrahedron Lett.* **1994,** 35, (51), 9501-9504.
47. Xu, Z.; Byun, H. S.; Bittman, R., Synthesis of photopolymerizable long-chain conjugated diacetylenic acids and alcohols from butadiyne synthons. *J. Org. Chem.* **1991,** 56, (25), 7183-7186.
48. Sieval, A. B.; Linke, R.; Zuilhof, H.; Sudhölter, E. J. R., High-quality alkyl monolayers on silicon surfaces. *Adv. Mater.* **2000,** 12, (19), 1457-1460.
49. Allongue, P.; de Villeneuve, C. H.; Morin, S.; Boukherroub, R.; Wayner, D. D. M., The preparation of flat H-Si(111) surfaces in 40% NH4F revisited. *electrochem. acta* **2000,** 45, 4591-4598.
50. Yang, M.; Teeuwen, R. L. M.; Giesbers, M.; Baggerman, J.; Arafat, A.; De Wolf, F. A.; Van Hest, J. C. M.; Zuilhof, H., One-step photochemical attachment of NHS-terminated monolayers onto silicon surfaces and subsequent functionalization. *Langmuir* **2008,** 24, (15), 7931-7938.
51. de Smet, L. C. P. M.; Pukin, A. V.; Sun, Q.-Y.; Eves, B. J.; Lopinski, G. P.; Visser, G. M.; Zuilhof, H.; Sudhölter, E. J. R., Visible-light attachment of SiC linked functionalized organic monolayers on silicon surfaces. *Appl. Surf. Sci.* **2005,** 252, (1), 24-30.
52. Brunner, H.; Mayer, U.; Hoffmann, H., External reflection infrared spectroscopy of anisotropic adsorbate layers on dielectric substrates. *App. Spectrosc.* **1997,** 51, (2), 209-217.
53. Hasegawa, T.; Takeda, S.; Kawaguchi, A.; Umemura, J., Quantitative analysis of uniaxial molecular orientation in Langmuir-Blodgett films by infrared reflection spectroscopy. *Langmuir* **1995,** 11, (4), 1236-1243.
54. Love, J. C.; Estroff, L. A.; Kriebel, J. K.; Nuzzo, R. G.; Whitesides, G. M., Self-Assembled Monolayers of Thiolates on Metals as a Form of Nanotechnology. *Chem. Rev.* **2005,** 105, 1103-1169.
55. Stöhr, J., *NEXAFS Spectroscopy*. Springer-Verlag: Berlin, 1992; Vol. 25.
56. Weidner, T.; Shaporenko, A.; Ballav, N.; Ulman, A.; Zharnikov, M., Modification of Alkaneselenolate Monolayers by Low-Energy Electrons. *J. Phys. Chem. C* **2008,** 112, (4), 1191-1198.
57. *For the beam damage study at the C K-edge, the 280 eV to 320 eV energy range was repeatedly scanned and analyzed. In addition, the partial electron yield at 285 eV was monitored over time to rule out damage related changes in the first seconds. No changes in the spectra were observed within 15 minutes, which is more than the exposure time in the longest carbon scans performed within this work. This studied proved that the pre-edge feature observed near 285 eV is not caused by beam damage.*

58. Outka, D. A.; Stöhr, J.; Rabe, J. P.; Swalen, J. D., The orientation of Langmuir-Blodgett monolayers using NEXAFS. *J. Chem. Phys.* **1988,** 88, (6), 4076.
59. Weiss, K.; Bagus, P. S.; Wöll, C., Rydberg transitions in X-ray absorption spectroscopy of alkanes: The importance of matrix effects. *J. Chem. Phys.* **1999,** 111, (15), 6834-6845.
60. Väterlein, P.; Fink, R., Analysis of the x-ray absorption spectra of linear saturated hydrocarbons using the Xα scattered-wave method. *J. Chem. Phys.* **1998,** 108, (8), 3313.
61. Cabarcos, O. M.; Shaporenko, A.; Weidner, T.; Uppili, S.; Dake, L. S.; Zharnikov, M.; Allara, D. L., Physical and electronic structure effects of embedded dipoles in self-assembled monolayers: Characterization of mid-chain ester functionalized alkanethiols on Au{111}. *J. Phys. Chem. C* **2008,** 112, (29), 10842-10854.
62. Laibinis, P. E.; Whitesides, G. M., ω-Terminated alkanethiolate monolayers on surfaces of copper, silver, and gold have similar wettabilities. *J. Am. Chem. Soc.* **1992,** 114, (6), 1990-1995.
63. Rong, H.-T. F., S.; Yang, Y.-J.; Zharnikov, M.; Buck, M.; Wuhn, M.; Wöll, C.; Helmchen, G., On the Importance of the Headgroup Substrate Bond in Thiol Monolayers: A Study of Biphenyl-Based Thiols on Gold and Silver. *Langmuir* **2001,** 17, (5), 1582-1593.
64. Scheres, L.; Rijksen, B.; Giesbers, M.; Zuilhof, H., Molecular Modeling of Alkyl and Alkenyl Monolayers on Hydrogen-Terminated Si(111). *Langmuir* **2011,** 27, (3), 972-980.
65. Sieval, A. B.; van den Hout, B.; Zuilhof, H.; Sudhölter, E. J. R., Molecular Modeling of Alkyl Monolayers on the Si(111) Surface. *Langmuir* **2000,** 16, (7), 2987-2990.
66. Yuan, S.-L.; Cai, Z.-T.; Jiang, Y.-S., Molecular simulation study of alkyl monolayers on the Si(111) surface. *New J. Chem.* **2003,** 27, (3), 626-633.

Supporting Information to Chapter 2

Table of Contents

Supporting Information to Chapter 2 52
S.2.1 Modeling studies in materials studio 52
S.2.2 DFT calculations of XPS binding energies 53
S.2.3 References 54

S.2.1 Modeling studies in materials studio

The modeling of the monolayers on silicon was performed following the procedures as described previously.[1, 2] Since the packing energies were combined with the binding energies, only one series of coverage patterns was used. In order to allow comparison with literature values, a single set of patterns from ref. 1 (A series, See Figure S1) was used.

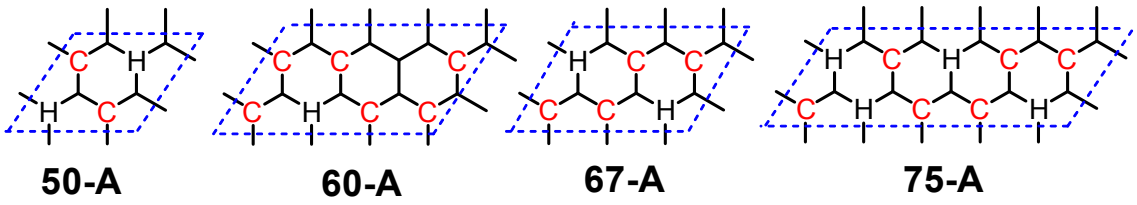

Figure S1. Patterns used in monolayer simulations.

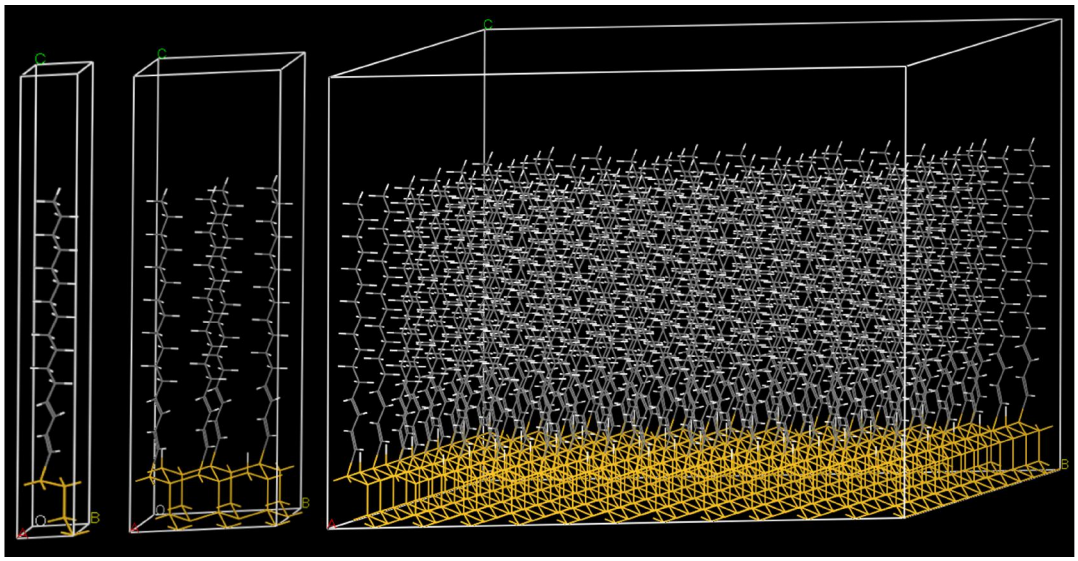

Figure S2. Construction of monolayer geometries from a single unit cell (left) to the desired pattern (middle), and finally the entire monolayer (right).

Unit cells were constructed, with dimensions $a = b = 3.840$ Å, $c = 35$ Å, $a = b = 90°$, and $g = 120°$ (See Figure S2). The cells were expanded to larger cells (2 × 2, 2 × 3, 2 × 4 or 2 × 5) and chains were replaced by hydrogen to achieve the desired pattern. The cells were then expanded to supercells of 12 × 12 units (33, 50, 67 and 75% surface coverage) and 10 × 15 units (60% surface coverage).[3]

The geometries were optimized using the polymer consistent force field (PCFF) (bottom two rows of Si atoms were constrained) as implemented in the Discover package in Materials Studio, using the ultrafine settings of the smart minimizer routine (line width 0,01 and convergence 10^{-5}, VdW and coulomb, atom centered and long-range correction switched off).

S.2.2 DFT calculations of XPS binding energies

XPS binding energies were estimated by calculating the orbital energies of molecular analogues of chains attached to a silicon surface which was mimicked by a $Si(SiH_3)_3$ group (See Figure S3). The geometries were optimized with B3LYP/6-311G(d,p), using the Gaussian 09 package.[4] The carbon binding energies were then estimated by calculating the 1s core energy versus the average of the 2p valence orbital energies (mimicking the Fermi level).

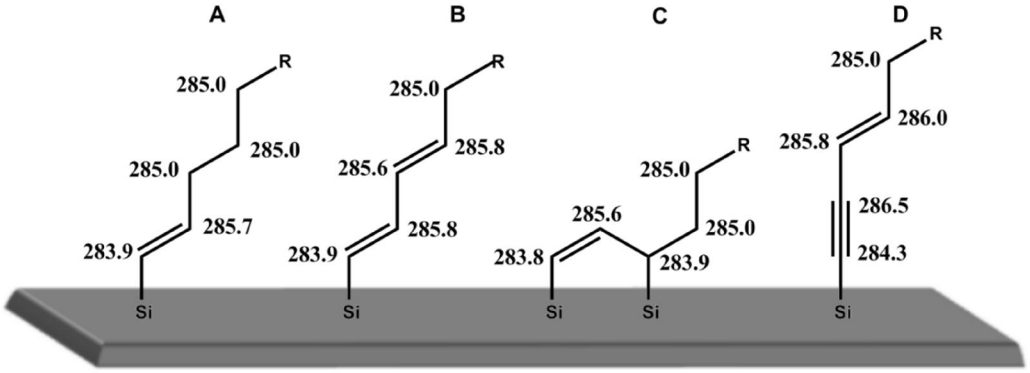

Figure S3. Self-Assembled monolayers on Si(111); A) hexadecenyl layers and B-D) possible modes of attachment of hexadeca-3-en-1-ynes. Calculated binding energies per carbon atom are depicted in eV (R = $C_{11}H_{23}$).

The calculations show that the peaks at 283.8 eV can be attributed to carbons attached to silicon. (both 283.9 eV, See Figure S3). Sp^2 hybridized carbons, show a binding energy around 285.7 eV, as the stronger electronegativity will increase the binding energy. Regular sp^3 hybridized carbons give a binding energy of 295.0 eV. Calculations of the binding energies of the hexadecenyl chain attached to the surface give three peaks: at

283.9 eV for the carbon attached to the silicon, at 285.0 eV for the aliphatic carbons, and at 285.8 eV for the sp^2 carbons, in the ratio of 1 : 14 : 1 (See Fig. S3A). The different attachment modes of the 3-en-1-yne give a very different pattern of binding energies. Terminal attachment (Fig. 3B) gives three peaks (binding energies for the sp^2 hybridized carbons at 285.6-285.8 eV) in a ratio of 1:3:14. Double attachment (Fig. 3C) gives two carbons attached to silicon, which results in a ratio of 2:1:15. Another possibility is terminal attachment with retention of the triple bond (Fig. 3D). The triple bond results in distinct peaks at 284.3 eV for the carbon connected to silicon, and at 286.5 eV for the other sp hybridized carbon.

S.2.3 References

1. Scheres, L.; Rijksen, B.; Giesbers, M.; Zuilhof, H., Molecular Modeling of Alkyl and Alkenyl Monolayers on Hydrogen-Terminated Si(111). *Langmuir* **2011,** 27, (3), 972-980.
2. Sieval, A. B.; Opitz, R.; Maas, H. P. A.; Schoeman, M. G.; Meijer, G.; Vergeldt, F. J.; Zuilhof, H.; Sudhölter, E. J. R., Monolayers of 1-Alkynes on the H-Terminated Si(100) Surface. *Langmuir* **2000,** 16, (26), 10359-10368.
3. Scheres, L.; Giesbers, M.; Zuilhof, H., Self-Assembly of Organic Monolayers onto Hydrogen-Terminated Silicon: 1-Alkynes Are Better Than 1-Alkenes. *Langmuir* **2010,** 26, (13), 10924-10929.
4. Frisch, M. J. T., G. W.; Schlegel, H. B.; Scuseria, G. E.; Robb, M. A.; Cheeseman, J. R.; Scalmani, G.; Barone, V.; Mennucci, B.; Petersson, G. A.; Nakatsuji, H.; Caricato, M.; Li, X.; Hratchian, H. P.; Izmaylov, A. F.; Bloino, J.; Zheng, G.; Sonnenberg, J. L.; Hada, M.; Ehara, M.; Toyota, K.; Fukuda, R.; Hasegawa, J.; Ishida, M.; Nakajima, T.; Honda, Y.; Kitao, O.; Nakai, H.; Vreven, T.; Montgomery, Jr., J. A.; Peralta, J. E.; Ogliaro, F.; Bearpark, M.; Heyd, J. J.; Brothers, E.; Kudin, K. N.; Staroverov, V. N.; Kobayashi, R.; Normand, J.; Raghavachari, K.; Rendell, A.; Burant, J. C.; Iyengar, S. S.; Tomasi, J.; Cossi, M.; Rega, N.; Millam, N. J.; Klene, M.; Knox, J. E.; Cross, J. B.; Bakken, V.; Adamo, C.; Jaramillo, J.; Gomperts, R.; Stratmann, R. E.; Yazyev, O.; Austin, A. J.; Cammi, R.; Pomelli, C.; Ochterski, J. W.; Martin, R. L.; Morokuma, K.; Zakrzewski, V. G.; Voth, G. A.; Salvador, P.; Dannenberg, J. J.; Dapprich, S.; Daniels, A. D.; Farkas, Ö.; Foresman, J. B.; Ortiz, J. V.; Cioslowski, J.; Fox, D. J. *Gaussian 09, Revision A.1*, Gaussian, Inc., Wallingford CT.: 2009.

CHAPTER 3

Mono-Fluorinated Alkyne-Derived SAMs on Oxide-Free Si(111) Surfaces: Preparation, Characterization and Tuning of the Si Workfunction

Organic monolayers derived from ω-fluoro-1-alkynes of varying carbon chain lengths (C_{10}-C_{18}) were prepared on Si(111) surfaces, resulting in changes of the physical and electronic properties of the surface. Analysis of the monolayers using XPS, Infrared Reflection Absorption Spectroscopy, ellipsometry and static water contact angle measurements provided information regarding the monolayer thickness, the tilt angle, and the surface coverage. Additionally, PCFF molecular mechanics studies were used to obtain information on the optimal packing density and the layer thickness, which were compared to the experimentally found data. From the results it can be concluded that the monolayers derived from longer chain lengths are more ordered, possess a lower tilt angle, and have a higher surface coverage than monolayers derived from shorter chains. We also demonstrate that by substitution of an H by F atom in the terminal group, it is possible to controllably modify the surface potential and energy barrier for charge transport in a full metal/monolayer-semiconductor (MOMS) junction.

This Chapter has been published as:

"Mono-Fluorinated Alkyne-Derived SAMs on Oxide-Free Si(111) Surfaces: Preparation, Characterization and Tuning of the Si Workfunction". Sidharam P. Pujari, Esther van Andel, Omer Yaffe, David Cahen, Tobias Weidner, Cees J. M. van Rijn, and Han Zuilhof. *Langmuir* **2013** 29 (2), 570-580

Table of Contents

3 Mono-Fluorinated Alkyne-Derived SAMs on Oxide-Free Si(111) Surfaces: Preparation, Characterization and Tuning of the Si Workfunction 55
3.1 INTRODUCTION 57
3.2 EXPERIMENTAL SECTION 59
3.2.1 Materials 59
3.2.2 Monolayer formation 60
3.3 Monolayer characterization 60
3.3.1 Static water and hexadecane contact angles 60
3.3.2 X-ray Photoelectron Spectroscopy (XPS) 60
3.3.3 Infrared Reflection Absorption Spectroscopy (IRRAS) 61
3.3.4 Ellipsometry 61
3.3.5 Contact Potential Difference (CPD) 61
3.3.6 Current-Voltage (I-V) 61
3.3.7 Near Edge X-ray Absorption Fine Structure (NEXAFS) 62
3.3.8 Molecular modeling 62
3.4 RESULTS AND DISCUSSION 64
3.4.1 Static contact angles 64
3.4.2 X-ray photoelectron spectroscopy 65
3.4.3 Infrared reflection absorption spectroscopy 68
3.4.4 Near Edge X-Ray Absorption Fine Structure (NEXAFS) 69
3.4.5 Controlled modification of the surface/interface potential and its application in metal/monolayer/semiconductor (MOMS) junctions 70
3.4.6 Molecular modeling 72
3.5 CONCLUSIONS 75
3.6 REFERENCES 76

3.1 INTRODUCTION

Molecular electronics describes molecules that assist as active elements (switching, sensing, current rectifiers, etc.) in electronic devices or passivate surfaces.[1] One practical example of molecular electronics is a glucose sensor that is based on the electrochemical detection of glucose via the action of electrode-bound glucose oxidase.[2] In numerous other examples, the molecules themselves are designed to match the properties of traditional solid-state devices like in molecular current rectifiers[3] and molecule-based tunnel junctions (resistors).[4-11]

Although considerable progress has been made in the development of organic thin film-based electronics, it is currently not commercially competitive with traditional silicon technology. In addition, there are problems associated with device stability, efficiency, and lifetime.[12-14] One strategy that is pursued to achieve a device that circumvents these problems, involves the use of covalently bound, self-assembled monolayers (SAMs) on inorganic surfaces to fine-tune the properties of the inorganic surface and of the interface, formed with such modified surface.[11,15-21] Features of SAMs that are attractive for this purpose include a high degree of chemical robustness, good passivating properties, low bias voltage, ease of formation, and above all, the ability to manipulate their structural and dipolar characteristics through design and synthesis.[20,22-24]

In many Micro-Electro-Mechanical Systems (MEMS) / Nano-Electro-Mechanical Systems (NEMS) applications Si-based materials are used.[25] However, direct use of native Si-based materials result in the oxidation of these materials, and functionalization of that oxide with an organic monolayer thus yields an intermediary, insulating layer between the Si and the functionality of interest. Treatment of Si surfaces with covalently bound stable monolayers addresses each of these issues: it hampers undesired surface oxidation during processing provides a direct electronic coupling between the Si surface and the organic functionality via hydrosilylation,[17,26,27] and monolayers that are directly linked to Si surfaces with a Si-C linkage are chemically and thermally more stable than alkoxyl (Si-O-C) monolayers.[28] Especially the possibility to obtain highly dense monolayers on oxide-free Si provides significant opportunities, as reviewed recently.[29-31] In addition, it has been shown that the interface state density of such well-prepared Si-organic monolayer interfaces is very low.[32,33] However, the studies over bond formation between silicon and carbon via radical chain mechanisms are well-documented.[34] The Si-C bond formation are irreversible which is different than the well-known thiol-Au bond. For thermodynamic equilibrium it is required that the bonding is reversible and there is an equilibrium between the free and bonded components.[35]

The work of various research groups shows that organic molecules having different tail groups (i.e. C-C, C=C, C≡C bonds) react differently with the Si substrate, and this influences the resulting monolayer packing densities on Si(111) surfaces.[31, 36] Experimental data[37] as well as a molecular modeling study[38] revealed that alkenyl monolayers derived from 1-alkynes are of better quality than alkyl monolayers derived from 1-alkenes. 1-Alkynes[37,39] and ynenes (HC≡C-CH=CHR)[40] turned out to be more reactive, and the resulting monolayers possess an improved packing density and higher surface coverage.[37,40] The differences in packing density can be explained by the compactness of the resulting Si-bound -CH=CH- moiety that decreases steric repulsion near the surface in comparison to Si-bound $–CH_2$-CH_2 moieties. Secondly, sp^2-hybridized carbon atoms form a stronger Si-C bond with H-terminated Si surfaces than the sp^3 C atoms resulting from alkene attachment.[38]

Apart from the Si-C forming moiety, also the chain length and terminal group of the precursor molecules will influence the properties of the resulting monolayers.[34,37,38,41] End groups that are bulky or electrically repulsive decrease the packing density and, hence, increase the susceptibility to oxidation of the underlying substrate.[42] Functionalization with small end groups is therefore expected to help achieve a high packing density, which makes terminal fluorine functionalization highly interesting. Fluorinated monolayers are unique in their low surface energies and their ability to reduce Van der Waals interactions.[43-46] This property results from the low polarizability and high ionization potential of the carbon-fluorine bond.[44,47] In addition, the presence of dipolar groups in the monolayer can also have a large effect on the electrical properties of the junction.[21,32,33]

Functionalized monolayers thus may provide a tunable means to affect the work function. Fluorinated monolayers are expected to increase the work function of almost any surface,[19, 48-50] and the hypothesis in this paper is that this increase can be tuned to a high degree by using terminal F-functionalization of monolayers, composed of Si-bound alkenyl chains of different lengths.

Here, we prepared monolayers made from five different ω-fluorinated 1-alkynes of different lengths (F-$(CH_2)_{8-16}$-C≡CH), onto oxide-free, hydrogen-terminated Si(111), see Figure 1. These monolayers were characterized experimentally by X-ray photoelectron spectroscopy (XPS), infrared reflection absorption spectroscopy (IRRAS), ellipsometry, near edge X-Ray absorption fine structure (NEXAFS), and contact angle measurements. In addition, molecular modeling was used to obtain information about the packing density and layer thickness. Finally using the n-Si-alkyl chain/Hg junction, where Hg contacts a monolayer of a series of organic molecules,[17] current-voltage studies were performed to obtain information about a stepwise tunable Si work function.

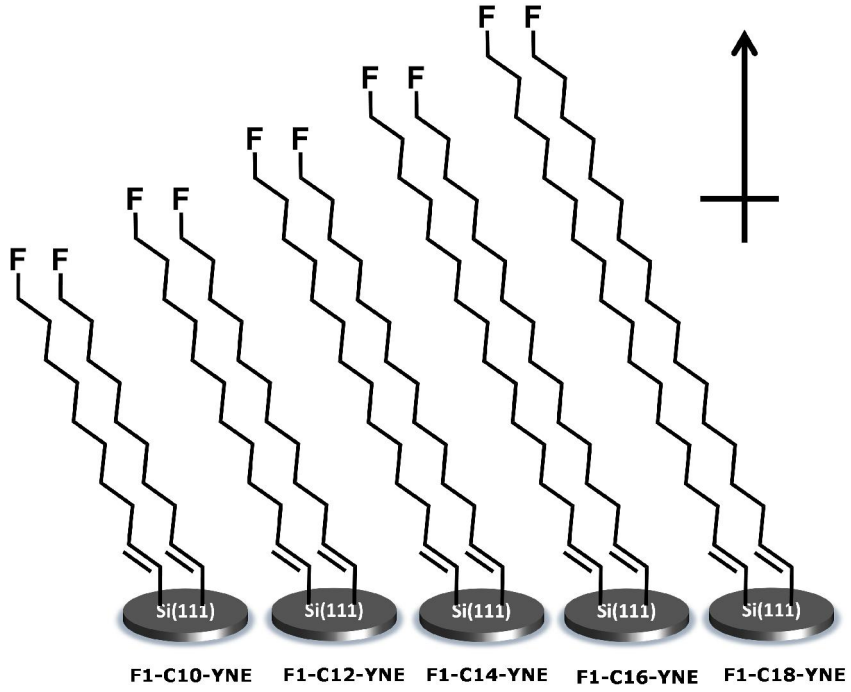

Figure 1. Monolayers on Si(111) used in the current study.

3.2 EXPERIMENTAL SECTION

3.2.1 Materials

Five mono-ω-fluorinated 1-alkynes were used. The synthesis procedures and spectra of 10-fluorodec-1-yne (F1-C10-yne), 12-fluorotetradec-1-yne (F1-C12-yne), 14-fluorotetradec-1-yne (F1-C14-yne), 16-fluorohexadec-1-yne (F1-C16-yne) and 18-fluorooctadec-1-yne (F1-C18-yne) can be found in the *Supporting Information S.3.2 to S.3.6*. All chemicals were used as received, with the following specifications and sources: n-hexadecane (Sigma Aldrich, 99%), sulphuric acid (Sigma Aldrich, 95 - 97%), hydrogen peroxide (Acros Organics, 35%), ammonium fluoride (Riedel-de Haën, 40%, semiconductor grade VLSI PURANAL Honeywell 17600), acetone (Aldrich, semiconductor grade VLSI PURANAL Honeywell 17617), deionized water (resistivity 18.3 MΩ cm), pentane (VWR, 95%). Silicon wafers, with a 0.2^{o} miscut angle along the <112> plane, were (111)-oriented, n-type, phosphorus-doped and with a specific resistance of 1-10 Ωcm, as purchased from Siltronix (France).

3.2.2 Monolayer formation

A three-necked flask was charged with 2 mL of mono-ω-fluorinated 1-alkyne and purged with argon under reduced pressure for 30 min, while being heated to 80 °C. Si(111) wafers were cut in 1 × 1 cm pieces. The surfaces were cleaned using air plasma (Harrick Scientific Products, Inc. Pleasantville, NY) for 10 min and the surfaces were subsequently sonicated for 15 min in pure acetone. The surfaces were rinsed with water and transferred to freshly prepared piranha solution (H_2SO_4/H_2O_2 3:1). After 20 min, the surfaces were thoroughly rinsed with water and dried with a stream of argon. Subsequently, the substrates were etched in argon-saturated 40% aqueous ammonium fluoride solution for 15 min. The surfaces were again rinsed with water and dried with a stream of argon. The samples were rinsed with argon-saturated water, and finally blown dry with a stream of argon. These samples were then immediately transferred into the flask, which was immediately depressurized again. The reaction mixture was kept at 80 °C overnight. The sample was then removed from the flask and immediately extensively rinsed with pentane and CH_2Cl_2, sonicated for 5 min in CH_2Cl_2 to remove physisorbed molecules, and blown dry with a stream of dry argon. The surfaces were directly used for surface characterization or stored in the glove box until surface characterization.

3.3 Monolayer characterization

3.3.1 Static water and hexadecane contact angles

Static water and hexadecane contact angles were measured with an automated Krüss DSA 100 goniometer. At least six small droplets (3.0 μL) were dispensed and the contact angles were determined by a Tangent 2 fitting model. The error in the determined contact angles is approximately 1^o.

3.3.2 X-ray Photoelectron Spectroscopy (XPS)

XPS spectra were recorded on a JPS-9200 photoelectron spectrometer (JEOL, Japan). The analysis was performed under ultra-high vacuum conditions using a monochromatic Al Kα source at 12 kV and 20 mA and an analyzer pass energy of 10 eV. A takeoff angle φ (angle between the sample and the detector) of 80^o was used. For an exact determination of the atomic C/Si ratio of organic monolayers on Si(111), the influence of X-ray photo diffraction (XPD) on the XPS signal had to be accounted for.[37, 51] It has been shown that the variations of the Si2p intensity were similar after each periodic variation of 120° on a hydrogen-terminated Si(111) surface, and this arises three times, symmetrically, on the crystalline silicon (111) substrate.[51] Therefore, the samples were

rotated 120° around the surface normal, yielding rotationally averaged C1s and Si2p spectra. The rotation X-ray photoelectron emissions yielded a truly quantitative C/Si ratio, which is now independent of the orientation of the sample.[40] All XPS spectra were evaluated by Casa XPS software (version 2.3.15). The binding energies were calibrated on the hydrocarbon (CH_2) peak with a binding energy of 285.0 eV.

3.3.3 Infrared Reflection Absorption Spectroscopy (IRRAS)

IRRAS spectra were recorded on a Bruker Tensor 27 FT-IR spectrometer using a commercial variable angle reflection unit (Auto Seagull, Harrick Scientific). A Harrick grid polarizer was installed in front of the detector and was used to measure the spectra with *p*-polarized (parallel) respect to the plane of incidence at the sample surface. All spectra were obtained at an incident angle of 68° with respect to the sample. 2048 scans were made. The resolution was set at 4 cm^{-1}. All spectra were recorded at room temperature in dry nitrogen atmosphere. A slight linear baseline correction was applied.

3.3.4 Ellipsometry

The ellipsometric thickness of the modified surfaces was measured using a rotating Sentech Instruments (Type SE-400) ellipsometer, operating at 632.8 nm (He–Ne laser), and an angle of incidence of 70°. The optical constants of a freshly etched H-terminated Si(111) surface were taken as n = 3.821 and k = 0.051.[37] The thicknesses of the monolayers were determined with a planar three layer (ambient, monolayer, substrate) isotropic model, with assumed refractive indices of 1.00 and 1.44 for ambient and the monolayer, respectively. The reported values are the average of at least 8 measurements and the error is less than 1 Å.

3.3.5 Contact Potential Difference (CPD)

CPD measurements were performed with a custom-made Kelvin Probe set-up, based on a commercial Besocke Delta Phi Kelvin probe + controller, which are placed in a glove box with controlled 10% relative humidity. The surface potential of the monolayers was measured, relative to that of a vibrating Au grid that was calibrated prior to the measurements against freshly peeled highly ordered pyrolytic graphite (HOPG).

3.3.6 Current-Voltage (I-V)

I-V measurements were performed on n-Si/monolayer/Hg junctions, formed by placing a Hg (99.9999% purity) drop on the monolayer, using a controlled growth hanging mercury drop (HMD) electrode (Polish Academy of Sciences, Poland). The samples were

contacted on the back by applying In-Ga eutectic, after scratching the surface with a diamond knife. Measurements were carried out in a controlled environment glove box with 10% relative humidity. The contact area between the Hg drop and the monolayer (typically 0.6 mm in diameter) was determined using an optical microscope and used to calculate the current density (J). Measurements were made with a Keithley 6430 sub-fA current/voltage source-measure unit. Several scans from -1 to +1 V (applied to Hg) were measured for each junction with a scan rate of 20 mV/s. At least 7 junctions were made on each sample, and the results represent the average of all the measurements. None of the measurements was rejected.

3.3.7 Near Edge X-ray Absorption Fine Structure (NEXAFS)

NEXAFS spectra were collected at the National Synchrotron Light Source (NSLS) U7A beamline at Brookhaven National Laboratory, using an elliptically polarized beam with ~85% p-polarization. This beam line utilizes a monochromator and 600 l/mm grating provides a full-width at half-maximum (FWHM) resolution of ~0.15 eV at the carbon K-edge. The monochromator energy scale was calibrated using the intense C1s - π^* transition at 285.35 eV of a graphite transmission grid placed in the path of the X-rays. Partial electron yield was monitored by a detector with the bias voltage maintained at -150 V. Samples were mounted to allow rotation and allow changing the angle between the sample surface and the synchrotron X-rays. The NEXAFS angle is defined as the angle between the incident light and the sample surface. The spectra were brought to the standard form by linear pre-edge background subtraction and normalizing to the unity edge jump, defined by a horizontal plateau, 40–50 eV above the absorption edge.

3.3.8 Molecular modeling

For the molecular modeling study, the same method is followed as reported by Scheres and co-workers.[38] In short, Materials Studio software (version 5.0) was used to construct and optimize the monolayers. All monolayers were formed from five standard cells containing a decenyl chain (representing the bonding situation obtained after attachment of one of the alkynes) attached in an all-*trans* conformation to four Si atoms. The Si atoms represent the first four layers of the Si substrate and this substrate model was obtained by cleaving a Si crystal along the (111) plane. The structures were placed in a box to obtain the standard unit cell (as depicted in Figure 2). The standard cells were copied in the directions of the Si substrate to form larger unit cells. By replacing some of the attached chains with hydrogen atoms, different substitution patterns and substitution percentages were obtained.

Unit cells were copied to form the final big simulation cells, representing the whole modified Si surface. The unit cells and the big simulation cells were optimized, using a polymer consistent force field (PCFF) (bottom two rows of Si atoms were constrained) as present in the Forcite module package in Materials Studio, using the ultra-fine settings of the "Smart Minimizer" routine, "high-convergence" criteria and periodic boundary conditions.

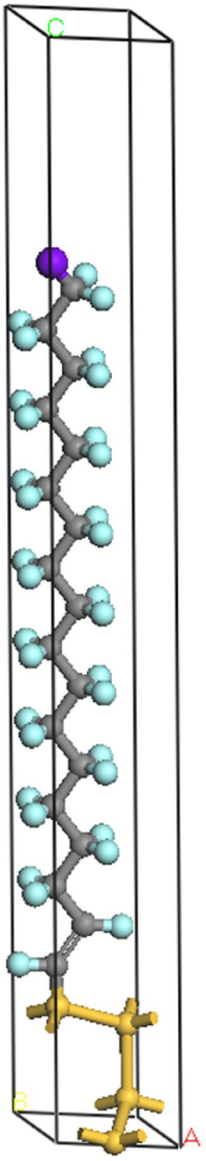

Figure 2. Structure ball and stick model of the F1-C18-yne unit cell. The color coding scheme is yellow (silicon atom), gray (carbon atom), light-blue (hydrogen atom) and purple (fluorine atom at the top).

3.4 RESULTS AND DISCUSSION

Monolayers with different chain lengths were studied to determine the influence of chain length on the quality of mono-ω-fluorinated 1-alkyne-derived monolayers. To this end five different mono-ω-fluorinated 1-alkynes were synthesized with total chain lengths C_{10}, C_{12}, C_{14}, C_{16} and C_{18}. The synthesis and characterization of these compounds is provided in the *Appendix B.3.2 to B.3.6*, and they will be referred to as F1-C10-yne, F1-C12-yne, F1-C14-yne, F1-C16-yne and F1-C18-yne, respectively. These alkynes were attached to oxide-free, hydrogen-terminated Si(111) at 80 °C under an inert atmosphere, according to the procedure described by Scheres et al.,[34, 37, 52] which resulted in covalently bound monolayers with Si-C=C bonds near the surface (see Figure 1).

3.4.1 Static contact angles

The obtained monolayers were analyzed with static water and hexadecane contact angle measurements to probe polar and dispersive interactions with the surface, respectively (Table 1). With an increase in chain length the static water contact angle increases from 94° (C_{10}) to 110° (C_{18}). While the data for F1-C18-yne are similar to the data for non-fluorinated C_{18} chains, for shorter chains the contact angle is somewhat lower than for non-fluorinated alkynes (~110-111° for non-fluorinated C_{12}-C_{18} 1-alkynes.[37, 38] This increase in hydrophobicity with increasing chain lengths for the mono-F monolayers is likely caused by a higher monolayer density, as discussed below in more detail.

Table 1. Static contact angle measurements for water and hexadecane of F1-C10-yne, F1-C12-yne, F1-C14-yne, F1-C16-yne and F1-C18-yne Monolayers on H-Si(111)

Monolayers	Contact Angle (°)±1	
	Water	Hexadecane
F1-C10-yne	94	39
F1-C12-yne	96	41
F1-C14-yne	106	43
F1-C16-yne	110	46
F1-C18-yne	110	46

The static hexadecane contact angle increased slightly from 39° (C_{10}) to 46° (C_{18}). These slight increases likely reflect two opposing trends. On the one hand they reflect a decrease in the dispersive interaction between the increasing amount of fluorine atoms and hexadecane as caused by the increasing density of F atoms on the surface. To some degree

this is counterbalanced by the effect of an increase of the C-C-C-F torsion angle with increased packing density, as observed by modeling (see *Supporting Information S.3.7*), and more in-depth studies would be needed to probe this balance more in detail.[53]

3.4.2 X-ray photoelectron spectroscopy

Figure 3 presents the results of XPS analyses of surfaces modified with a series of F_1-C_x-YNEs of various chain lengths (x = 10, 12, 14, 16 and 18). Detailed investigation of the C1s and Si2p regions of the XPS spectra (Figure 3A and 3C, respectively) confirms the successful formation of the surface F1-Cx-YNE. The C1s and Si2p narrow scans are aligned at the baseline to show the differences in the various monolayers. In the deconvoluted C1s narrow scan (Figure 3B), the peak at 283.7 eV corresponds to the carbon, bound to the silicon substrate, while a higher binding energy contribution at 287.9 eV is assigned to the carbon, bound to fluorine. The peak at 285.9 eV corresponds to the carbon, which is next to the carbon bound to fluorine and the large peak at 285.0 eV – which was used as reference peak – corresponds to the rest of the predominant aliphatic chain. In addition, the C1s XPS spectrum of (*E*)-$F(CH_2)_{14}CH{=}CH{-}Si(SiH_3)_3$ (see overlapped DFT in Figure 3B) was simulated using a B3LYP/6-311G(d,p)-derived method,[54] yielding a reasonable agreement with experiment. In narrow Si2p spectra (Figure 3C), the attenuation of the doublet Si2p3/2 and Si2p1/2 at 99.5 and 100.1 eV, due to an increased attenuation of the Si substrate signal upon thickening of the monolayer, becomes clearly visible after monolayer attachment to the surface. For all monolayers a completely flat baseline within 103 - 104 eV was obtained, indicating a (nearly) oxide-free Si surface.

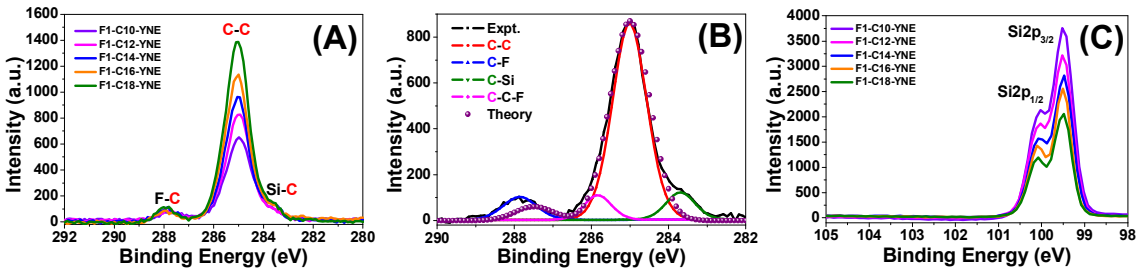

Figure 3. XPS spectra of mono-ω-fluorinated 1-alkyne-derived monolayers on H-terminated Si(111). (A) C1s narrow scan of monolayers derived from F1-Cx-YNE. (B) C1s narrow scan of F1-C16-YNE with deconvolution peaks and overlapped with B3LYP/6-311G(d,p)-simulated C1s spectrum of (*E*)-$F(CH_2)_{14}CH{=}CH{-}Si(SiH_3)_3$, and (C) Si2p region of monolayers derived from F1-Cx-YNE (x = 10 – 18).

Quantitative information on the packing density was obtained from XPS data, via rotational averaging of the observed C/Si ratio of the different monolayers to correct for any diffraction effects caused by the crystallinity of the Si substrate.[55, 56] Since variations in the C/Si ratio up to 1 - 2 % can be observed, rotational averaging was carried out by measuring this ratio at 13 angles over a 120° range, corresponding to the symmetry of the Si substrate.[37, 40, 51] These ratios are then converted into monolayer thicknesses (d_{ML}) by the following equation:[37]

$$d_{ML}(\text{Å}) = \lambda_{ML}^{Si} \sin(\varphi) \ln(1 + C/Si) \tag{1}$$

with λ_{ML}^{Si} = attenuation length of Si 2p photoelectrons in the organic monolayers (λ_{ML}^{Si} = 39.5 Å), and φ = takeoff angle between the surface and the detector (in this experiment: φ = 90°). For all monolayers, the C/Si ratios and the corresponding calculated thicknesses are shown in Table 2. As evident, the C/Si ratio and the derived thicknesses increase monotonously with increasing chain length.

The surface coverage and tilt angle was calculated by comparing the formed monolayers with a previous study on alkane-thiol monolayer on gold.[57] Tilt angles can be easily converted to monolayer thicknesses and vice versa (with Equation 2). The surface coverage can therefore also be calculated with monolayer thicknesses. The surface coverage of the monolayers was calculated with the following equation:[37, 51]

$$\theta_{ML} = \frac{d_{ML} \times D_{Au}}{d_{TH(30^o)} \times D_{Si}} \tag{2}$$

in which D_{Au} is the surface density of chains in a perfect alkane-thiol monolayer on gold with a tilt angle of 30° ($D_{Au} = 4.65 \cdot 10^{14}$ cm^{-2}), D_{Si} is the surface atom density on Si(111) ($D_{Si} = 7.8 \cdot 10^{14}$ cm^{-2}) and $d_{TH(30°)}$ is the theoretical thickness of an organic monolayer on Si with a tilt angle of 30°. The theoretical thickness can be calculated with the following equation.[37, 51, 58]

$$d_{TH}(\text{Å}) = 1.89 + \left(\frac{\text{n}}{2} - 1\right) 2.54 \cos(\theta) + 1.56 \sin(35.5° + \theta) \tag{3}$$

where n is the number of carbon atoms per alkyne chain and θ is the tilt angle of the chains.

The monolayer thickness was also obtained by ellipsometry, NEXAFS (using NEXAFS-derived values of tilt angles) and by molecular modeling studies (Material Studio); see Figure 4. All these measurements show that the monolayer thickness increases monotonously with increasing chain length, and display an increase in thickness of ca. 10 Å in going from C10 to C18. There are some systematic variations between the different methods, but overall experiments and theory in good agreement and the observed monolayer thicknesses comparable to reported values for non-fluorinated monolayers.[37]

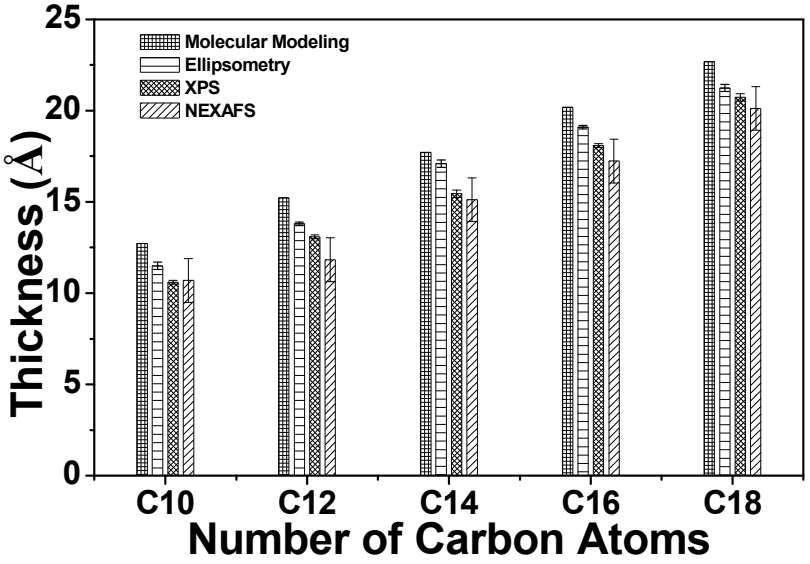

Figure 4. Molecular modeling studies at 60 % coverage (orange) estimated thickness compared with measured by ellipsometry (red column), XPS (green column), and NEXAFS (blue column) of F_1-C_x-YNE (x = 10 – 18) monolayers on H-Si(111).

The surface coverage was calculated for the prepared monolayers, the results are shown in Table 2. The calculated surface coverage ranges from 51 ± 2 % for the F1-C10-yne up to 58 ± 2 % for F1-C18-yne monolayers. This is somewhat lower than the reported 55 - 65% for non-fluorinated C12 - C18 1-alkynes,[37, 38] but still appreciably higher than obtained for any 1-alkene-derived monolayer, for which values between 50 - 55% for C_{16}/C_{18} monolayers are more typical.[37] The observed values are the balance between having the narrower CH=CH moiety (in comparison to CH_2-CH_2) near the Si surface and having the polar and slightly larger C-F moiety at the terminus.[43] The surface coverage increases with increasing chain length of monolayers. This is supported by data from IRRAS, NEXAFS and molecular modeling (which will be explained in the next section).

Table 2. Quantitative XPS Data of F1-C10-yne, F1-C12-yne, F1-C14-yne, F1-C16-yne and F1-C18-yne Monolayers on H-Si(111). Atomic C/Si Ratios, Resulting Monolayer Thicknesses d_{ML} and Surface Coverages (θ_{ML}).

Monolayers	C/Si ratio	SAM thickness, Expt.(d_{ML} (Å))	SAM thickness, Theory(d_{TH} (Å))	Surface coverage, θ_{ML} (%)
F1-C10-yne	23.8/76.2	10.6	12.3	51
F1-C12-yne	28.5/71.5	13.1	14.5	54
F1-C14-yne	32.7/67.3	15.5	16.8	55
F1-C16-yne	37.1/62.9	18.1	19.1	56
F1-C18-yne	41.2/58.8	20.7	21.3	58

3.4.3 Infrared reflection absorption spectroscopy

The absence of -CH_3 peak at 2950 cm^{-1} confirms that the formed monolayers are indeed -CH_2F terminated. Analysis of the CH_2 stretch vibrations of the prepared monolayers by IRRAS reveals a high degree of short-range ordering of the monolayers. The peak positions for the anti-symmetric stretching ($\upsilon_a CH_2$, anti-sym) at 2918 ± 1 cm^{-1} and the symmetric stretching ($\upsilon_s CH_2$, sym) at 2851 ± 1 cm^{-1} for the F1-C16-yne-derived and F1-C18-yne-derived monolayer are indicative of densely packed layers with a high degree of short-range ordering, in which all chains adopt a trans conformation.[59, 60] As depicted in Figure 5, the peaks of the methylene stretching vibrations shift to higher wavenumbers with decreasing chain length, to 2922 cm^{-1} for the F1-C10-yne derived monolayer (see Table 3). This is attributed to a lower packing density for the monolayers derived from shorter alkynes.[37]

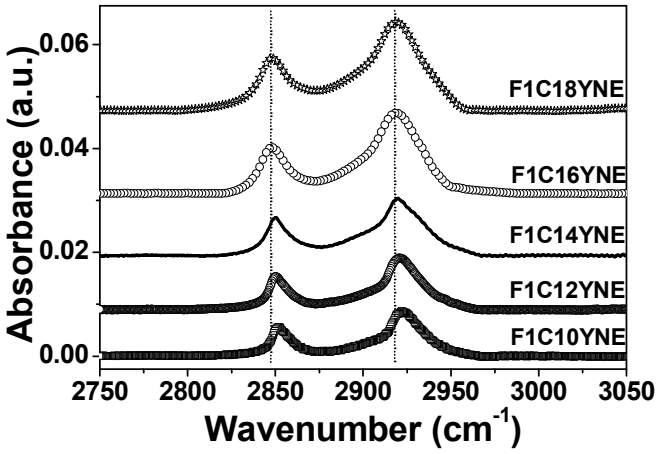

Figure 5. IRRAS spectra (CH_2 stretching area) for F1-C10-yne, F1-C12-yne, F1-C14-yne, F1-C16-yne and F1-C18-yne monolayers on H-Si(111).

Table 3. IRRAS ν_a-CH_2 anti-symmetric and ν_s-CH_2 symmetric frequencies with p-Polarized Light, of the F1-C10-yne, F1-C12-yne, F1-C14-yne, F1-C16-yne and F1-C18-yne Monolayers on H-Si(111).

Monolayers	Wavenumbers (cm^{-1})	
	ν_a-CH_2 anti-symmetric	ν_s-CH_2 symmetric
F1-C10-yne	2922.1	2852.2
F1-C12-yne	2920.1	2849.2
F1-C14-yne	2918.7	2848.8
F1-C16-yne	1918.2	2847.8
F1-C18-yne	1918.4	2847.4

3.4.4 Near Edge X-Ray Absorption Fine Structure (NEXAFS)

NEXAFS spectra were taken at the Carbon *K*-edge to determine the chain lengths of dipolar mono-ω-fluorinated 1-alkyne-derived molecules of SAMs on silicon. Data were acquired at 90°, 70°, 55°, 30° and 20° and are presented in Figure 6 (A-E). NEXAFS spectroscopy is known to be a powerful tool in the investigation of organic molecules at surfaces. It provides unique information both on the empty orbitals of organic molecules and on their orientation with respect to the substrate.[40, 61] On the basis of previous findings on Si(111) surfaces[40, 62] the first pronounced peak at 284.7 eV is associated to the π*(C=C) resonance involving the C atoms of the alkene; the second peak at 287.4 eV is assigned to transitions involving the σ* C-H atoms in the methylene units, and the peaks around ~293.2 and ~303.0 eV are assigned to (C-C/σ*, C-F/σ*) and C=C/σ* resonances respectively. Castner et al.[63] reported the C-F* peak in Teflon (PTFE) and assigned the sharp peak at 292.3 eV to the C-F* absorption, and the peaks at 295.7 and 299.0 eV to the C-C* and other C-F* absorption, respectively. In contrast we did not observe these specific peaks for C-F* at these positions, likely because of signal/noise issues with only one fluorine atom buried in the C-C/σ* and C=C/σ* resonance peak.

In figure 6 (A-E) all fluorinated monolayers have the same peak energies and shapes, indicating that Si-C=C, C-H, C-C, and C-F bonds are in very similar chemical environments. Note that these are normalized spectra; however, in absolute terms, the π*(C=C) peak is stronger for F1-C10-YNE (A), F1-C12-YNE (B) and F1-C14-YNE (C) than for F1-C16-YNE (D) and F1-C18-YNE (E). The σ* C-H, C-C/σ*, and C-F/σ* peaks are stronger for F1-C16-YNE (D) and F1-C18-YNE (E) because the molecules are much more densely packed in the SAM structure than for F1-C10-YNE (A), F1-C12-YNE (B) and F1-C14-YNE (C).

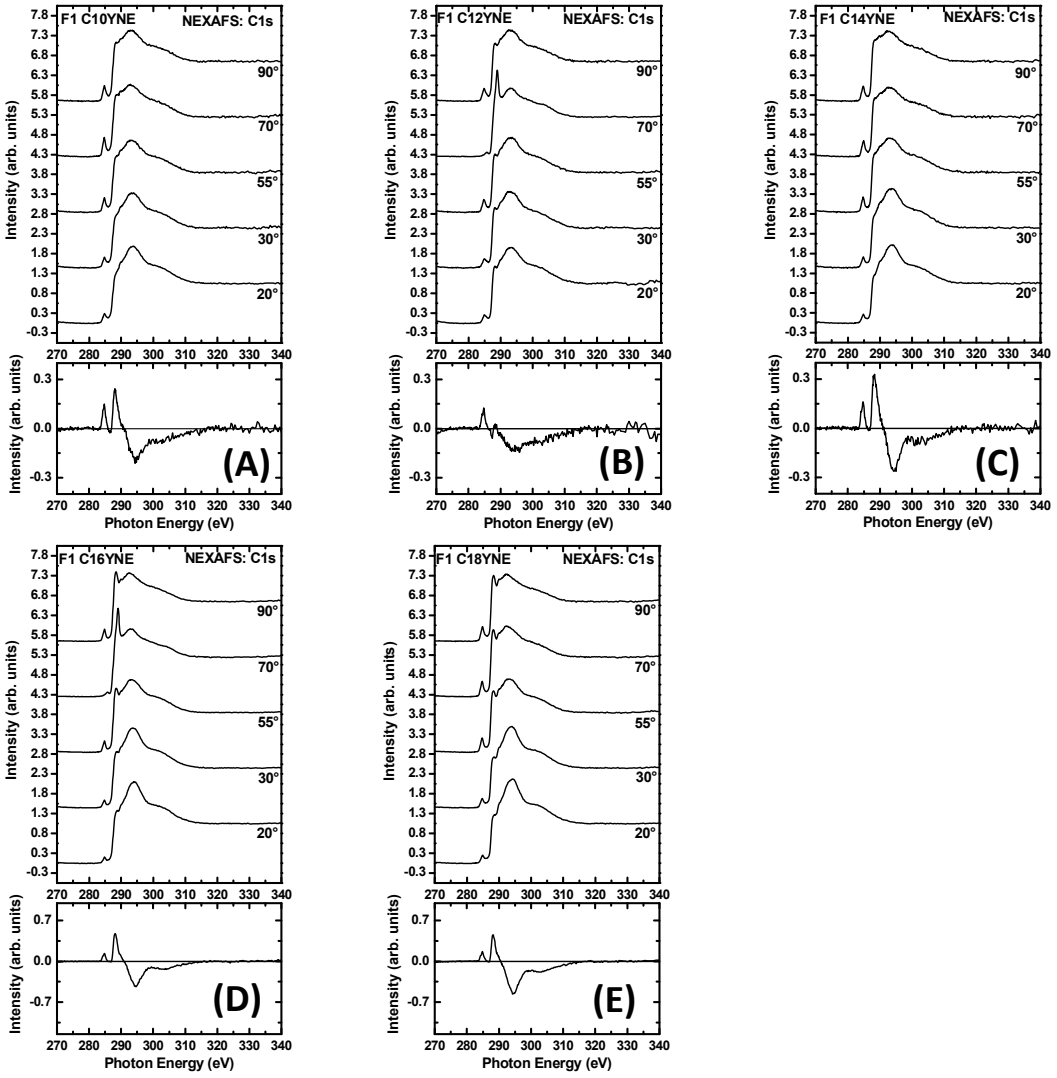

Figure 6. C K-edge NEXAFS spectra of SAMs prepared from F1-C10-YNE (A), F1-C12-YNE (B), F1-C14-YNE (C), F1-C16-YNE (D), and F1-C18-YNE (E) at 25 °C under ambient light, acquired at X-ray absorption spectra taken at different angles (90°, 70°, 55°, 30°, and 20°) between the surface plane and the electric field vector.

3.4.5 Controlled modification of the surface/interface potential and its application in metal/monolayer/semiconductor (MOMS) junctions

To demonstrate the potential application of the chemical modification (substituting H with an F atom in the terminal CH_3 group) of the molecular monolayer in possible future electronic devices, we compared the J-V behavior of a junction with the modified F1-C16-yne monolayer with that of the previously reported C16-yne monolayers (Figure 7).[33]

We showed previously that organic monolayers on oxide-free Si play two important roles in determining the J-V behavior of a MOMS junction.[17, 19, 64] The first is electronic passivation of the Si surface, i.e., reducing the density of surface states. This makes the Si surface more similar to an ideal surface that acts according to the Schottky-Mott limit, as given in eq 4:[65]

$$\phi_{b,n} = \Phi_m - \chi_{sc} \quad (4)$$

where $\phi_{b,n}$ is the barrier for charge transport inside the semiconductor, Φ_m is the metal work function, and χ_{sc} is the semiconductor electron affinity.

The second important role is that of introducing a surface dipole that strongly depends on the dipole of the precursor molecule, as used for monolayer formation. Once the surface is electronically passivated, eq 4 shows that the barrier for charge transport ($\phi_{b,n}$) depends on the semiconductor electron affinity (χ_{sc}), which in turn depends on the surface dipole that is introduced by the monolayer.

Substituting an H with an F atom in the terminal group of the alkenyl chain is expected to increase the work function (thus increasing the electron affinity) of the Si-monolayer surface. This increase is due to the direction of the bond dipole between C-F in comparison to C-H.[66] Indeed, multiple CPD measurements indicate that the work function of the F1-C16-yne sample is 100 ± 20 meV larger than that of the previously reported C16-yne sample (the error represents the standard deviation between measurements). According to eq 4, the higher work function should be expressed as a lower barrier for transport in the full MOMS junction. From the data presented in Figure 7 it is clear that $\phi_{b,n}$ is indeed 100 meV lower for the F1C16-yne monolayer than for the non-fluorinated monolayer[65], which is consistent with the work function, obtained from CPD measurements. The agreement between the CPD and J-V results indicates that the electronic passivation of the Si surface is indeed of high quality, which is attributed to the high density of the molecular monolayer obtained from 1-alkynes. Furthermore, it demonstrates how the surface potential of Si can be controllably modified by chemical modification of the monolayer and that the modification of the surface potential can be translated into interface modification in a full MOMS junction.

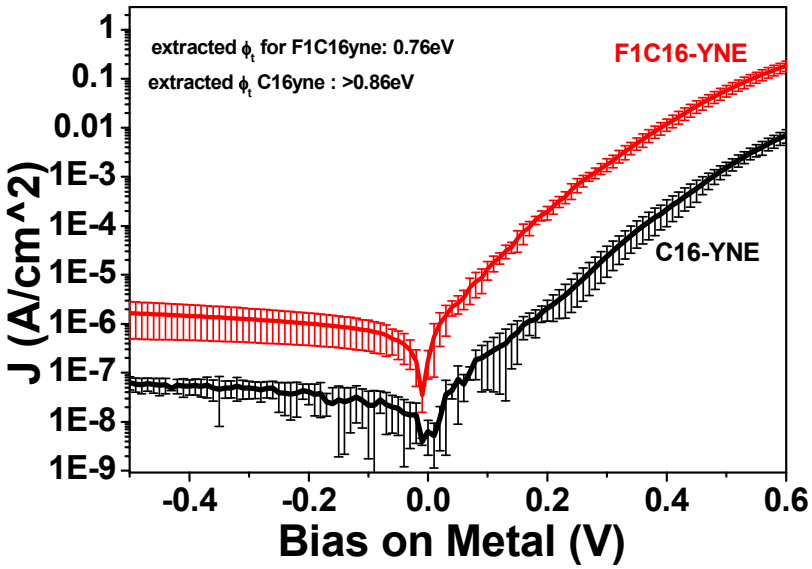

Figure 7. Comparison between the J-V curves of Hg/F1C16-YNE-Si (red) and Hg/C16-YNE-Si (black) junctions.

3.4.6 Molecular modeling

Finally, all experimentally prepared monolayers were studied by molecular modeling. Furthermore, the influence of molecule chain lengths with different substitution percentages and substitution patterns were studied. The different substitution percentages were 25, 33, 40, 50, 60, 67 and 75%. The 50-75% unit cells were used as reported by Scheres et al.[38]

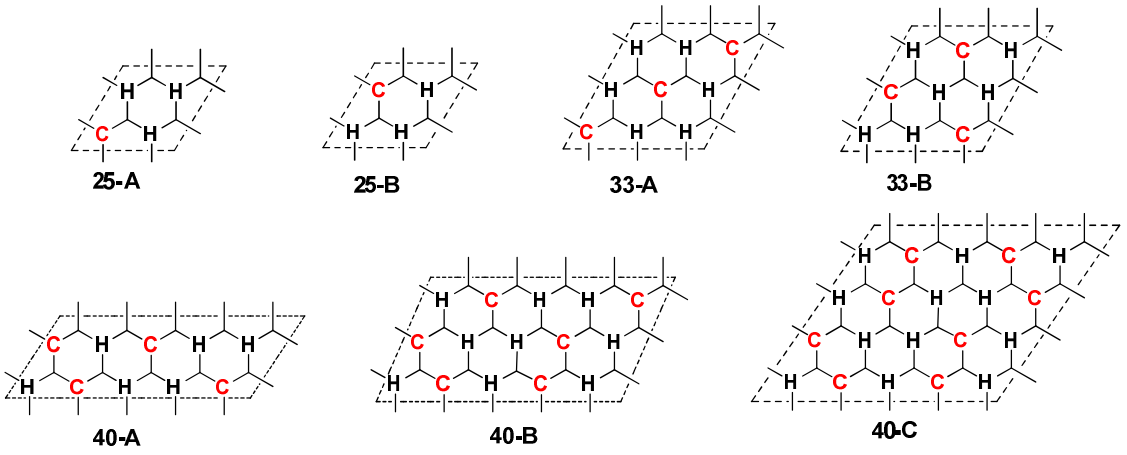

Figure 8. Overview of the unit cells with 25, 33 and 40% substitution. Each C (in red) represents an attached chain and each H corresponds to an unoccupied H-Si site.

The unit cells with 25, 33 and 40% coverage are depicted in Figure 8. Two different unit cells were made for the 25 and 33% substitution percentages and three unit cells for all other substitution percentages. The different unit cells per surface coverage have different substitution patterns (denoted as A, B and C). A top view of the unit cells is depicted in Figure 8. Each H represents an unoccupied position and each C an attached chain. The unit cells were copied in the plane of the silicon substrate until the simulations cells were 10 × 15 or 12 × 15 attachment places in size. These cells are large enough to give data that are independent of the number of chains.[38, 68]

Periodic boundary conditions were used to mimic an infinitely large surface, which is not affected by edge effects. An example of an optimized enlarged unit cell is shown in Figure 9. To study the interchain interactions, the packing energy per chain is calculated. The packing energy is the energy that is consumed or released by adding a chain, close to another chain. The packing energy can be calculated with the following equation:

$$E_{packing} = \frac{E_{chains}}{n} - E_{relaxed.chain} \tag{5}$$

With E_{chains} the total potential energy of all chains in an optimized simulation cell, n the total number of chains in the same unit cell and $E_{relaxed\ chain}$ is the potential energy of a single free optimized alkene, which represents an attached alkyne chain. To obtain the potential energy of the chains the silicon layer has to be cut off, i.e., all Si-C bonds were cleaved. It turned out that by adding hydrogen atoms to the carbons that were linked to the Si atoms, the conformations of the chains were altered. This is unwanted because then the information about the interchain interactions is lost. It was therefore examined if the formed radicals could also be used for the comparison of the monolayers. This is done by measuring the angles between the double bond and the remaining hydrogen after the removal of the silicon layer, see Figure 10. By measuring these angles, it could be seen whether the radicals of different chain lengths were treated in the same way and, thereby, whether the packing energies could be compared.

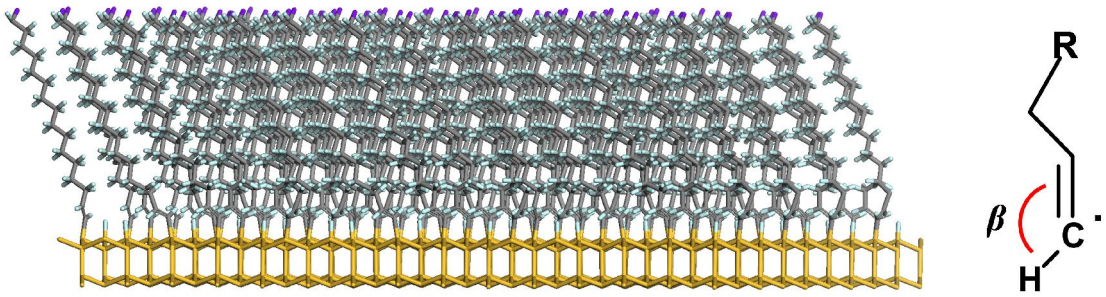

Figure 9. (left) Side view of simulation cell 60A after enlargement and optimization with F1-C16-yne. Yellow is silicon, gray is carbon, purple is fluorine and light blue is hydrogen. (right) Angle (*β*) measured after removal of the silicon layer.

Three angles per monolayer were measured and averaged. The results are shown in Figure 10 (A). Three main conclusions can be drawn from this plot. First, all angles are between 116.0 and 119.5°, which is only a small deviation from the normal sp^2 hybridized orbitals. This indicates that the program treated the radicals as almost normal bonds. Secondly, the measured angles per surface coverage are within one degree.

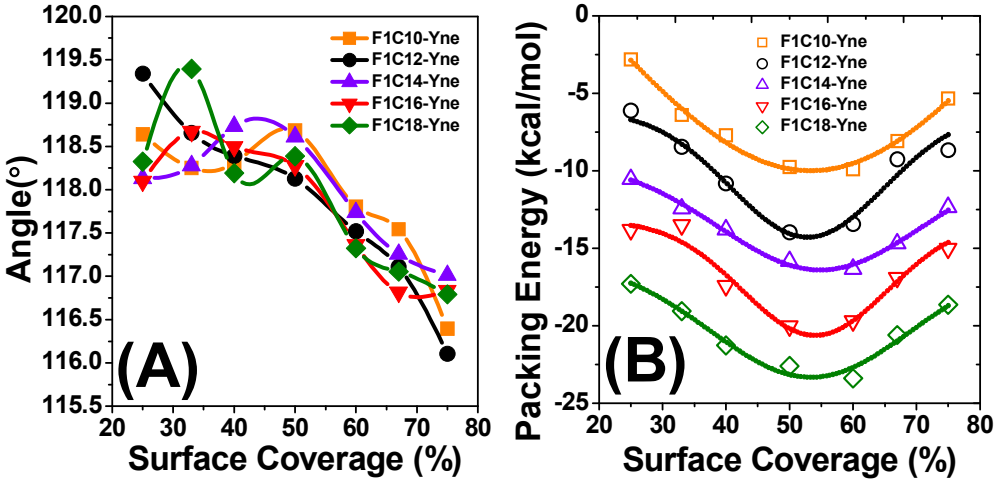

Figure 10. (A) Averaged angles (*β*) between the double bound and remaining hydrogen after removal of the silicon layer of the F1-C10-yne, F1-C12-yne, F1-C14-yne, F1-C16-yne and F1-C18-yne monolayers at different substitution percentages. (B) Averaged packing energies of F1-C10-yne, F1-C12-yne, F1-C14-yne, F1-C16-yne and F1-C18-yne monolayers on H-Si(111) at different surface coverages. The lines are added as a guide to the eye.

This result shows that the radicals of different alkenyl chains are treated in the same way. It allows us therefore to compare the packing energies calculated for the different chain lengths. However, the absolute values of the packing energy may be incorrect. Finally it can be seen that that the angles decrease with increasing surface coverage. This trend is ascribed to the smaller tilt angles with higher substitution percentages.[37, 38] In

Figure 10 (B), the packingenergies shown are calculated by the 'radical approach'. The monolayers are formed by a meandering functionalization[37, 58, 69, 70] and it therefore occurs via a near-random process.[38] It is therefore likely that experimentally the monolayer possess several substitution patterns. Therefore, the packing energies of the two or three unit cells were averaged for each surface coverage. The minima of the packing energies lie between 50 and 60%, which is just slightly higher than the experimentally found surface coverage of the monolayers. The trend is not very clear, but the surface coverage also increases slightly, if the monolayers are built from longer chain lengths. The optimized C-C-C-F torsional angles are shown to increase slightly with respect to chain length from 160° (C10) to 166° (C18) at 60 % surface coverage, implying that the fluorine atoms are rotated more and more "away" from the surface with increasing chain length. This result is in line with the ellipsometry-derived thickness, IRRAS and contact angle measurements. In addition, the packing energies of longer chains are lower for each substitution percentage. This is attributed to the more favorable Van der Waals interactions that occur if longer chains are placed next to one another. As stated by Scheres et al.,[38] the packing energy itself is not always sufficient to verify whether a certain substitution percentage or substitution pattern is favorable or not. The binding energy is the main driving force for monolayer formation, which is not included in the packing energy, but in the current cases all monolayers were formed from the same type of 1-alkynes. Therefore trends in the packing energies are expected to accurately mimic the overall energy of monolayer formation, and yield that for mono-F alkyne-derived monolayers the surface coverage is around 55%.

3.5 CONCLUSIONS

A series of mono-ω-fluorinated 1-alkyne-derived monolayers of various thicknesses was prepared on oxide-free hydrogen-terminated Si(111) were obtained from mono-ω-fluorinated 1-alkynes. A combination of experimental and theoretical studies shows that high-quality monolayers can be obtained (e.g. monolayer derived from F1-C18-yne has a packing density of 58 ± 2 %). It was demonstrated that by substitution of CH_3 to CH_2F in the terminal group, it is possible to controllably and stepwise modify the surface potential and barrier for charge transport in a full metal/monolayer-semiconductor (MOMS) junction. The work function of silicon surfaces can thus be altered to accommodate specific application needs, and therefore this technique extends the potential of using Si-C derived monolayers in the fabrication of MEMS and NEMS derived electronic devices.

3.6 REFERENCES

1. Heath, J. R., Molecular Electronics. *Annual Review of Materials Research* **2009,** 39, (1), 1-23.
2. Csoeregi, E.; Quinn, C. P.; Schmidtke, D. W.; Lindquist, S.-E.; Pishko, M. V.; Ye, L.; Katakis, I.; Hubbell, J. A.; Heller, A., Design, Characterization, and One-Point in vivo Calibration of a Subcutaneously Implanted Glucose Electrode. *Anal. Chem.* **1994,** 66, (19), 3131-3138.
3. Aviram, A.; Ratner, M. A., Molecular Rectifiers. *Chem. Phys. Lett.* **1974,** 29, (2), 277-283.
4. Polymeropoulos, E. E.; Sagiv, J., Electrical Conduction through Adsorbed Monolayers. *The Journal of Chemical Physics* **1978,** 69, (5), 1836-1847.
5. Yoon, H. J.; Shapiro, N. D.; Park, K. M.; Thuo, M. M.; Soh, S.; Whitesides, G. M., The Rate of Charge Tunneling through Self-Assembled Monolayers is Insensitive to Many Functional Group Substitutions. *Angew. Chem. Int. Ed.* **2012,** 51, (19), 4658-4661.
6. Joachim, C.; Gimzewski, J. K.; Aviram, A., Electronics using Hybrid-Molecular and Mono-Molecular Devices. *Nature* **2000,** 408, (6812), 541-548.
7. Nitzan, A.; Ratner, M. A., Electron Transport in Molecular Wire Junctions. *Science* **2003,** 300, (5624), 1384-1389.
8. Tao, N. J., Electron Transport in Molecular Junctions. *Nature Nanotechnology* **2006,** 1, (3), 173-181.
9. Song, H.; Reed, M. A.; Lee, T., Single Molecule Electronic Devices. *Adv. Mater.* **2011,** 23, (14), 1583-1608.
10. Ulgut, B.; Abruña, H. D., Electron Transfer through Molecules and Assemblies at Electrode Surfaces. *Chem. Rev.* **2008,** 108, (7), 2721-2736.
11. Shpaisman, H.; Seitz, O.; Yaffe, O.; Roodenko, K.; Scheres, L.; Zuilhof, H.; Chabal, Y. J.; Sueyoshi, T.; Kera, S.; Ueno, N.; Vilan, A.; Cahen, D., Structure Matters: Correlating Temperature Dependent Electrical Transport Through Alkyl Monolayers with Vibrational and Photoelectron Spectroscopies. *Chemical Science* **2012,** 3, (3), 851-862.
12. Finklea, H. O.; Avery, S.; Lynch, M.; Furtsch, T., Blocking Oriented Monolayers of Alkyl Mercaptans on Gold Electrodes. *Langmuir* **1987,** 3, (3), 409-413.
13. Everett, W. R.; Welch, T. L.; Reed, L.; Fritsch-Faules, I., Potential-Dependent Stability of Self-Assembled Organothiols on Gold Electrodes in Methylene Chloride. *Anal. Chem.* **1995,** 67, (2), 292-298.
14. McCulloch, I.; Heeney, M.; Bailey, C.; Genevicius, K.; MacDonald, I.; Shkunov, M.; Sparrowe, D.; Tierney, S.; Wagner, R.; Zhang, W.; Chabinyc, M. L.; Kline, R. J.; McGehee, M. D.; Toney, M. F., Liquid-Crystalline Semiconducting Polymers with High Charge-Carrier Mobility. *Nature Materials* **2006,** 5, (4), 328-333.
15. Cahen, D.; Yaffe, O.; Scheres, L.; Segev, L.; Biller, A.; Ron, I.; Salomon, E.; Giesbers, M.; Kahn, A.; Kronik, L.; Zuilhof, H.; Vilan, A., Hg/Molecular Monolayer-Si Junctions: Electrical Interplay between Monolayer Properties and Semiconductor Doping Density. *Journal of Physical Chemistry C* **2010,** 114, (22), 10270-10279.
16. Yaffe, O.; Qi, Y.; Scheres, L.; Puniredd, S. R.; Segev, L.; Ely, T.; Haick, H.; Zuilhof, H.; Vilan, A.; Kronik, L.; Kahn, A.; Cahen, D., Charge Transport Across Metal/Molecular (Alkyl) Monolayer-Si Junctions is Dominated by the LUMO Level. *Physical Review B - Condensed Matter and Materials Physics* **2012,** 85, (4), 045433.
17. Yaffe, O.; Scheres, L.; Puniredd, S. R.; Stein, N.; Biller, A.; Lavan, R. H.; Shpaisman, H.; Zuilhof, H.; Haick, H.; Cahen, D.; Vilan, A., Molecular Electronics at Metal/Semiconductor Junctions. Si Inversion by Sub-Nanometer Molecular Films. *Nano Lett.* **2009,** 9, (6), 2390-2394.
18. Gozlan, N.; Tisch, U.; Haick, H., Tailoring the Work Function of Gold Surface by Controlling Coverage and Disorder of Polar Molecular Monolayers. *Journal of Physical Chemistry C* **2008,** 112, (33), 12988-12992.

19. Toledano, T.; Biller, A.; Bendikov, T.; Cohen, H.; Vilan, A.; Cahen, D., Controlling Space Charge of Oxide-Free Si by in Situ Modification of Dipolar Alkyl Monolayers. *The Journal of Physical Chemistry C* **2012,** 116, (21), 11434-11443.
20. Vilan, A.; Shanzer, A.; Cahen, D., Molecular Control Over Au/GaAs Diodes. *Nature* **2000,** 404, (6774), 166-168.
21. Hotchkiss, P. J.; Jones, S. C.; Paniagua, S. A.; Sharma, A.; Kippelen, B.; Armstrong, N. R.; Marder, S. R., The Modification of Indium Tin Oxide with Phosphonic Acids: Mechanism of Binding, Tuning of Surface Properties, and Potential for Use in Organic Electronic Applications. *Acc. Chem. Res.* **2012,** 45, (3), 337-346.
22. Ashkenasy, G.; Cahen, D.; Cohen, R.; Shanzer, A.; Vilan, A., Molecular Engineering of Semiconductor Surfaces and Devices. *Acc. Chem. Res.* **2002,** 35, (2), 121-128.
23. Cahen, D.; Hodes, G., Molecules and Electronic Materials. *Adv. Mater.* **2002,** 14, (11), 789-798.
24. Salomon, A.; Cahen, D.; Lindsay, S.; Tomfohr, J.; Engelkes, V. B.; Frisbie, C. D., Comparison of Electronic Transport Measurements on Organic Molecules. *Adv. Mater.* **2003,** 15, (22), 1881-1890.
25. Maboudian, R.; Ashurst, W. R.; Carraro, C., Tribological Challenges in Micromechanical Systems. *Tribology Letters* **2002,** 12, (2), 95-100.
26. Salomon, A.; Boecking, T.; Seitz, O.; Markus, T.; Amy, F.; Chan, C.; Zhao, W.; Cahen, D.; Kahn, A., What is the Barrier for Tunneling through Alkyl Monolayers? Results from n- and p-Si-Alkyl/Hg Junctions. *Adv. Mater.* **2007,** 19, (3), 445-450.
27. Seitz, O.; Bocking, T.; Salomon, A.; Gooding, J. J.; Cahen, D., Importance of Monolayer Quality for Interpreting Current Transport through Organic Molecules: Alkyls on Oxide-Free Si. *Langmuir* **2006,** 22, (16), 6915-6922.
28. Sano, H.; Maeda, H.; Ichii, T.; Murase, K.; Noda, K.; Matsushige, K.; Sugimura, H., Alkyl and Alkoxyl Monolayers Directly Attached to Silicon: Chemical Durability in Aqueous Solutions. *Langmuir* **2009,** 25, (10), 5516-5525.
29. Li, Y.; Calder, S.; Yaffe, O.; Cahen, D.; Haick, H.; Kronik, L.; Zuilhof, H., Hybrids of Organic Molecules and Flat, Oxide-Free Silicon: High-Density Monolayers, Electronic Properties, and Functionalization. *Langmuir* **2012,** 28, (26), 9920-9929.
30. Rijksen, B.; Caipa Campos, M. A.; Paulusse, J. M. J.; Zuilhof, H., Silicon Radical Surface Chemistry. In *Encyclopedia of Radicals in Chemistry, Biology and Materials*, John Wiley & Sons, Ltd: 2012; p 2081.
31. Ciampi, S.; Harper, J. B.; Gooding, J. J., Wet Chemical Routes to the Assembly of Organic Monolayers on Silicon Surfaces via the Formation of Si-C bonds: Surface Preparation, Passivation and Functionalization. *Chem. Soc. Rev.* **2010,** 39, (6), 2158-2183.
32. Faber, E. J.; de Smet, L. C. P. M.; Olthuis, W.; Zuilhof, H.; Sudhölter, E. J. R.; Bergveld, P.; van den Berg, A., Si-C Linked Organic Monolayers on Crystalline Silicon Surfaces as Alternative Gate Insulators. *ChemPhysChem* **2005,** 6, (10), 2153-2166.
33. Yaffe, O.; Scheres, L.; Segev, L.; Biller, A.; Ron, I.; Salomon, E.; Giesbers, M.; Kahn, A.; Kronik, L.; Zuilhof, H.; Vilan, A.; Cahen, D., Hg/Molecular Monolayer−Si Junctions: Electrical Interplay between Monolayer Properties and Semiconductor Doping Density. *The Journal of Physical Chemistry C* **2010,** 114, (22), 10270-10279.
34. Scheres, L.; Giesbers, M.; Zuilhof, H., Self-Assembly of Organic Monolayers onto Hydrogen-Terminated Silicon: 1-Alkynes are Better than 1-Alkenes. *Langmuir* **2010,** 26, (13), 10924-10929.
35. Schlenoff, J. B.; Li, M.; Ly, H., Stability and Self-Exchange in Alkanethiol Monolayers. *J. Am. Chem. Soc.* **1995,** 117, (50), 12528-12536.
36. Puniredd, S. R.; Assad, O.; Haick, H., Highly Stable Organic Modification of Si(111) Surfaces: Towards Reacting Si with Further Functionalities while Preserving the Desirable Chemical Properties of Full Si−C Atop Site Terminations. *J. Am. Chem. Soc.* **2008,** 130, (29), 9184-9185.

37. Scheres, L.; Giesbers, M.; Zuilhof, H., Organic Monolayers onto Oxide-Free Silicon with Improved Surface Coverage: Alkynes versus Alkenes. *Langmuir* **2010,** 26, (7), 4790-4795.
38. Scheres, L.; Rijksen, B.; Giesbers, M.; Zuilhof, H., Molecular Modeling of Alkyl and Alkenyl Monolayers on Hydrogen-Terminated Si(111). *Langmuir* **2011,** 27, (3), 972-980.
39. Ng, A.; Ciampi, S.; James, M.; Harper, J. B.; Gooding, J. J., Comparing the Reactivity of Alkynes and Alkenes on Silicon (100) Surfaces. *Langmuir* **2009,** 25, (24), 13934-13941.
40. Rijksen, B.; Pujari, S. P.; Scheres, L.; van Rijn, C. J. M.; Baio, J. E.; Weidner, T.; Zuilhof, H., Hexadecadienyl Monolayers on Hydrogen-Terminated Si(111): Faster Monolayer Formation and Improved Surface Coverage Using the Enyne Moiety. *Langmuir* **2012,** 28, (16), 6577-6588.
41. Robinson, G. N.; Freedman, A.; Graham, R. L., Reactions Of Fluorine-Atoms With Self-Assembled Monolayers Of Alkanethiolates. *Langmuir* **1995,** 11, (7), 2600-2608.
42. Cohen, Y. S.; Vilan, A.; Ron, I.; Cahen, D., Hydrolysis Improves Packing Density of Bromine-Terminated Alkyl-Chain, Silicon−Carbon Monolayers Linked to Silicon. *The Journal of Physical Chemistry C* **2009,** 113, (15), 6174-6181.
43. Barriet, D.; Lee, T. R., Fluorinated Self-Assembled Monolayers: Composition, Structure and Interfacial Properties. *Current Opinion in Colloid & Interface Science* **2003,** 8, (3), 236-242.
44. Drummond, C. J.; Georgaklis, G.; Chan, D. Y. C., Fluorocarbons: Surface Free Energies and Van der Waals Interaction. *Langmuir* **1996,** 12, (11), 2617-2621.
45. Chaudhury, M. K., Interfacial Interaction between Low-Energy Surfaces. *Materials Science & Engineering R-Reports* **1996,** 16, (3), 97-159.
46. Sheparovych, R.; Motornov, M.; Minko, S., Low Adhesive Surfaces that Adapt to Changing Environments. *Adv. Mater.* **2009,** 21, (18), 1840-1844.
47. Pujari, S. P.; Spruijt, E.; Stuart, M. A. C.; Rijn, C. J. M. v.; Paulusse, J. M. J.; Zuilhof, H., Ultra-low Adhesion and Friction of Fluoro-Hydro Alkyne Derived Self-Assembled Monolayers on Si(111). **in preparation**
48. Campbell, I. H.; Rubin, S.; Zawodzinski, T. A.; Kress, J. D.; Martin, R. L.; Smith, D. L.; Barashkov, N. N.; Ferraris, J. P., Controlling Schottky Energy Barriers in Organic Electronic Devices Using Self-Assembled Monolayers. *Physical Review B* **1996,** 54, (20), R14321-R14324.
49. Bruner, E. L.; Koch, N.; Span, A. R.; Bernasek, S. L.; Kahn, A.; Schwartz, J., Controlling the Work Function of Indium Tin Oxide: Differentiating Dipolar from Local Surface Effects. *J. Am. Chem. Soc.* **2002,** 124, (13), 3192-3193.
50. Alloway, D. M.; Graham, A. L.; Yang, X.; Mudalige, A.; Colorado, R.; Wysocki, V. H.; Pemberton, J. E.; Randall Lee, T.; Wysocki, R. J.; Armstrong, N. R., Tuning the Effective Work Function of Gold and Silver Using ω-Functionalized Alkanethiols: Varying Surface Composition through Dilution and Choice of Terminal Groups. *The Journal of Physical Chemistry C* **2009,** 113, (47), 20328-20334.
51. Wallart, X.; de Villeneuve, C. H.; Allongue, P., Truly Quantitative XPS Characterization of Organic Monolayers on Silicon: Study of Alkyl and Alkoxy Monolayers on H-Si(111). *J. Am. Chem. Soc.* **2005,** 127, (21), 7871-7878.
52. Scheres, L.; Arafat, A.; Zuilhof, H., Self-Assembly of High-Quality Covalently Bound Organic Monolayers onto Silicon. *Langmuir* **2007,** 23, (16), 8343-8346.
53. Graupe, M.; Takenaga, M.; Koini, T.; Colorado, R.; Lee, T. R., Oriented Surface Dipoles Strongly Influence Interfacial Wettabilities. *J. Am. Chem. Soc.* **1999,** 121, (13), 3222-3223.
54. Manova, R. K.; Pujari, S. P.; Weijers, C. A. G. M.; Zuilhof, H.; van Beek, T. A., Copper-Free Click Biofunctionalization of Silicon Nitride Surfaces via Strain-Promoted Alkyne–Azide Cycloaddition Reactions. *Langmuir* **2012,** 28, (23), 8651-8663.
55. Westphal, C., The Study of the Local Atomic Structure by Means of X-ray Photoelectron Diffraction. *Surf. Sci. Rep.* **2003,** 50, (1–3), 1-106.
56. Bonzel, H. P., Studies of adsorbed molecules by X-ray photoelectron diffraction (XPD). *Prog. Surf. Sci.* **1993,** 42, (1–4), 219-229.

57. Laibinis, P. E.; Bain, C. D.; Whitesides, G. M., Attenuation of Photoelectrons in Monolayers of n-Alkanethiols Adsorbed on Copper, Silver, and Gold. *The Journal of Physical Chemistry* **1991,** 95, (18), 7017-7021.
58. Linford, M. R.; Fenter, P.; Eisenberger, P. M.; Chidsey, C. E. D., Alkyl Monolayers On Silicon Prepared From 1-Alkenes And Hydrogen-Terminated Silicon. *J. Am. Chem. Soc.* **1995,** 117, (11), 3145-3155.
59. Porter, M. D.; Bright, T. B.; Allara, D. L.; Chidsey, C. E. D., Spontaneously Organized Molecular Assemblies. 4. Structural Characterization of n-Alkyl Thiol Monolayers on Gold by Optical Ellipsometry, Infrared Spectroscopy, and Electrochemistry. *J. Am. Chem. Soc.* **1987,** 109, (12), 3559-3568.
60. Aswal, D. K.; Lenfant, S.; Guerin, D.; Yakhmi, J. V.; Vuillaume, D., Self Assembled Monolayers on Silicon for Molecular Electronics. *Anal. Chim. Acta* **2006,** 568, (1-2), 84-108.
61. Stöhr, J.; Outka, D. A., Determination of Molecular Orientations on Surfaces from the Angular Dependence of Near-Edge X-ray-Absorption Fine-Structure Spectra. *Physical Review B* **1987,** 36, (15), 7891-7905.
62. Lee, M. V.; Lee, J. R. I.; Brehmer, D. E.; Linford, M. R.; Willey, T. M., Unanticipated C═C Bonds in Covalent Monolayers on Silicon Revealed by NEXAFS. *Langmuir* **2009,** 26, (3), 1512-1515.
63. Gamble, L. J.; Ravel, B.; Fischer, D. A.; Castner, D. G., Surface Structure and Orientation of PTFE Films Determined by Experimental and FEFF8-Calculated NEXAFS Spectra. *Langmuir* **2002,** 18, (6), 2183-2189.
64. Har-Lavan, R.; Yaffe, O.; Joshi, P.; Kazaz, R.; Cohen, H.; Cahen, D., Ambient organic molecular passivation of Si yields near-ideal, Schottky-Mott limited, junctions. *AIP Advances* **2012,** 2, (1), 012164-13.
65. Sze, S. M.; Ng, K. K., *Physics of Semiconductor Devices*. 3 ed.; John Wiley & Sons: 2006.
66. Wu, K.-Y.; Tao, Y.-T.; Huang, H.-W., Tuning hole injection and charge recombination with self-assembled monolayer on silver anode in top-emitting organic light-emitting diodes. *Appl. Phys. Lett.* **2007,** 90, (24), 241104.
67. *$f_{b,n}$ was extracted by using the thermionic emmssion transport model on the reverse (negative) bias current density*.
68. Pei, Y.; Ma, J.; Jiang, Y., Formation Mechanisms and Packing Structures of Alkoxyl and Alkyl Monolayers on Si(111): Theoretical Studies with Quantum Chemistry and Molecular Simulation Models. *Langmuir* **2003,** 19, (18), 7652-7661.
69. Cicero, R. L.; Chidsey, C. E. D.; Lopinski, G. P.; Wayner, D. D. M.; Wolkow, R. A., Olefin Additions on H−Si(111): Evidence for a Surface Chain Reaction Initiated at Isolated Dangling Bonds. *Langmuir* **2001,** 18, (2), 305-307.
70. Eves, B. J.; Sun, Q.-Y.; Lopinski, G. P.; Zuilhof, H., Photochemical Attachment of Organic Monolayers onto H-Terminated Si(111): Radical Chain Propagation Observed via STM Studies. *J. Am. Chem. Soc.* **2004,** 126, (44), 14318-14319.

Supporting Information to Chapter 3

Table of Contents

Supporting Information to Chapter 3 80
S.3.1 EXPERIMENTAL SECTION 81
S.3.1.1 Materials 81
S.3.1.2 Analysis 81
S.3.2 Synthesis of 10-fluorodec-1-yne 82
S.3.2.1 Dec-9-yn-1-ol (1a) 82
S.3.2.2 Dec-9-ynyl 4-methylbenzenesulfonate (1b) 83
S.3.2.3 10-Fluorodec-1-yne (1c) 83
S.3.3 Synthesis of 12-fluorododec-1-yne 84
S.3.3.1 Dodec-11-yn-1-ol (2a) 84
S.3.3.2 Dodec-11-ynyl 4-methylbenzenesulfonate (2b) 85
S.3.3.3 12-Fluorotetradec-1-yne (2c) 85
S.3.4 Synthesis of 14-fluorotetradec-1-yne 86
S.3.4.1 2-Tetradec-2-ynoxytetrahydropyran (3a) 86
S.3.4.2 Tetradec-2-yn-1-ol (3b) 87
S.3.4.3 Tetradec-13-yn-1-ol (3c) 87
S.3.4.4 Tetradec-13-ynyl 4-methylbenzenesulfonate (3d) 88
S.3.4.5 14-Fluorotetradec-1-yne (3e) 88
S.3.5 Synthesis of 16-fluorohexadec-1-yne 89
S.3.5.1 Hexadec-15-yn-1-ol (4a) 89
S.3.5.2 Hexadec-15-ynyl 4-methylbenzenesulfonate (4b) 89
S.3.5.3 16-Fluorohexadec-1-yne (4c) 90
S.3.6 Synthesis of 18-fluorooctadec-1-yne 90
S.3.6.1 Octadec-2-yn-1-ol (5a) 91
S.3.6.2 Octadec-17-yn-1-ol (5b) 91
S.3.6.3 Octadec-17-ynyl-4-methylbenzenesulfonate (5c) 91
S.3.6.4 18-Fluorooctadec-1-yne (5d) 92
S.3.7 Torsional angle measured of C-C-C-F 92

S.3.1 EXPERIMENTAL SECTION

S.3.1.1 Materials

Tetrahydro-2-(2-propynyloxy)-2H-pyran (THP, Aldrich, 98%), n-butyllithium (BuLi, 1.6 M in hexane, Aldrich), *p*-toluenesulfonic acid monohydrate (PTSA, Aldrich, 98%), potassium fluoride (KF, Sigma, +99.5%), 18-crown-6 (Fluka, +99.0%), 2-decyn-1-ol (Aldrich, 97%), 1-bromoundecane (Aldrich, 98%), 1-bromopentadecane (Aldrich, 97%), potassium tert-butoxide (*t*-BuOK, Aldrich) pyridine (Acros Organics, reagent ACS), Acetonitrile (Acros Organics, +99.5%), methanol (MeOH, VWR, +99.8%), 1,3-diaminopropane (Aldrich, +99%), 9-dodecyn-1-ol (ABCR, 97%), silica gel 60 (Fluka) and p-toluenesulfonyl chloride (TsCl, Molekula) were used as received. Tetrahydrofuran (THF, VWR, 99%) was distilled from sodium benzophenone and stored on sodium wires. Hexamethylphosphoramide (HMPA, Aldrich, 99%) was dried over Linde type molecular sieves of 4Å. Dichloromethane (DCM, Fisher Chemical, +99%) was distilled before use.

S.3.1.2 Analysis

All reactions were monitored by thin layer chromatography (TLC) and carried out on 0.25 mm silica gel PET foil plates with a medium pore size of 60 Å and a fluorescent indicator of 254 nm. Vanillin coloring reagent and heat were used as developing agents. The synthesized compounds were purified by automatic column chromatography with the Biotage Isolera One UV-VIS Flash Purification System using Biotage SNAP Cartridges (KP-Sil 50 g or 100 g).

^{1}H-NMR (400 MHz) and ^{13}C-NMR (100 MHz) spectra were recorded on a Bruker 400 MHz spectrometer with $CDCl_3$ as solvent and internal standard (^{1}H-NMR: 7.26 ppm and ^{13}C-NMR: 77.16 ppm). In the reported data below the following abbreviations are used: s = singlet, d = doublet, t = triplet, q = quartet, quin = quintet, m = multiplet. Chemical shifts are reported in ppm. High resolution mass spectra were recorded using Electron Spray Ionization (ESI) or Direct Analysis in Real Time (DART) ionization coupled to a high resolution mass spectrometer from Thermo Scientific. Samples were measured in acetone.

Attenuated total reflectance (ATR) infrared spectra of pure compounds were recorded on a Alpha-P spectrometer from Bruker. The wavenumbers are reported in reciprocal centimeters and the appearances are denoted as weak (w), medium (m) or strong (s).

The purities of the synthesized compounds were checked with GC-MS using an Agilent HP-5MS column (30 m × 0.250 mm × 0.25 μm). If necessary, the final products were

subsequently purified by preparative HPLC using an Altima C_{18} column (250 × 22 mm) to afford 100% pure compounds.

S.3.2 Synthesis of 10-fluorodec-1-yne

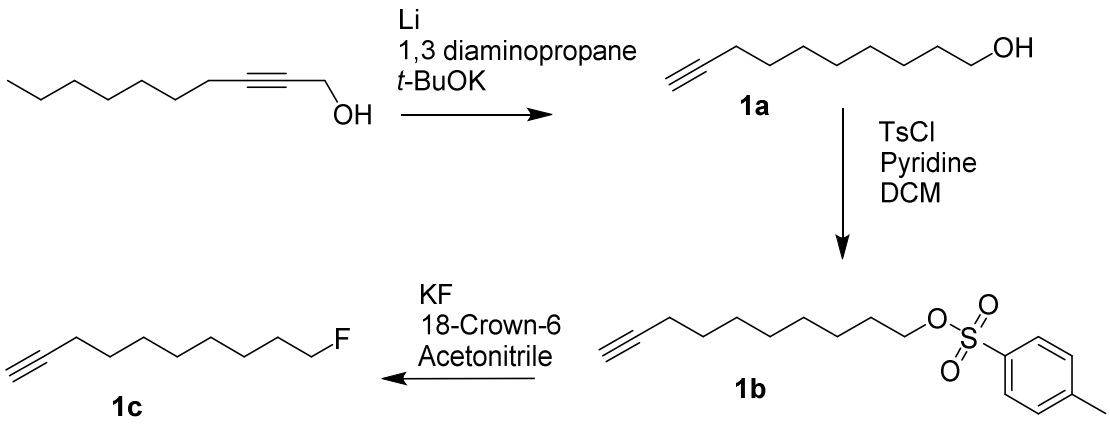

S.3.2.1 Dec-9-yn-1-ol (1a)

To a three-necked round-bottom flask, which was flushed with nitrogen and closed with a calcium chloride tube, small pieces of Li (2.73 g, 389.28 mmol) and 186 ml of 1,3-diaminopropane were added. The mixture was allowed to stir and heated in an oil bath at 70 ˚C until the blue color discharges (1 h) and a white suspension was formed. After cooling down to room temperature, potassium tert-butoxide (29.12 g, 259.52 mmol) was added to the mixture. The mixture was stirred for 20 min and then dec-2-yn-1-ol (10 g, 64.88 mmol) was added. Residual dec-2-yn-1-ol was washed into the mixture with a small portion of 1,3-diaminipropane (15 ml). The reaction mixture was stirred overnight at room temperature. Plenty of ice water was added to the reaction mixture and the mixture was extracted with ether three times. The organic layers were combined, washed with brine and water and dried over anhydrous $MgSO_4$. The solvent was removed under reduced pressure. The residue was purified by automatic column chromatography (heptane : ethyl acetate = 5:1) to afford dec-9-yn-1-ol (7.44 g, 48.23 mmol, 74%) as a clear oil. The reaction was monitored with TLC (heptane : ethyl acetate = 5:1).

^{1}H-NMR (δ_{ppm}): 3.60-3.57 (t, 2H, R-C*H*$_2$-OH), 2.17-2.12 (dt, 2H, R-C*H*$_2$-C≡C-H), 1.95 (s, 1H, R-O*H*), 1.92-1.90 (t, 1H, R-C≡C-*H*), 1.56-1.46 (m, 4H, alkyl), 1.39-1.30 (m, 8H, alkyl). ^{13}C-NMR (δ_{ppm}): 84.77 (1C, R-*C*≡C-H), 68.19 (1C, R-C≡*C*-H), 62.90 (1C, R-*C*H$_2$-OH), 32.77 (1C, alkyl), 29.23 (1C, alkyl), 29.20 (1C, alkyl), 28.72 (1C, alkyl), 28.50 (1C, akyl), 25.76 (1C, alkyl), 18.42 (1C, alkyl). IR (cm^{-1}): 3346 (m, OH), 3307, 624 (m, s,

C≡*C*-*H*), 2928, 2855, 1463 (s, s, m, CH_2), 2117 (w, C≡C). MS (DART): calculated for $C_{10}H_{22}ON$ (M + NH_4) 172.1696, found 172.1695.

S.3.2.2 Dec-9-ynyl 4-methylbenzenesulfonate (1b)

To a 250 ml three-necked round-bottom flask, flushed with nitrogen, was added dec-9-yn-1-ol (7.34 g, 47.62 mmol) at 0 ˚C, to dichloromethane (58 ml) and pyridine (7.6 ml). The mixture was stirred at 25 ˚C for 10 min. The flask was cooled down to 0 ˚C with an ice bath and p-toluenesulfonyl chloride (13.57 g, 71.43 mmol) was added to the reaction mixture. The mixture was stirred at 0 ˚C for 1 hour and then overnight at room temperature. The reaction was quenched with 35 ml of water at 0 ˚C and then warmed to 23 ˚C. The resulting layers were separated and the aqueous layer was washed with DCM. The combined organic layers were washed with brine and water and dried over $MgSO_4$. The solvent was removed by rotary evaporation. The crude extract was purified with automatic column chromatography (heptane : ethyl acetate = 13:1). The solvents were removed under reduced pressure to afford a white solid of dec-9-ynyl 4-methylbenzenesulfonate (10.25 g, 33.23 mmol, 70%). The reaction was monitored with TLC (heptane : ethyl acetate = 9:1).

^{1}H-NMR (δ_{ppm}): 7.80-7.78 (d, 2H, Ph), 7.36-7.34 (d, 2H, Ph), 4.04-4.00 (t, 2H, R-C*H*$_2$-OTs), 2.45 (s, 3H, R-Ph-C*H*$_3$), 2.19-2.14 (m, 2H, R-C*H*$_2$-C≡C-H), 1.94-1.93 (t, 1H, R-C≡C-*H*), 1.67-1.60 (m, 2H, alkyl), 1.53-1.46 (m, 2H, alkyl), 1.39-1.27 (m, 8H, alkyl). ^{13}C-NMR (δ_{ppm}): 144.58 (1C, Ph), 133.28 (1C, Ph), 129.76 (2C, Ph), 127.84 (2C, Ph), 84.57 (1C, R-*C*≡C-H), 70.58 (1C, R-*C*H$_2$-OTs), 68.12 (1C, R-C≡*C*-H), 28.77, 28.75, 28.71, 28.48, 28.32 (5C, alkyl), 25.23 (1C, alkyl), 21.58 (1C, R-*C*H$_3$), 18.31 (1C, alkyl). IR (cm^{-1}): 3290, 662 (m, s, C≡*C*-*H*), 2930, 2857, 1464 (m, m, m, CH_2), 2116 (w, C≡C),1174, 1356 (s, s, S=O). MS (DART): calculated for $C_{17}H_{28}O_3NS$ (M + NH_4) 326.1784, found 326.1785.

S.3.2.3 10-Fluorodec-1-yne (1c)

In a three-necked round-bottom flask, equipped with a condenser and a dropping funnel, potassium fluoride (3.86 g, 66.48 mmol) and 18-crown-6 (17.56 g, 66.48 mmol) were dissolved in 60 ml of acetonitrile. Nitrogen was flushed through the mixture. The solution was heated to 60 ˚C with an oil bath. A solution of dec-9-ynyl 4-methylbenzenesulfonate (10.11 g, 33.24 mmol) in 65 ml of acetonitrile was drop wise added. The solution was refluxed for 24 h and after that, additional equivalents of potassium fluoride (1.93 g, 33.24 mmol) and 18-crown-6 (8.78 g, 33.24 mmol) were added. The reaction mixture was refluxed for another 24 h. The solvent was removed by

rotary evaporation. The residue was dissolved in ether and washed with water. The organic layers was dried with $MgSO_4$ and the solvent was removed under reduced pressure. The residue was purified by automatic column chromatography (heptane) to afford 10-fluorodec-1-yne (3.80 g, 24.33 mmol, 73%) as a clear oil. The reaction was monitored with TLC (heptane).

^{1}H-NMR (δ_{ppm}) 4.43-4.40 (t, 1H, F-C*H*$_2$-R), 4.32-4.28 (t, 1H, F-C*H*$_2$-R), 2.13-2.09 (dt, 2H, R-C*H*$_2$-C≡C-H), 1.87-1.85 (t, 1H, R-C≡C-*H*), 1.70-1.55 (m, 2H, alkyl), 1.49-1.42 (m, 2H, alkyl), 1.35-1.27 (m, 8H, alkyl). ^{13}C-NMR (δ_{ppm}): 85.10, 83.47 (1C, F-*C*H$_2$-R), 84.79 (1C, R-*C*≡C-H), 68.23 (1C, R-C≡*C*-H), 30.62-30.43 (1C, R-*C*H$_2$-CH$_2$-F), 29.23 (1C, alkyl), 29.10 (1C, alkyl), 28.75 (1C, alkyl), 28.75 (1C, alkyl), 25.28-25.24 (1C, R-*C*H$_2$-CH$_2$-CH$_2$-F), 18.51 (1C, alkyl). IR (cm^{-1}): 3304, 627 (m, s, C≡*C*-*H*), 2931, 2858, 1464 (s, s, m, CH$_2$), 2118 (w, C≡C). MS (DART): calculated for $C_{10}H_{21}NF$ (M + NH_4) 174.1653, found 174.1655.

S.3.3 Synthesis of 12-fluorododec-1-yne

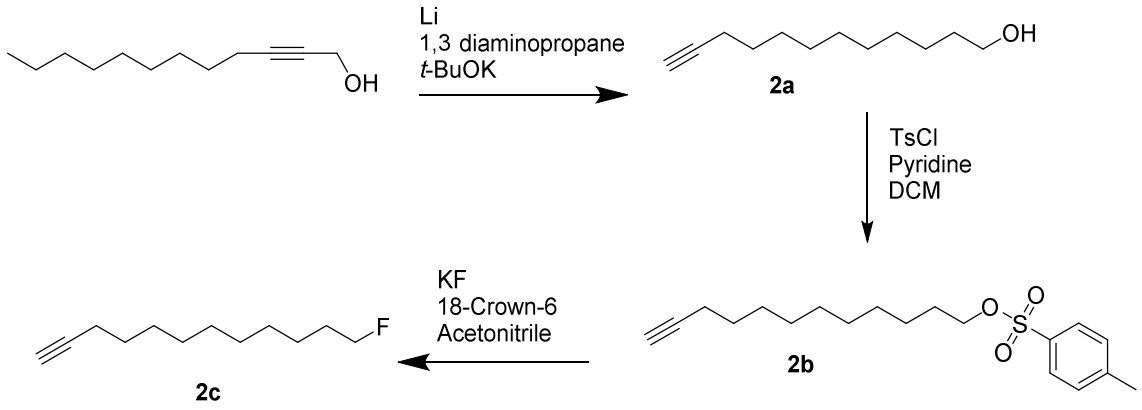

S.3.3.1 Dodec-11-yn-1-ol (2a)

The procedure described for dec-9-yn-1-ol **(1a)** was used with 9-dodecyn-1-ol (12.00 g, 65.83 mmol), lithium (2.74 g, 390.59 mmol), potassium *tert*-butoxide (29.5 g, 262.90 mmol) and 187 ml of 1,3-diaminopropane to afford dodec-11-yn-1-ol (10.44 g, 57.27 mmol, 87%).

^{1}H-NMR (δ_{ppm}): 3.61-3.57 (t, 2H, R-C*H*$_2$-OH), 2.17-2.12 (dt, 2H, R-C*H*$_2$-C≡C-H), 1.91-1.90 (t, 1H, R-C≡C-*H*), 1.77 (s, 1H, R-O*H*), 1.56-1.45 (m, 4H, alkyl), 1.38-1.26 (m, 12H, alkyl). ^{13}C-NMR (δ_{ppm}): 84.71 (1C, R-*C*≡C-H), 68.04 (1C, R-C≡*C*-H), 62.89 (1C, R-*C*H$_2$-OH), 32.72 (1C, alkyl), 29.49 (1C, alkyl), 29.36 (2C, alkyl), 29.03, 28.69, 28.44, 25.70, 18.34 (5C, alkyl). IR (cm^{-1}): 3310, 628 (m, s, C≡*C*-*H*), 2924, 2853, 1463 (s, s, m,

CH_2), 2118 (w, C≡C). MS (DART): calculated for $C_{12}H_{26}ON$ (M + NH_4) 200.2009, found 200.2010.

S.3.3.2 Dodec-11-ynyl 4-methylbenzenesulfonate (2b)

The procedure described for dec-9-ynyl 4-methylbenzenesulfonate **(1b)** was used with dodec-11-yn-1-ol (10.42 g, 57.16 mmol), pyridine (9.25 ml, 114.45 mmol), 69 ml of dichloromethane and p-toluenesulfonyl chloride (16.36 g, 86.11 mmol) to give dodec-11-ynyl 4-methylbenzenesulfonate (12.57 g, 37.36 mmol, 65%).

^{1}H-NMR (δ_{ppm}): 7.74-7.72 (d, 2H, Ph), 7.30-7.28 (d, 2H, Ph), 3.97-3.94 (t, 2H, R-C*H*$_2$-OTs), 2.39 (s, 3H, R-Ph-C*H*$_3$), 2.13-2.12 (dt, 2H, R-C*H*$_2$-C≡C-H), 1.92 (t, 1H, R-CH$_2$-C≡C-*H*), 1.60-1.53 (quin, 2H, alkyl), 1.48-1.41 (quin, 2H, alkyl), 1.37-1.23 (m, 12H, alkyne) ^{13}C-NMR (δ_{ppm}): 144.55 (1C, Ph), 133.27 (1C, Ph), 129.74 (2C, Ph), 127.82 (2C, Ph), 84.67 (1C, R-*C*≡C-H), 70.62 (1C, R-*C*H$_2$-OTs), 68.04 (s, 1C, R-C≡*C*-H), 29.24 (2C, alkyl), 28.95, 28.82, 28.76, 28.63, 28.40 (5C, alkyl), 25.26 (1C, alkyl), 21.57 (1C, alkyl), 18.33 (1C, alkyl). IR (cm^{-1}): 3292, 664 (m, s, C≡*C*-*H*), 2927, 2855, 1465 (s, s, m, CH_2), 2116 (w, C≡C), 1176, 1359 (s, s, S=O). MS (DART): calculated for $C_{19}H_{32}O_3NS$ (M + NH_4) 354.2097, found 354.2102.

S.3.3.3 12-Fluorotetradec-1-yne (2c)

The procedure described for 10-fluorodec-1-yne **(1c)** was used with dodec-11-ynyl 4-methylbenzenesulfonate (12.57 g, 37.36 mmol), potassium fluoride (4.33 g, 74.53 mmol and 2.17 g, 37.36 mmol), 18-crown-6 (19.7 g, 74.53 mmol and 9.85 g, 37.36 mmol) and 60 and 75 ml of acetonitrile to afford 12-fluorododec-1-yne (6.63 g, 35.98 mmol, 95%). The product was purified with subsequently automatic column chromatography and preparative HPLC to afford a colorless oil.

^{1}H-NMR (δ_{ppm}): 4.51-4.48 (t, 1H, F-C*H*$_2$-R), 4.39-4.36 (t, 1H, F-C*H*$_2$-R), 2.20-2.16 (dt, 2H, R-C*H*$_2$-C≡C-H), 1.94-1.93 (t, 1H, R-C≡C-*H*), 1.72-1.64 (m, 2H, alkyl), 1.54-1.51 (m, 2H, alkyl), 1.41-1.30 (m, 12H, alkyl). ^{13}C-NMR (δ_{ppm}): 85.00, 83.37 (1C, F-*C*H$_2$-R), 84.74 (1C, R-*C*≡C-H), 68.02 (1C, R-C≡*C*-H), 30.48-30.29 (1C, R-*C*H$_2$-CH$_2$-F), 29.41, 29.34, 29.18, 29.03, 28.70, 28.46 (6C, alkyl), 25.28-25.24 (1C, R-*C*H$_2$-CH$_2$-CH$_2$-F), 18.51 (1C, alkyl). IR (cm^{-1}): 3305, 627 (m, s, C≡*C*-*H*), 2927, 2855, 1464 (s, s, m, CH_2), 2117 (w, C≡C). MS (DART): calculated for $C_{12}H_{25}NF$ (M + NH_4) 202.1966, found 202.1969.

S.3.4 Synthesis of 14-fluorotetradec-1-yne

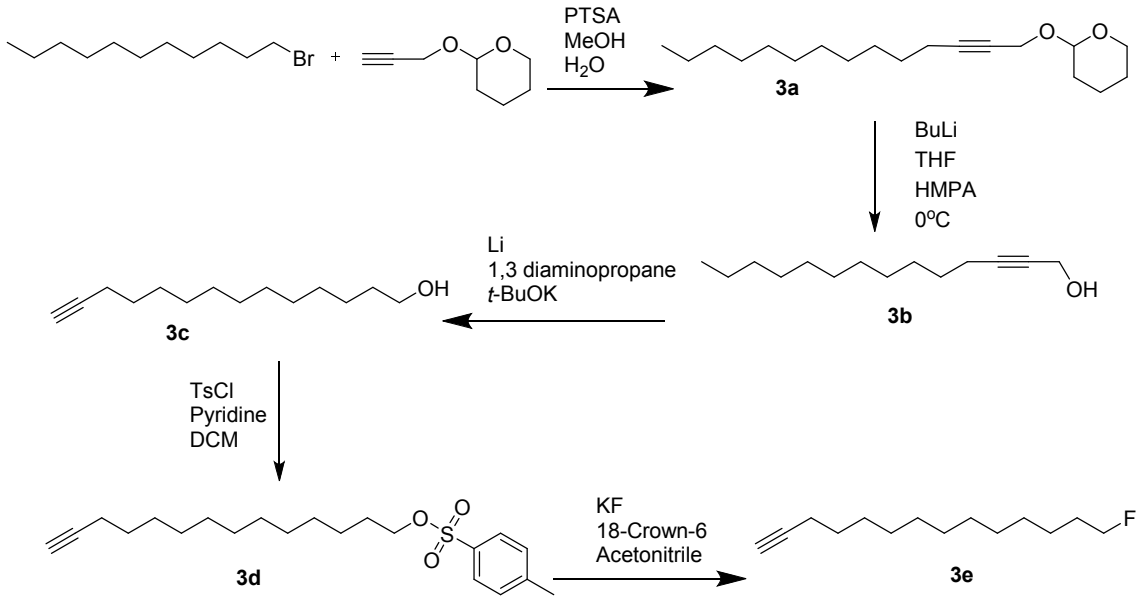

S.3.4.1 2-Tetradec-2-ynoxytetrahydropyran (3a)

In an oven-dried 500 ml three-necked round-bottom flask, a solution of tetrahydro-2-(2-propynyloxy)-2H-pyran (11.95 ml, 85.00 mmol) in 212 ml of dry THF was cooled to 0 ˚C in an ice bath. The mixture was flushed with nitrogen and the round-bottom flask was closed with a calcium chloride tube. The mixture was treated with *n*-butyllithium in hexane (16.02 ml of a 1.6 M solution) Thereafter, 1-bromoundecane (18.97 ml, 85.00 mmol) in 149 ml of dry HMPA was added at 0 ˚C. The reaction mixture was stirred overnight at room temperature. The reaction was quenched with 50 ml of saturated aqueous NH_4Cl solution and extracted with heptane. The combined organic layers were washed with demineralized water and dried over $MgSO_4$. The solvent was removed by rotary evaporation. Remaining starting material was removed using a with silica gel filled glass filter (heptane). After that, the residue was purified by automatic column chromatography (heptane: ethyl acetate = 9:1). The solvents were removed under reduced pressure to afford 2-tetradec-2-ynoxytetrahydropyran (8.26 g, 28.05 mmol, 33%) as a clear oil. The reaction was monitored with TLC (heptane : ethyl acetate = 9:1).

^{1}H-NMR (δ_{ppm}): 4.82-4.80 (t, 1H, R-O-C*H*-O-R), 4.30-4.18 (tq, 2H, R-C≡C-C*H*$_2$-O-R), 3.88-3.82, 3.55-3.50 (m, 2H, R-O-CR-O-C*H*$_2$-CH$_2$-R), 2.23-2.19 (tt, 2H, R-CH$_2$-C≡C-R), 1.897-1.47 (m, 6H, alkyl), 1.38-1.26 (m, 18H, akyl), 0.90-0.86 (t, 3H, R-CH$_3$). ^{13}C-NMR (δ_{ppm}): 96.81 (1C, R-O-C*H*-O-R), 86.94 (1C, R-C≡*C*-CH$_2$-O-R), 75.89 (1C, R-*C*≡C-CH$_2$-O-R), 62.16 (1C, R-C≡C-*C*H$_2$-O-R), 54.82 (1C, R-O-CR-O-*C*H$_2$-CH$_2$-R),

32.07, 30.49, 29.77, 29.68, 29.49, 29.29, 29.05, 28.79, 25.57, 22.84, 19,32, 18.99 (13C, alkyl and ring structure), 14.25 (1C, R-*C*H_3). IR (cm^{-1}): 2922, 2852, 1463 (s, s, m, CH_2), 2217 (w, C≡C), 1117 (s, C-O). MS (DART): calculated for $C_{19}H_{38}O_2N$ (M + NH_4) 312.2897, found 312.2902.

S.3.4.2 Tetradec-2-yn-1-ol (3b)

The reaction was carried out in a 250 ml three-necked round-bottom flask which was flushed with nitrogen gas and closed with a calcium chloride tube. *p*-Toluenesulfonic acid monohydrate (1.87 g, 9.85 mmol) was added to a solution of 2-tetradec-2-ynoxytetrahydropyran (5.80 g, 19.70 mmol) and 100 ml of methanol. The reaction mixture was stirred overnight at room temperature. The reaction was checked with TLC (heptane: ethyl acetate 8:2). If still starting material remains, another portion of PTSA can be added. The reaction was quenched with 10 ml of ice cold demineralized water. The methanol was removed by rotary evaporation. More water was added and the mixture was extracted with ether. The organic layers were washed with saturated NaCl solution and dried over anhydrous $MgSO_4$. The solvent was removed under reduced pressure and the remaining residue was purified by automatic column chromatography (heptane: ethyl acetate = 9:1) to give tetradec-2-yn-1-ol (3.05 g, 14.51 mmol, 74%) as a white wax-like solid. The reaction was monitored with TLC (heptane : ethyl acetate = 8:2).

^{1}H-NMR (δ_{ppm}): 4.27-4.25 (td, 2H, RC≡C-C*H*$_2$-OH), 2.24-2.19 (tt, 2H, R-C*H*$_2$-C≡CR), 1.55-1.49 (quin, 2H, R-C*H*$_2$-CH_2-C≡CR), 1.40-1.27 (m, 17H, alkyl/R-O*H*), 0.91-0.87 (t, 3H, R-C*H*$_3$). ^{13}C-NMR (δ_{ppm}): 86.88 (1C, R-C≡*C*-CH_2-OH), 78.42 (1C, R*C*≡C-CH_2-OH), 51.63 (1C, R-*C*H_2-OH), 32.07, 29.77, 29.67, 29.48, 29.30, 29.03, 28.77, 22.83, 18.89 (10C, alkyl), 14.26 (1C, R-C*H*$_3$). IR (cm^{-1}): 3294 (m, OH), 2955, 2871 (m, m, CH_3), 2915, 2849, 1470 (s, s, s, CH_2), 2119 (w, C≡C). MS (DART): calculated for $C_{14}H_{30}ON$ (M + NH_4) 228.2322, found 228.2324.

S.3.4.3 Tetradec-13-yn-1-ol (3c)

The procedure described for dec-9-yn-1-ol **(1a)** was used with tetradec-2-yn-1-ol (5.81 g, 27.64 mmol), lithium (1.16 g, 165.84 mmol), potassium *tert*-butoxide (12.40 g, 110.56 mmol) and 79 ml of 1,3-diaminopropane to afford tetradec-13-yn-1-ol (4.80 g, 22.84 mmol, 83%)

^{1}H-NMR (δ_{ppm}): 3.67-3.63 (t, 2H, R-C*H*$_2$-OH), 2.19-2.13 (dt, 2H, R-C*H*$_2$-C≡C-H), 1.95-1.94 (t, 1H, RC≡C-*H*), 1.61-1.45 (m, 4H, alkyl), 1.41-1.28 (m, 17H, alkyl). ^{13}C-NMR (δ_{ppm}): 84.79 (1C, R-*C*≡C-H), 67.99 (1C, RC≡*C*-H), 62.92 (1C, R-*C*H_2-OH), 32.80 (1C, alkyl), 29.56, 29.54, 29.52, 29.46, 29.40, 29.07, 28.73, 28.48 (8C, alkyl) 25.72 (1C,

alkyl), 1837 (1C, alkyl). IR (cm^{-1}): 3312 (m, OH), 3287, 628 (m, C≡*C*-*H*), 2923, 2853, 1462 (s, s, m, CH_2), 2118 (w, C≡C). MS (DART): calculated for $C_{14}H_{30}ON$ (M + NH_4) 228.2322, found 228.2321.

S.3.4.4 Tetradec-13-ynyl 4-methylbenzenesulfonate (3d)

The procedure described for dec-9-ynyl 4-methylbenzenesulfonate **(1b)** was used with tetradec-13-yn-1-ol (4.67 g, 22.22 mmol), pyridine (3.59 ml, 44.44 mmol), *p*-toluenesulfonylchloride (5.07 g, 26.69 mmol) and 27 ml of dichloromethane to give tetradec-13-ynyl 4-methylbenzenesulfonate (3.32 g, 9.12 mmol). The product was obtained with a good yield.

^{1}H NMR (δ_{ppm}): 7.80-7.78 (d, 2H, Ph), 7.35-7.33 (d, 2H, Ph), 4.03-4.00 (t, 2H, R-C*H*$_2$-OTs), 2.45 (s, 3H, R-Ph-C*H*$_3$), 2.2-2.16 (dt, 2H, R-C*H*$_2$-C≡C-H), 1.94-1.92 (t, 1H, RC≡C-*H*), 1.66-1.60 (quin, 2H, alkyl), 1.56-1.48 (quin, 2H, alkyl), 1.39-1.22 (m, 16H, alkyl). ^{13}C NMR (δ_{ppm}): 144.56 (1C, Ph), 133.32 (1C, Ph), 129.76 (2C, Ph), 127.85 (2C, Ph), 84.73 (1C, R-*C*≡C-H), 70.66 (1C, R-*C*H$_2$-OTs), 68.02 (1C, RC≡*C*-H), 29.48 (1C, alkyl), 29.42 (2C, alkyl), 29.33, 29.05, 28.89, 28.80, 28.71, 28.46, 25.30, 21.59, 18.37 (9C, alkyl). IR (cm^{-1}): 3293, 663 (m, s, C≡*C*-*H*), 2918, 2851, 1471 (s, s, m, CH_2), 2116 (w, C≡C), 1173, 1354 (s, s, S=O). MS (DART): calculated for $C_{21}H_{36}O_3NS$ (M + NH_4) 382.2410, found 382.2410.

S.3.4.5 14-Fluorotetradec-1-yne (3e)

The procedure described for 10-fluorodec-1-yne **(1c)** was used with tetradec-13-ynyl 4-methylbenzenesulfonate (3.20 g, 8.79 mmol), potassium fluoride (1.02g, 17.55 mmol and 0.51 g, 8.78 mmol), 18-crown-6 (4.64 g, 17.55 mmol and 2.32 g, 8.78 mmol) and 18 and 16 mol of acetonitrile to afford 14-fluorotetradec-1-yne (1.44 g, 6.78 mmol, 77%). The product was purified by preparative HPLC. A pure colorless oil was obtained.

^{1}H NMR (δ_{ppm}) 4.51-4.48 (t, 1H, F-C*H*$_2$-R), 4.39-4.36 (t, 1H, F-C*H*$_2$-CH$_2$), 2.21-2.16 (m, 2H, R-C*H*$_2$-C≡C-H), 1.94-1.93 (t, 1H, R-C≡C-*H*), 1.76-1.63 (m, 2H, alkyl), 1.57-1.49 (m, 2H, alkyl), 1.41-1.29 (m, 16H, alkyl). ^{13}C NMR (δ_{ppm}): 85.01, 83.38 (1C, F-*C*H$_2$-R), 84.76 (1C, R-*C*≡C-H), 68.00 (1C, R-C≡*C*-H), 30.50, 30.31 (1C, FCH$_2$-*C*H$_2$-R), 29.53, 29.48, 29.46, 29.22, 29.08, 28.74, 28.49 (8C, alkyl), 25.16, 25.11 (1C, FCH$_2$-CH$_2$-*C*H$_2$-R), 18.38 (1C, alkyl). IR (cm^{-1}): 3310, 626 (m, s, C≡*C*-*H*), 2924, 2854, 1465 (s, s, m, CH_2), 2119 (w, C≡C). MS (DART): calculated for $C_{14}H_{29}NF$ (M + NH_4) 230.2279, found 230.2280.

S.3.5 Synthesis of 16-fluorohexadec-1-yne

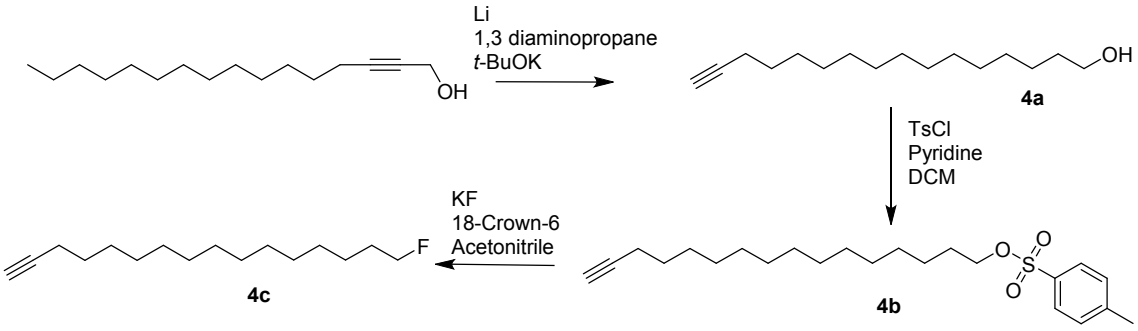

S.3.5.1 Hexadec-15-yn-1-ol (4a)

The procedure described for dec-9-yn-1-ol **(1a)** was used with hexadec-7-yn-1-ol (20 g, 83.9. mmol), Lithium (3.49 g, 503.3 mmol), 1,3 diaminopropane (240 mL) and potassium *tert*-butoxide (37.6 g, 335.54 mmol) to give hexadec-15-yn-1-ol as a colorless oil (13.95 g, 58.51 mmol, 73%)

^{1}H-NMR (δ_{ppm}) 3.62-3.59 (t, 2H, R-C*H*$_2$-OH), 2.17-2.13 (dt 2H, R-C*H*$_2$-C≡C-H), 1.91-1.90 (t, 1H, R-C≡C-*H*), 1.61 (s, 1H, R-O*H*), 1.56-1.46 (m, 4H, Alkyl), 1.38-1.24 (m, 20H, alkyl). ^{13}C-NMR (400 MHz, $CDCl_3$, δ_{ppm}): 85.08 (1C, R-*C*≡C-H), 68.34 (1C, C≡*C*-H), 63.29 (1C, R-*C*H$_2$-OH), 33.10 (1C, alkyl), 29.93, 29.92, 29.90 (5C, alkyl), 29.80 (1C, alkyl), 29.74 (1C, alkyl), 29.41 (1C, alkyl), 29.06 (1C, alkyl), 28.81 (1C, alkyl), 26.06 (1C, alkyl), 18.70 (1C, alkyl). IR (cm^{-1}): 3286, 628 (m, s, C≡*C*-*H*), 2917, 2849, 1472 (s, s, m, CH_2), 2114 (w, C≡C). MS (DART): calculated for $C_{16}H_{31}O$ (M + H) 239.2375, found 239.2367.

S.3.5.2 Hexadec-15-ynyl 4-methylbenzenesulfonate (4b)

The procedure described for dec-9-ynyl **(1b)** was used with hexadec-15-yn-1-ol (10.00 g, 42.0 mmol) and *p*-toluenesulfonyl chloride (9.60 g, 50.4 mmol) to give hexadec-15-ynyl 4-methylbenzenesulfonate as a white solid (13.35 g, 34.04 mmol, 81%):

^{1}H-NMR (δ_{ppm}): 7.79-7.77 (d, 2H, Ph), 7.34-7.32 (d, 2H, Ph), 4.03-3.99 (t, 2H, R-C*H*$_2$-OTs), 2.44 (s, 3H, R-Ph-C*H*$_3$), 2.19-2.15 (m 2H, R-C*H*$_2$-C≡C-H), 1.93-1.91 (t, 1H, R-C≡C-*H*), 1.65-1.58 (m, 2H, alkyl), 1.54-1.48 (m, 2H, alkyl), 1.41-1.21(m, 20H, alkyl). ^{13}C NMR (δ_{ppm}): 144.90 (1C, Ph), 133.67 (1C, Ph), 130.10 (1C, Ph), 128.19 (1C, Ph), 85.09 (1C, R-*C*≡C-H), 71.00 (1C, R-*C*H$_2$-OTs), 68.35 (1C, R-C≡*C*-H), 29.90, 29.89, 29.80, 29.79, 29.69, 29.42, 29.24, 29.15, 29.07, 28.82 (13C, alkyl), 25.64 (1C, alkyl), 21.92 (1C, alkyl), 18.71 (1C, alkyl). IR (cm^{-1}): 3288, 667 (m, s, C≡*C*-*H*), 2916, 2850,

1472 (s, s, m, CH_2), 2116 (w, C≡C), 1175, 1357 (s, s, S=O). MS (ESI): calculated for $C_{23}H_{36}O_3NaS$ (M + Na) 415.2283, found 415.2273.

S.3.5.3 16-Fluorohexadec-1-yne (4c)

The procedure described for 10-fluorodec-1-yne **(1c)** was used with potassium tert-butoxide (3.26 g, 56.09 mmol and 1.62 g, 28.04 mmol) and 18-crown-6 (14.8 g, 56.09 mmol and 7.4 g, 28.04 mmol) in 50 ml of acetonitrile and hexadec-15-ynyl 4-methylbenzenesulfonate (11.0 g, 28.04 mmol) in 55 mL of acetonitrile to give 16-fluorohexadec-1-yne (6.40 g, 26.64 mmol, 95%) as a clear oil.

^{1}H-NMR (δ_{ppm}) 4.49-4.46 (t, 1H, F-C*H*$_2$-R), 4.37-4.34 (t, 1H, F-C*H*$_2$-R), 2.19-2.15 (m, 2H, R-C*H*$_2$-C≡C-H), 1.92-1.91(t, 1H, R-C≡C-*H*), 1.74-1.61 (m, 2H, alkyl), 1.55-1.48 (m, 2H, alkyl), 1.40-1.26 (m, 20H, alkyl). ^{13}C-NMR (δ_{ppm}): 85.29, 83.66 (1C, F-*C*H$_2$-R), 85.05 (1C, R-*C*≡C-H), 68.35 (1C, R-C≡*C*-H), 30.86, 30.67 (1C, alkyl), 29.96, 29.93, 29.89, 29.85 (6C, alkyl), 29.59 (1C, alkyl), 29.45 (1C, alkyl), 29.10 (1C, alkyl), 28.85 (1C, alkyl), 25.52, 25.47 (1C, F-CH$_2$-*C*H$_2$-R), 18.73 (1C, alkyl). IR (cm^{-1}): 3311, 626 (m, s, C≡*C*-*H*), 2923, 2853, 1465 (s, s, m, CH_2), 2117 (w, C≡C). MS (ESI): calculated for $C_{16}H_{30}NF$ (M + H) 241.2332, found 241.2325.

S.3.6 Synthesis of 18-fluorooctadec-1-yne

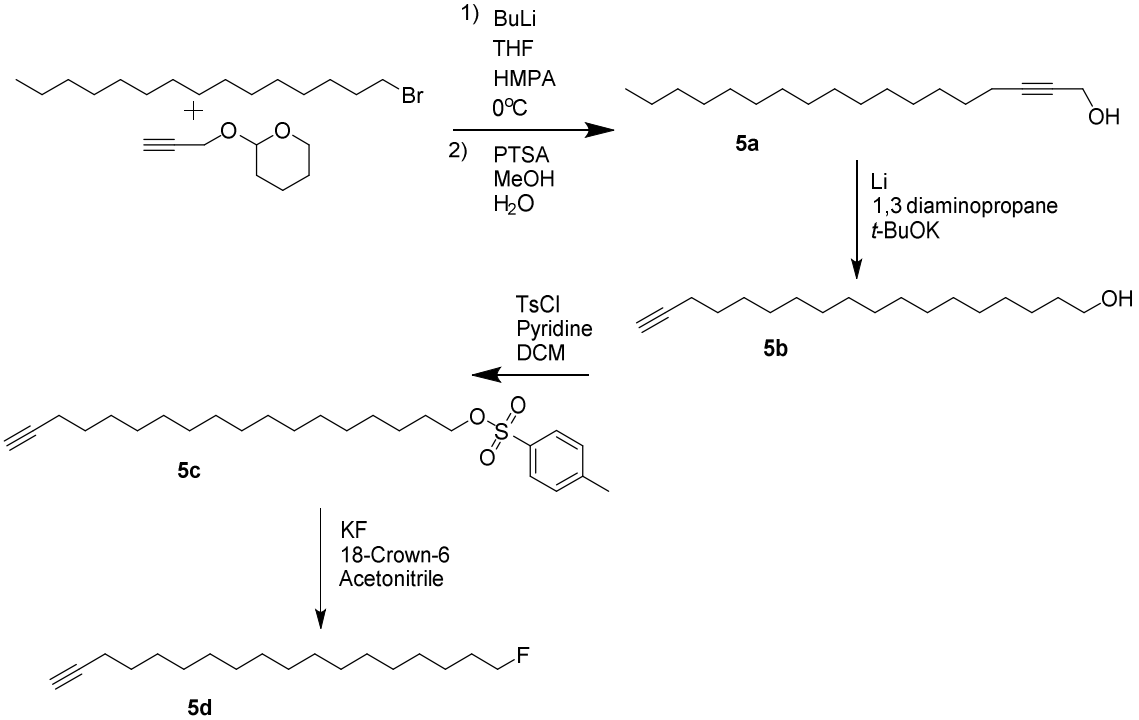

S.3.6.1 Octadec-2-yn-1-ol (5a)

The procedure described for 2-tetradec-2-ynoxytetrahydropyran **(3a)** was used with THP (11.91 g, 85.00 mmol) in 212 ml of dry THF, n-butyl lithium (10.89 g, 170.00 mmol) and 1-bromopentadecane (24.26 g, 85.00 mmol) in 149 ml of HMPA. The product was directly used in the next step without purification. The procedure described for tetradec-2-yn-1-ol **(3b)** was used with *p*-toluenesulfonic acid monohydrate (8.08 g, 42.50 mmol).

^{1}H-NMR (δ_{ppm}): 4.26-4.25 (t, 2H, RC≡C-C*H*$_2$-OH), 2.23-2.19 (m, 2H, R-C*H*$_2$-C≡CR), 1.52-1.47 (quin, 2H, R-C*H*$_2$-CH$_2$-C≡CR), 1.39-1.26 (m, 25H, alkyl), 0.90-0.86 (t, 3H, R-C*H*$_3$). ^{13}C-NMR (δ_{ppm}): 86.66 (1C, RC≡*C*-CH$_2$-OH), 78.24 (1C, R*C*≡C-CH$_2$-OH), 51.41 (1C, R-*C*H$_2$-OH), 31.92 (1C, alkyl), 29.69 (3C, alkyl), 29.65 (3C, alkyl), 29.63, 29.52, 29.35, 29.14, 28.88 (5C, alkyl), 22.68, (1C, alkyl), 18.72 (1C, alkyl), 14.71 (1C, alkyl). IR (cm^{-1}): 3302 (m, OH), 2954, 2871 (m, m, CH$_3$), 2914, 2848, 1470 (s, s, s, CH$_2$), 2118 (w, C≡C). MS (DART): calculated for $C_{18}H_{38}ON$ (M + NH$_4$) 284.2948, found 284.2950.

S.3.6.2 Octadec-17-yn-1-ol (5b)

The procedure described for dec-9-yn-1-ol **(1a)** was used with lithium (0.39 g, 56.07 mmol), 29 mol of 1,3-diaminopropane, potassium tert-butoxide (4.53 g, 37.38 mmol) and octadec-2-yn-1-ol (2.49 g, 9.35 mmol) to give octadec-17-yn-1-ol (1.20 g, 4.51 mmol, 48%).

^{1}H-NMR (δ_{ppm}): 3.64-3.61 (t, 2H, R-C*H*$_2$-OH), 2.19-2.15 (dt, 2H, R-C*H*$_2$-C≡C-H), 1.93-1.92 (t, 1H, RC≡C-*H*), 1.60-1.44 (m, 4H, alkyl), 1.40-1.25 (m, 25H, alkyl). ^{13}C-NMR (δ_{ppm}): 84.77 (1C, R-*C*≡C-H), 67.99 (1C, RC≡*C*-H), 62.91 (1C, R-*C*H$_2$-OH), 32.79 (1C, alkyl), 29.63, 29.58, 29.48, 29.42, 29.09, 28.74, 28.48 (13C, alkyl) 25.72 (1C, alkyl), 18.37 (1C, alkyl). IR (cm^{-1}): 3286, 628 (m, s, R-C≡*C*-*H*), 2917, 2849, 1472 (s, s, m, CH$_2$), 2115 (w, C≡C). MS (DART): calculated for $C_{18}H_{38}ON$ (M + NH$_4$) 284.2948, found 284.2953.

S.3.6.3 Octadec-17-ynyl-4-methylbenzenesulfonate (5c)

The procedure described for dec-9-ynyl 4-methylbenzenesulfonate **(1b)** was used with octadec-17-yn-1-ol (1.20 g, 4.51 mmol), pyridine (0.70 ml, 9.01 mmol), p-toluenesulfonylchloride (0.88 g, 4.61 mmol) and 50 ml of dichloromethane to give octadec-17-ynyl-4-methylbenzenesulfonate (1.20 g, 2.85 mmol, 63%).

^{1}H-NMR (δ_{ppm}): 7.79-7.77 (d, 2H, Ph), 7.35-7.32 (d, 2H, Ph), 4.03-4.00 (t, 2H, R-C*H*$_2$-OTs), 2.44 (s, 3H, R-Ph-C*H*$_3$), 2.19-2.15 (dt, 2H, R-C*H*$_2$-C≡C-H), 1.93-1.92 (t, 1H,

R-CH_2-C≡C-*H*), 1.66-1.59 (quin, 2H, alkyl), 1.55-1.49 (quin, 2H, alkyl), 1.44-1.21 (m, 24H, alkyne) ^{13}C-NMR (δ_{ppm}): 144.56 (1C, Ph), 133.32 (1C, Ph), 129.76 (2C, Ph), 127.85 (2C, Ph), 84.73 (1C, R-*C*≡C-H), 70.67 (1C, R-*C*H_2-OTs), 68.02 (1C, R-C≡*C*-H), 29.61 (4C, alkyl), 29.57 (2C, alkyl), 29.47, 29.36, 29.09, 28.90, 28.80, 28.73, 28.48 (7C, alkyl), 25.30 (1C, alkyl), 21.58 (1C, alkyl), 18.37 (1C, alkyl). IR (cm^{-1}): 3293 (m, s, C≡*C*-*H*), 2916, 2850, 1471 (s, s, m, CH_2), 2115 (w, C≡C). MS (DART): calculated for $C_{25}H_{44}NO_3S$ (M + NH_4) 438.3036, found 438.3032.

S.3.6.4 18-Fluorooctadec-1-yne (5d)

The procedure described for 10-fluorodec-1-yne **(1c)** was used with potassium tert-butoxide (3.26 g, 5.70 mmol and 1.62 g, 2.85 mmol) and 18-crown-6 (14.8 g, 5.70 mmol and 7.4 g, 2.85 mmol) in 10 ml of acetonitrile and hexadec-15-ynyl 4-methylbenzenesulfonate (1.2 g, 2.85 28.04 mmol) in 12 mL of acetonitrile to afford 18-fluorooctadec-1-yne (0.6 g, 2.23 mmol, 78%)

^{1}H-NMR (δ_{ppm}) 4.50-4.47 (t, 1H, F-C*H*$_2$-R), 4.38-4.35 (t, 1H, F-C*H*$_2$-R), 2.20-2.15 (m, 2H, R-C*H*$_2$-C≡C-H), 1.93-1.92 (t, 1H, R-C≡C-*H*), 1.75-1.62 (m, 2H, alkyl), 1.56-1.49 (quin, 2H, alkyl), 1.41-1.27 (m, 24H, alkyl). ^{13}C NMR (δ_{ppm}): 84.92, 83.28 (1C, F-*C*H_2-R), 84.67 (1C, R-*C*≡C-H), 67.98 (1C, R-C≡*C*-H), 30.50, 30.30 (1C, FCH_2-*C*H_2-R), 29.59, 29.57, 29.52, 29.49, 29.48, 29.22, 29.08, 28.74, 28.64, 28.48 (12C, alkyl), 25.16, 25.10 (1C, FCH_2-CH_2-*C*H_2-R), 18.36 (1C, alkyl). IR (cm^{-1}): 3311, 627 (m, s, C≡*C*-*H*), 2923, 2853, 1465 (s, s, m, CH_2), 2118 (w, C≡C). MS (DART): calculated for $C_{18}H_{37}NF$ (M + NH_4) 286.2905, found 286.2915.

S.3.7 Torsional angle measured of C-C-C-F

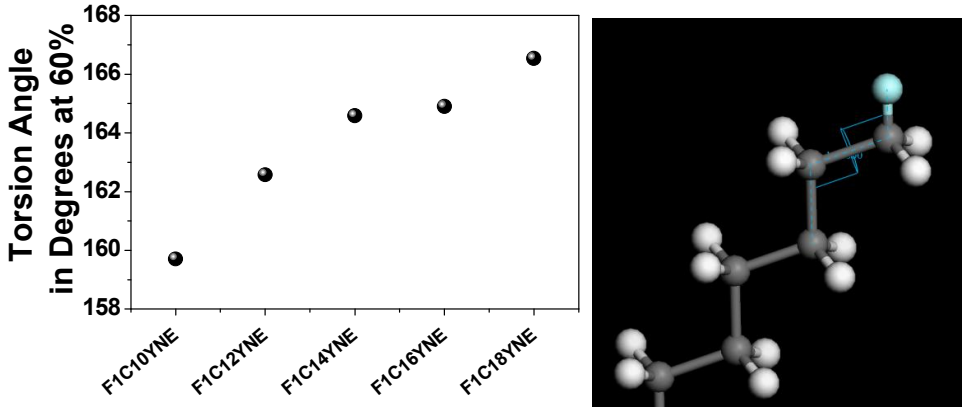

Figure S1. (Left) Simulation cells of surface coverage of 60 % after optimization and average torsional angle of C-C-C-F, (Right) torsional angle measured of C-C-C-F.

CHAPTER 4

Ultra-Low Adhesion and Friction of Fluoro-Hydro Alkyne-Derived Self-Assembled Monolayers on H-terminated Si(111)

New fluorine-containing terminal alkynes were synthesized and self-assembled onto Si(111) substrates to obtain fluorine-containing organic monolayers. The monolayers were analyzed in detail by ellipsometry, X-ray photoelectron spectroscopy (XPS), Fourier transform infrared reflection absorption spectroscopy (FT-IRRAS), static water contact angle measurements (CA) and atomic force microscopy (AFM). The SAMs exhibit excellent hydrophobicity, with static water contact angles up to 119° and low critical surface tensions of 5 - 20 mN/m, depending on the number of F atoms per molecule. IRRAS confirmed the formation of highly ordered monolayers, as indicated by the anti-symmetric and symmetric stretching vibrations of the CH_2 moieties at 2918 - 2920 cm^{-1} and 2850 - 2851 cm^{-1}, respectively. Upon increasing the number of fluorine atoms in the alkyne chains from 0 to 17, the adhesion of bare silica probes to the SAMs in air reduces from 11.6±0.20 mJ/m^2 for fluorine-free (F0) alkyne monolayers to as low as 3.2±0.03 mJ/m^2 for a heptadecafluoro-hexadecyne (F17) based monolayer. Likewise, the friction coefficient decreases from 5.7×10^{-2} to 1.2×10^{-2}. The combination of high ordering, excellent hydrophobicity, low adhesion and low friction make these fluoro-hydro alkyne-derived monolayers highly promising candidates for use in high-performance micro-electronic devices.

This Chapter has been published as:

"Ultralow Adhesion and Friction of Fluoro-Hydro Alkyne-Derived Self-Assembled Monolayers on H-Terminated Si(111)". Sidharam P. Pujari, Evan Spruijt, Martien A. Cohen Stuart, Cees J. M. van Rijn, Jos M. J. Paulusse, and Han Zuilhof. Langmuir **2012** 28 (51), 17690-17700

Table of Contents

4 Ultra-Low Adhesion and Friction of Fluoro-Hydro Alkyne-Derived Self-Assembled Monolayers on H-terminated Si(111) 93
4.1 INTRODUCTION 95
4.2 EXPERIMENTAL SECTION 97
4.2.1 Materials 97
4.2.2 Hydrogen-Terminated Si(111) surfaces 98
4.2.3 Preparation of Fluoro-Hydro Alkyne Derived Monolayers on Si(111) 98
4.3 MONOLAYER CHARACTERIZATION 98
4.3.1 Contact Angle Measurements 98
4.3.2 Ellipsometry 99
4.3.3 Atomic Force Microscopy 99
4.3.4 X-ray Photoelectron Spectroscopy (XPS) 100
4.3.5 Infrared Reflection Absorption Spectroscopy (IRRAS) 100
4.3.6 Molecular modeling 100
4.4 RESULTS AND DISCUSSION 101
4.4.1 Synthesis of Fluoro-Hydro Alkynes 101
4.4.2 Monolayer formation 102
4.4.3 Infrared Reflection-Absorption Spectroscopy 106
4.4.4 Adhesion and Friction 107
4.4.5 Molecular Modeling 112
4.5 CONCLUSIONS 113
4.6 REFERENCES 113

4.1 INTRODUCTION

Studies on low adhesion and low frictional surfaces are particularly important for high performance technological devices. One of the great challenges in many micro-component devices, such as micro-and nano-electro-mechanical systems (MEMS and NEMS), is to reduce adhesion and friction to surfaces as much as possible, while keeping the surface highly robust and resistant against wear. The typical dimensions of MEMS and NEMS are a few to several hundreds of microns and they are primarily made from silicon. At these small scales, surface properties, such as Van der Waals and capillary forces, greatly influence the performance of these mechanical systems.[1-3] Without a suitable surface modification Si shows high friction, adhesion, and wear.[4-6] Therefore, several types of thin films have been investigated as coating for Si with enhanced tribological properties of silicon.[7] In particular, thin organic fluorocarbon-hydrocarbon films have been found to produce low-adhesion and low-friction lubricants.[8-12] In practice, polytetrafluoroethylene (PTFE) is now the primary coatings material in many micro-electro-mechanical systems.[5] However, these films are not covalently bound to the silicon and are therefore prone to wear. Moreover, PTFE films are relatively thick, which may still lead to high adhesion and friction forces when high loads are applied and the films are compressed. Here, we report on ultra-thin covalently bound fluoro-hydro alkyne-derived monolayers as high quality, low-adhesion and low-friction surface coatings on silicon for use in micro-component devices.

Densely packed organic monolayers, which are covalently bound via Si-CH=C linkages to crystalline silicon surfaces without an interfacial silicon oxide (SiO_2) layer, are receiving increasing interest,[13-15] mainly due to the potential of Si-C bound monolayers for application in micro- and nano-electronics, as well as in bio-chemical sensors.[16-22] This field has recently been reviewed.[23] With the advent of nanotechnology, lubricating monolayers are highly desired because they are covalently attached to the substrate, therefore not easily damaged and even if they break, do not yield particulates that may cause damage. Among the different organic monolayers grafted on the surface, fluorinated organic thin films have drawn much attention due to their outstanding chemical stability, thermal stability, unique wettability, and non-adhesive properties.[24, 25] On a nanometer scale, the physical state of thin film systems may be influenced by a number of forces, including intermolecular interactions between molecules making up the film,[26] surface interactions in adsorbed films, and solvent interactions in detached film systems.[27]

The formation of a dipole between the last fluorinated carbon (R-CH_2-$\mathbf{CF_2}$-R^1) and the first methylene group (R-$\mathbf{CH_2}$-CF_2-R^1) in fluorinated organic monolayers causes the electronegative groups to be oriented normal to the surface. This gives rise to an important

decrease in adhesion to and friction of the fluorinated monolayers. In addition, fluorination leads to an enhancement of the hydrophobicity and oleophobicity.[28, 29] The diverse effects that varying degrees of fluorination cause as well as the ratio between fluorocarbons and hydrocarbons, are under extensive study, with the aim to improve the tribological properties and to enhance the hydrophobicity of these monolayers.[30-32]

A range of synthetic methods has been successfully used to prepare covalently bound monolayers on solid surfaces. For silicon, extensive reviews are provided by Gooding et al.[33, 34] and Zuilhof et al.[23, 35] The formation of a silicon-carbon bond via hydrosilylation is a key step in the coating of a silicon surface with a monolayer, as it greatly improves both packing and stability of SAMs.[34] Grafting of alkynes onto the Si surface can be achieved in various ways.[36-41] The mildest approach already allows for the preparation of high-quality covalently bound organic monolayers at room temperature.[42] As the assembly on the silicon surface progresses, interchain steric hindrance of CH_2 and CF_2 becomes dominant and prevents the bonding of alkyl chains to every silicon atom of the substrate. Since the resistance towards oxidation depends on the density of monolayer packing,[15] a technique to develop tightly packed monolayers is desired in order to minimize water penetration, oxide formation, and consequently, degradation of the silicon substrate.

In this paper, we prepare alkyne-based SAMs, which are known to be stable and to form densely packed monolayers.[23, 43] By contrast, alkene-based SAMs, in which a Si- CH_2-CH_2 single bond allows for higher degree of free rotation around the chain axis, give rise to a lower packing density. Apart from the enhanced rotation, the saturation of the carbon chain is another important feature: when an alkyne is attached to silicon, an alkene (Si-CH=C linkage) remains, which takes up a smaller volume and thus causes less interchain repulsion than caused by the Si-CH_2-CH_2 linkage that is formed upon attaching an alkene to silicon. The enhanced packing density of alkyne-derived monolayers compared to alkene is furthermore due to the smaller tilt angle with respect to the surface normal, and higher ordering of the remaining alkene moieties, facilitated by attractive π-π interactions.[15] Finally, it is remarked that the packing density increases with longer carbon chains for alkyne-derived monolayers as well as alkene-derived monolayers.[13, 44-46]

Studying the characteristics of our S-CH=C linked monolayers together with the requirements for ultra-low surface tensions and adhesion properties, we expect that partially fluorinated monolayers on hydrogenated, oxide-free Si (H-Si) surface will combine several of the highly desirable characteristics strived for in this field. The current paper presents the synthesis of novel fluoro-hydro alkynes with a varying number of fluorine atoms (#F atoms: 0 – 17) at a constant chain length (C_{16}) (**Figure 1**), and their application in monolayer formation onto oxide-free H-Si(111) surfaces. The resulting

monolayers are characterized by ellipsometry, X-ray photoelectron spectroscopy (XPS), Fourier transform infrared reflection absorption spectroscopy (FT-IRRAS), advancing, and static water contact angle measurements (CA) and critical surface tension measurements. Subsequently, the adhesion and friction of these monolayers were studied as a function of fluorine content by colloidal probe atomic force microscopy (CP-AFM), to reveal unprecedentedly low surface tensions and adhesion properties.

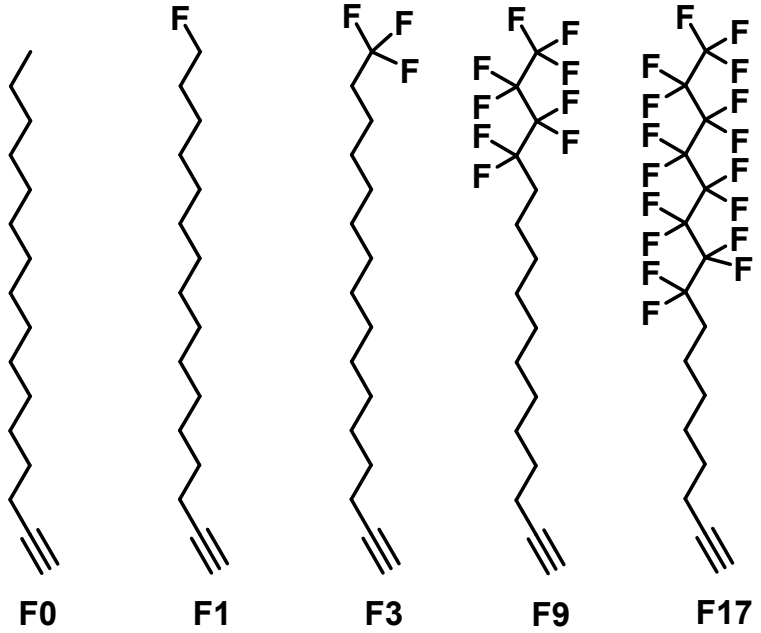

Figure 1. Fluoro-hydro alkynes employed in monolayer formation.

4.2 EXPERIMENTAL SECTION

4.2.1 Materials

The synthetic procedures and spectroscopic characterization for hexadec-1-yne (F0), 16-fluorohexadec-1-yne (F1), 16,16,16-trifluorohexadec-1-yne (F3), 13,13,14,14, 15,15,16,16,16-nonafluoro-hexadec-1-yne (F9), and 9,9,10,10,11,11,12,12,13,13,14, 14,15,15,16,16,16-heptadecafluoro-hexadec-1-yne (F17) are described in the *Supporting Information S.4.2 to S.4.5*. For rinsing and contact angle measurements, Milli-Q water (resistivity 18.3 MΩ×cm) was used. Hexadecane (C16, 99%); tetradecane (C14, 99%); dodecane (C12, 99%); decane (C10, 99%); heptane (C7, 99%); and hexane (C6, 99%) are used to determine the critical surface tension and were obtained from Aldrich and used as received. Sulfuric acid (Sigma Aldrich, 95-97%), hydrogen peroxide (Acros Organics,

35%), ammonium fluoride (Riedel-de Haën, 40%, semiconductor grade VLSI PURANAL Honeywell 17600), and acetone (Aldrich, semiconductor grade VLSI PURANAL Honeywell 17617) were used as received. Silicon wafers were (111)-oriented single-side and doubly polished 500 - 550 μm thick, phosphorus-doped n-type, and have a resistivity of 2.0 - 8.0 Ω×cm with a 0.2° miscut angle along the <112> plane (Siltronix).

4.2.2 Hydrogen-Terminated Si(111) surfaces

Hydrogen-terminated Si(111) surfaces ("H-Si") were prepared by chemical etching as previously reported.[45, 47] All liquid reagents were continuously purged with an argon flow. N-type Si(111), was cut into an appropriately size substrate (10 × 10 mm^2) and subsequently cleaned in a sonication bath with acetone and then with Milli-Q water. The Si wafer was oxidized in freshly prepared piranha solution (H_2SO_4/H_2O_2 3 : 1) for at least 20 min. After piranha treatment, the substrates were immersed immediately in water and rinsed thoroughly, followed by drying with a stream of argon. Subsequently, the substrates were etched in an argon-saturated 40% aqueous NH_4F solution for 15 min, rinsed by Milli-Q water, and finally dried with a stream of argon.

4.2.3 Preparation of Fluoro-Hydro Alkyne Derived Monolayers on Si(111)

A three-necked flat-bottom flask, connected with a thin capillary as the argon inlet and a reflux-condenser connected to a vacuum pump, was charged with individual neat fluoro-hydro alkyne (Scheme 1), flushed with argon, and heated to 80 °C in order to remove traces of oxygen and moisture. The freshly etched Si(111) substrate was placed in fluoro-hydro alkyne. The reaction was carried out at 80 °C, under an argon atmosphere at an argon pressure of 2 - 5 mbar for 16 h. After the reaction had been stopped, the modified surfaces were rinsed and sonicated with CH_2Cl_2 for 5 min to remove any physisorbed fluoro-hydro alkynes.

4.3 MONOLAYER CHARACTERIZATION

4.3.1 Contact Angle Measurements

Contact angle measurements were performed on a Krüss DSA 100 contact angle goniometer with an automated drop dispenser and image video capture system. The static contact angles of six small droplets 3.0 μL volume of liquid, dispensed on modified silicon surfaces with a microliter syringe with stainless steel needle (diameter = 0.51 mm), were determined using a Tangent 2 fitting model. The digital drop images were processed by the image analysis system, which calculated both the left and right contact angles from the drop shape with an accuracy of ±1.0°. For advancing contact angle determinations on

the same polymer samples droplets of 1 µL total volume were applied at 10 µL/min and monitored by video recording. Reported angles are averaged over at least five droplets

4.3.2 Ellipsometry

The thickness of the modified silicon surfaces (in the dry state) was measured using a rotating analyzer ellipsometer (Sentech Instruments type SE-400), operating at 632.8 nm (He–Ne laser), with an angle of incidence of 70°. The optical constants of the substrate were determined with a piece of freshly etched H-Si(111) (n = 3.819 and k = 0.057). The thicknesses of the monolayers were determined with a planar three-layer (ambient, monolayer, substrate) isotropic model with a refractive index for the organic monolayers of 1.46 (F0), 1.44 (F1), 1.40 (F3), 1.38 (F9), and 1.35 (F17).[48] The reported values for the layer thickness are the average of eight measurements taken at different locations on the substrate with an error < 1 Å.

4.3.3 Atomic Force Microscopy

Force measurements are performed on a Nanoscope IIIA AFM (Digital Instruments) equipped with a PicoForce scanner. Spherical silica particles (R = 3.0 µm, rms roughness value of 6.83 ± 2.06 nm)[49] were attached to triangular standard silicon nitride cantilevers (Bruker probes, NP-B, spring constant between 0.10 and 0.16 N/m) using Norland optical adhesive 61, and cured by UV light (365 nm). Before use, the colloidal probes were cleaned by excessive amounts of ethanol followed by 5 min air plasma cleaning. Both adhesion and friction measurements were carried out in air, at relative humidity of 44 ± 2 %.

Adhesion forces were measured using a scan range of 1.0 µm for modified surfaces and 10 µm for oxide surfaces at a scan rate of 0.5 Hz. At least 200 separate force curves were recorded for every surface. For each cantilever the normal spring constant was determined using the thermal tuning method introduced by Hutter and Bechhoefer,[50] correcting for non-ideality of the spring and the fact that the deflection sensitivity was measured for a supported cantilever.[51] The overall error in measured adhesion forces is the sum of uncertainties in the voltage measurement, deflection sensitivity, and spring constant, and was estimated to be ±10%.[32, 52]

Friction forces were obtained from trace and retrace of 5 × 5 µm^2 lateral force images under varying normal loads (F_N = 0 to 80 nN). The lateral force images are measured at a constant speed of 5 µm/s under a 90° angle with respect to the cantilever's long axis. The average lateral force difference signal ($[\mu_{trace} - \mu_{retrace}]/2$, in V) was converted directly into friction force, following the method of Liu et al.[53] Cantilevers were calibrated using the

reversible bending of a 8.9 μm thick glass fiber, leading to a lateral conversion factor of approximately 17.7 nN/V. The overall error in the conversion factor determined in this way, was estimated to be 15%.[53]

4.3.4 X-ray Photoelectron Spectroscopy (XPS)

XPS measurements were performed using a JPS-9200 photoelectron spectrometer (JEOL, Japan). A monochromatic Al Kα X-ray source (hν = 1486.7 eV) 12 kV and 20 mA using an analyzer pass energy of 10 eV was used. The base pressure in the chamber during measurements was 3×10^{-7} Torr, and spectra were collected at room temperature. The intensity of XPS core level electron was measured as the peak area after standard background subtraction according to the linear procedure. The takeoff angle φ (angle between sample and detector) of 80° is defined with a precision 1°. The typical sample size was 1×1 cm^2. All XPS spectra were evaluated using the Casa XPS software (version 2.3.15). The symmetrical GL(30) line shape was employed, which is constituted of a Gaussian (70%) and a Lorentzian (30%) component. The FWHM of each component was constrained to ~1.0 eV. The relative areas of each component peak were fixed by the stoichiometry of the main hydrocarbon (CH_2), which were assigned as aliphatic carbon to a binding energy of 285.00 eV.

4.3.5 Infrared Reflection Absorption Spectroscopy (IRRAS)

IRRA spectra were recorded on a Bruker Tensor 27 FT-IR spectrometer using a variable angle reflection unit (Auto Seagull, Harrick Scientific). A Harrick grid polarizer was installed in front of the detector and was used to record spectra with p-polarized (parallel) radiation with respect to the plane of incidence at the sample surface. All spectra were obtained at an incident angle of 68° (2048 scans). The resolution was set at 2 cm^{-1} per modulation center. The final spectra were obtained using a piranha-oxidized reference surface as background. Data were collected as differential reflectance versus wavenumber. All spectra were recorded at room temperature in dry atmosphere.

4.3.6 Molecular modeling

For the molecular modeling study, the same method is followed as reported by Scheres et al.[43, 54] In short, Materials Studio software (version 5.0) was used to construct and optimize the monolayers. All monolayers were formed from five standard cells containing a decenyl chain (representing one of the alkynes) attached in all-trans conformation to four Si atoms. The Si atoms represent the first four layers of the Si substrate and it was obtained by cleaving a Si crystal along the (111) plane. The structures were placed in a

box to obtain the standard cells. The standard cells were copied in the directions of the Si substrate to form larger unit cells. By replacing some of the attached chains by hydrogen atoms, different substitution patterns and substitution percentages were obtained. All unit cells were finally copied to form the final big simulation cells, representing the whole modified Si surface. The unit cells and the big simulation cells were optimized using a polymer consistent force field (PCFF) with the "Smart Minimizer" routine and "high-convergence" criteria. Periodic boundary conditions were applied.

4.4 RESULTS AND DISCUSSION

4.4.1 Synthesis of Fluoro-Hydro Alkynes

The synthesized fluoro-hydro alkynes are depicted in Figure 1. Fluorine-free 1-hexadecyne (**F0**) was obtained by tosylation of 1-tetradecanol, followed by nucleophilic substitution with lithium acetylide. **F3** was synthesized in six steps (see Scheme 1; full experimental details in *Supporting Information S.4.4*), consisting of coupling of THP-protected propargyl alcohol to 1-bromododecane, followed by deprotection of the THP-group affording pentadec-2-yn-1-ol. Isomerization of pentadec-2-yn-1-ol afforded the terminal alkyne, which was again tosylated and subsequently converted into the corresponding iodide, to increase reactivity for the final reaction with Me_3SiCF_3 to yield **F3**. A similar procedure was followed for preparing **F1** from commercially available hexadec-7-yn-1-ol. After isomerization and tosylation, treatment with KF afforded **F1**. The heptadecafluoro alkyne **F9** was obtained via a four step reaction (see in *Supporting Information S.4.2* Scheme S1). Radical chain addition of 1,1,1,2,2,3,3,4,4-nonafluoro-4-iodobutane to 9-decene-1-ol afforded 11,11,12,12,13,13,14,14,14-nonafluoro-9-iodotetradecan-1-ol, and was followed by reduction of the iodide to give the reduced 11,11,12,12,13,13,14,14,14-nonafluorotetradecan-1-ol. Tosylation of 11,11,12,12,13,13,14,14,14-nonafluoro-tetradecan-1-ol was followed by nucleophilic substitution with lithium acetylide to obtain fluoro-hydro-alkyne **F9**. **F17** was synthesized following the same procedure, but starting with 1,1,1,2,2,3,3,4,4,5,5,6,6,7,7,8,8-heptadecafluoro-8-iodooctane and 5-hexen-1-ol.

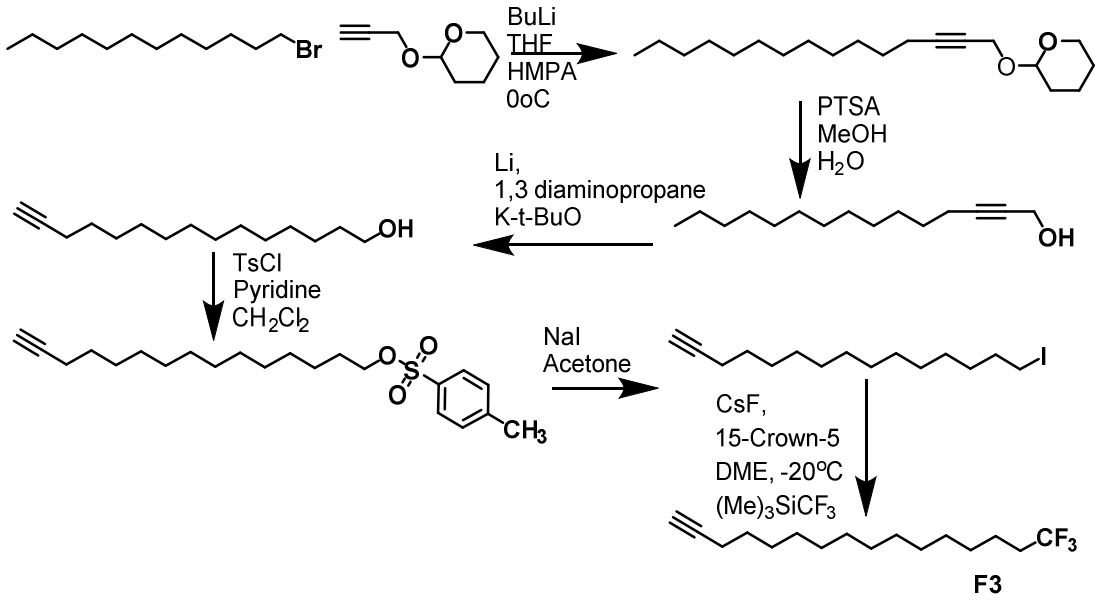

Scheme 1. Synthetic procedure used to create fluoro-hydro alkynes (**F3** is given as an example).

4.4.2 Monolayer formation

In search of a mild and generally applicable method for grafting the newly synthesized fluoro-hydro containing alkynes onto Si substrates, different reaction times and temperatures were investigated (data not shown). Typically, the Si substrate was immersed in neat alkyne under oxygen-free and water-free conditions. While high-quality monolayers were formed on Si(111) with **F0** even at room temperature and ambient light,[42] the modification with fluorinated alkynes were not completed under these conditions, and physisorption dominated based on weak Van der Waals interaction or hydrogen bonding between C-F···H-C.[55] Hence, grafting of the fluorinated alkynes required reaction conditions of at least 80 °C for 16 h.

Advancing and static water contact angle measurements were determined for all monolayers (see *Supporting Information S.4.6* **Table S1**). The hexadecyne (**F0**) based monolayer displayed a static water contact angle of 110°, in agreement with earlier observed values.[42] The hydrophobicity of the SAMs based on **F1** - **F17** are typical for the presence of fluorinated moieties.[28] The water contact angle rises with increasing number of fluorines in the monolayer (static water contact angle up to 119° for **F17**), and compares favorably with that of PTFE = (115°). For **F9** and **F17** higher contact angles were observed, because of weak dipole-dipole interaction between the CF_3 terminus and water molecules. In comparison, a PTFE surface displays a lower static water contact

angle, because the CF_2 groups are less capable of reducing the surface energy than CF_3 groups.[56] The lower polarizability of fluorine compared to hydrogen leads to very weak Van der Waals interactions among the CF_3 terminus and polar water molecules.[57] There has been a number of studies on the influence of terminal groups.[58, 59] Colorado et al. obtained for a Au..S-$(CH_2)_{15}$-x$(CF_2)_xCF_3$ series of monolayers a smaller contact angle (108°) for x = 0 (comparable to our **F3** monolayer; θ = 113°).[28] This lower contact angle is likely due to a more horizontal organization of the CH_2-CF_3 terminus, thus exposing the CH_2 moiety. In our case, the monolayer is likely more organized, presenting only the CF_3 group head up, yielding a higher hydrophobicity.)

From the advancing water contact angle the apparent work of adhesion can be calculated. **Figure 2** shows how the work of adhesion decreases with an increasing number of fluorine atoms. The strongest decrease occurs between **F3** and **F9**, as discussed above. Between **F9** and **F17** little change is observed.

A similar trend is found in the critical surface tension of the monolayers. Critical surface tensions are obtained from Zisman plots of static contact angles of a series of linear alkanes on the monolayers. A Zisman plot can be used to investigate the surface energy of a low-energy solid surface.[60] When the surface energy of the solid is comparable to that of the liquid, a transition from partial to complete wetting is observed. Surfaces with very low surface energies are difficult to wet and may never reach complete wetting.

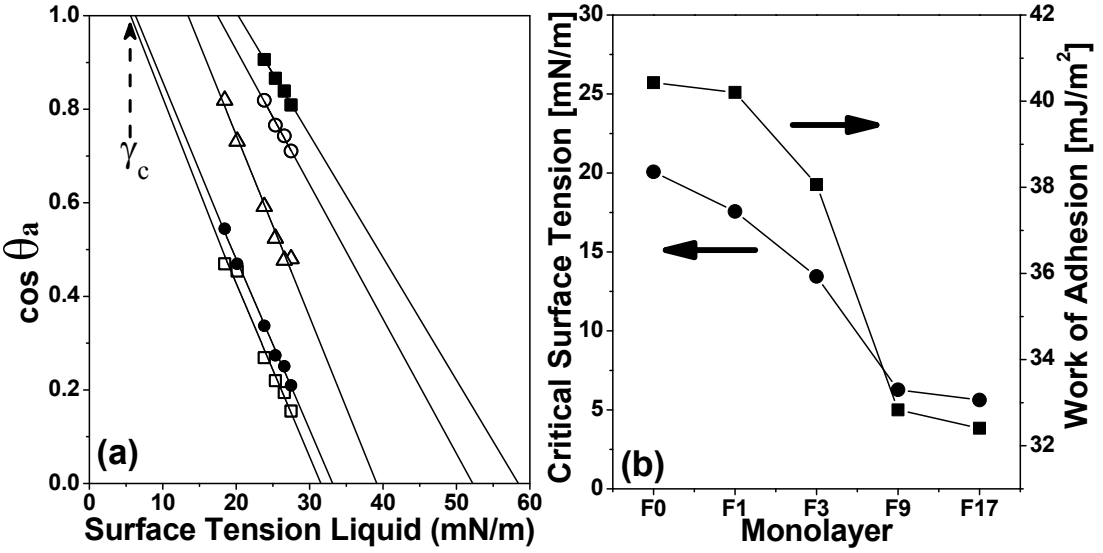

Figure 2. (a) Zisman plot showing the linear regression of cos *θ* vs different n-alkanes (from C6 to C16) on **F17** (empty squares), **F9** (circles), **F3** (empty triangles), **F1** (circles empty), and **F0** (squares) monolayers on H-terminated Si(111). The line coefficient r^2 = 0.98 ± 0.01 indicates a high degree of

confidence. (b) Critical surface tension (circles) and work of adhesion (squares) on SAMs derived from the hexadecyne series as a function of the total number of fluorine atoms per chain. Critical surface tensions (γ_c) are obtained from extrapolation to cos θ = 1 at 24 ± 2 °C.

In that case, measuring the wetting contact angle (θ) for different values of the liquid surface tension (γ_L) and extrapolating to cos θ = 1, *i.e.* complete wetting, will yield a critical surface tension (γ_c), which is a measure for the solid surface energy and an essential parameter in many practical applications.[61] In general, the critical surface tension and the details of the extrapolation depend on the molecular characteristics of the liquid.[61] However, in a homologous series of simple molecular liquids, such as *n*-alkanes, the Van der Waals forces dominate the liquid surface energy, and Zisman found that cos θ depends linearly on γ_L.[60] Using this approach, Zisman determined critical surface tensions for a variety of solids with a low-energy surface. The lowest critical surface tension found was 6 mN/m for condensed monolayers of perfluorolauric acid on platinum, whereas Teflon has a critical surface tension of 18.5 mN/m.

The monolayers under current study stand out by displaying extraordinarily low surface tensions. **Figure 2a** shows Zisman plots for the fluoro-hydro alkyne-derived monolayers F0 to F17, using a homologous series of n-alkanes. In all cases, a linear relation is found between cos(θ) and γ_L, in agreement with the original findings of Zisman.[60] The corresponding critical surface tensions are shown in **Figure 2b**. Surfaces with a low critical surface tension are expected to suffer least from adhesion to the surface, which is desirable in many microelectronic devices. First of all, the critical surface tension for **F0** is found to be 20.1 mN/m, which is lower than characteristic values reported for CH_3-termination in literature (22 - 24 mN/m),[62] revealing the high organization of the monolayer. Increasing the number of F atoms in the monolayer further decreases the critical surface tension to 5.6±0.21 mN/m for **F17**, which is – as far as we know – currently the lowest for any solid surface. Consequently, only condensed inert gases would show complete wetting on this surface.[60, 63]

Table 1 summarizes monolayer thicknesses measured by ellipsometry as well as XPS.[13] The observed refractive index (RI) of the **F17** monolayer on Si(111) is close to that of the analogous F_{17} silane reported by Geer et al.[48] Monolayers prepared from compounds **F9** and **F17** display slightly lower thicknesses than those obtained from **F0**, **F1** and **F3.** The relaxed fluoro-hydro alkyne molecules in the SAMs are most likely not straight, but helical and bent, similar to fluorinated alkyl thiols on Au. Such monolayers were reported to display tilt angles of 30 - 35° with respect to the surface normal.[31, 64, 65] The lower thicknesses may also relate to differences in the effective cross-sectional area of the -CF_2-

CF_3 and -CH_2-CH_3 moieties (28 Å^2 and 18 Å^2, respectively), and fit it less optimally with the intersite distances on the Si(111) surface.[66]

Table 1. XPS Data Atomic C/Si Ratios and XPS and Ellipsometry Thickness.

Monolayer	C/Si	C/F ratio Theory	C/F ratio Expt.	XPS Thickness [nm]	Ellipsometry Thickness [nm]	Refractive index
F0	40.9/59.1	--	--	2.07	2.09	1.46
F1	38.7/61.3	16.0	15.0	2.01	2.02	1.44
F3	38.4/61.6	5.3	5.2	1.91	1.95	1.40
F9	37.2/62.8	1.8	1.9	1.84	1.91	1.39
F17	37.8/62.2	0.9	1.0	1.89	1.93	1.35

The fluoro-hydro alkyne-derived monolayers were analyzed by XPS as well, and the resulting C_{1s} and Si_{2p} high-resolution spectra of an **F9**-based monolayer are depicted in **Figure 3**. The peak labels in the spectra correspond to the carbon atoms having different environments in the modified monolayer which was deconvoluted into six distinct components. The hydrocarbon CH_2 C_{1s} (2) calibrated at a binding energy of 285.0 eV corresponds to carbon atoms involved in CH_2 moieties of **F9**, whereas signal (1) at 283.6 eV is assigned to the carbon bound to the less electronegative Si.[42] The relative intensity of this Si-C signal is ~1/16 of the total C signal, in line with expectations. C_{1s} signal (3) at 286.1 eV corresponds to the methylene carbon atom involved in the -CF_2-***C***H_2- group. The shoulder peak observed at 290.9 eV corresponds to the -***C***F_2-CH_2- group (4). C_{1s} signal (5) at 291.6 eV corresponds to the other CF_2 groups, whereas the highest binding energy (293.8 eV) is observed for the terminal CF_3 group (**Figure 3b)**. [636363]This assignment is in excellent agreement with computational C_{1s} and F_{1s} XPS data obtained by B3LYP/6-311G(d,p) calculations (*Supporting Information S.4.7.1* **Figure S4**).[67]

The Si_{2p} high-resolution spectrum (**Figure 3a**) shows binding energies of the Si $2p_{1/2}$ and Si $2p_{3/2}$ doublet at 100.1 and 99.5 eV, respectively. Importantly, no contribution related to oxide or suboxide species in the energy range 101 - 104 eV was observed, indicating the oxide-free nature of the silicon substrate underneath this partially fluorinated monolayer. Whereas excellent surface passivation has been shown before for alkyne-derived **F0** monolayers,[13] apparently fluorination does not hamper the formation of a fully surface-covering monolayer.

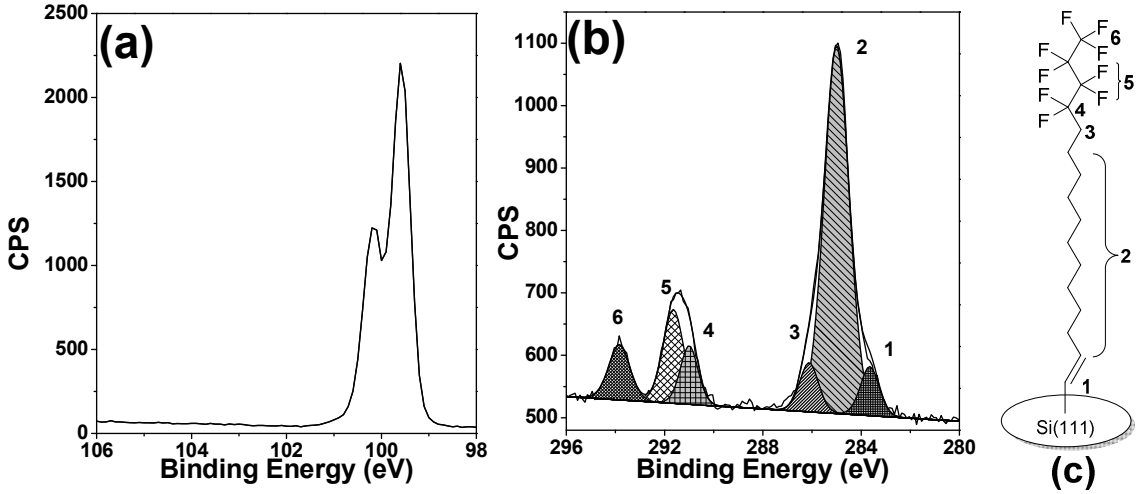

Figure 3. High-resolution XPS data of a **F9**-based monolayer on an oxide-free H-Si(111) surface. a) Si 2p and b) C 1s. (c) Schematic representation of **F9** monolayer on Si(111).

4.4.3 Infrared Reflection-Absorption Spectroscopy

Qualitative differences in the conformational order of the alkyl chains in the monolayers were evaluated using infrared reflection-adsorption spectroscopy (IRRAS) by monitoring the anti-symmetric and symmetric CH_2 stretching vibrations (**Figure 4a**).[13, 68, 69] For increases in fluorine content from **F0** to **F17**, the SAMs exhibited slightly increasing values for the anti-symmetric CH_2 stretching vibrations from 2918 to 2920 cm^{-1}, as well as symmetric stretching vibrations ranging from 2850 to 2851 cm^{-1}. The low values observed for **F0** are – as reported before[13] – attributed to the high degree of short-range ordering in these monolayers. Since higher values of this peak frequencies are typically correlated with diminished ordering, it may be thought that the higher values observed for e.g. **F17** display a reduced ordering. However, another, electronic factor comes into play here. The increased electronegativity of the chain yields an upward shift of the CH_2 stretching vibrations, as exemplified by B3LYP/6-311G(d,p) data obtained for frequencies of the C-H stretching vibrations of model compounds CH_3-$(CH_2)_7$-$(CH_2)_7CH_3$ (i.e. n-hexadecane), and CH_3-$(CH_2)_7$-$(CF_2)_7CF_3$ using scaled (0.9679)[70] optimized B3LYP/6-311G(d,p) data. As can be seen (**Figure 4b**) fluorination by itself decreases the C-H stretching vibration frequencies by approximately 3 cm^{-1}. If one thus compensates for this electronic effect on the CH_2 stretching vibrations, the degree of ordering in our fluorinated monolayers seems to equal that observed for **F0**, pointing to highly ordered monolayers throughout the entire fluoro-hydro alkyne series. This high ordering, of

course, does not imply identical conformations, as the **F9** and **F17** chains may well display helical conformations.[71]

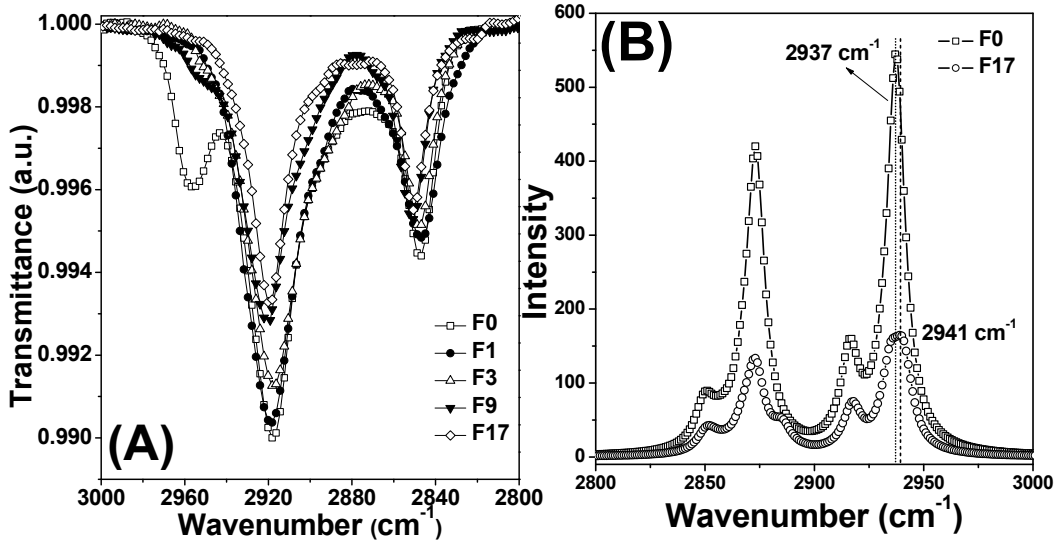

Figure 4. (a) IRRAS spectra (between 2800 and 3000 cm^{-1}) for fluorinated monolayers on H-Si(111). (b) DFT calculations of relevant vibrational frequencies of CH_3-$(CH_2)_7$-$(CX_2)_7CX_3$, for X = H and F)) optimized by B3LYP/6-311G(d,p) using a scaling factor of 0.9679.

4.4.4 Adhesion and Friction

To assess the adhesion and friction characteristics of the modified Si(111) surfaces atomic force microscopy was used. Both adhesion to and friction on surfaces greatly influence the performance of micro-electronic devices. Colloidal probe AFM allows measuring both properties with high accuracy. The colloidal probe acts as a model solid object that can interact with the modified surfaces. Previously, covalently bound alkene SAMs and adsorbed fluorine-containing surface coatings have been shown to reduce adhesion and increase lubrication significantly in solution.[52, 72] However, most devices operate in air or vacuum, where adhesion is expected to be much larger. Moreover, capillary condensation may occur between surfaces that are hydrophilic enough, leading to even stronger adhesive interactions. Under these conditions a candidate surface coating should still effectively reduce adhesion and provide sufficient lubrication. Therefore, fluoro-hydro alkyne-derived monolayers were subjected to the most stringent adhesion and friction test by carrying out the AFM measurements in air with a smooth silica probe as a hydrophilic solid particle.

The fluorinated monolayers under current study display very low adhesion forces. Figure 5 shows the adhesion of a silica probe particle to the monolayers when the surfaces are compressed at a load of 10 nN. Adhesion forces decrease with increasing fluorine content in the monolayers from 35 nN (11.6±0.20 mJ/m^2) for the F0-based monolayer to as low as 9.8 nN (3.2±0.03 mJ/m^2) for the F17-based monolayer. This is as far as we know the lowest adhesion force observed for any flat surface. This low adhesion is attributed to the high degree of ordering in the monolayer, which allows little reorganization within the monolayer to increase attractive interactions between the monolayer and the probe. Only in the case of F0 monolayers a small, non-zero attraction was measured upon approach of the surfaces.

The measured adhesion originates from Van der Waals interactions between the probe particle and the fluoro-hydro alkyne-coated Si(111) surface. Stable water capillary bridges cannot be formed, due to the high water contact angle of the SAMs and the low relative humidity.[73] The low adhesion forces and thus low surface energies of the F9- and F17-based monolayers confirm the low polarizability of the terminal CF_2-CF_3 groups. The F9- and F17-based monolayers show lower a adhesion than (-$(CH_2)_n$-CF_2-CF_3) SAMs on silica surfaces, and are even comparable to rough surfaces of PEG-grafted and fluorinated nanoparticles in air.[72] Clearly, the high quality of these monolayers further reduces the surface energy and leads to minimal adhesion. Combining these monolayers with structured surfaces would thus be highly interesting for the construction of robust superhydrophobic surfaces.

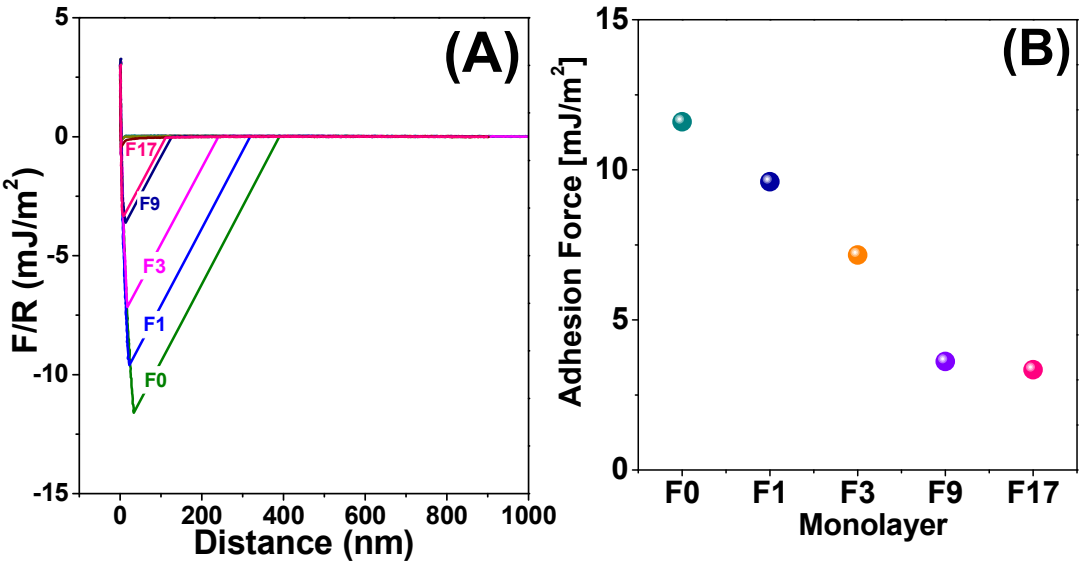

Figure 5. (B) Representative force-distance curves for SAMs with different fluorinated

monolayers. In all cases a load of 10 nN is applied. (B) The adhesion force, defined as the minimum in the force-distance plot, for different monolayers.

The low thickness of the monolayers compared to other PTFE coatings[74] leads to a limited compressibility and this suggests that the adhesion will not increase significantly when the applied load is increased. **Figure 6** shows the increase in adhesion with increasing load for all monolayers in air. Indeed, adhesion increases only slightly (30%), with the increase being largest for the **F0**-based monolayer. The increasing adhesion originates from elastic compression of the surfaces, which yields a larger contact area between the solid probe and the monolayers. The JKR model can be used to predict the load deformation of compressed surfaces when their interaction is governed by short-range adhesion only.[75] In this case, the total compression is determined by three materials with very different elastic moduli: the silica probe, the Si(111) substrate and the fluoro-hydro alkyne-derived monolayer. Therefore, a two-layer substrate JKR model was used in which a transition function describes the change of elastic modulus of the substrate from the top of the SAM (150 - 300 MPa) to deep inside the Si(111) (160 GPa).[76] The solid lines in **Figure 6** represent fits of the data to this modified JKR model with a fixed layer thickness of 2.0 nm in all cases. The elastic modulus of the monolayer decreases with increasing fluorine content by a total factor of two (from **F0** to **F17**). This decrease may be explained by a higher order and crystallinity of **F0**, **F1** and **F3**-based monolayers than of **F9** and **F17**-based monolayers. In addition, the model gives a prediction for the compression of the SAM and the area of contact between the silica probe and the SAM as a function of normal load. Using these values, the work of adhesion between the silica probe and the fluoro-hydro alkyne-coated Si(111) and an effective Hamaker constant can be calculated using the Derjaguin approximation. A typical indentation of the SAM at a normal load of 10 nN is 1.3 nm, leading to a contact area of 0.030 μm^2. Combined with the adhesion forces in **Figure 5**, the effective Hamaker constant is found to decrease from 15.4 $k_B T$ for the **F0-**derived monolayer to 5.1 $k_B T$ for the monolayer obtained from **F17**. There is a good agreement between the Hamaker constant for the **F0** monolayer with the theoretical prediction for the interaction between a silica probe and Si(111) covered by a crystalline hydrocarbon layer.[77]

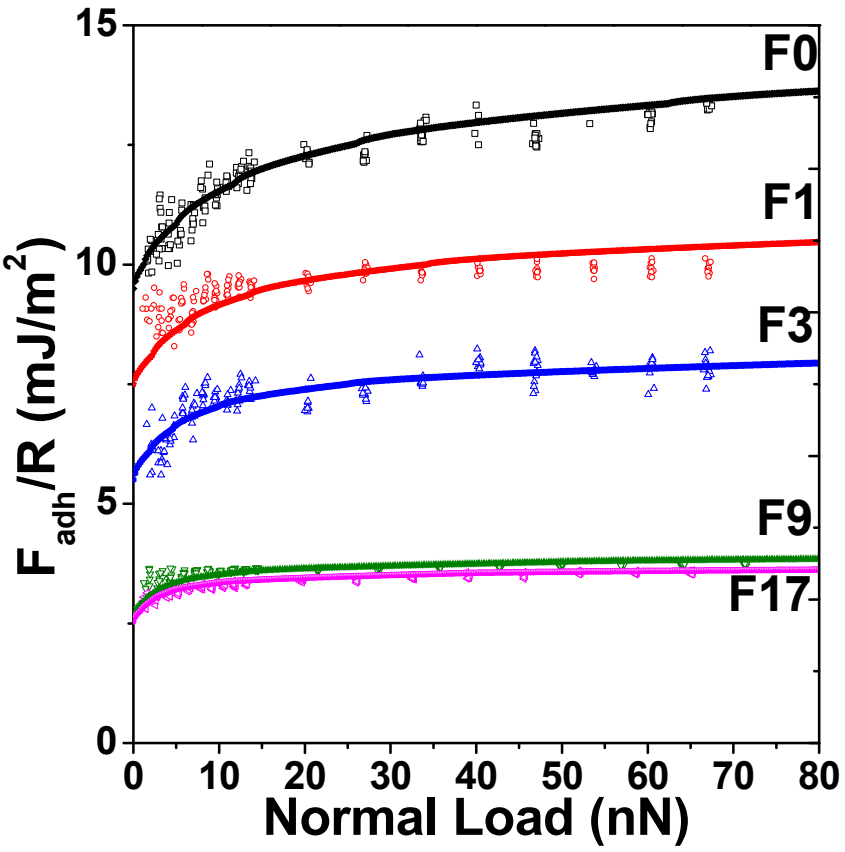

Figure 6. Adhesion forces of a colloidal silica probe as a function of normal load for different monolayers. Solid lines are fits of the data with a JKR model of a soft layer with 1.8 nm thickness on top of H-Si(111).

Besides adhesion, friction of laterally moving or rolling objects on the surfaces of microelectronic devices is an important aspect that governs their performance. Minimal friction coefficients or high lubrication are desirable. The lateral friction force on the fluorinated monolayers was measured using the same colloidal probe set-up as for the adhesion measurements. The load was varied from 0 to 75 nN and the lateral friction was recorded on several 5 × 5 μm^2 areas (see *Supporting Information S.4.8* **Figure S5**). The mean friction forces are depicted in **Figure 7**. The friction forces follow an apparent Gaussian distribution around the mean values and the typical relative standard deviation is shown in **Figure 7(A)** as well. Variations between the mean friction forces on three independently modified surfaces were found to be smaller than the variations in friction force on one surface. The friction coefficients are calculated from the slopes of the data in **Figure 7(B)**. At zero load a small but nonzero friction results from the adhesion between probe and monolayer. The magnitude of this apparent adhesion, obtained by extrapolating to zero friction force, is lower than the adhesion found in normal force measurements

(**Figure 6**). This is probably due to the weak stick-slip nature of the frictional motion, for which the mean friction force can be lower than for smooth sliding.[78, 79]

This friction at zero load decreases with increasing fluorine content, in agreement with the adhesion measurements. For **F0**-based monolayers a friction coefficient of $5.7 \cdot 10^{-2}$ is found, in good agreement with the results for SAMs on gold.[52] Upon increasing the fluorine content in the monolayers, the friction coefficient decreases to the rather low value of $1.2 \cdot 10^{-2}$ for **F17**-based monolayers. These values are comparable with data reported for $C_{16}H_{33}$ thiol monolayers on Au ($3.0 \cdot 10^{-3}$), and $C_{16}H_{33}$ alcohol monolayers on silicon ($1.3 \cdot 10^{-2}$).[80] Interestingly, for SAMs on Au the friction coefficient goes up with an increase in fluorination [81] or shows no change,[52] in marked contrast with our data. Kim et al. have summarized the factors that can influence friction: (i) chemical structure and binding to organic molecule to substrate, (ii) packing density and order of monolayer, (iii) gauche conformation and or surface coverage, (iv) mechanical properties such as elastic constant, rigidity of the monolayer, (v) terminal polar or non-polar functional groups, and (vi) surface dipole orientations.[66, 82] In this case, the fluorine-rich monolayers (especially **F9** and **F17**) are expected to have a lower polarizability at their surface, as a result of the dipole orientation of the last fluorinated carbon and the first methylene group (R-**CH_2-CF_2**-R^1), are densely packed and display a high short-range organization, leading to an overall low friction coefficient.

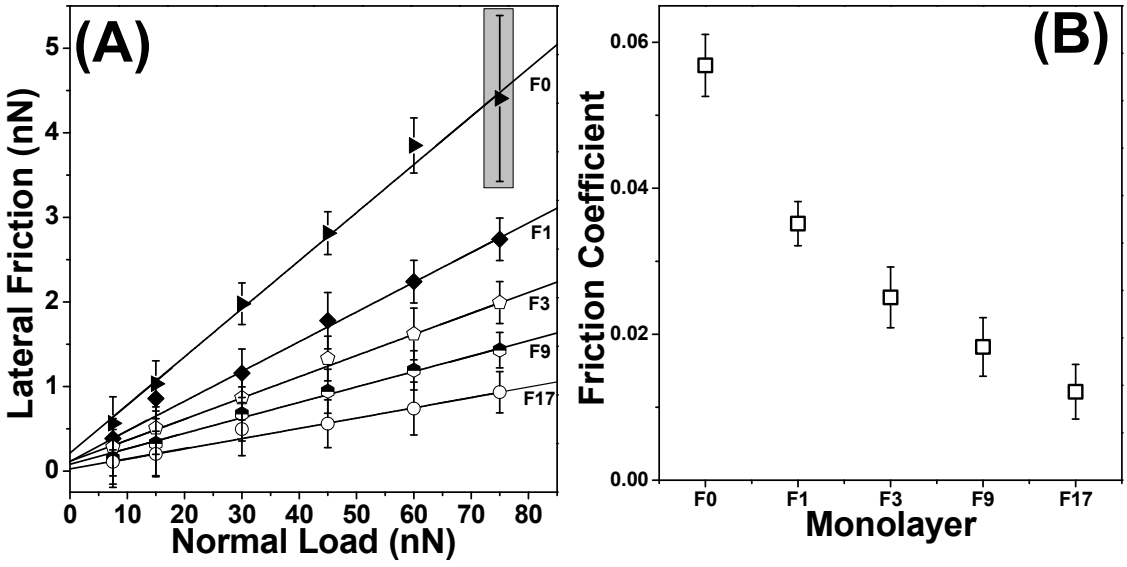

Figure 7. (A) Lateral friction force of fluorinated SAMs on Si(111), as a function of applied normal load. The error bars represent the standard deviation in mean friction force between three independently modified surfaces. The highlighted error bar at a normal load of 75 nN shows the relative variation in the friction force on a single surface (see *Supporting Information S.4.8* Figure S5).

(B) The friction coefficients, obtained from the slope of the friction force versus normal load, for different monolayers.

4.4.5 Molecular Modeling

To substantiate the optimum substitution percentages of the fluoro-hydro alkyne-derived monolayers on H-Si(111), and to investigate the structural differences between different fluorinated monolayers, models of the monolayers were studied by molecular mechanics (see *Supporting Information S.4.9* **Figure S6-S7**). Packing energies of SAMs on H-Si(111) for different surface coverage are depicted in **Figure 8**. The average packing energy per chain was then calculated according to the literature,[43, 54] and the optimal surface coverage obtained after fitting to a parabolic function. The optimum surface coverage decreases from 56% for **F0**, to 42% for **F17**, due to the larger cross section of the CF_2/CF_3 moieties. These values are confirmed by the experimentally determined monolayer thicknesses (displayed in **Table 1**), with a clear trend in the direction of greater surface coverage for the **F0** as compared to the F17.

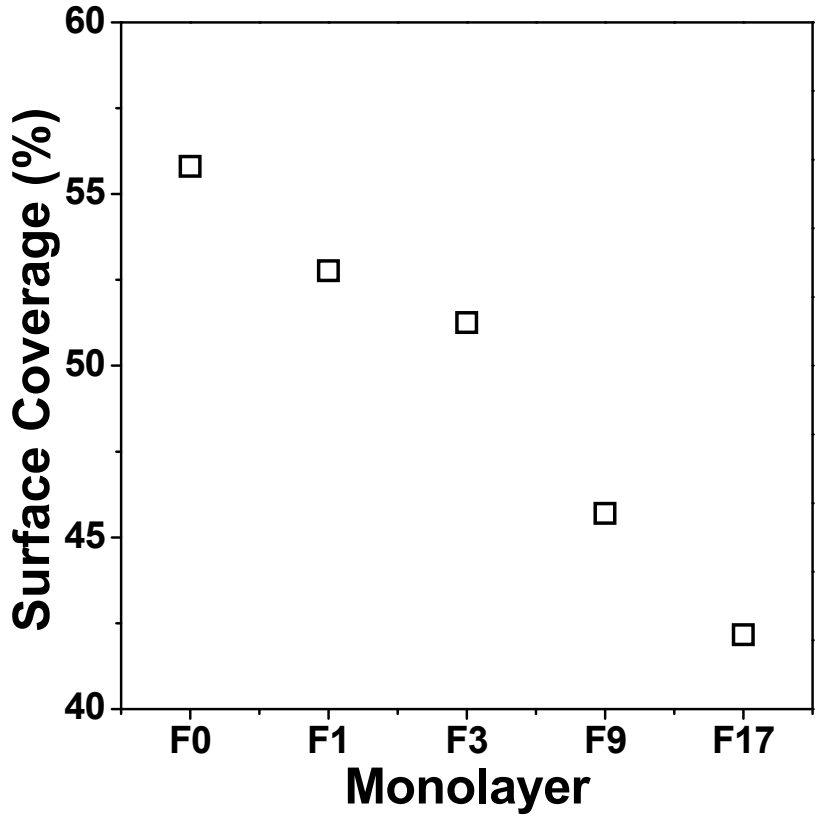

Figure 8. Surface coverage for fluoro-hydro alkyne-derived monolayers **F0** to **F17** on H-Si(111).

4.5 CONCLUSIONS

Partially fluorinated, Si-CH=C bound monolayers on oxide-free Si(111) surfaces display an extremely low surface tension and adhesion. Such self-assembled organic monolayers are uniform and densely packed, and characterized by a high degree of short-range ordering. This set of properties yields a highly uniform, upward presentation of CF_3 moieties, yielding this low interaction with the outside world, as evidenced by a critical surface tension of 5.6±0.21 mN/m, adhesion forces of 3.2±0.03 mJ/m^2 and a friction coefficient of $1.2 \cdot 10^{-2}$ for an **F17** monolayer (Si-(HC=CH)-$(CH_2)_6$-C_8F_{17}). Each of these values is either the lowest currently measured for any flat surface, or close to it. The present study suggests that fluoro-hydro alkyne-derived monolayers on silicon surfaces significantly expand the scope of strong covalently bound nanometer monolayers and display significant potential in MEMS/NEMS applications.

4.6 REFERENCES

1. Hans-Jürgen Butt, M. K., *Surface and Interfacial Forces*. Wiley-VCH: 2010; p 436.
2. Israelachvili, J. N., In *Intermolecular and Surface Forces*, Third ed.; Elsevier Inc.: 2010; pp 253-289.
3. Kristiansen, K.; Zeng, H.; Wang, P.; Israelachvili, J. N., Microtribology of Aqueous Carbon Nanotube Dispersions. *Advanced Functional Materials* **2011,** 21, (23), 4555-4564.
4. Ren, S. L.; Yang, S. R.; Wang, J. Q.; Liu, W. M.; Zhao, Y. P., Preparation and Tribological Studies of Stearic Acid Self-assembled Monolayers on Polymer-coated Silicon Surface. *Chemistry of Materials* **2004,** 16, (3), 428-434.
5. Palacio, M.; Bhushan, B., Ultrathin Wear-Resistant Ionic Liquid Films for Novel MEMS/NEMS Applications. *Advanced Materials* **2008,** 20, (6), 1194-1198.
6. Prioli, R.; Jacobsohn, L. G.; da Costa, M.; Freire, F. L., Nanotribological Properties of Amorphous Carbon-Fluorine Films. *Tribology Letters* **2003,** 15, (3), 177-180.
7. Tsukruk, V. V., Molecular Lubricants and Glues for Micro- and Nanodevices. *Advanced Materials* **2001,** 13, (2), 95-108.
8. Bhushan, B.; Israelachvili, J. N.; Landman, U., Nanotribology: Friction, Wear and Lubrication at the Atomic Scale. *Nature* **1995,** 374, (6523), 607-616.
9. McGuiggan, P. M., Friction and Adhesion Measurements Between a Fluorocarbon Surface and a Hydrocarbon Surface in Air. *Journal of Adhesion* **2004,** 80, (5), 395-408.
10. Socoliuc, A.; Gnecco, E.; Maier, S.; Pfeiffer, O.; Baratoff, A.; Bennewitz, R.; Meyer, E., Atomic-Scale control of Friction by Actuation of Nanometer-Sized Contacts. *Science* **2006,** 313, (5784), 207-210.
11. Carpick, R. W.; Salmeron, M., Scratching the Surface: Fundamental Investigations of Tribology with Atomic Force Microscopy. *Chemical Reviews* **1997,** 97, (4), 1163-1194.
12. Mo, Y. F.; Turner, K. T.; Szlufarska, I., Friction Laws at the Nanoscale. *Nature* **2009,** 457, (7233), 1116-1119.

13. Scheres, L.; Giesbers, M.; Zuilhof, H., Organic Monolayers onto Oxide-Free Silicon with Improved Surface Coverage: Alkynes versus Alkenes. *Langmuir* **2010,** 26, (7), 4790-4795.
14. Ng, A.; Ciampi, S.; James, M.; Harper, J. B.; Gooding, J. J., Comparing the Reactivity of Alkynes and Alkenes on Silicon (100) Surfaces. *Langmuir* **2009,** 25, (24), 13934-13941.
15. Puniredd, S. R.; Assad, O.; Haick, H., Highly Stable Organic Monolayers for Reacting Silicon with further Functionalities: The Effect of the C-C Bond Nearest the Silicon Surface. *Journal of the American Chemical Society* **2008,** 130, (41), 13727-13734.
16. Halik, M.; Klauk, H.; Zschieschang, U.; Schmid, G.; Dehm, C.; Schutz, M.; Maisch, S.; Effenberger, F.; Brunnbauer, M.; Stellacci, F., Low-voltage Organic Transistors with an Amorphous Molecular Gate Dielectric. *Nature* **2004,** 431, (7011), 963-966.
17. Zigah, D.; Herrier, C.; Scheres, L.; Giesbers, M.; Fabre, B.; Hapiot, P.; Zuilhof, H., Tuning the Electronic Communication between Redox Centers Bound to Insulating Surfaces. *Angewandte Chemie-International Edition* **2010,** 49, (18), 3157-3160.
18. Hunger, R.; Fritsche, R.; Jaeckel, B.; Jaegermann, W.; Webb, L. J.; Lewis, N. S., Chemical and Electronic Characterization of Methyl-terminated Si(111) Surfaces by High-Resolution Synchrotron Photoelectron Spectroscopy. *Phys. Rev. B* **2005,** 72, (4), 045317.
19. Faucheux, A.; Gouget-Laemmel, A. C.; de Villeneuve, C. H.; Boukherroub, R.; Ozanam, F.; Allongue, P.; Chazalviel, J. N., Well-defined Carboxyl-terminated Alkyl Monolayers Grafted onto H-Si(111): Packing Density from a Combined AFM and Quantitative IR Study. *Langmuir* **2006,** 22, (1), 153-162.
20. Maboudian, R.; Ashurst, W. R.; Carraro, C., Tribological Challenges in Micromechanical Systems. *Tribology Letters* **2002,** 12, (2), 95-100.
21. Seitz, O.; Vilan, A.; Cohen, H.; Hwang, J.; Haeming, M.; Schoell, A.; Umbach, E.; Kahn, A.; Cahen, D., Doping Molecular Monolayers: Effects on Electrical Transport Through Alkyl Chains on Silicon. *Advanced Functional Materials* **2008,** 18, (14), 2102-2113.
22. Böcking, T.; Kilian, K. A.; Gaus, K.; Gooding, J. J., Modifying Porous Silicon with Self-Assembled Monolayers for Biomedical Applications: The Influence of Surface Coverage on Stability and Biomolecule Coupling. *Advanced Functional Materials* **2008,** 18, (23), 3827-3833.
23. Li, Y.; Calder, S.; Yaffe, O.; Cahen, D.; Haick, H.; Kronik, L.; Zuilhof, H., Hybrids of Organic Molecules and Flat, Oxide-Free Silicon: High-Density Monolayers, Electronic Properties, and Functionalization. *Langmuir* **2012,** 28, (26), 9920-9929.
24. Faucheux, A.; Gouget-Laemmel, A. C.; Allongue, P.; de Villeneuve, C. H.; Ozanam, F.; Chazalviel, J. N., Mechanisms of Thermal Decomposition of Organic Monolayers Grafted on (111) Silicon. *Langmuir* **2007,** 23, (3), 1326-1332.
25. Collins, G.; Kolesnik, M.; Krstic, V.; Holmes, J. D., Germanium Nanowire Synthesis from Fluorothiolate-Capped Gold Nanoparticles in Supercritical Carbon Dioxide. *Chemistry of Materials* **2010,** 22, (18), 5235-5243.
26. Mitsuya, M.; Sato, N., Energy Shift for Core Electron Levels of Chemisorbed Molecules Observed by X-ray Photoelectron Spectroscopy in the Course of Monolayer Growth on a Si(111) Surface. *Langmuir* **1999,** 15, (6), 2099-2102.
27. Cheng, Y. A.; Zheng, B.; Chuang, P. H.; Hsieh, S. C., Solvent Effects on Molecular Packing and Tribological Properties of Octadecyltrichlorosilane Films on Silicon. *Langmuir* **2010,** 26, (11), 8256-8261.
28. Colorado, R.; Lee, T. R., Wettabilities of Self-Assembled Monolayers on Gold Generated from Progressively Fluorinated Alkanethiols. *Langmuir* **2003,** 19, (8), 3288-3296.

29. Mezger, M.; Sedlmeier, F.; Horinek, D.; Reichert, H.; Pontoni, D.; Dosch, H., On the Origin of the Hydrophobic Water Gap: An X-ray Reflectivity and MD Simulation Study. *Journal of the American Chemical Society* **2010,** 132, (19), 6735-6741.
30. Rodenstein, M.; Zurcher, S.; Tosatti, S. G. P.; Spencer, N. D., Fabricating Chemical Gradients on Oxide Surfaces by Means of Fluorinated, Catechol-Based, Self-Assembled Monolayers. *Langmuir* **2010,** 26, (21), 16211-16220.
31. Tamada, K.; Ishida, T.; Knoll, W.; Fukushima, H.; Colorado, R.; Graupe, M.; Shmakova, O. E.; Lee, T. R., Molecular Packing of Semifluorinated Alkanethiol Self-assembled Monolayers on Gold: Influence of Alkyl Spacer Length. *Langmuir* **2001,** 17, (6), 1913-1921.
32. te Riet, J.; Smit, T.; Coenen, M. J. J.; Gerritsen, J. W.; Cambi, A.; Elemans, J.; Speller, S.; Figdor, C. G., AFM Topography and Friction Studies of Hydrogen-Bonded Bilayers of Functionalized Alkanethiols. *Soft Matter* **2010,** 6, (15), 3450-3454.
33. Ciampi, S.; Harper, J. B.; Gooding, J. J., Wet Chemical Routes to the Assembly of Organic Monolayers on Silicon Surfaces via the Formation of Si-C bonds: Surface Preparation, Passivation and Functionalization. *Chem. Soc. Rev.* **2010,** 39, (6), 2158-2183.
34. Gooding, J. J.; Ciampi, S., The molecular level modification of surfaces: from self-assembled monolayers to complex molecular assemblies. *Chem. Soc. Rev.* **2011,** 40, (5), 2704-2718.
35. Rijksen, B.; Caipa Campos, M. A.; Paulusse, J. M. J.; Zuilhof, H., Silicon Radical Surface Chemistry. In *Encyclopedia of Radicals in Chemistry, Biology and Materials*, John Wiley & Sons, Ltd: 2012; p 2081.
36. Buriak, J. M., Silicon-Carbon Bonds on Porous Silicon Surfaces. *Advanced Materials* **1999,** 11, (3), 265-267.
37. Buriak, J. M., Organometallic Chemistry on Silicon and Germanium Surfaces. *Chemical Reviews* **2002,** 102, (5), 1271-1308.
38. Hurley, P. T.; Ribbe, A. E.; Buriak, J. M., Nanopatterning of Alkynes on Hydrogen-Terminated Silicon Surfaces by Scanning Probe-induced Cathodic Electrografting. *Journal of the American Chemical Society* **2003,** 125, (37), 11334-11339.
39. de Smet, L.; Stork, G. A.; Hurenkamp, G. H. F.; Sun, Q. Y.; Topal, H.; Vronen, P. J. E.; Sieval, A. B.; Wright, A.; Visser, G. M.; Zuilhof, H.; Sudhölter, E. J. R., Covalently Attached Saccharides on Silicon Surfaces. *Journal of the American Chemical Society* **2003,** 125, (46), 13916-13917.
40. Sun, Q. Y.; de Smet, L.; van Lagen, B.; Giesbers, M.; Thune, P. C.; van Engelenburg, J.; de Wolf, F. A.; Zuilhof, H.; Sudhölter, E. J. R., Covalently Attached Monolayers on Crystalline Hydrogen-Terminated Silicon: Extremely Mild Attachment by Visible Light. *Journal of the American Chemical Society* **2005,** 127, (8), 2514-2523.
41. Sun, Q. Y.; de Smet, L.; van Lagen, B.; Wright, A.; Zuilhof, H.; Sudhölter, E. J. R., Covalently Attached Monolayers on Hydrogen Terminated Si(100): Extremely Mild Attachment by Visible Light. *Angewandte Chemie-International Edition* **2004,** 43, (11), 1352-1355.
42. Scheres, L.; Arafat, A.; Zuilhof, H., Self-assembly of High-Quality Covalently Bound Organic Monolayers onto Silicon. *Langmuir* **2007,** 23, (16), 8343-8346.
43. Scheres, L.; Rijksen, B.; Giesbers, M.; Zuilhof, H., Molecular Modeling of Alkyl and Alkenyl Monolayers on Hydrogen-Terminated Si(111). *Langmuir* **2011,** 27, (3), 972-980.

44. Linford, M. R.; Fenter, P.; Eisenberger, P. M.; Chidsey, C. E. D., Alkyl Monolayers On Silicon Prepared From 1-Alkenes And Hydrogen-Terminated Silicon. *J. Am. Chem. Soc.* **1995,** 117, (11), 3145-3155.
45. Sieval, A. B.; Linke, R.; Zuilhof, H.; Sudhölter, E. J. R., High-Quality Alkyl Monolayers on Silicon Surfaces. *Advanced Materials* **2000,** 12, (19), 1457-1460.
46. Rijksen, B.; van Lagen, B.; Zuilhof, H., Mimicking the Silicon Surface: Reactivity of Silyl Radical Cations toward Nucleophiles. *Journal of the American Chemical Society* **2011,** 133, (13), 4998-5008.
47. Allongue, P.; de Villeneuve, C. H.; Morin, S.; Boukherroub, R.; Wayner, D. D. M., The Preparation of Flat H-Si(111) Surfaces in 40% NH4F Revisited. *electrochemica acta* **2000,** 45, 4591-4598.
48. Geer, R. E.; Stenger, D. A.; Chen, M. S.; Calvert, J. M.; Shashidhar, R.; Jeong, Y. H.; Pershan, P. S., X-Ray and Ellipsometric Studies of Self-Assembled Monolayers of Fluorinated Chlorosilanes. *Langmuir* **1994,** 10, (4), 1171-1176.
49. Banerjee, S.; Mulder, P.; Kleijn, J. M.; Cohen Stuart, M. A., Effect of Surface Roughness and Softness on Water Capillary Adhesion in Apolar Media. *The Journal of Physical Chemistry A* **2012,** 116, (25), 6481-6488.
50. Hutter, J. L.; Bechhoefer, J., Calibration of Atomic-Force Microscope Tips. *Rev. Sci. Instrum.* **1993,** 64, (7), 1868-1873.
51. Stark, R. W.; Drobek, T.; Heckl, W. M., Thermomechanical Noise of a Free v-shaped Cantilever for Atomic-Force Microscopy. *Ultramicroscopy* **2001,** 86, (1-2), 207-215.
52. Te Riet, J.; Smit, T.; Gerritsen, J. W.; Cambi, A.; Elemans, J.; Figdor, C. G.; Speller, S., Molecular Friction as a Tool to Identify Functionalized Alkanethiols. *Langmuir* **2010,** 26, (9), 6357-6366.
53. Liu, W. H.; Bonin, K.; Guthold, M., Easy and Direct Method for Calibrating Atomic Force Microscopy Lateral Force Measurements. *Rev. Sci. Instrum.* **2007,** 78, (6), 063707.
54. Rijksen, B.; Pujari, S. P.; Scheres, L.; van Rijn, C. J. M.; Baio, J. E.; Weidner, T.; Zuilhof, H., Hexadecadienyl Monolayers on Hydrogen-Terminated Si(111): Faster Monolayer Formation and Improved Surface Coverage Using the Enyne Moiety. *Langmuir* **2012,** 28, (16), 6577-6588.
55. Frechette, J.; Maboudian, R.; Carraro, C., Thermal Behavior of Perfluoroalkylsiloxane Monolayers on the Oxidized Si(100) Surface. *Langmuir* **2006,** 22, (6), 2726-2730.
56. van de Grampel, R. D.; Ming, W.; Gildenpfennig, A.; Laven, J.; Brongersma, H. H.; de With, G.; van der Linde, R., Quantification of Fluorine Density in the Outermost Atomic Layer. *Langmuir* **2004,** 20, (1), 145-149.
57. Song, X. Y.; Zhai, J.; Wang, Y. L.; Jiang, L., Fabrication of Superhydrophobic Surfaces by Self-assembly and their Water-Adhesion Properties. *Journal of Physical Chemistry B* **2005,** 109, (9), 4048-4052.
58. Bain, C. D.; Troughton, E. B.; Tao, Y. T.; Evall, J.; Whitesides, G. M.; Nuzzo, R. G., Formation of Monolayer Films by the Spontaneous Assembly of Organic Thiols from Solution onto Gold. *Journal of the American Chemical Society* **1989,** 111, (1), 321-335.
59. Folkers, J. P.; Laibinis, P. E.; Whitesides, G. M., Self-Assembled Monolayers of Alkanethiols on Gold: Comparisons of Monolayers Containing Mixtures of Short- and Long-chain Constituents with Methyl and Hydroxymethyl Terminal Groups. *Langmuir* **1992,** 8, (5), 1330-1341.

60. Zisman W, A., Relation of the Equilibrium Contact Angle to Liquid and Solid Constitution. In *Contact Angle, Wettability, and Adhesion*, AMERICAN CHEMICAL SOCIETY: 1964; Vol. 43, pp 1-51.
61. de Gennes, P. G., Wetting: Statics and Dynamics. *Rev. Mod. Phys.* **1985,** 57, (3), 827-863.
62. Baier, R. E.; Shafrin, E. G.; Zisman, W. A., Adhesion: Mechanisms That Assit or Impede It. *Science* **1968,** 162, (3860), 1360-1368.
63. Nishino, T.; Meguro, M.; Nakamae, K.; Matsushita, M.; Ueda, Y., The Lowest Surface Free Energy Based on −CF3 Alignment. *Langmuir* **1999,** 15, (13), 4321-4323.
64. Ulman, A., Formation and Structure of Self-assembled Monolayers. *Chemical Reviews* **1996,** 96, (4), 1533-1554.
65. Schonherr, H.; Ringsdorf, H.; Jaschke, M.; Butt, H. J.; Bamberg, E.; Allinson, H.; Evans, S. D., Self-assembled Monolayers of Symmetrical and Mixed Alkyl Fluoroalkyl Disulfides on Gold .2. Investigation of Thermal Stability and Phase Separation. *Langmuir* **1996,** 12, (16), 3898-3904.
66. Kim, H. I.; Koini, T.; Lee, T. R.; Perry, S. S., Systematic Studies of the Frictional Properties of Fluorinated Monolayers with Atomic Force Microscopy: Comparison of CF_3- and CH_3-Terminated Films. *Langmuir* **1997,** 13, (26), 7192-7196.
67. Yang, M.; Teeuwen, R. L. M.; Giesbers, M.; Baggerman, J.; Arafat, A.; de Wolf, F. A.; van Hest, J. C. M.; Zuilhof, H., One-Step Photochemical Attachment of NHS-Terminated Monolayers onto Silicon Surfaces and Subsequent Functionalization. *Langmuir* **2008,** 24, (15), 7931-7938.
68. Hostetler, M. J.; Stokes, J. J.; Murray, R. W., Infrared Spectroscopy of Three-Dimensional Self-Assembled Monolayers: N-alkanethiolate Monolayers on Gold Cluster Compounds. *Langmuir* **1996,** 12, (15), 3604-3612.
69. Snyder, R. G.; Strauss, H. L.; Elliger, C. A., Carbon-Hydrogen Stretching Modes and the Structure of n-alkyl Chains. 1. Long, Disordered Chains. *Journal of Physical Chemistry* **1982,** 86, (26), 5145-5150.
70. Andersson, M. P.; Uvdal, P., New Scale Factors for Harmonic Vibrational Frequencies Using the B3LYP Density Functional Method with the Triple-ζ Basis Set 6-311+G(d,p). *The Journal of Physical Chemistry A* **2005,** 109, (12), 2937-2941.
71. Shaporenko, A.; Cyganik, P.; Buck, M.; Ulman, A.; Zharnikov, M., Self-Assembled Monolayers of Semifluorinated Alkaneselenolates on Noble Metal Substrates. *Langmuir* **2005,** 21, (18), 8204-8213.
72. Sheparovych, R.; Motornov, M.; Minko, S., Low Adhesive Surfaces that Adapt to Changing Environments. *Adv. Mater.* **2009,** 21, (18), 1840-1844.
73. Butt, H. J.; Kappl, M., Normal Capillary Forces. *Advances in Colloid and Interface Science* **2009,** 146, (1-2), 48-60.
74. Bhushan, B., *Handbook of Nanotechnology*. 2 ed.; Springer-Verlag New York, LLC: 2007; p 1222.
75. Maugis, D., Adhesion of Spheres - The JRK-DMT Transition using a Dugdale Model. *Journal of Colloid and Interface Science* **1992,** 150, (1), 243-269.
76. Shulha, H.; Kovalev, A.; Myshkin, N.; Tsukruk, V. V., Some Aspects of AFM Nanomechanical Probing of Surface Polymer Films. *European Polymer Journal* **2004,** 40, (5), 949-956.
77. Lyklema, J., *Fundamentals of Interface and Colloid Science: Fundamentals*. Academic Press Ltd, London. : 1991; Vol. 1.

78. Urbakh, M.; Klafter, J.; Gourdon, D.; Israelachvill, J., The nonlinear nature of friction. *Nature* **2004,** 430, (6999), 525-528.
79. Wu-Bavouzet, F.; Clain-Burckbuchler, J.; Buguin, A.; De Gennes†, P. G.; Brochard-Wyart, F., Stick-Slip: Wet Versus Dry. *The Journal of Adhesion* **2007,** 83, (8), 761-784.
80. Kim, H. I.; Boiadjiev, V.; Houston, J. E.; Zhu, X. Y.; Kiely, J. D., Tribological Properties of Self-Assembled Monolayers on Au, SiOx and Si Surfaces. *Tribology Letters* **2001,** 10, (1-2), 97-101.
81. Houston, J. E.; Doelling, C. M.; Vanderlick, T. K.; Hu, Y.; Scoles, G.; Wenzl, I.; Lee, T. R., Comparative Study of the Adhesion, Friction, and Mechanical Properties of CF3- and CH3-Terminated Alkanethiol Monolayers. *Langmuir* **2005,** 21, (9), 3926-3932.
82. Park, B.; Lorenz, C. D.; Chandross, M.; Stevens, M. J.; Grest, G. S.; Borodin, O. A., Frictional Dynamics of Fluorine-Terminated Alkanethiol Self-Assembled Monolayers. *Langmuir* **2004,** 20, (23), 10007-10014.

Supporting Information to Chapter 4

Table of Contents

Supporting Information to Chapter 4 119
S.4.1 Synthesis and characterization. 120
S.4.1.1 General procedures. 120
S.4.2 Synthesis of 13,13,14,14,15,15,16,16,16-Nonafluoro-hexadec-1-yne (F9) 121
S.4.2.1 11,11,12,12,13,13,14,14,14-nonafluoro-9-iodotetradecan-1-ol (1a). 121
S.4.2.2 11,11,12,12,13,13,14,14,14-Nonafluoro-tetradecan-1-ol (1b). 122
S.4.2.3 Toluene-4-sulfonic acid 11,11,12,12,13,13,14,14,14-nonafluoro-tetradecyl ester (1c). 122
S.4.2.4 13,13,14,14,15,15,16,16,16-nonafluoro-hexadec-1-yne (1d). 123
S.4.3 9,9,10,10,11,11,12,12,13,13,14,14,15,15,16,16,16-heptadecafluorohexadec-1-yne (F17). 124
S.4.3.1 7,7,8,8,9,9,10,10,11,11,12,12,13,13,14,14,14-heptadecafluoro-5-iodotetradecan-1-ol (2a). 124
S.4.3.2 7,7,8,8,9,9,10,10,11,11,12,12,13,13,14,14,14-heptadecafluorotetradecan-1-ol (2b). 125
S.4.3.3 7,7,8,8,9,9,10,10,11,11,12,12,13,13,14,14,14-heptadecafluorotetradecyl 4-methylbenzenesulfonate (2c). 125
S.4.3.4 9,9,10,10,11,11,12,12,13,13,14,14,15,15,16,16,16-heptadecafluorohexadec-1-yne (2d). 125
S.4.4 16,16,16-trifluorohexadec-1-yne (F3) 126
S.4.4.1 2-(Pentadec-2-yn-1-yloxy)tetrahydro-2H-pyran (3a). 127
S.4.4.2 Pentadec-2-yn-1-ol (3b). 127
S.4.4.3 Pentadec-14-yn-1-ol (3c). 128
S.4.4.4 Pentadec-14-yn-1-yl 4-methylbenzenesulfonate (3d). 128
S.4.4.5 15-iodopentadec-1-yne (3e). 128
S.4.4.6 16,16,16-trifluorohexadec-1-yne (4f). 129
S.4.5 16-fluorohexadec-1-yne 129
S.4.6 Contact angle 130
S.4.7 XPS and DFT calculation of C1s and F1s binding energy. 130
S.4.7.1 DFT calculation of XPS chemical shifts of carbon and fluorine atoms 130

S.4.8 Friction image 132
S.4.9 Molecular modeling (Material studio)..... 132
S.4.10 References 134

S.4.1 Synthesis and characterization.

S.4.1.1 General procedures.

Commercially available reagents were purchased and used as supplied. Dichloromethane was distilled from $CaCl_2$ stored away from bright light in a brown bottle with Linde type 4Å molecular sieves, in an atmosphere of dry argon. Diethyl ether, heptane, ethyl acetate, DMSO (dimethyl sulfoxide), acetic acid were degassed before use. Reactions were monitored by thin-layer chromatography (TLC) carried out on 0.25 mm silica gel foils 60 F254 plates using UV light as visualizing agent and ceric ammonium molybdate (CAM) and vanilla stain and heat as developing agents.

^{1}H NMR (400 MHz), ^{13}C NMR (100 MHz) and ^{19}F NMR (376 MHz) spectra were recorded on a Bruker 400 spectrometer and calibrated using residual undeuterated solvent ($CDCl_3$: δ_H = 7.26 ppm, δ_C = 77.36 ppm) as an internal reference.[1] The following abbreviations were used to designate the multiplicities: s = singlet, d = doublet, t = triplet, q = quartet, quin = quintet, m = multiplet. Elemental analysis was carried out using DART (Direct Analysis in Real Time) mass spectrometer[2-4] Samples for DART was prepared by adding a solution of the corresponding compound in toluene (1 mL, c=10 mg/mL). IR spectra (Bruker). were recorded in the range of 400-4000 cm^{-1} for the synthesized compounds in a KBr disk Heptadecafluoro-1-iodooctane (98%) was purchased from Fluka, 2,2-azobis(isobutyronitrile)(AIBN) was purchased from Acros and recrystallized in acetone, nonafluoro-1-iodobutane (98%), 5-hexen-1-ol (98%), 9-decen-1-ol (98%), and lithium acetylide ethylenediamine complex (90%), was purchased from Merck used as received.

S.4.2 Synthesis of 13,13,14,14,15,15,16,16,16-Nonafluoro-hexadec-1-yne (F9)

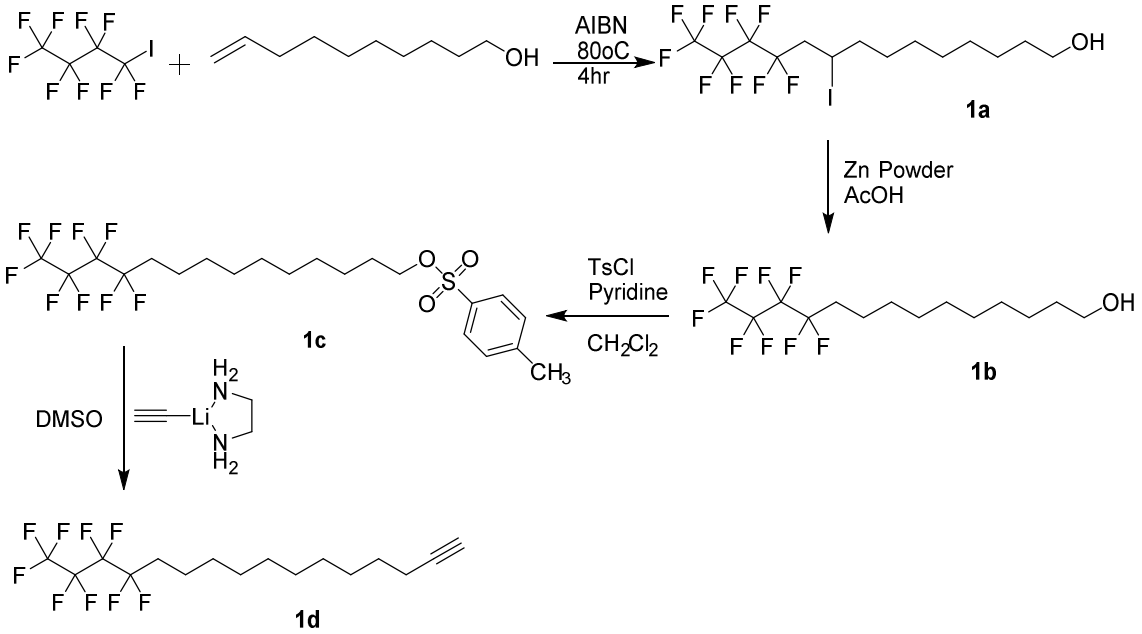

Scheme S1. Synthetic routes for 13,13,14,14,15,15,16,16,16-Nonafluoro-hexadec-1-yne (F9).

S.4.2.1 11,11,12,12,13,13,14,14,14-nonafluoro-9-iodotetradecan-1-ol (1a).

Nonafluoro-1-iodobutane (15.0 g, 43.4 mmol), 9-decen-1-ol (6.64 g, 42.5 mmol) and 2,2-azobis(isobutyronitrile) (2.08 g, 12.69 mmol) was added without using any solvent under a flow of argon, in a two necked 250 mL round bottom flask equipped with a condenser and heated at 65 ºC for 1 hr. The mixture was stirred overnight at 80 ºC. The progress of the reaction was monitored by thin layer chromatography. After completion of the reaction flask has cooled to room temperature. The product was purified by silica column chromatography (Rf = 0.50, heptane/ethyl acetate 1:1.5). the product was obtained as clear oil as 96% yield 20.45 gm, 40.7 mmol, of 11,11,12,12,13,13,14,14,14-nonafluoro-9-iodotetradecan-1-ol (**1a**):

1H NMR (400 MHz, CDCl3,) δ in ppm: 4.36-4.29 (m, 1H, CHI), 3.65-3.62(t, 2H, CH2-OH), 2.99-2.70 (m, 2H, CF2-CH2), 1.88-1.68 (m, 2H, alkyl), 1.64-1.54 (m, 4H, alkyl), 1.44-1.33 (m, 9H, alkyl, OH). 13C NMR (100 MHz, CDCl3, δ ppm): 122.08-105.94 (m, 4C, CF3-CF2-CF2-CF2), 63.09 (s, 1C, CH2-OH), 41.96, 41.76, 41.55 (t, 1C, CF_2-CH_2), 40.48, 40.46 (d, 1C, alkyl), 32.87 (s, 1C, alkyl), 29.66 (s, 1C, alkyl), 29.44, 29.42 (d, 2C, alkyl), 28.55 (s, 1C, alkyl), 25.81 (s, 1C, alkyl), 20.83 (s, 1C, alkyl). FTIR

(neat, cm^{-1}): 3345 (CH_2-*OH*), 2931 (ν_a CH_2), 2879 (ν_s CH_2), 1235 (ν_a CF_2), 1135 (ν_a CF_2). HRMS (DART-TOF) $[M - H]^-$ calcd. for $C_{14}H_{19}F_9IO$, 501.0336; found, 501.0329.

S.4.2.2 11,11,12,12,13,13,14,14,14-Nonafluoro-tetradecan-1-ol (1b).

The (19.77 g, 39.36 mmol) of 11,11,12,12,13,13,14,14,14-nonafluoro-9-iodotetradecan-1-ol (**1a**) was dissolved in 100 ml of glacial acetic acid (HOAc). Zinc dust (7.55 g 118.10 mmol) was added at room temperature under argon. The mixture was stirred for 16 hr. The solution was then vacuum-filtered through a Buchner funnel, and 1.0 M NaOH was added to the acidic solution until the mixture exhibited a neutral pH as indicated by pH paper. The mixture was extracted with diethyl ether (3 x 100 mL), and the solution was washed with water (2 x 100 mL), saturated aqueous $NaHCO_3$ solution (1 x 100 mL), and brine (1 x 100 mL), and then dried over $MgSO_4$. Removal of the solvent afforded the crude **1b**. The crude product was purified by column chromatography on silica gel (R_f = 0.54, heptane/ethyl acetate 1:1). Yield 12.45 g, 33.10 mmol, 84% of 11,11,12,12,13,13,14,14,14-Nonafluoro-tetradecan-1-ol (**1b**) as white solid:

^{1}H NMR (400 MHz, $CDCl_3$, δ_{ppm}): 3.63-3.60 (t, 2H, C*H*$_2$-OH), 2.09-1.96 (m, 2H, CF_2-C*H*$_2$), 1.68 (s, 1H, -O*H*), 1.62-1.52(m, 4H, alkyl), 1.36-1.29 (m, 12H, alkyl). ^{13}C NMR (100 MHz, $CDCl_3$, δ_{ppm}): 122.23-105.77 (m, 4C, *C*F_3-*C*F_2-*C*F_2-*C*F_2), 63.10 (s, 1C, *C*H_2-OH), 32.91 (s, 1C, alkyl), 31.16, 30.93, 30.72 (t, 1C, CF_2-*C*H_2), 29.62, 29.52, 29.43, 29.33, 29.22 (m, 5C, alkyl), 25.87 (s, 1C, alkyl), 20.23, 20.20, 20.16 (t, 1C, alkyl). HRMS (DART-TOF) $[M - H]^-$ calcd for $C_{14}H_{20}F_9O$, 375.1370; found, 375.1367.

S.4.2.3 Toluene-4-sulfonic acid 11,11,12,12,13,13,14,14,14-nonafluoro-tetradecyl ester (1c).

To an oven-dried and argon-purged 250 mL round-bottom flask were added the 11,11,12,12,13,13,14,14,14-nonafluoro-tetradecan-1-ol (**1b**) (12.45 g, 33.10 mmol) at 0 ^{o}C in absolute dichloromethane (DCM) (40 mL) pyridine (5.33mL, 66.19 mmol) and the mixture was stirred at 25 °C for 10 min. The flask was cooled to 0 °C with an ice bath, and recrystallized p-toluenesulfonyl chloride (9.46 g, 49.64 mmol) was added to the reaction. The mixture was stirred at 0°C for 1 h, then kept at room temperature for 3 hr. The reaction was quenched with distilled water at 0 °C and warmed to 23 °C. The layers were separated, and the aqueous layer was extracted with ether. The combined organic layers were washed with brine and dried over MgSO4. The mixtures was sequentially washed with 2 N HCl (10 mL), saturated $NaHCO_3$ solution (2 x 25 mL) and (3 x 50 mL) water. The organic layer extract was dried ($MgSO_4$), concentrated in vacuo, and purification of the crude product by silica gel column chromatography (R_f = 0.52,

Heptane/EtOAc, 2:1) afforded 13.11 g, 24.72 mmol, 75% of the Toluene-4-sulfonic acid 11,11,12,12,13,13,14,14,14-nonafluoro-tetradecyl (**1c**) as a white solid: ^{1}H NMR (400 MHz, $CDCl_3$, δ_{ppm}): 7.80-7.78 (d, 2H, Ph), 7.34-7.33 (d, 2H, Ph), 4.04-4.00 (t, 2H, C*H*$_2$-OTs), 2.45 (s, 3H, Ph-C*H*$_3$), 2.11-1.97 (m, 2H, CF_2-C*H*$_2$), 1.67-1.55 (m, 4H, Alkyl), 1.38-1.24(m, 12H, alkyl). ^{13}C NMR (100 MHz, $CDCl_3$, δ_{ppm}): 144.75 (s, 1C, Ph), 133.49 (s, 1C, Ph), 129.93 (s, 1C, Ph), 128.03 (s, 1C, Ph), 121.88-105.34 (m, 4C, *C*F_3-*C*F_2-*C*F_2-*C*F_2), 70.79 (s, 1C, *C*H_2-OTs), 31.16, 30.94, 30.71 (t, 1C, CF_2-*C*H_2), 29.40, 29.33, 29.28, 29.19, 29.02, 28.98 (m, 6C, alkyl), 25.47 (s, 1C, alkyl), 21.74 (s, 1C, Ph-*C*H_3), 20.24, 20.21, 20.17 (t, 1C, alkyl). HRMS (DART-TOF) $[M - H]^-$ calcd for $C_{21}H_{26}O_3F_9S$, 529.1459; found, 529.1465.

S.4.2.4 13,13,14,14,15,15,16,16,16-nonafluoro-hexadec-1-yne (1d).

To an oven-dried, three-necked, round-bottom flask equipped with a magnetic stirring bar, argon line, pressure-equalizing dropping funnel and reflux condenser, protected from moisture by a calcium chloride-filled drying tube was flushed with argon and charged with lithium acetylide ethylenediamine (2.14 g, 23.23 mmol) dimethyl sulfoxide was then added to make the slurry ~2 M in lithium acetylide ethylenediamine (11 mL of DMSO). The solution was rapidly stirred under a dry argon atmosphere and the temperature was brought to 0 ^{o}C in ice bath. The toluene-4-sulfonic acid 11,11,12,12,13,13,14,14,14-nonafluoro-tetradecyl (**1c**) (9.47 g, 17.87 mmol) was dissolved in 20 mL dimethyl sulfoxide then added dropwise for 25 min with the temperature maintained 0 ^{o}C external cooling. When the addition was complete the reaction mixture was heated to 50 ^{o}C for four hours. The brown mixture was hydrolyzed with 60 mL of H_2O, and the aqueous phase was extracted with heptane (3 x 100 mL). The organic layer was washed with brine solution and dried over $MgSO_4$. The solvent was evaporated in vacuo to yield a colorless oil was obtained after by purification by silica gel column chromatography (R_f = 0.54, Heptane) afforded 5.53 g, 14.39 mmol, 80% of the 13,13,14,14,15,15,16,16,16-Nonafluoro-hexadec-1-yne (**1d**): ^{1}H NMR (400 MHz, $CDCl_3$, δ_{ppm}): 2.21-2.17 (m, 2H, Alkyl), 2.12-1.99 (m, 2H, CF_2-C*H*$_2$), 1.95-1.93 (t, 1H, C≡C-*H*), 1.64-1.50 (m, 4H, Alkyl), 1.42-1.31(m, 12H, alkyl). ^{13}C NMR (100 MHz, $CDCl_3$, δ_{ppm}): 121.89-105.36 (m, 4C, *C*F_3-*C*F_2-*C*F_2-*C*F_2), 84.88 (s, 1C, *C*≡C-H), 68.19 (s, 1C, C≡*C*-H), 31.18, 30.96, 30.73 (t, 1C, CF_2-*C*H_2), 29.51, 29.44, 29.33, 29.24, 29.19, (m, 5C, alkyl), 28.86 (s, 1C, alkyl), 28.62 (s, 1C, alkyl), 20.25, 20.22, 20.18 (t, 1C, alkyl). 18.54 (s, 1C, alkyl); HRMS (DART-TOF) $[M + H]^+$ calcd for $C_{16}H_{22}F_9$, 385.1578; found, 385.1560. ^{19}F NMR (500 MHz, $CDCl_3$,

δppm): -82.26, -82.28, -82.30 (triplet); -115.72, -115.75, -115.78, -115.81, -115.85 (pentet or quintet); -125.66 (singlet); -127.34, -127.22, -127.25(triplet).

S.4.3 9,9,10,10,11,11,12,12,13,13,14,14,15,15,16,16,16-heptadecafluorohexadec-1-yne (F17).

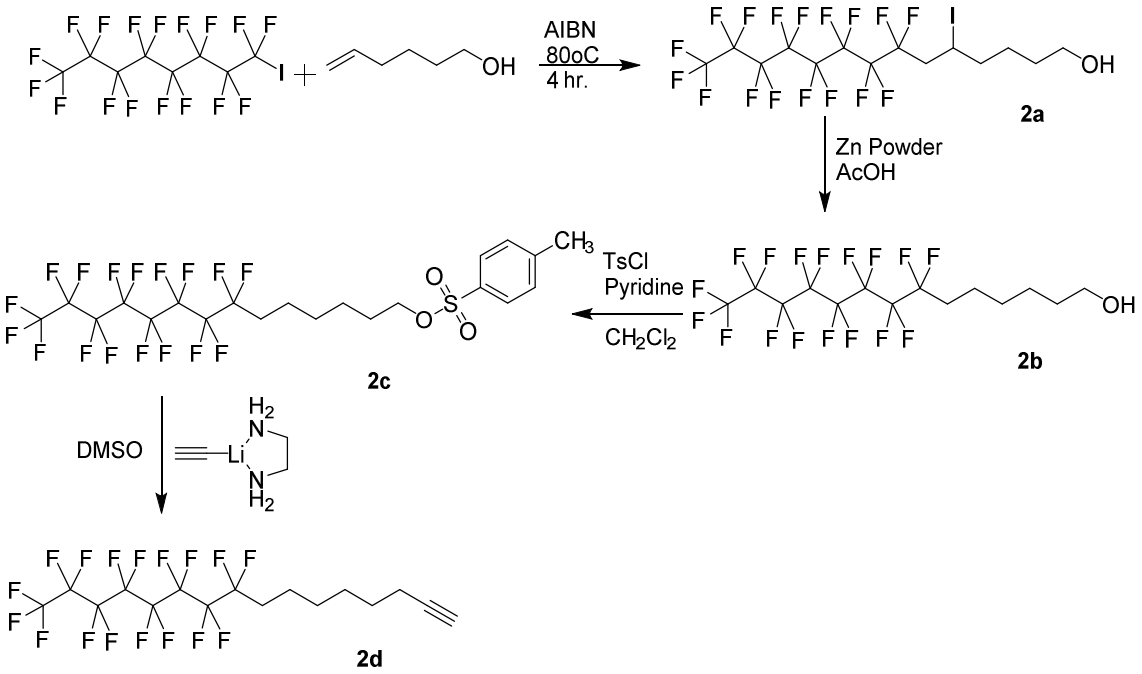

Scheme S2. Synthetic routes for 9,9,10,10,11,11,12,12,13,13,14,14,15,15,16,16,16-heptadecafluorohexadec-1-yne (F17).

S.4.3.1 7,7,8,8,9,9,10,10,11,11,12,12,13,13,14,14,14-heptadecafluoro-5-iodotetradecan-1-ol (2a).

The procedure described for 11,11,12,12,13,13,14,14,14-nonafluoro-9-iodotetradecan-1-ol (**1a**) was used with Heptadecafluoro-1-iodooctane (41.34 g 75.71 mmol) and 5-Hexen-1-ol (7.36 g, 73.45 mmol) to give 7,7,8,8,9,9,10,10,11,11,12,12,13,13,14,14,14-heptadecafluoro-5-iodotetradecan-1-ol (**2a**) as an off-white solid (38.73 g, 59.96 mmol, 82%): ^{1}H NMR (400 MHz, $CDCl_3$, δ_{ppm}): 4.37-4.30 (m, 1H, C*H*I), 3.70-3.3.66(q, 2H, C*H*$_2$-OH), 3.00-2.71 (m, 2H, CF_2-C*H*$_2$), 1.92-1.77 (m, 2H, alkyl), 1.69-1.47 (m, 5H, alkyl, OH). ^{13}C NMR (100 MHz, $CDCl_3$, δ_{ppm}): 121.93-105.64 (m, 8C, *C*F_3-*C*F_2-*C*F_2-*C*F_2-*C*F_2-*C*F_2-*C*F_2-*C*F_2), 62.65 (s, 1C, *C*H_2-OH), 42.07, 41.86, 41.66 (t, 1C, CF_2-*C*H_2), 40.24, 40.22 (d, 1C, alkyl), 31.69 (s, 1C, alkyl), 26.16 (s, 1C, alkyl), 20.53 (s, 1C, alkyl). HRMS (DART-TOF) $[M - H]^-$ calcd for $C_{14}H_{11}OF_{17}I$, 644.9583; found, 644.9587.

S.4.3.2 7,7,8,8,9,9,10,10,11,11,12,12,13,13,14,14,14-heptadecafluorotetradecan-1-ol (2b).

The procedure described for 11,11,12,12,13,13,14,14,14-Nonafluoro-tetradecan-1-ol (**1b**) was used with 7,7,8,8,9,9,10,10,11,11,12,12,13,13,14,14,14-heptadecafluoro-5-iodotetradecan-1-ol (36.75 g 56.89 mmol) and zinc powder (10.91 g, 107.67 mmol) to give 7,7,8,8,9,9,10,10,11,11,12,12,13,13,14,14,14-heptadecafluorotetradecan-1-ol (**2b**) as an off-white solid (27.87 g, 53.59 mmol, 94%): ^{1}H NMR (400 MHz, $CDCl_3$, δ_{ppm}): 3.66-3.63 (t, 2H, C*H*$_2$-OH), 2.12-1.99 (m, 2H, CF_2-C*H*$_2$), 1.68-1.52 (m, 4H, alkyl), 1.43-1.40 (m, 5H, alkyl). ^{13}C NMR (100 MHz, $CDCl_3$, δ_{ppm}): 122.17-105.29 (m, 8C, *C*F_3-*C*F_2-*C*F_2-*C*F_2-*C*F_2-*C*F_2-*C*F_2-*C*F_2), 62.90 (s, 1C, *C*H_2-OH), 32.60 (s, 1C, alkyl), 31.60, 31.00, 30.78 (t, 1C, CF_2-*C*H_2), 29.05 (m, 1C, alkyl), 25.59 (s, 1C, alkyl), 20.27 (t, 1C, alkyl). HRMS (DART-TOF) $[M - H]^-$ calcd for $C_{14}H_{12}F_{17}O$, 519.0617; found, 519.0616.

S.4.3.3 7,7,8,8,9,9,10,10,11,11,12,12,13,13,14,14,14-heptadecafluorotetradecyl 4-methylbenzenesulfonate (2c).

The procedure described for Toluene-4-sulfonic acid 11,11,12,12,13,13,14,14,14-nonafluoro-tetradecyl ester (**1c**) was used with 7,7,8,8,9,9,10,10,11,11,12,12,13,13, 14,14,14-heptadecafluorotetradecan-1-ol (**2b**) (10.00 g 19.23 mmol) and p-Toluenesulfonyl chloride (4.03 g, 21.15 mmol) to give 7,7,8,8,9,9,10,10,11,11,12,12, 13,13,14,14,14-heptadecafluorotetradecyl 4-methylbenzenesulfonate (**2c**) as an shine white solid (10.27gm, 15.24 mmol, 79%): ^{1}H NMR (400 MHz, $CDCl_3$, δ_{ppm}): 7.79-7.77 (d, 2H, Ph), 7.35-7.33 (d, 2H, Ph), 4.05-4.02 (t, 2H, C*H*$_2$-OTs), 2.44 (s, 3H, Ph-C*H*$_3$), 2.07-1.94 (m, 2H, CF_2-C*H*$_2$), 1.69-1.62 (m, 2H, Alkyl), 1.58-1.51 (m, 2H, Alkyl), 1.40-1.28 (m, 4H, alkyl). ^{13}C NMR (100 MHz, $CDCl_3$, δ_{ppm}): 144.91(s, 1C, Ph), 133.44(s, 1C, Ph), 129.97 (s, 1C, Ph), 128.02 (s, 1C, Ph), 121.59-105.70(m, 8C, *C*F_3-*C*F_2-*C*F_2-*C*F_2), 70.40 (s, 1C, *C*H_2-OTs), 31.10, 30.88, 30.65 (t, 1C, CF_2-*C*H_2), 28.72 (s, 1C, alkyl), 28.53 (s, 1C, alkyl), 25.23 (s, 1C, alkyl), 21.64 (s, 1C, Ph-*C*H_3), 20.15, 20.12, 20.08 (t, 1C, alkyl). FTIR (neat, cm^{-1}): 2978, 2954 (phenyl), 2926 (ν_a CH_2), 2865 (ν_s CH_2), 1216 (ν_a CF_2), 1134 (ν_a CF_2). HRMS (DART-TOF) $[M - H]^-$ calcd for $C_{21}H_{18}F_{17}O_3S$, 673.0705; found, 673.0710.

S.4.3.4 9,9,10,10,11,11,12,12,13,13,14,14,15,15,16,16,16-heptadecafluorohexadec-1-yne (2d).

The procedure described for 13,13,14,14,15,15,16,16,16-Nonafluoro-hexadec-1-yne (**1d**) was used with 7,7,8,8,9,9,10,10,11,11,12,12,13,13,14,14,14-

heptadecafluorotetradecyl 4-methylbenzenesulfonate (**2c**) (10.29 g 15.27 mmol) and lithium acetylide ethylenediamine (2.25 g, 24.44 mmol) to give 9,9,10,10,11,11,12,12,13,13,14,14,15,15,16,16,16-heptadecafluorohexadec-1-yne (2d) as an shine white solid (4.84 g, 8.99 mmol, 60%): ^{1}H NMR (400 MHz, $CDCl_3$, δppm): 2.21-2.19 (m, 2H, Alkyl), 2.14-2.00 (m, 2H, CF_2-CH_2), 1.96-1.95 (t, 1H, C≡C-H), 1.66-1.52 (m, 4H, Alkyl), 1.50-1.40(m, 4H, alkyl). ^{13}C NMR (100 MHz, $CDCl_3$, δppm): 121.42-105.15(m, 8C, CF_3-CF_2-CF_2-CF_2-CF_3-CF_2-CF_2-CF_2), 84.26 (s, 1C, C≡C-H), 68.31 (s, 1C, C≡C-H), 31.05, 30.82, 30.60 (t, 1C, CF_2-CH_2), 28.54 (s, 1C, alkyl), 28.21, 28.09 (d, 2C, alkyl), 20.03, 19.99, 19.96 (t, 1C, alkyl). 18.26 (s, 1C, alkyl); HRMS (DART-TOF) [M + NH4] calcd for C16H13F17, 546.10895; found, 546.10720. ^{19}F NMR (500 MHz, $CDCl_3$, δppm): -82.05, -82.07, -82.09 (triplet); -115.53, -115.56, -115.60, -115.63, -115.66 (pentet or quintet); -112.91, -123.11 (doublet); -123.91 (singlet); -124.70 (singlet); -127.31, -127.34, -127.36 (triplet).

S.4.4 16,16,16-trifluorohexadec-1-yne (F3)

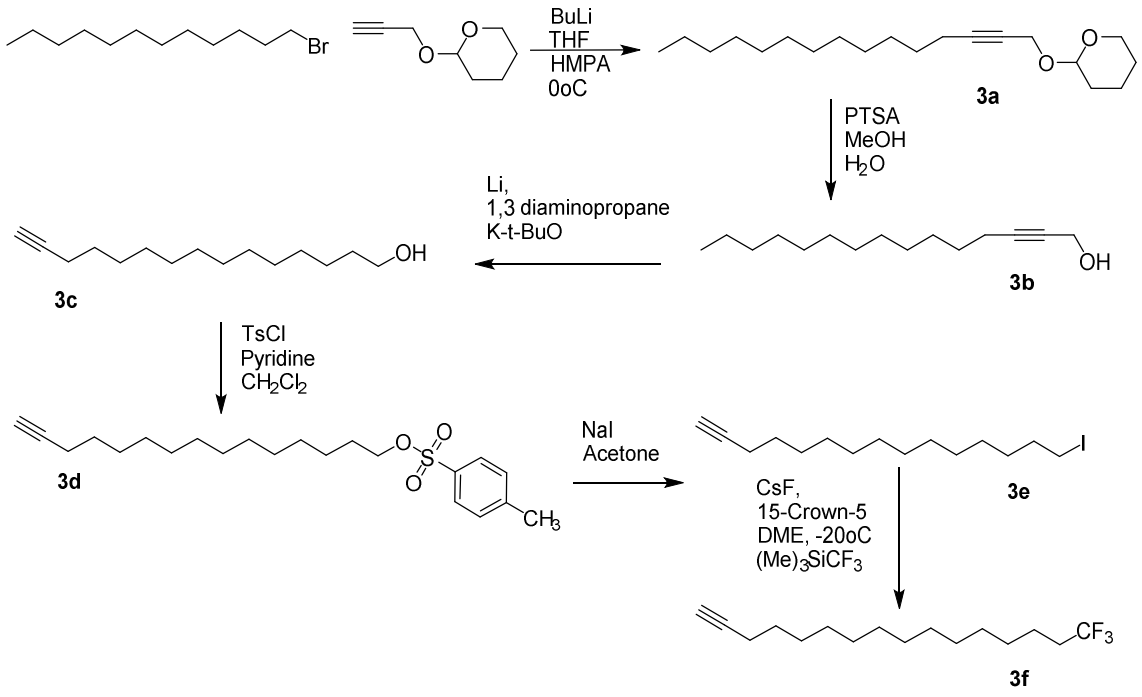

Scheme S3. Synthetic routes for 16,16,16-trifluorohexadec-1-yne (**F3**).

S.4.4.1 2-(Pentadec-2-yn-1-yloxy)tetrahydro-2H-pyran (3a).

To an oven-dried and argon-purged 100 mL round-bottomed flask were added the a solution of tetrahydro-2-(2-propynyloxy)-2H-pyran (0.98 mL, 6.98 mmol) in dry THF (20 mL) was cooled to 0 °C in an ice bath and treated with 1.6 M solution of n-butyllithium in hexane (1.89 mL, 8.02 mmol). Thereafter, 1-bromoalkane (1.93 mL 8.02 mmol) in dry distilled HMPA (14 mL) was added at 0 °C and the resulting reaction mixture stirred 1.5 h at room temperature. The reaction was quenched with saturated aqueous NH_4Cl solution followed by extraction with pentane. The combined organic extracts were washed with water and dried ($MgSO_4$). The residue was purified by column chromatography to afford 2-(pentadec-2-yn-1-yloxy)tetrahydro-2H-pyran (**3a**) (0.69 g, 2.23 mmol) as a clear oil: (hepatane/EtOAc=9:1). . ^{1}H NMR (400 MHz, $CDCl_3$, δ_{ppm}) 4.82-4.80(t, 1H, O-C*H*-O), 4.27-4.18(m, 2H, alkyl), 3.84-3.81(m, 1H, alkyl), 3.53-3.50(m, 1H, alkyl), 2.23-2.18(m, 2H, alkyl), 1.73-1.64(m, 2H, alkyl), 1.63-1.46(m, 6H, alkyl), 1.38-1.26(m, 18H, alkyl), 0.89-0.26(t, 3H, CH_2-C*H*$_3$). ^{13}C NMR (100 MHz, $CDCl_3$, δ_{ppm}): 96.61 (s, 1C, C≡*C*-CH_2-O-), 86.73 (s, 1C, *C*≡C-CH_2-O-), 61.97 (s, 1C, alkyl), 54.63 (s, 1C, alkyl), 31.89(s, 1C, alkyl), 30.30 (s, 1C, alkyl), 29.66, 29.60, 29.51, 29.32, 29.11, 28.86, 28.60 (m, 8C, alkyl), 25.39 (s, 1C, alkyl), 22.65 (s, 1C, alkyl), 19.13(s, 1C, alkyl), 18.80 (s, 1C, alkyl), 14.07 (s, 1C, CH_2-*C*H_3). HRMS (DART-TOF) [M + NH_4] calcd for $C_{20}H_{40}O_2N$, 326.3059; found, 326.3043.

S.4.4.2 Pentadec-2-yn-1-ol (3b).

To a 0.61 g (1.96 mmol) solution of 2-(pentadec-2-yn-1-yloxy)tetrahydro-2H-pyran (**3a**) in 10 mL methanol was added 0.19 g (0.98 mmol) of 4-toluene sulfonic acid monohydrate at room temperature. The mixture was allowed to stir overnight at room temperature and then quenched with 10 mL of ice-cold water. The organic layer was washed with saturated NaCl and dried over anhydrous $MgSO_4$. The solvent was removed by rotary evaporation. The residue was purified by silica column chromatography (9:1, heptane/ether) to give 0.362 g (83%) of a light yellow oil: (9:1, heptane/ether). ^{1}H NMR (400 MHz, $CDCl_3$, δ_{ppm}): 4.25-4.24 (t, 2H, HO-C*H*$_2$-), 2.22-2.18 (m, 2H, C≡C-C*H*$_2$-CH_2), 1.60-1.59 (t, 1H, *HO*-CH_2-), 1.53-1.46 (m, 2H, alkyl), 1.38-1.26 (m, 18H, alkyl), 0.89-0.86 (t, 3H, CH_2-C*H*$_3$). ^{13}C NMR (100 MHz, $CDCl_3$, δ_{ppm}): 87.02 (s, 1C, C≡*C*-CH_2-OH), 78.62 (s, 1C, CH_2-*C*≡C-CH_2-OH), 51.77 (s, 1C, CH_2-OH), 32.26 (s, 1C, alkyl), 30.00, 29.97, 29.86, 29.69, 29.49, 29.23, 28.96 (m, 8C, alkyl), 23.02(s, 1C, alkyl), 19.08(s, 1C, alkyl), 14.44 (s, 1C, CH_2-*C*H_3). HRMS (DART-TOF) [M + H]$^+$ calcd for $C_{15}H_{29}O$, 225.2218; found, 225.2205.

S.4.4.3 Pentadec-14-yn-1-ol (3c).

The procedure described for dec-9-yn-1-ol (Appendix B **1a**) was used with Pentadec-2-yn-1-ol (**4b**) (0.307 g 1.37 mmol), lithium, 0.06 g (8.01 mmol), 1,3 diaminopropane 10 mL and potassium tert-butoxide (0.61 g, 5.47 mmol) to give Pentadec-14-yn-1-ol (**4c**) as an clear oil (0.276 g, 1.23 mmol, 90%): ^{1}H NMR (400 MHz, $CDCl_3$, δ_{ppm}) 3.64-3.61 (t, 2H, C*H*$_2$-OH), 2.19-2.15 (dt 2H, CH_2-C*H*$_2$-C≡C-H), 1.93-1.92 (t, 1H, C≡C-*H*), 1.59-1.48 (m, 4H, Alkyl), 1.45-1.26 (m, 19H, alkyl). ^{13}C NMR (100 MHz, $CDCl_3$, δppm): 85.14(s, 1C, *C*≡C-H), 68.36 (s, 1C, C≡*C*-H), 63.40 (s, 1C, -*C*H_2-OH), 33.15 (s, 1C, alkyl), 29.94, 29.91, 29.82, 29.76(m, 6C, alkyl), 29.44(s, 1C, alkyl), 29.09(s, 1C, alkyl), 28.84(s, 1C, alkyl), 26.08(s, 1C, alkyl), 18.73 (s, 1C, alkyl). HRMS (DART-TOF) $[M + H]^+$ calcd for $C_{15}H_{29}O$, 225.2218; found, 225.2207.

S.4.4.4 Pentadec-14-yn-1-yl 4-methylbenzenesulfonate (3d).

The procedure described for Toluene-4-sulfonic acid 11,11,12,12,13,13,14,14,14-nonafluoro-tetradecyl ester (**1c**) was used with Pentadec-14-yn-1-ol **3c** (0.195 g 0.87 mmol) and p-Toluenesulfonyl chloride (0.18 g , 0.95 mmol) to give Pentadec-14-yn-1-yl 4-methylbenzenesulfonate (**3d**) as an shine white solid 0.31 g, 0.82 mmol, 93%): ^{1}H NMR (400 MHz, $CDCl_3$, δ_{ppm}): 7.80-7.78 (d, 2H, Ph), 7.35-7.33 (d, 2H, Ph), 4.04-4.00 (t, 2H, C*H*$_2$-OTs), 2.45 (s, 3H, Ph-C*H*$_3$), 2.20-2.16 (dt, 2H, CH_2-C*H*$_2$-C≡C-H), 1.94-1.92 (t, 1H, C≡C-*H*), 1.66-1.60 (m, 2H, alkyl), 1.56-1.49 (m, 2H, alkyl), 1.40-1.22(m, 18H, alkyl). ^{13}C NMR (100 MHz, $CDCl_3$, δ_{ppm}): 144.93 (s, 1C, Ph), 133.71 (s, 1C, Ph), 130.13(s, 1C, Ph), 128.24 (s, 1C, Ph), 85.15 (s, 1C, *C*≡C-H), 71.04 (s, 1C, *C*H_2-OTs), 68.38 (s, 1C, C≡*C*-H), 29.90, 29.82, 29.72 (m, 5C, alkyl), 29.45 (s, 1C, alkyl), 29.28 (s, 1C, alkyl), 29.19 (s, 1C, alkyl), 29.11 (s, 1C, alkyl), 28.85 (s, 1C, alkyl), 25.68 (s, 1C, alkyl), 21.97 (s, 1C, alkyl), 18.75 (s, 1C, alkyl). HRMS (DART-TOF) $[M + H]^+$ calcd for $C_{22}H_{35}O_3S$, 379.2307; found, 379.2294.

S.4.4.5 15-iodopentadec-1-yne (3e).

To a stirred mixture of sodium iodide (1.64 g, 10.95 mmol) in acetone (100 mL), a solution of 14-yn-1-yl 4-methylbenzenesulfonate (**3d**) (2.07 g, 5.47 mmol) in acetone (25 mL) was added and the reaction mixture was stirred and heated under reflux for 8 h under nitrogen atmosphere and then concentrated in vacuo to remove the acetone. The obtained residue was diluted with water and extracted with ethyl acetate (2 x 40 mL). The combined ethyl acetate extract was washed with water, brine and dried over Na_2SO_4. The concentration of organic layer in vacuo followed by silica gel column chromatographic purification of the resulting residue using ethyl acetate/heptane (1:5) as an eluent afforded

pure product 15-iodopentadec-1-yne (**3e**) as a colorless oil (1.86 g, 5.57 mmol, 99%). ^{1}H NMR (400 MHz, $CDCl_3$, δ_{ppm}): 3.05-3.02 (t, 2H, C*H*$_2$-I), 2.08-2.01(dt, 2H, CH_2-C*H*$_2$-C≡C-H), 1.79-1.78(t, 1H, C≡C-H), 1.71-1.63 (m, 2H, alkyl), 1.41-1.33 (m, 2H, alkyl), 1.25-1.07 (m, 18H, alkyl). ^{13}C NMR (100 MHz, $CDCl_3$, δ_{ppm}): 84.61(s, 1C, *C*≡C-H), 67.82(s, 1C, C≡*C*-H), 33.40 (s, 1C, alkyl), 30.32 (s, 1C, alkyl), 29.37, 29.33, 29.28, 29.22 (m, 6C, alkyl), 28.90 (s, 1C, alkyl), 28.60 (s, 1C, alkyl), 28.35 (s, 1C, alkyl), 18.21 (s, 1C, alkyl), 7.07 (s, 1C, -*C*H_2-I). HRMS (DART-TOF) $[M + H]^+$ calcd for $C_{15}H_{28}I$, 335.1256; found, 335.1250.

S.4.4.6 16,16,16-trifluorohexadec-1-yne (4f).

Under an argon atmosphere, a mixture of dried CsF (1.62 g, 10.77 mmol) 15-crown-5 (2.13 mL, 10.77 mmol) and dry 1,2-dimethoxyethane (DME) 25 mL was stirred for 5 min at -20 ºC (ice:NaCl 33:66). Then a mixture of Me_3SiCF_3 (1.58 mL, 10.77 mmol) and 15-iodopentadec-1-yne (**3e**) (1.80 g, 5.39 mmol) in 25 mL DME was slowly added to the reaction flask. The reaction temperature was raised to 10 ºC in 4 hr, followed by adding H_2O (20 mL) to the reaction mixture. The organic phase was combined and washed with saturated NaCl(Brine), then dried over anhydrous Na_2SO_4. The solvent was evaporated under vacuum. The residue was purified by silica gel column chromatography (Heptane) to afford 17,17,17-trifluoroheptadec-1-yne **3f** (1.30 g, 4.76 mmol 88%) as colorless oil. ^{1}H NMR (400 MHz, $CDCl_3$, δ_{ppm}): 2.20-2.16 (m, 2H, CH_2-C*H*$_2$-C≡C-H), 2.10-2.00 (m, 2H, CF_3-C*H*$_2$), 1.94-1.93 (t, 1H, C≡C-*H*), 1.57-1.49 (m, 4H, Alkyl), 1.40-1.25(m, 12H, alkyl). ^{13}C NMR (100 MHz, $CDCl_3$, δ_{ppm}): 141.11, 126.55, 110.78, 103.68(q, 1C, *C*F_3-CH_2-), 85.17(s, 1C, *C*≡C-H), 68.37(s, 1C, C≡*C*-H), 34.41, 34.19, 33.96, 33.73(q, 1C, CF_3-*C*H_2), 30.05, 29.92, 29.88, 29.83, 29.70, 29.53, 29.45, 29.11, 28.84 (m, 11C, alkyl), 22.21, 22.19, 22.17, 22.15(q, 1C, CF_3-CH_2-*C*H_2-). 18.75 (s, 1C, alkyl). HRMS (DART-TOF) $[M + H]^+$ calcd for $C_{16}H_{28}F_3$, 277.2143; found, 277.2152. ^{19}F NMR (500 MHz, $CDCl_3$, δppm): -67.48, -67.50, -67.52 (triplet).

S.4.5 16-fluorohexadec-1-yne

Experimental procedure explained in Supporting Information S.3.5 Synthesis of 16-fluorohexadec-1-yne. ^{19}F NMR (500 MHz, $CDCl_3$, δppm): -218.81, -218.86, -218.91, -218.96, -219.01, -219.06, -219.11 (septet).

S.4.6 Contact angle

Table S1. Advancing (θ_a) and Static Contact Angles of Liquids on Fluoro-Hydro Alkyne Monolayers on Si(111) [a,b,c.]

Monolayers	Water	1,5 pentanol	C16	C14	C12	C10	C7	C6
F0	116 [110]	79	37	34	30	26	[a]	[a]
F1	116 [113]	81	45	42	40	37	[a]	[a]
F3	118 [115]	95	61	62	58	54	43	35
F9	123 [117]	99	78	76	74	70	62	57
F17	124 [119]	104	81	79	77	74	63	62

[a] Not measurable. [b] The number in square brackets denotes static contact angles measurement. [c] Contact angle error < ±2°.

S.4.7 XPS and DFT calculation of C1s and F1s binding energy.

S.4.7.1 DFT calculation of XPS chemical shifts of carbon and fluorine atoms

The assignment of the C_{1s} XPS spectra is supported by density functional theory B3LYP/6-311G(d,p) calculations of the core orbital energy levels by "initial state approximation". The absolute values of calculated binding energies cannot be compared directly with the experimental data because of the difference in reference energies in theory and experiment. As a point of reference the CH_2 moiety in the center of the aliphatic hydrocarbon chain was positioned at a binding energy of 285 eV. For every carbon atom, a gaussian centered at the corresponding binding energy was used with a fwhm of 1.0437 eV. The sum of all Gaussians gave the simulated XPS spectra. Electronic Core Level Calculations: All calculations were done using the GAUSSIAN09 program.[5,6] The geometries of the different systems were optimized at the B3LYP/6-311G(d,p) level of theory. Natural bond orbital (NBO) analysis was employed to obtain the core orbital energies.

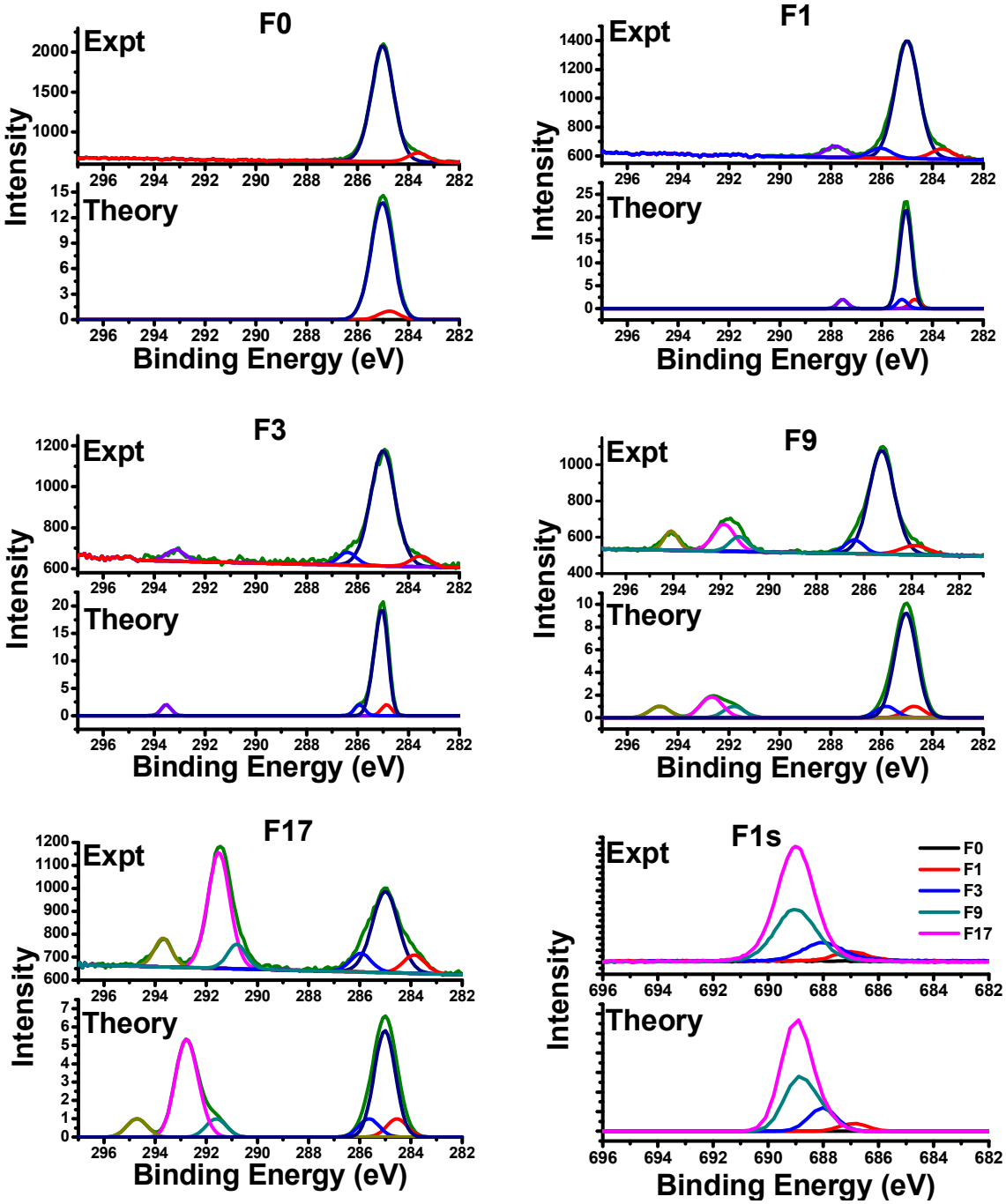

Figure S4. Experimental and calculated (DFT) core level C_{1s} XPS spectra of **F0, F1, F3, F9,** and **F17** alkyne monolayer on H-Si(111); the bottom right spectra are of the F_{1s}.

S.4.8 Friction image

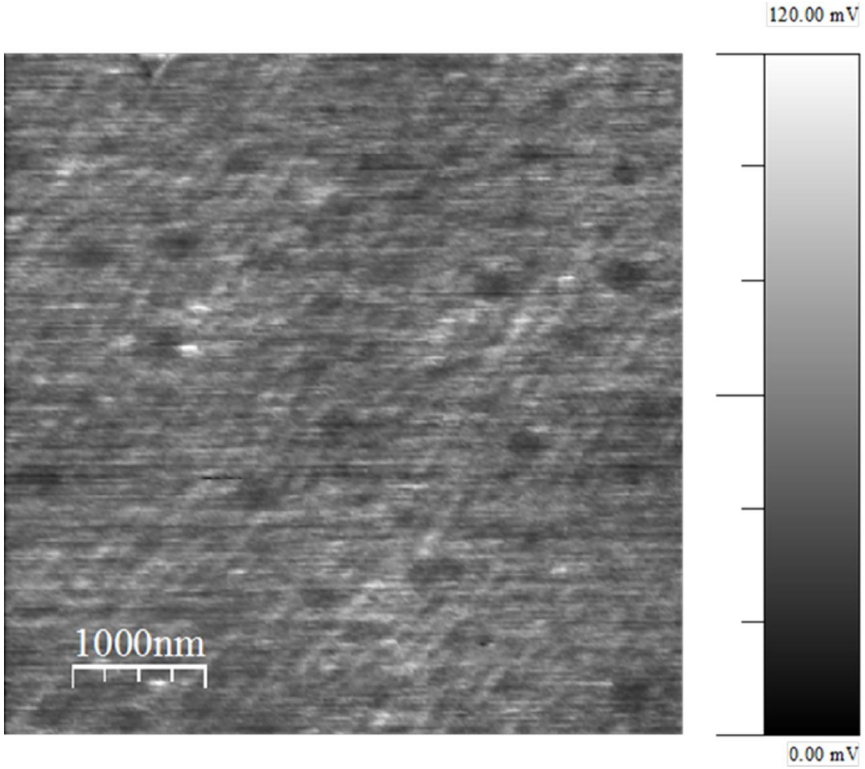

Figure S5. AFM friction images with lateral force mode on the **F9** SAMs**.**

S.4.9 Molecular modeling (Material studio)

The average packing energy per chain was then calculated according to [$E_{packing}$ = (E_{chains}/n)-E_{single}] in which E_{chains} is the total packing energy of the layer, n is the number of chains in the layer, and E_{single} is the energy of a separately optimized chain.[7,8]

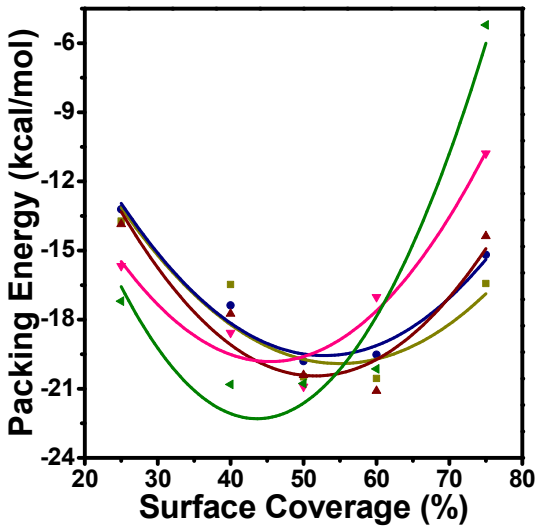

Figure S6. Average packing energies of fluoro-hydro alkyne derived (■) F0, (●) F1, (▲) F3, (▼) F9, and (◀) F17 monolayers on Si(111); the fits are to parabolic functions.

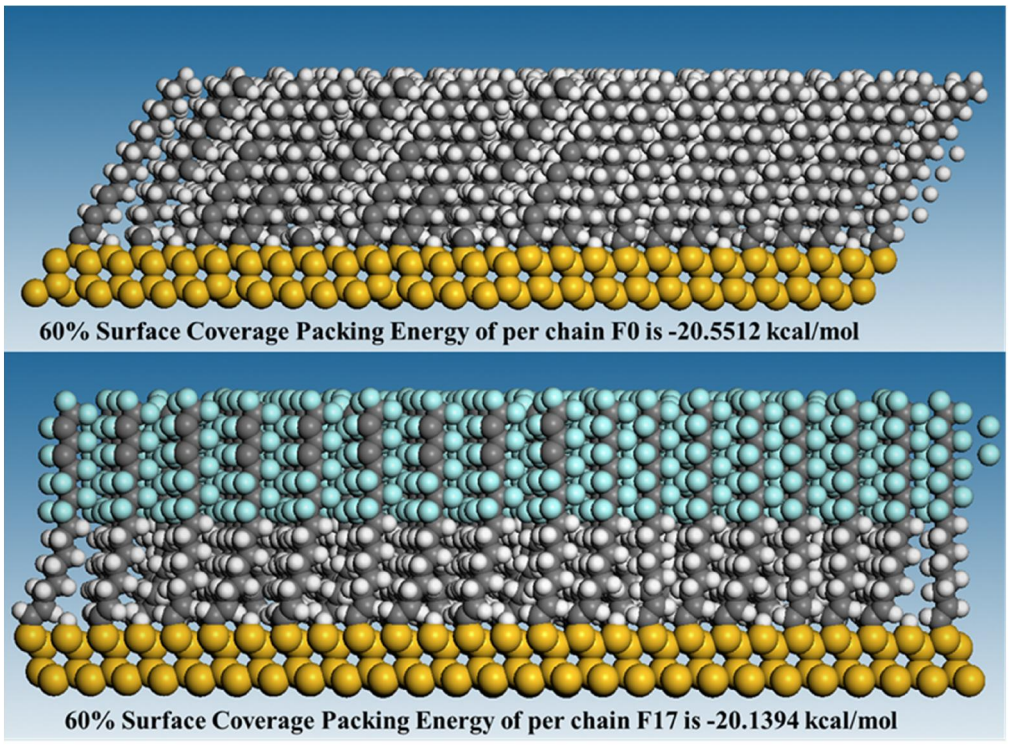

Figure S7. Side view of simulation cell 60A after optimization. The gold color represent (Silicon), gray (carbon), white (hydrogen), and aqua(fluorine). Top is **F0** and bottom **F17** optimized model on Si(111).

S.4.10 References

[1] Gottlieb, H. E.; Kotlyar, V.; Nudelman, A. *The Journal of Organic Chemistry* **1997**, *62*, 7512-7515.

[2] Petucci, C.; Diffendal, J.; Kaufman, D.; Mekonnen, B.; Terefenko, G.; Musselman, B. *Analytical Chemistry* **2007**, *79*, 5064-5070.

[3] Morlock, G.; Ueda, Y. *Journal of Chromatography A* **2007**, *1143*, 243-251.

[4] Cody, R. B. *Analytical Chemistry* **2009**, *81*, 1101-1107.

[5] Frisch, M. J. T., G. W.; Schlegel, H. B.; Scuseria, G. E.; Robb, M. A.; Cheeseman, J. R.; Scalmani, G.; Barone, V.; Mennucci, B.; Petersson, G. A.; Nakatsuji, H.; Caricato, M.; Li, X.; Hratchian, H. P.; Izmaylov, A. F.; Bloino, J.; Zheng, G.; Sonnenberg, J. L.; Hada, M.; Ehara, M.; Toyota, K.; Fukuda, R.; Hasegawa, J.; Ishida, M.; Nakajima, T.; Honda, Y.; Kitao, O.; Nakai, H.; Vreven, T.; Montgomery, Jr., J. A.; Peralta, J. E.; Ogliaro, F.; Bearpark, M.; Heyd, J. J.; Brothers, E.; Kudin, K. N.; Staroverov, V. N.; Kobayashi, R.; Normand, J.; Raghavachari, K.; Rendell, A.; Burant, J. C.; Iyengar, S. S.; Tomasi, J.; Cossi, M.; Rega, N.; Millam, N. J.; Klene, M.; Knox, J. E.; Cross, J. B.; Bakken, V.; Adamo, C.; Jaramillo, J.; Gomperts, R.; Stratmann, R. E.; Yazyev, O.; Austin, A. J.; Cammi, R.; Pomelli, C.; Ochterski, J. W.; Martin, R. L.; Morokuma, K.; Zakrzewski, V. G.; Voth, G. A.; Salvador, P.; Dannenberg, J. J.; Dapprich, S.; Daniels, A. D.; Farkas, Ö.; Foresman, J. B.; Ortiz, J. V.; Cioslowski, J.; Fox, D. J. In Gaussian 09, Revision A.1; Gaussian, Inc., Wallingford CT.: **2009**.

[6] E. D. Glendening , A. E. R., J. E. Carpenter , F. Weinhold NBO, version 3.1.

[7] Scheres, L.; Rijksen, B.; Giesbers, M.; Zuilhof, H. *Langmuir* **2011**, *27*, 972-980.

[8] Rijksen, B.; Pujari, S. P.; Scheres, L.; van Rijn, C. J. M.; Baio, J. E.; Weidner, T.; Zuilhof, H. *Langmuir* **2012**, *28*, 6577-6588.

CHAPTER 5

Highly Wear-Resistant Ultra-Thin Per-fluorinated Organic Monolayers on Silicon (111) Surfaces

This study reports on fluorine-containing alkyne-derived monolayers onto Si(111) substrates to obtain densely packed, highly wear-resistant surfaces. The nano-wear properties were measured using atomic force microscopy (AFM). The presence of the fluorinated monolayers was found to enhance the wear properties of the silicon surfaces, with a decrease of the depth of wear scratches of up to 120 times as compared to the unmodified surface. Ultimately, the scratch depth was only 6 nm for a heptadecafluoro-alkyl based monolayer for scratching normal forces as high as 38 μN.

This Chapter is submitted for publication as:

"Highly Wear-Resistant Ultra-Thin Per-fluorinated Organic Monolayers on Silicon (111) Surfaces". Sidharam P. Pujari, and Han Zuilhof. Applied Surface Science, **2013** *Accepted (Ms. Ref. No.: APSUSC-D-13-02378)*.

Table of Contents

5 Highly Wear-Resistant Ultra-Thin Per-fluorinated Organic Monolayers on Silicon (111) Surfaces 135
5.1 INTRODUCTION 137
5.2 EXPERIMENTAL METHODS AND TEST PROCEDURE 139
5.2.1 Monolayer formation 139
5.2.2 Wear Resistance 139
5.3 RESULTS AND DISCUSSION 140
5.3.1 Wear mark at lower load 140
5.3.2 Wear mark at higher load 141
5.3.3 Bond dissociation energy and chain deformation 142
5.3.4 Wear in silicon nitride tips sliding on monolayers 144
5.4 CONCLUSIONS 145
5.5 REFERENCES 145

5.1 INTRODUCTION

Silicon and other electronic materials are increasingly being used to manufacture devices which can achieve mechanical operations.[1-4] Several typical integrated circuit (IC) preparation methods are used, especially layer deposition, lithography, etching, doping, together with special etching and bonding processes. With these approaches 3D MEMS/NEMS can be generated. The combination of various specific parts such as motors, gears, and actuators enables the manufacturing of micro-machines.[5] At small scales like this, the surface-to-volume ratios are very high, and surface forces become highly important, especially for in intrinsically rather brittle materials as silicon. As a result, stiction and wear form technical barriers for the production of good Si-based devices.[6, 7]

A pair of solid surfaces in contact exhibits two types of stiction: release-related stiction and in-use stiction. In-use stiction happens during the process when two surfaces come into contact. If adhesion forces go beyond the restoring forces, the surfaces will not separate, causing device failure. Organic monolayers are widely used to minimize release-related stiction in MEMS fabrication. The effects of organic monolayers on friction and wear of Si, SiC, SiN and CrN based surfaces were studied in more detail by various research groups.[4, 8-11] As a result, outstanding wear resistance properties were developed on fluorinated alkyne-derived monolayers onto SiC and CrN surfaces, caused by the strong C-O-C and Cr-O-C covalent bond and high monolayer density.[9, 11, 12]

The wear resistance is a key factor for organic coatings to be used as nanometer-scale lubricants. In particular, ultrathin organic monolayers have been shown to efficiently lubricate surfaces while showing low adhesion, low friction and low wear resistance.[9, 11, 13-16] Jennings and co-worker[16] studied the tribological stability of various alkyl silane monolayer films on silicon by using pin-on-disk tribometry at ambient conditions. For monolayers derived from *n*-octadecyltrichlorosilane, a critical load was identified to be approximately 250 mN (200 MPa, 4 mm diameter), above which failure of films occurred within 100 cycles of testing. In fact, on H-terminated Si(111) surfaces, fluorinated alkyne-derived monolayers have recently even been shown to yield the lowest friction and adhesion forces of any flat surface, reducing the adhesion and friction by a factor of ~4 compared to polytetrafluoroethylene (PTFE).[17] This is highly relevant, since PTFE is used as a primary key coating material in many MEMS/NEMS.[18] However, those polymer films are not covalently bound to the surface and therefore vulnerable to high wear.[19] Moreover, PTFE coatings are relatively thick, which may eventually lead to high adhesion and friction forces when high loads are applied and the films are compressed.[19]

In those early investigations, wear tests were carried out using a traditional pin-on-disk or ball-on-disk tribotester under relatively large normal loads ranging from 0.1 to 0.15 N.[20] Thus, the relevance of these tests is questionable for MEMS/NEMS applications. With the development of AFM techniques,[1, 9, 11] researchers successfully characterized the nano-tribological properties of organic monolayers and polymer coatings. Previous studies showed that silane monolayers improved wear resistance properties on Si(111).[8] However, the stability of silane-based monolayers is eventually diminished at physiological pH,[21] due to the hydrolytic liability of Si-O bonds. In addition, the relatively low dissociation energy of Si-O bonds accounts for the weak mechanical stability of silane monolayers at high normal loads, whilst the higher dissociation energy of Si-C bonds might strengthen the monolayer stability.[11, 22] However, to the best of our knowledge, no detailed wear study has been reported yet of covalently attached, Si-C linked monolayers on silicon, nor of a systematic variation of the fluorine content in such monolayers.

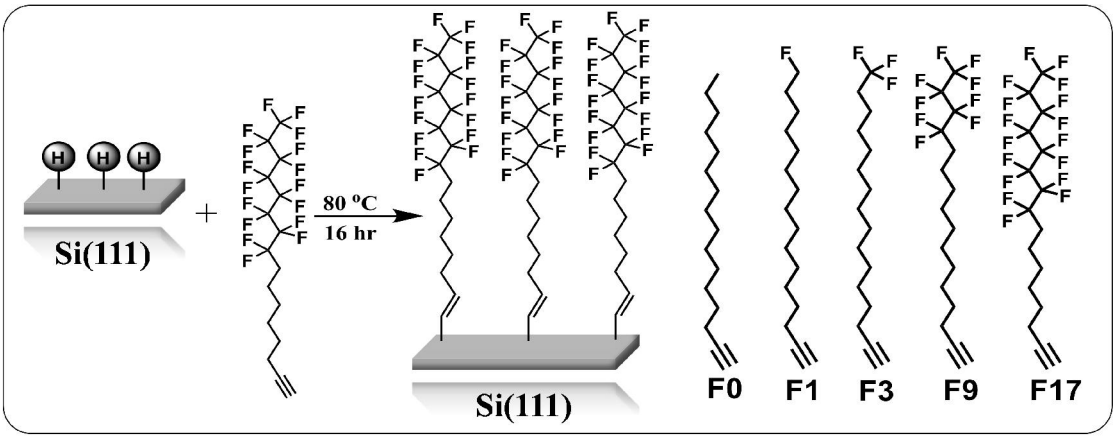

Figure 1. Schematic depiction of the fluorinated organic monolayers on Si(111) and the wear study detailed in this paper.

In a previous study of fluorinated monolayers on the Si(111)surface the focus was mainly on the physical properties of this system, specifically adhesion, surface tension, and friction forces as a function of the number of fluorine atoms in the organic monolayer.[17] Since these systems thus yielded such superb adhesion and friction properties, it is of interest to also study their wear properties in detail. In this work therefore the surface chemistry and wear resistance of Si(111) surfaces coated with a covalently bound alkyne-derived monolayer are investigated using AFM and SEM. Specifically, various C_{16} monolayers are studied - to warrant a constant layer thickness - with a varying number of fluorine atoms (#F atoms = 0 – 17) as shown in Figure 1. The

results outline the potential of covalently attached fluorinated monolayers as high-quality lubricants.

5.2 EXPERIMENTAL METHODS AND TEST PROCEDURE

5.2.1 Monolayer formation

Perfluorinated alkyne-derived monolayers on NH_4F-etched Si(111) surfaces were prepared as described in detail elsewhere.[17] In brief, a piece of an n-type Si(111) wafer was first rinsed several times with acetone, followed by sonication for 10 min in acetone. The Si wafer was then oxidized in freshly prepared piranha solution (H_2SO_4/H_2O_2 3:1) for at least 20 min. After piranha treatment, the substrates were immersed immediately in water and rinsed thoroughly, followed by drying with a stream of argon. Subsequently, the Si(111) substrates were etched in an argon-saturated 40% aqueous NH_4F solution for 15 min under an argon atmosphere. After being etched, the samples were rinsed with water and finally blown dry with a stream of nitrogen. A three-necked flat-bottomed flask connected to a thin capillary as the argon inlet and to a reflux condenser connected to a vacuum pump was charged with individual neat fluoro-hydro alkyne (Scheme 1), flushed with argon, and heated to 80 °C in order to remove traces of oxygen and moisture. The freshly etched Si(111) substrate was placed in fluoro-hydro alkyne. The reaction was carried out at 80 °C under an argon atmosphere at an argon pressure of 2 – 5 mbar for 16 h. After the reaction had been stopped, the modified surfaces were rinsed and sonicated with CH_2Cl_2 for 5 min to remove any physisorbed fluoro-hydro alkynes. The monolayers were extensively analyzed by XPS, IR and contact angle measurements, as described elsewhere.[17, 23, 24]

5.2.2 Wear Resistance

Nanowear/machining experiments on single-crystal silicon(111) were conducted by using an Asylum MFP-3D atomic force microscope (AFM) in contact mode. All AFM measurements were carried out in ambient conditions (temperature = 25 °C, relative humidity = 40%), and at least in duplicate. Rectangular silicon cantilevers a with spring constant of 49 N/m were used in this study. The radius of the tip is about 20 nm, which was confirmed by scanning electron microscope (SEM). Organic monolayers were scanned in a direction vertical to the long axis of the cantilever beam with a scanning speed of 1 μm/s during the nanowear and at a resolution of 258 × 258 pixels. In all wear experiments, an area of 200 × 200 nm^2 was scanned at normal loads ranging from 1 to 35 μN for one scan cycle. A force was applied at one edge of the scan area till the other edge. All AFM scanning experiments were performed vertical (90°) to the long axis of the cantilever at a scan velocity of 1 Hz. The wear images and corresponding wear depth measurements were done with a larger specimen

surface area. The specimen area was scanned before and after the nanowear test, using the same silicon nitride (Si_3N_4) tip at a normal load of about 392 nN.

5.3 RESULTS AND DISCUSSION

5.3.1 Wear mark at lower load

Fluoro-hydro alkynes were covalently attached to oxide-free hydrogen-terminated silicon surfaces via Si-C=C bonds.[23, 25] This type of organic monolayers are typically densely packed, display a high degree of short-range ordering as indicated from IRRAS spectroscopy data, and exhibit remarkable hydrophobic properties including static water contact angles up to 123°.[17] The resulting monolayers were first studied by adhesion and frictional force measurements at low forces from 5 to 75 nN. Under this lower force these monolayers did not show any nano-wear properties, as e.g. shown by an AFM topographic image after applied normal load 75 nN (Figure **2**).

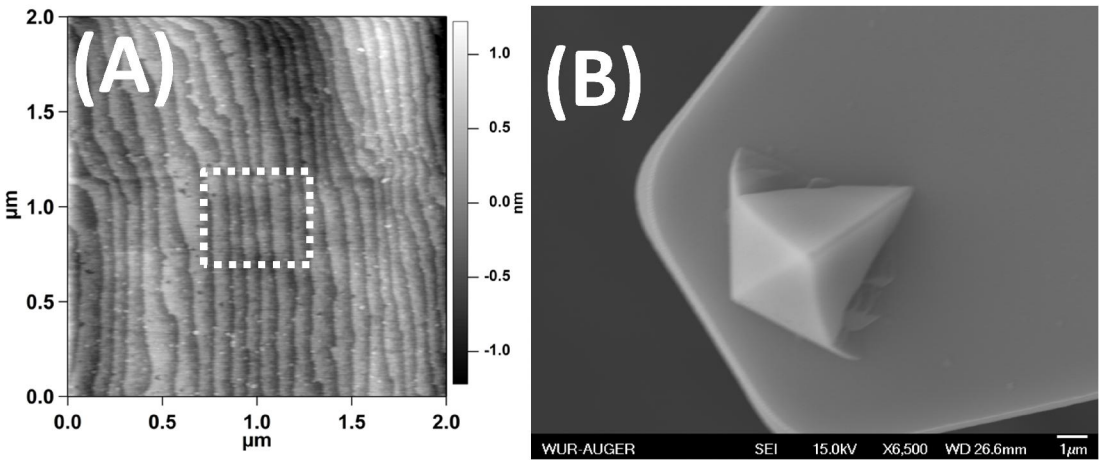

Figure 2. (A) AFM topographic image after an applied normal load of 75 nN; marked area 200 × 200 nm^2 and use of same silicon nitride (Si_3N_4) tip at a normal load of about 5 nN to obtain the image. (B) SEM image of silicon nitride (Si_3N_4) tip; tip spring constant = 0.12 N/m.

While an interesting result by itself, it stimulated us to push to the limits of wear resistance under significantly higher, industrially relevant forces. Therefore the current study was extended to extreme loads from 8 to 38 µN force (Figure **3)**. Typical wear marks with the size of 200 × 200 nm^2, generated at different normal loads for one scan cycle, were subsequently imaged by AFM at scan velocities from 0.5 to 2 Hz (0.2 to 1

μm/s) in contact mode. There was no dependence on the scanning speed obtained at a given normal force, which is in agreement with result shown by Bhushan et al.[26] The same cantilever was used for the AFM imaging of the wear mark. The scan area for imaging the wear marks was 2 × 2 μm^2 or 1 × 1 μm^2, and the normal load was about 394 nN.

5.3.2 Wear mark at higher load

The surface topography images of the wear marks for four different loads (11.8, 15.7, 19.6 and 27.4 μN) for the **F17** monolayer are shown in Figure 3A to D. Increasing the normal force from 8 μN to 27 μN resulted in the change of the wear depth from 0.3 nm to 1.8 nm, which is close to the thickness of the monolayers. If the force was further increased to 31 μN and 38 μN, the wear depth increased drastically to 3.1 nm and 6.1 nm, respectively. The increasing wear depths by growing forces are consistent with the results of Bhushan et al.[8, 18, 27] Interestingly, the observed wear depth is negligible under normal forces up to 8 μN. Apparently, up to these already quite significant loads, the monolayers can undergo orientation changes that can accommodate the applied force. The scratching depth only increases with a further increase in the normal force to above 8 μN. In the range from 8 to 23 μN, the wear depth increases slowly from 0.2 to 2 nm with a rate of about 0.15 nm/μN. In addition, the wear fragments produced at higher loads throughout the wear marking are not sticky, and could be moved out of the scan area by the light load during the AFM topographic scan (lower load 392 nN; no observed stick slip effect). It should be remarked that these monolayer-coated Si surfaces perform superiorly over uncoated Si.[4] At a force of 6 μN, the monolayer-coated samples are still basically undamaged, while an uncoated Si surface displays already scratching marks of 8 nm deep. For higher loads this difference becomes even larger: for loads of ca. 20 μN, the uncoated Si surfaces would display data points off the scale, while none of the monolayer-coated samples displays wear marks of more than a nanometer, i.e. typically show only some damaging of the organic coating.

Only for loads above 25 μN do we observe the monolayer-coated surfaces to break down, but even then a force of 38 μN induces less damage to a **F17**-coated Si surface than a 6 μN force to a non-coated sample. In more detail, Figure **3F** shows that with the higher loads from 24 to 38 μN, the wear depth for **F0**, **F1** and **F3** coated surfaces increases rapidly, from 2 nm to 30 nm with a slope of about 2.0 - 2.8 nm/ μN. The fluorinated monolayers **F9** and **F17** showed an even better wear resistance: at loads from 24 to 38 μN, the wear depth only increases gradually from 2 to 5 nm with a slope of about 0.3 nm/ μN. As suggested,[17] a fluoro-hydro monolayer (**F9** and **F17**) is more rigid than more hydrocarbon-like monolayers (**F0**, **F1** and **F3**). These results are in good agreement with previously reported findings for

alkyl monolayers on Si surfaces.[30] However, all these monolayers display a highly beneficial wear-resisting effect, even when the hard AFM tip penetrates into the monolayer, or - at higher loads (critical load) - into the Si surface. In this condition, **F9** and **F17** monolayers do not only help as protective monolayer, but also reduce wear by acting to minimize friction between the tip and substrate.

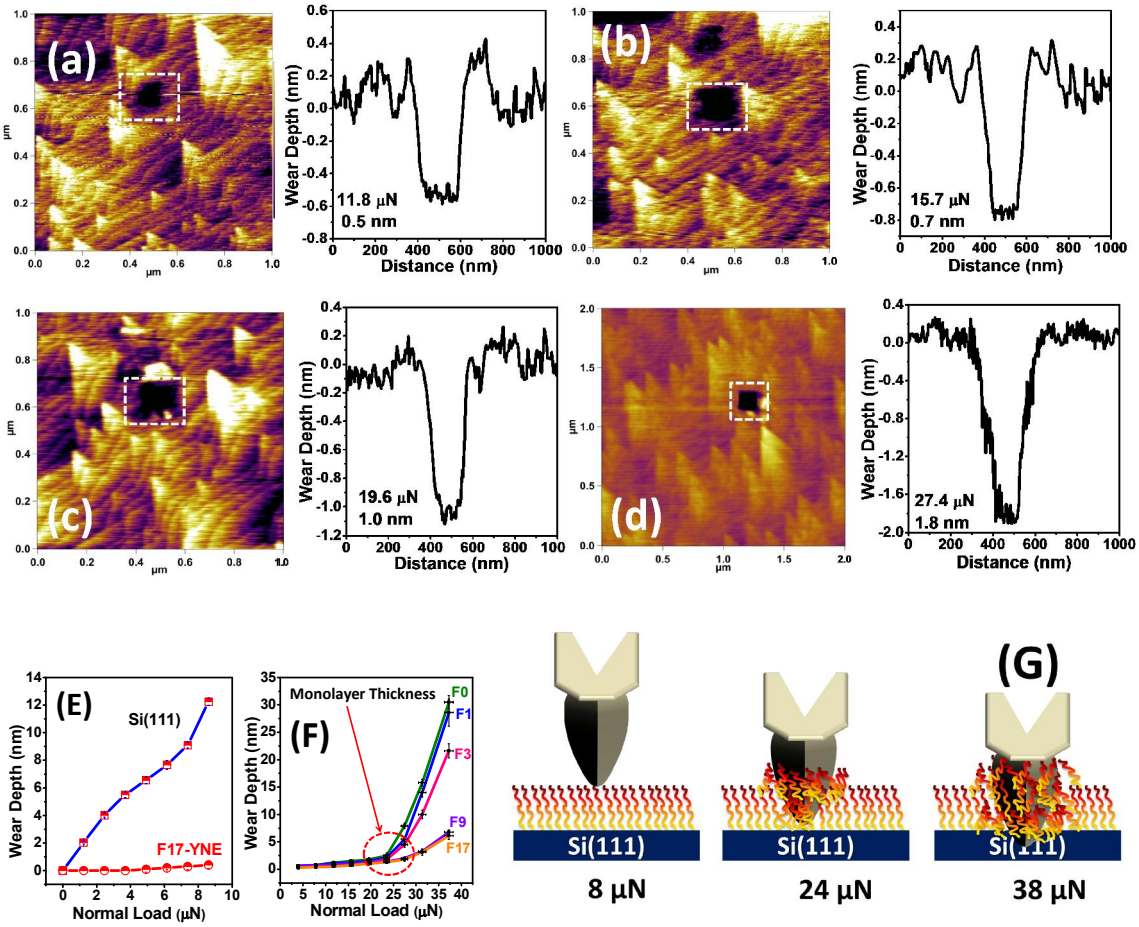

Figure 3. (A to D) AFM images of wear marks produced at different normal load after one scan cycle, the normal force and the average wear depth are shown on the right side. (E and F) Wear depth as a function of normal load on unmodified Si(111) and on a F17 monolayer (E), and comparison between various fluoro-hydro monolayers at lower load after one scan cycle (F). Schematic depiction of the wear mechanism of monolayers (G) with increasing normal load, yielding nanowear-induced depths from ~0.3 nm (8 µN) to ~6.1 nm (38 µN).

5.3.3 Bond dissociation energy and chain deformation

The different rates of depth increase in different load ranges may be attributed to different material removal mechanisms, like bond dissociation energy and chain deformation. Only at the critical normal loads from 24 to 38 µN, the Si_3N_4 tip approaches the interface to sever

monolayers away from the substrate. This might be due to the interface chemical adsorption bond strength. For uncoated Si this is the Si-O bond [242.7 kJ/mol], which is effectively the top layer, and which is generally weaker than the other chemical bonds in monolayers (see Table 1**)**. For Si-C bound monolayers with many C-C bonds the relevant bond strengths [C-C bond: 418 kJ/mol; Si-C=C bond: 360 kJ/mol; C-F bond: 475 kJ/mol] are higher than the Si-Si [340 kJ/mol] and Si-O [242.7 kJ/mol] bonds.[1] This explains why the rigid fluorinated monolayers have higher wear resistance as compared with non-fluorinated monolayers and unmodified Si(111) surfaces. In fact, these fluorinated monolayers display even better wear resistance properties (critical normal load > 24 μN) than previously reported by Bhushan et al. for monolayers of fluorinated and non-fluorinated SAMs on aluminium surfaces (critical normal loads - 20 μN).[31] They hypothesized that the shearing of the monolayers occurred due to the weak interfacial bonds. We think that our data support that hypothesis, and that the combination of the high density of the fluorinated monolayers under study,[17] and the use of Si-C=C linking groups (vide infra) may give rise to the currently observed high wear resistance.

TABLE 1. **Bond strengths of the chemical bonds in monolayers.**[28, 29]

Bond	Bond strength kJ/mol	Bond	Bond strength kJ/mol
Si─O	242.7	Si─C═C	~360
Si─Si	340	Si─C─C	360, 435
Si─H	393	C═C─C	418
C═C	682	C─CH_2F	368
C─C	347	C─CH_3	301
CH_2─CF_2	~ >347	C─CF_3	423.4
C─F	475	C─H	414

In addition, Shchukin et al.[32] reported that the C–C bond strength increases when the hydrogen is replaced with fluorine. When the maximum force required for bond cleavage is taken as a measure for bond strength, this could be a possible explanation for the higher wear resistance of fluorinated monolayers **F9** and **F17.** In addition, the high density of strong Si-C=C bonds in this well-ordered dense monolayer additionally offers a significant resistance to water or other chemical penetration that would otherwise lead to the formation of monolayer-weakening oxide layers during mechanical movements.

5.3.4 Wear in silicon nitride tips sliding on monolayers

Furthermore, the radius of curvature sharp tip (Figure 4A) before measurement is < 20 nm (limits of resolution of our instrumentation). However, the SiN_x tip undergoes a gradual change in tip shape with scanning upon AFM imaging in contact mode and after extensively applied higher forces from 1 to 38 μN. SEM imaging (Figure 4B) indeed confirms that the tip became blunt, with the sharpness reduced by roughly a factor 5, yielding a radius of the AFM tip of about 110 nm, analogous to previous work done by various research groups.[33-35] To avoid this degradation problem each single measurement thus was, and needs to be, measured with a new AFM tip.

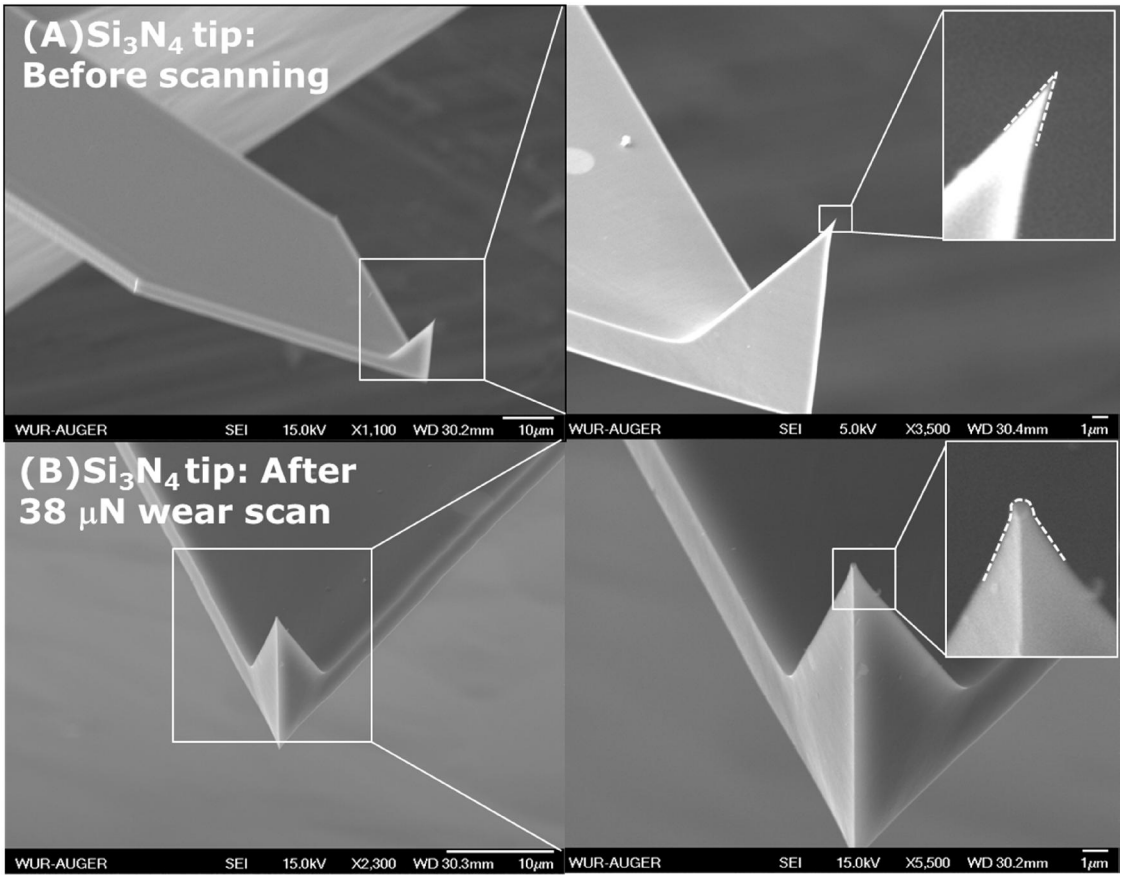

Figure 4. SEM images of a Si_3N_4 tip before (A) and after (B) wear tests for 9 cycles in ambient conditions with various normal loads (1-38 μN); the AFM tip radius changed from ~20 nm (before) to ~111 nm (after).

5.4 CONCLUSIONS

Covalently bound, densely packed fluoro-alkyl monolayers on Si(111) [e.g. ~Si-CH=CH-$(CH_2)_6$-$(CF_2)_8CF_3$] surfaces display an excellent wear resistance. Typically, no wear marks are seen to AFM-induced pressures of 8 μN, while even for pressures up to 24 μN the underlying Si is hardly damaged. Below these critical normal loads, the SAMs can accommodate the external forces by reorientation of the chains. These Si-C=C bound monolayers display such excellent wear-resistance due to the high bond strengths of the involved chemical bonds, and the high density of the monolayers that minimizes external penetration. Due to these superior wear resistance properties, fluoro-alkyl monolayers show a robustness that makes them useful for application in MEMS/NEMS.

5.5 REFERENCES

1. Bhushan, B., *Handbook of Nanotechnology*. 2 ed.; Springer-Verlag New York, LLC: 2007; p 1222.
2. Petersen, K. E., Silicon as a Mechanical Material. *Proceedings of the IEEE* **1982,** 70, (5), 420-457.
3. Tseng, A. A., A comparison study of scratch and wear properties using atomic force microscopy. *Appl. Surf. Sci.* **2010,** 256, (13), 4246-4252.
4. Sundararajan, S.; Bhushan, B., Micro/nanotribology of ultra-thin hard amorphous carbon coatings using atomic force/friction force microscopy. *Wear* **1999,** 225–229, Part 1, (0), 678-689.
5. Quake, S. R.; Scherer, A., From micro- to nanofabrication with soft materials. *Science* **2000,** 290, (5496), 1536-1540.
6. Maboudian, R.; Ashurst, W. R.; Carraro, C., Tribological challenges in micromechanical systems. *Tribol. Lett* **2002,** 12, (2), 95-100.
7. Baker, M. A.; Li, J., The influence of an OTS self-assembled monolayer on the wear-resistant properties of polysilicon based MEMS. *Surf. Interface Anal.* **2006,** 38, (4), 863-867.
8. Liu, H.; Bhushan, B., Investigation of nanotribological properties of self-assembled monolayers with alkyl and biphenyl spacer chains (Invited). *Ultramicroscopy* **2002,** 91, (1–4), 185-202.
9. Pujari, S. P.; Scheres, L.; Weidner, T.; Baio, J. E.; Cohen Stuart, M. A.; van Rijn, C. J. M.; Zuilhof, H., Covalently Attached Organic Monolayers onto Silicon Carbide from 1-Alkynes: Molecular Structure and Tribological Properties. *Langmuir* **2013,** 29, (12), 4019–4031.
10. Bhushan, B.; Israelachvili, J. N.; Landman, U., Nanotribology: Friction, wear and lubrication at the atomic scale. *Nature* **1995,** 374, (6523), 607-616.
11. Pujari, S. P.; Li, Y.; Regeling, R.; Zuilhof, H., Tribology and Stability of Organic Monolayers on CrN: A Comparison among Silane, Phosphonate, Alkene, and Alkyne Chemistries. *Langmuir* **2013**, DOI:10.1021/la401981b.

12. Pujari, S. P.; Scheres, L.; Lagen, B. v.; Zuilhof, H., Organic Monolayers from 1-Alkynes Covalently Attached to Chromium Nitride: Alkyl and Fluoroalkyl Termination. *Langmuir* **2013**, DOI:10.1021/la401978h.
13. McGuiggan, P. M., Friction and adhesion measurements between a fluorocarbon surface and a hydrocarbon surface in air. *J. Adhes.* **2004,** 80, (5), 395-408.
14. Liu, H.; Bhushan, B., Nanotribological characterization of molecularly thick lubricant films for applications to MEMS/NEMS by AFM. *Ultramicroscopy* **2003,** 97, (1–4), 321-340.
15. Carpick, R. W.; Salmeron, M., Scratching the surface: Fundamental investigations of tribology with atomic force microscopy. *Chem. Rev.* **1997,** 97, (4), 1163-1194.
16. Booth, B. D.; Vilt, S. G.; Lewis, J. B.; Rivera, J. L.; Buehler, E. A.; McCabe, C.; Jennings, G. K., Tribological Durability of Silane Monolayers on Silicon. *Langmuir* **2011,** 27, (10), 5909-5917.
17. Pujari, S. P.; Spruijt, E.; Cohen Stuart, M. A.; van Rijn, C. J. M.; Paulusse, J. M. J.; Zuilhof, H., Ultralow Adhesion and Friction of Fluoro-Hydro Alkyne-Derived Self-Assembled Monolayers on H-Terminated Si(111). *Langmuir* **2012,** 28, (51), 17690-17700.
18. Tao, Z.; Bhushan, B., Degradation Mechanisms and Environmental Effects on Perfluoropolyether, Self-Assembled Monolayers, and Diamondlike Carbon Films. *Langmuir* **2005,** 21, (6), 2391-2399.
19. Sawyer, W. G.; Freudenberg, K. D.; Bhimaraj, P.; Schadler, L. S., A study on the friction and wear behavior of PTFE filled with alumina nanoparticles. *Wear* **2003,** 254, (5–6), 573-580.
20. DePalma, V.; Tillman, N., Friction and wear of self-assembled trichlorosilane monolayer films on silicon. *Langmuir* **1989,** 5, (3), 868-872.
21. Silverman, B. M.; Wieghaus, K. A.; Schwartz, J., Comparative Properties of Siloxane vs Phosphonate Monolayers on A Key Titanium Alloy. *Langmuir* **2004,** 21, (1), 225-228.
22. Marcinko, S.; Fadeev, A. Y., Hydrolytic Stability of Organic Monolayers Supported on TiO2 and ZrO2. *Langmuir* **2004,** 20, (6), 2270-2273.
23. Scheres, L.; Giesbers, M.; Zuilhof, H., Self-Assembly of Organic Monolayers onto Hydrogen-Terminated Silicon: 1-Alkynes Are Better Than 1-Alkenes. *Langmuir* **2010,** 26, (13), 10924-10929.
24. de Smet, L. C. P. M.; Pukin, A. V.; Sun, Q.-Y.; Eves, B. J.; Lopinski, G. P.; Visser, G. M.; Zuilhof, H.; Sudhölter, E. J. R., Visible-light attachment of SiC linked functionalized organic monolayers on silicon surfaces. *Appl. Surf. Sci.* **2005,** 252, (1), 24-30.
25. Li, Y.; Calder, S.; Yaffe, O.; Cahen, D.; Haick, H.; Kronik, L.; Zuilhof, H., Hybrids of Organic Molecules and Flat, Oxide-Free Silicon: High-Density Monolayers, Electronic Properties, and Functionalization. *Langmuir* **2012,** 28, (26), 9920-9929.
26. Bhushan, B., Nanoscale tribophysics and tribomechanics. *Wear* **1999,** 225–229, Part 1, (0), 465-492.
27. Bhushan, B.; Liu, H., Nanotribological properties and mechanisms of alkylthiol and biphenyl thiol self-assembled monolayers studied by AFM. *Phys. Rev. B* **2001,** 63, (24), 245412.
28. Zhao, Z.; Bhushan, B.; Kajdas, C., Tribological performance of PFPE and X-1P lubricants at head–disk interface. Part II. Mechanisms. *Tribol. Lett* **1999,** 6, (2), 141-148.
29. Kerr, J. A., Bond Dissociation Energies by Kinetic Methods. *Chem. Rev.* **1966,** 66, (5), 465-500.

30. Kasai, T.; Bhushan, B.; Kulik, G.; Barbieri, L.; Hoffmann, P., Micro/nanotribological study of perfluorosilane SAMs for antistiction and low wear. *J Vac Sci Technol B Microelectron Nanometer Struct Process Meas Phenom* **2005,** 23, (3), 995-1003.
31. Bhushan, B.; Cichomski, M.; Hoque, E.; DeRose, J.; Hoffmann, P.; Mathieu, H., Nanotribological characterization of perfluoroalkylphosphonate self-assembled monolayers deposited on aluminum-coated silicon substrates. *Microsys. Technol.* **2006,** 12, (6), 588-596.
32. Ponomareva, T. P.; Yushchenko, V. S.; Shchukin, E. D., Calculation of carbon-carbon bond deformation curves for fluorinated ethylenes and the corresponding carbocations. *J. Struct. Chem.* **1995,** 36, (1), 29-35.
33. Liu, J.; Notbohm, J. K.; Carpick, R. W.; Turner, K. T., Method for Characterizing Nanoscale Wear of Atomic Force Microscope Tips. *ACS Nano* **2010,** 4, (7), 3763-3772.
34. Kopycinska-Müller, M.; Geiss, R. H.; Hurley, D. C., Contact mechanics and tip shape in AFM-based nanomechanical measurements. *Ultramicroscopy* **2006,** 106, (6), 466-474.
35. Killgore, J. P.; Geiss, R. H.; Hurley, D. C., Continuous Measurement of Atomic Force Microscope Tip Wear by Contact Resonance Force Microscopy. *Small* **2011,** 7, (8), 1018-1022.

CHAPTER 6

Covalently Attached Organic Monolayers onto Silicon Carbide from 1-Alkynes: Molecular Structure and Tribological Properties

In order to achieve improved tribological and wear properties at semiconductor interfaces, we have investigated the thermal grafting of both alkylated and fluorine-containing (C_xF_{x+1})-(CH_2)$_n$-) 1-alkynes and 1-alkenes onto silicon carbide (SiC). The resulting monolayers display static water contact angles up to 120°. The chemical composition of the covalently bound monolayers was studied by X-ray photoelectron spectroscopy (XPS), infrared reflection absorption spectroscopy (IRRAS), and near-edge X-ray absorption fine structure (NEXAFS) spectroscopy. These techniques indicate the presence of acetal groups at the organic-inorganic interface of alkyne-modified SiC surfaces. The tribological properties of the resulting organic monolayers with fluorinated or non-fluorinated endgroups were explored using atomic force microscopy (AFM). It was found that the fluorinated monolayers exhibit a significant reduction of adhesion forces, friction forces and wear resistance compared with non-fluorinated molecular coatings and especially bare SiC substrates. The successful combination of hydrophobicity and excellent tribological properties makes these strongly bound, fluorinated monolayers promising candidates for application as a thin film coating in high-performance micro-electronic devices.

This Chapter has been published as:

"Covalently Attached Organic Monolayers onto Silicon Carbide from 1-Alkynes: Molecular Structure and Tribological Properties." Sidharam P. Pujari, Luc Scheres, Tobias Weidner, Joe E. Baio, Martien A. Cohen Stuart, Cees J. M. van Rijn, and Han Zuilhof. Langmuir **2013** 29 (12), 4019-4031

Table of Contents

6 Covalently Attached Organic Monolayers onto Silicon Carbide from 1-Alkynes: Molecular Structure and Tribological Properties 149
6.1 INTRODUCTION 151
6.2 MATERIALS AND METHODS 153
6.2.1 Materials 153
6.2.2 Monolayer formation 153
6.3 MONOLAYER CHARACTERIZATION 154
6.3.1 Contact angle 154
6.3.2 Ellipsometry 154
6.3.3 X-ray Photoelectron Spectroscopy (XPS) 155
6.3.4 Near-edge X-ray absorption (NEXAFS) 155
6.3.5 Infrared reflection absorption spectroscopy (IRRAS) 155
6.3.6 Atomic force microscope (AFM) 156
6.4 RESULTS AND DISCUSSION 156
6.4.1 Etching of SiC by HF. 156
6.4.2 Water Contact Angle and Monolayer Thickness 157
6.4.3 Infrared Reflection Absorption Spectroscopy 159
6.4.4 X-ray Photoelectron Spectroscopy (XPS) 162
6.4.5 Near Edge X-ray Absorption Fine Structure (NEXAFS) 165
6.4.6 Atomic Force Microscopy (AFM) 166
6.4.6.1 Adhesion 168
6.4.6.2 Friction 170
6.4.6.3 Wear 172
6.5 CONCLUSIONS 175
6.6 REFERENCES 175

6.1 INTRODUCTION

Due to its remarkable physico-chemical stability, mechanical hardness and the large band gap (2.0 eV ≲ Eg ≲ 7.0 eV, depending on polytype), silicon carbide (SiC) is one of the most used semiconductor materials for building high-performance microelectronic devices.[1-3] SiC has a higher breakdown electric field than silicon (0.3 and 3.0 MV/cm, respectively).[1] Consequently SiC has been considered as a possible alternative for Si under high temperature and highly oxidative conditions.[4] In addition, also the physical properties of SiC such as low friction coefficient, high wear resistance, and chemical inertness make this material attractive for micromechanical device applications.[5, 6]

The modification of SiC with covalently bound organic monolayers is an attractive and rapidly growing research area from both fundamental and applied perspectives. So far, four approaches have been developed for the formation of dense and well-defined organic monolayers onto SiC for biofunctionalization: 1) photochemical attachment (254 nm) of 1-alkenes,[7-9] 2) thermal grafting of 1-alkenes,[10, 11] 3) radical attachment using 2,2′-azobisisobutyronitrile (AIBN),[12] and 4) silane chemistry.[13-15] The attachment of 1-alkynes onto SiC has not been investigated systematically, but seems interesting as recently it has been found that on oxide-free silicon the use of 1-alkynes provided significant improvements in term of reaction rate, surface coverage and (oxidative) stability compared to the analogous 1-alkene-derived surfaces.[16-18]

Such increased stability would also be of interest for tribological studies. Understanding adhesion, friction and wear at the molecular scale is of significant importance for many regular applications, including nanoscale modules that laterally slide over a surface, such as in MEMS/NEMS. Many inorganic surfaces display relatively high adhesion and friction forces due to a native oxide layer present on top, which yields H-bond formation and capillary forces with surface-bound water, and thereby greatly influences the tribological performance of these mechanical systems.[19, 20] Therefore, thin organic films on silicon, alumina and gold surfaces have been investigated, to obtain reduced adhesive forces and friction coefficients at both the micro- and nanoscale.[20, 21] In particular, ultrathin organic fluorinated monolayers have been found to yield lubricating surfaces with low adhesion, low friction and low wear resistance.[21-23] In fact, fluorinated monolayers on Si surfaces[24, 25] have been found to even yield the lowest friction coefficient for any solid surface, even about 4x lower than Teflon.[25] However, to the best of our knowledge, no tribological study of covalently attached organic monolayers onto SiC has been reported yet. In practice, polytetrafluoroethylene (PTFE) is now the primary coating material in many micro-electromechanical systems.[26] These films are, however, not covalently bound to the surface and are therefore susceptible to wear. Moreover,

PTFE films are relatively thick, which may eventually lead to high adhesion and friction forces when high loads are applied and the films are compressed.

Finally, the prospect of covalent bonding also induced us to study the nature of the bonding of the organic monolayer to the surface. Such bonding is by no means trivial to predict. Whereas 1-alkynes react with a hydrogen-terminated Si(111) surface under exclusive formation of Si-C=C-bonds,[16] on aluminium oxide alkynes R-C≡C-H react under formation of a surface-bound R-C(OH)-COOH moiety.[27] Since HF etching of SiC yields OH-terminated surfaces,[28] it is not clear which binding mode could be expected for this. For comparison, for the binding of 1-alkenes to SiC the development of CH_3-bands in the IR spectrum upon the attachment of 'CH_3-free' alkenes like H_2C=CH-$(CH_2)_n$F, prompted the hypothesis of binding via ~OC(CH_3)H-R groups, i.e. a Markovnikov-type addition.[7, 10]

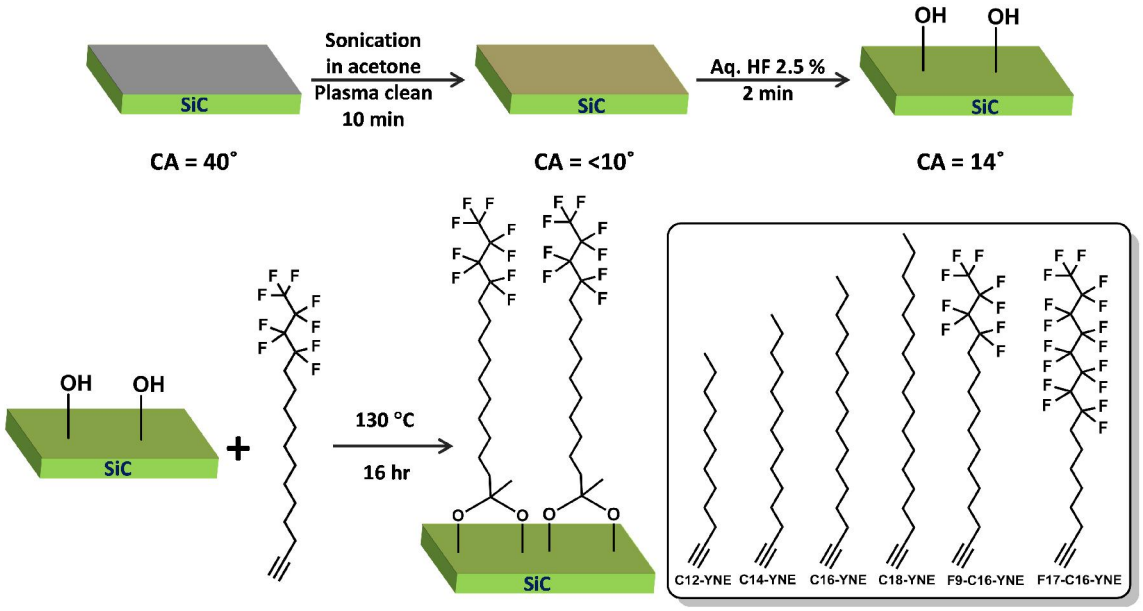

Scheme 1. Schematic representation of the preparation of hydroxyl-terminated SiC surface by wet chemistry method and reacted with F9-C16-YNE at 130 °C for 16 hr. Bottom right (inset): alkynes used to modify the SiC with identical conditions.

The goal of this study is to investigate whether 1-alkynes could be bound to silicon carbide surfaces in such a manner that this would provide improved access to low adhesion, low friction and high wear resistance properties on SiC surfaces. Here, we report a method for the thermally induced formation of novel covalently bound, 1-alkyne-

derived (fluorinated and non-fluorinated) monolayers on HF-etched 3C-SiC surfaces (see Scheme 1). The structure of the resulting monolayers is investigated in detail by XPS, water contact angle, IRRAS, AFM, and NEXAFS measurements, which are complemented by ab-initio calculations. This combination of data leads to a detailed proposal for the mode of attachment for 1-alkynes onto SiC. Finally, the resulting modified SiC surfaces are studied in view of their remarkable tribological properties and wear resistance, to outline their potential to further improve the performance of micro-electronic devices.

6.2 MATERIALS AND METHODS

6.2.1 Materials

Acetone (semiconductor grade VLSI PURANAL Honeywell 17617), dichloromethane (DCM, Fisher), hydrogen peroxide (Acros Organics, 35%), Milli-Q water (resistivity 18.3 MΩ cm), and pentane (VWR, 95%) were used as received. Hydrofluoric acid (HF, Merck, 40%) was diluted with deionized water to get a 2.5% solution (Warning: Hydrofluoric acid is an extremely corrosive acid: HF readily penetrates human skin, allowing it to destroy soft tissues and decalcify bone, and should be handled with extreme care!). Stoichiometric polycrystalline 3C-SiC films (thickness 183 nm, surface rms roughness determined with AFM 2.11 ± 0.2 nm) were obtained by chemical vapor deposition (CVD) on Si(100),[29] as generous gifts by Prof. Roya Maboudian, University of California, Berkeley, USA. 1-Hexadecene (Aldrich, ≥99%, C16-ENE), 1-dodecyne (Aldrich, 98% C12-YNE), 1-tetradecyne (Aldrich, ≥97%, C14-YNE), and 1-hexadecyne (ABCR, Germany 90%, C16-YNE) were purified by column chromatography (hexane) to remove trace amounts of 1-bromoalkane or other impurities, and subsequently distilled twice under reduced pressure before use. The synthesis procedure for 1-octadecyne (C18-YNE) has been described in detail elsewhere.[30] 13,13,14,14,15,15,16,16,16-Nonafluorohexadec-1-yne (F9-C16-YNE) and 9,9,10,10,11,11,12,12,13,13,14,14,15,15,16,16,16-heptadeca-fluorohexadec-1-yne (F17-C16-YNE) were synthesized and purified according to previously published procedures.[25]

6.2.2 Monolayer formation

Pieces of SiC (1 × 1 cm^2) wafers were first rinsed several times with acetone (p.a. grade). These samples were sonicated for 10 min in acetone, and then dried with a stream of argon. The samples were further cleaned using air plasma (Harrick PDC-002 setup) for 10 min. Subsequently, the SiC substrates were etched in 2.5% aqueous HF solution for 2

min.[7, 10] After etching, the samples were thoroughly rinsed with Milli-Q water and finally blown dry with a stream of argon. The monolayer preparation is described elsewhere.[10] These freshly etched and dried surfaces were then quickly transferred into a three-necked flask, which was charged with 2 mL of alkyne or alkene. This setup was purged with argon under reduced pressure (10 mbar) for 30 min, while being heated up to 80 °C, and the reaction mixture was kept at 130 °C for 16 h. The modified samples were removed from the flask and immediately rinsed extensively with pentane and DCM, sonicated for 5 min in DCM to remove physisorbed molecules and blown to dry using an argon stream. The modified surfaces were directly subjected to surface characterization unless specified otherwise.

6.3 MONOLAYER CHARACTERIZATION

6.3.1 Contact angle

Contact angle measurements were performed on a Krüss DSA 100 contact angle goniometer with an automated drop dispenser and image video capture system. The static contact angles of six small droplets (3.0 μL volume of deionized water) dispensed on modified silicon surfaces, were determined using the implemented Tangent 2 fitting model. The digital drop images were processed by the image analysis system, which calculated both the left and right contact angles from the drop shape with an accuracy of ±1.0°. For advancing contact angle determinations on the same samples droplets of 1 μL total volume were applied at 1 μL/min, and monitored by video recording. Reported angles are the average of at least five droplets.

6.3.2 Ellipsometry

To measure the thickness of the organic layer on top of the silicon carbide surfaces (in the dry state), a rotating analyzer ellipsometer from Sentech Instruments (Type SE-400) was used. The operating wavelength was 632.8 nm (He–Ne laser), and the incident angle was 70°. The optical constants of the substrate were determined with a piece of freshly etched SiC, and yielded refractive index (n_s = 3.38) and imaginary refractive index (k_s = 0.54). These refractive indices were very high as compared to the literature value of 2.64 for SiC,[31] because the optical model does not include the thin film of (non-stoichiometric) oxycarbide layers.[28] Monolayer thicknesses were determined with a planar three-layer (ambient, monolayer, substrate) isotropic model with a refractive index of 1.46 for the organic monolayers.[10] The reported values for the layer thicknesses are the average of

minimum eight measurements taken at different locations on the substrate with an error ±3 Å.

6.3.3 X-ray Photoelectron Spectroscopy (XPS)

XPS measurements were performed using a JPS-9200 photoelectron spectrometer (JEOL, Japan). A monochromatic Al Kα X-ray source (hν = 1486.7 eV) 12 kV and 20 mA using an analyzer pass energy of 10 eV was used. The base pressure in the chamber during measurements was 3×10^{-7} Torr, and spectra were collected at room temperature. The takeoff angle φ (angle between sample and detector) of 80° is defined with a precision 1°. The intensity of core level electrons was measured as the peak area after a standard, linear background subtraction. The typical sample size was 1×1 cm^2. All XPS spectra were fitted using the Casa XPS software (version 2.3.15).

6.3.4 Near-edge X-ray absorption (NEXAFS)

NEXAFS spectra were collected at the National Synchrotron Light Source (NSLS) U7A beamline at Brookhaven National Laboratory, using an elliptically polarized beam with ~85% p-polarisation. This beam line utilizes a monochromator and 600 l/mm grating providing a full-width at half-maximum (FWHM) resolution of ~0.15 eV at the carbon *K*-edge. The monochromator energy scale was calibrated using the intense C 1s–π* transition at 285.35 eV of a graphite transmission grid placed in the path of the X-rays. Partial electron yield was monitored by a detector with the bias voltage maintained at −150 V. Samples were mounted to allow rotation and changing the angle between the sample surface and the synchrotron X-rays. The NEXAFS angle is defined as the angle between the incident light and the sample surface. The spectra were brought to the standard form by linear pre-edge background subtraction and normalising to the unity edge jump defined by a horizontal plateau 40–50 eV above the absorption edge. The SAM spectra were normalized to spectra of reference SiC substrate to remove blurring of the overlayer spectra by carbon in the substrate material.

6.3.5 Infrared reflection absorption spectroscopy (IRRAS)

IRRAS was performed on a Bruker TENSOR 27, using a Harrick Auto SeaguII™ sample holder and a MCT (Mercury, Cadmium, Telluride) detector. Measurements were done using the Auto SeaguII Pro v1.50 software. P-polarized spectra were recorded at a mirror angle of 68°. Per measurement 2048 scans were taken at a resolution of 4 cm^{-1}. The spectra were analyzed using the Opus 6.5 software. The final spectra were obtained as the raw data divided by the data recorded on a plasma-oxidized reference surface as

background. All spectra were recorded at room temperature in a dry, nitrogen atmosphere. A linear baseline correction was applied.

6.3.6 Atomic force microscope (AFM)

Tribological and wear testing experiments were performed using an Asylum MFP-3D atomic force microscope (AFM) in contact and tapping mode. All AFM measurement were carried out under ambient conditions (25 °C, relative humidity = 40 %). For adhesion and friction measurements, the experimental setup and procedure have been described previously.[25] Nanowear/machining experiments were performed using diamond-like carbon (DLC) coating on tip side of the cantilever, 15 nm thick; aluminum coating on detector side of the cantilever, 30 nm thick, cantilevers with spring constant of 43 N/m (Tap300DLC Budgetsensors). The radius of the tip was about 100 nm, as confirmed by scanning electron microscopy (SEM). Self-assembled monolayers (SAMs) were scanned in a direction perpendicular to the long axis of the cantilever beam with a scanning speed of 50 μN/s during the nanowear and at a resolution of 480 × 480 pixels. In all wear experiments, an area of 25 μm × 25 μm was scanned at normal loads ranging from 1 to 14 μN for one scan cycle. A force was applied from one edge of the scan area to the other edge. All AFM scans were performed at a 90° angle to the long axis of the cantilever at a velocity of 0.5 Hz. The wear images and corresponding wear depth measurements were done with a larger specimen surface area. The latter was scanned before and after the nanowear test; using the same DLC tip the wear marks were observed by scanning a larger 50 μm × 50 μm area with the wear mark at the center at zero normal load.

6.4 RESULTS AND DISCUSSION

6.4.1 Etching of SiC by HF.

Scheme **1** shows the various alkynes and alkene that were attached to SiC surfaces via thermally induced monolayer formation. Pieces of freshly oxidized oxycarbide (SiC_xO_y) wafers were etched with aq. 2.5% HF (2 min), and subsequently exhibited a static contact angle (SCA) of 14° (see Table 1). As previously reported, this hydrophilicity might be attributed to the formation of a high density hydroxyl-terminated SiC surface.[8, 14, 28] Moreover, Dhar et al. reported contact angles for the C and Si face of 3C-SiC are 24 ± 1° and 4 ± 1°, respectively,[28] considerably more hydrophilic than freshly etched H-terminated Si(111) which has a contact angle of ~83°.[18]

To confirm the absence of silicon oxide layer after HF etching, the etched SiC surfaces were studied with X-ray photoelectron spectroscopy (XPS).[10, 28] Table **1** shows the peak assignment and elemental concentration (in Atom %) derived from the XPS measurements (see *Supporting Information S.6.2* Figure S2) after each step of the SiC etching procedure. According to Dhar et al. the C-face of SiC shows a binding energy of C1s in the top surface carbon layer at 283.6 eV and a Si2p core level component at 100.1 eV, which indicates that each surface silicon atom is bound to one oxygen atom.[28] The percentage of oxygen significantly decreased after etching with HF (from 31.4% to 7.6%). After etching ~1 oxygen monolayer was obtained, this was determined using the intensity of the measured O1S core levels on etched SiC, which is in accordance with data reported earlier by Dhar et al. [28] (see *Supporting Information S.6.3*). A survey scan showed the appearance of a small fluorine signal (0.5%) after the etching step assigned to Si-F bonds.[10, 28]

Table 1. Sequential Wetting behavior and XPS-derived elemental composition (in atom %) after series of surface treatments.

Substrate	Contact Angle	C1s (283.6 eV)	Si2p (100.1 eV)	O1s (532.6 eV)	F1s (686.9 eV)
Bare SiC[a]	40°	32.5%	42.6%	24.9%	--
Air Plasma cleaning	<10°[b]	26.3%	42.3%	31.4%	--
2 min in 2.5 % HF	14°	43.8%	48.1%	7.6%	0.5%

[a] After 5 min sonication in acetone. [b] 10° is limit of measurement

6.4.2 Water Contact Angle and Monolayer Thickness

The etched SiC wafers were immersed in deoxygenated neat fluorinated or non-fluorinated alkynes and alkene at 130 °C for 16 h to obtain covalently bound monolayers on SiC.[10] Static and advancing water contact angle measurements are a quick and useful tool in monolayer characterization. It can be used in particular to study the stability and quality of the monolayers. The static and advancing water contact angles as determined for the alkyne and alkene derived monolayers are shown in Table **2**.[7, 10] The static water contact angles of the methyl-terminated monolayers were in the range of θ = 106 - 111°, analogous to observations made for covalently bound monolayers on Si(100),[30] SiC,[7, 10] SiN,[7] and Si(111)[17, 18, 32] and thiols on gold.[33] As expected, the static water contact angle

was higher for the fluorinated monolayers (θ = 116 - 120°), due to the low Van der Waals interactions between water and F-containing alkyl chains.[25, 34]

The advancing water contact angles of the methyl-terminated layers were in the range of θ = 110 - 117°, similar results were observed for methyl-terminated monolayers on Au,[33] while for the fluorinated monolayers values of θ = 124 - 126° were found. Subsequently, these wettability data can be used to calculate the work of adhesion (W_A) of a surface. The work of adhesion is the reversible free energy associated with the creation and destruction of interfaces. In case of water drops on solid surfaces, W_A can be calculated using the Young−Dupré equation:[35]

$$W_A = \gamma_{LV}(1 + cos\,\theta_a) \qquad (1)$$

where θ_a is the advancing water contact angle, γ_{LV} is the surface tension of the air/water interface and approximately 72.8 mN/m. Table 2 show the calculated works of adhesion using Equation (1) as a function of chain length for the CH_3 and CF_3-terminated monolayers on SiC. For all monolayers, the total work of adhesion decreases with increasing chain length. The decrease in W_A is related to a decrease in the intercalation of water as the interface becomes more highly ordered.[36] For comparison a C_{16} alkene-derived monolayer was also prepared, which showed static and advancing contact angles of 106° and 110°, respectively, which was significantly lower than obtained for the corresponding C16-YNE-derived monolayer: 110° and 115°, respectively. This suggests that the packing density of alkyne-derived monolayers on SiC is indeed better than obtainable with 1-alkenes. The work of adhesion is very low for fluorinated monolayers F9-C16-YNE (advancing contact angle = 124°; 32.1 mJ/m^2) and F17-C16-YNE (advancing contact angle = 126°; 30.0 mJ/m^2), e.g in comparison to literature values for poly(tetrafluoroethylene) (PTFE), 34.2 mJ/m^2,[36] and similar to *Wa* values for fluorinated thiols on gold surfaces, 30.0 mJ/m^2.[34] These contact angles are slightly higher, and work of adhesion data slightly lower than for similar fluorinated alkyne-derived monolayers on Si(111) (for F17-C16-YNE advancing contact angle = 123.7°; Wa = 32.4 mJ/m^2),[25] and most probably induced by the difference in surface roughness of SiC (R_a = 2 nm) and Si(111) (R_a = 0.1 nm).[37]

Table 2. Wettabilities and Ellipsometric Thickness of Alkyne-Derived Monolayers on SiC: Static Water Contact Angle (SCA), Advancing Water Contact Angle (ACA), work of adhesion (W_A) and Ellipsometry Thickness.

Monolayers	SCA (θ) ± 1°	ACA (θ) ± 2°	Work of Adhesion WA [mJ/m^2]	Ellipsometry thickness ± 3 Å
C12-YNE	107	110	47.9	15
C14-YNE	109	112	45.5	16
C16-YNE	110	115	42.0	19
C18-YNE	111	117	39.7	24
F9-C16-YNE	116	124	32.1	17
F17-C16-YNE	120	126	30.0	16

In addition, the monolayer thicknesses obtained by ellipsometry measurements on SiC are shown in Table **2**. Previously our group reported on difficulties to distinguish between various layer thicknesses and optical constants by ellipsometry on SiC, and we found monolayer thicknesses of about 70% lower than theory values for 1-docosene on SiC.[10] These problems could be related to the optical constants used in the ellipsometry. We determined for freshly HF-etched SiC the refractive index N_s = 3.38 and imaginary refractive index K_s = 0.54. Using these values, the observed ellipsometric layer thicknesses range from 15 ± 3 Å for C12-YNE to 24 ± 3 Å for C18-YNE. These values are in excellent agreement with predicted values as obtained via molecular mechanics calculations in Materials Studio for a fully extended, configuration of the molecules oriented normal to the surface: 15 Å for C12-YNE to 23 Å for C18-YNE.

6.4.3 Infrared Reflection Absorption Spectroscopy

Infrared reflection absorption spectroscopy (IRRAS) is a useful technique that not only provides direct evidence for the presence of particular functional groups at the monolayer terminus, but also gives an indication about the mode of attachment of monolayers on these reflective substrates. In Figure 1, selected ranges of the IRRAS data for C18-YNE, C16-ENE and F17-YNE monolayers on SiC are depicted, showing among other absorptions, clear stretching peaks assigned to CH_2 (antisymmetric and symmetric) and CH_3, (Figure 1).

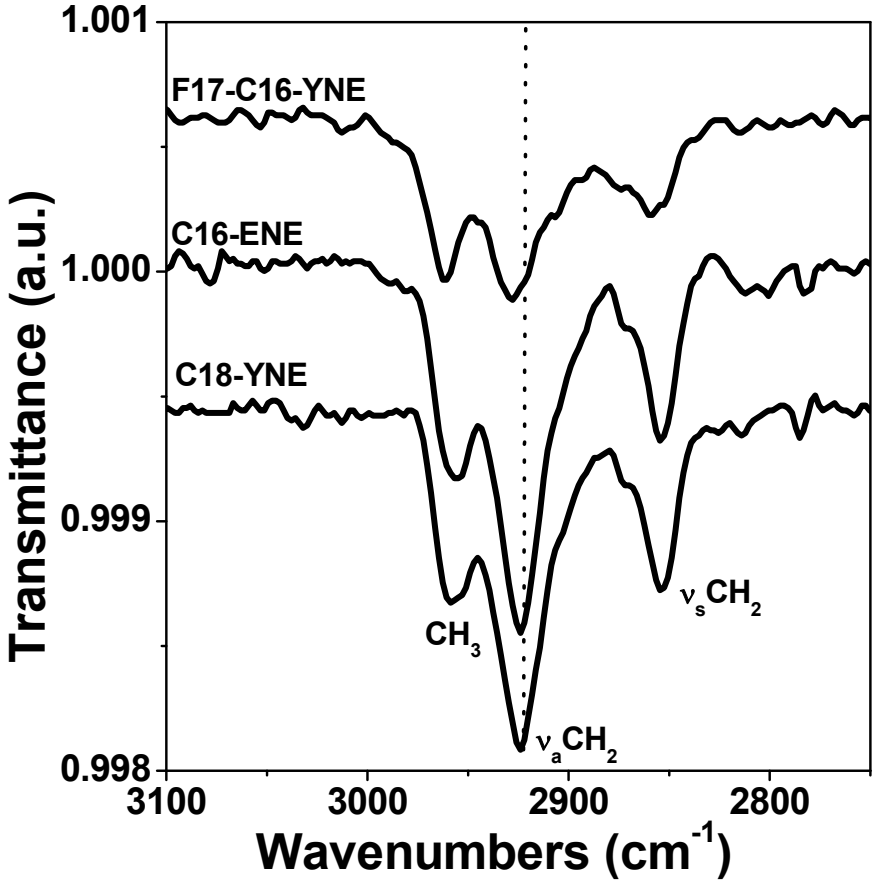

Figure 1. IRRA spectrum in dry air of C18-YNE (bottom), C16-ENE (middle), and F17-C16-YNE (top) derived monolayer on SiC at 130 °C for 16 h only C-H stretching region after spectra are shown after linear baseline correction.

The positions of the antisymmetric (ν_a CH_2) and symmetric (ν_s CH_2) methylene stretching can be used to distinguish between monolayers that display short-range order (~2918/2850 cm^{-1}) or disorder (~2928/2854 cm^{-1}).[38] It is obvious that F17-C16-YNE monolayers are disordered, with CH_2 stretching frequencies of 2927.6 and 2853.5 cm^{-1}, respectively. For C12-YNE to C18-YNE monolayers ν_a CH_2 stretching decreased monotonously from 2925.0 to 2922.5 cm^{-1}, and ν_s CH_2 stretching decreased monotonously from 2852.9 to 2851.1 cm^{-1} (Table 3), indicating a low to intermediate short-range ordering. This shift in wavenumber suggests that the longer alkynes result in a more dense molecular coating than the shorter alkynes. Interestingly, a C_{16} alkene-derived monolayer displayed IRRAS peaks at about the same positions as the C12-YNE, i.e. confirming that alkyne-derived monolayer are denser and thus display a higher degree of short-range order. Similar IRRAS peaks were observed for alkenes on as Si_xN_4,[7] SiC,[10] and fluorinated thiols on Au.[39]

Table 3. IRRAS peaks of Antisymmetric (ν_a CH_2) and Symmetric Methylene Stretching (ν_s CH_2) and Antisymmetric Methyl Stretching (ν_a CH_3) for Alkyne-Derived Monolayers.

Monolayers	[ν_a (CH_2)]	[ν_s (CH_2)]	[ν_a (CH_3)]
C12-YNE	2925.0	2852.9	2962.0
C14-YNE	2924.2	2852.6	2961.5
C16-YNE	2923.5	2851.3	2960.6
C18-YNE	2922.5	2851.1	2960.3
F9-C16-YNE	2925.3	2852.5	2962.1
F17-C16-YNE	2927.6	2853.5	2962.5

Rosso et al. reported that 11-fluoroundec-1-ene reacted with hydroxyl-terminated SiC surfaces via a Markovnikov addition, given the development of IR-visible methyl peaks during monolayer formation.[10] This -CH_3 peak around 2960 cm^{-1} was also observed in the case of the alkyne-terminated monolayers, both for the methyl-terminated ones as well as for the CF_3-terminated ones (Figure 1 and Table 3). Given the stability of a CF_3 moiety under these reaction conditions, we propose also for 1-alkyne derived monolayers the formation of surface-bound methyl groups. Figure 2 depicts schematically our hypothesis of an alkyne reacts with a hydroxyl-terminated SiC surface. Most probably, nucleophilic attack of the alkyne π bond on H-O-C (from SiC surface) (Figure 2a) leads to the formation of a vinyl carbocation at the most substituted position, following the Markovnikov selectivity, and then to enol ether formation (Figure 2b) Subsequently, this enol ether can either remain on the surface as is, or be protonated by another surface-bound proton, yielding an –O-$C^+(CH_3)$R ion, which can attack a neighboring hydroxyl group to yield a stable six-membered ring (Figure 2c). Hence, it is hypothesized that alkynes react twice to hydroxyl-terminated silicon carbide substrates via a double Markovnikov addition.

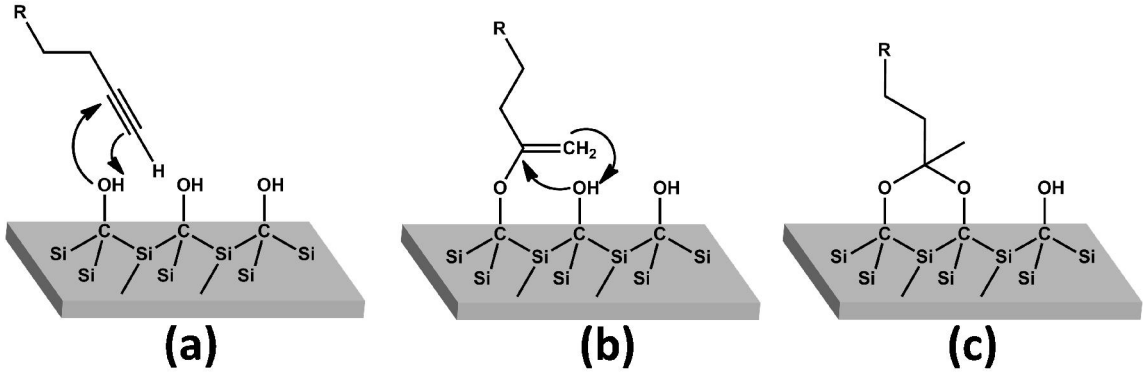

Figure 2. Proposed mechanism of the reaction between an alkyne and an OH-terminated SiC surface.

6.4.4 X-ray Photoelectron Spectroscopy (XPS)

The results of XPS analysis carried out on the C16-ENE and C16-YNE samples are shown in Figure 3. Detailed investigation of the C1s and Si2p region of the XPS spectra (Figure 3A - D, respectively) further confirm the formation of C16-ENE and C16-YNE derived monolayers on SiC.

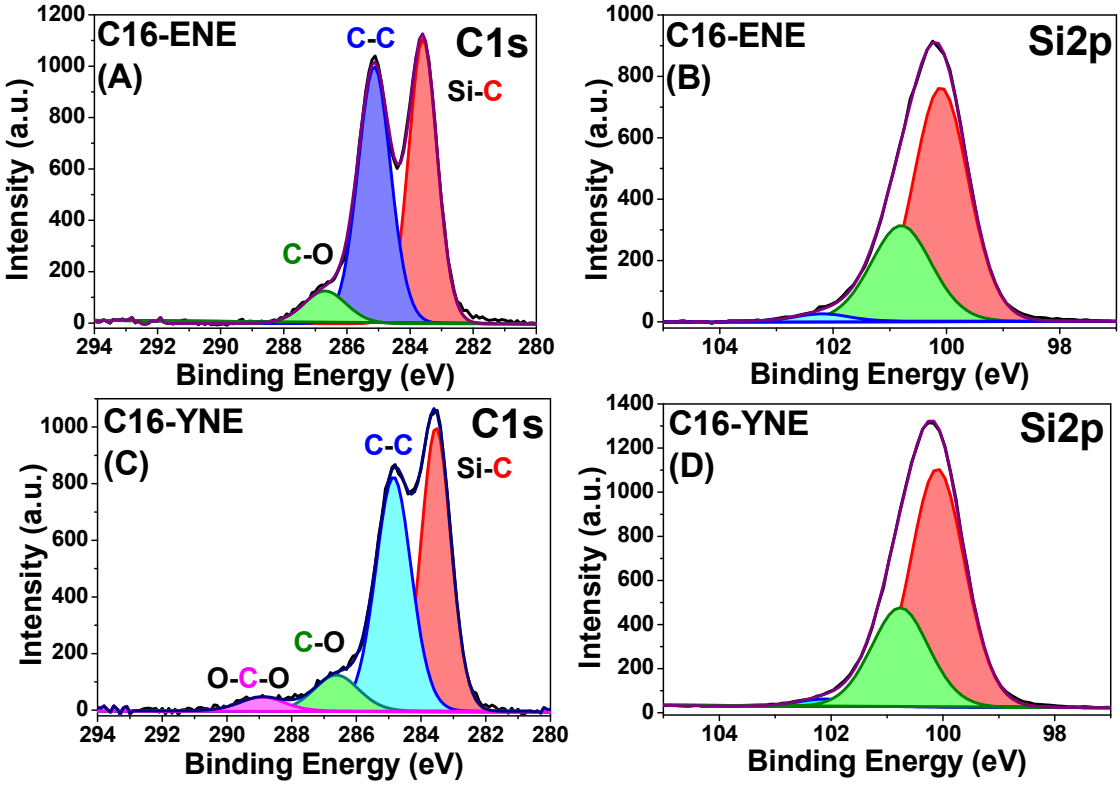

Figure 3. Narrow-scan C1s and Si2p XPS data of C16-ENE (top) and C16-YNE (bottom) derived monolayers on SiC.

The emissions from the C1s core levels of C16-ENE (Figure 3A) are in line with the formation of –O-CH(CH_3)-R monolayer structures, as explained in detail elsewhere.[40] The C1s narrow scan of C16-YNE is shown in Figure 3C and reveals the same three contributions as for C16-ENE onto SiC; however, the C16-YNE spectrum clearly also shows a fourth peak and was therefore deconvoluted into four main contributions. For the first three contributions, the assignment is similar to C16-ENE, but a new peak at 289.0 eV is also present, and is attributed to an acetal-like linkage (O-C-O) to the SiC surface, an assignment in good agreement with literature values for acetyl-protected derivatives.[41, 42] This was confirmed by DFT-simulated XPS spectra (B3LYP/6-311G(d,p) level), which

showed that a C-O peak is to be expected at 287.3 eV, while an acetal (O-C-O) carbon atom should yield a peak at 289.2 eV, in near-perfect agreement with experiment. The DFT data for the C16-ENE and C16-YNE attachments are provided in the *Supporting Information S.6.1* Figure S1.

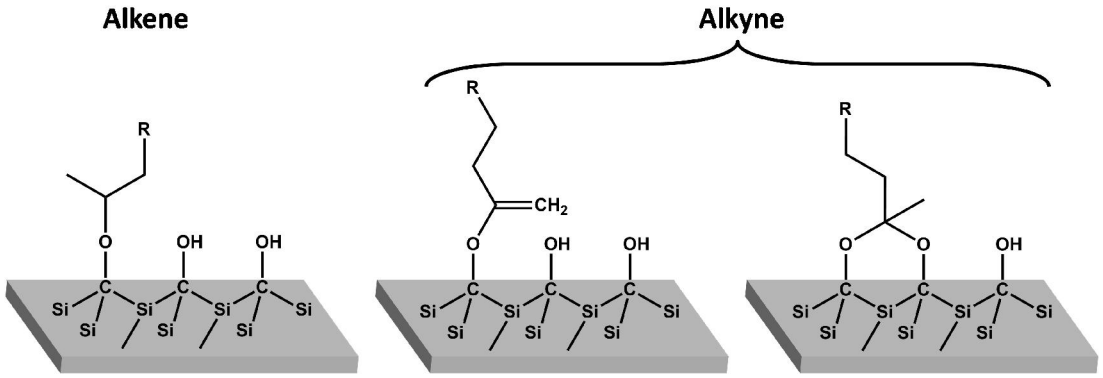

Figure 4. Schematic representation of the monolayer structure for 1-alkenes[10] and 1-alkynes reacting with a hydroxyl-terminated SiC surface.

Since a narrow scan C1s XPS spectrum of a freshly etched SiC surface shows no significant carbon peaks at 287 - 290 eV, and the ratio of the peak areas of the different carbons (-C-O and =C-O versus O-C-O) of the alkyne-derived monolayer is approximately 2.6 : 1, it is likely that the alkyne functionality reacts in a Markovnikov-type addition reaction to either one (to remain sp^2-hybridized) or two (to become sp^3-hybridized) hydroxyl carbons on the SiC surfaces, as shown in Figure 4. Unfortunately, the signal/noise ratio in the IRRAS data in Figure 1 is such that these data cannot confirm this assignment. Similar addition reactions have been reported in organic synthesis using metal-catalyzed additions of oxygen nucleophiles to alkenes and alkynes,[43] and therefore, from these spectra, it is concluded that the acetal and ether peak were uniquely associated with the attachment of alkynes on HO-terminated SiC via a Markovnikov-type addition reaction.

The Si2p narrow scan of the SiC modified with C16-ENE and C16-YNE reveals a broad peak at ca. 100 eV (see Figure 3B and D), which can be deconvoluted into three main peaks, as reported earlier.[10] The main component at 100.1 eV corresponds to bulk silicon in SiC, the second peak at 100.9 eV to surface silicon - because every surface Si atom is bounded to one oxygen atom only - and the third and weakest peak at 102.0 eV is typical of a residual silicon oxycarbide layer.[44] This oxycarbide layer was weakly visible even on freshly prepared SiC surfaces (after 2.5% HF etching). In addition, there is no sign of SiO_2 around 103 - 104 eV after modification.[44]

Table 4. XPS C 1s Binding Energies, Curve Fittings in % and Calculated Thickness of Fluorinated and Non-Fluorinated 1-Alkyne-derived Monolayers.

Species & Binding energy [eV]	C12 YNE	C14 YNE	C16 YNE	C18 YNE	F9C16 YNE[a]	F17C16 YNE[a]
Si─*C* [283.6]	59.6	52.3	44.3	38.9	55.9	52.9
C─*C* [285.0]	28.1	35.6	44.0	51.7	28.3	16.6
C─O [286.7]	9.8	9.5	8.4	7.3	--	--
O─*C*─O [289.0]	2.5	2.6	3.3	2.1	2.2	1.9
C─O, *C*H_2-CF_2 [286.4]	--	--	--	--	7.1	4.5
─*C*F_2─ [292.0]	--	--	--	--	4.7	18.4
─*C*F_3 [294.3]	--	--	--	--	1.8	5.7
Monolayer Thickness (nm)	1.5	1.8	2.3	2.6	1.6	1.8

[a] for F9C16YNE and F17C16YNE narrow scan XPS are shown in *Supporting Information S.6.4* Figure S4.

By averaging the observed (C-H + C-O + C-F)/Si-C ratio in the C1s narrow scan, quantitative information on the monolayer thickness can obtained by XPS. Of course, on this rough surface, these XPS results can only provide a rough estimate of the thickness, as the outcome strongly depends on the attenuation length and atomic density of the substrate and the monolayers.[8] The corresponding data are shown in Table 4. Subsequently, these ratios can be converted into monolayer thicknesses (t) by the following equation:[7]

$$t = \lambda_{CH}.\cos(\theta).ln\left(1 + \frac{I_{CH}.\rho_S.\lambda_S}{I_S.\rho_{CH}.\lambda_{CH}}\right) \qquad (2)$$

where θ is the take-off angle between the surface plane and the detector, I_{CH} (C-H, C-O, or C-F) and I_S (Si-C) are the intensities of the C1s narrow scan XPS signal from the organic film (I_{CH}) and from the substrate (I_S), respectively. The ρ_{CH} and ρ_S are the elemental densities of carbon in the monolayer and in the SiC substrate, and were estimated at 0.054 and 0.08 mol.cm^{-3}, respectively. The attenuation length of C1s photoelectrons in alkyl monolayers is λ_{CH} = 2.8 nm (data form alkanethiols on gold surface),[45] and the attenuation length of C1s photoelectrons in SiC is λ_S = 2.35 nm.[46] For all monolayers, the (C-H, + C-O + C-F)/Si-C ratios and the corresponding calculated thicknesses are shown in Table 4. As evident for non-fluorinated monolayers, the Si-C contribution (283.6 eV) decreases with increasing chain length and thicknesses increase linearly with increasing chain length. In addition, we would like to note that in general the XPS-determined thicknesses are higher than the thicknesses obtained by ellipsometry (see Table 2).

6.4.5 Near Edge X-ray Absorption Fine Structure (NEXAFS)

NEXAFS spectra can provide information about the chemical bonds and their orientation and order on surfaces by probing characteristic absorption resonances related to electronic transitions from atomic core levels to unoccupied molecular orbitals.[47] Figure 5 shows carbon *K*-edge NEXAFS spectra of C16-YNE monolayers on SiC recorded at different X-ray incidence angles. The spectra exhibit the expected absorption edge related to the transition of C1s core level electrons into continuum states and a number of absorption resonances. A strong Rydberg/C-H (R*) resonance visible near 288.0 eV is mostly related to the alkyl chains. Broad σ* resonances related to C–C and C-O bonds are present at higher photon energies (293 eV and 302 eV, respectively). Chemical impurities such as C=O a common contaminant in low fidelity SAMs - are not detectable. An interesting finding is the presence of a pronounced π*(C=C) resonance near 284.8 eV assigned to C=C groups in the SAM. This observation clearly supports our the hypothesis stated in Figure 5, that both vinyl ether and acetyl formation takes place upon SAM binding, which underlines the coexistence of mono- and bidentate surface coordination.

NEXAFS also probes structural parameters of the film by monitoring intensity variations of resonances with the X-ray incidence angle, and, thus, the angle between the X-ray electric field vector and the transition dipole moment (TDM) of the respective chemical bond.[47] This effect, the so-called linear dichroism of X-ray absorption, can be directly observed in difference spectra between normal (90°) and glancing (20°) X-ray incidence angles. The difference spectrum in Figure 5 shows a weak but discernible

dichroism for the C–H resonances near 288 eV. Since a strong dichroism is a signature of well-aligned films, the weak dichroism underlines the results of the IR analysis in that C16-YNE forms films on SiC with a slight short-range order. This is also in line with the roughness of the SiC substrate (see also AFM data below), which, will also decrease the apparent overall film order. The positive sign of the difference signal indicates a mostly upright orientation of the alkyl chains. The lack of a significant difference peak for the C=C groups (284.8 eV) indicates a relatively low degree of chain alignment close to substrate surface.

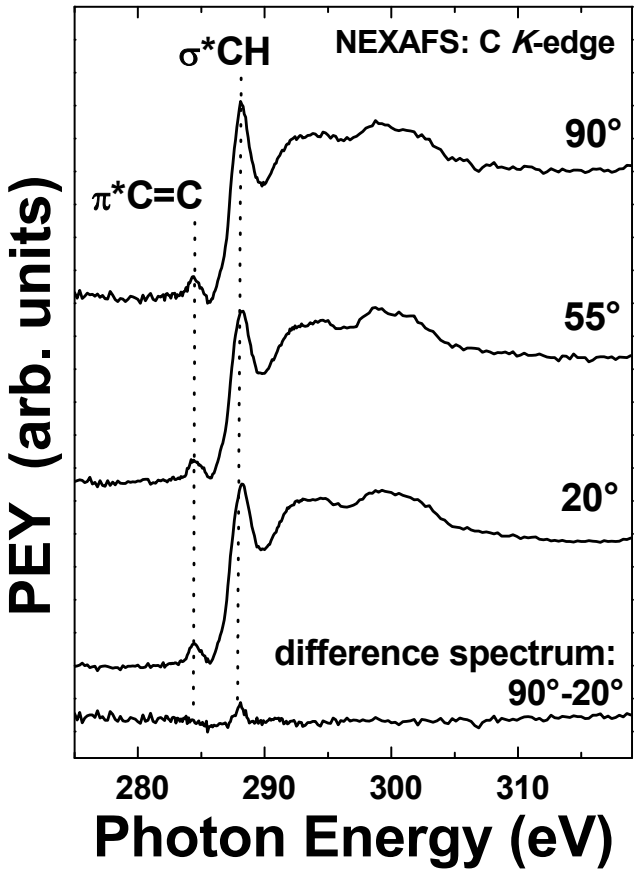

Figure 5. NEXAFS C *K*-edge spectra of C16-YNE monolayers on SiC surfaces at different X-ray incidence angles, along with a difference spectrum of spectra recorded at 90° and 20°.

6.4.6 Atomic Force Microscopy (AFM)

To explore the ability of modified SiC surfaces for application in high-performance MEMS/NEMS devices, atomic force microscopy has been used to examine the nanotribology properties of these modified SiC surfaces.[23] In general, the adhesion,

friction and wear of a film that is deposited onto a surface depend on the top layer of this film (monolayer, lubricants or polymer). In addition, tip shape, materials and applied normal force might also affect the outcome of these measurements.[20] A colloidal probe or spherical AFM probe allows a precise measurement of adhesion and friction forces on the surface. Moreover, such a probe shape allows an easy a comparison between experimental results and theoretical models such as the Derjaguin-Muller-Toporov (DMT) or the Johnson-Kendall-Roberts (JKR) models.[48] The Van der Waals forces intensify the elastic contact area between the colloidal probe and the modified surfaces.[49] As described in literature, covalently bound alkyl monolayers on various substrates have been studied with colloidal probes in different environments, such as solution phases[50] and air.[51] However, most of the high-performance MEMS/NEMS devices were analyzed in air, where typically higher adhesion and friction force are expected due to capillary condensation in air. Moreover, low-surface energy materials possess lower capillary condensing properties, which implies a lower adhesion and lower friction on the surfaces.

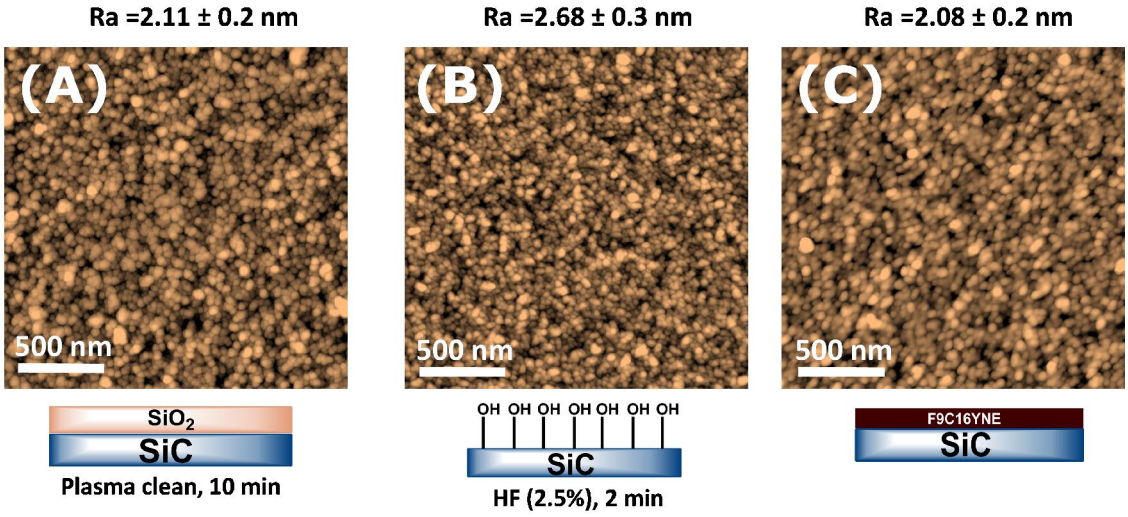

Figure 6. Tapping-mode atomic force microscope (AFM) of SiC surfaces. (A) after 10 min oxygen plasma cleaning, (B) after 2 min 2.5 % HF etching, and (C) after modification with F9-C16-YNE.

SiC is a very hard ceramic material that has high wear resistance properties as compared to Si.[5] Therefore with the aim to obtain superior tribological properties fluorinated alkyne-derived monolayers were prepared and subjected to adhesion and friction tests by AFM in air with a smooth silica probe as hydrophilic solid particle. For wear resistance studies by AFM a sharp diamond-like carbon (DLC) tip was used. A DLC tip is typically used for wear testing on surfaces, because it is virtually fully resistant to wear at the macroscale.[52]

All nano-tribological measurements were done on modified SiC surfaces with similar roughness (R_a = ~2 nm). Figure 6 shows the AFM topographical height image of SiC substrates after various activation processes: 10 min air plasma cleaning of SiC (Figure 6A); 2.5% HF etching for 2 min (Figure 6B), and after modification with F9-C16-YNE (Figure 6C). We found that the surface roughness increases to 2.68 ± 0.3 nm after etching with 2.5% HF (2 min). After monolayer grafting, the roughness slightly reduced again to 2.08 ±0.2 nm, indicating formation of a cushioning monolayer.

6.4.6.1 Adhesion

The adhesion force measurements between a silica sphere and the modified SiC surfaces are shown in Figure 7. The force required to detach the silica particle from the modified surface (pull-off force) is given as a function of advancing water contact angles (see Table 2). A clear trend is observed for C12-YNE to C18-YNE monolayers: the lower the contact angle the higher the adhesion force. For instance, the adhesion force for the C12-YNE monolayer is 13.1 mJ/m^2 (39.3 nN), whereas for C18-YNE 10.4 mJ/m^2 (31.3 nN) was found (Figure 7A). The adhesion force between the organic monolayer and silica probe is mostly non-bonding (electrostatic, hydrogen bond, and Van der Waals) in origin. The attraction of the silica probe to a rough surface is much weaker than to a smooth surface, due to the reduced contact area between the surface and the silica probe.[20] In case of fluorinated monolayers F9-C16-YNE and F17-C16-YNE, in fact, extremely low adhesion forces were observed 2.2 mJ/m^2 (6.7 nN) and 1.9 mJ/m^2 (5.9 nN), respectively. These findings were consistent with published work on more rough surfaces of PEG-grafted and fluorinated nanoparticles,[50] poly(perfluoroalkyl methacrylate) film,[53] and nano-patterned fluorinated surfaces.[54] The intrinsic properties of these covalently bound fluorinated monolayers, become evident in the comparison with atomically flat Si(111) surface modified with F9-C16-YNE and F17-C16-YNE: those show the lowest measured adhesion for any flat surface (3.6 mJ/m^2 (10.8 nN) and 3.2 mJ/m^2 (9.8 nN)),[25] while those slightly higher adhesion values are most probably caused by the maximal contact area between the silica probe and the ultra-smooth Si(111) surfaces. The very low intrinsic adhesion force observed here for the fluorinated monolayers on SiC is attributed to the weak Van der Waals forces between the probe particle and the fluorocarbon SiC surface, and follows the decrease in surface energy in the order of CH_2 (36 mNm^{-1}) > CH_3 (30 mNm^{-1}) > CF_2 (23 mNm^{-1}) > CF_3 (15 mNm^{-1}).[53]

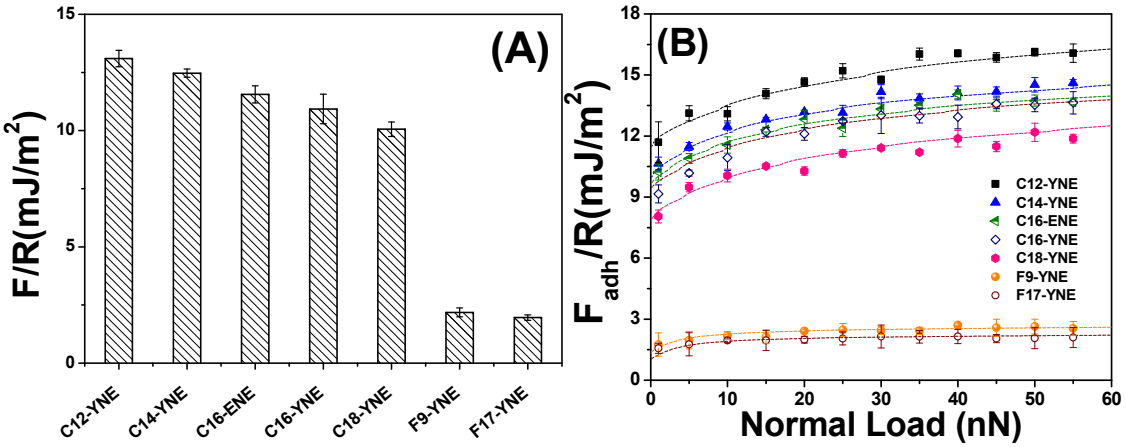

Figure 7. (A) Mean forces of adhesion as measured from pull-off curves ~200 of each monolayers at 10 nN force. (B) Adhesion forces of a colloidal silica probe as a function of normal load for different monolayers. Solid lines are fits of the data with a JKR model of a soft layer with 15 Å to 24 Å thickness on top of SiC.

These denser and more ordered ultra-thin monolayers have a lower compressibility as compared to conventional polymer coated surfaces, because the adhesion is not increasing significantly with higher normal loading force.[20] Figure 7B shows that with increasing normal load the adhesion raises for both non-fluorinated and fluorinated monolayers only up to 25%. At any stage at the same applied normal load the adhesion is considerably smaller for fluorinated monolayers as compared to non-fluorinated monolayers. These adhesion force are very low in comparison to literature values, for e.g. perfluorophosphonate monolayers on Al/Si surface the adhesion shows 17 nN to a Si_3N_4 tip.[55] Analogously, monolayers made of F17-C16-YNE on hydrogen-terminated Si(111) showed an increase in adhesion up to 30% with respect to those on SiC. This might be due to the fact that Si(111) is atomically flat surface and therefore the contact area between silica probe and the surface is larger. Also the Young's modulus is higher for SiC as compared to Si(111), resulting in a lower elastic compression for SiC.[20]

The solid lines in Figure 7B represent fits of the data to this modified JKR model with a fixed layer thickness as determined by to XPS and ellipsometry measurements. The elastic modulus of the monolayer decreases in fluorinated monolayers by a total factor of 2 as compared to non-fluorinated monolayers. In addition, the model gives a prediction for the compression of the monolayer and the area of contact between the silica probe and the monolayer as a function of normal load. Using these values, the work of adhesion between the silica probe and the monolayers and an effective Hamaker constant can be calculated using a Derjaguin approximation. A typical indentation of the monolayer at a normal load of 10 nN is 1.3 nm, leading to a contact area of 0.030 μm^2. Combining these values with

the adhesion forces in Figure 7A, the effective Hamaker constant is calculated to range from 44.6 k_BT (C12-YNE) to 67.29 k_BT (C18-YNE), and decreases to 7.49 k_BT for fluorinated monolayers. Although, of course, the SiC roughness leads to lower Van der Waal forces, these results show a very low Hamaker constant for the fluorinated surfaces as compared to bare SiC surface, for which values in range of 60-107 k_BT have been observed.[56]

6.4.6.2 Friction

Covalently bound fluorinated monolayers hold great promise in nano-lubrication. Therefore, the lateral friction force on the fluorinated and non-fluorinated monolayers was measured using the same silica probe set-up as for the adhesion measurements. The normal load was increased from 0 to 65 nN, and the corresponding lateral friction was recorded on several 5×5 μm^2 areas at a scan rate of 0.5 Hz. Due to use of a low scan speed of 6.22 μm/s on the surface, we observed boundary friction but not hydrodynamic friction. As shown in Figure 8A, the average frictional forces are linearly proportional to the normal loads, with a slope that can be correlated to the friction coefficient values in Figure 8B. The friction at zero load decreases for the fluorinated monolayers, which is in agreement with the adhesion measurements, whereas the friction coefficient for non-fluorinated monolayers varies from 0.013 (C12-YNE) to 0.020 (C18-YNE), in good agreement with the results for monolayers on Si(111).[57] For the fluorinated monolayers, the friction coefficient remarkably decreases to 0.008 for F17-C16-YNE and 0.01 for F9-C16-YNE, The three major factors for this decrease in friction are: 1) fluorinated monolayers are expected to have a lower polarizability at their surface; 2) due to the surface roughness, it could be that there is significant stick-slip motion of the probe on the surface. In that case the net friction for the trace and retrace might be the same, and 3) higher Young's modulus materials decrease the friction coefficient.[5] The overall resulting low friction coefficient value of covalently bound fluorinated monolayers indicates this system to have excellent lubrication properties in air. Also, no wear was observed even at a maximum force of 65 nN. For bare SiC a friction coefficient of 0.02 is found, which is in good agreement with the experimental results for polished SiC (Rms = 0.89 nm)[5] and molecular dynamics (MD) simulations on SiC, which yield a value of 0.02 ± 0.01.[58]

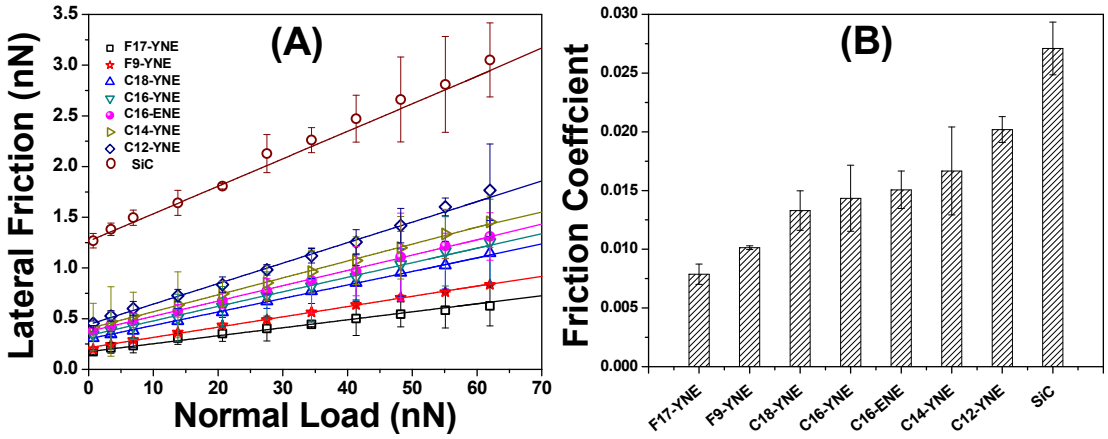

Figure 8. Lateral friction forces of SAMs. (A) Representative lateral friction force data versus applied normal load for the all fluorinated and non-fluorinated SAMs on SiC. [The solid lines are linear regression lines.] (B) The friction coefficients for different monolayers, obtained from the slope of the friction force versus normal load.

The correlation between the dynamic friction coefficient and the adhesion energy F/R (in mJ/m^2) is shown in Figure 9. The adhesion energy was taken at constant applied load of 10 nN force for different monolayers. For the fluorinated monolayers (point 1, 2), we observed that the adhesion energy (F/R) is around 2 mJ/m^2 and the dynamic friction coefficient is small (between 0.008 – 0.010). In case of non-fluorinated monolayers (point 3-7), we observe that the adhesion energy (F/R) is higher than ~10 mJ/m^2, and that there is also a rapid increase in the friction coefficient. Clearly, the friction coefficient is correlated to the properties of the surface, showing that the sliding of the probe over the surface causes dissipative molecular bonding and debonding events (both normally noncovalent in nature) to occur. The larger the adhesion forces, the larger the energy barrier associated with debonding events and the higher the friction coefficient. This is in line with a sum of a constant term and an Arrhenius term:

$$FC = FC\ (0) + k_f e^{A\,W_{adh}/kt} \qquad (3)$$

where A is an effective contact area, k is Boltzmann's constant and t is the absolute temperature and k_f a constant. The data shown in the inset to Figure 9 is calculated by using the equation 3. The effective contact area (A) calculated from the slope of the linear line is shown in the inset to Figure 9. An effective contact area of 30 nm^2 was found for the silica colloidal probe, which was used to measure adhesion and friction on rough SiC

modified surfaces. A possible explanation of such low contact area is the low elastic–plastic deformation of such organic monolayers.

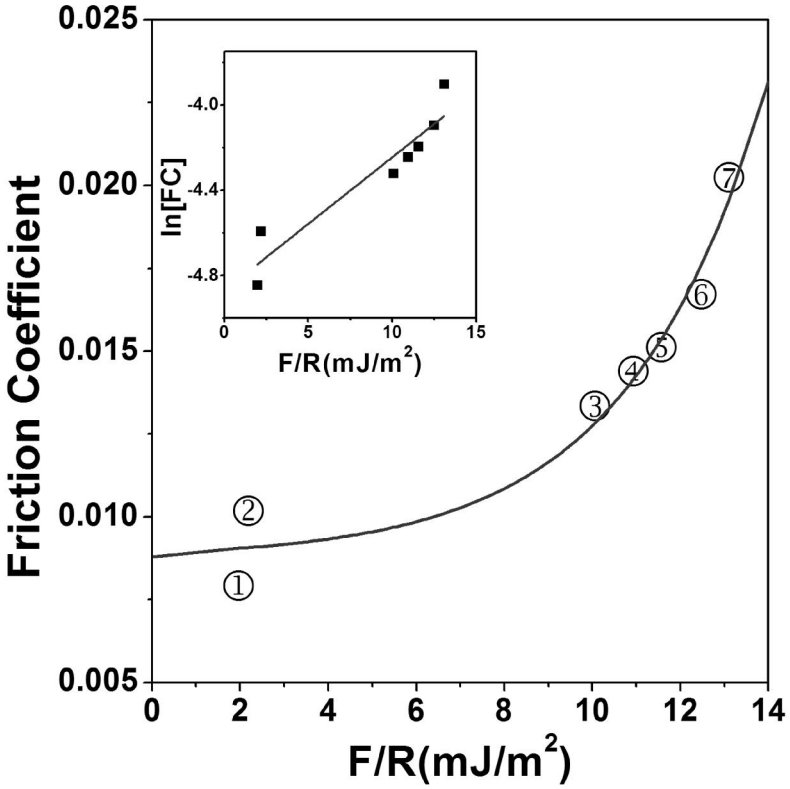

Figure 9. Correlation between dynamic friction coefficient and adhesion energy F/R(mJ/m^2) at applied normal load 10 nN on different monolayers on SiC (from F17-YNE (①), F9-YNE (②), C18-YNE (③), C16-YNE (④), C16-ENE (⑤), C14-YNE (⑥), and C12-YNE (⑦).The inset shows the linear Arrhenius plot drawn with natural log of friction coefficient verses adhesion energy. The obtained slope gives the effective contact area of probe to the surface.

6.4.6.3 Wear

As explained in earlier section the resulting monolayers have been characterized for their nano-lubrication properties by the frictional force measurements at pressures from 0 to 65 nN. In this range of force these monolayers do not show any wear marks. This is already an interesting result, but to further proof the potential of the wear properties of these monolayers, experiments at higher normal forces were carried out. The applied normal load was in the range of 1 μN to 14 μN (Figure 10 and Figure 11**)**. Typical wear marks with the size of 25 × 25 μm were generated during one scan cycle, and subsequently imaged by AFM at scan velocity of 0.5 Hz in contact mode. The same cantilever was used for the AFM imaging of the wear mark. The scan area for imaging the wear marks was 50 × 50 μm^2, and zero normal load was applied to capture the image. The

surface topography images of the wear marks are depicted in Figure 11. At higher load, the wear fragments produced throughout the wear marking area are not sticky, and could be moved out of the scan area by the light load during scanning (no stick slip effect was observed).

The observed wear-induced depth increases linearly with an increasing normal load, as is shown in Figure 10. The surfaces modified with organic monolayers showed a lower wear-induced depth than unmodified SiC, even at a high normal force (14 μN). In short chain length non-fluorinated monolayers, the wear depth is greater than for the longer chain length monolayers (2.8 nm and 1.5 nm for C12-YNE and C18-YNE, respectively). This decrease in wear-induced depth is attributed to a more dense monolayer. The fluorinated monolayers clearly exhibit extreme wear resistivity compared to the non-fluorinated monolayers, indicating that fluorinated monolayers significantly improve the mechanical properties of the surface. The enhanced wear resistivity of fluorinated monolayers is at least partially due less cleavage of the top layer, $-(CF_2)_nCF_3$,[59] because the strength of the $-CF_2-CF_3$ bond (dissociation energy ~423 kcal/mol) is higher than that for the $-CH_2-CH_3$ bond (~301 kcal/mol). For both fluorinated and non-fluorinated monolayers, increasing the chain length decreases the wear-induced depth for any given normal load, similar to what Bhushan et al. observed with modified Al and Si oxide surfaces.[59]

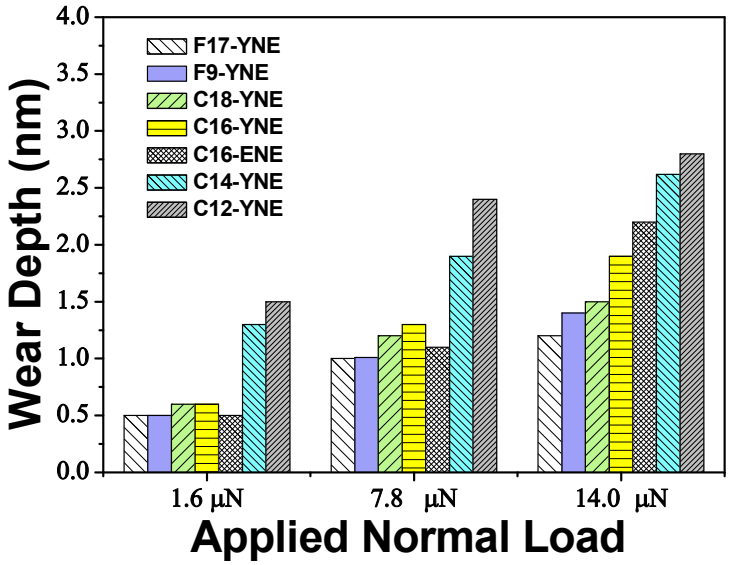

Figure 10. Wear depth for single cycle at various loads and for evolution of wear at different monolayers on SiC.

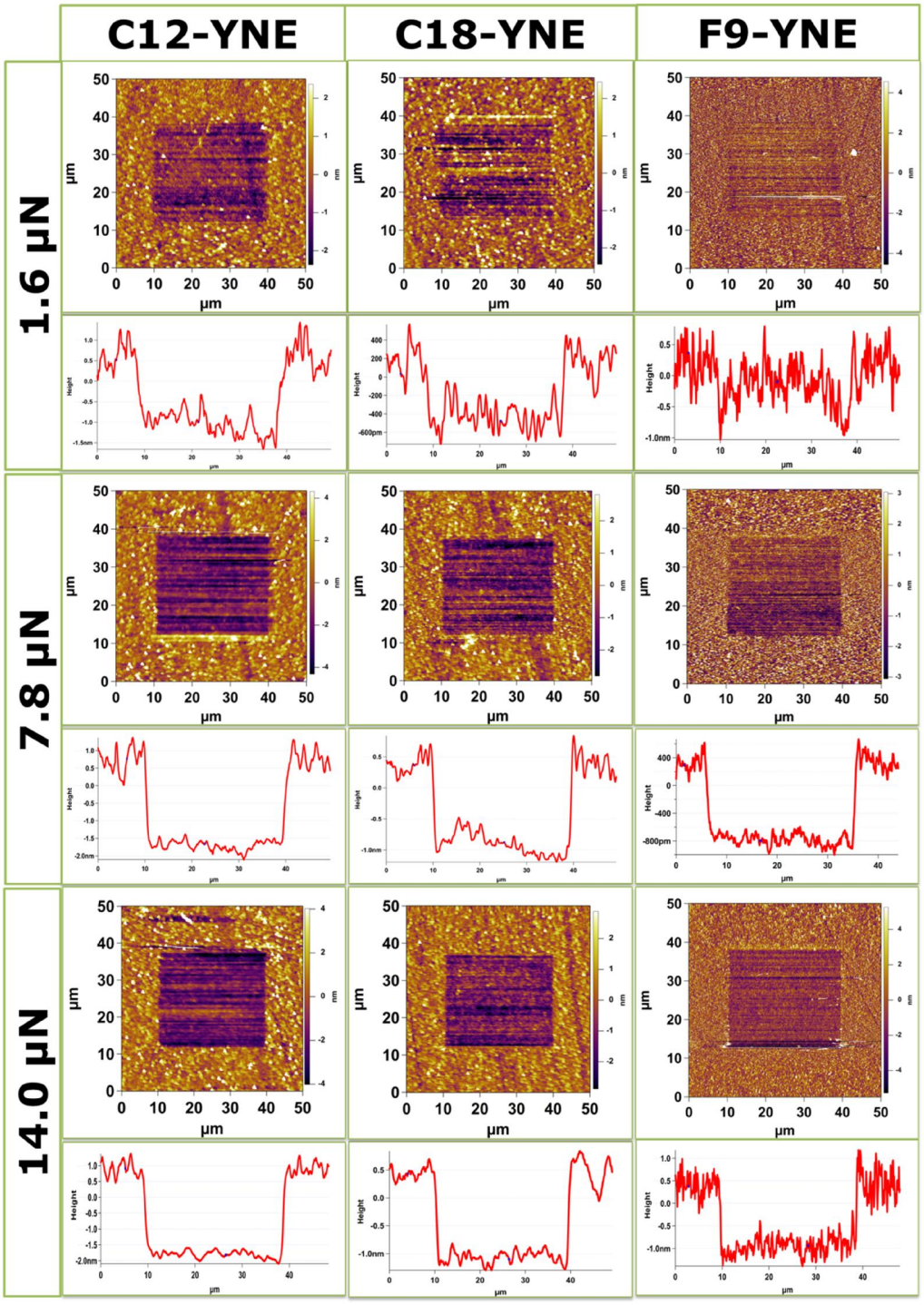

Figure 11. AFM images of wear marks produced at different normal load after one scan cycle, the normal pressure and the average wear depth are shown on the bottom side of the figure (profile width: 50 micron for all images; the square drawn to test the wear resistance is 25 × 25 micron).

6.5 CONCLUSIONS

In this work, we have successfully demonstrated the formation of covalently bound, highly stable fluorinated and non-fluorinated monolayers via the thermal reaction of 1-alkynes with SiC substrates. The alkyne group reacts with the hydroxyl-terminated surface via a double Markovnikov addition, forming a doubly bound, acetal-containing heteroatomic six-membered ring. This suggests a new pathway for the reaction mechanism of un-substituted hydrocarbons with hydroxyl-terminated surfaces. In addition, fluorinated monolayers on SiC were shown to display minimal friction (friction coefficient down to 0.008) and adhesion energies. In combination with the extraordinary wear resistance of SiC surfaces that are coated with these fluorinated monolayers, this shows that these covalently bound fluorinated monolayers on SiC provide a promising alternative to currently used stable lubricants in high-performance micro-electronic devices.

6.6 REFERENCES

1. Peter Friedrichs; Tsunenobu Kimoto; Lothar Ley; Pensl, G., *Silicon Carbide*. WILEY-VCH: Weinheim, 2010; Vol. 1.
2. Casady, J. B.; Johnson, R. W., Status of silicon carbide (SiC) as a wide-bandgap semiconductor for high-temperature applications: A review. *Solid-State Electronics* **1996,** 39, (10), 1409-1422.
3. Yang, N.; Zhuang, H.; Hoffmann, R.; Smirnov, W.; Hees, J.; Jiang, X.; Nebel, C. E., Nanocrystalline 3C-SiC Electrode for Biosensing Applications. *Analytical Chemistry* **2011,** 83, (15), 5827-5830.
4. Chalker, P. R., Wide bandgap semiconductor materials for high temperature electronics. *Thin Solid Films* **1999,** 343-344, (1-2), 616-622.
5. Sundararajan, S.; Bhushan, B., Micro/nanotribological studies of polysilicon and SiC films for MEMS applications. *Wear* **1998,** 217, (2), 251-261.
6. Lantz, M. A.; Gotsmann, B.; Jaroenapibal, P.; Jacobs, T. D. B.; O'Connor, S. D.; Sridharan, K.; Carpick, R. W., Wear-Resistant Nanoscale Silicon Carbide Tips for Scanning Probe Applications. *Advanced Functional Materials* **2012,** 22, (8), 1639-1645.
7. Rosso, M.; Giesbers, M.; Arafat, A.; Schroën, K.; Zuilhof, H., Covalently Attached Organic Monolayers on SiC and Si_xN_4 Surfaces: Formation Using UV Light at Room Temperature. *Langmuir* **2009,** 25, (4), 2172-2180.
8. Qin, G.; Zhang, R.; Makarenko, B.; Kumar, A.; Rabalais, W.; Lopez Romero, J. M.; Rico, R.; Cai, C., Highly stable, protein resistant thin films on SiC-modified silicon substrates. *Chemical Communications* **2010,** 46, (19), 3289-3291.
9. Steenackers, M.; Sharp, I. D.; Larsson, K.; Hutter, N. A.; Stutzmann, M.; Jordan, R., Structured Polymer Brushes on Silicon Carbide. *Chemistry of Materials* **2010,** 22, (1), 272-278.

10. Rosso, M.; Arafat, A.; Schroen, K.; Giesbers, M.; Roper, C. S.; Maboudian, R.; Zuilhof, H., Covalent Attachment of Organic Monolayers to Silicon Carbide Surfaces. *Langmuir* **2008,** 24, (8), 4007-4012.
11. Schoell, S. J.; Howgate, J.; Hoeb, M.; Auernhammer, M.; Garrido, J. A.; Stutzmann, M.; Brandt, M. S.; Sharp, I. D., Electrical passivation and chemical functionalization of SiC surfaces by chlorine termination. *Applied Physics Letters* **2011,** 98, (18).
12. Iijima, M.; Kamiya, H., Surface Modification of Silicon Carbide Nanoparticles by Azo Radical Initiators. *The Journal of Physical Chemistry C* **2008,** 112, (31), 11786-11790.
13. Schoell, S. J.; Hoeb, M.; Sharp, I. D.; Steins, W.; Eickhoff, M.; Stutzmann, M.; Brandt, M. S., Functionalization of 6H-SiC surfaces with organosilanes. *Applied Physics Letters* **2008,** 92, (15).
14. Howgate, J.; Schoell, S. J.; Hoeb, M.; Steins, W.; Baur, B.; Henrich, S.; Nickel, B.; Sharp, I. D.; Stutzmann, M.; Eickhoff, M., Photocatalytic cleavage of self-Assembled organic monolayers by UV-lnduced charge transfer from GaN Substrates. *Advanced Materials* **2010,** 22, (24), 2632-2636.
15. Williams, E. H.; Davydov, A. V.; Motayed, A.; Sundaresan, S. G.; Bocchini, P.; Richter, L. J.; Stan, G.; Steffens, K.; Zangmeister, R.; Schreifels, J. A.; Rao, M. V., Immobilization of streptavidin on 4H–SiC for biosensor development. *Applied Surface Science* **2012,** 258, (16), 6056-6063.
16. Li, Y.; Calder, S.; Yaffe, O.; Cahen, D.; Haick, H.; Kronik, L.; Zuilhof, H., Hybrids of Organic Molecules and Flat, Oxide-Free Silicon: High-Density Monolayers, Electronic Properties, and Functionalization. *Langmuir* **2012,** 28, (26), 9920-9929.
17. Scheres, L.; Arafat, A.; Zuilhof, H., Self-Assembly of High-Quality Covalently Bound Organic Monolayers onto Silicon. *Langmuir* **2007,** 23, (16), 8343-8346.
18. Scheres, L.; Giesbers, M.; Zuilhof, H., Organic Monolayers onto Oxide-Free Silicon with Improved Surface Coverage: Alkynes versus Alkenes. *Langmuir* **2010,** 26, (7), 4790-4795.
19. Butt, H. J.; Kappl, M., *Surface and Interfacial Forces*. Wiley-VCH: Weinheim, Germany,: 2010.
20. Bhushan, B., *Handbook of Nano-technology*. Springer: Berlin, 2007.
21. Liu, H.; Bhushan, B., Nanotribological characterization of molecularly thick lubricant films for applications to MEMS/NEMS by AFM. *Ultramicroscopy* **2003,** 97, (1–4), 321-340.
22. McGuiggan, P. M., Friction and adhesion measurements between a fluorocarbon surface and a hydrocarbon surface in air. *Journal of Adhesion* **2004,** 80, (5), 395-408.
23. Carpick, R. W.; Salmeron, M., Scratching the surface: Fundamental investigations of tribology with atomic force microscopy. *Chemical Reviews* **1997,** 97, (4), 1163-1194.
24. Pujari, S. P.; van Andel, E.; Yaffe, O.; Cahen, D.; Weidner, T.; van Rijn, C. J. M.; Zuilhof, H., Mono-Fluorinated Alkyne-Derived SAMs on Oxide-Free Si(111) Surfaces: Preparation, Characterization and Tuning of the Si Workfunction. *Langmuir* **2013**, 10.1021/la303403v.
25. Pujari, S. P.; Spruijt, E.; Stuart, M. A. C.; van Rijn, C. J. M.; Paulusse, J. M. J.; Zuilhof, H., Ultralow Adhesion and Friction of Fluoro-Hydro Alkyne-Derived Self-Assembled Monolayers on H-Terminated Si(111). *Langmuir* **2012,** 28 (51), 17690-17700.
26. Tao, Z. H.; Bhushan, B., Degradation mechanisms and environmental effects on perfluoropolyether, self-assembled monolayers, and diamondlike carbon films. *Langmuir* **2005,** 21, (6), 2391-2399.

27. ter Maat, J.; Regeling, R.; Ingham, C. J.; Weijers, C. A. G. M.; Giesbers, M.; de Vos, W. M.; Zuilhof, H., Organic Modification and Subsequent Biofunctionalization of Porous Anodic Alumina Using Terminal Alkynes. *Langmuir* **2011,** 27, (22), 13606-13617.
28. Dhar, S.; Seitz, O.; Halls, M. D.; Choi, S.; Chabal, Y. J.; Feldman, L. C., Chemical Properties of Oxidized Silicon Carbide Surfaces upon Etching in Hydrofluoric Acid. *Journal of the American Chemical Society* **2009,** 131, (46), 16808-16813.
29. Roper, C. S.; Radmilovic, V.; Howe, R. T.; Maboudian, R., Single-Source Chemical Vapor Deposition of SiC Films in a Large-Scale Low-Pressure CVD Growth, Chemical, and Mechanical Characterization Reactor. *J. Electrochem. Soc.* **2006,** 153, (8), C562-C566.
30. Sieval, A. B.; Opitz, R.; Maas, H. P. A.; Schoeman, M. G.; Meijer, G.; Vergeldt, F. J.; Zuilhof, H.; Sudhölter, E. J. R., Monolayers of 1-Alkynes on the H-Terminated Si(100) Surface. *Langmuir* **2000,** 16, (26), 10359-10368.
31. Shaffer, P. T. B.; Naum, R. G., Refractive Index and Dispersion of Beta Silicon Carbide. *J. Opt. Soc. Am.* **1969,** 59, (11), 1498-1498.
32. Rijksen, B.; Pujari, S. P.; Scheres, L.; van Rijn, C. J. M.; Baio, J. E.; Weidner, T.; Zuilhof, H., Hexadecadienyl Monolayers on Hydrogen-Terminated Si(111): Faster Monolayer Formation and Improved Surface Coverage Using the Enyne Moiety. *Langmuir* **2012,** 28, (16), 6577-6588.
33. Bain, C. D.; Troughton, E. B.; Tao, Y. T.; Evall, J.; Whitesides, G. M.; Nuzzo, R. G., Formation of monolayer films by the spontaneous assembly of organic thiols from solution onto gold. *Journal of the American Chemical Society* **1989,** 111, (1), 321-335.
34. Colorado, R.; Lee, T. R., Wettabilities of Self-Assembled Monolayers on Gold Generated from Progressively Fluorinated Alkanethiols. *Langmuir* **2003,** 19, (8), 3288-3296.
35. Fox, H. W.; Zisman, W. A., The spreading of liquids on low energy surfaces. I. polytetrafluoroethylene. *Journal of Colloid Science* **1950,** 5, (6), 514-531.
36. Lee, S.; Park, J.-S.; Lee, T. R., The Wettability of Fluoropolymer Surfaces: Influence of Surface Dipoles. *Langmuir* **2008,** 24, (9), 4817-4826.
37. Ramos, S. M. M.; Charlaix, E.; Benyagoub, A.; Toulemonde, M., Wetting on nanorough surfaces. *Physical Review E* **2003,** 67, (3), 031604.
38. Nuzzo, R. G.; Dubois, L. H.; Allara, D. L., Fundamental studies of microscopic wetting on organic surfaces. 1. Formation and structural characterization of a self-consistent series of polyfunctional organic monolayers. *Journal of the American Chemical Society* **1990,** 112, (2), 558-569.
39. Zhang, S.; Jamison, A. C.; Schwartz, D. K.; Lee, T. R., Self-Assembled Monolayers Derived from a Double-Chained Monothiol Having Chemically Dissimilar Chains. *Langmuir* **2008,** 24, (18), 10204-10208.
40. Hijikata, Y.; Yaguchi, H.; Yoshikawa, M.; Yoshida, S., Composition analysis of SiO2/SiC interfaces by electron spectroscopic measurements using slope-shaped oxide films. *Applied Surface Science* **2001,** 184, (1–4), 161-166.
41. Dhayal, M.; Ratner, D. M., XPS and SPR Analysis of Glycoarray Surface Density. *Langmuir* **2009,** 25, (4), 2181-2187.
42. Manova, R. K.; Pujari, S. P.; Weijers, C. A. G. M.; Zuilhof, H.; van Beek, T. A., Copper-Free Click Biofunctionalization of Silicon Nitride Surfaces via Strain-Promoted Alkyne–Azide Cycloaddition Reactions. *Langmuir* **2012,** 28, (23), 8651-8663.
43. Li, M.; Hua, R., $Ru_3(CO)_{12}$-Catalyzed Reactions of Catechols with Alkynes: An Atom-Economic Process for the Synthesis of 2,2-Disubstituted 1,3-Benzodioxoles from the

Double Addition of the O−H Bond Across a Triple Bond. *The Journal of Organic Chemistry* **2008,** 73, (21), 8658-8660.
44. Gao, D.; Carraro, C.; Howe, R. T.; Maboudian, R., Polycrystalline silicon carbide as a substrate material for reducing adhesion in MEMS. *Tribology Letters* **2006,** 21, (3), 226-232.
45. Lamont, C. L. A.; Wilkes, J., Attenuation Length of Electrons in Self-Assembled Monolayers of n-Alkanethiols on Gold. *Langmuir* **1999,** 15, (6), 2037-2042.
46. Krawczyk, M.; Zommer, L.; Kosiński, A.; Sobczak, J. W.; Jablonski, A., Measured electron IMFPs for SiC. *Surface and Interface Analysis* **2006,** 38, (4), 644-647.
47. Stöhr, J., *NEXAFS Spectroscopy*. Springer-Verlag: Berlin, 1992; Vol. 25.
48. Maugis, D., Adhesion of spheres: The JKR-DMT transition using a dugdale model. *Journal of Colloid And Interface Science* **1992,** 150, (1), 243-269.
49. Cappella, B.; Dietler, G., Force-distance curves by atomic force microscopy. *Surface Science Reports* **1999,** 34, (1–3), 1-104.
50. Sheparovych, R.; Motornov, M.; Minko, S., Low Adhesive Surfaces that Adapt to Changing Environments. *Advanced Materials* **2009,** 21, (18), 1840-1844.
51. te Riet, J.; Smit, T.; Gerritsen, J. W.; Cambi, A.; Elemans, J. A. A. W.; Figdor, C. G.; Speller, S., Molecular Friction as a Tool to Identify Functionalized Alkanethiols. *Langmuir* **2010,** 26, (9), 6357-6366.
52. Bhaskaran, H.; Gotsmann, B.; Sebastian, A.; Drechsler, U.; Lantz, M. A.; Despont, M.; Jaroenapibal, P.; Carpick, R. W.; Chen, Y.; Sridharan, K., Ultralow nanoscale wear through atom-by-atom attrition in silicon-containing diamond-like carbon. *Nat Nano* **2010,** 5, (3), 181-185.
53. Tsibouklis, J.; Graham, P.; Eaton, P. J.; Smith, J. R.; Nevell, T. G.; Smart, J. D.; Ewen, R. J., Poly(perfluoroalkyl methacrylate) Film Structures: Surface Organization Phenomena, Surface Energy Determinations, and Force of Adhesion Measurements. *Macromolecules* **2000,** 33, (22), 8460-8465.
54. Burton, Z.; Bhushan, B., Hydrophobicity, Adhesion, and Friction Properties of Nanopatterned Polymers and Scale Dependence for Micro- and Nanoelectromechanical Systems. *Nano Letters* **2005,** 5, (8), 1607-1613.
55. Hoque, E.; DeRose, J. A.; Hoffmann, P.; Mathieu, H. J.; Bhushan, B.; Cichomski, M., Phosphonate self-assembled monolayers on aluminum surfaces. *The Journal of Chemical Physics* **2006,** 124, (17), 174710.
56. Israelachvili, J. N., In *Intermolecular and Surface Forces*, Third ed.; Elsevier Inc.: 2010; pp 253-289.
57. Liu, H.; Bhushan, B., Investigation of nanotribological properties of self-assembled monolayers with alkyl and biphenyl spacer chains. *Ultramicroscopy* **2002,** 91, (1–4), 185-202.
58. Mishra, M.; Szlufarska, I., Analytical Model for Plowing Friction at Nanoscale. *Tribology Letters* **2012,** 45, (3), 417-426.
59. Bhushan, B.; Cichomski, M.; Hoque, E.; DeRose, J.; Hoffmann, P.; Mathieu, H., Nanotribological characterization of perfluoroalkylphosphonate self-assembled monolayers deposited on aluminum-coated silicon substrates. *Microsystem Technologies* **2006,** 12, (6), 588-596.

Supplementary information to Chapter 6

Table of Contents

Supplementary information to Chapter 6 179

S.6.1 Density functional theory (DFT) 179

S.6.2 XPS data of bare SiC and 2.5 % HF etched SiC surfaces 181

S.6.3 Coverage of oxygen layer after HF etching 182

S.6.4 XPS spectra of fluorinated monolayers on SiC 183

S.6.1 Density functional theory (DFT)

Electronic core level calculations were used to simulate core levels of C 1s XPS spectra. All electronic core level calculations were done with the GAUSSIAN09 program.[1] The effect of the bulk substrate on Si-C-O-C bound monolayers was mimicked by attaching the organic species to a $(SiH_3)_3C–O-$ moiety. The geometries of the different systems were optimized at the B3LYP/6-311G(d,p) level of theory. Natural bond orbital (NBO) analysis[2] was employed to obtain the core orbital energies. Assuming that the core orbital energy levels are directly related to the binding energies of the core electrons, the DFT calculations can be compared with the XPS spectrum. Because of the difference in reference energy between theory and experiment,[3] absolute values of calculated binding energies were referenced to the measured BE of CH_2 moieties in the aliphatic hydrocarbon chain by multiplying with a scaling factor (1.0438).[4] An assumption for equal contribution by each carbon atom was made and for every carbon atom a Gaussian centered at the corresponding BE was used with an fwhm of 0.94 eV. The simulated XPS spectra were used to facilitate the peak fitting procedure for overlapping contributions in the experimental XPS data.

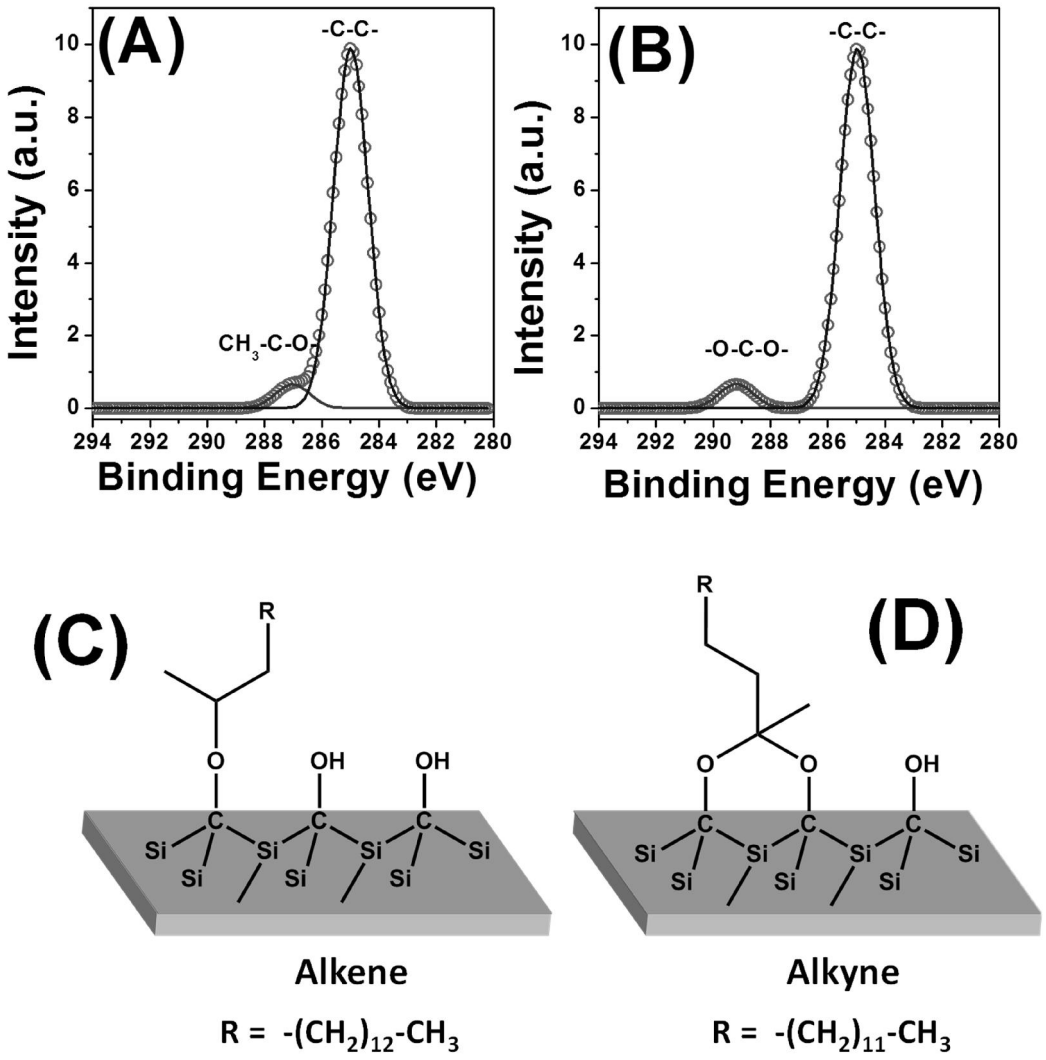

Figure S1. DFT Simulated core level C1s XPS-spectra for the hexadecene (A) monolayer (C) and hexadecyne (B) monolayer (D).

S.6.2 XPS data of bare SiC and 2.5 % HF etched SiC surfaces

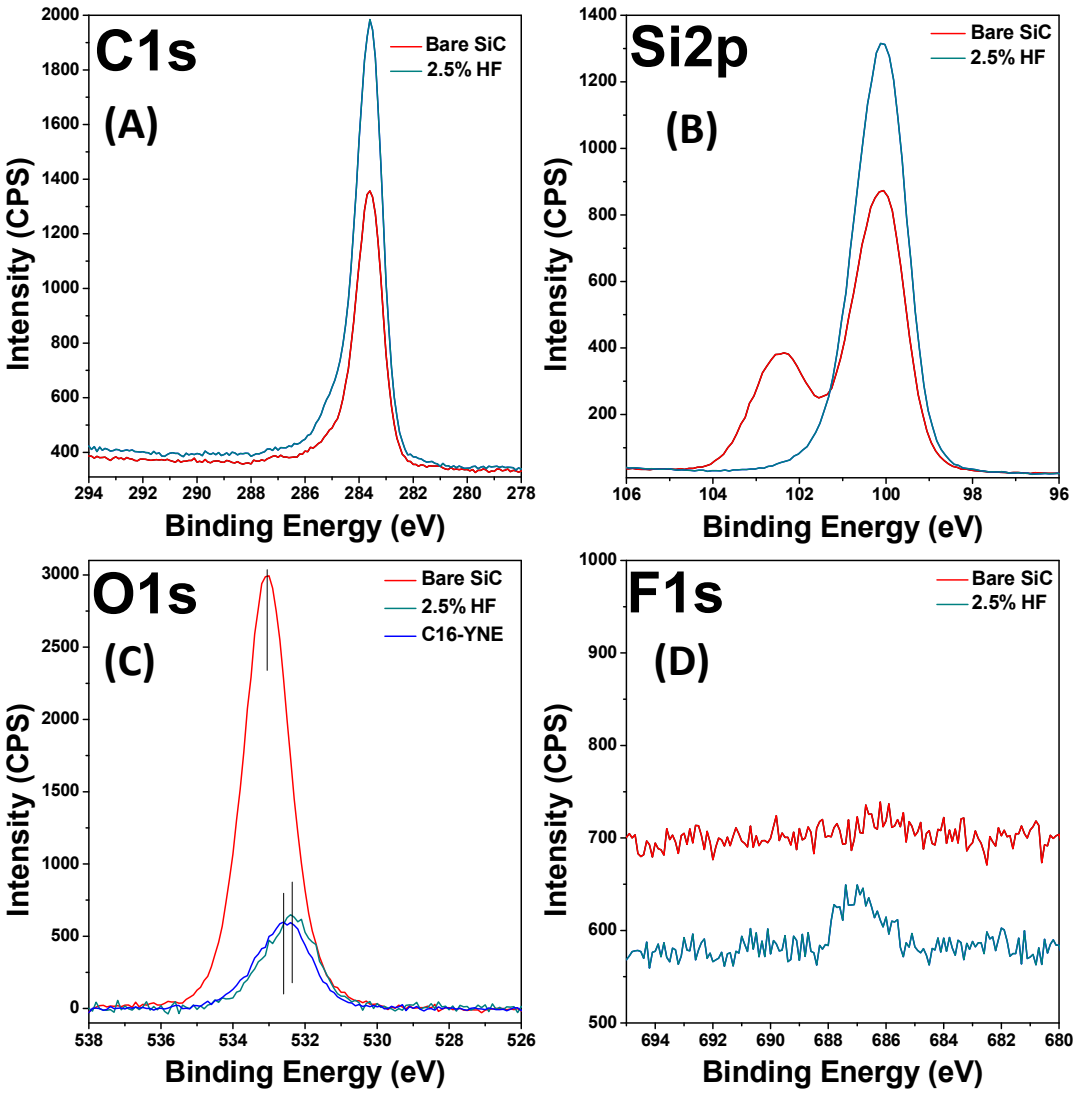

Figure S2. Narrow-scan C1s (A) and Si2p (B), O1s (C), and F1s (D) XPS data of bare SiC and 2.5 % HF etched SiC surfaces. O1s narrow-scan spectra of C16-YNE derived monolayers on SiC only compare the after modification changes.

S.6.3 Coverage of oxygen layer after HF etching

According to Dhar *et al*. the estimated coverage of oxygen layer after HF etching C-term. SiC is 0.93 ±0.1 ML. Using these method in our system we found similar results that is **1.03 ±0.14** ML. Assuming that the last layer of the SiC sample is composed of these two components (see figure R3) (e.g. expt-1 - $\%C1s_{283.6}$ = 7.10% and $Si2p_{101.1}$ = 2.11%) the coverage of oxygen can then be derived from the intensity of the measured O1s core levels as follows:

2.5 % HF etch	*C1s*	*C1s*	*C1s*	*Si2p*	*Si2p*	*O1s*
Binding Energy (eV)	283.6	284.8	286.2	100.1	101.3	532.6
Extpt.1 % of components	36.95	7.10	0.85	44.85	2.11	8.14
Extpt.2 % of components	37.02	6.20	0.85	44.10	2.07	9.76

Expt.1

$\%O1s_{532.6}$ / ($\%C1s_{283.6}$ + $\%Si2p_{101.1}$) = [8.14% / (7.10%+2.11%)] ≈ **0.88 ±0.1 ML**

Expt.2

$\%O1s_{532.6}$ / ($\%C1s_{283.6}$ + $\%Si2p_{101.1}$) = [9.76% / (6.2%+2.07%)] ≈ **1.18 ±0.1 ML**

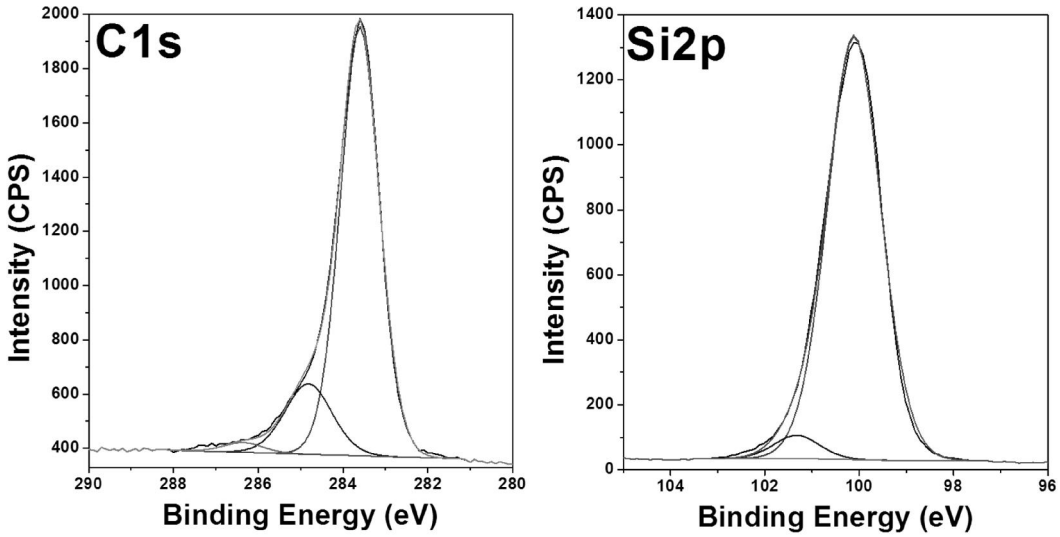

Figure S3. C1s (left) and Si2p (right) deconvolution XPS spectra of 2.5% HF etching on SiC surfaces.

S.6.4 XPS spectra of fluorinated monolayers on SiC

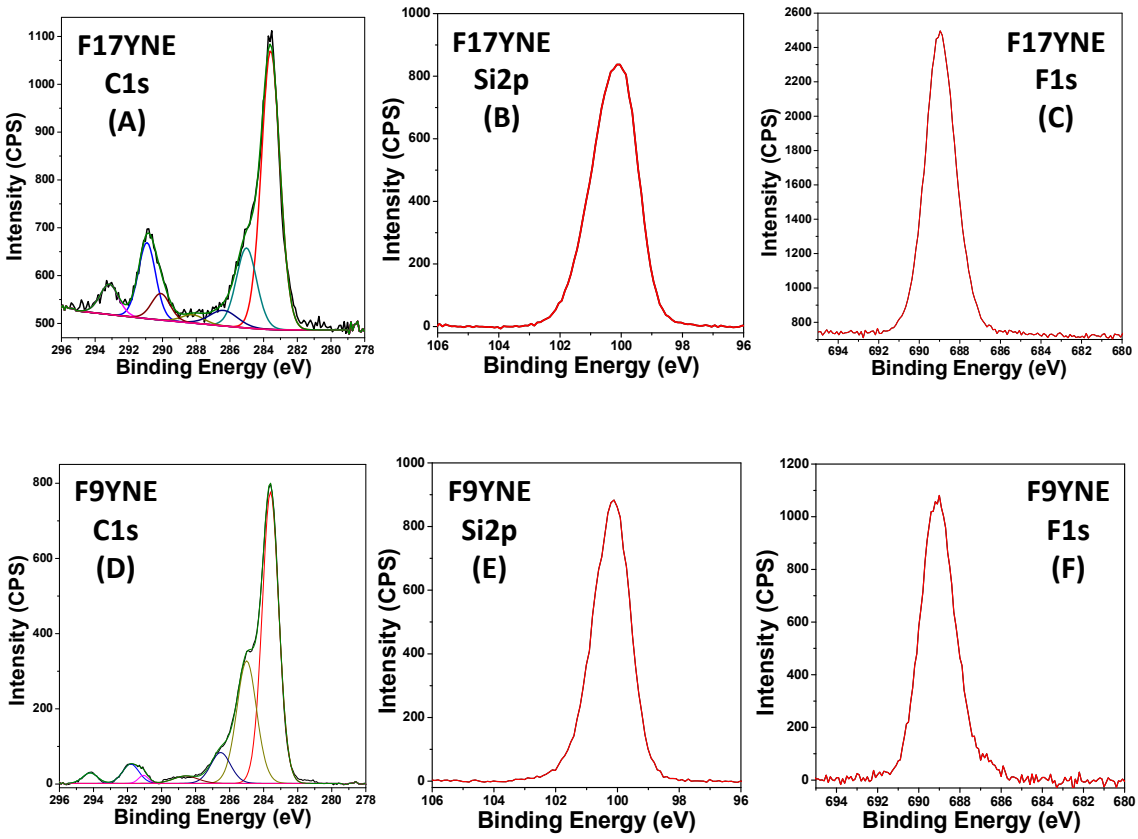

Figure S4. Narrow-scan C1s, Si2p, F1s XPS data of F17YNE (top) and F9YNE (bottom) derived monolayers on SiC.

1. Frisch, M. J. T.,et.al. *Gaussian 09, Revision A.1*, Gaussian, Inc., Wallingford CT.: 2009.
2. Glendening, E. D.; Reed, A. E.; Carpenter, J. E.; Weinhold, F. *NBO*, Version 3.1.
3. Tielens, F.; Costa, D.; Humblot, V.; Pradier, C.-M., Characterization of ω-Functionalized Undecanethiol Mixed Self-Assembled Monolayers on Au(111): A Combined Polarization Modulation Infrared Reflection−Absorption Spectroscopy/X-ray Photoelectron Spectroscopy/Periodic Density Functional Theory Study. *The Journal of Physical Chemistry C* **2007,** 112, (1), 182-190.
4. Manova, R. K.; Pujari, S. P.; Weijers, C. A. G. M.; Zuilhof, H.; van Beek, T. A., Copper-Free Click Biofunctionalization of Silicon Nitride Surfaces via Strain-Promoted Alkyne–Azide Cycloaddition Reactions. *Langmuir* **2012,** 28, (23), 8651-8663.

CHAPTER 7

Organic Monolayers from 1-Alkynes Covalently Attached to Chromium Nitride: Alkyl and Fluoroalkyl Termination

Strategies to modify chromium nitride (CrN) surfaces are important because of the increasing applications of these materials in various areas such as hybrid electronics, medical implants, diffusion barrier layers, corrosion inhibition, and wettability control. The present work presents the first surface immobilization of alkyl and perfluoro-alkyl (from C_6 to C_{18}) chains onto CrN substrates using appropriately functionalized 1-alkynes, yielding covalently bound, high-density organic monolayers with excellent hydrophobic properties and a high degree of short-range order. The obtained monolayers were characterized in detail by water contact angle, X-ray photoelectron spectroscopy (XPS), ellipsometry, and Infrared Reflection Absorption Spectroscopy (IRRAS).

This Chapter is submitted for publication as:

"Organic Monolayers from 1-Alkynes Covalently Attached to Chromium Nitride: Alkyl and Fluoroalkyl Termination" Sidharam P. Pujari, Luc Scheres, Barend van Lagen, and Han Zuilhof. *Langmuir* **2013,** in press, DOI:10.1021/la401978h

Table of Contents

7 Covalently Attached Organic Monolayers from 1-Alkynes onto Chromium Nitride: Alkyl and Fluoroalkyl Termination 185

7.1 INTRODUCTION 187

7.2 MATERIALS AND METHODS 190

7.2.1 Materials 190

7.2.2 Monolayer formation 190

7.2.3 Surface characterization 191

7.3 RESULTS AND DISCUSSION 192

7.3.1 Plasma-oxidized CrN surfaces 192

7.3.2 Kinetic study of the attachment of 1-alkynes and 1-alkenes onto plasma-activated CrN surface 194

7.3.3 Wettability and ellipsometric thickness 195

7.3.4 Monolayer Ordering 198

7.3.4.1 Infrared Reflection Absorption Spectroscopy (IRRAS) 198

7.3.5 Mode of Attachment 201

7.3.6 Fluorinated Monolayers 204

7.4 CONCLUSIONS 205

7.5 REFERENCES 206

7.1 INTRODUCTION

Surface modification using nanostructures such as organic monolayers has become an elegant and frequently used route to enhancing surface properties such as resistance to wear, corrosion, passivation and oxidation.[1-3] This has great potential for micro- and nanoelectromechanical systems (MEMS and NEMS) made of non-metallic materials such as silicon nitride (SiN) and silicon carbide (SiC). Compared to main group nitrides and carbides, SiN-derived and SiC-derived ceramics modified with organic monolayers are useful in many important engineering applications, particularly because of their high corrosion resistance and hardness. However, these materials also suffer from a low fracture toughness and high sintering temperatures.[4] As a consequence, there is an ongoing search for alternative materials with improved properties. CrN is such an upcoming material, with at least five properties of interest that provide the potential to replace the ceramics mentioned above: 1) outstanding wear[5] and high-temperature corrosion resistance that protects the material from chemical attack and tarnishing,[6] and even greater than that of TiN, presently the most commonly used hard coating.[7] 2) low friction coefficient, which makes it ideal for die cast and plastic molding components helping to reduce galling.[6] 3) a greater hardness (25 GPa or HK 2800), and not shattering as easily, as other ultrahard, but nonmetallic carbides or diamonds.[8] 4) low electrical resistivity (640 μΩ cm) and high melting point (~1770 °C for 1:1 CrN).[9] 5) unlike hexavalent chromium, CrN is rather biocompatible, with minimal toxicity. This allows its use in medical implants and corrosion-resistant steels that are now becoming commercially available.[6] Such use would likely become even more promising if the surface properties of CrN could be tuned to be optimal for high-wear conditions, or could be fine-tuned to minimize the response by the immune system upon placement of a medical implant in the body. Such applications would require a precisely tuned modification of the surface, such as that obtainable via covalently attached organic monolayers or polymers.

Chemical modifications via the covalent attachment of organic monolayers are employed via a wide variety of approaches, depending on the nature of the substrate. This includes, for example, the adsorption of alkanethiols, dialkyl disulfides and dialkyl sulfides on gold[10] and GaAs(001),[11] fatty acids[12] and alkenes[13] on indium tin oxide (ITO), alkenes on oxide-free Cu,[14] alkanephosphonic acids on titanium,[15] and organosilanes on silicon surfaces used for the development of MEMS and NEMS.[16] However, although interesting for a wide variety of properties - ranging from electronic modification such as band bending and surface dipoles to mechanical changes including friction and adhesion control, these monolayers are not always very stable. This need for a high stability of

these molecular coatings in real-life applications motivated researchers to use other interesting functional groups such as alkynes on SiC and SiN surfaces, which show a very high stability (e.g. stable in refluxing acid at pH <0). This high stability is induced by two factors:[17] 1) the strong and nonpolar covalent bond between Si and C,[18-20] and 2) the high chemical stability of SiC and SiN, which effectively hampers the loss of the monolayer via etching of the substrate (i.e. minimizes the formation of monolayer defects via the 'eating away' of the underlying material by acid or base).[21]

To our knowledge, only a few studies have been reported that describe the formation of organic monolayers on native-oxide-covered Cr surfaces.[22-26] For example, to study the electrical properties of ferrocene-containing monolayers, the attachment of these functional groups was achieved via isonitrile and thiol groups.[23] Monolayers derived from sulfonic acid, hydroxamic acid, and carboxylic acids were studied to obtain lithography-based surface patterning, and the reactivity of these moieties toward the surface was investigated.[24, 25] However, none of these monolayers are very stable, and they are easily desorbed in air, upon sonication and even upon room-temperature rinsing in organic solvents.[23, 27] The study of monolayer formation on chromium-rich surfaces is also relevant from a catalysis point of view. For example, chromium-containing catalysts are frequently used, but the catalyst might suffer from poisoning due to fouling by a variety of unsaturated compounds, including thiophenes, pyridine, and carboxylic acid-terminated molecules.[28] Monolayers derived from silanes currently display the highest quality (yielding e.g. a NEXAFS-determined tilt angle of 9.3° ± 1.3° for monolayers of octadecyltrimethoxysilane),[24] although they are somewhat slow to form (more than 3 days),[25] and whereas they are slightly more stable, all silane-based monolayers are typically prone to hydrolytic detachment reactions.

To circumvent such hydrolytic reactivity and to obtain a wider access to surface-modified substrates, our group has recently shown the potential of the modification with 1-alkenes or 1-alkynes of hydroxyl-terminated surfaces such as silica,[29] indium tin oxide (ITO),[13] alumina,[30] and silicon carbide (SiC).[20] On such surfaces, the surface properties (wettability, and surface dipole/band bending) can be tuned in great detail via modification of the top group. For example, replacement of the terminal $-CH_3$ by a $-CF_3$ group strongly diminishes the adhesion and friction forces on hydroxyl-terminated SiC,[20] analogous to observations made for fluorinated monolayers on Si.[31, 32] The extremely high hardness and mechanical robustness of CrN, therefore suggest that the development of novel monolayer chemistry may also allow the development of CrN with extremely low friction and adhesion properties, which would open up new applications of this material. In addition, biofunctional monolayers may significantly widen the biological use

of these materials. The growing interest in CrN and other Cr-containing surfaces thus motivated us to study the analogous monolayer formation with these precursors on oxide-covered CrN.

In this chapter, we describe for the first time the formation of stable organic monolayers on plasma-activated, hydroxyl-terminated CrN surfaces through covalent bond formation with anchoring alkyne molecules. We describe the use of various 1-alkynes to form monolayers on hydroxyl-terminated CrN surfaces via Cr-O-C linkages under thermal conditions (Figure 1). We compare various approaches to activating CrN and then outline the optimal conditions for monolayer formation. Subsequently, the kinetics are discussed for alkyne- and alkene-derived monolayers. Then, the monolayer structure is analyzed by ellipsometry, wetting properties, and detailed IR measurements as a function of the reactive group and the length of the alkyl chain. Subsequently, the mode of binding to the surface was studied by IR and XPS measurements and compared to monolayers derived from 1-hexadecene and 2-hydroxyhexadecanoic acid (2HHDA). Finally, various degrees of alkyl fluorination were used to study the influence of fluorination on the monolayer formation, packing of the monolayer, and wetting properties. The results outline the potential of such covalently bound monolayers on CrN for a wide range of follow-up studies.

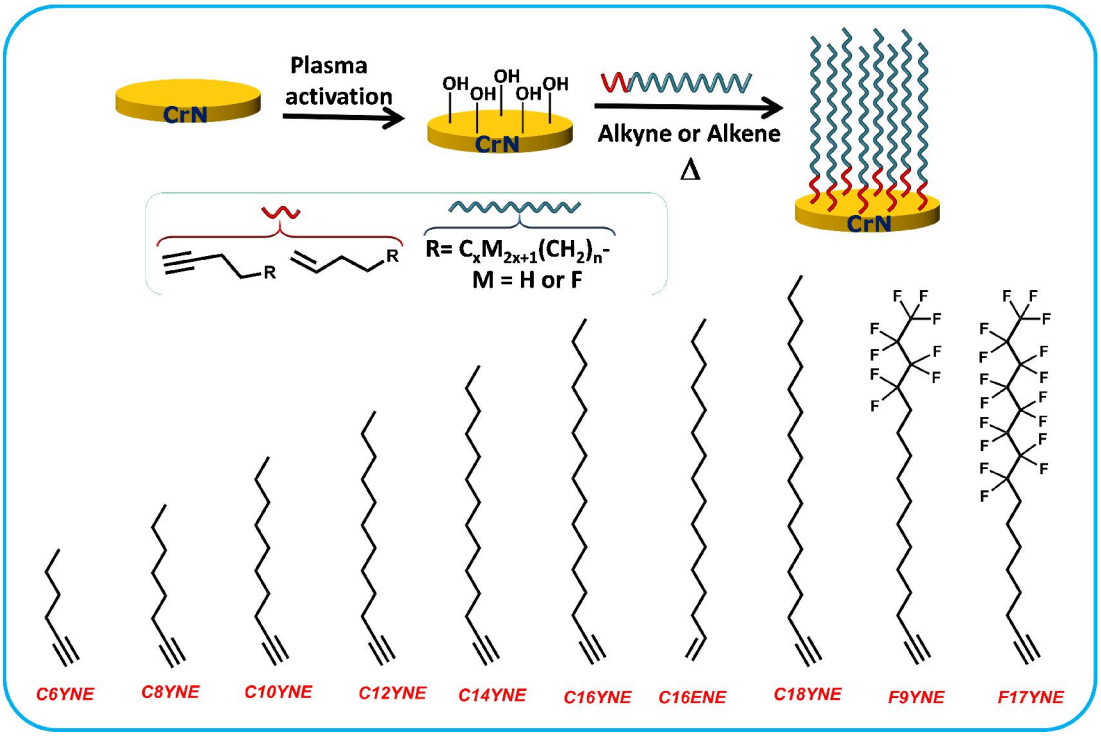

Figure 1. Schematic representation of the formation of alkyne and alkene-derived fluorinated and nonfluorinated organic monolayers on a plasma-activated, hydroxyl-terminated CrN surface.

7.2 MATERIALS AND METHODS

7.2.1 Materials

Acetone (semiconductor-grade VLSI PURANAL Honeywell 17617), dichloromethane (DCM, Fisher), and other solvents used were either of analytical grade or distilled prior to use. The wafers with nonstoichiometric chromium nitride films (thickness 1 μm, surface root-mean-square (rms) roughness determined with AFM ~5.0 nm) were obtained by sputter deposition on Si(100). Short-chain-length molecules 1-hexyne (Aldrich, 97%, C6YNE), 1-octyne (Aldrich, 98%, C8YNE), and 1-decyne (Aldrich, 98%, C10YNE) were purified by distillation before use. The longer chain length alkynes 1-dodecyne (Aldrich, 98%, C12YNE), 1-tetradecyne (Aldrich, ≥97%, C14YNE), and 1-hexadecyne (ABCR, Germany, 90%, C16YNE) were purified by column chromatography (hexane) to remove trace amounts of 1-bromoalkane or other impurities and subsequently distilled twice under reduced pressure before use. 1-Hexadecene (Aldrich, ≥99%, C16ENE) was purified by distillation under reduced pressure before use. 1-Octadecyne[20] (C18YNE), 13,13,14,14,15,15,16,16,16-nonafluoro-hexadec-1-yne[31] (F9YNE) and 9,9,10,10,11,11, 12,12,13,13,14,14,15,15,16,16,16-heptadecafluoro-hexadec-1-yne[31] (F17YNE) were synthesized using literature procedures. 2-Hydroxyhexadecanoic acid (ABCR, 95%, 2HHDA), and palmitic acid (Sigma, >99%, PMA) were used as received.

7.2.2 Monolayer formation

A chromium nitride (CrN) epilayer on a Si(100) substrate was diced into 10 mm × 10 mm wafers with a diamond-tipped pen. The CrN surface was first cleaned by rinsing several times with dichloromethane and sonication for 10 min in acetone. Subsequently, the samples were further activated using an air plasma (PDC-002 plasma cleaner, Harrick Scientific Products, Inc. Ossining, NY) for 10 min (0.3 SCFH air flow, 29.6 W power, at 300 mTorr pressure) to remove adventitious organic contamination. After being activated, the samples were blown dry with a stream of argon. These freshly plasma-activated and dried surfaces were then quickly transferred to a screw-capped bottle under argon atmosphere, which was charged with 1 mL of alkynes at 100 °C for 16 h, or for the time and at the temperature indicated at the text. After reaction, the samples were removed from the flask, rinsed extensively with DCM, and sonicated for 5 min in acetone to remove physisorbed reagents. Samples were stored in a glovebox between measurements, rinsed with fresh DCM, and blown dry with argon immediately before characterization.

2-Hydroxyhexadecanoic acid (2HHDA)-modified surfaces were prepared using an activation process as similar to that described elsewhere.[30] In this case, after plasma

activation the samples were rinsed in ethanol and immersed in a 1 mM solution of 2-hydroxyhexadecanoic acid in ethanol at 65 °C for 16 h. This same procedure was used to prepare palmitic acid (PMA)-derived monolayers.

7.2.3 Surface characterization

The static and advancing water contact angles of the bare and modified CrN surfaces were measured using the sessile drop method on a DSA100 optical contact angle meter (Krüss instrument). The thickness of the alkynes grafted onto the CrN substrate was determined using a Sentech Instruments (type SE-400) automated ellipsometry. The optical constants of the substrate were determined with a piece of freshly plasma-oxidized CrN refractive index of $n_s = 2.73$ and an imaginary refractive index of $k_s = 2.48$. Each reported values of the layer thicknesses is the average of a minimum of eight measurements taken at different locations on the substrate with an error ± 0.3 nm. The elemental composition of the modified CrN surfaces was determined by X-ray photoelectron spectroscopy (XPS) using a JPS-9200 photoelectron spectrometer (JEOL, Japan). All spectra were corrected with a slight linear background before fitting. All XPS spectra were evaluated using the Casa XPS software (version 2.3.15) and the C1s hydrocarbon CH_2 peak was calibrated at a binding energy (BE) of 285.0 eV. Calculated atomic percentages were normalized by the corresponding atomic sensitivity factors [C1s (1.00), Cr2p (10.6), N1s (1.80), O1s (2.93), F1s (4.43), S2p (1.68) and Cl2p (2.29); http://www.casaxps.com/] for the X-rays incident at 80° from the analyzer: as shown in Table 1 (vide infra). Infrared reflection absorption spectroscopy (IRRAS) spectra were measured using a Bruker TENSOR 27 equipped with a liquid-nitrogen-cooled MCT (Mercury, Cadmium, Telluride) detector using a Harrick Auto SeaguII^{TM} with a variable angle (10 - 85°) attachment. For our experiments, the angle of p-polarized light incidence was 80° with respect to the surface normal. Typically, 2048 scans were taken at a resolution of 4 cm^{-1} for each spectrum, and from the resulting spectrum a background spectrum was divided by a plasma-oxidized CrN reference sample. The topography of the plasma-activated CrN surfaces was studied with an Asylum MFP-3D atomic force microscope (AFM) in tapping mode. Note that all characterization techniques were performed after acetone or dichloromethane rinsing and sonication for 5 min.

7.3 RESULTS AND DISCUSSION

7.3.1 Plasma-oxidized CrN surfaces

Plasma-oxidized CrN surfaces were used to yield alkyne-derived monolayers onto CrN surfaces via thermal initiation (Figure 1). The aim of the air-generated plasma was to remove any carbon contamination from the surface, while simultaneously introducing surface hydroxylation. In general, the plasma process results in an oxide layer that is only a few atomic layers thick and introduces hydroxyl termination. The static contact angle (SCA) of untreated (as-received) CrN substrates of 106° was reduced to <10° after plasma activation, demonstrating the conversion of an adventitious carbon-contaminated, hydrophobic CrN surface to a clean, hydrophilic surface consisting primarily of hydroxyl-terminated groups.[17, 33, 34] The hydrophobic nature of untreated Cr-derived surfaces was previously described for chromium oxynitride (contact angle: ~90°),[35] and has been ascribed to the high chromium content as well as surface roughness of 6.1 ± 0.1 nm as shown in *Supporting Information figure* S2.

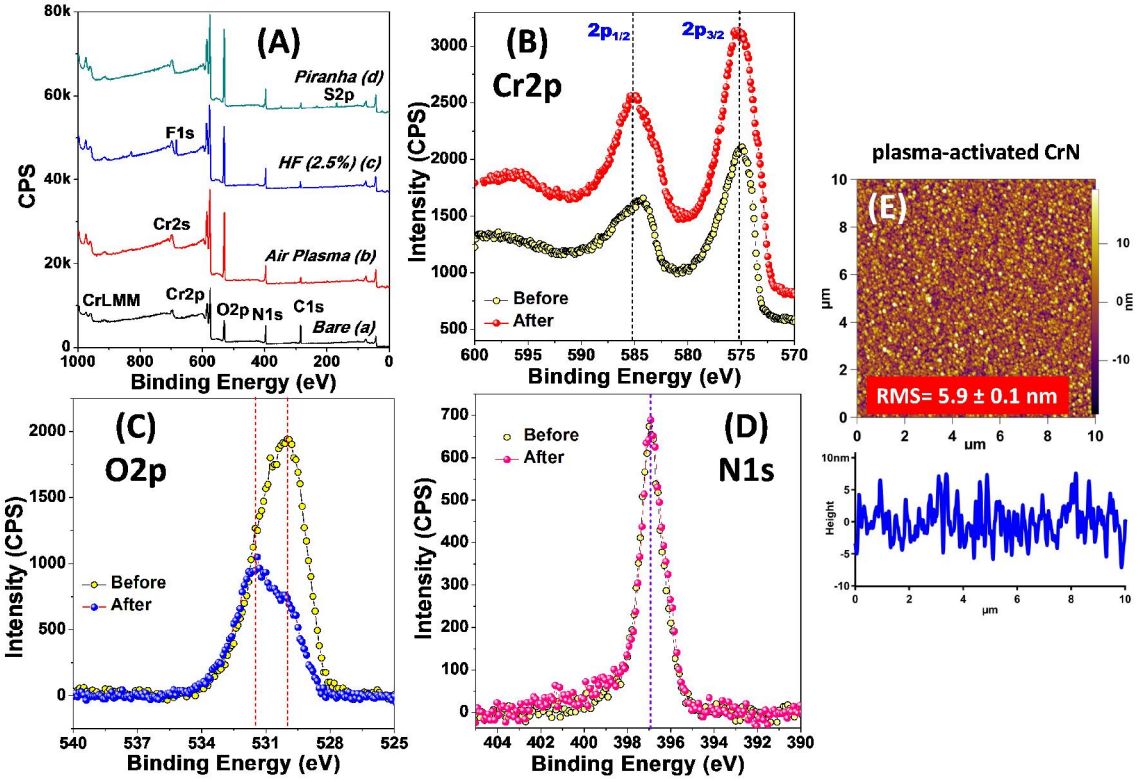

Figure 2. (A) XPS wide scans measured on CrN surface with various treatment: a) bare (before activation), b) after air plasma activation for 10 min, c) HF (2.5%) for 2 min, d) piranha for 10 min. (B)

XPS Cr2p narrow scan of CrN and after plasma treatment. (C) XPS O1s narrow scan of CrN before and after plasma treatment. (D) XPS N1s narrow scan of CrN before and after plasma treatment. (E) AFM tapping mode image of plasma-activated CrN surface.

In addition to plasma activation, we also studied common wet chemical activation routines such as, like 2.5% aqueous HF, piranha solution (H_2SO_4:H_2O_2) and concentrated HCl. As shown in Table 1, a concentrated HCl solution also created a hydrophilic CrN substrate with water contact angles below 10°; however, this surface treatment yields other elemental contaminations (e.g. Cl) resulting from surface complexation and CrN dissolution.[36] As also demonstrated by the XPS wide scans in Figure 2A, etching with 2.5% HF leaves trace amounts of fluorine on the surface whereas piranha solution introduces sulfur. Such etching remnants are not found upon plasma activation, but even for that method (as for all the others) after the full surface etching procedure, some persistent carbon contamination remains on the CrN surface, as detected by XPS (BE = 285.0 eV). Altough its nature cannot be certified beyond doubt, it is different from that of chromium carbide (CrC), which appears at 283.2 eV in the C1s XPS narrow scan.[37] The Cr2p XPS narrow scan of an air-plasma activated CrN sample, as depicted in Figure 2B, displays a broad Cr2p peak in the region of 570 eV to 605 eV. Typically, components around 577 ($2p_{3/2}$) and 587 eV ($2p_{1/2}$) are assigned to chromium in a nitrogen and/or oxygen environment (chromium oxynitride CrN_xO_y, Cr_2O_3, and CrO(OH)).[38,39, 40] XPS analysis of our chromium nitride samples suggests a bulk nonstoichiometric Cr/N composition of roughly 2:1, with significant oxidation products on the surface and some unremovable carbon (*vide infra*). Upon plasma activation, the %C goes down, while the %O goes up (see Table 1). This oxidation step does not yield significant differences in the formal oxidation state of Cr, as the Cr2p XPS narrow scan is basically identical before and after the plasma treatment. The overall chemical reaction is thus the "burning away" of carbon contaminants, and the replacement of N with O. Given the increased %O and the sharp decrease in the water contact angle, we conclude that activating the surface with air plasma introduces oxygen-containing functional groups on the surface, most likely hydroxyl moieties. This is confirmed by the O1s narrow scan in Figure 2C, which showed that upon plasma treatment the O1s peak shifts slightly to higher binding energies (the peak maximum moves from 530 eV to 532 eV), as expected for the formation of $Cr(OH)_x$ compounds from the original oxynitride; cf. the O1s binding energy of Cr_2O_3 is 530.0 eV, whereas that of CrO(OH) is 531.6 eV, whereas organic compounds show XPS O1s peaks around 533.0 eV.[27] Finally, AFM analysis reveals slight changes in surface roughness upon air plasma treatment, with an rms surface roughness of 5.9 ± 0.1 nm (Figure 2E).

Table 1. Static water contact angle and XPS-based elemental composition (in atom %) of chromium nitride after various surface treatments

Surface Treatments	C1s (285eV)	Cr2p (575.0 eV)	N1s (397 eV)	O1s (531 eV)	Other (F1s(684 eV) S2p (168 eV))	Contact angle (°)
Untreated CrN	37.2	26.8	17.2	18.7	--	106
Air Plasma	9.2	33.3	16.4	41.1	--	<10
HF (2.5%)[a]	8.7	33.3	16.1	36.2	F1s, 5.6	<10
Piranha[a]	8.2	30.3	15.4	42.6	S2p, 3.3	<10
1 M HCl	10.0	32.5	15.1	40.3	Cl2p, 2.1	

[a] The CrN substrate was pretreated with 10 min of air plasma.

7.3.2 Kinetic study of the attachment of 1-alkynes and 1-alkenes onto plasma-activated CrN surface

Freshly plasma-activated CrN surfaces were modified at 100 °C with pure 1-alkene or 1-alkyne. To this aim, freshly plasma-activated CrN wafers were placed in screw-capped bottle with 1 - 2 mL of an alkene or alkyne, which was put in a water or oil bath to reach the required temperature. The resulting surfaces were analyzed by water contact angle, XPS and IR measurements. As depicted in Figure 1, nine different nonfluorinated and fluorinated 1-alkenes and 1-alkynes of different chain lengths were used.

The degree of completion and progress of monolayer formation can be expressed through the XPS atomic ratio of C1s to Cr2p, N1s, and O2p, respectively. In addition, the development of the surface wettability was evaluated via static water contact angle measurements. A kinetics study was carried out by keeping one parameter – viz. time or temperature – constant while varying the other. The resulting kinetics of the reaction of 1-hexadecene and 1-hexadecyne on the hydroxyl-terminated CrN surface are shown in Figure 3. As shown in Figure 3A, for both 1-alkenes and 1-alkynes, the water contact angle gradually increases with temperature. Clearly, monolayer formation proceeds faster with 1-hexadecyne than with 1-hexadecene. For the fixed reaction time of 12 h, a limiting contact angle of 110° was obtained at 100 °C or higher for 1-hexadecyne, while for 1-hexadecene the attachment required 12 h of reaction at 160 °C to be complete. In line with this, the C1s composition (Figure 3B) initially increases gradually while approaching an asymptotic value at 100 and 160 °C for 1-hexadecyne and 1-hexadecene, respectively.

The higher reactivity of alkynes is likely due to a combination of the higher nucleophilicity of alkynes versus that of alkenes, and the increased ease of oxidation of alkynes versus that of alkenes. Interestingly, as the data in Figure 3C show, the carbon content for the 1-alkyne reaches a constant value after 12 h at 100 °C. This likely means that at that (and lower) temperatures, likely no multilayer formation takes place because this would lead to a continuous increase in the C1s signal over time, as observed for a wide variety of other oxide surfaces such as glass,[41] SiC[19] and TiO_2.[42]

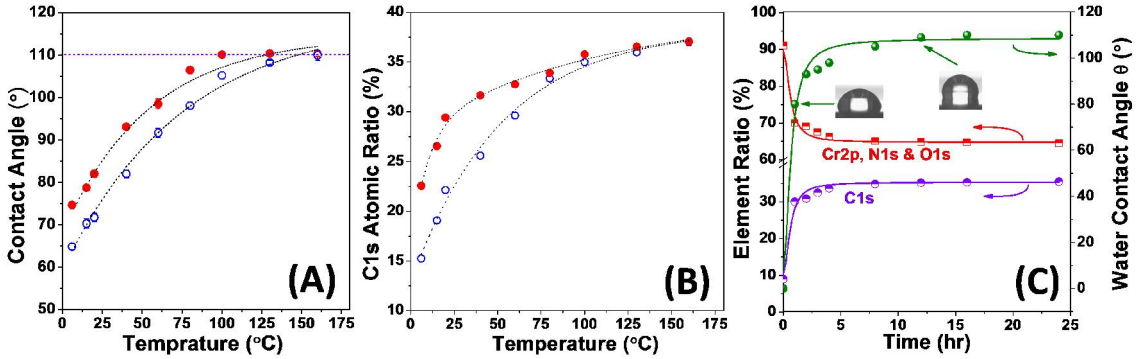

Figure 3. (A) Static water contact angle of organic monolayers derived from 1-hexadecene (blue open circles) and 1-hexadecyne (red filled circles) on hydroxyl-terminated CrN as a function of the reaction temperature at 12 h. (B) XPS C1s atomic ratio and (C) hexadecyne-derived monolayers on the CrN surface with different times at 100 °C with symbols for XPS elemental ratio Cr2p, N1s, and O1s (red, half-filled squares), C1s (purple, half-filled circle) and static water contact angle (green, filled circle). The lines in A-C are guides to the eye. Contact angle data points in the graph represent an average of two independent series of experiments. Each series consists of two separately prepared (partially completed) monolayers. Contact angle values were obtained by measuring at 3-4 different spots on the surface, per monolayer. See *Supporting Information S.7.3 Table S1 and S2*.

7.3.3 Wettability and ellipsometric thickness

The wettability of optimally modified CrN surfaces (12 h at 100 °C) was monitored by contact angle measurements with water and hexadecane. The water contact angle strongly depends on the molecular structure, surface roughness, and packing density of the monolayer. In general, a densely packed $-CF_3$ or $-CH_3$ terminated monolayer always results in water contact angles ≥110°. The water contact angle deceases with decreasing packing density. Table 2 shows the static contact angle (SCA) and advancing contact angle (ACA) water on the fluorinated and nonfluorinated alkyne-derived and alkene-derived monolayers as a function of chain length. Henceforth, the respective monolayers are referred to by their number of carbon or fluorine atoms and reactive group on the surface that is, as C6YNE, C8YNE, C10YNE, C12YNE, C14YNE, C16YNE, C18YNE, F9YNE, and F17YNE for the various alkyne-derived monolayers, and C16ENE for the

hexadecene-derived monolayers. Static water contact angles ≥110° were obtained for alkyne monolayers with more than 12 carbons per chain (>C12), whereas the alkynes with fewer than 10 carbon atoms per chain (<C10) reveal static water contact angles lower than 110°. The advancing water contact angles were larger than 112° for chain length of >C12, while those of the <C10 were lower than 112°. In studies with alkanethiols on gold, alkyne, and alkene monolayers on Si similar water contact angles in the range of 110° - 115° have been reported for densely packed alkyl monolayers with methyl termination.[43, 44] This indicates for shorter alkynes that the packing density at optimal attachment is less than fully dense, but that for the C12 and longer alkynes a densely packed monolayer is formed. Interestingly, the static water contact angle of these densely packed layers are significantly higher than obtainable for analogous C16 monolayers on various other ceramic surfaces of similar roughness, e.g. SiC (SCA = 107°), and SiN (SCA = 106°),[18, 20] which points to the high quality of these chromium nitride-bound monolayers.

Table 2. Static contact angles (SCA) and advancing contact angles (ACA) of water and ellipsometric thicknesses of alkyne-derived monolayers on hydroxyl-terminated CrN (12 h at 100 °C).

Monolayers	Water Contact angle (±1°)		Monolayer Thickness (±0.3 nm)[a]	Estimated Thickness[b]
	SCA	ACA		
$CH{\equiv}C\text{-}C_4H_9$	85°	91°	0.6	0.75
$CH{\equiv}C\text{-}C_6H_{13}$	93°	98°	0.8	1.00
$CH{\equiv}C\text{-}C_8H_{17}$	102°	106°	1.0	1.26
$CH{\equiv}C\text{-}C_{10}H_{21}$	110°	112°	1.6	1.51
$CH{\equiv}C\text{-}C_{12}H_{25}$	108°	112°	1.8	1.76
$CH{\equiv}C\text{-}C_{14}H_{29}$	110°	116°	1.9	2.19
$CH{\equiv}C\text{-}C_{16}H_{33}$	112°	116°	2.2	2.27
$CH{\equiv}C\text{-}C_{16}H_{24}F_9$	116°	128°	1.7	--
$CH{\equiv}C\text{-}C_{16}H_{16}F_{17}$	119°	130°	1.6	--

[a] Refractive index of activated CrN surface used to determine the ellipsometric thickness: n_s =2.73 and k_s = 2.45. [b]Nominal thicknesses computed by ChemBio3D for "all-trans", vertically aligned alkyl chains from Cr to $-CH_3$

For the fluorinated monolayers, static water contact angles as high as 116° and 119° were obtained for F9YNE and F17YNE, respectively. Analogously, advancing water contact angles of 128° and 130° were obtained, indicating the high quality of these modified surfaces, especially given the unchanged surface roughness (rms = 5.7 ± 0.1 nm, as confirmed by AFM See *Supporting Information S.7.3 Figure S2*) in comparison to that of the plasma-activated CrN surface (rms = 6.1 ± 0.1 nm) displayed in Figure 2E. This is similar to what is observed on modified SiC surfaces.[20] These contact angles display the low van der Waals interactions between water and these -CF_3 containing monolayers. These results are similar to previously reported monolayers on H-Si(111) and SiC surfaces.[20, 31] In addition, the contact angles to hexadecane (surface tension = 27 mN/m) were measured. For all CH_3-terminated monolayers both the hexadecane SCA and ACA are <10°, whereas for the CF_3-terminated monolayers the hexadecane contact angles are around 40°. This indicates that CH_3-terminated monolayers are oleophilic whereas the CF_3 monolayers are only somewhat more oleophobic. These values of <10° and 40° for the –CH_3 and –CF_3 monolayer are somewhat lower than the values of 37° and 81° for the analogous monolayers on Si(111).[31] Becasue the final wetting state is the Wenzel state in both cases,[45] we attribute this to the higher surface roughness of CrN (RMS = 5.7 ± 0.1 nm See *Supporting Information S.7.3 Figure S2*) versus that of Si(111) (~0.1 nm). A combination of hydrophobic and oleophilic properties as obtained for our CH_3-terminated materials might be useful for oil and water separation in the oil refinery industry.[46]

Ellipsometry was used to determine the thickness of the obtained monolayers on the CrN surface. First, the optical constants of the freshly plasma activated CrN substrate were determined to be n_s = 2.73 ± 0.02 and k_s = 2.45 ± 0.02. These values are similar to the ones obtained by the same technique for the effective refractive index (RI) for a range of chromium oxides of n_s = 2.6 and k_s = 2.18 - 2.55, as found by other researchers.[47] The thicknesses of monolayers reported here were determined with these RI values as determined on the same unmodified CrN substrate. In addition, we note that the accuracy of measurement of the thickness might be affected by the substrate roughness.[48] The observed monolayer thicknesses range from 0.6 ± 0.3 nm to 2.2 ± 0.3 nm for C6YNE to C18YNE monolayers, respectively. This is in line with the formation of dense monolayers with all-*trans* alkyl chains, and confirms the lack of multilayer formation for any of the materials. Furthermore, the estimated film thicknesses are lower than the estimated thickness based on "all trans" conformations, and may be related to a previously reported contraction of monolayers on surfaces with nanoscopic roughness.[49] However, for C16ENE the maximum ellipsometric thickness was determined to be 1.7 ± 0.3 nm, which

indicates a slightly less dense monolayer and might be related to a lower coverage as compared to that of the C16YNE monolayer (1.9 ± 0.3 nm).

7.3.4 Monolayer Ordering

7.3.4.1 Infrared Reflection Absorption Spectroscopy (IRRAS)

To examine in more detail the structure of the organic monolayers, we employed IRRAS. This allows to derive information regarding the short-range order and packing density, the overall molecular orientation (tilt angle), and the presence of functional groups within the monolayers.[50] In Figure 4, the C-H stretching vibration peaks for short chain C6YNE (Figure 4A) and long chain C18YNE (Figure 4B) are depicted. For comparison purposes, with relevant modes assigned, the exact IR peak positions are shown in Figure 4C. To extract quantitative information concerning the methylene bands, this spectral region was deconvoluted.[33, 51] Five independent C-H stretch vibrations are distinguished. First, the antisymmetric and symmetric CH_2 stretch vibrations are observed around 2920 and 2852 cm^{-1}, respectively. In addition, we also observed a Fermi resonance peak of $\nu_s CH_{2\,(FR)}$ at 2894 - 2901 cm^{-1} the symmetric stretching of CH_3 at 2871 - 2876 cm^{-1}, and the in-plane and out-of-plane antisymmetric CH_3 stretches at 2954 - 2964 cm^{-1}. The detailed peak positions and interpretation thereof will be discussed in more detail below (Figure 4A and 4B).

The exact position of the anti-symmetric (ν_a CH_2) and symmetric (ν_s CH_2) methylene stretching vibrations for the long chain C18YNE appear at ~2919.8/2849.6 cm^{-1}, whereas for the short chain C6YNE layers these vibrations are detected at ~2927.8/2856.6 cm^{-1}, as shown in Figure 4C.[52, 53] These values indicate a remarkably high degree of short-range order for the long alkyne-derived monolayers, while the short alkyne-based monolayers are typically disordered. For organic monolayers (from C12YNE to C18YNE) on Si[54] and SiC[20] surfaces similar peak shifts from short-chain and disordered to long-chain and ordered monolayers have been reported. In line with the contact angle data (*vide supra*) the wavenumbers obtained for the C18YNE indicate that monolayers on CrN are ordered like those on H-terminated Si(111) surfaces, and significantly more ordered than those on e.g. SiC. Batteas et al. have shown that for a nanoparticle-like film with nanoparticles of > 40 nm the nanoparticle size no longer has any bearing on the monolayer assembly, and that the surface appears essentially flat to an individual molecule.[49, 55] In our case, the large-scale roughness of the CrN (nanoparticle like film diameter ~250 nm as shown by

AFM, see *Supporting Information S.7.3 Figure S2*) thus does not affect the observed high order of the monolayers.

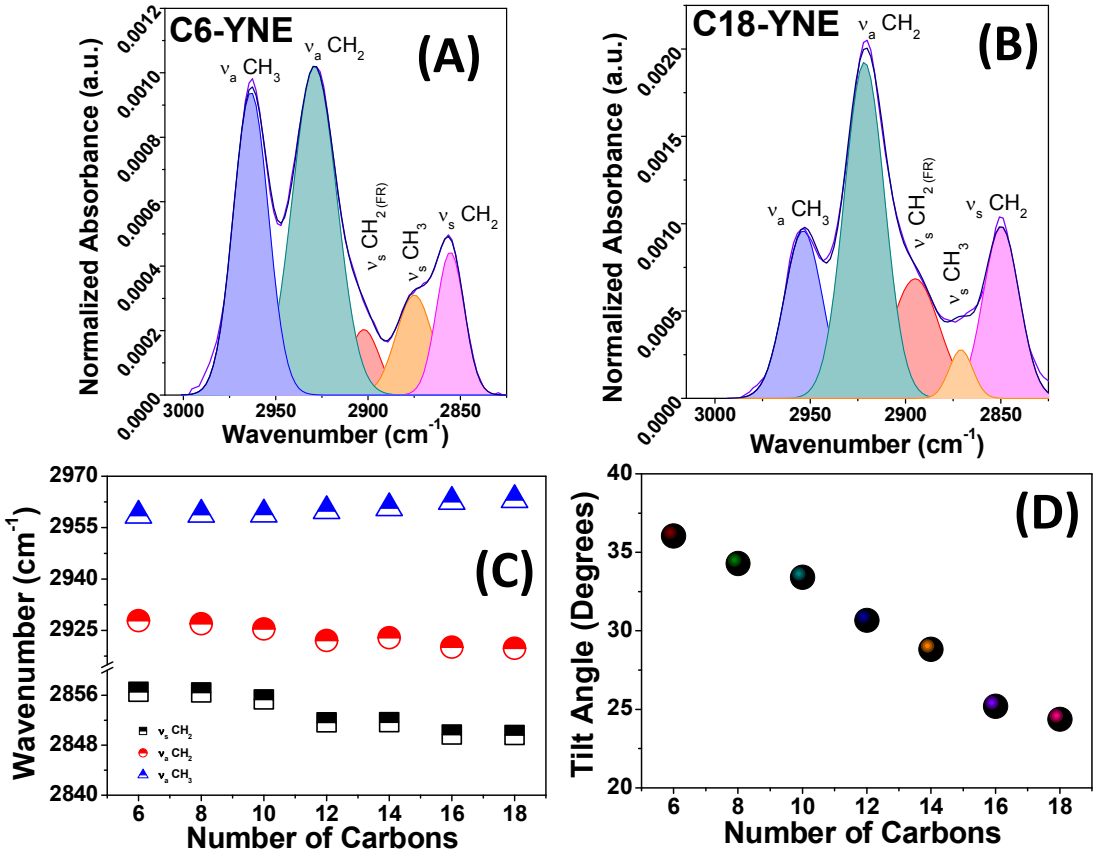

Figure 4. Deconvoluted IRRAS spectrum: (A) C6YNE, (B) C18YNE monolayers on CrN surfaces spectra most visible peak are deconvoluted, and (C) overview peak position of C8YNE to C18YNE monolayers symmetric methylene stretch (νa CH_2, half-filled square), anti-symmetric methylene stretch (νa CH_2, half-filled circle), and anti-symmetric methylene stretch (νa CH_3, half-filled triangle). (D) Tilt angle with respect to the surface normal for varying molecular lengths, calculated with eq 1.

The relative peak areas of the anti-symmetric methylene stretch (ν_a CH_2) and anti-symmetric methyl stretch (ν_a CH_3) can be used to estimate the average chain tilt angles (see Figure 4D) with respect to the surface normal via the following equation:[50]

$$\frac{I(CH_2)}{I(CH_3)} = \frac{2}{3}\, m\, \frac{cos^2\,(90° - \alpha)}{cos^2(35° - \alpha)} \qquad \text{Equation 1}$$

where *I* is the peak area, m is the number of methylene groups, α is the tilt angle, and 90° and 35° the direction of the stretches with respect to the molecular axis. On this surface, the IR data that can be obtained are particularly nice, which here allows for a proper deconvolution of the absorption components that cannot be obtained on many other surfaces. In Figure 4D the resulting tilt angles are shown, and it is evident that the average chain tilt decreases with increasing chain length, from 36° for C8YNE to 24° for C18YNE layers, suggesting a crystalline densely packed monolayer structure composed of mainly fully extended all-trans chains.

Yet another IR-based parameter to provide information about the structure of the monolayer is the precise position of the antisymmetric CH_3 peak. This anti-symmetric CH_3 stretch appears at 2964 cm^{-1} when it occurs in-plane (terminal C-C bond parallel to the surface normal) and at 2954 cm^{-1} when it is out-of-plane (terminal C-C bond parallel to the surface). In the IRRAS spectra, the in-plane anti-symmetric stretching band has a low intensity for the C18YNE as compared to out-of-plane anti-symmetric stretch.[56] Firstly, the modes of the anti-symmetric stretching band are clearly seen for the methyl group (-CH_3) direction of $\perp$ C-CH_3 bond, in plane C-C backbone in the C-H stretching region for C6YNE-C18YNE are 2958 and 2963 cm^{-1}, respectively.[57, 58] Due to more favorable interchain van der Waals interactions, C18YNE-derived monolayers exhibit similar packing densities as long chain thiol-based monolayers on gold, as described by Nuzzo and co-workers,[57-59] as clearly revealed by the low relative intensity of the in-plane CH_3 stretching mode compared to the antisymmetric CH_2 vibration, corresponding to an average chain tilt angle of 25° with respect to the surface normal. On the other hand, short C6YNE monolayers, lacking the interchain van der Waals stabilization, are more tilted with respect to the surface normal as confirmed by the more pronounced out-of-plane CH_3 stretching vibration. It is obvious that increasing chain length induces more favorable interchain Van der Waals interactions, significantly improves the ordering, and therefore might enhance the overall stability of the monolayer. This is in excellent agreement with average chain tilted angles extracted from the IR data as given in Figure 4D. Moreover, for C16ENE-derived monolayers (modification conditions: 160 °C for 16 h) an average chain tilt angle of 30.4° was deduced, which is approximately 5° higher than for C16YNE layers, as shown in Table 3. This tilt angle is in the same order as for C12YNE-derived monolayers, and confirms that alkyne-derived monolayers are more densely packed, and display a higher degree of short-range order. Analogous information on the average chain tilt angle can in principle be obtained from the effective thickness by ellipsometry. Taking the ellipsometry thickness for C6YNE (0.75 nm) and C18YNE (2.20 nm) monolayers yields estimated tilt angles of 14.5° and 20.5°, respectively. However, in our experience

ellipsometry thickness data typically overestimate the monolayer thickness,[54] making this a less reliable source of information.

Table 3. IRRAS peaks of 1-hexadecene (C16ENE) derived monolayers on CrN surfaces with varying different reaction temperature for 16 h. Tilt angle calculated using anti-symmetric methylene and methyl peak area according to equation 1.

Reaction Temp.	ν_a CH_2	ν_s CH_2	ν_a CH_3	C=O	Tilt angle
100 °C	2926.6	2855.4	2859.5	1739.7	35.3°
130 °C	2924.5	2853.2	2860.2	1741.2	34.1°
160 °C	2921.1	2850.7	2961.7	1741.6	30.4°

Finally, IRRAS was used to study the influence of the reaction temperature on the reactivity and resulting packing density of 1-alkene-derived monolayers. Comparison of the data depicted in Table 3 and Figure 4, clearly demonstrates that in comparison with 1-alkene monolayers, 1-alkyne monolayers are denser and more ordered already at lower reaction temperatures (100 °C). This is e.g. evidenced by the position of the antisymmetric methylene stretching vibrations (CH_2 ν_a) and the IR derived tilt angle: C16YNE at 100 °C gives CH_2 ν_a = 2918 cm^{-1} with tilt angle ~24°, while C16ENE even at 160 °C results in CH_2 ν_a = 2921.1 cm^{-1} with tilt angle ~30.4°**.** Furthermore, a clear temperature-dependent peak shift was found for the methylene stretching modes from 100 to 160 °C. This trend indicates a gradual transition from a disordered, liquid-like assembly at 100 °C towards a denser, closer-packed monolayer structure at 160 °C. In line with this, the tilt angle decreases for this alkene-derived monolayer with increasing reaction temperature from 35.3° to 30.4°. This increased order at elevated modification temperatures is attributed to the higher activation energy required to fill the finally vacant sites in an almost complete monolayer.

7.3.5 Mode of Attachment

To investigate the monolayer structure further, detailed analyses with XPS were performed. The XPS wide scans after modification with CH_3-$(CH_2)_n$-C≡CH (n = 3 – 15) on plasma-activated CrN surfaces are shown in Figure 5A, whereas the C1s narrow scans are displayed in Figure 5B. As expected for monolayer formation without contributions of multilayer formation, both the wide and C1s narrow scans show that the peak intensity for C1s (at BE of 285 eV) correlates well with the number of carbons in the chain. The C1s spectra are deconvoluted into three main peaks (see Figure 6C): (i) the alkyl peak at 285.0

eV, (ii) a peak assigned to –<u>C</u>-C=O around 286.7 eV, and (iii) a –<u>C</u>=O peak at 288.5 eV. For all of these CH_3-$(CH_2)_n$-C≡CH (n = 3 – 15) derived monolayers, a peak area ratio of n+1 : 1 : 1 was obtained, which closely resembled the expected ratio. This was confirmed by DFT-simulated XPS spectra (B3LYP/6-311G(d,p) level),[60] which showed that a C=O peak is to be expected at 289.5 eV, while –***<u>C</u>***-C=O carbon atom should yield a peak at 287.6 eV, in close to agreement with experiment. The DFT data for the C16-YNE and 2HHDA attachments are provided in the *Supporting Information S.7.1 Figure S1*. We note that similar data with carbonyl-related peaks were observed for the attachment of 1-alkynes on alumina surfaces,[30] while this contrasts strongly with the formation of the signals obtained for Si-CH=CH-bound monolayers obtained from 1-alkynes on H-terminated Si(111) surfaces.[3, 61]

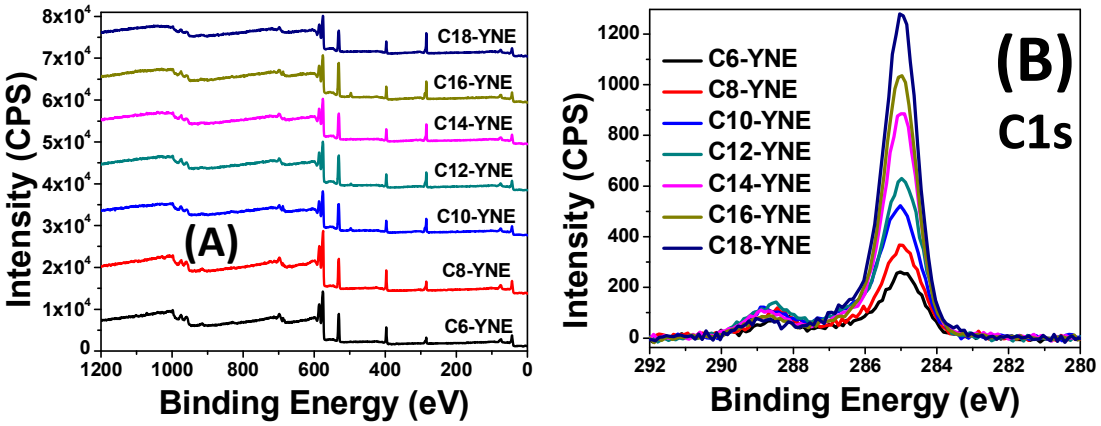

Figure 5. XPS data measured on monolayers derived from CH_3-$(CH_2)_n$-C≡CH (n = 3 – 15) on plasma-activated CrN surfaces. (A) wide scans, (B) C1s narrow scans.

Stimulated by earlier work in our group on the oxidative binding of C16YNE on porous anodic alumina,[30] we also used 2-hydroxyhexadecanoic acid (2HHDA) as a reference. Ter Maat et al. observed a remarkable resemblance between the XPS and IR spectra obtained from C16YNE-modified and 2HHDA-modified porous anodic alumina surfaces.[30] Analogously, as shown in Figure 6A and 6B, the IRRAS spectra of 2HHDA and C16YNE modified CrN show great similarity, both possessing clear absorptions at 1720 and 1444 cm^{-1}, assigned to C=O stretching and C-H bending vibrations, respectively. In addition to IRRAS, the XPS C1s narrow scans confirm the oxidative binding structures of alkynes and alkenes onto plasma-activated CrN surfaces. As shown in Figure 6 C and D, the peak positions and peak area of the C1s narrow scan of a C16YNE-derived monolayer are in excellent agreement with the C1s narrow scan of a 2HHDA monolayer. These results imply the oxidative adsorption of terminal alkynes on plasma-activated CrN surfaces under the formation of 2-hydroxy-carboxylic acids (see Figure 6).

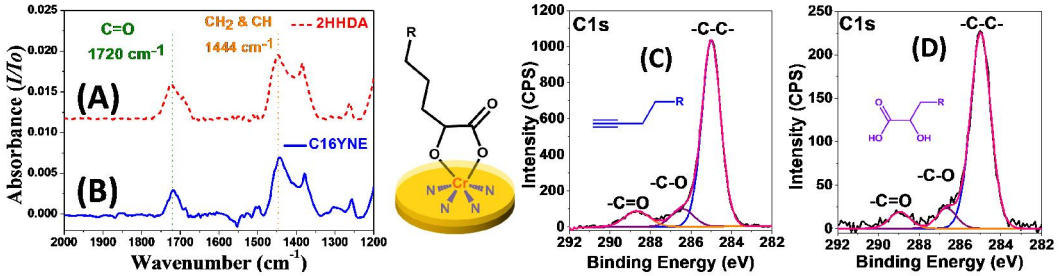

Figure 6. (A) IRRAS spectra of a 2HHDA-derived monolayer dotted line and (B) C16YNE-monolayer on freshly plasma-oxidized CrN surfaces after baseline correction. Schematic representation (left side) of the binding of 2HHDA onto the oxidized CrN surface, resulting from the oxidative adsorption of terminal alkyne functionality. (C & D) XPS C1s narrow scan of (C) 1-hexadecyne (C16YNE), (D) 2-hydroxyhexadecanoic acid (2HHDA) monolayers on plasma-activated CrN surfaces, together with the indicated deconvolution.

Analogously, the chemical bonding of alkene-derived monolayers onto CrN surface was also studied. IRRAS shows the formation of strong C=O stretching mode around 1742 cm^{-1}, which also suggests an oxidative addition reaction of 1-alkenes onto plasma-activated CrN, in good agreement with the binding of palmitic acid (PMA) on alumina surfaces.[62] In addition, the C1s narrow scan for C16ENE and palmitic acid (PMA) monolayers (figure 7 C and D) displays a high degree of similarity, supporting the IRRAS data.

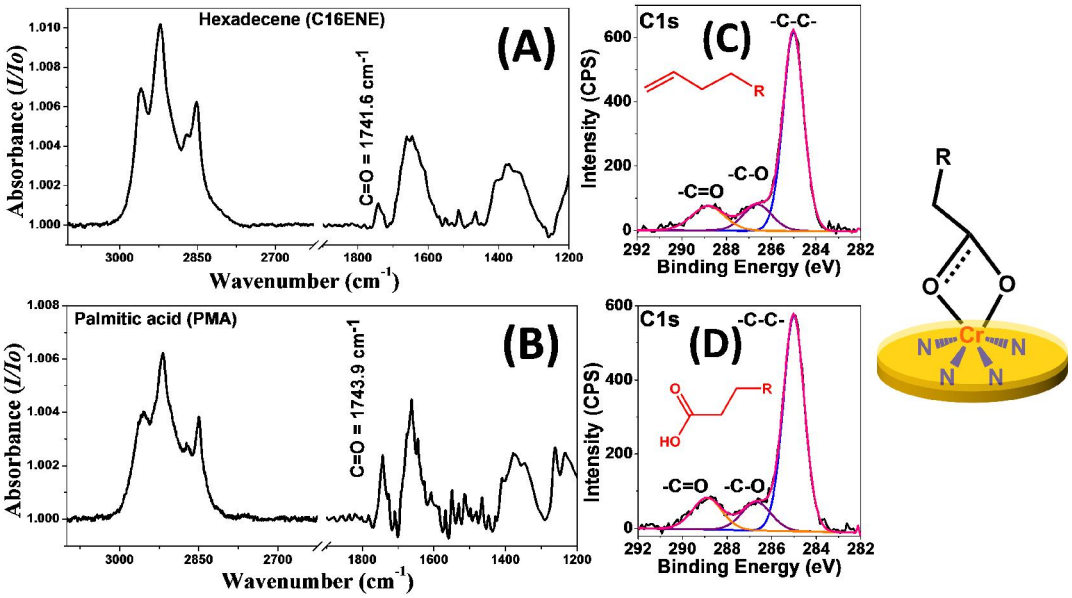

Figure 7. IRRAS spectra of the C-O region and C-H region of hexadecene-derived monolayers (A) and PMA monolayers (B) on plasma-activated CrN surfaces, with a schematic depiction of the mode of binding for alkene-derived monolayers. (C & D) XPS C1s narrow scan of (C) 1-hexadecene

(C16ENE) and (D) palmitic acid (PMA) derived monolayers on plasma-activated CrN surfaces, together with the indicated deconvolution.

The proposed chemical bonding for both alkyne and alkene on freshly oxidized CrN is shown in Figure 6 and 7. Most probably, these structures can be explained by the nucleophilic attack of the π bond of the alkene/alkyne functionality on surface hydroxyl groups present on the CrN surface after plasma activation and subsequent oxidation of the alkyne/alkene. Interestingly, the carbonyl group formation likely uses the oxygen present on chromium oxynitride surface becasue this oxidatively adsorbed monolayer is formed even upon rigorous exclusion of oxygen from the reaction vessel. This finding is strongly supported by the analogous reaction of 1-alkynes on the η-alumina surface, which also displays surface-bound carbonyl groups.[30] In contrast, alkynes were shown to bind to the silicon carbide surface via a double Markovnikov addition,[20] but that bonding situation yields significantly different spectra.

7.3.6 Fluorinated Monolayers

Compared to the hydrogenated C16YNE layers, the fluorinated alkyne-derived monolayers (F9YNE and F17YNE) are somewhat more disordered, as shown by the positions of the antisymmetric (2924 cm^{-1} and 2926 cm^{-1}) and symmetric (2852 cm^{-1} and 2853 cm^{-1}) methylene stretching vibrations, respectively. Such high wavenumbers for the CH_2 stretches are due to the $CF_{2/3}$ part of the chains adopting helical conformations, with a relatively large footprint, which allows for a concomitantly lower order of the CH_2 moieties as compared to that of the nonfluorinated chains. In addition, for fluorinated monolayers F9YNE, the thickness is 1.7 ± 0.3 nm, and for F17YNE it is 1.6 ± 0.3 nm (see Table 2). This is again in line with a somewhat reduced monolayer density, as was e.g. also observed for fluorinated monolayers on hydroxyl-terminated SiC.[20] The fluorohydro alkyne-derived (F9YNE) monolayers were also analyzed by XPS, and the resulting C1s and F1s high-resolution spectra are depicted in Figure 8. The C1s narrow scan was deconvoluted into seven distinct components representing the different carbon atoms in the fluoro monolayer. The C1s contributions at a binding energy of 285.0 eV correspond to carbon atoms involved in CH_2 moieties of F9YNE. The signal at 286.3 eV corresponds to -CF_2-***C***H_2- group, whereas the -***C***F_2-CH_2- signal is found at 290.7 eV. In between the two carbonyl related peaks show up at ~287.2 eV for –***C***H_2-C=O and at 288.8 eV for -C=O. Finally, the C1s signal at 292.1 eV corresponds to the other CF_2 groups, whereas the highest binding energy (294.4 eV) was observed for the terminal CF_3 group. In addition, the C1s XPS spectrum of F9YNE (see in Figure 8B) was simulated using a B3LYP/6-

311G(d,p)-derived method, yielding a reasonable agreement with experiment (See *Supporting Information S.7.1 Figure S1*). The F 1s region (see figure 8B) displays a single peak at 689.2 eV, which is consistent with what is previously reported for other substrates.[31, 32] Similar features were also found for the F17YNE-derived monolayers. The XPS wide scan C/F atomic ratio calculated as an average of three different sample modifications was C1s(16)/F1s(9) = 1.86 ± 0.10 for F9YNE. and C1s(16)/F1s(17) = 0.78 ± 0.2 for F17YNE is, which is in excellent agreement with theoretical values of 1.77 and 0.94, respectively.

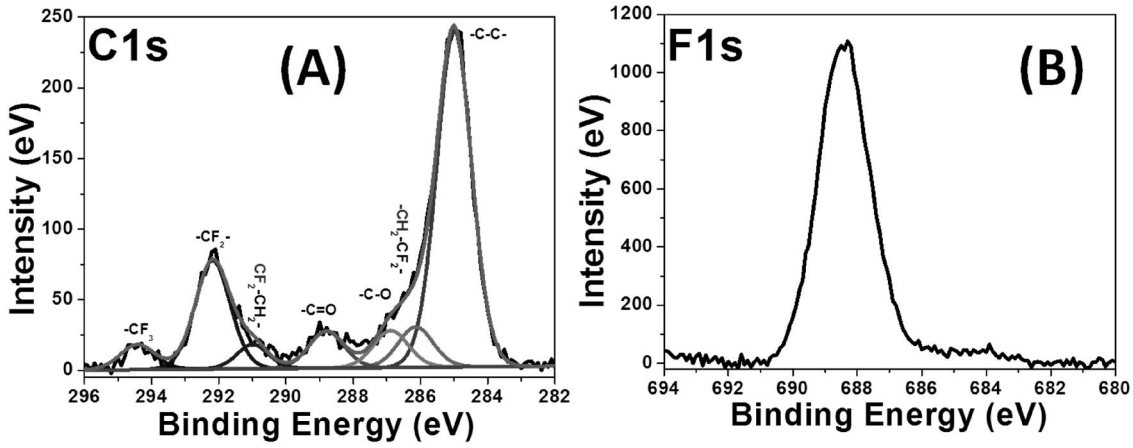

Figure 8. High-resolution XPS data of a F9YNE monolayer on plasma-activated CrN surface modified at 100 °C for 16 h. (A) C1s narrow scan; (B) F1s narrow scan.

7.4 CONCLUSIONS

We have developed a novel method for obtaining high-quality, covalently bound monolayers on CrN surfaces via the thermal reaction of 1-alkynes with air plasma-activated CrN surfaces. The monolayers are readily formed (8 - 12 h), and are densely packed with a high degree of short-range order. Analogous monolayers can be derived from 1-alkenes, but these are of lower quality. Initial binding studies indicate an oxidative adsorption mode of attachment, with the concomitant formation of surface-bound C=O groups. These monolayers thus provide substantial potential for further studies that would combine the unique properties of CrN (chemical stability and mechanical robustness) with the tunability of covalently attached monolayers.

7.5 REFERENCES

1. Bhushan, B., *Handbook of Nanotechnology*. Springer: Berlin, 2007.
2. Butt, H. J.; Cappella, B.; Kappl, M., Force measurements with the atomic force microscope: Technique, interpretation and applications. *Surf. Sci. Rep.* **2005,** 59, (1-6), 1-152.
3. Li, Y.; Calder, S.; Yaffe, O.; Cahen, D.; Haick, H.; Kronik, L.; Zuilhof, H., Hybrids of Organic Molecules and Flat, Oxide-Free Silicon: High-Density Monolayers, Electronic Properties, and Functionalization. *Langmuir* **2012,** 28, (26), 9920-9929.
4. Padture, N. P., In Situ-Toughened Silicon Carbide. *J. Am. Ceram. Soc.* **1994,** 77, (2), 519-523.
5. Nie, X.; Zhang, P.; Weiner, A. M.; Cheng, Y.-T., Nanoscale Wear and Machining Behavior of Nanolayer Interfaces. *Nano Lett.* **2005,** 5, (10), 1992-1996.
6. Su, Y. L.; Yao, S. H.; Leu, Z. L.; Wei, C. S.; Wu, C. T., Comparison of tribological behavior of three films - TiN, TiCN and CrN - Grown by physical vapor deposition. *Wear* **1997,** 213, (1-2), 165-174.
7. Hones, P.; Zakri, C.; Schmid, P. E.; Levy, F.; Shojaei, O. R., Oxidation resistance of protective coatings studied by spectroscopic ellipsometry. *Appl. Phys. Lett.* **2000,** 76, (22), 3194-3196.
8. Chen, I. W.; Rosenflanz, A., A tough SiAlON ceramic based on α-Si_3N_4 with a whisker-like microstructure. *Nature* **1997,** 389, (6652), 701-704.
9. Toth, L. E., *Transition Metal Carbides and Nitrides*. Academic Press Inc., U. S: 1971.
10. Vericat, C.; Vela, M. E.; Benitez, G.; Carro, P.; Salvarezza, R. C., Self-assembled monolayers of thiols and dithiols on gold: New challenges for a well-known system. *Chem. Soc. Rev.* **2010,** 39, (5), 1805-1834.
11. Jun, Y.; Zhu, X. Y.; Hsu, J. W. P., Formation of Alkanethiol and Alkanedithiol Monolayers on GaAs(001). *Langmuir* **2006,** 22, (8), 3627-3632.
12. Karsi, N.; Lang, P.; Chehimi, M.; Delamar, M.; Horowitz, G., Modification of indium tin oxide films by alkanethiol and fatty acid self-assembled monolayers: A comparative study. *Langmuir* **2006,** 22, (7), 3118-3124.
13. Li, Y.; Zuilhof, H., Photochemical Grafting and Patterning of Organic Monolayers on Indium Tin Oxide Substrates. *Langmuir* **2012,** 28, (12), 5350-5359.
14. Caipa Campos, M. A.; Trilling, A. K.; Yang, M.; Giesbers, M.; Beekwilder, J.; Paulusse, J. M. J.; Zuilhof, H., Self-Assembled Functional Organic Monolayers on Oxide-Free Copper. *Langmuir* **2011,** 27, (13), 8126-8133.
15. Helmy, R.; Fadeev, A. Y., Self-Assembled Monolayers Supported on TiO_2: Comparison of $C_{18}H_{37}SiX_3$ (X = H, Cl, OCH_3), $C_{18}H_{37}Si(CH_3)_2Cl$, and $C_{18}H_{37}PO(OH)_2$. *Langmuir* **2002,** 18, (23), 8924-8928.
16. Jones, R. L.; Harrod, B. L.; Batteas, J. D., Intercalation of 3-Phenyl-1-proponal into OTS SAMs on Silica Nanoasperities to Create Self-Repairing Interfaces for MEMS Lubrication. *Langmuir* **2010,** 26, (21), 16355-16361.
17. Seitz, O.; Fernandes, P. G.; Tian, R.; Karnik, N.; Wen, H.-C.; Stiegler, H.; Chapman, R. A.; Vogel, E. M.; Chabal, Y. J., Control and stability of self-assembled monolayers under biosensing conditions. *J. Mater. Chem.* **2011,** 21, (12), 4384-4392.
18. Rosso, M.; Giesbers, M.; Arafat, A.; Schroën, K.; Zuilhof, H., Covalently Attached Organic Monolayers on SiC and Si_xN_4 Surfaces: Formation Using UV Light at Room Temperature. *Langmuir* **2009,** 25, (4), 2172-2180.

19. Rosso, M.; Arafat, A.; Schroën, K.; Giesbers, M.; Roper, C. S.; Maboudian, R.; Zuilhof, H., Covalent Attachment of Organic Monolayers to Silicon Carbide Surfaces. *Langmuir* **2008,** 24, (8), 4007-4012.
20. Pujari, S. P.; Scheres, L.; Weidner, T.; Baio, J. E.; Stuart, M. A. C.; Rijn, C. J. M. v.; Zuilhof, H., Covalently Attached Organic Monolayers onto Silicon Carbide from 1-Alkynes: Molecular Structure and Tribological Properties. *Langmuir* **2013,** 29, (12), 4019–4031.
21. Wang, X.; Landis, E. C.; Franking, R.; Hamers, R. J., Surface Chemistry for Stable and Smart Molecular and Biomolecular Interfaces via Photochemical Grafting of Alkenes. *Acc. Chem. Res.* **2010,** 43, (9), 1205-1215.
22. Fadeev, A. Y.; McCarthy, T. J., A New Route to Covalently Attached Monolayers: Reaction of Hydridosilanes with Titanium and Other Metal Surfaces. *J. Am. Chem. Soc.* **1999,** 121, (51), 12184-12185.
23. Clot, O.; Wolf, M. O., Spontaneous Adsorption of 4-Ferrocenylphenyl Isocyanide and 11-Mercaptoundecanoyl Ferrocene on Chromium. *Langmuir* **1999,** 15, (24), 8549-8551.
24. Hild, R.; David, C.; Müller, H. U.; Völkel, B.; Kayser, D. R.; Grunze, M., Formation and Characterization of Self-assembled Monolayers of Octadecyltrimethoxysilane on Chromium: Application in Low-Energy Electron Lithography. *Langmuir* **1998,** 14, (2), 342-346.
25. Anac, I.; McCarthy, T. J., Chemical modification of chromium oxide surfaces using organosilanes. *J. Colloid Interface Sci.* **2009,** 331, (1), 138-142.
26. Lancaster, S.; Kakade, S.; Mani, G., Microrough Cobalt–Chromium Alloy Surfaces for Paclitaxel Delivery: Preparation, Characterization, and In Vitro Drug Release Studies. *Langmuir* **2012,** 28, (31), 11511-11526.
27. Raman, A.; Quiñones, R.; Barriger, L.; Eastman, R.; Parsi, A.; Gawalt, E. S., Understanding Organic Film Behavior on Alloy and Metal Oxides. *Langmuir* **2009,** 26, (3), 1747-1754.
28. Khodakov, Y. S.; Vinogradova, E. F.; Tulupov, V. A.; Minachev, K. M., Relation between the hydrogenating and dehydrogenating activity of chromium oxide catalysts and their basicity. *Bulletin of the Academy of Sciences of the USSR, Division of chemical science* **1971,** 20, (12), 2700-2701.
29. Vong, T.; Schoffelen, S.; van Dongen, S. F. M.; van Beek, T. A.; Zuilhof, H.; van Hest, J. C. M., A DNA-based strategy for dynamic positional enzyme immobilization inside fused silica microchannels. *Chemical Science* **2011,** 2, (7), 1278-1285.
30. ter Maat, J.; Regeling, R.; Ingham, C. J.; Weijers, C. A. G. M.; Giesbers, M.; de Vos, W. M.; Zuilhof, H., Organic Modification and Subsequent Biofunctionalization of Porous Anodic Alumina Using Terminal Alkynes. *Langmuir* **2011,** 27, (22), 13606-13617.
31. Pujari, S. P.; Spruijt, E.; Stuart, M. A. C.; van Rijn, C. J. M.; Paulusse, J. M. J.; Zuilhof, H., Ultralow Adhesion and Friction of Fluoro-Hydro Alkyne-Derived Self-Assembled Monolayers on H-Terminated Si(111). *Langmuir* **2012,** 28, (51), 17690-17700.
32. Pujari, S. P.; van Andel, E.; Yaffe, O.; Cahen, D.; Weidner, T.; van Rijn, C. J. M.; Zuilhof, H., Mono-Fluorinated Alkyne-Derived SAMs on Oxide-Free Si(111) Surfaces: Preparation, Characterization and Tuning of the Si Workfunction. *Langmuir* **2013,** 29, (2), 570-580.
33. Bin, X.; Zawisza, I.; Goddard, J. D.; Lipkowski, J., Electrochemical and PM-IRRAS Studies of the Effect of the Static Electric Field on the Structure of the DMPC Bilayer Supported at a Au(111) Electrode Surface. *Langmuir* **2004,** 21, (1), 330-347.

34. Weckhuysen, B. M.; Wachs, I. E.; Schoonheydt, R. A., Surface Chemistry and Spectroscopy of Chromium in Inorganic Oxides. *Chem. Rev.* **1996,** 96, (8), 3327-3350.
35. Rawal, S. K.; Chawla, A. K.; Jayaganthan, R.; Chandra, R., Optical and hydrophobic properties of co-sputtered chromium and titanium oxynitride films. *Appl. Surf. Sci.* **2011,** 257, (21), 8755-8761.
36. Reartes, G. B.; Morando, P. J.; Blesa, M. A.; Hewlett, P. B.; Matijevic, E., Reactivity of Chromium Oxide in Aqueous Solutions. 2. Acid Dissolution. *Langmuir* **1995,** 11, (6), 2277-2284.
37. Teghil, R.; Santagata, A.; De Bonis, A.; Galasso, A.; Villani, P., Chromium carbide thin films deposited by ultra-short pulse laser deposition. *Appl. Surf. Sci.* **2009,** 255, (17), 7729-7733.
38. Salvi, A. M.; Castle, J. E.; Watts, J. F.; Desimoni, E., Peak fitting of the chromium 2p XPS spectrum. *Appl. Surf. Sci.* **1995,** 90, (3), 333-341.
39. Aouadi, S. M.; Schultze, D. M.; Rohde, S. L.; Wong, K. C.; Mitchell, K. A. R., Growth and characterization of Cr2N/CrN multilayer coatings. *Surf. Coat. Technol.* **2001,** 140, (3), 269-277.
40. Lippitz, A.; Hübert, T., XPS investigations of chromium nitride thin films. *Surf. Coat. Technol.* **2005,** 200, (1–4), 250-253.
41. ter Maat, J.; Regeling, R.; Yang, M.; Mullings, M. N.; Bent, S. F.; Zuilhof, H., Photochemical Covalent Attachment of Alkene-Derived Monolayers onto Hydroxyl-Terminated Silica. *Langmuir* **2009,** 25, (19), 11592-11597.
42. Franking, R.; Hamers, R. J., Ultraviolet-Induced Grafting of Alkenes to TiO2 Surfaces: Controlling Multilayer Formation. *The Journal of Physical Chemistry C* **2011,** 115, (34), 17102-17110.
43. Linford, M. R.; Chidsey, C. E. D., Alkyl monolayers covalently bonded to silicon surfaces. *J. Am. Chem. Soc.* **1993,** 115, (26), 12631-12632.
44. Bansal, A.; Li, X.; Yi, S. I.; Weinberg, W. H.; Lewis, N. S., Spectroscopic Studies of the Modification of Crystalline Si(111) Surfaces with Covalently-Attached Alkyl Chains Using a Chlorination/Alkylation Method. *J. Phys. Chem. B* **2001,** 105, (42), 10266-10277.
45. Koishi, T.; Yasuoka, K.; Fujikawa, S.; Ebisuzaki, T.; Xiao, C. Z., Coexistence and transition between Cassie and Wenzel state on pillared hydrophobic surface. *Proceedings of the National Academy of Sciences of the United States of America* **2009,** 106, (21), 8435-8440.
46. Feng, L.; Zhang, Z.; Mai, Z.; Ma, Y.; Liu, B.; Jiang, L.; Zhu, D., A super-hydrophobic and super-oleophilic coating mesh film for the separation of oil and water. *Angew. Chem. Int. Ed.* **2004,** 43, (15), 2012-2014.
47. Machaggah, S. M.; Kivaisi, R. T.; Lushiku, E. M., Ellipsometric studies of obliquely deposited chromium films. *Solar Energy Materials* **1989,** 19, (3–5), 315-321.
48. Ramsey, D. A.; Ludema, K. C., The influences of roughness on film thickness measurements by Mueller matrix ellipsometry. *Rev. Sci. Instrum.* **1994,** 65, (9), 2874-2881.
49. Ewers, B. W.; Batteas, J. D., Molecular Dynamics Simulations of Alkylsilane Monolayers on Silica Nanoasperities: Impact of Surface Curvature on Monolayer Structure and Pathways for Energy Dissipation in Tribological Contacts. *J. Phys. Chem. C* **2012,** 116, (48), 25165-25177.
50. Levine, I.; Weber, S. M.; Feldman, Y.; Bendikov, T.; Cohen, H.; Cahen, D.; Vilan, A., Molecular Length, Monolayer Density, and Charge Transport: Lessons from Al–AlOx/Alkyl–Phosphonate/Hg Junctions. *Langmuir* **2011,** 28, (1), 404-415.

51. Leitch, J.; Kunze, J.; Goddard, J. D.; Schwan, A. L.; Faragher, R. J.; Naumann, R.; Knoll, W.; Dutcher, J. R.; Lipkowski, J., In Situ PM-IRRAS Studies of an Archaea Analogue Thiolipid Assembled on a Au(111) Electrode Surface. *Langmuir* **2009,** 25, (17), 10354-10363.
52. Snyder, R. G.; Strauss, H. L.; Elliger, C. A., Carbon-hydrogen stretching modes and the structure of n-alkyl chains. 1. Long, disordered chains. *J. Phys. Chem.* **1982,** 86, (26), 5145-5150.
53. MacPhail, R. A.; Strauss, H. L.; Snyder, R. G.; Elliger, C. A., Carbon-hydrogen stretching modes and the structure of n-alkyl chains. 2. Long, all-trans chains. *J. Phys. Chem.* **1984,** 88, (3), 334-341.
54. Scheres, L.; Giesbers, M.; Zuilhof, H., Organic Monolayers onto Oxide-Free Silicon with Improved Surface Coverage: Alkynes versus Alkenes. *Langmuir* **2010,** 26, (7), 4790-4795.
55. Jones, R. L.; Pearsall, N. C.; Batteas, J. D., Disorder in Alkylsilane Monolayers Assembled on Surfaces with Nanoscopic Curvature. *J. Phys. Chem. C* **2009,** 113, (11), 4507-4514.
56. Nuzzo, R. G.; Dubois, L. H.; Allara, D. L., Fundamental studies of microscopic wetting on organic surfaces. 1. Formation and structural characterization of a self-consistent series of polyfunctional organic monolayers. *J. Am. Chem. Soc.* **1990,** 112, (2), 558-569.
57. Nuzzo, R. G.; Zegarski, B. R.; Dubois, L. H., Fundamental studies of the chemisorption of organosulfur compounds on gold(111). Implications for molecular self-assembly on gold surfaces. *J. Am. Chem. Soc.* **1987,** 109, (3), 733-740.
58. Nuzzo, R. G.; Fusco, F. A.; Allara, D. L., Spontaneously organized molecular assemblies. 3. Preparation and properties of solution adsorbed monolayers of organic disulfides on gold surfaces. *J. Am. Chem. Soc.* **1987,** 109, (8), 2358-2368.
59. Dubois, L. H.; Nuzzo, R. G., Synthesis, Structure, And Properties Of Model Organic-Surfaces. *Annu. Rev. Phys. Chem.* **1992,** 43, 437-463.
60. Giesbers, M.; Marcelis, A. T. M.; Zuilhof, H., Simulation of XPS C1s Spectra of Organic Monolayers by Quantum Chemical Methods. *Langmuir* **2013,** 29, (15), 4782-4788.
61. Scheres, L.; Giesbers, M.; Zuilhof, H., Self-Assembly of Organic Monolayers onto Hydrogen-Terminated Silicon: 1-Alkynes Are Better Than 1-Alkenes. *Langmuir* **2010,** 26, (13), 10924-10929.
62. Allara, D. L.; Nuzzo, R. G., Spontaneously organized molecular assemblies. 2. Quantitative infrared spectroscopic determination of equilibrium structures of solution-adsorbed n-alkanoic acids on an oxidized aluminum surface. *Langmuir* **1985,** 1, (1), 52-66.

Supporting Information to Chapter 7

Table of Contents

Supporting Information to Chapter 7 210

S.7.1 Density Functional Theory (DFT)..... 210

S.7.2 Kinetic study of the attachment of 1-alkynes and 1-alkenes onto plasma-activated CrN surface: 211

S.7.3 AFM image and roughness: 211

S.7.1 Density Functional Theory (DFT)[1]

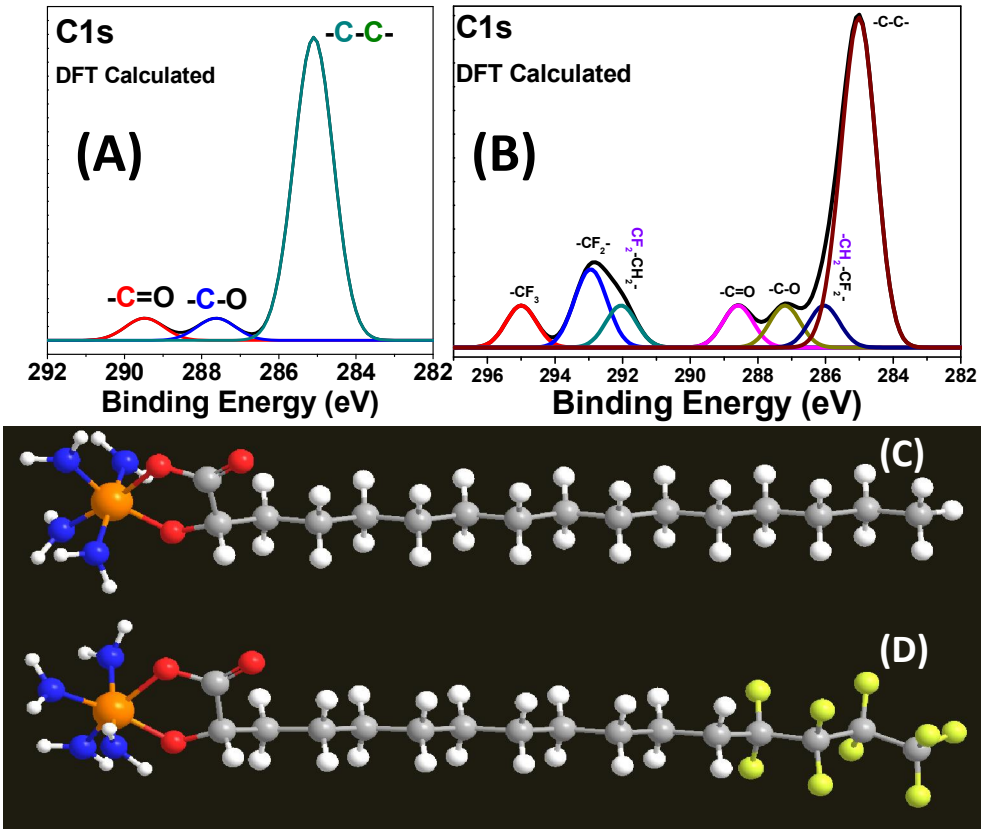

Figure S1. (A) Simulated XPS spectra of C16YNE (A and C) and F9YNE (B and D) using the B3LYP/6-311G(d,p)-calculated binding energies corrected with slope and offset. Color code: blue (nitrogen), orange (chromium), red (oxygen), gray (carbon), white (hydrogen), and yellow (fluorine).

S.7.2 Kinetic study of the attachment of 1-alkynes and 1-alkenes onto plasma-activated CrN surface:

Table S1. Static water contact angle of organic monolayers derived from 1-hexadecene and 1-hexadecyne on hydroxyl-terminated CrN as function of reaction temperature at 12 h.

Contact angle : effects of temperature (Figure 3A)									
1-hexadecene					**1-hexadecyne**				
Temp. °C	Surf-I	Std(± °)	Surf-II	Std(± °)	**Temp. °C**	Surf-I	Std(± °)	Surf-II	Std(± °)
6	64.5	0.8	65.2	0.6	**6**	75.0	0.6	74.3	0.6
15	71.1	1.4	69.5	0.8	**15**	78.5	0.6	79.0	0.6
20	71.8	0.8	71.7	1.2	**20**	81.7	1.0	82.4	0.6
40	81.5	1.1	82.5	0.8	**40**	93.0	0.6	93.2	0.7
60	90.7	1.0	92.6	1.2	**60**	97.5	1.1	99.5	1.2
80	98.0	0.7	98.2	0.9	**80**	106.5	0.7	106.4	0.9
100	105.4	0.6	105.0	1.0	**100**	110.2	0.6	110.0	0.6
130	108.7	0.6	107.8	0.5	**130**	110.0	0.5	110.7	0.5
160	109.4	0.9	110.5	1.3	**160**	110.4	0.7	110.2	0.6

Table S2. Hexadecyne-derived monolayers on the CrN surface with different time at 100 °C for static water contact angle.

Contact angle : Time (hr) at 100 oC (Figure 3C)				
1-hexadecyne				
Time (hr)	Surf-I	Std(± °)	Surf-II	Std(± °)
0.0	0.0	0.0	0.0	0.0
1.0	80.1	*0.4*	*81.0*	0.8
2.0	92.7	*0.6*	*92.5*	1.2
3.0	95.2	*0.7*	*95.0*	0.8
4.0	99.0	*0.6*	*98.0*	1.2
8.0	105.3	*0.5*	*105.4*	0.9
12.0	109.6	*0.6*	*109.4*	1.0
16.0	110.0	*1.0*	*110.0*	0.5
24.0	110.2	0.6	110.0	1.3

S.7.3 AFM image and roughness:

Figure S2 shows the AFM topographical height image of CrN substrates after various activation processes and alkyne modification: Bare (before activation) acetone cleaning of CrN (Figure S2A), 10 min air plasma activation (Figure S2B), after modification with C16YNE (Figure S2C), and after modification with F9YNE (Figure S2D). We found that the surface roughness decreases to 5.9 ± 0.1 nm after air plasma activation 10 min. After

monolayer grafting, the roughness slightly reduced again in both C16YNE and F9YNE to 5.8 ± 0.1 nm and 5.7 ± 0.1 nm, demonstrating that the formation of a cushioning monolayer. The similar effect we observed in the SiC surfaces.[2]

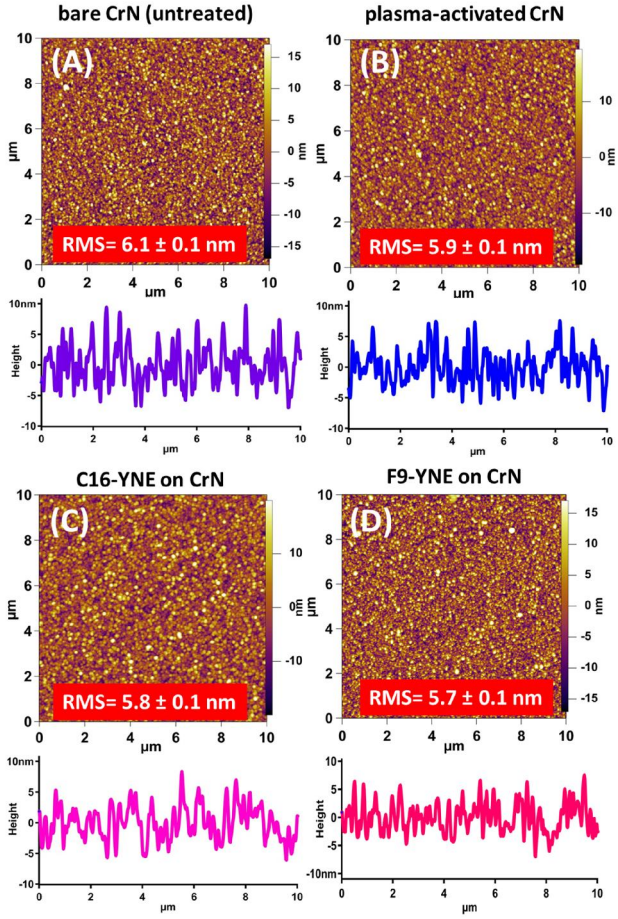

Figure S2. AFM tapping mode topographic images of CrN surface. (A) bare CrN (untreated) surface, (B) air plasma activation for 10 min, (C) after modification with C16YNE on CrN surfaces, and (D) after modification with F9YNE on CrN surfaces. Section Analyses for corresponding surfaces shown in below.

1. Giesbers, M.; Marcelis, A. T. M.; Zuilhof, H., Simulation of XPS C1s Spectra of Organic Monolayers by Quantum Chemical Methods. *Langmuir* **2013,** 29, (15), 4782-4788.

2. Pujari, S. P.; Scheres, L.; Weidner, T.; Baio, J. E.; Stuart, M. A. C.; Rijn, C. J. M. v.; Zuilhof, H., Covalently Attached Organic Monolayers onto Silicon Carbide from 1-Alkynes: Molecular Structure and Tribological Properties. *Langmuir* **2013,** 29, (12), 4019–4031.

CHAPTER 8

Tribology and Stability of Organic Monolayers on CrN: A Comparison among Silane, Phosphonate, Alkene, and Alkyne Chemistries

The fabrication of chemically and mechanically stable monolayers on the surfaces of various inorganic hard materials is crucial to the development of biomedical/electronic devices. In this chapter, monolayers based on the reactivity of silane, phosphonate, 1-alkene, and 1-alkyne moieties were obtained on the hydroxyl-terminated chromium nitride surface. Their chemical stability and tribology were systematically investigated. The chemical stability of the modified CrN surfaces was tested in aqueous media at 60 °C at pH 3, pH 7 and pH 11, and monitored by static water contact angle measurements, X-ray photoelectron spectroscopy (XPS), ellipsometry, and Fourier transform infrared reflection absorption spectroscopy (FT-IRRAS). The tribological properties of the resulting organic monolayers with different end groups (fluorinated or nonfluorinated) were studied using atomic force microscopy (AFM). It was found that the fluorinated monolayers exhibit a dramatic reduction of adhesion and friction force as well as excellent wear resistance compared to those of nonfluorinated coatings and bare CrN substrates. The combination of remarkable chemical stability and superior tribological properties makes these fluorinated monolayers promising candidates for the development of robust high-performance devices.

This Chapter is submitted for publication as:

'*Tribology and Stability of Organic Monolayers on CrN: A Comparison among Silane, Phosphonate, Alkene, and Alkyne Chemistries'*. Sidharam P. Pujari, Yan Li, Remco Regeling, and Han Zuilhof. *Langmuir* **2013,** in press, DOI: 10.1021/la401981b

Table of Contents

8 Tribology and Stability of Organic Monolayers on CrN: A Comparison among Silane, Phosphonate, Alkene, and Alkyne Chemistries 213
8.1 INTRODUCTION 215
8.2 MATERIALS AND METHODS 218
8.2.1 Materials 218
8.2.2 Monolayer formation 218
8.2.3 Chemical Stability 218
8.2.4 Monolayer Characterization 219
8.2.5 Tribological experiments 219
8.3 RESULTS AND DISCUSSION 221
8.3.1 Monolayer formation 221
8.3.2 Wettability and Ellipsometric Thickness 221
8.3.3 IRRAS and XPS 222
8.3.4 Chemical Stability 224
8.3.5 Tribology 226
8.3.5.1 Adhesion 227
8.3.5.2 Friction 228
8.3.5.3 Wear 230
8.4 CONCLUSIONS 233
8.5 REFERENCES 233

8.1 INTRODUCTION

Chromium nitride (CrN) is a material of significant industrial importance, due to a unique combination of interesting properties, including a low friction coefficient, a low wear rate, a high thermal stability and corrosion resistance, and a large bulk modulus (K_0 ≈ 361 GPa).[1-4] Another important property of CrN is its high electrical conductivity, which enables the application as anode material for high-temperature fuel cells.[5] Recently, CrN has also been heavily investigated for biomaterials, such as artificial joints, medical devices (armamentarium) and cutting tools.[6] There is a great demand for lower-adhesion, friction, and wear hard materials with stable lubricants under high load conditions. Such demands occur in micro-and nano-electro-mechanical systems (MEMS and NEMS) and in miniature motors with nano/micronewton loads or harsh chemical environments.[7-11] In this regard, it is noteworthy that many inorganic surfaces display relatively high adhesion and friction forces and a low wear resistance. This is due to a native oxide layer present on top of the surface, which yields H-bonding interactions and capillary forces with surface-bound water, thereby exhibiting a negative influence on the tribological performance of these mechanical systems.[9] Overcoming these constraints represents a critical challenge for the quality and performance assurance of many manufacturing processes.[12]

With the ongoing further miniaturization of moving components in many technological devices, the need has arisen to control the tribology to an unprecedented level. One approach to this has been the attachment of nanometer-thick organic monolayers to the surfaces of various materials.[9,13-15] Such organic monolayers provide the chance to modify and enhance the tribological properties. The incorporation of chemical functionalities at the top of the monolayer allows for systematic variation of the chemical and physical properties of the exposed SAM surface, making SAMs a powerful tool for controlled surface modification.[16,17] To investigate the tribological properties of a thus-modified surface with nanometer-scale features accurately, AFM has been widely used.[18-20]

Through recent investigations of the adhesion, friction, and wear behavior of densely packed monolayers,[16, 21] it has been recognized that the adhesion energy can be significantly reduced within the nanometer-scale ranges.[22] The adhesion/friction strength (force or energy) is well known to be highly dependent on numerous factors, such as the terminal group (e.g. $-CH_3$ or $-CF_3$), chain length, packing, and density of monolayers.[22] The obtained interaction strengths are also dependent on the surface properties of the AFM tip that is used during such measurements. For example, an AFM tip modified with a monolayer shows an increase in adhesion/friction forces with increases in chain length as a result of the more effective interdigitation that occurs between the surface monolayer

and the modified probe.[23] However, in the case where a nonmodified Si_3N_4 probe was used, higher adhesion/friction forces were detected with decreasing chain length. This was attributed to the formation of disordered monolayers with loosely packed structures and weaker van der Waals interactions in the case of the shorter chains. This allows stronger molecular contact between the inorganic probe and the monolayer as a result of the increased ease of surface penetration into the shorter-chain-length monolayer.[22]

The schematic treatment of SAM-forming monomers highlights three domains: a surface-anchoring group that typically responsible for the achieved stability, a hydrocarbon chain (typically polymethylene) to promote monolayer packing and organization, and a terminal functional group that ultimately defines the exposed surface functionality and dominates the resulting tribology. Various anchoring groups, such as thiols, alcohols, alkynes, alkenes, siloxanes, and phosphonates, can readily self-assemble on a wide variety of active surfaces having hydrogen, metal, hydroxyl- and/or oxide termination, making them particularly attractive for surface modification in a variety of applications.[21, 24-28] However, each type of monolayer has advantages and disadvantages. Regarding the chemical stability, for example, thiol-, carboxylate-, siloxane-, and phosphonate-derived monolayers on metal oxide surfaces typically show poor stability in aqueous environments as a result of the protonation of the carboxylate group at low pH and hydrolysis at pH > 9.[29] Phosphonate-derived monolayers on ITO electrode studied in three different media. They show that monolayers are in PBS solution are more stable than in pure water, and extremely stable under ambient air conditions. This improved stability of phosphonate monolayers in PBS solution was attributed to the stabilized pH in this system, as hydrolysis can be catalyzed under acidic or basic conditions.[30] However, silane-based monolayers on Ti-6Al-4V at physiological pH are liable to hydrolyze surface Si-O bonds.[31] On the contrary, alkene/alkyne-derived covalently attached layers exhibit remarkable stability in aqueous environments with pH ranging from 1 to 10.[27, 28, 32, 33]

In particular, ultrathin organic fluorinated monolayers have been found to yield lubricating surfaces with low adhesion, low friction and low wear resistance.[34] In fact, coating SiC and Si surfaces with covalently linked fluorinated monolayers yields the lowest friction coefficient for any solid surface, even about 4 times lower than for Teflon.[16, 21] In addition, fluorinated monolayers increase the wear resistance by 5 times on SiC surfaces and even up to 20 times on Si surfaces.[21, 35] Despite these significant successes, to the best of our knowledge, neither systematic study of covalently attached organic monolayers on CrN nor their tribology has yet been reported. In practice, polytetrafluoroethylene (PTFE) is now the primary coating material of CrN in many microelectromechanical systems.[36] However, these films are not covalently bound to the

surface and are therefore susceptible to wear. Moreover, PTFE films are relatively thick, which may eventually lead to high adhesion and friction forces when high loads are applied and the films are compressed.

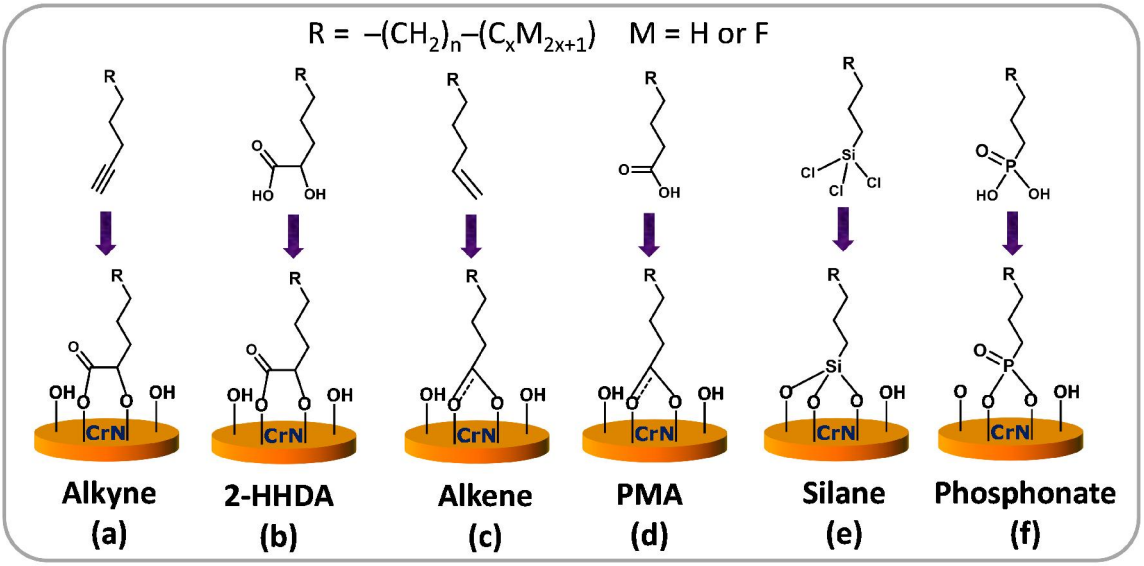

Figure 1. Schematic representation of tentative chemical binding structures of the anchoring groups (alkyne or 2-hydroxyl acid, alkene or carboxylic acid, silane, and phosphonate) used in this work (*n* + x = 16 or 18). Method of monolayer formation: (a) pure 1-alkyne, 100 °C, 16 hr, (b) 1 mM 2-HHDA (2-hydroxyhexadecanoic acid) in ethanol, 65 °C, 16 h, (c) pure 1-hexadecene, 160 °C, 16 hr, (d) 1 mM PMA (palmitic acid) in ethanol, 65 °C, 16 h, (e) 1 mM ODTS (trichloro(octadecyl)silane) in dry cyclohexane, 25 °C , 30 min, and (f) 1 mM HDPA (hexadecylphosphonic acid) in dry THF, 60 °C, 3 h.

In this chapter, we investigate the chemical stability and tribological (adhesion, friction, and wear) of a series of covalently linked organic monolayers on CrN. These properties were studied as a function of different anchoring groups and varying chain length and with the replacement of the methyl group by the fluorinated terminal group (Figure 1). To test the chemical stability, we used three different media: acid (pH 3), base (pH 11) and neutral water, all at 65 °C. The tribology was studied by colloidal probe atomic force microscopy (CP-AFM), to reveal the enhancements provided by the surface coatings, while and DLC (diamond-like carbon)-coated probes were used to study the reduction of the wear resistance. The obtained results provide a valuable reference for the development of high-performance devices or CrN and other robust inorganic materials.

8.2 MATERIALS AND METHODS

8.2.1 Materials

Wafers with nonstoichiometric chromium nitride films (thickness 1 μm, surface root-mean-square (rms) roughness determined with AFM ~5.0 nm) obtained by sputter deposition on Si(100) were kindly provided by ASML The Netherlands B.V. 1-Hexadecene (≥99%, C16ENE), 1-hexyne (97%, C6YNE), 1-octyne (98%, C8YNE), 1-decyne (98%, C10YNE), 1-dodecyne (98%, C12YNE), and 1-tetradecyne (≥97%, C14YNE), were purchased from Aldrich and purified by distillation before use. 1-Hexadecyne and 1-octadecyne (C18YNE) were synthesized according to literature procedures.[16] 2-Hydroxyhexadecanoic acid (ABCR, 95%, 2HHDA), trichloro(octadecyl)silane (Aldrich, >90%, ODTS), hexadecylphosphonic acid (Aldrich, 97%, HDPA), and N-ethyldiisopropylamine (Aldrich, 98%) were used as received. 13,13,14,14,15,15,16,16,16-Nonafluorohexadec-1-yne (F9YNE) and 9,9,10,10,11,11, 12,12,13,13,14,14,15,15,16,16,16-heptadecafluorohexadec-1-yne (F17YNE) were synthesized using literature procedures.[16] Other reagents or solvents were purchased from major chemical suppliers and used as received unless otherwise noted.

8.2.2 Monolayer formation

CrN samples (10 mm × 10 mm) were cut from a Si(100) substrate with a CrN epilayer, and these surfaces were first cleaned by rinsing with dichloromethane followed by sonication for 10 min in acetone. Subsequently, the samples were further activated using air plasma (PDC-002-plasma cleaner, Harrick Scientific Products, Inc. Ossining, NY) for 10 min (0.3 SCFH air flow, 29.6 W power, at 300 mTorr pressure), to remove any organic contaminations and to obtain a hydroxyl-terminated surface. After being activated, the samples were dried under a stream of argon. These freshly etched and dried surfaces were then quickly transferred to a screw-capped bottle under an argon atmosphere, which was charged with 1 mL of alkynes, and subsequently heated to 100 °C for 16 h. After the thermal reaction, the samples were removed from the flask, immediately rinsed extensively with DCM, sonicated for 5 min in acetone to remove physisorbed reagents and dried under a stream of argon. Samples were stored in a glovebox (O_2, H_2O < 0.1 ppm) between measurements. Samples were rinsed with fresh DCM and blown dry with argon immediately before any characterization.

2-Hydroxyhexadecanoic acid (2HHDA)-derived monolayers and palmitic acid (PMA)-derived monolayers were prepared using a similar activation process. In this case, after plasma activation the samples were rinsed in ethanol, and immersed in a 1 mM solution of

2-hydroxyhexadecanoic acid or palmitic acid in ethanol at 65 °C for 16 h.[26] Trichloro(octadecyl)silane-derived monolayers were obtained upon immersing plasma-oxidized CrN surfaces in 10 ml of 1 mM trichloro(octadecyl)silane (ODTS) in anhydrous cyclohexane [dried with molecular sieves 4 Å] in the presence of Hunig's base (N-ethyldiisopropylamine) (1 mM). The reaction was allowed to proceed for 10 min at room temperature, after which time the CrN surface was removed, washed with water, ethanol, and dichloromethane, and dried under argon. Hexadecylphosphonic acid (HDPA)-derived monolayers were obtained by immersing plasma-oxidized CrN surfaces in a 1 mM solution of HDPA in tetrahydrofuran (THF) in a simple glass tube.[37] The solution was heated in a water bath to 60 °C until complete evaporation of THF was achieved (~3 h). After modification, the surfaces were washed with water, ethanol, and dichloromethane, and the samples were dried under a stream of argon. Then this HDPA-modified surface was cured in a vacuum oven at 140 °C for 1 h.

8.2.3 Chemical Stability

We carried out chemical stability (desorption kinetics) experiments by placing the modified surfaces in glass vials having rubber stoppers. The desorption kinetics procedures for organic monolayers have been described in detail elsewhere.[32] The stability of these monolayers was measured at 65 °C in three different aqueous media: deionized water, at pH 3 (HCl solution), and at pH 11 (NaOH solution). In all cases, the surfaces were rinsed with fresh deionized water and dichloromethane, dried in a flow of dry argon and stored under vacuum (~10 mbar) for 30 min before the measurement. These surfaces were characterized using contact angle measurements, XPS, IRRAS and ellipsometry. After these measurements, the samples were transferred back to the same vial filled with freshly prepared solutions for continuation of stability study.

8.2.4 Monolayer Characterization

The static and advancing water contact angles were measured with an automated Krüss DSA 100 goniometer. At least six small droplets of 3.0 μl deionized water were dispensed and the contact angles were determined using a Tangent 2 fitting model. The error in the contact angles is < 1°. The ellipsometric thicknesses were measured with a Sentech Instruments (Type SE-400) ellipsometer, operating at 632.8 nm (He-Ne-laser) and an angle of incidence of 70°. First the optical constants of the substrate were determined with a piece of freshly plasma-oxidized CrN surfaces (n_s = 2.73 and k_s = 2.48). The thicknesses of the monolayers were determined with a planar three-layer (ambient, organic monolayer, substrate) isotropic model with assumed refractive indices of 1.00 and 1.46 for

ambient and the organic monolayer, respectively. The reported values for the layer thicknesses are the average of at least eight measurements taken at various locations on the substrate with an error of ± 3 Å. The elemental composition of the modified CrN surfaces was determined by X-ray photoelectron spectroscopy (XPS) using a JPS-9200 Photoelectron Spectrometer (JEOL, Japan). High-resolution spectra were obtained under UHV conditions using monochromatic Al Kα X-ray radiation at 12 kV and 20 mA, using an analyzer pass energy of 10 eV. All high-resolution spectra were corrected with a linear background before fitting. All XPS spectra were evaluated using the Casa XPS software (version 2.3.15). Infrared Reflection Absorption Spectroscopy (IRRAS) spectra were obtained using an IR-ATR Bruker TENSOR 27. A Harrick Auto SeaguII^{TM} grid polarizer was installed in front of the detector and was used to record spectra with p-polarized (parallel) radiation with respect to the plane of incidence at the sample surface with a MCT (Mercury, Cadmium, Telluride) detector and a grazing angle (80°) attachment. Typically, 2048 scans were taken at a resolution of 4 cm^{-1} for each spectrum. The final spectra were obtained using a plasma-activated CrN reference surface as background. Data were collected as differential reflectance versus wavenumber. All spectra were recorded at room temperature in dry nitrogen atmosphere.

8.2.5 Tribological experiments

Tribological experiments were performed using an Asylum MFP-3D atomic force microscope (AFM) in contact and tapping mode. All AFM measurements were carried out in ambient conditions (25 °C, relative humidity = 40 %). For adhesion and friction measurements, the experimental setup and procedure have been described previously.[16] Nanowear/machining experiments were performed using a diamond-like carbon (DLC) tip, with a 15 nm thick DLC coating on the tip side of the cantilever, and an 30 nm thick aluminum coating on the detector side of the cantilever. The cantilevers had a spring constant of 43 N/m (Tap300DLC Budgetsensors), and a tip radius of ca. 100 nm, as confirmed by scanning electron microscopy (SEM). Self-assembled monolayers (SAMs) were scanned in a direction perpendicular to the long axis of the cantilever beam with a scanning speed of 50 μN/s (0.5 Hz) during the nanowear and at a resolution of 480 × 480 pixels. In all wear experiments, an area of 25 μm × 25 μm was scanned at larger loads ranging from 1 to 14 μN for one scan cycle. A force was applied from one edge of the scan area to the other edge. All AFM scans were performed at a 90° angle to the long axis of the cantilever at a velocity of 0.5 Hz. The wear images and corresponding wear depth measurements were obtained with a larger specimen surface area. The latter was scanned before and after the nanowear test; using the same DLC tip the wear marks were observed

by scanning a larger 50 μm × 50 μm area with the (25 μm × 25 μm) wear mark at the center at zero normal load.

8.3 RESULTS AND DISCUSSION

8.3.1 Monolayer formation

The reactions of a an air plasma-activated chromium nitride surface with various alkynes, alkenes, 2-hydroxyhexadecanoic acid (2HHDA), palmitic acid (PMA), trichloro(octadecyl)silane (ODTS) and hexadecylphosphonic acid (HDPA) have been investigated. The tentative structures of the surface anchoring groups used are indicated in **Figure 1**. The aim of the variation of the surface anchoring group is twofold: study of the structure of the resulting monolayers, and investigation of the chemical and mechanical stability of the self-assembled monolayers on CrN. Monolayers derived from 1-alkynes, 1-alkenes, 2-hydroxycarboxylic acids (2HHDA) and palmitic acid (PMA) were prepared according to standard procedures (see for details the Chapter 7).[38] Briefly, C16YNE and C16ENE monolayers were prepared on plasma-activated CrN surfaces by heating the alkyne/alkene for 16 hr to 100 °C and 160 °C, respectively. 2HHDA and PMA monolayers were prepared using the same procedure: after plasma activation the samples were rinsed in ethanol, and immersed in a 1 mM solution of 2-hydroxyhexadecanoic acid or palmitic acid in ethanol at 65 °C for 16 h. Phosphonic acid (HDPA) monolayer formation was achieved in analogy to a procedure from Chabal and co-workers and cured at 140 °C for 1 hr.[37] ODTS-derived monolayers were prepared from a 1 mM silane solution in cyclohexane at room temperature for 10 min, in the presence of Hunig's base (N-ethyldiisopropylamine) (1 mM). After the formation of ODTS and HDPA derived monolayers, these were thoroughly washed with ethanol, water and DCM. The washing step was performed to make sure that this process was not leaving any residue that could affect contact angle determinations.

8.3.2 Wettability and Ellipsometric Thickness

Water contact angle and ellipsometric thickness measurements of the freshly prepared surfaces were performed to ascertain the resulting monolayer quality. A dense, methyl-terminated monolayer on CrN typically yields static water contact angles of ~ 110° and advancing water contact angles of ~115°, as observed for C16YNE, C16ENE, and ODTS. In line with this, ODTS (C_{18} silane) monolayers on CrN show a advancing contact angle of 115°. This is, in fact, significantly higher than the 105° (ODTS (C_{18} silane)) previously

obtained on CrN from solution (toluene, 70 °C, 3 days), [39] or the 103° (HDTS (C_{16} silane)) obtained from vapor phase deposition.[40] Monolayers prepared from 2HHDA, PMA and HDPA exhibit slight lower contact angles (static ~107° and advancing ~112°). These results are consistent with observations made on analogous surface OH-bound monolayers on oxide surfaces studied by our lab[21, 26, 27] and other groups.[41-43]

Additionally, ellipsometric thickness measurements were performed to investigate the monolayer quality. The thickness of the all monolayers under study was 1.7 - 2.5 ± 0.3 nm, which in all cases agreed within experimental error with the theoretical estimated thickness (assuming an all-trans orientation of the chains) of 1.8 - 2.2 nm as shown in **Table 1**. Combined with the contact angle data, this indicates the formation of densely packed organic monolayers for all six anchoring groups.

Table 1. Characterization of Methyl-Terminated Monolayers with Six Anchor Groups on CrN: Static and Advancing Water Contact Angle (θ_{H2O}) and Ellipsometry Thicknesses (data in triplicate).

Monolayers	Static Contact Angle error ± 1°	Advancing Contact Angle error ± 1°	Ellipsometric Thickness error ± 0.3 nm
C16YNE	110	116	1.9
C16ENE	109	115	1.7
2HHDA	107	112	1.8
PMA	107	112	1.7
ODTS	110	115	2.5
HDPA	107	112	2.0

8.3.3 IRRAS and XPS

The structures of monolayers formed were characterized in more detail by IRRAS and XPS spectroscopy. IR absorption provides direct evidence for the presence of the expected chemical groups on the surface, and the degree of short-range ordering,[25] whereas XPS can provide detailed information on the bonding situation, as has been shown elsewhere for the C16YNE, C16ENE, 2HHDA, and PMA monolayers on plasma-activated CrN.[38] **Figure 2** presents the FT-IRRAS spectra for ODTS (open square, purple) and HDPA (open circle, red), showing the C–H vibrations in anti-symmetric ν_a-CH_2 (2918, 2921 cm^{-1}) and symmetric ν_s-CH_2 (2848 cm^{-1}) stretching modes. These values indicate highly ordered ODTS monolayers, whereas HDPA yields monolayers with

intermediate short-range order. Similar data are reported for alkyl phosphonic acids, adsorbed onto other substrates such as TiO_2, GaAs, HfO_2, $La_{2/3}Sr_{1/3}MnO_3$ and Al_2O_3.[37, 44-46]

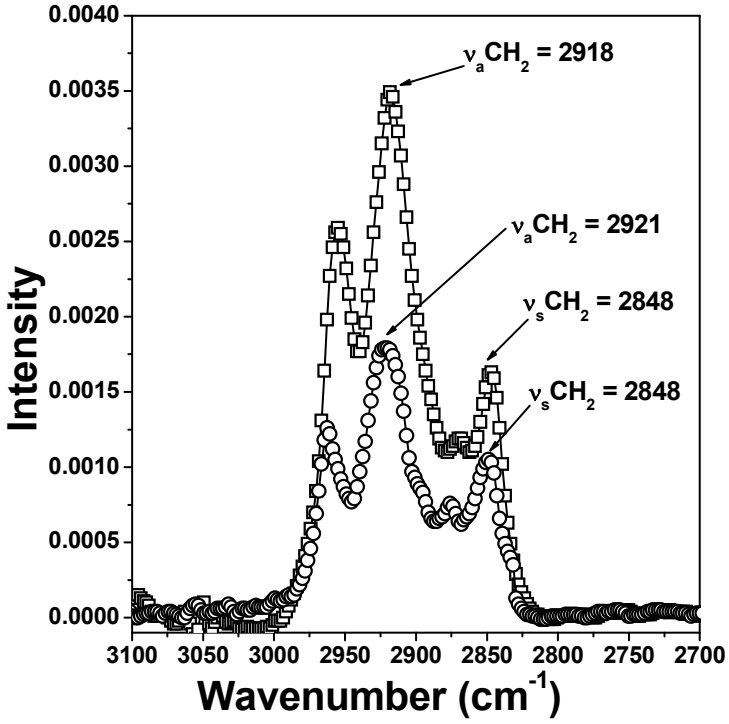

Figure 1. FT-IRRAS characterization of C–H stretching region, showing a spectra of **ODTS** (open square, purple) and **HDPA** (open circle, red) after the baseline correction.

XPS was used to characterize the structure of ODTS and HDPA modified CrN surfaces. C1 and Si2p XPS spectra of ODTS on CrN are given in **Figure 3A** and **3B**, respectively. The C1s signal contributes only one peak binding energy at 285.0 eV that can be assigned to the carbon of the aliphatic chain (C-C/C-H). The binding energy for Si2p is found at 102.3 eV, while the calculated Si/C atomic ratio is 1.0 : 18.9, i.e. in good agreement with theoretical expectations (1 : 18). The Cr : C : N : O : Si ratio is 21.0 : 36.0 : 13.3 : 20.9 : 1.9, which is very close to C18YNE monolayers is Cr : C : N : O ratio is 22.3 : 36.8 : 18.4 : 22.5, indicating formation of a monolayer. We also note here that if the reaction time exceeds more than 10 min, then multilayer formation is observed.

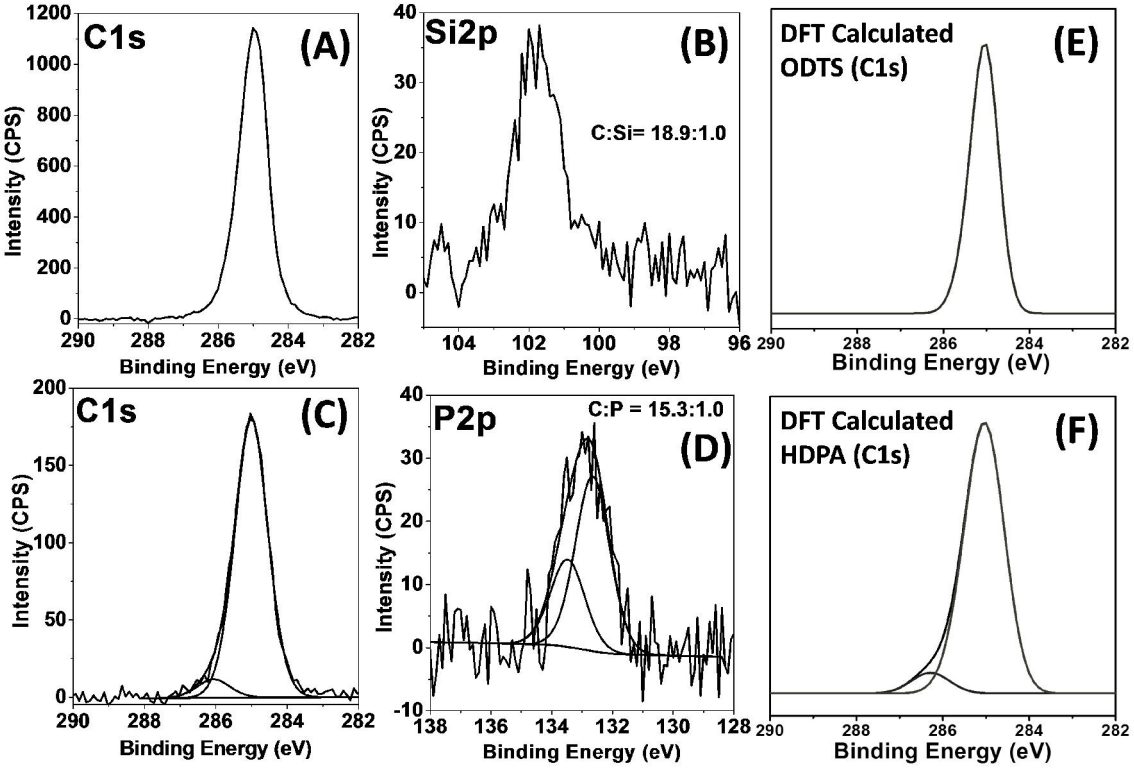

Figure 2. XPS narrow scan spectra of CrN surfaces. ODTS monolayer: (A) C1s spectrum, (B) Si2p spectrum. HDPA monolayer: (C) C1s spectrum, (D) P2p spectrum, the curves were fitted taking into account the spin-orbit splitting of 0.8 eV and ratio of $2p_{1/2}$:$2p_{3/2}$ components as 0.5, and simulated XPS spectra of C1s using the B3LYP/6-311G(d,p)-calculated binding energies for ODTS (E) and HDPA (F).

For the HDPA monolayer C1s and P2p XPS narrow scan spectra are shown in **Figures 3C** and **3D**. The C1s spectra are deconvoluted in to two main peaks: (i) the **C**-**C** peak at 285.0 eV corresponds to CH_2 moieties; (ii) the shoulder at 286.1 eV is attributed to the carbon bonded to phosphorus, CH_3–$(CH_2)_{14}$–**C**H_2–$PO(OH)_2$. This shift towards higher energy is likely due to an inductive electron attractive effect on this carbon by the three oxygen atoms connected to phosphorus in the $PO(OH)_2$ group. Furthermore, the C1s XPS spectrum of ODTS and HDPA (see DFT in Figure 3E and 3F respectively) was simulated using a B3LYP/6-311G(d,p)-derived method,[47] which showed that a **C**–P peak in HDPA is to be expected at 286.2 eV, yielding an excellent agreement with experiment. In addition, the deconvolution of the high-resolution scan of P2p (**Figure 3D**) fitted two peaks: (i) the $2p_{3/2}$ peak at around 132.7 eV (66.5%), and (ii) the $2p_{1/2}$ peak at around 133.5 eV (33.5%).[48] The observed P/C atomic ratio is 1.0 : 15.3, i.e are within the limits of the obtained signal/noise ratio in good agreement with theoretical expectations (1 : 16).

8.3.4 Chemical Stability

Since these experiments constituted the first systematic modification of the CrN surface by a range of organic monolayers, the chemical stability of the modified surfaces was investigated in various chemical environments. In general, the stability of monolayers is dependent on the binding state of the anchoring group, chemical environment, susceptibility to hydrolysis under thermal conditions[49] or just in water,[30,50] and on the stability of the substrate itself.[26, 51, 52] In order to study the stability of the attached monolayers in aqueous environments, we immersed grafted films in deionized water, and in solutions of pH 3 and pH 11, all at in 65 °C. **Figure 4** shows the XPS C 1s/Cr 2p vs immersion time for each medium; in each case the data are normalized to the height at the start of the experiment. Data are shown for four different anchoring groups (alkene, alkyne, silane and phosphate) attached on CrN.

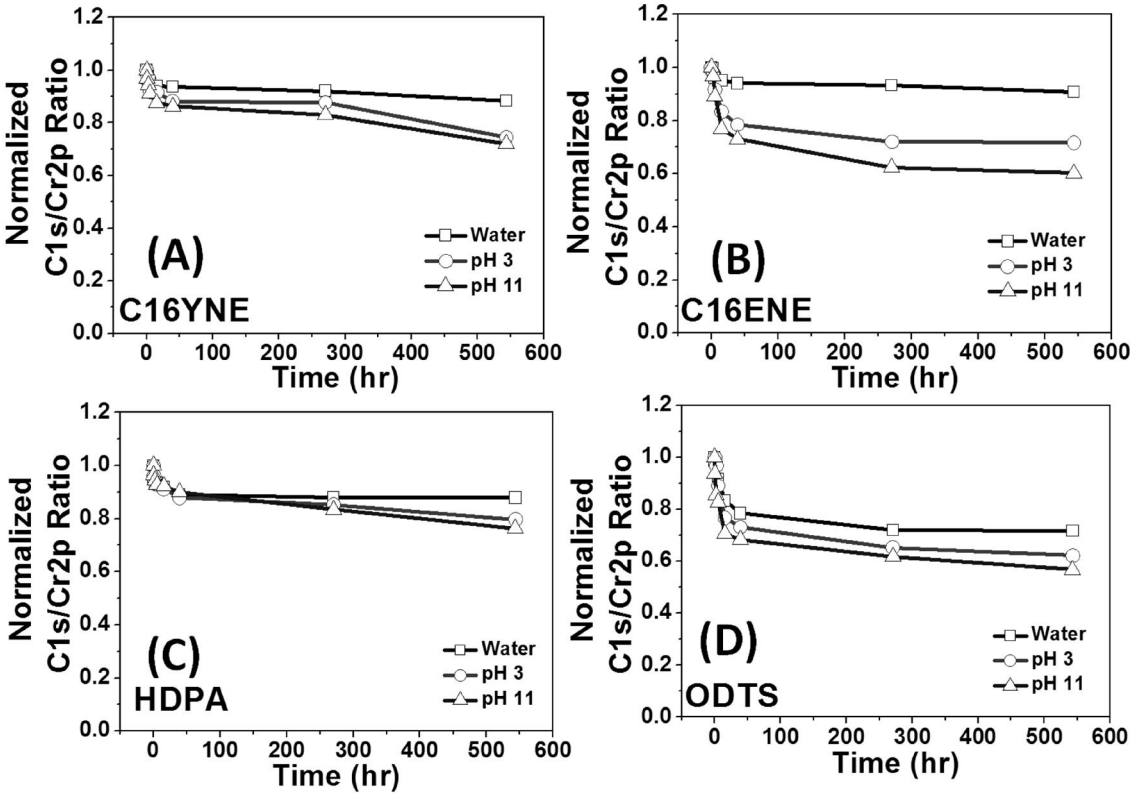

Figure 4. XPS-derived desorption kinetics of monolayers with different anchoring groups using wide scan C 1s and Cr 2p elemental composition of C16YNE (A), C16ENE (B), HDPA (C), and ODTS (D), on CrN surfaces in deionized (DI) water (black squares), at pH 3 (red circles), at pH 11 (blue triangles).

All monolayers on CrN were remarkably more stable compared to the analogous monolayers on other oxide substrates. For example, in neutral water, upon immersion for 40 h at 65 °C only ~7% loss of the alkyne-derived C16YNE monolayers was noted (**Figure 4A**), while the alkene-derived C16ENE monolayer and the HDPA monolayer decayed ~9% and ~8%, respectively (**Figure 4B,** and **C**). In contrast, the ODTS (**Figure 4D**) monolayer was degraded upto ~22% under same conditions. This edge acuity is slightly larger than observed through IRRAS technique (see supporting information Figure S1). It might be due to the slight organic contamination in stability study used water, which cannot be observed in IRRAS due to the low signal to noise ratio. In addition, upon prolonged immersion for 24 days, a loss of (carbon content) in total ~12% was observed for C16-YNE monolayers. Also in warm acid or base the C16YNE monolayers were found to be most stable: after an initial loss of ~12% within in the 40 h, prolonged immersion for 24 days leads to an overall loss of ~26%. The increased loss has been attributed to protonation and deprotonating of the surface ligands,[32] and follow-up reactions. HDPA monolayers were also shown similar stability under these conditions.

The alkene-derived C16ENE monolayers were slightly less stable, and least stability was observed for the silane-based materials, in line with the low stability of Cr-O-Si bonds.[51] The monolayers prepared from 2HHDA and PMA display just a slightly lower stability than the respective C16YNE and C16ENE monolayers (see supporting information Figure S2), in line with the chemical similarity between these monolayers. The monolayers formed by C16YNE and C16ENE shown better stability than previously studied on alumina surfaces.[26] Because the Cr-O-C bond is stronger compared to Al-O-C bond, thus providing a more stable attachment.[53] Again, XPS results show that C16YNE and HDPA layers exhibit excellent stability in neutral, acidic, and basic condition. Overall, these six monolayers display a very good long-term stability in warm water, with the stability order C16YNE ~ 2HHDA > HDPA ~ PMA > C16-ENE > ODTS.

8.3.5 Tribology

Adhesion, friction, and wear on surfaces greatly influence the performance of micro-electronic devices with moving components. To assess the adhesion, friction and wear characteristics of the modified CrN surfaces, atomic force microscopy (AFM) was used. Colloidal probe AFM (see **Figure 5A**) allows measuring both adhesion and friction properties with high accuracy. The colloidal probe acts as a model solid object with well-defined contact area that can interact with the modified surfaces. While many tribological studies have been performed in solution, most devices do in fact operate in air or vacuum, where adhesion is expected to be much larger. Moreover, capillary condensation may

occur between surfaces that are leading to even stronger adhesive interactions. Under these conditions, an ideal surface coating should not only effectively reduce the adhesion, but also provide sufficient lubrication. Therefore, non-fluorinated and fluorinated alkyne, alkene, silane, and phosphonic-derived monolayers were subjected to a stringent adhesion/friction test, namely examination by AFM measurements in air with a smooth silica probe as a model for a hydrophilic solid particle.

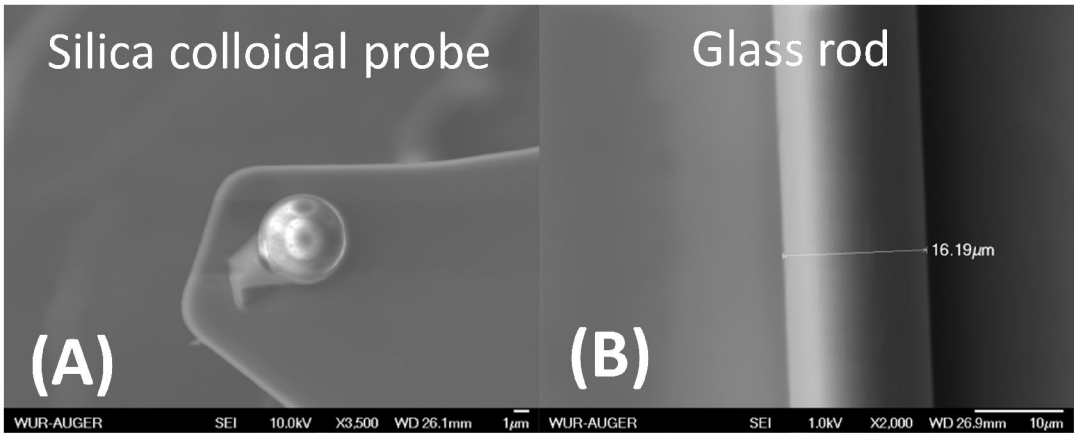

Figure 5. Scanning electron microscopy images: (A) AFM silicon nitride cantilever with a silica colloidal particle (R= 3 μm) glued to its tip. (B) SEM image of glass fiber one end fixed on glass substrate to estimate the torsional spring constant for friction measurements.

8.3.5.1 Adhesion

Figure 6 shows the adhesion of a silica probe particle to the monolayers when the surfaces are compressed at a load of 10 nN. Adhesion forces decrease with increasing chain length of the monolayers, *i.e.*, from 8.85 ± 0.95 mJ/m^2 for the C6YNE (0.6 ± 0.3 nm) derived monolayer to as low as 6.78 ± 0.63 mJ/m^2 for the C12YNE-derived monolayer (1.6 ± 0.3 nm). A further increase of the monolayer thickness, up to 2.2 nm (C18YNE, 6.24 ± 0.78 mJ/m^2) slightly decrease the adhesion force. This is attributed to a higher degree of ordering and hence a more closely packed molecular layer. Several studies have reported on the effect of the length of the monolayer-forming chains on the adhesion force.[23, 54] Generally, a decrease of the adhesion force is found as the chain length increased,[55] which is in agreement with our result. Similar results are observed on monolayers obtained from C16ENE, 2HHDA ODTS, and HDPA, namely 6.42 ± 0.60, 6.34 ± 0.81, 6.62 ± 1.24 and 6.85 ± 0.85 mJ/m^2, respectively. For fluorinated alkyne-derived monolayer adhesion forces as low as 3.32 ± 0.34 mJ/m^2 and 2.99 ± 0.17 mJ/m^2 were obtained, for the F9YNE and F17YNE monolayers, respectively.

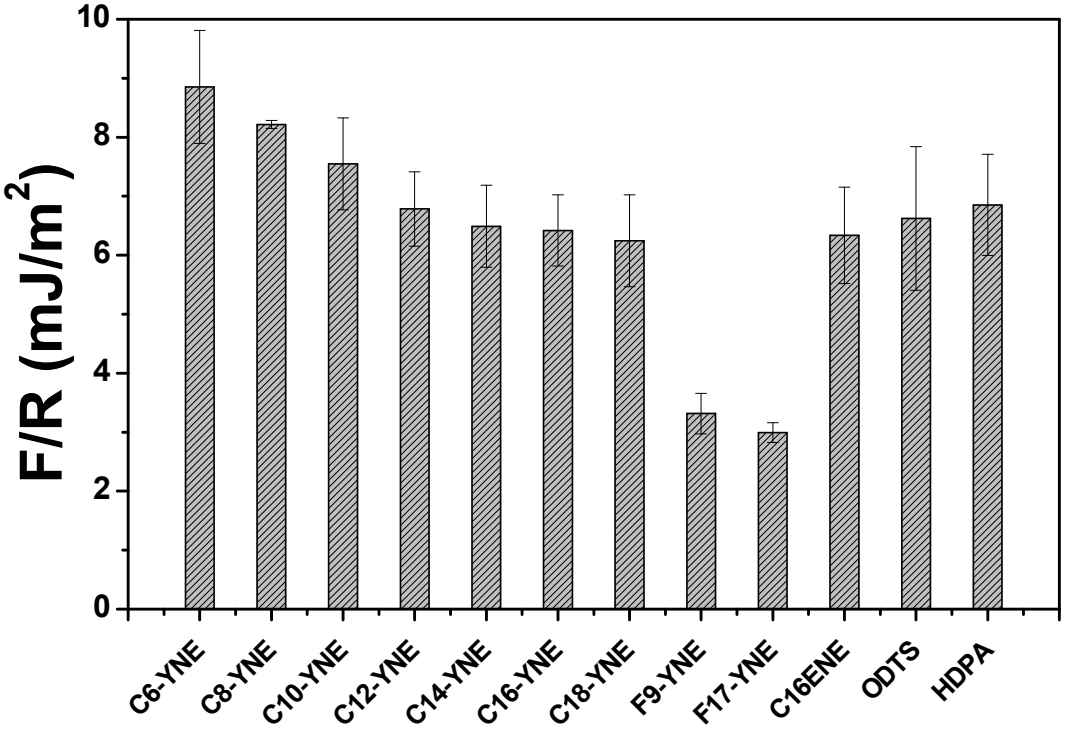

Figure 6. Mean value of adhesion forces as measured from pull-off curves: ~200 of each monolayer at 10 nN force.

These adhesion forces are considerably lower than the recently published results for analogous high-density monolayers on flat Si(111) and SiC.[16, 21] The main reason for the current, lower adhesion energy can be attributed by the lower roughness of Si(111) (0.1 nm) and SiC (2.0 nm),[16, 21] as a higher surface roughness reduces the surface contact area to the spherical particle.

8.3.5.2 Friction

Besides adhesion, the friction of laterally moving or rolling objects on the surfaces of microelectronic devices is an important aspect that can govern device performance. Minimal friction coefficients, or high lubrication, are often desirable, and the monolayers under study display excellent behavior in this category. The lateral friction force on the monolayers was measured using the same colloidal probe setup as for the adhesion measurements. The average lateral force difference signal ([μtrace – μretrace]/2, in V) was converted directly into friction force, following the method of Liu et al.[56] The **Figure 5B** shows the SEM image of a representative glass fiber, which was used to calibrate the cantilever. The cantilever calibration method is explained in more detail in the supporting information (Figure S3).

Figure 7A shows the friction coefficient of alkyne-derived monolayers of varying chain length, as well as the combination with fluorinated and non-fluorinated, whereas **Figure 7B** shows the effects of a different anchoring group attached to hydroxyl-terminated CrN surfaces. The friction coefficients are compared with unmodified plasma cleaned bare CrN surfaces as shown in **Figure 7B**. A significant decrease in the friction coefficient is observed upon lengthening the monolayer-forming chains: from C6YNE (0.0133 ± 0.0006) to C18YNE (0.0057 ± 0.0004). A further decrease of the friction coefficient is observed for F9YNE and F17YNE, which display extremely low friction coefficients (for F9YNE = 0.0028 ± 0.0007 and for F17YNE = 0.0028 ± 0.0006). These values are low, not just compared to the non-fluorinated surfaces mentioned above, but also as compared to analogous monolayers on Si(111)[16] (for F9YNE = 0.01826 ± 0.0040 and for F17YNE = 0.0121 ± 0.0037) and SiC[21] (for F9YNE = 0.0101 ± 0.0001 and for F17YNE = 0.0079 ± 0.0008).

The major factors, which may cause the decrease in friction are:[32] (1) packing density and terminal groups (alkylated versus fluorinated) of the monolayer, (2) the surface roughness, as this determines the contact area with the probe. As discussed above, monolayers are composed of molecules with different chemical structures. The carbon backbone is similar, but different anchoring groups are used that affect the packing density, and in turn, the friction coefficient. **Figure 7B** shows that friction coefficient of C16YNE is slightly lower than that of monolayers derived from other anchoring groups. This is because, as discussed previously, an increased packing density decreases the friction coefficient, as defects form more readily in less dense monolayers during sliding. Flater et al. attributed an increase in the friction coefficient to several factors: defects create a more rough surface, expose a larger fraction of methylene groups to the surface, and create additional channels for frictional energy dissipation during sliding.[57] The defects in the chains most likely form outside of the area of contact, where there is more free volume.

Such solid, ultralow-friction coefficient materials are interesting for application in high-performance devices, because they act as superior stable lubricants. For unmodified, plasma-cleaned bare CrN surfaces, a friction coefficient of 0.0734 ± 0.0006 was found, which is roughly 25 times higher than our fluorinated surfaces, due to highly hydrophilic groups such as hydroxyls on the interface. The friction coefficient we obtained on bare CrN was in good agreement with literature.[58]

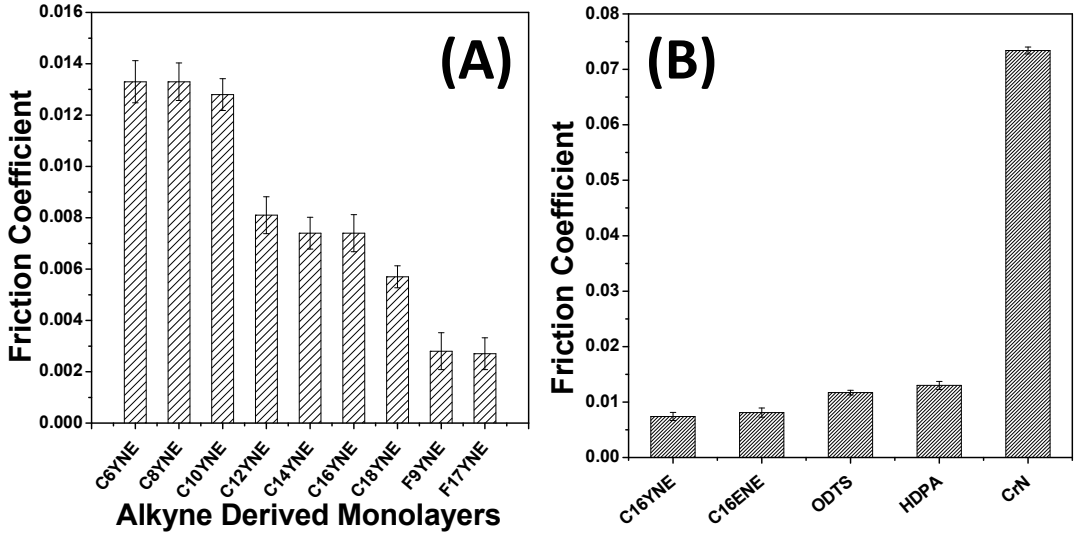

Figure 7. Friction coefficient of SAMs. (A) The friction coefficients for different alkyne derived fluorinated and non-fluorinated monolayers. (B) The friction coefficients for different monolayers, obtained from the slope of the friction force versus normal load.

8.3.5.3 Wear

As discussed above the adhesion and frictional force measurements were carried out at a lower pressure from 5 nN to 75 nN. At this lower force, these monolayers did not show any nano-wear effects. While that was a nice result by itself, the more relevant question for practical industrial application might be the wear resistance under significantly higher pressures. Therefore, the current wear study was carried out at high loads from 1.6 - 14.0 μN (**Figure 8** and **9**).

A typical 25 × 25 μm^2 wear mark on monolayers with different anchoring groups – generated at a normal load of 7.8 μN (5 volt) for one scan cycle and imaged using AFM with a scan size of 50 × 50 μm^2 – is shown in **Figure 8A-E**. The cross line profile of wear marks indicates the uniform removal of material at the bottom of the wear mark. The AFM image of the wear mark did not shows any debris at the edges, swiped during AFM scanning. Thus, the debris is loose or powdered (not sticky) and it may be removed during the AFM scanning.

The effects of the wear resistance (at various normal loads) and different anchoring groups are shown in **Figure 8F**, which demonstrates that the C16YNE monolayer performs better than other monolayers. Silane (ODTS) and phosphate (HDPA) monolayers display a critical load – at which the monolayer is just removed by the scratching tip – at ca. 3 μN, which is similar to shorter chain alkyne-derived monolayers on CrN. Compared to the monolayers on CrN, the approximated critical normal load is

lower than for SiC and Si(111),[16, 21] but higher than for silane and thiol monolayers on gold, silicon and alumina surfaces.[9, 10, 17] The likely explanation is packing density, interface chemical adsorption bond strength of anchoring groups surfaces.[9, 10, 17] Bare CrN surfaces shows a wear depth that is more than two order of magnitude higher (at 14 μN: 12.2 ± 0.6 nm) as compared to modified surfaces. These results are consistent with the literature values for nano-multilayer carbon and CrN surfaces.[1]

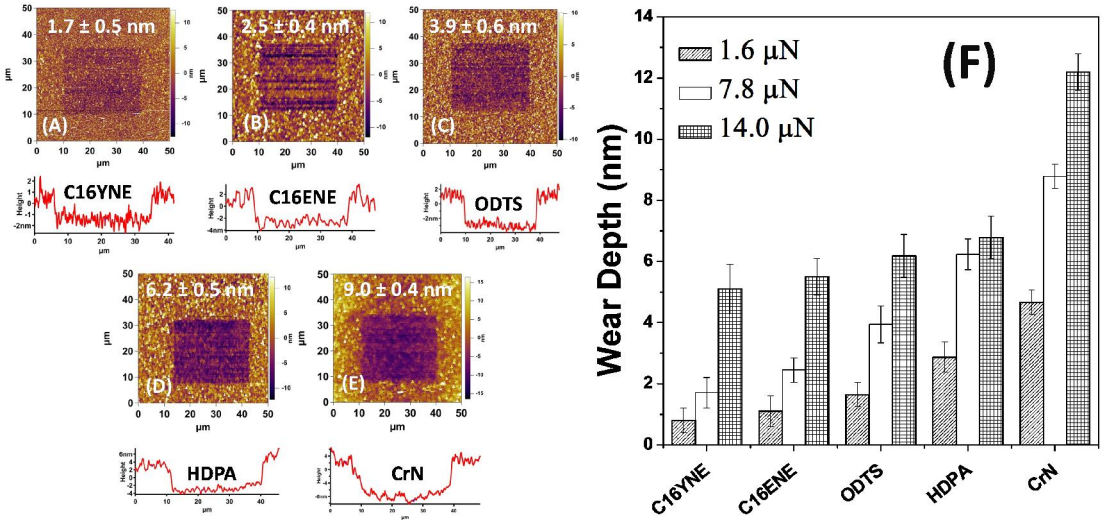

Figure 8. Wear images on various modified CrN surfaces studied at 5 volt (7.8 μN force); wear mark size: 25 × 25 μm^2, and image size: 50 × 50 μm^2. (A) C16YNE, (B) C16ENE, (C) ODTS, (D) HDPA CrN surfaces. (F) Wear depth for single cycle of at various normal loads for different anchoring groups on modified CrN surfaces and the plasma-activated, bare CrN surface.

Wear depth as a function of normal load was shown in **Figure 9**, which indicates the wear depth increased with the rising of loads on monolayer on CrN. The wear property is not only influenced by the molecular chain length, but also the terminal functional group In the completely testing range, the longer of the molecular chain and terminal head group, the better the wear resistance. Among them, the F17YNE monolayer on CrN exhibits the best wear resistance. For all of the tested monolayers, there appears to be a critical normal load in the wear depth. For shorter chain (C6 - C14), the critical normal load is ~3 μN. These results are consistent with the monolayers reported by Bhushan et. al. for monolayers on silicon, gold and alumina surfaces.[10, 17] However, for longer chain and fluorinated monolayer, the approximated critical normal load is > 7.8 μN as shown in **Figure 9**, indicating a very high wear resistance of these fluoro-alkyne-modified CrN surfaces.

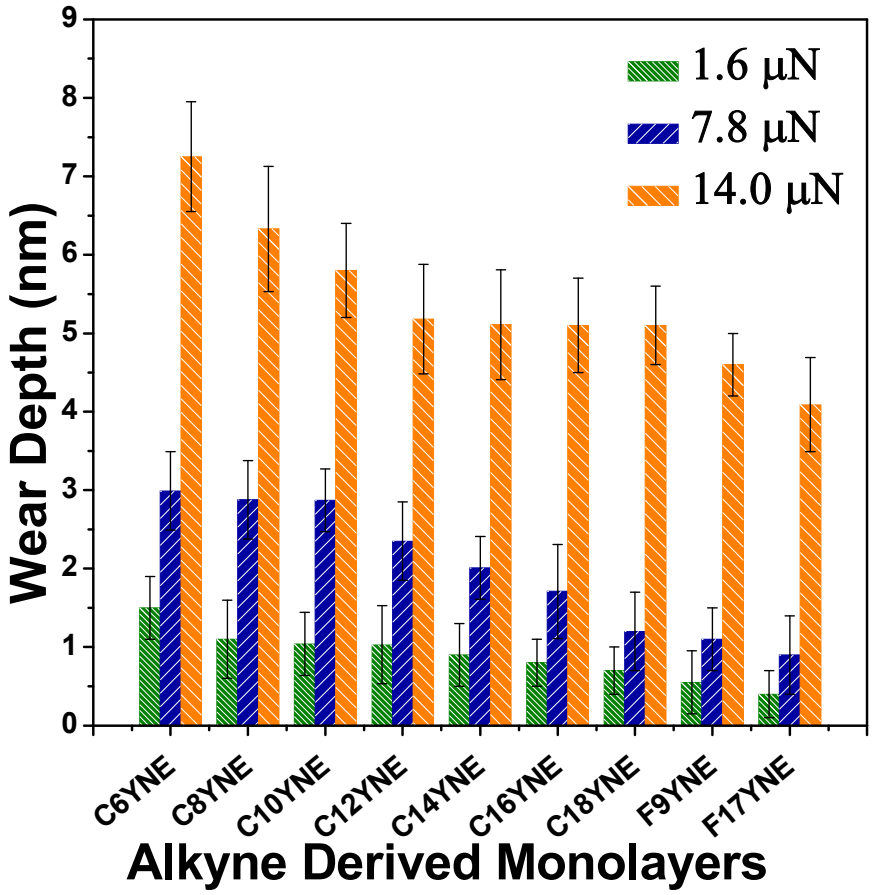

Figure 9. Wear depth for single cycle of at various normal loads and for evolution of wear at alkyne-derived fluorinated and non-fluorinated monolayers on CrN.

A two-dimensional computer-controlled piezo transducer was used that can apply and monitor normal and lateral forces on an AFM DLC (diamond-like carbon) tip (see SEM image in **Figure 10A**), with a force resolution in the nano/micro-Newton range during sliding and scanning motions. This ability affords unique opportunities, outside the function of visualization alone, for investigation of the wear properties of these nanometer-thick monolayers. **Figure 10B** shows the tip wear of a DLC tip with a spring constant of about 43 ± 3 N/m, after a single 25 × 25 μm^2 contact mode scan with an applied load of 14 µN. After these high load (wear mark generation) and low load (wear mark imaging) AFM scans, giving a scanning distance of 512 mm, the tip apex of the DLC probe was slightly worn as shown in **Figure 10B**. The effect of just this one 'wear mark generation – wear mark imaging' cycle shows the mechanical robustness of CrN

surfaces, as DLC is very hard itself. This induced us to use a new DLC tip for every measurement to ensure the same pressure on the surfaces.

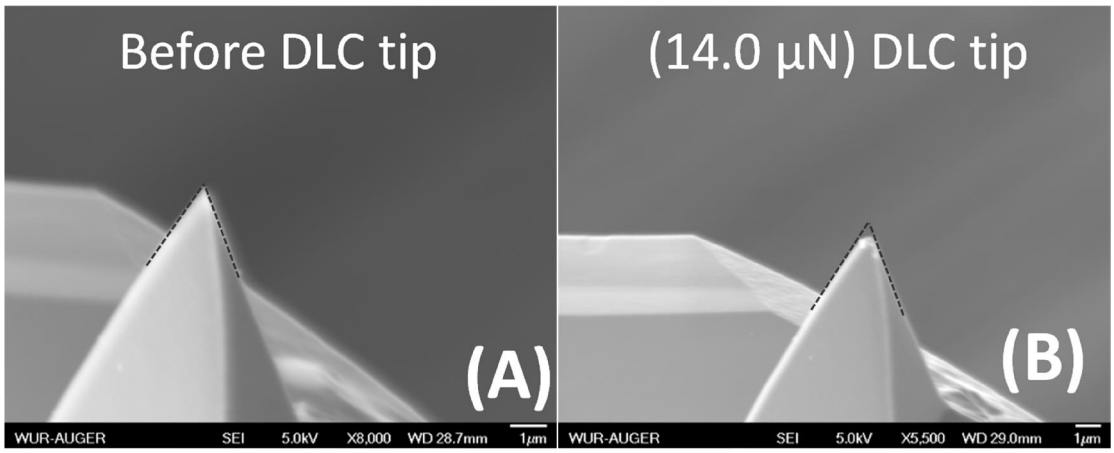

Figure 10. Comparative SEM images of DLC tip (A) before use and (B) after applying force 14 μN (9 volt) and acquiring AFM image on modified CrN surfaces.

8.4 CONCLUSIONS

Fluorine-containing alkyne-derived monolayers on CrN yield a superior chemical stability and wear resistance. This conclusion was reached via a systematic study of the chemical and mechanical properties of modified CrN by varying the anchoring group, chain length and most importantly fluorinated and non-fluorinated carbon chain. The chemical stability of monolayers in warm aqueous solution at various pH was found to be: alkyne ~ 2-hydroxy carboxylic acids > phosphonic acids > alkenes ~ carboxylic acids > silanes. Molecules with at least 12 carbon atoms in the chain were found to exhibit less adhesion, friction and higher wear resistance when compared to molecules with shorter chain lengths, as the latter display a lower packing density and reduced hydrophobicity. Finally, fluorinated monolayers on CrN demonstrate excellent tribological properties, thus making them ideal candidates for application in high-performance devices.

8.5 REFERENCES

1. Nie, X.; Zhang, P.; Weiner, A. M.; Cheng, Y.-T., Nanoscale Wear and Machining Behavior of Nanolayer Interfaces. *Nano Lett.* **2005,** 5, (10), 1992-1996.

2. Rivadulla, F.; Bãobre-López, M.; Quintela, C. X.; Pĩeiro, A.; Pardo, V.; Baldomir, D.; López-Quintela, M. A.; Rivas, J.; Ramos, C. A.; Salva, H.; Zhou, J. S.; Goodenough, J. B., Reduction of the bulk modulus at high pressureinCrN. *Nature Mater.* **2009,** 8, (12), 947-951.
3. Grossman, J. C.; Mizel, A.; Côté, M.; Cohen, M. L.; Louie, S. G., Transition metals and their carbides and nitrides: Trends in electronic and structural properties. *Phys. Rev. B* **1999,** 60, (9), 6343-6347.
4. McMillan, P. F., New materials from high-pressure experiments. *Nature Mater.* **2002,** 1, (1), 19-25.
5. Pozio, A.; Zaza, F.; Masci, A.; Silva, R. F., Bipolar plate materials for PEMFCs: A conductivity and stability study. *J. Power Sources* **2008,** 179, (2), 631-639.
6. Fuentes, G. G.; Rodriguez, R.; Avelar-Batista, J. C.; Housden, J.; Montalá, F.; Carreras, L. J.; Cristóbal, A. B.; Damborenea, J. J.; Tate, T. J., Recent advances in the chromium nitride PVD process for forming and machining surface protection. *J. Mater. Process. Technol.* **2005,** 167, (2-3), 415-421.
7. Hans-Jürgen Butt, M. K., *Surface and Interfacial Forces*. Wiley-VCH: 2010; p 436.
8. Israelachvili, J. N., In *Intermolecular and Surface Forces*, Third ed.; Elsevier Inc.: 2010; pp 253-289.
9. Bhushan, B., *Handbook of Nanotechnology*. 2 ed.; Springer-Verlag New York, LLC: 2007; p 1575-1631.
10. Bhushan, B.; Liu, H., Nanotribological properties and mechanisms of alkylthiol and biphenyl thiol self-assembled monolayers studied by AFM. *Phys. Rev. B* **2001,** 63, (24), 245412.
11. Colton, R. J., Nanoscale measurements and manipulation. *J. Vac. Sci. Technol., B* **2004,** 22, (4), 1609-1635.
12. Hutchings, I. M., *Tribology : Friction and Wear of Engineering Materials*. ELSEVIER LTD: 1992.
13. Flink, S.; van Veggel, F. C. J. M.; Reinhoudt, D. N., Sensor Functionalities in Self-Assembled Monolayers. *Adv. Mater.* **2000,** 12, (18), 1315-1328.
14. Gooding, J. J.; Mearns, F.; Yang, W.; Liu, J., Self-Assembled Monolayers into the 21st Century: Recent Advances and Applications. *Electroanalysis* **2003,** 15, (2), 81-96.
15. Wink, T.; J. van Zuilen, S.; Bult, A.; P. van Bennekom, W., Self-assembled Monolayers for Biosensors. *Analyst* **1997,** 122, (4), 43R-50R.
16. Pujari, S. P.; Spruijt, E.; Cohen Stuart, M. A.; van Rijn, C. J. M.; Paulusse, J. M. J.; Zuilhof, H., Ultralow Adhesion and Friction of Fluoro-Hydro Alkyne-Derived Self-Assembled Monolayers on H-Terminated Si(111). *Langmuir* **2012,** 58, (51), 17690-17700.
17. Liu, H.; Bhushan, B., Investigation of nanotribological properties of self-assembled monolayers with alkyl and biphenyl spacer chains (Invited). *Ultramicroscopy* **2002,** 91, (1–4), 185-202.
18. Rubio-Sierra, F. J.; Heckl, W. M.; Stark, R. W., Nanomanipulation by Atomic Force Microscopy. *Adv. Eng. Mater.* **2005,** 7, (4), 193-196.
19. Firtel, M.; Henderson, G.; Sokolov, I., Nanosurgery: observation of peptidoglycan strands in Lactobacillus helveticus cell walls. *Ultramicroscopy* **2004,** 101, (2–4), 105-109.
20. Wen, C. K.; Goh, M. C., AFM Nanodissection Reveals Internal Structural Details of Single Collagen Fibrils. *Nano Lett.* **2003,** 4, (1), 129-132.
21. Pujari, S. P.; Scheres, L.; Weidner, T.; Baio, J. E.; Stuart, M. A. C.; Rijn, C. J. M. v.; Zuilhof, H., Covalently Attached Organic Monolayers onto Silicon Carbide from 1-Alkynes: Molecular Structure and Tribological Properties. *Langmuir* **2013,** 29, (12), 4019–4031.

22. Hacker, C. A.; Anderson, K. A.; Richter, L. J.; Richter, C. A., Comparison of Si−O−C Interfacial Bonding of Alcohols and Aldehydes on Si(111) Formed from Dilute Solution with Ultraviolet Irradiation. *Langmuir* **2004,** 21, (3), 882-889.
23. van der Vegte, E. W.; Subbotin, A.; Hadziioannou, G.; Ashton, P. R.; Preece, J. A., Nanotribological Properties of Unsymmetrical n-Dialkyl Sulfide Monolayers on Gold: Effect of Chain Length on Adhesion, Friction, and Imaging. *Langmuir* **2000,** 16, (7), 3249-3256.
24. Li, Y.; Calder, S.; Yaffe, O.; Cahen, D.; Haick, H.; Kronik, L.; Zuilhof, H., Hybrids of Organic Molecules and Flat, Oxide-Free Silicon: High-Density Monolayers, Electronic Properties, and Functionalization. *Langmuir* **2012,** 28, (26), 9920-9929.
25. Ulman, A., Formation and Structure of Self-assembled Monolayers. *Chem. Rev.* **1996,** 96, (4), 1533-1554.
26. ter Maat, J.; Regeling, R.; Ingham, C. J.; Weijers, C. A. G. M.; Giesbers, M.; de Vos, W. M.; Zuilhof, H., Organic Modification and Subsequent Biofunctionalization of Porous Anodic Alumina Using Terminal Alkynes. *Langmuir* **2011,** 27, (22), 13606-13617.
27. Rosso, M.; Giesbers, M.; Arafat, A.; Schroën, K.; Zuilhof, H., Covalently Attached Organic Monolayers on SiC and SixN4 Surfaces: Formation Using UV Light at Room Temperature. *Langmuir* **2009,** 25, (4), 2172-2180.
28. Rosso, M.; Arafat, A.; Schroen, K.; Giesbers, M.; Roper, C. S.; Maboudian, R.; Zuilhof, H., Covalent Attachment of Organic Monolayers to Silicon Carbide Surfaces. *Langmuir* **2008,** 24, (8), 4007-4012.
29. Nazeeruddin, M. K.; Humphry-Baker, R.; Liska, P.; Grätzel, M., Investigation of Sensitizer Adsorption and the Influence of Protons on Current and Voltage of a Dye-Sensitized Nanocrystalline TiO2 Solar Cell. *J. Phys. Chem. B* **2003,** 107, (34), 8981-8987.
30. Jo, K.; Yu, H.-Z.; Yang, H., Formation kinetics and stability of phosphonate self-assembled monolayers on indium–tin oxide. *Electrochim. Acta* **2011,** 56, (13), 4828-4833.
31. Silverman, B. M.; Wieghaus, K. A.; Schwartz, J., Comparative Properties of Siloxane vs Phosphonate Monolayers on A Key Titanium Alloy. *Langmuir* **2004,** 21, (1), 225-228.
32. Franking, R. A.; Landis, E. C.; Hamers, R. J., Highly Stable Molecular Layers on Nanocrystalline Anatase TiO2 through Photochemical Grafting. *Langmuir* **2009,** 25, (18), 10676-10684.
33. Li, Y.; Zuilhof, H., Photochemical Grafting and Patterning of Organic Monolayers on Indium Tin Oxide Substrates. *Langmuir* **2012,** 28, (12), 5350-5359.
34. McGuiggan, P. M., Friction and adhesion measurements between a fluorocarbon surface and a hydrocarbon surface in air. *J. Adhes.* **2004,** 80, (5), 395-408.
35. Pujari, S. P.; Zuilhof, H., High Wear Resistant Ultra-Thin Dense Per-fluorinated Organic Monolayers on Silicon (111) Surface. *Appl. Surf. Sci.* **2013**, In Preparation.
36. Tao, Z. H.; Bhushan, B., Degradation mechanisms and environmental effects on perfluoropolyether, self-assembled monolayers, and diamondlike carbon films. *Langmuir* **2005,** 21, (6), 2391-2399.
37. Vega, A.; Thissen, P.; Chabal, Y. J., Environment-Controlled Tethering by Aggregation and Growth of Phosphonic Acid Monolayers on Silicon Oxide. *Langmuir* **2012,** 28, (21), 8046-8051.
38. Pujari, S. P.; Scheres, L.; Barend, L. v.; Zuilhof, H., Covalently Attached Organic Monolayers onto Chromium Nitride: Alkylated and Fluorinated 1-Alkynes. *Langmuir* **2013**, Submitted
39. Anac, I.; McCarthy, T. J., Chemical modification of chromium oxide surfaces using organosilanes. *J. Colloid Interface Sci.* **2009,** 331, (1), 138-142.

40. Fadeev, A. Y.; McCarthy, T. J., A New Route to Covalently Attached Monolayers: Reaction of Hydridosilanes with Titanium and Other Metal Surfaces. *J. Am. Chem. Soc.* **1999,** 121, (51), 12184-12185.
41. Hofer, R.; Textor, M.; Spencer, N. D., Alkyl Phosphate Monolayers, Self-Assembled from Aqueous Solution onto Metal Oxide Surfaces. *Langmuir* **2001,** 17, (13), 4014-4020.
42. Zwahlen, M.; Tosatti, S.; Textor, M.; Hähner, G., Orientation in Methyl- and Hydroxyl-Terminated Self-Assembled Alkanephosphate Monolayers on Titanium Oxide Surfaces Investigated with Soft X-ray Absorption. *Langmuir* **2002,** 18, (10), 3957-3962.
43. Allara, D. L.; Nuzzo, R. G., Spontaneously organized molecular assemblies. 1. Formation, dynamics, and physical properties of n-alkanoic acids adsorbed from solution on an oxidized aluminum surface. *Langmuir* **1985,** 1, (1), 45-52.
44. Levine, I.; Weber, S. M.; Feldman, Y.; Bendikov, T.; Cohen, H.; Cahen, D.; Vilan, A., Molecular Length, Monolayer Density, and Charge Transport: Lessons from Al–AlOx/Alkyl–Phosphonate/Hg Junctions. *Langmuir* **2011,** 28, (1), 404-415.
45. Spori, D. M.; Venkataraman, N. V.; Tosatti, S. G. P.; Durmaz, F.; Spencer, N. D.; Zürcher, S., Influence of Alkyl Chain Length on Phosphate Self-Assembled Monolayers. *Langmuir* **2007,** 23, (15), 8053-8060.
46. Shpaisman, H.; Salomon, E.; Nesher, G.; Vilan, A.; Cohen, H.; Kahn, A.; Cahen, D., Electrical Transport and Photoemission Experiments of Alkylphosphonate Monolayers on GaAs. *J. Phys. Chem. C* **2009,** 113, (8), 3313-3321.
47. Giesbers, M.; Marcelis, A. T. M.; Zuilhof, H., Simulation of XPS C1s Spectra of Organic Monolayers by Quantum Chemical Methods. *Langmuir* **2013,** 29, (15), 4782-4788.
48. Viornery, C.; Chevolot, Y.; Léonard, D.; Aronsson, B.-O.; Péchy, P.; Mathieu, H. J.; Descouts, P.; Grätzel, M., Surface Modification of Titanium with Phosphonic Acid To Improve Bone Bonding: Characterization by XPS and ToF-SIMS. *Langmuir* **2002,** 18, (7), 2582-2589.
49. Helmy, R.; Fadeev, A. Y., Self-Assembled Monolayers Supported on TiO2: Comparison of C18H37SiX3 (X = H, Cl, OCH3), C18H37Si(CH3)2Cl, and C18H37PO(OH)2. *Langmuir* **2002,** 18, (23), 8924-8928.
50. Gamble, L.; Jung, L. S.; Campbell, C. T., Interaction of Silane Coupling Agents with the TiO2(110) Surface. *Langmuir* **1995,** 11, (11), 4505-4514.
51. Marcinko, S.; Fadeev, A. Y., Hydrolytic Stability of Organic Monolayers Supported on TiO2 and ZrO2. *Langmuir* **2004,** 20, (6), 2270-2273.
52. Yang, W.; Auciello, O.; Butler, J. E.; Cai, W.; Carlisle, J. A.; Gerbi, J.; Gruen, D. M.; Knickerbocker, T.; Lasseter, T. L.; Russell Jr, J. N.; Smith, L. M.; Hamers, R. J., DNA-modified nanocrystalline diamond thin-films as stable, biologically active substrates. *Nature Mater.* **2002,** 1, (4), 253-257.
53. Chenite, A.; Selmani, A.; Yelon, A., X-ray photoelectron spectroscopy investigation of interfacial interactions in the Cr/BPDA-PDA and Ti/BPDA-PDA systems. *J. Vac. Sci. Technol., A* **1994,** 12, (2), 513-522.
54. Guo, L. I. Y. A.; Zhao, Y. A. P. U., Effect of chain length of self-assembled monolayers on adhesion force measurement by AFM. *J. Adhes. Sci. Technol.* **2006,** 20, (12), 1281-1293.
55. Lee, D. H.; Oh, T.; Cho, K., Combined Effect of Chain Length and Phase State on Adhesion/Friction Behavior of Self-Assembled Monolayers. *J. Phys. Chem. B* **2005,** 109, (22), 11301-11306.

56. Liu, W.; Bonin, K.; Guthold, M., Easy and direct method for calibrating atomic force microscopy lateral force measurements. *Rev. Sci. Instrum.* **2007,** 78, (6), 063707-7.
57. Flater, E. E.; Ashurst, W. R.; Carpick, R. W., Nanotribology of Octadecyltrichlorosilane Monolayers and Silicon: Self-Mated versus Unmated Interfaces and Local Packing Density Effects. *Langmuir* **2007,** 23, (18), 9242-9252.
58. Lee, D. H.; Kim, D.; Oh, T.; Cho, K., Phase State Effect on Adhesion Behavior of Self-Assembled Monolayers. *Langmuir* **2004,** 20, (19), 8124-8130.

Supporting Information to Chapter 8

Table of Contents

Supporting Information to Chapter 8 238

S.8.1 Chemical stability studied by IRRAS 238

S.8.2 Chemical stability of 2HHDA and PMA 238

S.8.3 Lateral Spring Constant (Cantilevers calibration) 239

S.8.1 Chemical stability studied by IRRAS

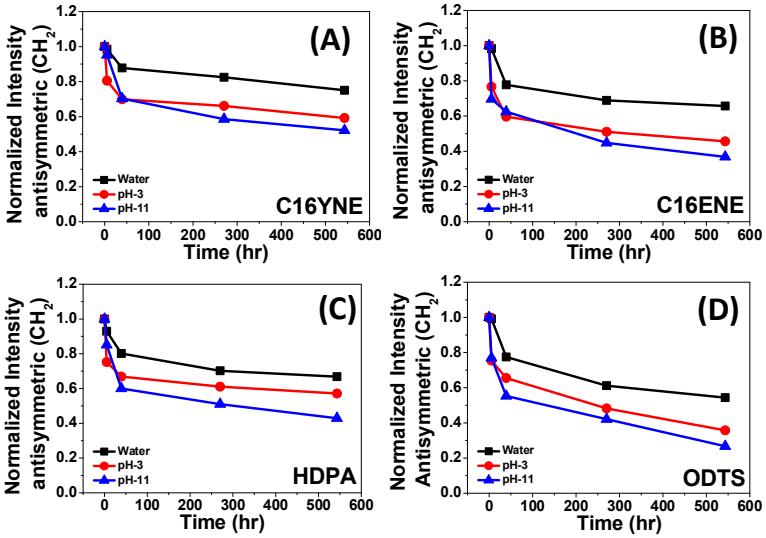

Figure S1. IRRAS-derived desorption kinetics at 65 °C of different anchoring types monolayers (C16YNE, C16ENE, HDPA and ODTS) on CrN surfaces in deionized (DI) water (black filled squares), at pH = 3 (red filled circles), at pH = 11 (blue filled triangles).

S.8.2 Chemical stability of 2HHDA and PMA

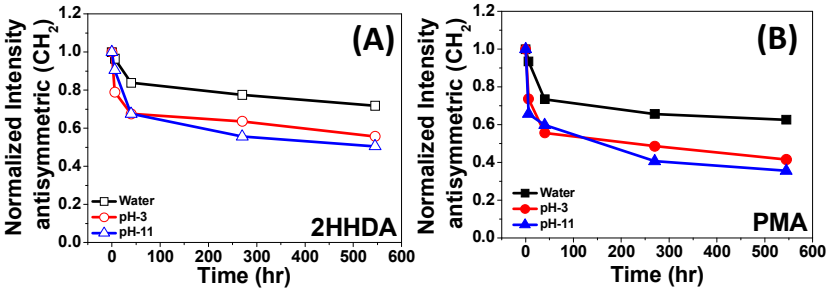

Figure S2. IRRAS-derived desorption kinetics of different anchoring types monolayers 2HHDA (left), and PMA (right) onto CrN surfaces studied under glass vials containing deionized (DI) water (black filled squares), an acidic solution at pH = 3 (red circles), a basic solution at pH = 11(blue triangles) at 65 °C oven.

S.8.3 Lateral Spring Constant (Cantilevers calibration)

Cantilevers were calibrated using the reversible bending of an 16.2-µm-thick glass fibre, as shown in **Figure 6B**. The bending force F for such a cantilever can be calculated via following equation. (Rev Sci Instrum. 2007 June; 78(6): 063707.)

$$F = \frac{3E_g \pi r^4}{4L^3} \Delta y$$

where E_g is the Young's modulus (6.80×10^{10} Pa); r is the radius (8.85×10^{-6} m); and L is the length of the glass fibre (1.60×10^{-3} m) and Δy is the slope of bending fibres trace and retrace see **Figure S3**. The calculated lateral conversion factor of approximately 17.7 nN/V. The overall error in the conversion factor determined in this way was estimated to be 6 %.

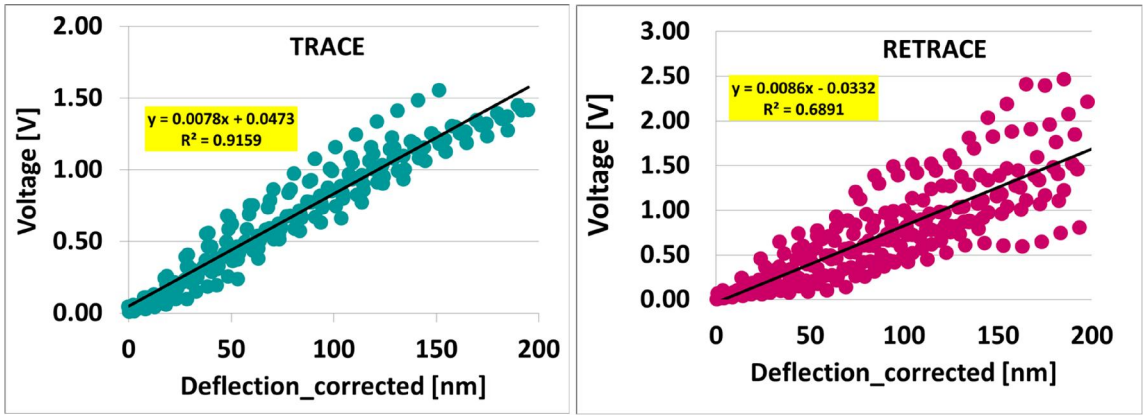

Figure S3. A plot of the lateral force (Volatge) vs the glass fiber defelction. The left corresponds to the trace (forward) and the right to the retrace (backward) motion of the cantiliver. The black line is the average of the curves. The slope of this curve corresponds to 1/Kc.

CHAPTER 9

Superoleophobic and Highly Stable Perfluorinated Monolayers on Polymer Surfaces

Superoleophobic polymer surfaces of polymethyl methacrylate (PMMA), polyether ether ketone (PEEK), and polydimethyl siloxane (PDMS) are fabricated in a two-step process: 1) plasma nanotexturing (i.e. ion-enhanced plasma etching with simultaneous roughening), with varying chemistry depending on the polymer, and subsequently 2) grafting of self-assembled perfluorododecyltrichlorosilane monolayers (SAMs). Depending on the absence or not of an etch mask (i.e. a polymer surface without or with colloidal microparticle self-assembly on it) random or ordered hierarchical micro and nanotexturing can be obtained. We demonstrate that highly stable organic monolayers can be grafted onto all these etched polymer surfaces. After the monolayer deposition, the initially hydrophilic polymeric surfaces become superoleophobic, with static contact angles for water >165°, soya oil >150° and hexadecane ~140° for all surfaces. This approach thus provides a simple and generic method to obtain superoleophobicity on polymers. Hydrolytic stability tests prove that this superoleophobicity is robust against degradation in water for more than 40 days.

This Chapter is submitted for publication as:

'*Superoleophobic and Highly Stable Perfluorinated Monolayers on Polymer Surfaces'*. Sidharam P. Pujari, K. Ellinas, Angeliki Tserepi, Evangelos Gogolides, and Han Zuilhof. Submitted **2013.**

Table of Contents

9 Superoleophobic and Highly Stable Perfluorinated Monolayers on Polymer Surfaces 241

9.1 INTRODUCTION 243

9.2 EXPERIMENTAL 245

9.2.1 Materials 245

9.2.2 Plasma-induced nanotexturing of polymers 245

9.2.3 Substrate reactivation 246

9.2.4 SAM Preparation 246

9.2.5 Contact Angle Measurements 246

9.2.6 Surface Characterization 247

9.2.7 Hydrolytic Stability tests of the monolayers 247

9.3 RESULTS AND DISCUSSION 248

9.3.1 Perfluorododecyltrichlorosilane monolayer on smooth polymer surfaces 248

9.3.1.1 Characterization of the modified smooth surfaces: XPS and IR. 248

9.3.1.2 Wettability of smooth untreated, plasma-activated, and FDTS-grafted polymer surfaces. 251

9.3.2 Wettability of Nanotextured Polymer Surfaces. 252

9.3.2.1 Random nanotextured PMMA, and PEEK surfaces. 252

9.3.2.2 Ordered hierarchical micro and nanotextured PMMA surface 254

9.3.2.3 Random nanotextured PDMS Surfaces 255

9.3.3 Stability testing of the fluorosilane-coated polymer surfaces 256

9.3.3.1 Hydrolytic Stability test on smooth non-plasma textured surfaces 256

9.3.3.2 Hydrolytic stability of plasma-micro and nanotextured surfaces 258

9.4 CONCLUSIONS 259

9.5 REFERENCES 260

9.1 INTRODUCTION

A major goal of surface and coating research is to design and fabricate self-cleaning surfaces, which repel not only water,[1] but also other low surface-energy liquids.[2] Nanostructuring as well as chemical modification of polymeric surfaces using low surface energy organic layers has been extensively studied and used to improve macroscopic as well as microscopic surface properties, such as coating adhesion, mechanical strength, suitability for microfluidics,[3, 4] and amphiphobicity.[5-7] Such "smart" modified polymers display a significant potential for a range of biomedical applications, in the semiconductor and automobile industry, in micro-contact printing,[8] as lubricant,[9] in protection against environmental fouling,[10] in self-cleaning,[10, 11], antifogging,[12] anti-icing,[13] and other useful properties.[14] Incorporation of such surfaces into miniaturized components allows further development of "smart" multifunctional devices and systems (MEMS/NEMS).[3]

With flat surfaces, the use of an ultra-low surface-energy coating is by itself not sufficient to achieve super-hydrophobic/oleophobic properties: with flat ultra-low adhesion, perfluorinated flat surfaces water contact angles (CA) up to ~120° can be obtained,[15] and the oleophobicity is typically worse. In order to obtain superhydrophobicity as well as superoleophobicity (contact angle with water and oil both > 150°, and small hysteresis), two factors are required: a) chemical surface modification using low-surface energy molecules,[15, 16] and b) a well-designed topography with re-entrant curvature structures with predesigned spacing and height.[17] Tuteja et al. designed a re-entrant curvature geometry using fluorinated polyhedral oligomeric silsesquioxane (POSS) coating material. They obtained a CA for hexadecane close to 150° by overhanging structures. However, fabrication by this method is labor intensive and expensive. Recently, many new methods to fabricate amphiphobic/superamphiphobic surfaces are found in the literature that follow either stochastic[18, 19] or biomimetic bottom-up approaches,[20] or microfabrication top-down approaches.[6] Typically these modifications are done on silicon and little work can be found on superamphiphobic polymer substrates. A recent review paper that includes all the progress made on polymers[21] stresses the need for a simple generic fabrication method that can be applied in almost any polymer substrate (PDMS, PMMA, PEEK and PS) with consistent results.

A facile method to obtain superamphiphobic polymers is to randomly plasma nanotexture surfaces and deposit a fluorocarbon plasma coating as shown by Gnanappa et al.[5] Another method to fabricate ordered, hierarchical topography is the use of colloidal lithography followed by plasma etching of the polymer and fluorocarbon plasma deposition, as shown by Ellinas et al.[22] We obtained a superamphiphobic PMMA surface,

exhibiting 168° and 153° static CAs for water and diiodomethane, respectively, and small hysteresis. However, the static contact angle measured with hexadecane was 'only' 101°, due to the non-minimized surface energy of the C_4F_8 plasma coating. This example showed that plasma treatment may be a generic technique towards superoleophobicity of polymeric surfaces, but that further improvements were required in order to obtain also high CAs towards alkanes.

In contrast to disordered fluorocarbon coatings with typical surface energy values of 18.5 mN/m (the surface energy for polytetrafluoroethylene (Teflon)),[23] much lower surface energies have been reported for ordered perfluoroalkyl monolayers, in fact as low as 5.6 mN/m for perfluorinated alkyne-derived monolayers on Si(111) surfaces.[15] To make use of this feature, perfluoroalkyl monolayers have been used for superoleophobic Si-containing inorganic surfaces.[24-26] Typically such surfaces require pre-activation to allow efficient attachment reactions, e.g. by HF or strong acids, which severely limits their use for polymers.

An alternative to surface-activating reactions in solution is plasma activation with subsequently covalent surface reaction with liquid-repellent perfluoroalkyl trichlorosilane-based materials. However, it is difficult to obtain perfluoroalkyl monolayers attached to the surface, since condensation of silanol is described to lead to the formation of cross-linked siloxane networks, covalently bound to the substrate through occasional condensation with surface silanol groups. First efforts to obtain such monolayers on polymers have been described in the literature.[27, 28]

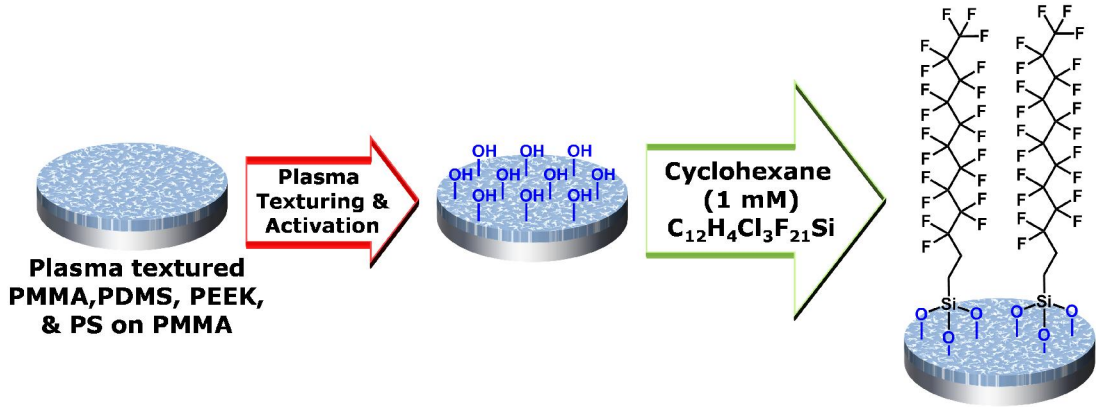

Figure 1. Two-step approach to obtain superoleophobic surfaces via plasma-induced texturing and follow-up reaction with FDTS ($Cl_3SiCH_2CH_2$-$C_{10}F_{21}$)

In the current paper, we combine the plasma-induced nanotexturing of polymeric surfaces with a covalently attached perfluorinated monolayer. The resulting stochastic or ordered surfaces were characterized in detail by IR spectroscopy and XPS analyses. Static

CAs and the concomitant hysteris are measured with a variety of liquids, ranging from water to hexadecane and soya oil, not just for freshly prepared samples, but also after prolonged (> 1 month) exposure to aqueous media. The resulting data show that non-degrading superoleophobicity can be produced on polymeric surfaces using a simple and generic technology suitable for most polymers.

9.2 EXPERIMENTAL

9.2.1 Materials

Optically transparent 2 mm thick PMMA plates were purchased from IRPEN (Spain), and opaque grey 1.5 mm thick PEEK plates from RTP Company (USA), and both were cleaned using isopropyl alcohol (IPA) and deionized (DI) water prior to plasma processing. PDMS prepolymer was mixed with its curing agent and a thickness of ~15-20 μm was coated on silicon wafer. 1H,1H,2H,2H-Perfluorododecyltrichlorosilane (FDTS, 97%, Aldrich) was used as received. Cyclohexane CHROMASOLV® Plus, for HPLC, ≥99.9% was purchased from Aldrich. Polysterene spheres 1 and 3 μm diameter were purchased from microParticles GmbH and were used as described elsewhere.[22]

9.2.2 Plasma-induced nanotexturing of polymers

Plasma processes were performed in the Micromachining Etching Tool (MET) from Alcatel at NCSR Demokritos, equipped with a helicon source (at 13.56 mHz) providing RF power up to 2,000 W. Typical values for the O_2 plasma used in the texturing of organic polymers were 1,900 W, 0.75 Pa, 100 sccm, –100 V bias voltage, 15 °C. Surfaces after the O_2 plasma treatment became amphiphilic. The same reactor was also used for the inorganic polymers etching using SF_6 chemistry at conditions: 1900 W, 1.33 Pa, 172 sccm, 15 °C, -100 V bias voltage. Under these anisotropic conditions polymers become nanotextured in a highly reproducible manner. Nanotexturing is mainly formed due to the anisotropic etching conditions and the simultaneous co-deposition of minute amounts of alumina fragments sputtered from the alumina Helicon reactor dome. Alumina is unetchable in oxygen or SF_6 plasmas, and when present in trace amounts, it initiates the formation of the “nanograss”-like structures locally, which grow gradually higher since alumina preferentially sticks to the protruding parts of the topography, causing a roughness instability, as discussed in detail elsewhere.[29] Similar nanotexturing results have been observed by other authors.[30, 31] We note that the nanotexture obtained after 1 min plasma texturing is dual scale comprising approximately 600 nm high columnar structures with 200 nm spacing , as well as shorter structures on the foot of the taller

columns with approximately 50 nm spacing.. For long plasma treatments, the resulting filamenetal nanostructures are not mechanically stable. To stabilize the PEEK and PMMA surfaces before hydrophobization, the surfaces were immersed into water and upon drying the nanofilaments coalesce in shorter more compact hierarchical microhills, due to capillary forces. Wetted-dried surfaces are mechanically stable and described elsewhere.[5] PDMS surfaces are stabilized during the silanization step, and there is no need for water immersion (see *Supporting Information S.9.4* figure S6 and section 3.2.3). To produce ordered hierarchical surfaces, polystyrene microspheres are spin-coated on polymer surfaces resulting in hexagonally packed microsphere arrays. The same plasma processes as before are performed, followed by a short isotropic oxygen plasma etching step to produce undercut profiles, as described in detail by Ellinas et al.[22] These surfaces do not need additional water-immersion stabilization.

9.2.3 Substrate reactivation

Since the plasma nanotexturing took place in Athens, and the follow-up SAM preparation was always performed in Wageningen several weeks later, a brief air plasma reactivation of the surface was necessary in order to regenerate OH or COOH groups lost due to ageing.[32] To this aim, a polymeric substrate was placed in the plasma reaction chamber (PDC-002 (plasma cleaner) PDC-FMG-2 (plasmaFlo), Harrick Scientific Products, Inc. Ossining, NY). The reaction chamber was pumped down to less than $(1.2 \pm 0.2) \times 10^{-2}$ mbar prior to the introduction of air plasma. Pieces of polymeric substrates were placed in the plasma cleaner and oxidized for 2 min with 0.3 SCFH air flow, 29.6 W power, at 300 mtorr pressure.

9.2.4 SAM Preparation

Polymeric substrates were degreased by immersion for 2 min in an ultrasonic bath containing ethanol and then allowed to dry in a stream of argon, and reactivated in the plasma as described in section 2.3. Immediately after removal from the plasma cleaner, these activated substrates were immersed for 60 min in a solution of 1 mM FDTS in cyclohexane, thoroughly rinsed with cyclohexane and dried in a stream of dry argon. Evidence for the successful surface modification was obtained from a detailed surface characterization (vide infra).

9.2.5 Contact Angle Measurements

Contact angle analysis was performed with a Krüss DSA 100 Contact Analyzer System. Static contact angle were measured using typically 5 μL droplets. Advancing, and

receding angles were measured as the droplet volume was continuously increased and decreased, to estimate contact angle hysteresis. The contact angle was determined with the software suite and via graphical fitting of the contact tangents method-2 (polynomial method) in the captured image. Both approaches gave the same nominal value, typically within 1°, and always within ±2°. For each sample, a minimum of four different readings in different spots on the surface were recorded.

9.2.6 Surface Characterization

An X-ray photoelectron spectrometer (XPS; JEOL JPS-9200 photoelectron spectrometer) was used for elemental composition of surfaces. The mono-chromatized Al-Kα X-ray source was operated at 12 kV and 20 mA. Photoelectrons were collected at a take-off angle of 80° relative to the sample surface. Wide-scan survey spectra were acquired using analyzer pass energy of 100 eV and a step size of 1 eV. To avoid any surface charging of the polymer surface, a charge neutralizer was employed at a setting of 5.1 A and 2.8 V. Atomic and mass percentages were calculated from the areas of representative elemental peaks using the library of relative sensitivity factors provided by the manufacturer. After a linear-type background subtraction, the raw spectra were fitted using nonlinear least squares fitting program adopting Gaussian−Lorentzian peak shapes for all the peaks. The atomic compositions were evaluated using sensitivity factors as provided by CasaXPS Version 2.3.15 software. Attenuated Total Reflectance Infrared (ATR-IR) Spectra were collected with an α ALPHA-P Bruker equipped with an exchangeable QuickSnap™ sampling and platinum ATR single reflection diamond ATR module. All spectra were built up from 150 scans (resolution: 1 cm^{-1}), and referenced to a clean plasma-activated polymer surface.

9.2.7 Hydrolytic Stability tests of the monolayers

We carried out the water stability experiments by placing the modified polymer surfaces inside a tailor-made glass beaker, which has two connections, one for fresh deionized (DI) water 2000 mL/day (25 °C), and another for draining (see circulating water bath Figure S7 in *Supporting Information S.9.5*). Samples remained in the bath for a pre-determined period, and then were taken out for contact angle measurement. In all cases, the surfaces were rinsed with fresh deionized water and ethanol, dried in a flow of dry argon and subjected to high vacuum (~10 mbar) for 30 min before the contact angle was measured. Samples were then returned to the same circulating water bath for monitoring of the stability for a longer period.

9.3 RESULTS AND DISCUSSION

9.3.1 Perfluorododecyltrichlorosilane monolayer on smooth polymer surfaces.

Smooth fluorinated polymer surfaces were for PMMA, PEEK and PDMS surfaces obtained by air plasma activation of the polymers, directly followed by reacting the –OH or COOH functionalized surfaces for 1 h with a solution of FDTS (1 mM, dry cyclohexane). This typically yielded formation of a smooth fluorinated monolayer upon a single immersion, as indicated below.

9.3.1.1 Characterization of the modified smooth surfaces: XPS and IR.

To characterize in detail the variation in the surface chemistry of the substrates – untreated, air plasma-activated, and FDTS-grafted smooth PDMS, PMMA, and PEEK substrates – they were analyzed by X-ray photoelectron spectroscopy (XPS). The XPS-based elemental analysis showed a decrease in the carbon composition at the surface after plasma activation and a clear increase of the oxygen content. This confirms the surface oxidation of the substrates. At this stage no visible F signal is present on any of the polymers. Upon subsequent grafting of FDTS, fluorine appears in the XPS data in line with monolayer attachment (see Table 1, and *Supporting Information S.9.2*, Figure S2-S4). The percentage of Si on PDMS substrates before and after plasma treatment remains approximately the same, while upon grafting of FDTS it is slightly decreased, in line with the formation of a signal-attenuating overlayer, i.e. the fluorinated monolayer (see *Supporting Information S.9.2* figure S2-S4). These data are analogous to data in the literature.[32]

Peak-fitted narrow-scan C1s spectra of FDTS-modified PEEK, PDMS, and PMMA are shown in Figure 2 a, c & e. A large shift (typically on the order of several eV) towards higher binding energies was typically observed in these XPS measurements due to surface charging of the polymer surfaces during the analysis. Therefore, all measurements required the use of a charge neutralizer, and the spectra were calibrated afterwards by setting the major C–C/C–H peak at 285.0 eV (PDMS & PMMA) and 284.7 eV (PEEK).[33]

The composition of all three modified surfaces was also confirmed in more detail by narrow scan C1s XPS measurements. The deconvolution of the C1s signal for the FDTS-functionalized PEEK revealed the contributions of seven main carbon signals. The main C1s signal is centered at 284.7 eV and was assigned to the contribution of aromatic C-C bonds together with C=C and Si-C carbon atoms. The chemical shifts relative to this peak

were quoted in parenthesis. The contributions of C1s electrons from C-O groups and $\underline{C}H_2$-CF_2 at 286.2 eV (ΔE = 1.5 eV) were too close together to be resolved and therefore were summed together. The peak at 287.2 eV (ΔE = 2.5 eV) was attributed to carbonyl carbon, while the small component at 289.2 eV is a characteristic shake-up satellite due to the π-π* transitions in aromatic groups. The signals and their corresponding percentage with high binding energies were assigned to the $\underline{C}F_2$-CH_2 at 290.7 eV (ΔE = 6.0 eV), $\underline{C}F_2$ at 291.8 eV (ΔE = 7.1 eV), and terminal -CF_3 groups at 294.0 eV (ΔE = 9.3 eV) (Figure 2a). The relative concentrations (%) of the peaks for FDTS-grafted PEEK are (C–H/C=C, Si-C) 48.2 %, $\underline{C}H_2$-CF_2 3.6 % and $\underline{C}$-O 16.5 %, the π-π* shake-up satellite 1.9 %, $\underline{C}F_2$-CH_2 2.9 %, CF_2-$CF_{2/3}$ 23.7 % and the CF_3 3.1 %.

Table 1. XPS-Based elemental composition of untreated, plasma-activated, and FDTS-grafted smooth PMMA, PDMS, and PEEK substrates (theoretical composition of untreated substates is shown in parentheses).

Substrate		PMMA	PDMS	PEEK
Untreated:	%C	74.3 (71.5)	46.5 (50)	87.6 (86.4)
	%O	25.7 (28.5)	24.6 (25)	12.4 (13.6)
	%Si	--	28.9 (25)	--
Plasma-activated:	%C	65.9	18.5	79.7
	%O	34.1	52.1	20.3
	%Si	--	29.4	--
FDTS grafted:	%C	54.3	24.9	55.2
	%O	11.1	25.5	9.3
	%Si	3.0	18.0	1.8
	%F	31.6	31.1	33.8

[a] See for survey scan XPS spectra the *Supporting Information S.9.2*, (Figure S2-S4).

For FDTS-modified PDMS, the C1s XPS spectrum was deconvoluted into five components (Figure 2c), with the chemical shift relative to the (C–H/C–C, Si-C) contribution and their percentage quoted in parentheses. Hydrocarbon C atoms (C–H/C–C, Si-C) were found at 285.0 eV (ΔE = 0 eV, 37.3 %), $\underline{C}H_2$-CF_2 at 286.6 eV (ΔE = 1.6 eV, 5.3 %), $\underline{C}F_2$-CH_2 at 291.2 eV (ΔE = 6.2 eV, 5.7 %), CF_2-$CF_{2/3}$ at 292.0 eV (ΔE = 7.0 eV, 45.9 %), and the terminal CF_3 moieties at 294.1 eV (ΔE = 9.1 eV, 5.7 %), as shown in Figure 2b.

The C1s deconvoluted spectrum of the FDTS-grafted PMMA substrate in Figure 2e represent the contributions of the C1s electrons from hydrocarbon (C-C/C-H and Si-C) at a binding energy of 285.0 eV (ΔE = 0 eV, 47.4%), with α-shifted carbon (C-C=O) and the $\underline{C}H_2$-CF_2 contributions summed together and found at 286.4 eV (ΔE = 1.4 eV, 14.6%). The methoxy group contribution is found at 287.5 eV (ΔE = 2.5 eV, 5.7%), while the carbonyl carbon in the ester group has a binding energy of 290.0 eV (ΔE = 5.0 eV, 6.2%). The components at 291.0 eV (ΔE = 6.0 eV, 2.8%), 292.0 eV (ΔE = 7.0 eV, 20.7%) and 294.2 eV (ΔE = 9.2 eV, 2.6%) were assigned to the $\underline{C}F_2$-CH_2, $\underline{C}F_2$-$\underline{C}F_{2/3}$ and $\underline{C}F_3$ groups, respectively.

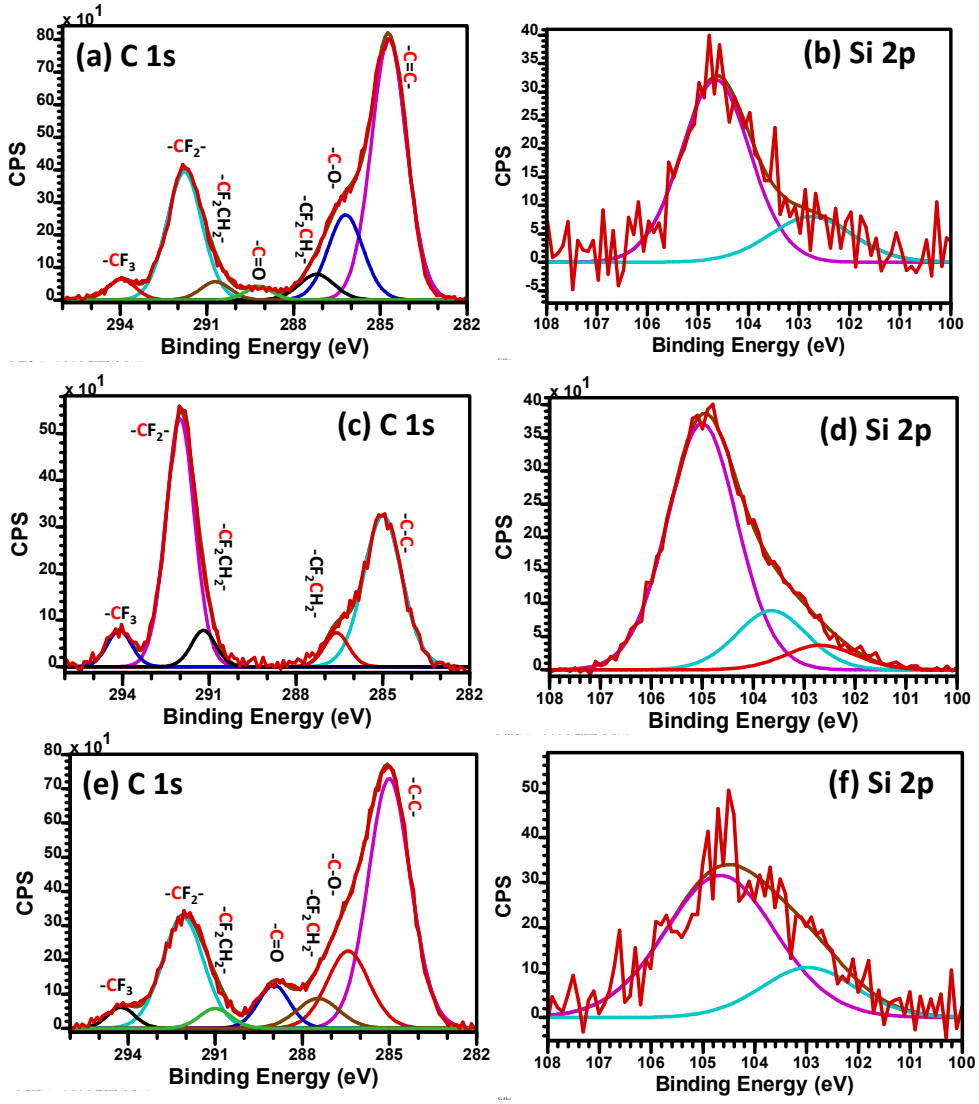

Figure 2. Peak-fitted C1s and Si2p XPS spectra of FDTS-modified PEEK (a & b), PDMS (c & d), and PMMA (e & f).

To estimate the relative coverage of these monolayers, one can compare the contribution of the clearly distinguishable contribution of the CF_3 group (one of the 12 C atoms of FDTS). If one of those CF_3 groups would be bound per polymer repeat unit on the surface (5 C for PMMA, 2 C for PDMS and 19 C for PEEK), then the CF_3 peak would constitute 5.8% on PMMA, 7.1% on PDMS, and 3.2% on PEEK. In fact, the CF_3 contributions amount to 2.6% on PMMA, 5.7% on PDMS and 3.1% on PEEK. This implies a somewhat denser monolayer formation on PDMS and PEEK than on PMMA.

To confirm the presence of Si-O, Si-C and O-Si-O bonds, the Si2p XPS peak was deconvoluted (Figure 2b, d & f) into two components at 102.7 eV (Si-C) and 104.6 eV (Si-O), respectively, in accordance with the incorporation of a silane on the PEEK and PMMA interfaces (Figure 2b and 2f, respectively). The experimental ratios of these two components (Si-O & Si-C) are 3.1 : 1, in close agreement with the theoretical ratio of 3 : 1. The deconvoluted Si2p XPS peak of FDTS-grafted PDMS revealed three contributions (Figure 2d). They were assigned to O-Si-O Si atoms at 105.0 eV, Si-O at 103 eV, and Si-C at 102.7 eV. The XPS narrow scans of the O1s and F1s regions further supported the successfully grafted polymer substrates (see *Supporting Information S.9.2*, Figure S2-S4).

The successful formation of a FDTS overlay was also confirmed by IR spectroscopy (see *Supporting Information S.9.6*, Figure S8). This revealed not only the appearance of characteristic C-H stretching vibrations (especially clear on PMMA), but also characteristic C-F absorptions in the 1130 – 1250 cm^{-1} region.[34]

9.3.1.2 Wettability of smooth untreated, plasma-activated, and FDTS-grafted polymer surfaces.

Contact angle (CA) measurements are sensitive indicators of the surface properties of a monolayer.[35-39] The obtained monolayers on smooth surfaces were analyzed with static CA measurements and a variety of test liquids, namely water, soya oil and hexadecane. Low-surface-tension liquids such as hexadecane (γ_{lv} = 27.5 mN/m) and soya oil (γ_{lv} = 34.1 mN/m) were chosen as probe liquids to observe the oleophobicity on the surface. Data for all relevant samples are summarized in Table 2. Before modification these surfaces were thoroughly rinsed in pentane and dried by an argon stream. The native PDMS had a water CA of 114°, while water contact angles of 82° and 60° were found for native PEEK and PMMA, respectively. Upon plasma-activation, these values drop, to <40°, which confirms formation of hydroxyl and carboxyl groups. After silanization, the water contact angles were increased, to 125° for PMMA, 123° for PDMS and 119° for PEEK. Such values are in line with the attachment of a fluorinated monolayer,[15, 26, 37, 40, 41] and imply the presence

of weak dipole-dipole interactions between the CF_3 terminus and water molecules. In comparison, a PTFE surface displays a lower static water CA (typically ~115°),[42] because the CF_2 groups are less capable of reducing the surface energy than CF_3 groups.[43] The lower polarizability of fluorine compared to hydrogen leads to weak Van der Waals interactions among the CF_3 terminus and polar water molecules.[15, 44, 45] The differences between the different polymer surfaces are attributed to the effects of differences in the AFM-observed surface roughnesses (PMMA: 1.7 nm, PDMS: 6.7, and PEEK: 5.5 nm) and the degree to which the polymer is swelled by cyclohexane, i.e. the solvent in which the FDTS attachment takes place, which affects the degree of fluorination.

Table 2. Static contact angle and hysteresis data on smooth PMMA, PDMS and PEEK before and after silanization. (Hysteresis is shown in parentheses.) (Error ±2°)

		PMMA	PDMS	PEEK
Bare surface (water)		60°	114°	82°
Soon after air plasma activation (water)		40°	25°	25°
After silanization	Water	125° (15°)	123 (17°)	119° (18°)
	Soya oil	90°	87°	92°
	Hexadecane	75°	76°	76°

After coating with FDTS, the polymer surfaces became repellent to soya oil and water, and contact angles for all surfaces.

9.3.2 Wettability of Nanotextured Polymer Surfaces.

In this section, we discuss the superhydrophobic and superoleophobic properties of the polymeric surfaces that were nanostructured in a hierarchical manner – either randomly or in an ordered fashion – using plasma-induced texturing (see section 2.2.),[22, 32, 46] and subsequently coated with a perfluorosilane-based monolayer.

9.3.2.1 Random nanotextured PMMA, and PEEK surfaces.

Oxygen plasma etching was used to micro-nano texture PMMA and PEEK surfaces, yielding a high-aspect ratio, random topography.[32] However, this topography is not stable upon immersion in water and drying, and eventually yields coalesced micro hills.[5, 47] Figure 3 shows PEEK and PMMA surfaces after texturing with O_2 plasma for 20 min, immersion in water, drying, subsequent plasma-induced reactivation and grafting by FDTS. The PMMA surface is affected during silane modification (swells slightly in cyclohexane), yielding small changes in the morphology, and penetration of monolayer-

forming silanes into the swelled polymer. In contrast, PEEK is not attacked by cyclohexane.

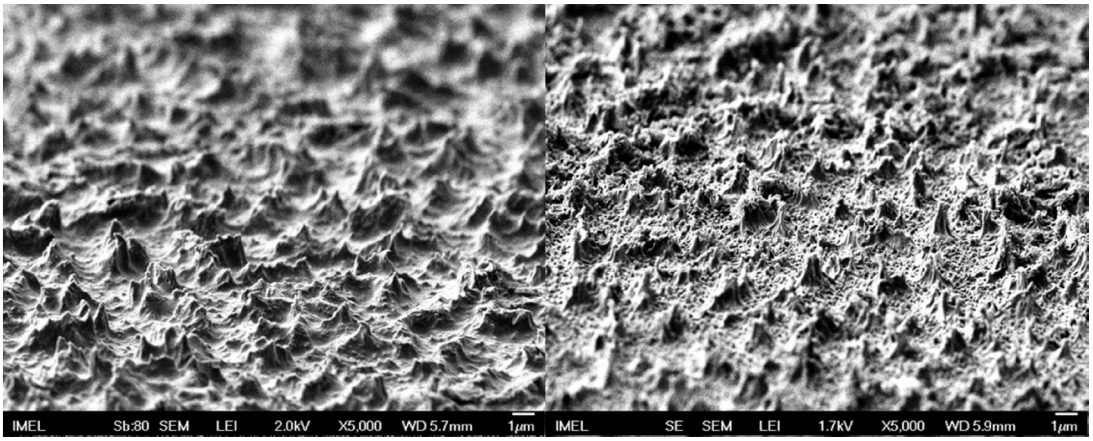

Figure 3. SEM images of micro-nano textured, water-immersed and dried PEEK (left) and PMMA (right) surfaces after perfluorosilane modification in cyclohexane (70 degrees tilted).

The dynamic contact angle measurements on micro-nano textured PMMA and PEEK after 20 min O_2 plasma treatment and subsequent FDTS grafting are provided in Table 3. Superoleophobicity is observed for all liquids tested, including hexadecane. This represents a significant improvement compared to plasma-deposited fluorocarbon coatings (using C_4F_8 plasma[5]). These findings of the current study are consistent and the PMMA data even improve slightly upon the superoleophobic surfaces reported by Zimmermann et al.,[24] who obtained a contact angle for hexadecane of 140° ± 5° on silicon nanofilaments with FOTS coatings.

Table 3. Static, advancing, receding contact angles and hysteresis (all: in degrees) for water, soya oil and hexadecane on silane-modified, hierarchical randomly rough surfaces of PMMA and PEEK.*

Liquid	Contact Angle	PMMA 20 min O_2 plasma	PEEK 20 min O_2 plasma
Water	Static	167◦	168◦
	Adv/Rec (Hyster)	168◦/166◦ (2◦)	168◦/166◦ (2◦)
Soya Oil	Static	157◦	159◦
	Adv/Rec (Hyster)	157◦/153◦ (4◦)	159◦/145◦ (14◦)
Hexadecane	Static	142◦	138◦
	Adv/Rec (Hyster)	145◦/135◦ (10◦)	142◦/130◦ (12◦)

* 5 μL liquid , error in Static ±2° advancing and receding ±5°

9.3.2.2 Ordered hierarchical micro and nanotextured PMMA surface.

Figure 4 shows SEM images of uniform, mushroom-like micropillars produced on PMMA by the combination of colloidal lithography using PS particles and plasma etching as described before.[22] These mushroom-like micropillars do not display any coalescence after immersion in water or silane solution for 1 h. High-resolution SEM images of surfaces show the same morphology before and after silanization (see *Supporting Information S.9.4*, Figure S5-S6).

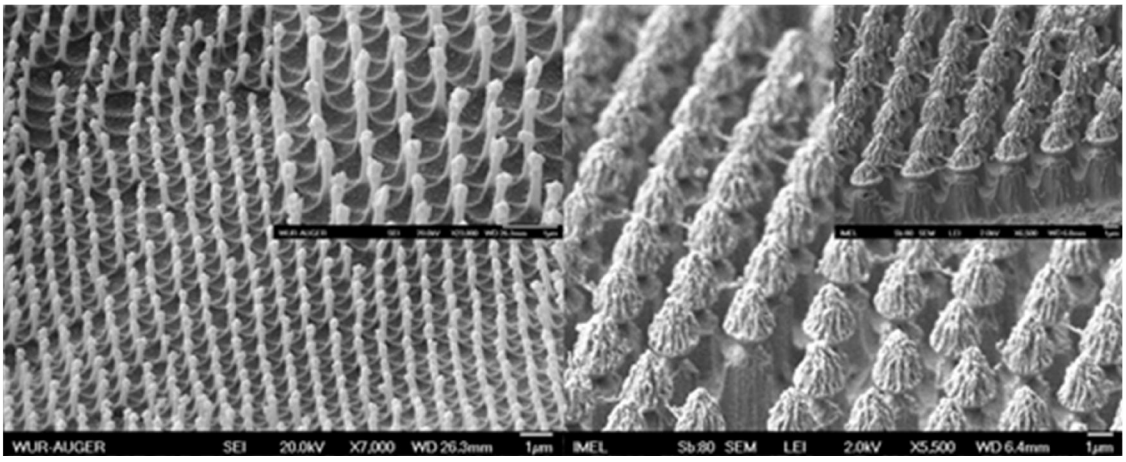

Figure 4. SEM images of PMMA surfaces (60 degrees tilted) displaying the hierarchical, hexagonically ordered packed pillars obtained upon plasma etching using (A) 1 μm and (B) 3 μm polystyrene particles.

The contact angle results are shown in Table 4 for FDTS-modified, ordered (using both 1 and 3 μm PS particles) PMMA surfaces. In addition, this table presents the comparison with contact angles from our previous reported work[13] (red font in parentheses) using the same re-entrant topography with the C_4F_8 plasma-deposited layer (film thickness 30 nm). In all cases the current CAs with water, soya oil or hexadecane are higher to significantly higher than previous results. This highlights the efficient functionalization with FDTS, which results in a high local CF_3 density concentration that yields a superhydrophobic material with a low surface energy. These CA results are better or equal to those obtained on POSS-coated surfaces, as reported by Tuteja et al.[17]

The contact angle hysteresis are for water <4°, soya oil ~7° and hexadecane ~10°. Such values indicate a Cassie or impregnating Cassie state. 5-μl water and soya oil drops roll-off easily from these surfaces, by tilting approximately for only ~1° for water, while <8° for soya. This rolling-off movements were captured in videos (see only pictures *Supporting Information S.9.1,* Figure S1).

Table 3. Contact angle measurements for water, soya oil and hexadecane on silane-modified hierarchical ordered PMMA surfaces with PS microparticles. Hystereris is shown in parenthesis for Adv/Rec measurements.

Solvent	Contact angle	1 μm PS on PMMA 1.30 min (anisotropic) +0.30 min (isotropic)	3 μm PS on PMMA 4.30 min (anisotropic) +1.30 min (isotropic)
Water	Static	166° [165°]	167° [168°]
($\gamma l\upsilon$ = 72.1 mN m^{-1})	Adv/Rec	168°/166° (2°) [≤ 2°]	168°/164° (4°) [≤ 5°]
Soya Oil	Static	153° [125°]	154° [134°]
($\gamma l\upsilon$ = 34.1 mN m^{-1})	Adv/Rec	159°/152° (7°)	157°/150°(7°) [>15°]
Hexadecane	Static	140° [96°]	142° [101°]
($\gamma l\upsilon$ = 27.5 mN m^{-1})	Adv/Rec	142°/133°(9°) [>30°]	143°/133°(10°) [>30°]

Note: The corresponding contact angles and hysteresis when a plasma-deposited fluorocarbon layer was used instead of the current FDTS grafting are shown in [square brackets], to reveal the improvement using the FDTS monolayer compared to reference [22].

[*] 5 μL liquid, uncertainty in static CA ±2°; receding CA: ±5°.

9.3.2.3 Random nanotextured PDMS surfaces

SF_6 plasma etching was used to texture PDMS surfaces, resulting in high aspect ratio topography. The resulting topography for 10 min plasma processing is shown in Figure 5. These surfaces are not stable upon water immersion. However, the silanization process is used for the stabilization of the topography (see also *Supporting Information S.9.4*, Figure S6). Similar results for stabilization of the topography have been also observed for other polymer surfaces and will be reported elsewhere.

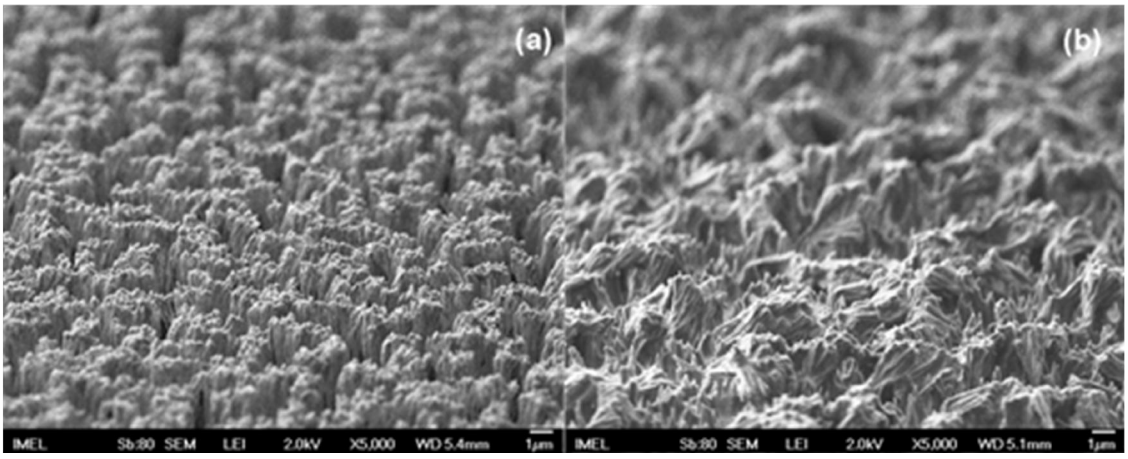

Figure 5. SEM images of SF_6 plasma-nanotextured PDMS surfaces (a) before silanization (b) after silanization. After 10 min SF_6 etching, the surface in (a) is modified with silane in cyclohexane (b).

The filamental topography that is produced after several minutes of plasma texturing (section 2.5) enhances the resulting oleophobicity. For example, the soya oil static contact angle upon texturing for 10 min becomes 152°. PDMS exhibits grass-like, re-entrant structures after the silanization, but the resulting surface is less homogeneous than PMMA and PEEK. As a result, PDMS exhibits a slightly lower CA with hexadecane than PMMA and PEEK, as indicated above. The static and advancing contact angle and the hysteresis for water, soya oil and hexadecane are shown in Table 4.

Table 4. Static, advancing and receding contact angles for water, soya oil and hexadecane on perfluorosilane-modified hierarchical randomly rough PDMS surfaces (in degrees).

Solvent	Contact angle	PDMS 10 min SF_6 plasma
Water	Static	167°
(γ_{lv}=72.1 mN/m)	Adv/Rec	168°/165° (3°)
Soya Oil	Static	152°
(γ_{lv}=34.1 mN/m)	Adv/Rec	157°/145° (12°)
Hexadecane	Static	135°
(γ_{lv}=27.5 mN/m)	Adv/Rec	142°/129° (13°)

* 5 μL liquid; uncertainty in static CA ±2°; receding CA: ±5°.

9.3.3 Stability testing of the fluorosilane-coated polymer surfaces

9.3.3.1 Hydrolytic Stability test on smooth non-plasma textured surfaces

For practical applications of such monolayer-coated polymeric surfaces, either in outdoor uses or inside microchannels, it is important that the monolayer is stable. The stability of the attached monolayers is dependent on the stability of the substrate itself, on the surface morphology, on the anchoring group, and on the environment. In order to study the stability of the attached monolayers in aqueous environments, monolayer-coated polymers were immersed in continuously flowing deionized water. The properties of the fluorinated layers were hardly influenced upon immersion for a day. Therefore long-term stability tests were performed by immersion of the modified surfaces in water for 40 days.

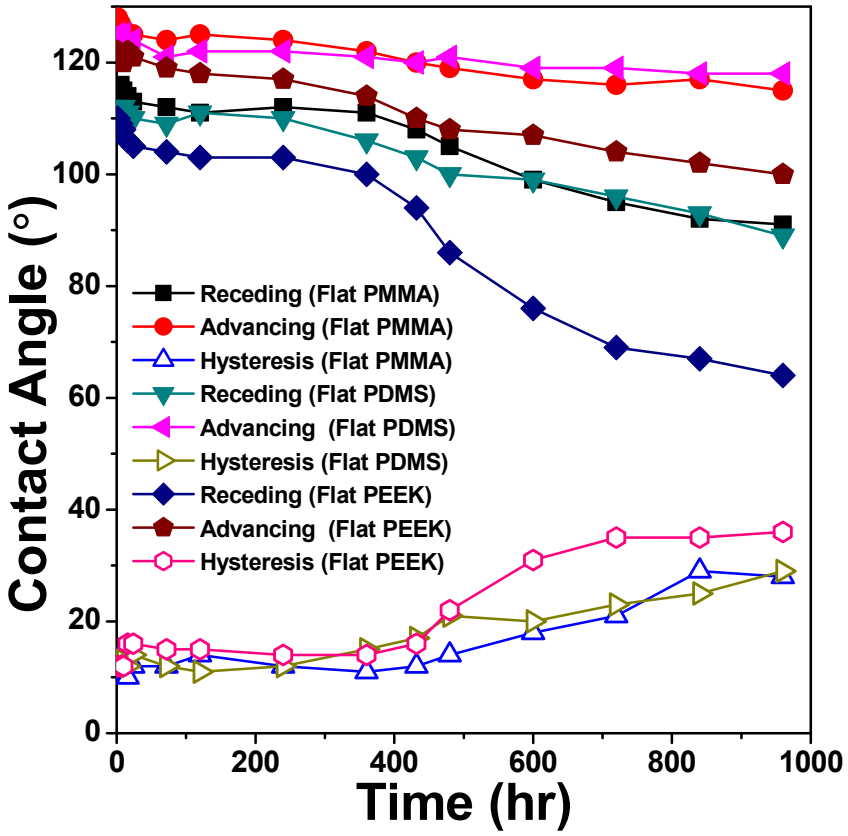

Figure 6. The advancing, receding and hysteresis water contact on smooth non-plasma textured surfaces of PMMA, PDMS, and PEEK.

First, the stability was studied on FDTS-modified smooth polymer surfaces, with the contact angle measurements as shown Figure 6. Figure 6 shows that PMMA and PDMS exhibit good hydrolytic stability. The advancing CAs of PMMA and PDMS decrease only slightly, from 128° to 115° and from 125° to 118°, respectively, while the receding CA decreases from 115° to 91° and from 112° to 89°, respectively. PEEK shows a smaller stability than PMMA and PDMS, and displays an increase in the CA hysteresis from 17° to 36°. We suspect that there are two main factors for the lower stability of PEEK: First, it is possible that not enough surface OH groups are generated by the plasma reactivation step on this polymer. Second, it is known that PEEK is not attacked by cyclohexane, while PMMA[48] and PDMS[49] are affected and probably slightly swelled by the solvent. We thus expect that silanization of PMMA and PDMS could extend a few nanometers from the surface into the swollen layer. Further swelling will be prevented since the multifunctional silylating agent causes crosslinking on the surface. This surface-only swelling and

silylation would make that layer more stable in hydrolysis, by analogy to surface silylation of photoresists which become stable (unetchable) in oxygen plasmas.[50]

9.3.3.2 Hydrolytic stability of plasma-micro and nanotextured surfaces

Figure 7 presents the advancing and receding CA of water on perfluorosilane-modified hierarchical plasma-textured surfaces. The stability of the perfluorosilane-coated PMMA surface is shown in Figure 7A. The advancing CA did not change upon immersion in water for 40 days (168° ± 2°), but the receding CA slightly decreased from 164° to 154°, and from 166° to 159°, for PMMA surfaces that were plasma-etched for 10 min and 20 min, respectively. As this indicates, especially the 20 min-etched PMMA shows a remarkably high resistance to water. This suggests that the SAM is densely packed over the whole surface and acts as a very good barrier to prevent water from attacking the hydrolysis of the Si-O-C bond that links the monolayer to the substrate. In Figure 7b, the monolayer stability of 10 min etched PEEK surfaces is shown. Both the advancing and receding CA are reduced after 40 days water flow over the PEEK surface. The advancing CA is reduced from 168° to 140° and the receding CA from 166° to 135°. This observation reflects that the perfluorosilane-derived monolayer is less stable on the plasma-textured PEEK surface than on PMMA, in line with the observations made for smooth PMMA and PEEK surfaces above.

The stability of ordered plasma-textured PMMA surfaces (using 1 or 3 μm PS particles as etch masks) are shown in Figure 7C. In this case, water flow for 40 days affected the surface wetability only slightly, with the advancing CA values remaining constantly high at 168°±1°, whereas the receding CA gradually decreased slightly, to approximately 162° ±1° after 40 days. Such low hysteresis suggests that multiscale roughness (roughness in the micron, hundred-nanometer, and ten-nanometer range) that is present in these overhanging pillars enhances the hydrolytic stability of these surfaces compared to the randomly textured surfaces.

The hydrolytic stability of the 10 min plasma-textured PDMS surface is shown in figure 7D. The data clearly show that also on PDMS the attachment of a perfluorosilane-derived monolayer coating effectively stabilizes the superoleophobicity of the surface. Even after 40 days in water, the advancing CA only reduces from 168° to 165°, while the hysteresis stays under 10°. This again shows that structuring the polymer surface in a hierarchical manner that encompasses both the nano and micrometer scale allows for the formation of a highly stable coating, with a concomitantly stable superoleophobicity.

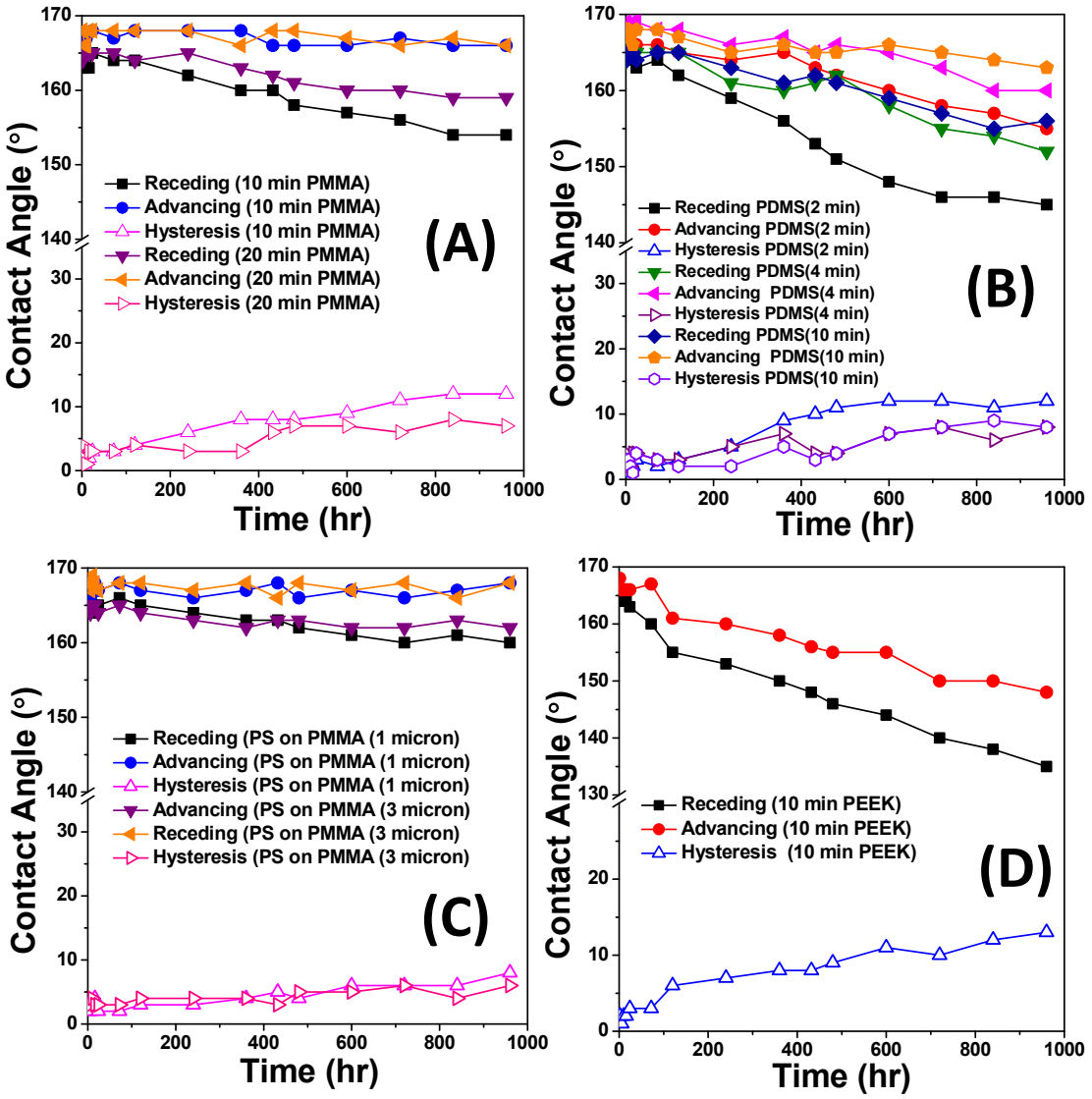

Figure 7. Advancing, receding and hysteresis contact angles of water used to study the layer desorption kinetics of different fluorinated silane modified hierarchical rough surfaces (A) 20 min plasma textured PMMA. (B) 20 min plasma-textured PEEK. (C) PMMA surfaces masked with 1 μm or 3 μm PS microparticles and plasma etched. (D) 10 min plasma-etched PDMS.

9.4 CONCLUSIONS

We have shown a generic method to produce superoleophobic polymer surfaces that display a high long-term stability in water. Our approach involves two steps: 1) Hierarchical nanotexturing of the surfaces (PEEK, PMMA and PDMS) by a plasma

etching step. Especially when plasma etching is performed using as a mask a self-assembled layer of monodisperse micrometer-sized particles, this yields an ordered micro and nanotextured surface structure. 2) Grafting of these etched surfaces with a perfluorosilane, which yields superoleophobic polymeric surfaces. Such surfaces display a long-term hydrolytic stability, with minimal loss of the superoleophobicity, as indicated by immersion measurements in water for a period of >40 days. This simple approach will allow the construction of a wide range of long-lasting superoleophobic surfaces, which are attractive for a variety of outdoor uses as well as in MEMS, microfluidics and (bio-) sensor applications.

9.5 REFERENCES

1. Li, X.-M.; Reinhoudt, D.; Crego-Calama, M., What do we need for a superhydrophobic surface? A review on the recent progress in the preparation of superhydrophobic surfaces. *Chem. Soc. Rev.* **2007,** 36, (8), 1350-1368.
2. Liu, K.; Tian, Y.; Jiang, L., Bio-inspired superoleophobic and smart materials: Design, fabrication, and application. *Prog. Mater Sci.* **2012,** 58, (4), 503–564.
3. Tsougeni, K.; Papageorgiou, D.; Tserepi, A.; Gogolides, E., "Smart'" polymeric microfluidics fabricated by plasma processing: controlled wetting, capillary filling and hydrophobic valving. *Lab on a Chip* **2010,** 10, (4), 462-469.
4. Tanzi, S.; Østergaard, P. F.; Matteucci, M.; Christiansen, T. L.; Cech, J.; Marie, R.; Taboryski, R., Fabrication of combined-scale nano- and microfluidic polymer systems using a multilevel dry etching, electroplating and molding process. *J. Micromech. Microeng.* **2012,** 22, (11), 115008.
5. Gnanappa, A. K.; Papageorgiou, D. P.; Gogolides, E.; Tserepi, A.; Papathanasiou, A. G.; Boudouvis, A. G., Hierarchical, Plasma Nanotextured, Robust Superamphiphobic Polymeric Surfaces Structurally Stabilized Through a Wetting–drying Cycle. *Plasma Processes Polym.* **2012,** 9, (3), 304-315.
6. Tuteja, A.; Choi, W.; Mabry, J. M.; McKinley, G. H.; Cohen, R. E., Robust omniphobic surfaces. *Proc. Natl. Acad. Sci. USA* **2008,** 105, (47), 18200-18205.
7. Susarrey-Arce, A.; Marín, Á. G.; Nair, H.; Lefferts, L.; Gardeniers, J. G. E.; Lohse, D.; van Houselt, A., Absence of an evaporation-driven wetting transition on omniphobic surfaces. *Soft Matter* **2012,** 8, (38), 9765-9770.
8. Zhao, H.; Law, K.-Y.; Sambhy, V., Fabrication, Surface Properties, and Origin of Superoleophobicity for a Model Textured Surface. *Langmuir* **2011,** 27, (10), 5927-5935.
9. Yao, X.; Gao, J.; Song, Y.; Jiang, L., Superoleophobic Surfaces with Controllable Oil Adhesion and Their Application in Oil Transportation. *Adv. Funct. Mater.* **2011,** 21, (22), 4270-4276.
10. Park, Y.-B.; Im, H.; Im, M.; Choi, Y.-K., Self-cleaning effect of highly water-repellent microshell structures for solar cell applications. *J. Mater. Chem.* **2011,** 21, (3), 633-636.
11. Howarter, J. A.; Youngblood, J. P., Self-Cleaning and Anti-Fog Surfaces via Stimuli-Responsive Polymer Brushes. *Adv. Mater.* **2007,** 19, (22), 3838-3843.

12. Gao, X.; Yan, X.; Yao, X.; Xu, L.; Zhang, K.; Zhang, J.; Yang, B.; Jiang, L., The Dry-Style Antifogging Properties of Mosquito Compound Eyes and Artificial Analogues Prepared by Soft Lithography. *Adv. Mater.* **2007,** 19, (17), 2213-2217.
13. Chuppina, S. V., Anti-Icing gradient organosilicate coatings. *Glass Phys. Chem* **2007,** 33, (5), 502-509.
14. Bhushan, B.; Jung, Y. C., Natural and biomimetic artificial surfaces for superhydrophobicity, self-cleaning, low adhesion, and drag reduction. *Prog. Mater Sci.* **2011,** 56, (1), 1-108.
15. Pujari, S. P.; Spruijt, E.; Cohen Stuart, M. A.; van Rijn, C. J. M.; Paulusse, J. M. J.; Zuilhof, H., Ultralow Adhesion and Friction of Fluoro-Hydro Alkyne-Derived Self-Assembled Monolayers on H-Terminated Si(111). *Langmuir* **2012,** 28, (51), 17690-17700.
16. Mabry, J. M.; Vij, A.; Iacono, S. T.; Viers, B. D., Fluorinated Polyhedral Oligomeric Silsesquioxanes (F-POSS). *Angew. Chem. Int. Ed.* **2008,** 120, (22), 4205-4208.
17. Tuteja, A.; Choi, W.; Ma, M.; Mabry, J. M.; Mazzella, S. A.; Rutledge, G. C.; McKinley, G. H.; Cohen, R. E., Designing Superoleophobic Surfaces. *Science* **2007,** 318, (5856), 1618-1622.
18. C-T Hsieh, F.-L. W., W-Y Chen, Contact Angle Hysteresis and Work of Adhesion of Oil Droplets on Nanosphere Stacking Layers. *J. Phys. Chem. C* **2009,** 113, 13683–13688.
19. A. Steele, I. B., E. Loth, Inherently Superoleophobic Nanocomposite Coatings by Spray Atomization. *Nano Lett.* **2009,** 9, (1), 501–505.
20. Sheen, Y.-C.; Huang, Y.-C.; Liao, C.-S.; Chou, H.-Y.; Chang, F.-C., New approach to fabricate an extremely super-amphiphobic surface based on fluorinated silica nanoparticles. *J. Polym. Sci., Part B: Polym. Phys.* **2008,** 46, (18), 1984-1990.
21. Xue, Z.; Liu, M.; Jiang, L., Recent developments in polymeric superoleophobic surfaces. *J. Polym. Sci., Part B: Polym. Phys.* **2012,** 50, (17), 1209-1224.
22. Ellinas, K.; Tserepi, A.; Gogolides, E., From Superamphiphobic to Amphiphilic Polymeric Surfaces with Ordered Hierarchical Roughness Fabricated with Colloidal Lithography and Plasma Nanotexturing. *Langmuir* **2011,** 27, (7), 3960-3969.
23. Waite, J. H., Nature's underwater adhesive specialist. *Int. J. Adhes. Adhes.* **1987,** 7, (1), 9-14.
24. Zimmermann, J.; Rabe, M.; Artus, G. R. J.; Seeger, S., Patterned superfunctional surfaces based on a silicone nanofilament coating. *Soft Matter* **2008,** 4, (3), 450-452.
25. Zhao, H.; Law, K.-Y., Directional Self-Cleaning Superoleophobic Surface. *Langmuir* **2012,** 28, (32), 11812-11818.
26. Pujari, S. P.; Scheres, L.; Weidner, T.; Baio, J. E.; Cohen Stuart, M. A.; van Rijn, C. J. M.; Zuilhof, H., Covalently Attached Organic Monolayers onto Silicon Carbide from 1-Alkynes: Molecular Structure and Tribological Properties. *Langmuir* **2013,** 29 (12), 4019-4031.
27. Brown, L.; Koerner, T.; Horton, J. H.; Oleschuk, R. D., Fabrication and characterization of poly(methylmethacrylate) microfluidic devices bonded using surface modifications and solvents. *Lab on a Chip* **2006,** 6, (1), 66-73.
28. Bhushan, B.; Hansford, D.; Lee, K. K., Surface modification of silicon and polydimethylsiloxane surfaces with vapor-phase-deposited ultrathin fluorosilane films for biomedical nanodevices. *J. Vac. Sci. Technol., A* **2006,** 24, (4), 1197-1202.
29. Kokkoris, G.; Gogolides, E., The potential of ion-driven etching with simultaneous deposition of impurities for inducing periodic dots on surfaces. *J. Phys. D: Appl. Phys* **2012,** 45, (16), 165204.

30. Mundo, R. D.; Palumbo, F.; d'Agostino, R., Influence of Chemistry on Wetting Dynamics of Nanotextured Hydrophobic Surfaces. *Langmuir* **2010,** 26, (7), 5196-5201.
31. Accardo, A.; Gentile, F.; Mecarini, F.; De Angelis, F.; Bughammer, M.; Di Fabrizio, E.; Riekel, C., In Situ X-ray Scattering Studies of Protein Solution Droplets Drying on Micro- and Nanopatterned Superhydrophobic PMMA Surfaces. *Langmuir* **2010,** 26, (18), 15057-15064.
32. Tsougeni, K.; Vourdas, N.; Tserepi, A.; Gogolides, E.; Cardinaud, C., Mechanisms of Oxygen Plasma Nanotexturing of Organic Polymer Surfaces: From Stable Super Hydrophilic to Super Hydrophobic Surfaces. *Langmuir* **2009,** 25, (19), 11748-11759.
33. Beamson, G.; Briggs, D., *High Resolution XPS of Organic Polymers: The Scienta ESCA300 Database*. John Wiley & Sons: 1992.
34. Lenk, T. J.; Hallmark, V. M.; Hoffmann, C. L.; Rabolt, J. F.; Castner, D. G.; Erdelen, C.; Ringsdorf, H., Structural Investigation of Molecular Organization in Self-Assembled Monolayers of a Semifluorinated Amidethiol. *Langmuir* **1994,** 10, (12), 4610-4617.
35. Fadeev, A. Y.; McCarthy, T. J., Trialkylsilane monolayers covalently attached to silicon surfaces: Wettability studies indicating that molecular topography contributes to contact angle hysteresis. *Langmuir* **1999,** 15, (11), 3759-3766.
36. Mundo, R. D.; Palumbo, F., Comments regarding 'an essay on contact angle measurements'. *Plasma Processes Polym.* **2011,** 8, (1), 14-18.
37. Gao, L.; McCarthy, T. J., Contact Angle Hysteresis Explained. *Langmuir* **2006,** 22, (14), 6234-6237.
38. Tavana, H.; Jehnichen, D.; Grundke, K.; Hair, M. L.; Neumann, A. W., Contact angle hysteresis on fluoropolymer surfaces. *Adv. Colloid Interface Sci.* **2007,** 134-135, 236-248.
39. Balkenende, A. R.; van de Boogaard, H. J. A. P.; Scholten, M.; Willard, N. P., Evaluation of Different Approaches To Assess the Surface Tension of Low-Energy Solids by Means of Contact Angle Measurements. *Langmuir* **1998,** 14, (20), 5907-5912.
40. Shibuichi, S.; Yamamoto, T.; Onda, T.; Tsujii, K., Super Water- and Oil-Repellent Surfaces Resulting from Fractal Structure. *J. Colloid Interface Sci.* **1998,** 208, (1), 287-294.
41. Onda, T.; Shibuichi, S.; Satoh, N.; Tsujii, K., Super-water-repellent fractal surfaces. *Langmuir* **1996,** 12, (9), 2125-2127.
42. Zhang, J.; Li, J.; Han, Y., Superhydrophobic PTFE Surfaces by Extension. *Macromol. Rapid Commun.* **2004,** 25, (11), 1105-1108.
43. van de Grampel, R. D.; Ming, W.; Gildenpfennig, A.; Laven, J.; Brongersma, H. H.; de With, G.; van der Linde, R., Quantification of fluorine density in the outermost atomic layer. *Langmuir* **2004,** 20, (1), 145-149.
44. Song, X. Y.; Zhai, J.; Wang, Y. L.; Jiang, L., Fabrication of superhydrophobic surfaces by self-assembly and their water-adhesion properties. *J. Phys. Chem. B* **2005,** 109, (9), 4048-4052.
45. Barriet, D.; Lee, T. R., Fluorinated self-assembled monolayers: composition, structure and interfacial properties. *Curr. Opin. Colloid Interface Sci.* **2003,** 8, (3), 236-242.
46. Vlachopoulou, M.-E.; Kokkoris, G.; Cardinaud, C.; Gogolides, E.; Tserepi, A., Plasma Etching of Poly(dimethylsiloxane): Roughness Formation, Mechanism, Control, and Application in the Fabrication of Microfluidic Structures. *Plasma Processes Polym.* **2013,** 10, (1), 29-40.
47. Skarmoutsou, A.; Charitidis, C. A.; Gnanappa, A. K.; Tserepi, A.; Gogolides, E., Nanomechanical and nanotribological properties of plasma nanotextured superhydrophilic and superhydrophobic polymeric surfaces. *Nanotechnology* **2012,** 23, (50), 505711.

48. Shen, J.-N.; Zheng, X.-C.; Ruan, H.-M.; Wu, L.-G.; Qiu, J.-H.; Gao, C.-J., Synthesis of AgCl/PMMA hybrid membranes and their sorption performance of cyclohexane/cyclohexene. *J. Membr. Sci.* **2007,** 304, (1–2), 118-124.
49. Hajsz, T.; Csetneki, I.; Filipcsei, G.; Zrinyi, M., Swelling kinetics of anisotropic filler loaded PDMS networks. *Phys. Chem. Chem. Phys.* **2006,** 8, (8), 977-984.
50. Kontziampasis, D.; Beltsios, K.; Tegou, E.; Argitis, P.; Gogolides, E., Optimized surface silylation of chemically amplified epoxidized photoresists for micromachining applications. *J. Appl. Polym. Sci.* **2010,** 117, (4), 2189-2195.

Supporting Information to Chapter 9

Table of Contents

Supporting Information to Chapter 9 264
S.9.1 Water Contact angle 264
S.9.2 X-ray photoelectron spectroscopy (XPS) 265
S.9.3 Atomic Force Microscopy (AFM) 268
S.9.4 Solvent effect on plasma nanotextured surfaces 268
S.9.5 Stability test experimental setup 271
S.9.6 IR spectroscopy of smooth polymeric samples 272
S.9.7 Reference 273

S.9.1 Water contact angle

Figure S1. Droplets (colored with different dyes) of water (γ/v = 72.1 mN/m), soya oil (γ/v = 34.1 mN/m), and Hexadecane (γ/v = 27.5 mN/m) on a FDTS modified textured polymer surfaces.

S.9.2 X-ray photoelectron spectroscopy (XPS)

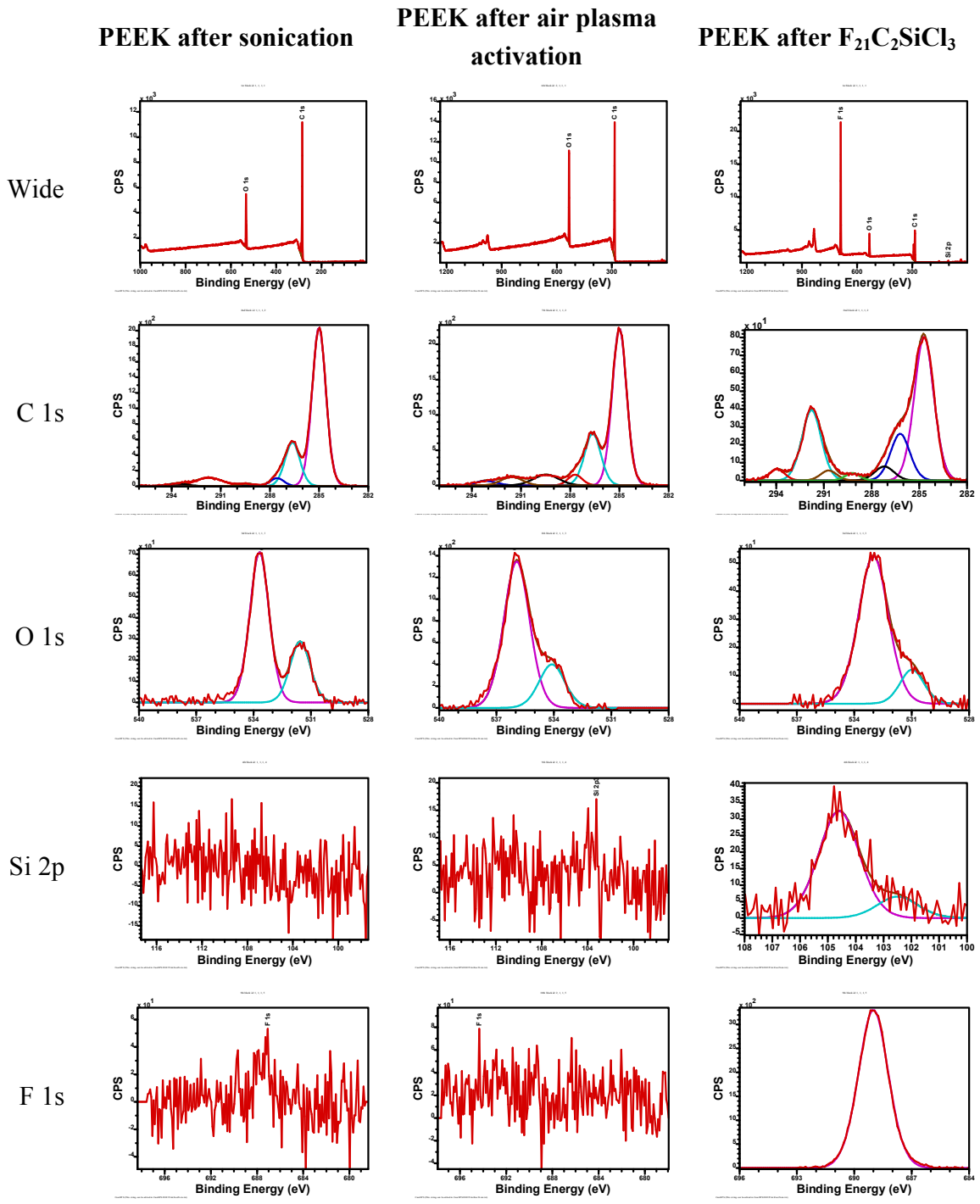

Figure S2. XPS spectra of bare, plasma-activated and FDTS modified PEEK surfaces

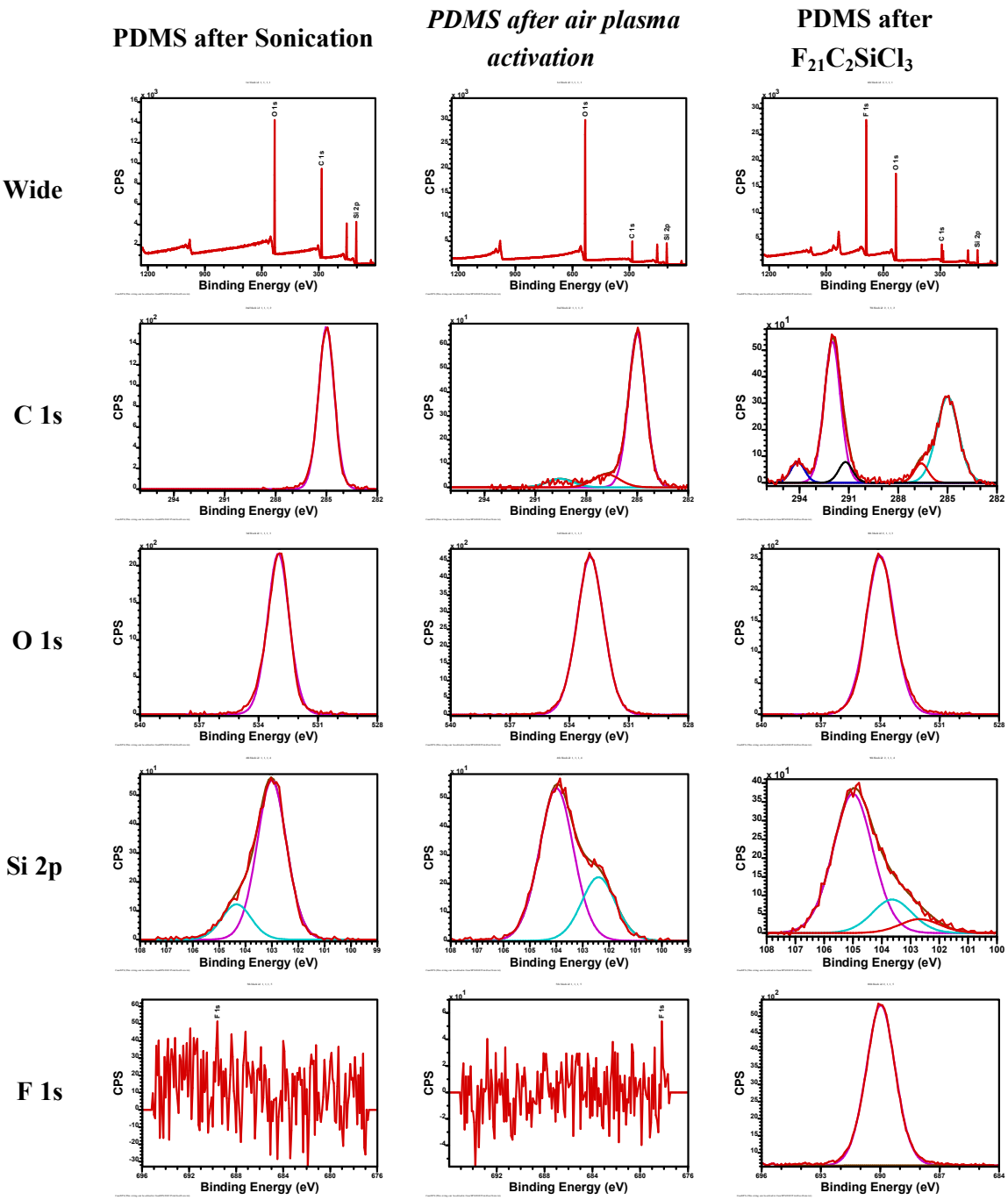

Figure S3. XPS spectra of bare, plasma-activated and FDTS modified PDMS surfaces.

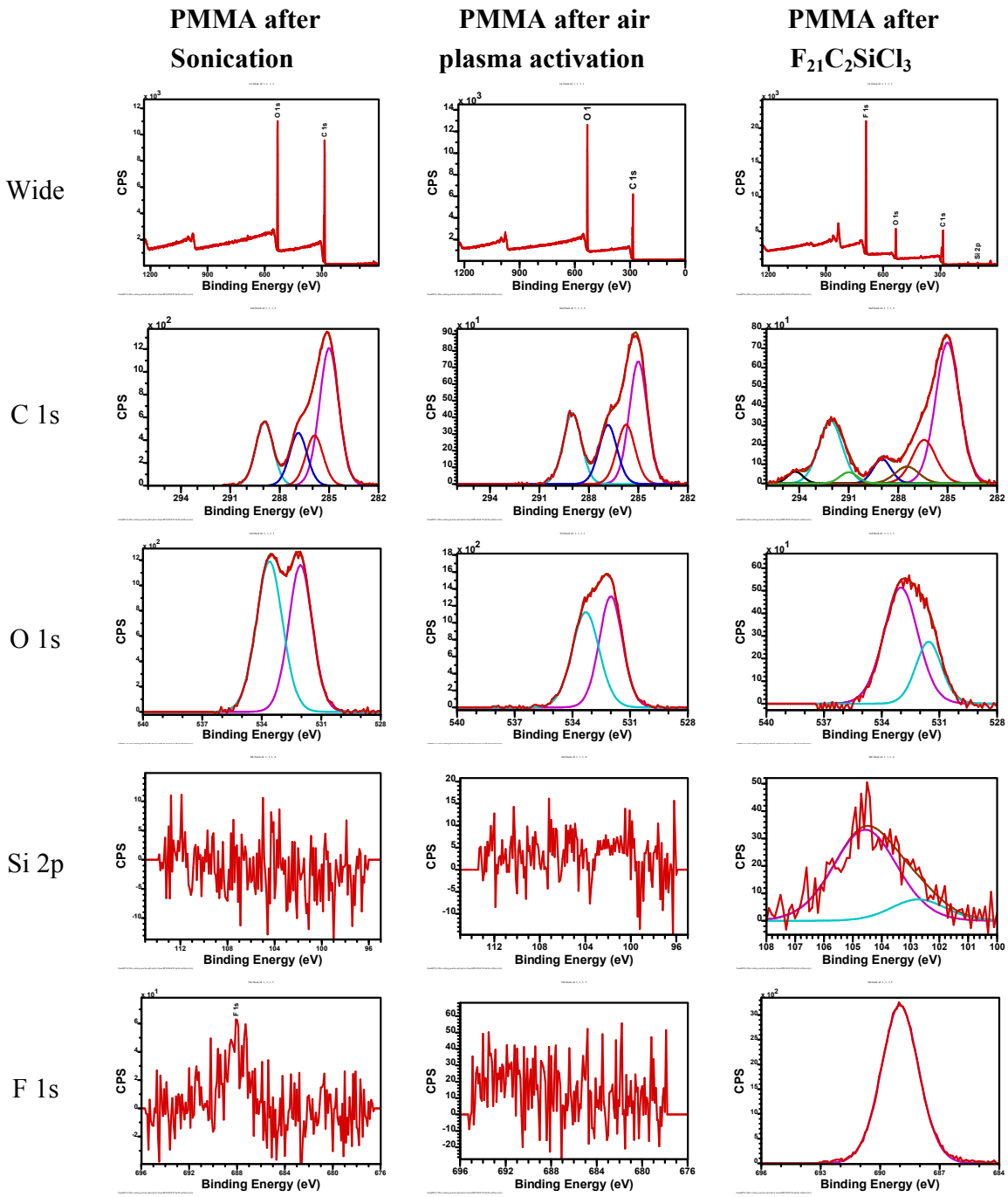

Figure S4. XPS spectra of bare, plasma-activated and FDTS modified PMMA surfaces.

S.9.3 Atomic Force Microscopy (AFM)

AFM of smooth polymer surfaces (as received, after air plasma activation, and after FDTS modification)

The surface topography was imaged using a scanning probe microscope (Jeol JSPM-5400) in tapping mode (AC-AFM) with a standard silicon cantilever (320 kHz, NSC35/AIBS, ULTRASHARP). The bare PMMA PEEK and PDMS surfaces were relatively smooth, with small roughness (Figure S2A). Upon air plasma activation some increased roughness is evident (see Figure S2B). .Such roughness features can be ascribed to a surface change during the plasma process, most likely cross-linking of the polymer-surface or preferential etching. Clearly the air plasma treatment is milder compared to oxygen plasma etching performed in vacuum, and roughness is much smaller compared to the rough topographies observed on PMMA and PEEK after O_2 plasma nanotexturing[1] The plasma treatment of polymer surfaces induces also removable nanoscale structures, such as tiny bubbles or low-molecular-weight fragments which form at the interface.[2, 3] The consecutive exposure to solvents (cyclohexane, pentane, water, ethanol) washes-off such low-molecular-weight fragments[3]. Similar behavior is observed on polystyrene and PMMA surfaces.[3 4]

After being modified by FDTS in cyclohexane solution, the PMMA, PEEK, and PDMS surfaces showed a correspondingly increased roughened character, which was shown is due to FDTS solution concentration interference[5] (Figure S2C).

S.9.4 Solvent effect on plasma nanotextured surfaces

The surface topography of plasma nanotextured samples was imaged using SEM microscopy to observe changes in the texture during the silanization process. For PMMA and PEEK, the surface was first immersed in water and dried, in order to stabilize the morphology using the capillary collapse phenomenon. For PDMS, no water immersion was done prior to silanization.

It is clear that small changes occur in all polymers as expected. In the case of PDMS and PMMA, the cyclohexane solution seems to affect the texture in a more severe way. More accurately, PDMS texture bends and sometimes breaks, a fact that proves that the solvent mildly attacks PDMS, while in PMMA it reduces the roughness, despite the prior water/drying immersion-stabilization process. On the contrary, during PEEK silanization process, the texture seems to be affected much less. This mild solvent attack in PMMA

and PDMS favours the coating stability and packing, while in PEEK the unstable coating leads in poor hydrolytic stability as shown in section 3.3.2.

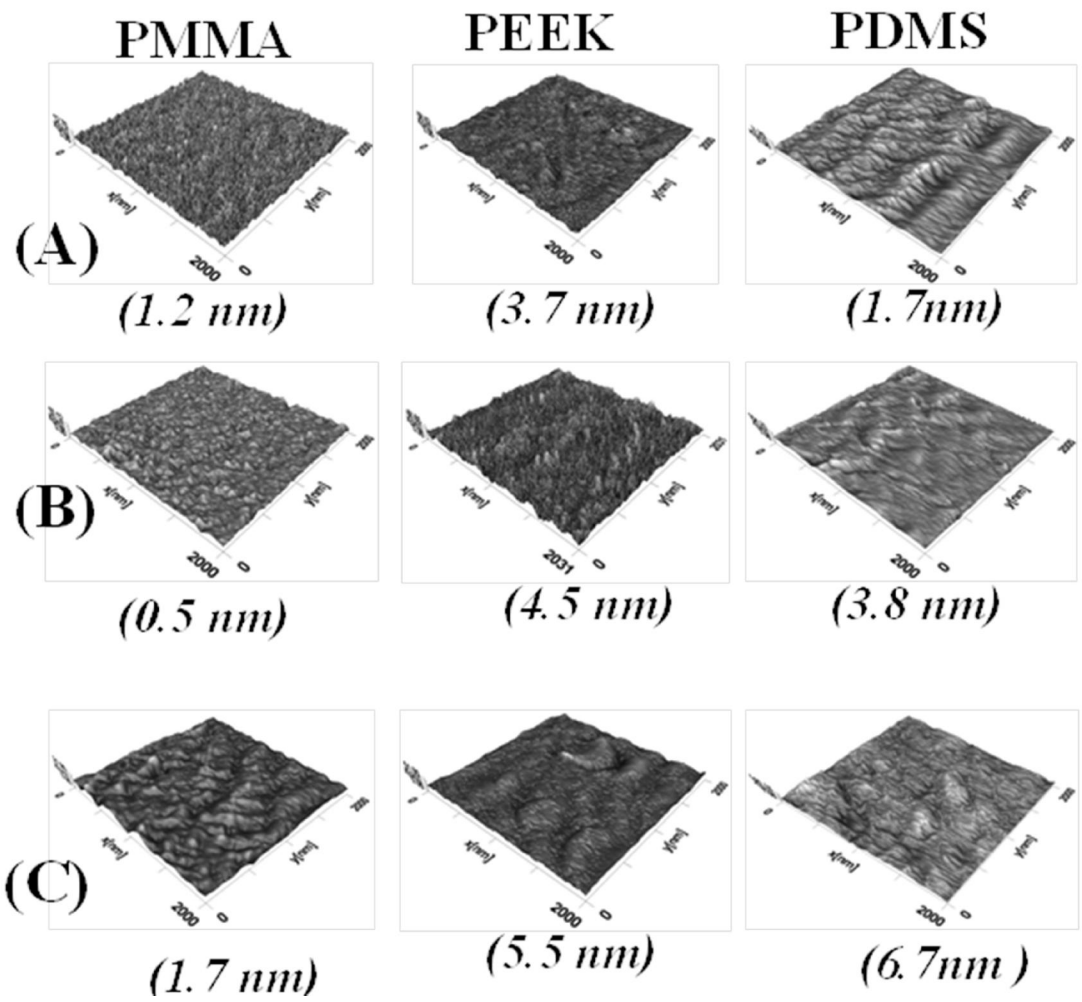

Figure S5. AFM images (2 μm × 2μm) of PMMA (left column), PEEK (middle column) and PDMS (right column); roughness are shown in parentheses. (A) bare substrate, (B) air plasma-activated substrate, and (C) after modification with FDTS.

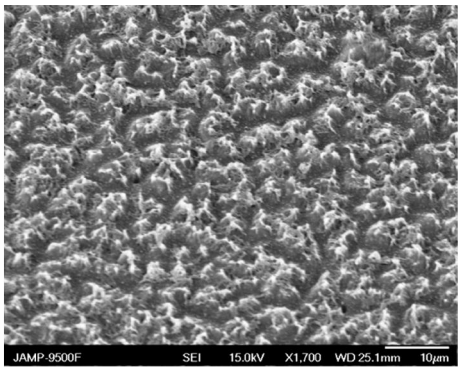

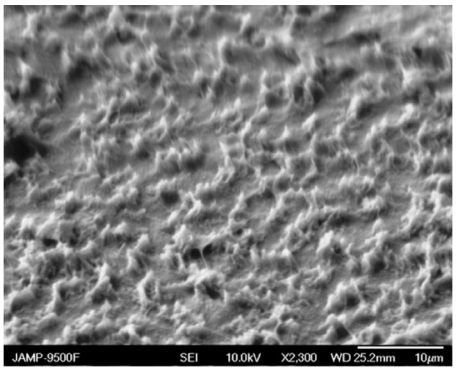

before silanization after silanization

Nanotextured PMMA for 20 min in O_2 plasma

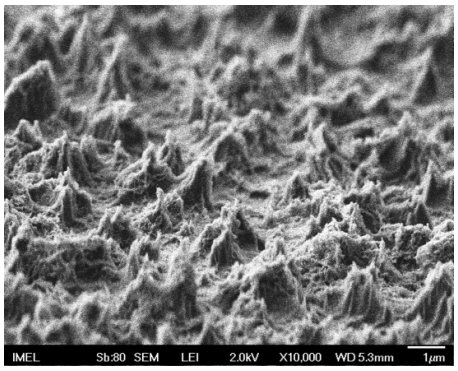

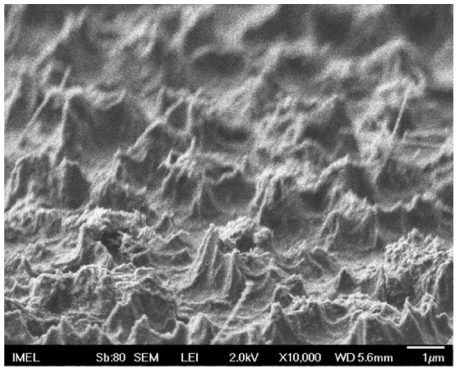

before silanization after silanization

Nanotextured PEEK for 20 min in O_2 plasma

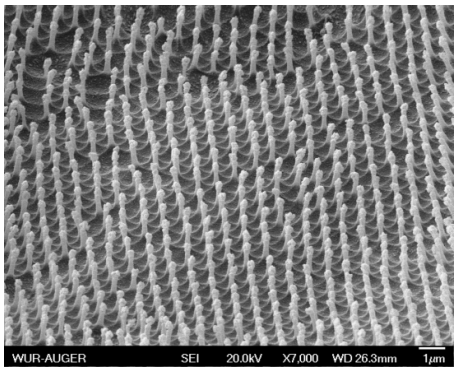

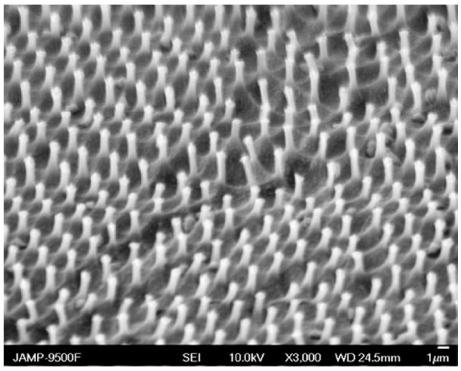

before silanization after silanization

Nanotextured PS (1μm) on PMMA for 2 min in O_2 plasma

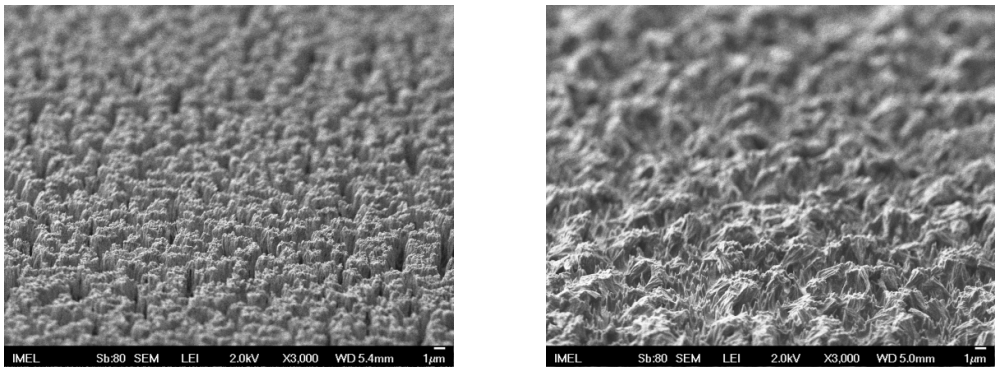

before silanization after silanization

Nanotextured PDMS for 10 min in SF_6 plasma

Figure S6. SEM images from all plasma nanotextured polymer surfaces before and after silanization in the cyclohexane solution

S.9.5 Stability test experimental setup

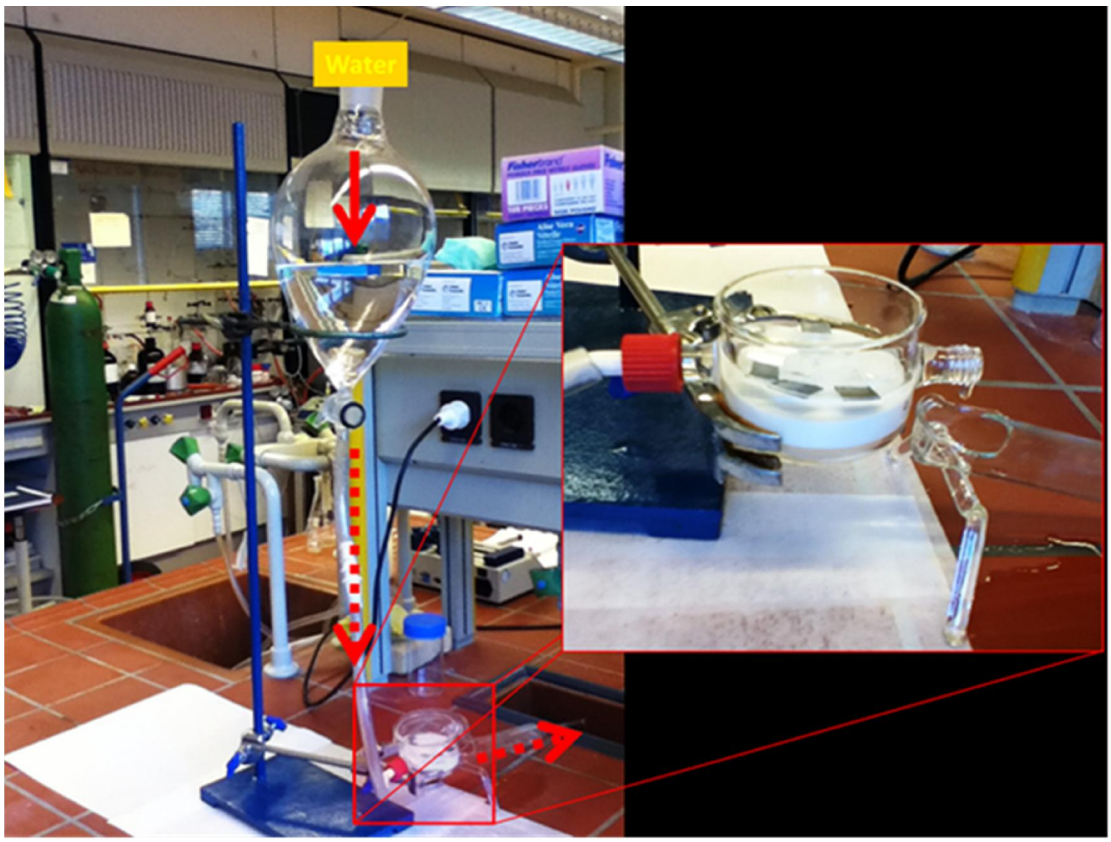

Figure S7: Setup for stability study of FDTS coated polymer surfaces. See the circulating water bath.

S.9.6 IR spectroscopy of smooth polymeric samples.

The fluorinated smooth PDMS, PMMA, and PEEK surfaces were characterized by ATR-IR spectroscopy (Figure S5). The C-H stretching is shown in Figure 1A. For PDMS, the peak at 2961 cm^{-1} can be assigned to methyl C-H bond stretching, and is present both for the untreated surface (not shown) and for FDTS-grafted surface, showing no obvious difference in the spectra in that region. For the modified PDMS and PEEK, the symmetric CH_2 stretching vibration peaks were not clearly observed in the present study, because of the order of magnitude lower intensity of this band. However, both bands were observed in the spectrum of PMMA at 2924 and 2852 cm^{-1} for anti-symmetric and symmetric CH_2, stretching vibrations, $\nu_a(CH_2,)$ and $\nu_s(CH_2)$, respectively. This spectrum matches earlier reports for PMMA surfaces coated with a monolayer of OTS,[6] as well as after deposition onto PMMA of alkyl carboxylic acid monolayers via Langmuir−Blodgett methods.[7] The ATR-FTIR spectra of the modified PDMS and PMMA surfaces displayed no clear infrared absorption over large areas in the region from 2000-400 cm^{-1} (Figure S5B). However, a band at ca. 1131 cm^{-1} was observed in the modified PMMA spectrum which was attributed to C-F stretching vibration. In the case of modified PDMS substrate, the signals at 1209 cm^{-1} and 1151 cm^{-1} were assigned to the C-F stretch vibrations. Figure S5 (C) for PEEK shows a clear indication for C-F stretch vibration at 1278 cm^{-1}, 1215 cm^{-1}, 1184 cm^{-1}, and 1155 cm^{-1}. This result confirmed that FDTS was successfully attached on these surfaces.

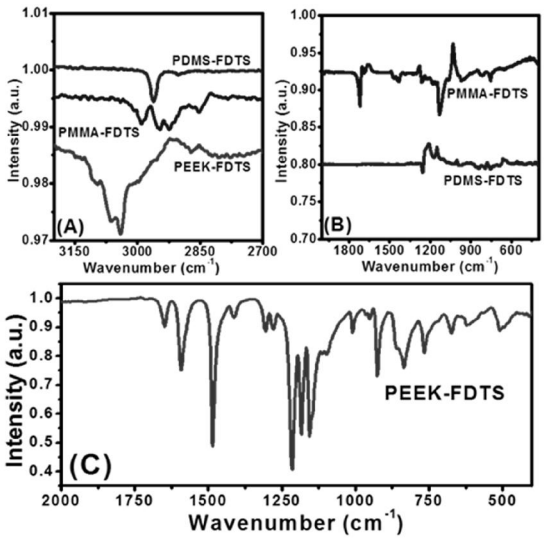

Figure S8. ATR-IR spectra of FDTS on PDMS, PMMA, and PEEK surfaces, (A) C-H stretching bands 2700-3200 cm-1; (B) fingerprint region of PMMA and PDMS; (C) fingerprint region of PEEK. These spectra were obtained from clean unmodified surfaces and subtracted from FDTS modified polymer spectra.

S.9.7 Reference

1. Tsougeni, K.; Vourdas, N.; Tserepi, A.; Gogolides, E.; Cardinaud, C., Mechanisms of Oxygen Plasma Nanotexturing of Organic Polymer Surfaces: From Stable Super Hydrophilic to Super Hydrophobic Surfaces. *Langmuir* **2009**, 25, (19), 11748-11759.
2. Chai, J.; Lu, F.; Li, B.; Kwok, D. Y., Wettability Interpretation of Oxygen Plasma Modified Poly(methyl methacrylate). *Langmuir* **2004**, 20, (25), 10919-10927.
3. Bonaccurso, E.; Graf, K., Nanostructuring Effect of Plasma and Solvent Treatment on Polystyrene. *Langmuir* **2004**, 20, (25), 11183-11190.
4. Chang, S. S.; Rodriguez, A. B.; Higgins, A. M.; Liu, C.; Geoghegan, M.; Sirringhaus, H.; Cousin, F.; Dalgleish, R. M.; Deng, Y., Control of roughness at interfaces and the impact on charge mobility in all-polymer field-effect transistors. *Soft Matter* **2008**, 4, (11), 2220-2224.
5. Popat, K. C.; Sharma, S.; Johnson, R. W.; Desai, T. A., AFM analysis of organic silane thin films for bioMEMS applications. *Surface and Interface Analysis* **2003**, 35, (2), 205-215.
6. Long, T. M.; Prakash, S.; Shannon, M. A.; Moore, J. S., Water-Vapor Plasma-Based Surface Activation for Trichlorosilane Modification of PMMA. *Langmuir* **2006**, 22, (9), 4104-4109.
7. Chen, S. H.; Frank, C. W., Infrared and fluorescence spectroscopic studies of self-assembled n-alkanoic acid monolayers. *Langmuir* **1989**, 5, (4), 978-987.

CHAPTER 10

General Discussion

This chapter gives a brief overview of the most striking achievements as presented in this thesis. In particular, the organic synthesis of new molecules, formation, tribology, wettability, and stability of organic monolayers on various inorganic and organic surfaces are discussed for the various approaches that were applied. We will focus on some preparation methods and highlight results obtained for specific surfaces. Remaining questions, additional ideas, and recommendation will also be addressed to enable further research.

Table of Contents

10 General Discussion 275

10.1 Introduction 277

10.2 Organic Monolayer Formation and Electronic Properties 277

10.3 Tribological Application 279

10.4 Conclusions 285

10.5 Reference 285

10.1 INTRODUCTION

Low adhesion and low frictional surfaces are particularly important for high performance technological devices. One of the great challenges in many micro-component devices is to reduce adhesion and friction to surfaces as much as possible, while keeping the surface highly robust and resistant against wear. At small dimensions surface properties, such as Van der Waals and capillary forces, greatly influence the performance of mechanical systems. Without a suitable surface modification uncoated substrates may show a high friction, a strong adhesion, and considerable wear. In particular, thin organic fluorocarbon-hydrocarbon films have been found to produce low-adhesion and low-friction lubricants. In practice, polytetrafluoroethylene (PTFE) is currently a primary coating material in many micro-electro-mechanical systems. However, these films are not covalently bound to the substrate and are therefore prone to wear and delamination. Moreover, PTFE films are relatively thick, which may still lead to high adhesion and friction forces when high loads are applied and films get compressed. Here we discuss in more detail on ultra-thin covalently bound fluoro-hydro alkyne-derived monolayers as high quality, low-adhesion and low-friction surface coatings for many applications.

10.2 ORGANIC MONOLAYER FORMATION AND ELECTRONIC PROPERTIES

As presented in previous chapters, we have succeeded in the formation of stable, covalently anchored novel fluorinated and non-fluorinated monolayers on Si(111), silicon carbide, chromium nitride, and on both organic polymeric (PEEK, PMMA, PS) and inorganic polymeric (PDMS) substrates with enhanced tribological properties. Monolayers could be formed chemically stable and with a high chain density; also their physical and theoretical predicted structures were discussed.

The principal process for monolayer formation was described in **chapter 2.** Here we showed that the novel molecule hexadecadienyl reacts faster with the silicon substrate molecules than alkyne molecules and that it possibly is a better reagent for dense monolayer formation. Organic monolayer formation on hydrogen-terminated silicon (H–Si) surfaces with the novel molecule gave a more dense monolayer as compared with the use of the hitherto best agents. It is anticipated that this might be due to the increased delocalization of β-carbon radicals by the enyne group. Monolayers formed at room temperature yielded plateau values for hexadec-3-en-1-yne and 1-hexadecyne after 8 and 16 h, respectively. The newly

developed monolayer chemistry could be useful for electrochemical sensing and/or passivation applications, facilitated through the high reactivity, high chain density, and fast formation of the monolayer under ambient conditions. It is still unknown what causes the higher packing density when using enynes: both π-π and/or Van der Waals interactions could contribute. To answer this question, shorter chain length (e.g. C10) monolayers were studied;. this would increase the π-π and depress the Van der Waals interactions.

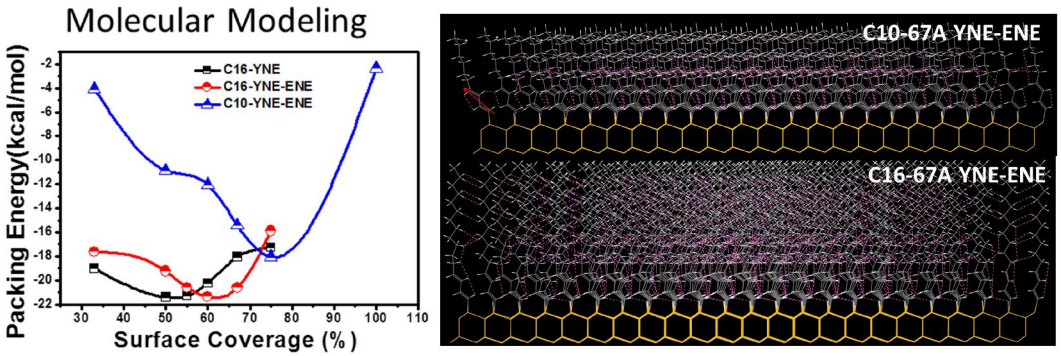

Figure 1. Preliminary molecular modeling results. Left average packing energy of C16-YNE (half-filled square), C16-YNE-ENE (half-filled circle) and C10-YNE-ENE (half-filled triangle). Right side view of simulation cell 67A after optimization. The pink dashed line represents the close contacts. Upper right C10-YNE-ENE and lower right C16-YNE-ENE.

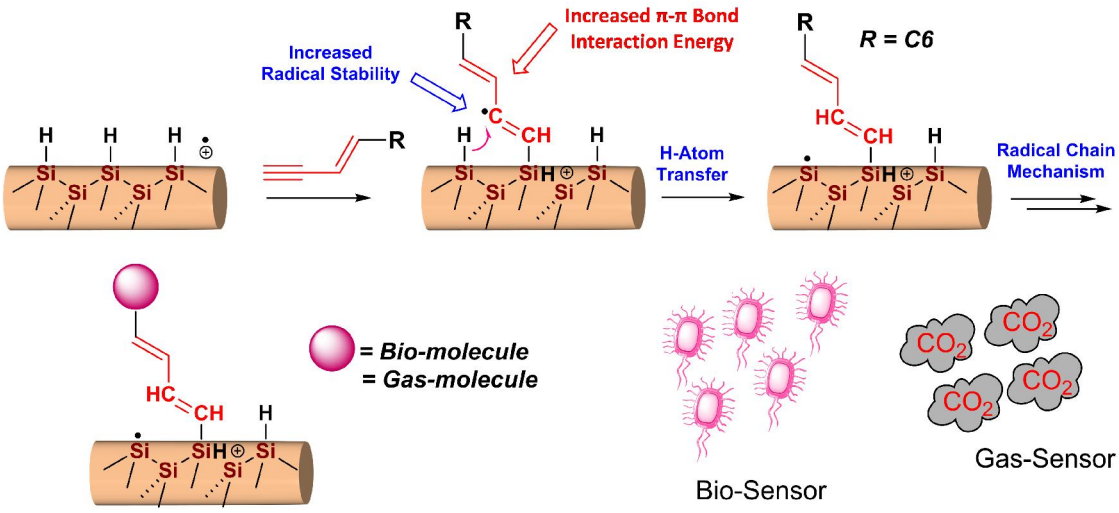

Figure 2. Schematic representations of silicon nano-wire (SiNW) modification with shorter chain length monolayers (e.g. C10), and sensing bio-molecule and gas molecules (eg. CO_2, NO_2…..).

In **Figure 1** we show preliminary results of molecular modeling of (C10-YNE-ENE) (half-filled triangle) molecules on Si(111) in comparison with C16-YNE (half-filled square) and C16-YNE-ENE(half-filled circle). The simulation clearly shows a higher surface coverage of

the short chain length C10-YNE-ENE monolayers. It favors the interpretation that Van der Waals radii of CH_2 groups higher close contacts in C16-YNE-ENE as compared to C10-YNE-ENE.

Application of these higher density and shorter chain length functional monolayers seem highly usefull in silicon nano-wire modification,[1] which might enhance sensitivity of bio-sensors[2] and/or gas sensors[3] as shown **figure 2**.[4] The electrical detection of biomolecular interactions in strong ionic solutions is difficult. In ionic solutions, a charged surface forms an electrical double layer that effectively screens the surface charges within the range of the Debye length (3 nm in 10 mM ionic solution).[4]

In **Chapter 3** we studied monolayer formation with mono-fluorinated (-CH_2F) alkyne molecules on Si(111). Such mono-fluorinated monolayers are characterized by low surface energies and have an ability to reduce the Van der Waals interaction. This originates from the low polarizability and high ionization potential of the carbon-fluorine bond. In addition, the presence of dipolar groups in the monolayer can also have a significant effect on the electrical properties of the junction. It is shown that high-quality monolayers can be obtained (e.g. a monolayer derived from F1-C18-yne has a packing density of 58 ± 2 %). It was demonstrated that by substitution of CH_3 to CH_2F in the terminal group, it is possible in a controlled manner to stepwise modify the surface potential and corresponding barrier for charge transport in a full metal/monolayer-semiconductor (MOMS) junction. A discrepancy was found for the dipolar effect in wettability; an anticipated trendline was not observed. The static hexadecane contact angle increased slightly from 39° (F1-C10-YNE) to 46° (F1-C18-YNE). These slight increases likely reflect two opposing trends. On the one hand they reflect a decrease in the dispersive interaction between the increasing amount of fluorine atoms and hexadecane as caused by the increasing density of F atoms on the surface.[5]

The exact effect on the wettability and exact orientation of F-CH_2- in this mono-fluorinated monolayer is still unclear and more in-depth studies will be needed and to probe this balance more in detail.[6] The interrelation between wettability, electronic structure, and exact orientation of the terminal groups would become more clear by e.g. substitution of groups on the surface (F-CH_2- substituted by X-CH_2- with X = D, I, Br, or Cl).

10.3 TRIBOLOGICAL APPLICATION

In **Chapter 4 and 5** novel fluoro-hydro alkynes with a varying number of fluorine atoms (#F atoms: 0 – 17) at a constant chain length (C16) were synthesized, high density

monolayer formation onto oxide-free H-Si(111) surfaces was performed and corresponding physical and tribological properties were characterized. The obtained F1-F17 monolayers displayed a hydrophobicity that is typical for fluorinated moieties. The water contact angle increased at higher fluorine content in the monolayer. For F17 a static water contact angle of 119° was measured, which is higher than PTFE = (115°). A PTFE surface displays a lower static water contact angle, because the CF_2 groups in PTFE are less capable of reducing the surface energy than the CF_3 groups present in F17.[7]

Monolayers based on F0 were characterized by a very low critical surface tension. Values of 20.1 mN/m were found, which is lower than characteristic values reported for CH_3-termination in literature (22 - 24 mN/m),[8] revealing the high organization of the monolayer. Increasing the number of F atoms in the monolayer further decreased the critical surface tension to 5.6 ± 0.21 mN/m for F17, which is – as far as we know – currently the lowest value for any solid surface. In view of possible applications for micro-devices the stability of these layers also in an aqueous environment have to be studied. Higher fluorinated alkyne induced monolayer formation on Si(111) seems interesting for both micro-nano fluidics and electronic devises. Special care should be taken for that alkynes are highly reactive to H-Si and other multi-fluorine components. Some Lab-on-Chip devices require hydrophobic fluidic channels and a sufficient chemical stability of these monolayers with a few nanometer thicknesses is desirable. In some cases Lab-on-Chip devices require a segmented flow with regions having a distinct hydrophobicity. Currently these fluidic channels are being modified using a fluorinated silane modification which is relatievely unstable in a basic environment. Another application of the fluoriated molecules is to use them in copper-catalyzed azide–alkyne cycloaddition (CuAAC) reactions, because the molecules are relatively easy to synthesize and soluble in polar aprotic/apolar solvents. The CuAAC chemistry is reliable and widely utilized, in both bio-medical and material chemistry.[9]

Moreover interfaces with a minimized surface energy have a great potential in MEMS/NEMS. It is shown that a highly uniform, upward presentation of CF_3 moieties, yields a very low interaction with the outside world, as evidenced by measured adhesion forces as low as 3.2 ± 0.03 mJ/m^2 and a friction coefficient of $1.2 \cdot 10^{-2}$ for an F17 monolayer (Si-(HC=CH)-(CH2)6-C8F17). Each of these values is either the lowest currently measured for any flat surface, or close to it. Furthermore, currently ongoing experiments in our lab to place on an atomically flat silicon surface a fluorinated polymer brush can further improve the tribological properties.[10]

Adhesive and friction forces can be measured with AFM using a molecularly modified colloidal probe. The organic monolayers (terminating with $-CH_3$ or $-CF_3$) can be placed in a lithographically defined pattern.[11] Adhesive interactions between unmodified silica (Si-OH) and those with a monolayer (CH_3/CH_3, CH_3/CF_3, CH_3/COOH, COOH/CF_3 or COOH/CH_3) can be easily compared. Also using a modified AFM probe with different functional groups is a more sensitive technique to characterize adhesional, frictional and chemical properties.[12]

As discussed in **Chapter 3** the electronic transport properties of fluorinated alkyne on silicon did show clearly a molecular dipole effect. Substituting the H with an F atom in the terminal group of the alkenyl chain revealed an increase of the workfunction (thus increasing the electron affinity) of the Si-monolayer surface. This increase is due to the altered direction/orientation of the C-F bond in comparison to that of the C-H bond. Examining the tuning of the Si workfunction at higher fluorine number with fixed number of carbon (See **figure 3**) still need to be studied in more detail.[13]

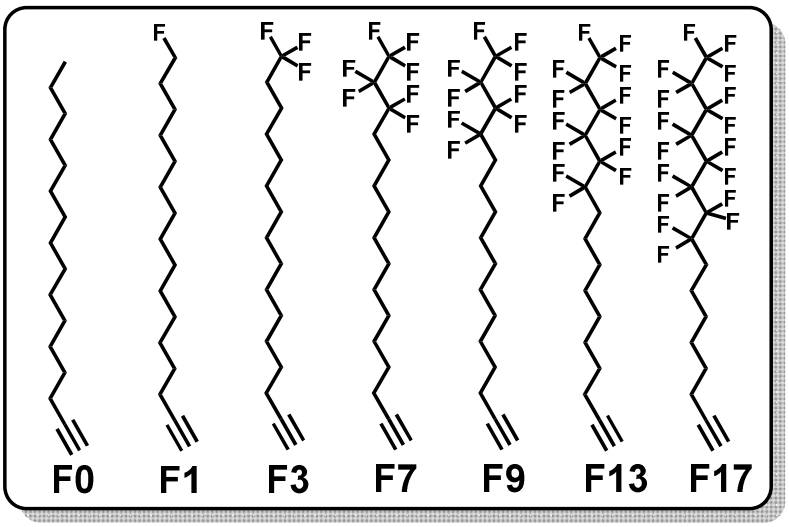

Figure 3. Tuning of the workfunction on Si substrates is possible with different novel synthesized fluorinated alkynes.

In **Chapter 6** both 1-alkynes (fluorinated and non-fluorinated) and 1-alkenes bound to silicon carbide surfaces provide improved access to low adhesion, low friction and high wear resistance properties. In literature only few results were shown for alkynes or alkenes reacting to hydroxyl terminated surfaces.[14, 15] Therefore it is still not clear how alkynes react to hydroxyl terminated[16] SiC surface. To guide (quantum) theoretical

understanding on the mechanistic structure more experiments may help. Our results show that the alkyne reacts twice to the hydroxyl-terminated silicon carbide substrates via a double Markovnikov addition. For future understanding deuterated alkyne or alkene chemistry may be helpful (see **Figure 4)** to elucidate the binding structure, especially via characterization of the corresponding infrared spectra.[17] In infrared spectra the C-D stretching band appears at a distinctive lower region 2200 cm^{-1}. The similar applies for using deuterated alkene.[18, 19]

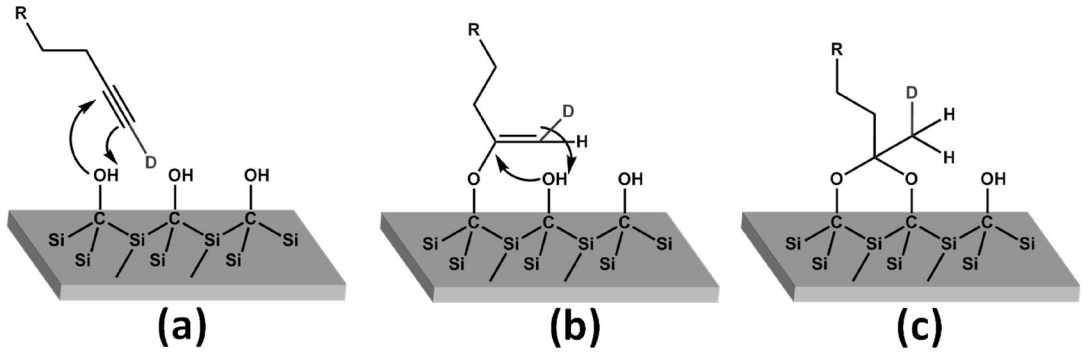

Figure 4. Proposed mechanism of the reaction between deuterated Alkyne (R-C≡C-D) and an OH-terminated SiC surface.

Fluorinated monolayers on SiC were shown to display minimal friction (friction coefficient down to 0.008) and corresponding low adhesion energies. In combination with the already low wear resistance of SiC surfaces itself; it is shown that these covalently bound fluorinated monolayers on SiC provide a promising alternative to currently used stable lubricants for high-performance micro-electronic devices. We will discuss here the example of an improved wafer chuck as can be used in wafer stepper lithography. Conventionally a wafer is clamped on a wafer chuck with a force originating from e.g. an applied vacuum or from a controlled electrostatic actuation method. Nowadays wafer chucks are being employed with a large number of mesas or flattened protrusions that define a second elevated surface (see Figure 5). The top surfaces of the mesas are therefore made of very hard and nonabrasive thin film substrate material, such as CrN, TiN, Si, SiC, SiN and SiSiC. The mesa top surface configuration defines a single plane for wafer support that is perfectly leveled and orientable into suitable directions with use of electrostatic clamping techniques. However even with a plurality of mesas providing a reduced contact surface, there remains a relatively large contact surface of the mesas physically in contact with the substrate. This may introduce a binding force, in the art known as "sticking", between the top faces of the mesas and the backside of the wafer.

Under vacuum operating conditions, such sticking may be considerable. In practice, this means that releasing the wafer from the wafer chuck can take a substantial amount of time causing a delay in the availability of the wafer stepper for a next lithographic round.

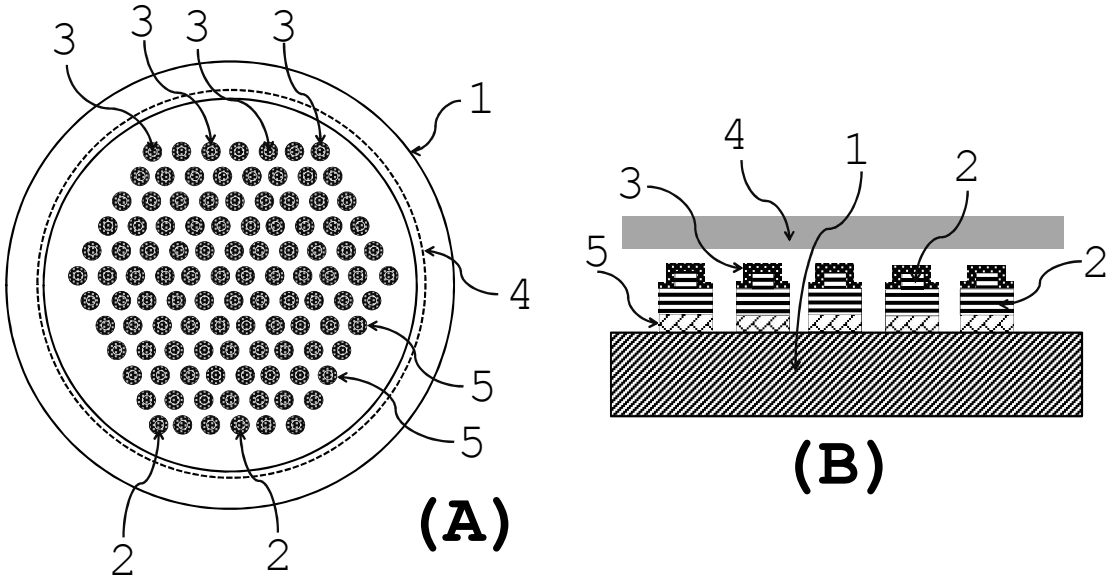

Figure 5. Shows a new generation wafer chuck, comprising a substrate with mesas defining a flat surface for clamping a wafer, A: Topview, B: Sideview.

As depicted in Figure 5 a fluorinated monolayer 3 is covalently bound to the top surface 2 of a substrate 1 having mesas 5 defining a flat surface for clamping a silicon wafer 4. The fluorinated monolayers exhibiting a minimum in friction and adhesion enable beneficially the lifting of the wafer from the wafer chuck in a controlled way with a minimal actuation force.

Also the developed high density, chemical and mechanical stable monolayers may be used in bio-chemical and bio-mechanical applications. For instance it would be readily possible to study further functionalizing of the monolayer by grafting it with a stable protein-repellent zwitterionic polymer brush. Schematic presentation as shown in **figure 6** for zwitterionic polymer brush grafted on SiC surfaces. [20, 21]

In **Chapter 7 and 8** for the first time, we have developed a novel method to obtain high-quality, covalently bound monolayers on CrN surfaces via the thermal reaction of 1-alkynes with an air plasma-activation of the CrN surface. We found in comparing alkyne and alkene, that the higher reactivity of 1-alkynes is attributed to the higher nucleophilicity of alkynes in comparison to that of alkenes. We also focused on the

ordering and mode of attachment of the alkene and alkyne molecules in the monolayers. Initial binding studies indicate an oxidative adsorption mode of attachment, with concomitant formation of surface-bound C=O groups. Difference in the alkyne and alkene chemistry for forming the monolayers needs further attention. In literature mechanistic information on both surface and catalyst may be available. Experimental observation might help for studying theoretical (quantum calculation) models of the CrN surface.

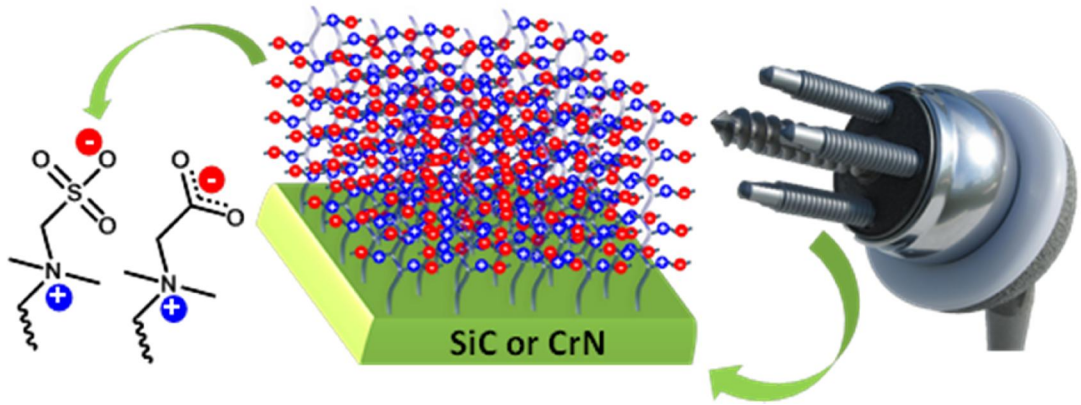

Figure 6. Schematic representations of zwitterionic (sulfobetaine or carboxybetaine) polymer brushes on SiC or CrN surfaces. Example of medical shoulder implant model (www.zimmer.com).

Furthermore, monolayers based on the reactivity of various anchoring groups like silane, phosphonate, 1-alkene and 1-alkyne moieties were obtained on the hydroxyl-terminated chromium nitride surface. We also investigated chemical stability and tribological properties (adhesion, friction, and wear) of organic monolayers on CrN. Strategies to modify chromium nitride (CrN) surfaces are important because of the increased applications of these materials in various areas such as hybrid electronics, medical implants, diffusion barrier layers, corrosion inhibition, and wettability control. Especially for medical (implant) application the modified substrate should be bio-compatibility. Zwitterionic polymer brush grafted on CrN surfaces have to be studied for antifouling properties, see **figure 6**. Modified CrN substrates has now been proven to comprise excellent tribological and chemical stable properties.

In **Chapter 9** we studied for the first time plasma-induced nanotexturing of polymeric surfaces with a covalently attached perfluorinated silane monolayer. Such surfaces displayed a long-term hydrolytic stability, with a minimal loss of superoleophobicity, as

indicated by immersion measurements in water for a period of >40 days. The resulting stochastic or ordered surfaces were characterized in detail by IR spectroscopy and XPS analyses with a variety of liquids, including water, hexadecane and soya oil. Our coatings can also be useful for other researchers, e.g. Tuteja et al.[22] We are thus confident that if a different low-surface energy coating is used similar results would be obtained with our structures as well.

10.4 CONCLUSIONS

The research described in this thesis evaluates the chemical stability and tribological properties of high quality homogeneously formed monolayers. Formation was performed using various anchoring and terminal groups(both fluorinated and non-fluorinated), and also on many different substrates. Fundamental understanding of the basic underlying chemical reaction mechanisms during formation has been obtained and this will not only bring progress in the scientific world, but will also enable a wide range of long-lasting chemical and mechanical stable modified surfaces, which are attractive for a variety of outdoor uses as well as in MEMS, medical, microfluidics and (bio-)sensor applications.

10.5 REFERENCE

1. Assad, O.; Puniredd, S. R.; Stelzner, T.; Christiansen, S.; Haick, H., Stable Scaffolds for Reacting Si Nanowires with Further Organic Functionalities while Preserving Si−C Passivation of Surface Sites. *Journal of the American Chemical Society* **2008,** 130, (52), 17670-17671.
2. McAlpine, M. C.; Agnew, H. D.; Rohde, R. D.; Blanco, M.; Ahmad, H.; Stuparu, A. D.; Goddard, W. A.; Heath, J. R., Peptide−Nanowire Hybrid Materials for Selective Sensing of Small Molecules. *Journal of the American Chemical Society* **2008,** 130, (29), 9583-9589.
3. Wan, J.; Deng, S.-R.; Yang, R.; Shu, Z.; Lu, B.-R.; Xie, S.-Q.; Chen, Y.; Huq, E.; Liu, R.; Qu, X.-P., Silicon nanowire sensor for gas detection fabricated by nanoimprint on SU8/SiO2/PMMA trilayer. *Microelectronic Engineering* **2009,** 86, (4–6), 1238-1242.
4. Elnathan, R.; Kwiat, M.; Pevzner, A.; Engel, Y.; Burstein, L.; Khatchtourints, A.; Lichtenstein, A.; Kantaev, R.; Patolsky, F., Biorecognition Layer Engineering: Overcoming Screening Limitations of Nanowire-Based FET Devices. *Nano Letters* **2012,** 12, (10), 5245-5254.
5. Lee, S.; Park, J.-S.; Lee, T. R., The Wettability of Fluoropolymer Surfaces: Influence of Surface Dipoles. *Langmuir* **2008,** 24, (9), 4817-4826.
6. Graupe, M.; Takenaga, M.; Koini, T.; Colorado, R.; Lee, T. R., Oriented Surface Dipoles Strongly Influence Interfacial Wettabilities. *Journal of the American Chemical Society* **1999,** 121, (13), 3222-3223.
7. van de Grampel, R. D.; Ming, W.; Gildenpfennig, A.; Laven, J.; Brongersma, H. H.; de With, G.; van der Linde, R., Quantification of Fluorine Density in the Outermost Atomic Layer. *Langmuir* **2004,** 20, (1), 145-149.

8. Baier, R. E.; Shafrin, E. G.; Zisman, W. A., Adhesion: Mechanisms That Assit or Impede It. *Science* **1968,** 162, (3860), 1360-1368.
9. Soules, A. l.; Ameduri, B.; Boutevin, B.; Calleja, G., Original Fluorinated Copolymers Achieved by Both Azide/Alkyne "Click" Reaction and Hay Coupling from Tetrafluoroethylene Telomers. *Macromolecules* **2010,** 43, (10), 4489-4499.
10. Nagendra S. Bhairamadgi; Pujari, S. P.; van Rijn, C. J. M.; Zuilhof, H., Superior Adhesion & Friction Properties of Fluoro-polymer Brushes on Si(111) Surfaces. **2013,** manuscript in preparation.
11. Frisbie, C. D.; Rozsnyai, L. F.; Noy, A.; Wrighton, M. S.; Lieber, C. M., Functional Group Imaging by Chemical Force Microscopy. *Science* **1994,** 265, (5181), 2071-2074.
12. Noy, A.; Vezenov, D. V.; Lieber, C. M., Chemical force microscopy. *Annu. Rev. Mater. Sci.* **1997,** 27, 381-421.
13. Alloway, D. M.; Hofmann, M.; Smith, D. L.; Gruhn, N. E.; Graham, A. L.; Colorado, R.; Wysocki, V. H.; Lee, T. R.; Lee, P. A.; Armstrong, N. R., Interface Dipoles Arising from Self-Assembled Monolayers on Gold: UV−Photoemission Studies of Alkanethiols and Partially Fluorinated Alkanethiols. *The Journal of Physical Chemistry B* **2003,** 107, (42), 11690-11699.
14. Franking, R.; Kim, H.; Chambers, S. A.; Mangham, A. N.; Hamers, R. J., Photochemical Grafting of Organic Alkenes to Single-Crystal TiO2 Surfaces: A Mechanistic Study. *Langmuir* **2012,** 28, (33), 12085-12093.
15. Dhar, S.; Seitz, O.; Halls, M. D.; Choi, S.; Chabal, Y. J.; Feldman, L. C., Chemical Properties of Oxidized Silicon Carbide Surfaces upon Etching in Hydrofluoric Acid. *Journal of the American Chemical Society* **2009,** 131, (46), 16808-16813.
16. ter Maat, J.; Regeling, R.; Ingham, C. J.; Weijers, C. A. G. M.; Giesbers, M.; de Vos, W. M.; Zuilhof, H., Organic Modification and Subsequent Biofunctionalization of Porous Anodic Alumina Using Terminal Alkynes. *Langmuir* **2011,** 27, (22), 13606-13617.
17. Ferguson, G. A.; Raghavachari, K.; Michalak, D. J.; Chabal, Y., Adsorbate−Surface Phonon Interactions in Deuterium-Passivated Si(111)-(1 × 1). *The Journal of Physical Chemistry C* **2008,** 112, (4), 1034-1039.
18. Luo, H.; Chidsey, C. E. D.; Chabal, Y., Infrared Spectroscopy of Covalently Bonded Species on Silicon Surfaces: Deuterium, Chlorine, and Cobalt Tetracarbonyl. *MRS Online Proceedings Library* **1997,** 477, 415.
19. de Smet, L. C. P. M.; Zuilhof, H.; Sudhölter, E. J. R.; Lie, L. H.; Houlton, A.; Horrocks, B. R., Mechanism of the Hydrosilylation Reaction of Alkenes at Porous Silicon: Experimental and Computational Deuterium Labeling Studies. *The Journal of Physical Chemistry B* **2005,** 109, (24), 12020-12031.
20. Nguyen, A. T.; Baggerman, J.; Paulusse, J. M. J.; Zuilhof, H.; van Rijn, C. J. M., Bioconjugation of Protein-Repellent Zwitterionic Polymer Brushes Grafted from Silicon Nitride. *Langmuir* **2011,** 28, (1), 604-610.
21. Gunkel, G.; Huck, W. T. S., Cooperative Adsorption of Lipoprotein Phospholipids, Triglycerides, and Cholesteryl Esters Are a Key Factor in Nonspecific Adsorption from Blood Plasma to Antifouling Polymer Surfaces. *Journal of the American Chemical Society* **2013**, (DOI: 10.1021/ja402126t).
22. Tuteja, A.; Choi, W.; Ma, M.; Mabry, J. M.; Mazzella, S. A.; Rutledge, G. C.; McKinley, G. H.; Cohen, R. E., Designing Superoleophobic Surfaces. *Science* **2007,** 318, (5856), 1618-1622.

Summary

Organic monolayers as described in this thesis are ultrathin (1 - 2 nm) layers of organic molecules covalently bound to an inorganic surface. To thoroughly understand and further improve the formation of monolayers detailed research is needed on corresponding anchoring molecules that provide the bond with the substrate. Knowledge has to be obtained in the precise mechanism of relevant reactions at the various interfaces that can be distinguished: molecule – substrate, liquid phase – forming monolayer, and in between monolayer-forming molecules. Selection of the right surface and anchoring molecules may provide a flexible tool to develop materials with desired properties both at the molecular and material level. Particularly in many micro and nano components, such as MEMS and NEMS, silicon is the main component material, and typical dimensions of such devices are a few to several 100s of microns. At these small scales, surface properties, such as Van der Waals and capillary forces, greatly influence the performance of these devices. Surface properties like minimal wear and low friction are therefore essential for application of tailor-made surfaces in these high-performance technological devices.

Several types of thin films have been investigated as coatings for inorganic surfaces with enhanced tribological properties. In particular, the nano-tribological behavior of fluorinated hydrocarbon-based organic coatings has been widely studied in order to produce durable and low-friction lubricant surfaces. These fluorinated hydrocarbon-based organic coatings on hard surfaces improve the tribological properties to a great extent. However (apart from silane coupling chemistry), those films are not covalently bound to the silicon and are therefore prone to wear. Fluorinated alkyne-derived monolayers on various surfaces will significantly expand their scope, as such monolayers are nanometer thin and strongly bound to the substrate, and display excellent tribological behavior. As such they display significant potential in MEMS/NEMS.

The aim of this thesis is to study the formation of such fluorinated monolayers on a variety of organic and inorganic surfaces, so as to minimize the surface energy with a greatly improved chemical stability in order to enable outstanding tribological properties.

In **Chapter 2**, we successfully developed a novel precursor, hexadeca-3-en-1-yne ($HC{\equiv}C\text{-}HC{=}CH\text{-}C_{12}H_{25}$), for the formation of high-quality monolayers on H-terminated silicon surfaces. Detailed kinetic and XPS studies show that hexadeca-3-en-1-yne reacts faster than the corresponding C_{16} alkyne and displays a higher packing density than the monolayers which had been reported up to now on H-Si(111). From Infrared and

NEXAFS studies, in combination with molecular modeling, our data confirm that the enyne-derived monolayers are more highly ordered, stable and densely packed than monolayers derived from the corresponding C_{16} alkyne (hexadecyne). These unique properties of enyne-derived monolayers make enynes (HC≡C-HC=CH-R) the agent of choice if a supreme monolayer quality is desired. Also a more stable oxide-free silicon interface is formed with an enyne-derived monolayer. This development facilitates a successful application of organic monolayers on silicon in electronic and biosensor devices.

In **Chapter 3**, we prepared a series of mono-ω-fluorinated 1-alkyne-derived monolayers of various thicknesses on oxide-free hydrogen-terminated Si(111). A combination of experimental and theoretical studies shows that high-quality monolayers can be obtained (e.g. a monolayer derived from F1-C18-yne has a packing density of 58 ± 2 %). It was demonstrated that by substitution of CH_3 to CH_2F in the terminal group, it is possible to controllably and stepwise modify the surface potential and barrier for charge transport in a full metal/monolayer-semiconductor (MOMS) junction. The work function of silicon surfaces can thus be altered to accommodate specific application needs, and therefore this technique extends the potential of using Si-C derived monolayers in the fabrication of MEMS and NEMS derived electronic devices.

Chapter 4, deals with the tribology of partially fluorinated monolayers grafted on oxide-free Si(111). These uniform and densely packed monolayers display a high degree of short-range ordering due to an upward presentation of the terminal CF_3 moieties. This resulted in a modified surface with an extremely low surface tension and adhesion as evidenced by the lowest critical surface tension currently measured for any flat surface, and correspondingly low adhesion forces, and friction coefficient. The present study expands the scope of application of strong covalently bound monolayers

Following **chapter 4**, in **Chapter 5** we focus on the nano-scale wear of such fluorinated monolayers. Covalently bound, densely packed fluoro-alkyl monolayers on Si(111) [e.g. ~Si-CH=CH-$(CH_2)_6$-$(CF_2)_8CF_3$] surfaces display an excellent wear resistance. Typically, no wear marks are seen to AFM-induced pressures of 8 μN, while even for pressures up to 24 μN the underlying Si is hardly damaged. Below these critical normal loads, the SAMs can accommodate the external forces by reorientation of the chains. These Si-C=C bound monolayers display such excellent wear-resistance due to the high bond strengths of the involved chemical bonds, and the high density of the monolayers that minimizes external penetration. Due to these superior wear resistance properties, fluoro-alkyl monolayers show a robustness that makes them useful for application in MEMS/NEMS.

Chapter 6 describs the formation of fluorinated and non-fluorinated monolayers of various chain lengths onto SiC surfaces, via a double Markovnikov addition, forming an acetal heteroatomic six membered ring. A new reaction mechanism for the reaction of un-substituted alkynes with hydroxyl-terminated surfaces is proposed. With the help of AFM studies we determined that fluorinated monolayers on SiC have a high durability, low adhesion and friction, as well as an extraordinary resistance to wear, when compared to non-fluorinated mono-layers.

In **Chapter 7**, we have developed a novel method to obtain high-quality, covalently bound monolayers on CrN surfaces via the thermal reaction of 1-alkynes with air plasma-activated CrN surfaces. The monolayers are readily formed (8 - 12 h), and are densely packed with a high degree of short-range order. Analogous monolayers derived from 1-alkenes are of lower quality. This was related in detail to the mode of attachment of 1-alkyne and 1-alkene derived monolayers. These monolayers provide substantial potential for further studies and can combine the unique material properties of CrN with the tunability of covalently attached monolayers.

Chapter 8 outlines a systematic chemical and mechanical stability study on CrN substrates with respect to anchoring, chain length-dependence, and structural changes in the fluorinated hydrocarbon. The chemical stability of the monolayer in aqueous solution on varying the pH was found in the following order: Alkyne ~ 2-hydroxy carboxylic acid > Phosphonic acid ~ Carboxylic acid > Alkene > Silane. Monolayers with longer chain length (# CH_2 units > 12) exhibited a lower adhesion, friction and higher wear resistance as compared to short chain (# CH_2 units < 12) monolayers. In conclusion, fluorinated monolayers on CrN were shown to have excellent tribological properties as compared to non-fluorinated counterparts.

Chapter 9 discusses the fabrication of superoleophobic polymer surfaces using a novel yet very simple two-step generic method of plasma etching followed by grafting of these etched surfaces with a perfluorosilane. These surfaces displayed a long-term hydrolytic stability, with minimal loss of the superoleophobicity, making them ideal candidates for application in a wide range of long-lasting superoleophobic surfaces, which are attractive for a variety of outdoor uses as well as in MEMS, microfluidics and (bio-) sensor applications.

Finally, in **Chapter 10** an overview is given of the most important findings presented in the thesis. Recommendation are being presented, as well as additional ideas on how to direct this research to novel fundamental aspects that are just getting within reach and also towards a wider industrial application of these exciting materials that demonstrate the ‘small is (very) beautiful’ theme.

Samenvatting

Onder organische monolagen, zoals beschreven in dit proefschrift, verstaan we ultradunne lagen (1-2 nm) van organische moleculen, die covalent gebonden zijn aan een anorganisch oppervlak (substraat). Om de vorming van deze monolagen diepgaand te kunnen begrijpen en om dit te verbeteren, is gedetailleerd onderzoek nodig naar moleculen met verschillende bindingsmogelijkheden met het anorganische oppervlak. Kennis moet worden vergaard over het precieze mechanisme van relevante reacties en interacties die aan alle betrokken grensvlakken plaats kunnen vinden, te weten: moleculen in oplossing met het anorganisch oppervlak en met de zich vormende monolaag en tussen de monolaag-vormende moleculen onderling. Door moleculen te gebruiken die de juiste reactiviteit voor een bepaald substraat bezitten kunnen gewenste oppervlakte-eigenschappen verkregen worden op zowel molecuulniveau (chemische reactiviteit) als materiaalniveau (fysische eigenschappen). Voor met name micro- en nano-componenten, zoals aanwezig in MEMS en NEMS, is silicium een belangrijk materiaal. De afmetingen van deze onderdelen variëren van enkele tot enkele honderden micrometers. Op deze kleine schaal spelen oppervlakte-eigenschappen, zoals Van der Waals krachten en capillaire werking, een grote rol in de prestaties van deze componenten. Oppervlakte-eigenschappen zoals slijtvastheid en lage wrijving zijn daarom essentieel voor de toepasbaarheid van deze op maat gemaakte anorganische oppervlakken in high-performance technologische apparaten.

Verschillende typen dunne lagen zijn onderzocht als coatings voor anorganische substraten om hun tribologische eigenschappen te verbeteren. Met name coatings gebaseerd op fluor-bevattende koolwaterstoffen zijn in detail onderzocht op hun nano-tribologische eigenschappen om duurzame en gladde oppervlakken met lage wrijving te produceren. Op harde oppervlakken verbeteren deze coatings gebaseerd op fluor-bevattende koolwaterstoffen de tribologische eigenschappen aanzienlijk. Behalve coatings gebaseerd op silaanchemie, zijn deze coatings echter niet covalent gebonden en zullen dus onderhevig zijn aan slijtage. Covalent gebonden fluor-bevattende monolagen op basis van alkynen kunnen gebonden worden aan verschillende oppervlakken en zullen beter presteren en breder inzetbaar zijn, omdat zulk soort monolagen ultradun zijn, sterk gebonden zijn aan het oppervlak en uitstekende tribologische eigenschappen laten zien. Hierdoor hebben deze monolagen veel potentie voor gebruik in MEMS en NEMS.

Het doel van dit proefschrift is om de vorming van zulke fluor-bevattende monolagen aan een breed scala van organische en anorganische oppervlakken te bestuderen om de

oppervlakte-energie te minimalizeren en tegelijkertijd de chemische stabiliteit te verbeteren om zodoende uitstekende tribologische eigenschappen mogelijk te maken.

In **hoofdstuk 2** is met succes een nieuwe precursor ontwikkeld voor de vorming van hoge kwaliteit monolagen op waterstof-getermineerd silicium (H-Si(111)), namelijk hexadeca-3-en-1-yn ($HC{\equiv}C\text{-}HC{=}CH\text{-}C_{12}H_{25}$). Gedetailleerd onderzoek naar de kinetiek van de reactie en analyse met XPS experimenten wijzen uit dat hexadeca-3-en-1-yn sneller reageert dan het overeenkomstige hexadec-1-yn ($HC{\equiv}C\text{-}C_{14}H_{29}$) en dat monolagen gevormd met hexadeca-3-en-1-yn de hoogste pakkingsgraad hebben van alle bekende monolagen op H-Si(111). Infrarood en NEXAFS metingen in combinatie met moleculair modelleren bevestigen dat de enyn monolagen beter geordend zijn, stabieler zijn en een hogere pakkingsgraad hebben dan overeenkomstige monolagen afgeleid van hexadec-1-yn. Deze unieke eigenschappen van enyn monolagen maken enynen ($HC{\equiv}C\text{-}HC{=}CH\text{-}R$) het beste reagens om monolagen met een extreem hoge kwaliteit te verkrijgen. Verder wordt een stabielere en beter zuurstof-vrij silicium oppervlak gevormd met de enyn monolaag. Deze ontwikkeling draagt bij aan succesvolle toepassing van organische monolagen op silicium in biosensors en electronische componenten.

In **hoofdstuk 3** wordt de synthese van een serie monolagen met verschillende lengtes op zuurstof-vrij H-Si(111) beschreven. Deze monolagen zijn gebaseerd op 1-alkynen, welke een enkel F-atoom hebben op de ω-positie. De combinatie van experimenteel en theoretisch onderzoek wijst uit dat monolagen van hoge kwaliteit verkregen worden (een monolaag gebaseerd op $F_1\text{-}C_{18}$-yne heeft bijvoorbeeld een pakkingsgraad van 58 ± 2 %). Door substitutie van de eindstandige CH_3 groep met CH_2F is het mogelijk om de oppervlaktepotentiaal en de ladingstransportbarrière op een gecontroleerde manier stapsgewijs aan te passen in een full metal/monolayer-semiconductor (MOMS) junction. De werkfunctie van siliciumoppervlakken kan zodoende worden aangepast aan de specifieke eisen van de toepassing. Hierdoor wordt de toepasbaarheid van monolagen op silicium carbide (SiC) voor fabricage van MEMS en NEMS onderdelen verhoogd.

Hoofdstuk 4 behandelt de tribologische eigenschappen van gedeeltelijk fluor-bevattende monolagen op zuurstof-vrij Si(111). Deze uniforme en dicht gepakte monolagen vertonen een hoge mate van korte afstand ordening doordat de terminale CF_3 groepen verticaal op het oppervlak staan. Dit resulteert in een gemodificeerd oppervlak met een extreem lage adhesie en oppervlaktespanning, blijkend uit de laagste kritische oppervlaktespanning ooit gemeten voor een vlak substraat, alsmede de ermee corresponderend lage adhesiekrachten en frictiecoëfficienten. Het huidige onderzoek verbreedt de toepassingsmogelijkheden van sterke covalent gebonden monolagen.

Als vervolg op hoofdstuk 4, wordt in **hoofdstuk 5** verder ingegaan op de slijtage op nanoschaal van zulke fluor-bevattende monolagen. Covalent gebonden, dichtgepakte fluor-alkyl monolagen op Si(111) [bijvoorbeeld ~Si-CH=CH-$(CH_2)_6$-$(CF_2)_8CF_3$] oppervlakken vertonen een uitstekende weerstand tegen slijtage. Er werd geen slijtage waargenomen bij AFM-geïnduceerde druk tot 8 μN, terwijl zelfs bij 24 μN het onderliggende Si substraat nauwelijks schade ondervindt. Beneden deze kritische belasting kan de monolaag de externe krachten opvangen door het heroriënteren van de ketens. Deze Si-C=C gebonden monolagen vertonen zulke uitstekende slijtagebestendige eigenschappen door de sterke chemische bindingen en de hoge pakkingsgraad van de monolagen, waardoor externe penetratie wordt geminimaliseerd. Deze superieure bestendigheid tegen slijtage maken fluor-alkyl monolagen robuust en nuttig voor MEMS/NEMS toepassingen.

In **hoofdstuk 6** wordt de synthese van al dan niet fluor-bevattende monolagen met verschillende ketenlengtes op silicium carbide (SiC) oppervlakken beschreven. Via een dubbele Markovnikov additie wordt hierbij een heterocyclische zesring met een acetaal gevormd. Een nieuw mechanisme voor de reactie van ongesubstitueerde alkynen met hydroxyl-getermineerde oppervlakken wordt voorgesteld. Met behulp van AFM is vastgesteld dat de fluor-bevattende monolagen in vergelijking met monolagen zonder fluoratomen op SiC een hogere duurzaamheid en lagere adhesie en frictie vertonen. Verder is een uitzonderlijk hoge bestendigheid tegen slijtage gevonden.

In **hoofdstuk 7** wordt een nieuwe methode beschreven om hoge kwaliteit, covalent gebonden monolagen op chromium nitride (CrN) oppervlakken te verkrijgen. In deze thermische reactie worden 1-alkynen gereageerd met plasma-geactiveerde CrN oppervlakken. De monolagen worden makkelijk gevormd (8 – 12 h) en hebben een hoge pakkingsgraad met een hoge mate van korte afstandsordening. Analoge monolagen, verkregen via de reactie van 1-alkenen met CrN oppervlakken leveren monolagen op met een lagere kwaliteit. Dit wordt in detail uitgelegd aan de hand van de reactiemechanismen van 1-alkynen en 1-alkenen met CrN oppervlakken. Deze monolagen vertonen potentieel voor verder onderzoek en kunnen de unieke materiaaleigenschappen van CrN combineren met de afstembaarheid van covalent gebonden monolagen.

In **hoofdstuk 8** wordt een systematische studie naar de chemische en mechanische stabiliteit van fluor-bevattende koolwaterstof monolagen op CrN substraten beschreven. Variabelen zijn de hechtingsmethode aan het oppervlak, ketenlengte en structuurveranderingen van de fluor-bevattende koolwaterstoffen. De chemische stabiliteit van de monolaag in waterige oplossingen met verschillende pH werd als volgt vastgesteld: Alkyne ~ 2-hydroxy carboxylic acid > Phosphonic acid ~ Carboxylic acid > Alkene >

Silane. Monolagen met een langere ketenlengte (> 12 CH_2 eenheden) vertonen een lagere adhesie, frictie en hogere slijtvastheid dan monolagen met korte ketens (< 12 CH_2 eenheden). Fluor-bevattende monolagen op CrN vertonen uitstekende tribologische eigenschappen vergeleken met monolagen zonder fluoratomen.

In **hoofdstuk 9** wordt de fabricage behandelt van superoleophobische polymeeroppervlakken, gemaakt met behulp van een nieuwe maar eenvoudige twee-staps procedure, waarin het oppervlak eerst geëtst wordt met plasma, gevolgd door reactie met een perfluorosilaan. Deze oppervlakken vertonen langdurige stabiliteit tegen hydrolyse met minimale afname in superoleophobiciteit. Dit maakt deze oppervlakken uitermate geschikt voor toepassingen waarbij een langdurige oleophobiciteit van het oppervlak wenselijk is, zoals in buitenhuistoepassingen, in MEMS onderdelen, microfluidica en (bio)sensoren.

Tenslotte geeft **hoofdstuk 10** een overzicht van de belangrijkste bevindingen van dit proefschrift. Aanbevelingen en nieuwwe ideeën worden aangegeven om dit onderzoek uit te breiden naar nieuwe, fundamentele aspecten, waarvan de bestudering pas recent binnen bereik zijn gekomen en naar bredere industriële toepassingen van deze materialen die het “klein is (heel) fijn” thema laten zien.

Overview of completed training activities

Discipline specific activities (courses, workshops, symposia, summer schools etc.)

⇒AVS 58th International Symposium and Exhibition (Oral)	Nashville Tennessee, USA,	2010
⇒NWO Lunteren meeting Netherlands (Poster)	Lunteren, Netherlands	2009, 2010
⇒SANAM 2011 Würzburg Germany (Poster)	Würzburg Germany	2011
⇒S.P.A.M. project review by the European Commission (Poster) (Oral)	Eindhoven, Netherlands	2011
⇒12th ASML Technology Conference. Neatherland (Poster)	Eindhoven, Netherlands	2011
⇒24th International Conference on SURFACE MODIFICATION TECHNOLOGIES (SMT 24) (Oral)	Dresden, Germany	2010
⇒CHAINS (Chemistry As Innovating Science) (Poster)	Maarssen, Netherlands	2011
⇒TransACTS conference Lunteren, Netherlands (Oral)	Lunteren, Netherlands,	2012
⇒Wageningen symposium on organic chemistry, Royal Netherlands Society of Chemistry (KNCV) (2013 - Oral)	Wageningen, Netherlands	2010-2013
⇒Advanced organic chemistry 1&2	ORC	2010- 2013
⇒Basic training surface cleanliness and conditioning by SRT 2 and TEP C , Alcatel Vacuum, Annecy, France	Annecy, France	2009
⇒Basic training surface conditioning and modification by SRT 3 and TEP A Wageningen University, Netherlands.	Wageningen, Netherlands.	2009
⇒Winter School on Lithography and complementary competences and advance training by SRT 1 and TEP A Delft University, Netherlands.	Delft, Netherlands.	2011
⇒Basic training surface conditioning and preparation by SRT 2 and TEP C , BESSY Berlin, Germany.	Berlin, Germany.	2010
⇒Ultra Clean Processing of Semiconductor Surfaces UCPSS 2010 conference Oostende Belgium	Oostende, Belgium	2010

General courses (language courses, presentation courses, statistics, etc.)

⇒WGS course: workshop Scientific Publishing (21 January 2011/ 19 Jun 2012)	Wageningen	2011 & 2012
⇒English language course at Regina Coeli 16 - 20 May 2011 (week 20).	Vught	2011
⇒WGS course: Reviewing a Scientific Paper (8 Nov 2012)	Wageningen	2012
⇒WGS course: Philosophy and Ethics of Food Science & Technology (2012)	Wageningen	2012
⇒WGS course: Techniques for Writing and Presenting a Scientific paper (Sept 2012)	Wageningen	2012
⇒WGS course: Career Orientation (9 - 15 September 2012)	Wageningen	2012
⇒WGS course: Career Perspectives (14, 21, 28 March and 4 and 11 April 2013)	Wageningen	2013

Optionals (participation in discussion groups, PhD excursions, MSc courses, etc.)

⇒PhD trip ORC Scotland and England 22/5/2011 to 28/5/2011	ORC	2011
⇒PhD trip ORC Switzerland and Germany 17/4/2013 to 26/4/2013	ORC	2013
⇒Group meetings	ORC	2009-2013
⇒Colloquia	ORC	2009-2013
⇒Preparing PhD research proposal	VLAG/ORC	2009-2013

Acknowledgements

"Kayakave Kailasa"
("Work is Worship")

This work would not have been possible without the help of many people. At this point I would like to thank all who contributed to this work and supported me during the last few years.

First of all, I would like to thank **Prof. Han Zuilhof** for giving me the opportunity to work in his group as well as to learn surface chemistry. It is really great to work with you. I have learned a lot of things from you, which not only include the basics of surface chemistry, but also how to deal with relevant research questions. I would also like to thank you for your supervision, helpful advice, inspiration and input for my work and for corrections of my thesis and paper writing.

Furthermore, I would like to thank **Prof. Cees van Rijn** for his guidance during my PhD and also for the useful discussions about industry-oriented research problems. My thanks also go to **Dr. Jos M. J. Paulusse** for his supervision and help in the initial stages of my research. Jos, I have learned lots of modern chemistry from you.

My special thanks to **Dr. Luc Scheres** for extensive scientific discussions during my PhD. Luc, thank you also for all the time you spent reading and correcting my texts. You were a great support for my research.

I would also like to extend my thanks to **Prof. Martien Cohen Stuart** and **Dr. Evan Spruijt** for the fruitful collaboration to study the tribological properties of different surfaces. Evan, you are a great scientist as well as a professional neighbor and I always enjoyed learning from you and discussing many things about tribological properties with you. I would also like to thank **Dr. Tobias Weidner** and **Dr. Joe E. Baio** (from Washington University, USA and Max Planck Institute for Polymer Research, Mainz, Germany) for their work on NEXAFS, which was a great addition to Chapters 3, 5 and 6. I am also grateful to **Prof. David Cohen** and **Dr. Omer Yaffe** from Weizmann Institute,

Israel, for studying the electronic properties of the monolayers (Chapter 3). I am obliged to **Prof. Evangelos Gogolides** and **Dr. Kosmas Ellinas** from Institute of Microelectronics, NCSR "Demokritos", Greece for the nice work they did with the superhydrophobic polymeric surfaces.

I would like to thanks all my colleagues in Laboratory of Organic Chemistry. Special thanks to Dr. Ton Marcelis, Dr. Teris van Beek, Dr. Maurice Franssen, Dr. Tom Wennekes and Prof. Michel Nielen, for all the advanced organic chemistry courses and for providing additional answers to many of my questions during the project.

I am indebted to Barend van Lagen, Marcel Giesbers, Remco Fokkink and Ed Snoek (JEOL) for their help with surface characterization techniques. Thanks to Frank Claassen, Remco Regeling, Elbert van der Klift and Ronald de Bruin for their help with analytical measurements and keeping laboratory equipment in good condition. I would like also thank to Cees van de Haar, Erik van Rozendaal and Anne-Marie Franssen-Hagebols, for their help while practical course teaching. Furthermore, I would also like to thank Elly Geurtsen, Aleida Ruisch and Anita ter Haar for their help with official documents.

Dr. Bart Rijksen, thank you for your help with synthesizing ene-yne molecules and also with the computational calculations. I also would like to thank Mabel A. Caipa Campos, Ankush T. Mane and Yan Li for their initial help for surface modification and fruitful discussions. I appreciate the help of Dr. Jacob Baggerman and Dr. Steven Calder with mathematical calculations.

I want to thank Esther, Quirijn, Naomi, Aljosha, and Hadas (Israel), the students who did their BSc or MSc thesis work under my guidance; for their hard work and quick understanding which supported me a lot with my scientific work. My special thanks to Ton, Bas and Aljosha for translating and correcting the PhD thesis summery from English to Dutch.

I would also like to thank my PhD colleagues from 2009 to 2013: Feng, Kim, Loes, Wouter, Jurjen, Ai, Bart, Willem, Nagesh, Sourav, Tin, Jacinthe, Jerome, Anke, Alexander, Umesh, Jaime, Radostina, Florine, Saurabh, Nagendra, Satesh, Bas, Aline, Wilco, Jorin, Sweccha, Yao, Tjerk, Rickdeb, Christie, and..... post-docs Hamilton, Denis, Nassir, Alonso, Kuldeep, Wang, and..…for all the scientific and non-scientific discussions we had together.

I would like to thank my entire group of Indian friends in Wageningen: Sourav, Nagesh, Umesh, Saurabh, Nagendra, Satesh, Sachin, Soumi, Surender, Rickdeb, Liyaqat, Rajesh, and..... for playing cricket, having discussions on many subjects and cooking Indian spicy food many times :-). Especially, I want to thank Nagendra for the almost three years that we spent in one office. He is a great polymer chemist and I discussed a lot of topics with him, especially about polymer brush synthesis (both fluorinated :-) and non-fluorinated). I want to thank Nagesh for his initial help to start up my life in Wageningen and for helping a lot in correcting my papers. I would like to thank Satesh for being such a nice neighbor and being a great help with computational chemistry.

I would also like to thank my best friend Radostina and her son Angie, for having lots of fun. I also thank Esther, Anke, Julian and Luc from Surfix for discussing the scientific, non-scientific and lot of other humorous stuff. I also thank Enid Tomkinson, for giving me English training while in Wageningen.

Finally, I want to thank my family members, parents (avva and appa), grandmother, my brothers, sisters, uncle, auntie and also my other friends from India for their immense support and guidance while reaching the goal I aimed for in the following manner:

"Take up one idea. Make that one idea your life - think of it, dream of it, live on that idea. Let the brain, muscles, nerves, every part of your body, be full of that idea, and just leave every other idea alone. This is the way to success."

-Swami Vivekananda

Wageningen, September 2013

Sidharam Pundlik Pujari

List of Publication

1. *Optical properties of a novel fluorene-based thermally stable conjugated polymer containing pyridine and unsymmetric carbazole groups.* Der-Jang Liaw, Kun-Li Wang, En-Tang Kang, Sidharam P. Pujari, Min-Hung Chen, Ying-Chi Huang, Bo-Cheng Tao, Kueir-Rarn Lee, and Juin-Yih Lai. Journal of Polymer Science Part A: Polymer Chemistry. **2009**, 47 (4), 991–1002

2. *A novel, conjugated polymer containing fluorene, pyridine and unsymmetric carbazole moieties: Synthesis, protonation and electrochemical properties.* Der-Jang Liaw, Kun-Li Wang, Sidharam P. Pujari, Ying-Chi Huang, Bo-Cheng Tao, Min-Hung Chen, Kueir-Rarn Lee, Juin-Yih Lai. Dyes and Pigments, **2009**, 82 (2), 109–117

3. *Biofunctional Silicon Nanoparticles by Means of Thiol-Ene Click Chemistry*. Loes Ruizendaal, Sidharam P. Pujari, Veronique Gevaerts, Jos M. J. Paulusse, and Han Zuilhof. Chemistry – An Asian Journal, **2011**, 6 (10), 2776 – 2786

4. *Hexadecadienyl Monolayers on Hydrogen-Terminated Si (111): Faster Monolayer Formation and Improved Surface Coverage Using the Enyne Moiety.* Bart Rijksen,/Sidharam P. Pujari, Luc Scheres, Cees J. M. van Rijn, Joe E. Baio, Tobias Weidner, Han Zuilhof. *Langmuir*, **2012**, 28 (16), 6577–6588

5. *Copper-Free Click Biofunctionalization of Silicon Nitride Surfaces via Strain-Promoted Alkyne–Azide Cycloaddition Reactions*. Radostina K. Manova, Sidharam P. Pujari, Carel A. G. M. Weijers, Han Zuilhof, and Teris A. van Beek. Langmuir, **2012**, 28 (23), 8651–8663

6. *Ultralow Adhesion and Friction of Fluoro-Hydro Alkyne-Derived Self-Assembled Monolayers on H-Terminated Si(111)*. Sidharam P. Pujari, Evan Spruijt, Martien A. Cohen Stuart, Cees J. M. van Rijn, Jos M. J. Paulusse, and Han Zuilhof. *Langmuir*, **2012**, 28 (51), 17690–17700

7. *Mono-Fluorinated Alkyne-Derived SAMs on Oxide-Free Si(111) Surfaces: Preparation, Characterization and Tuning of the Si Workfunction*. Sidharam P. Pujari, Esther van Andel, Omer Yaffe, David Cahen, Tobias Weidner, Cees J. M. van Rijn, and Han Zuilhof. *Langmuir*, **2013**, 29 (2), 570–580

8. *Covalently Attached Organic Monolayers onto Silicon Carbide from 1-Alkynes: Molecular Structure and Tribological Properties*. Sidharam P. Pujari, Luc Scheres, Tobias Weidner, Joe E. Baio, Martien A. Cohen Stuart, Cees J. M. van Rijn, and Han Zuilhof. Langmuir, **2013**, 29 (12), 4019–4031

9. *Effect of Doping Density on the Charge Rearrangement and Interface Dipole at the Molecule–Silicon Interface*. Omer Yaffe, Sidharam P. Pujari, Ofer Sinai, Ayelet Vilan, Han Zuilhof, Antoine Kahn, Leeor Kronik, Hagai Cohen, and David Cahen. *J. Phys. Chem. C*, **2013**, in press, DOI:10.1021/jp403177e.

10. *Covalently Attached Organic Monolayers from 1-Alkynes onto Chromium Nitride: Alkyl and Fluoroalkyl Termination*. Sidharam P. Pujari, Luc Scheres, Barend van Lagen, and Han Zuilhof. *Langmuir*, **2013,** in press, DOI:10.1021/la401978h

11. *Tribology and Stability of Organic Monolayers on CrN: A Comparison among Silane, Phosphonate, Alkene, and Alkyne Chemistries*. Sidharam P. Pujari, Yan Li, Remco Regeling, and Han Zuilhof. *Langmuir*, **2013,** in press, DOI:10.1021/la401981b

12. *Highly Wear-Resistant Ultra-Thin Per-fluorinated Organic Monolayers on Silicon (111) Surfaces*. Sidharam P. Pujari and Han Zuilhof. Applied Surface Science, **2013** *Accepted (Ms. Ref. No.: APSUSC-D-13-02378)*.

13. *Covalent Surface Modification of Oxide Surfaces*. Sidharam P. Pujari, Luc Scheres, Ton Marcelis, and Han Zuilhof. *Angewandte Chemie International Edition,* Submitted **2013**. (*Ms. Ref. No.: anie.201306709.* invited review paper)

14. *Light-Activated Electroactive Molecule-Based Memory Microcells Confined on Silicon Surface*. Bruno Fabre, Yan Li, Luc Scheres, Sidharam P. Pujari, and Han Zuilhof. *Angewandte Chemie International Edition*, *Submitted* **2013**.

15. *Superoleophobic and Highly Stable Perfluorinated Monolayers on Polymer Surfaces*. Sidharam P. Pujari, Ellinas, Kosmas, Tserepi, Angeliki, Gogolides, Evangelos and Han Zuilhof. *Submitted* **2013**.

16. *Adhesion and Friction Properties of Polymer Brushes: Effects of Fluorination and Thickness*. Nagendra S. Bhairamadgi, Sidharam P. Pujari, Cees J. M. van Rijn, and Han Zuilhof. *Submitted* **2013.**

17. *Hydrocarbon and Functionalized Short-Chain Alkynes to Expand the Palette of Gases and Liquids for Si(111) Surface Modification.* Sidharam P. Pujari, Aljosha Filippov, Satesh Gangarapu, and Han Zuilhof. *In Preparation* **2013.**

18. *H-terminated Si(111) Modification With Trans-enynes: High Quality and Stable Monolayer.* Sidharam P. Pujari, Naomi Vos, and Han Zuilhof. *In Preparation* **2013.**

19. *Adhesion and friction properties of (dry and wet) per-fluoro polymer brushes: effect of fluorine content*. Nagendra S. Bhairamadgi, Sidharam P. Pujari, Cees J. M. van Rijn, and Han Zuilhof. *Manuscript in Preparation* **2013.**

20. *Improved Nucleophile Properties of Alkenes to Enhance Monolayer Density on H-Si(111).* Hadas Alon, Sidharam P. Pujari, Satesh Gangarapu, Chaim Sukenik, and Han Zuilhof. *Manuscript in Preparation* **2013**.

About the author

Sidharam Pundlik Pujari was born on the June 1st 1982 in Solapur, (Akkalkot, Shaval) India. He received his bachelor's degree (2000-2003) in Chemistry from the Shivaji University (Sangameshwar College, Solapur), India and Master's degree (2003-2005) in Inorganic Chemistry (Bio-Inorganic) from the University of Pune (Department of Chemistry), India. After finishing his Master's degree, he worked (2005-2006) in Homogeneous Catalyst Division, National Chemical Laboratory (NCL) Pune, India. There after he started as a researcher in Taiwan (2007-2009) in the field of Polymer Chemistry, Chemical Engineering Division, National Taiwan University Science and Technology, Taipei (NTUST) under guidance of Prof. Der-Jang Liaw. Currently (2009-Present), he is a PhD student at the Lab. of Organic Chemistry, Wageningen University in the Netherlands, working in the field of Surface/Material Chemistry under the supervision of Prof. Dr. Han Zuilhof and Prof. Dr. Cees van Rijn. From the 1st September 2013, he will be working as Post-Doctoral Research Fellow (PDF) in the group Prof. Dr. Han Zuilhof in the Lab. of Organic Chemistry, Wageningen University in the Netherlands.

The research described in this was financially supported by the Marie Curie European Union FP7 project "Surface Physics for Advanced Materials (SPAM)"

Design & Layout: Sidharam Pundlik Pujari

Printed by: Wöhrmann Print Service B.V.